


Feng Xu · Tianjian Lu

Introduction to Skin Biothermomechanics and Thermal Pain

 Science Press
Beijing

 Springer


Feng Xu
Tianjian Lu

**Introduction to Skin Biothermomechanics and
Thermal Pain**

Feng Xu
Tianjian Lu

Introduction to Skin Biothermomechanics and Thermal Pain

With 126 figures

 Science Press
Beijing

 Springer

Authors

Feng Xu
Brigham Women's Hospital
Harvard Medical School Harvard University
Cambridge, MA, 02139, USA
Email: fxu2@rics.bwh.harvard.edu

Tianjian Lu
School of Aerospace
Xi'an Jiaotong University
Xi'an, Shaanxi, 710049, China
Email: tjlu@mail.xitu.edu.cn

ISBN 978-7-03-027077-1
Science Press Beijing

ISBN 978-3-642-13201-8 e-ISBN 978-3-642-13202-5
Springer Heidelberg Dordrecht London New York

Library of Congress Control Number: 2010927408

© Science Press Beijing and Springer-Verlag Berlin Heidelberg 2011

This work is subject to copyright. All rights are reserved, whether the whole or part of the material is concerned, specifically the rights of translation, reprinting, reuse of illustrations, recitation, broadcasting, reproduction on microfilm or in any other way, and storage in data banks. Duplication of this publication or parts thereof is permitted only under the provisions of the German Copyright Law of September 9, 1965, in its current version, and permission for use must always be obtained from Springer-Verlag. Violations are liable to prosecution under the German Copyright Law.

The use of general descriptive names, registered names, trademarks, etc. in this publication does not imply, even in the absence of a specific statement, that such names are exempt from the relevant protective laws and regulations and therefore free for general use.

Cover design: Frido Steinen-Broo, EStudio Calamar, Spain

Printed on acid-free paper

Springer is a part of Springer Science+Business Media (www.springer.com)

Preface

Advances in laser, microwave and similar technologies in medicine have led to recent developments of thermal treatments for disease and injury, involving skin tissue. In spite of the widespread use of thermal therapies in dermatology, they do not draw upon the detailed understanding of the biothermomechanical-neurophysiological behaviour, for none exists to date, even though each behavioural facet is somewhat established and understood. In view of this dilemma, a new research area emerges, which is the subject of this book: “Introduction to Skin Biothermomechanics and Thermal Pain”. This area is highly interdisciplinary, involving the subjects of engineering, biology and neurophysiology. This book is focused on the introduction of this new research area. According to the schematic relationship between the areas involved, this book is divided into four parts: PART I. Skin bioheat transfer and thermal damage; PART II. Skin biomechanics; PART III. Skin biothermomechanics; PART IV. Skin thermal pain.

The book is multidisciplinary with a market across several subject areas and will be interesting to a wide range of readers from lab bench to clinics. The book is primarily planned as a textbook and reference book. It targets three segments of readers:

- (1) Advanced students: this book primarily aimed at advanced graduate students in bioengineering, who have already some knowledge of engineering.
- (2) Researchers: researchers may find this book a good reference, e.g. data base of different properties of skin tissue. Besides skin tissue, the methodology in this book can also be very useful for researchers on other biological tissues.
- (3) Clinicians: the holistic methodology introduced in this book will be very helpful for clinicians to design, characterize and optimize strategies of delivering thermal therapies.

Feng Xu
Tianjian Lu
July 2010

Contents

Chapter 1 Introduction	1
1.1 Introduction	1
1.2 Skin Biothermomechanics and Thermal Pain	1
1.3 Outline of the Book	5
References	5
Chapter 2 Skin Structure and Skin Blood Flow	7
2.1 Introduction	7
2.2 Skin Structure	7
2.3 Skin Blood Perfusion	17
References	17
PART I SKIN BIOHEAT TRANSFER	
Chapter 3 Skin Bioheat Transfer and Skin Thermal Damage	23
3.1 Introduction	23
3.2 Skin Bioheat Transfer	25
3.3 Skin Thermal Damage	42
3.4 Summary	58
References	59
Chapter 4 Analysis of Skin Bioheat Transfer	69
4.1 Introduction	69
4.2 Skin Bioheat Transfer Analysis with Fourier Model	69
4.3 Skin Bioheat Transfer Analysis with Non-Fourier Models	73
4.4 Summary	79
References	80
PART II SKIN BIOMECHANICS	
Chapter 5 Skin Mechanical Behaviour	87
5.1 Introduction	87
5.2 Skin Behaviour under Stretch	87
5.3 Skin Behaviour under Compression	89
5.4 Skin Failure	90
5.5 Skin Friction	94
References	97

Chapter 6 Skin Biomechanics Experiments: Measurement and Influence of Different Factors	105
6.1 Introduction	105
6.2 <i>In Vivo</i> Measurements	114
6.3 <i>In Vitro</i> Measurements	118
6.4 Influence of Different Factors	127
6.5 Summary	139
References	139
Chapter 7 Skin Biomechanics Modeling	155
7.1 Introduction	155
7.2 Continuum Models and Phenomenological Models	158
7.3 Structural Models	179
7.4 Summary	196
References	198
PART III SKIN BIOTHERMOMECHANICS	
Chapter 8 Introduction of Skin Biothermomechanics	209
8.1 Introduction	209
8.2 Mechanism of Thermal Denaturation (Shrinkage) of Collagen	209
8.3 Properties Variations due to Thermal Denaturation of Collagen	212
References	217
Chapter 9 Analysis of Skin Biothermomechanics	221
9.1 Introduction	221
9.2 Theoretical Analysis of Thermal Stress	222
9.3 Analysis with Fourier Bioheat Transfer Models	226
9.4 Analysis with Non-Fourier Bioheat Transfer Models	244
9.5 Summary	258
9.6 Appendix	259
References	264
Chapter 10 Experimental Characterization of Skin Biothermomechanics	267
10.1 Introduction	267
10.2 Experimental Methodology	267
10.3 Thermal Denaturation of Collagen in Skin Tissue	282
10.4 Hydrothermal Tensile Tests	286
10.5 Hydrothermal Compressive Tests	290
10.6 Characterization of Skin Viscoelasticity with Static Tests	301

10.7 Summary and Limitations 312
 References 314

PART IV SKIN THERMAL PAIN

Chapter 11 Skin Thermal Pain Mechanism 327
 11.1 Introduction 327
 11.2 Definition of Pain and Pain Pathways 328
 11.3 Anatomy and Physiology of Nociceptors 329
 11.4 Theories of Thermal Pain 335
 References 337

Chapter 12 Physiological Features of Pain Sensation 343
 12.1 Introduction 343
 12.2 Role of C and $A\delta$ Nociceptors 343
 12.3 Influence of Stimulus Temperature on Pain 345
 12.4 Influence of Nociceptors Depth 345
 12.5 Influence of Temperature Change Rate on Pain 345
 12.6 Temporal Summation 347
 12.7 Influence of Stimulus Duration 350
 12.8 Spatial Summation 352
 12.9 Hyperalgesia and Tissue Damage 354
 12.10 Influence of Origin of Skin (Different Part in Body) 356
 12.11 Influence of Skin Type 357
 12.12 Gender Difference 358
 12.13 Influence of Age 360
 12.14 Summary 361
 References 361

Chapter 13 Skin Thermal Pain Modeling 375
 13.1 Introduction 375
 13.2 Model of Transduction 376
 13.3 Model of Transmission 389
 13.4 Model of Modulation and Perception 391
 13.5 Results and Discussion 394
 13.6 Summary 407
 References 408

Chapter 1

Introduction

1.1 Introduction

All biological bodies live in a thermal environment with no exception of human body, where skin is the interface with protecting function. It is the largest single organ of the body and plays a variety of important roles including sensory, thermoregulation and host defense etc. Among these roles, the most important one is the thermoregulation: skin functions thermally as a heat generator, absorber, transmitter, radiator, conductor and vaporizer. This thermoregulation function makes the skin an important barrier for the human body to various outside conditions. However, in extreme environment, people may feel uncomfortable or even pain due to extreme hot or cold. Obviously, skin fails in protecting the human body when the temperature is out of normal physiological range. Furthermore, in medicine, various thermal therapeutic methods have been used widely to cure disease/injury involving skin tissue, where the objective is to induce thermal injury precisely within skin tissue but without affecting the surrounding healthy tissue.

Then, questions come up. Why do human beings feel uncomfortable/pain in extreme thermal environment? What is happening in human body in extreme thermal environment? How to protect human body in extreme thermal environment? These questions have been addressed in this book.

1.2 Skin Biothermomechanics and Thermal Pain

1.2.1 What is skin thermomechanics and thermal pain?

Skin biothermomechanics and thermal pain is the study of the bio-thermal-mechanical-neurophysiological behaviors of skin tissue under different thermomechanical loadings.

1.2.2 Specialities of the problem

1) Thermal behaviour in skin tissue

Thermal behavior, or heat transfer, in skin is mainly a heat conduction process coupled to complicated physiological processes, including blood circu-

lation, sweating, metabolic heat generation, and sometimes heat dissipation via hair or fur above the skin surface. Thermal properties of skin vary in different layers; even within the same layer, there exists large non-homogeneity and anisotropy due to the presence of blood vessels. Both the physiological processes mentioned above and thermal properties of skin are influenced by a variety of factors such as temperature, damage, pressure, and age etc. To complicate matters, skin is an active, self-regulating system: heat transfer through the skin dramatically affects the state of skin, which can lead to the redistribution of skin blood flow over the cutaneous vascular network and counteractively influence the heat transfer in skin tissue.

2) Mechanical behaviour in skin tissue

Mechanical behavior of skin tissue is found to be heterogeneous, anisotropic, nonlinear, and viscoelastic *in vivo* because of its high non-homogenous structure and composition. It is affected by many factors such as age, gender, site, hydration etc. Furthermore, classical electrometric constitutive models are not suitable to describe the complicated mechanical behavior of skin tissue.

3) Thermomechanical behaviour in skin tissue

The major constituent of dry skin is collagen. During heating, due to thermal denaturation of collagen, there appears thermally induced mechanical stress, which in macro-scale is thermal shrinkage. The thermal shrinkage can be used as a convenient continuum metric of thermal damage^[1]. Hörmann & Schlebusch^[2] showed that gross shrinkage provides the same information on the kinetics of denaturation as many biochemical assays (albeit not the same detail on underlying mechanisms). It has been found that mechanical load is functionally as important as the temperature level during shrinkage^[3]. What's more, during denaturation, not only the structure, but also the hydration of collagen changes, thus, not surprisingly, thermal denaturation of a collagenoustissue can lead to remarkable changes in the mechanical, thermal, electrical, and optical properties. Thus, the strain, stress, temperature are highly correlated, in other words, the problem is fully coupled.

4) Thermal pain in skin

When skin is heated to a temperature beyond a critical value (≈ 43 °C), pain sensation (an unpleasant sensory and emotional experience) is evoked. Correspondingly, thermal damage of skin tissue causes cells to break down and to release a number of tissue byproducts and mediators, which will activate and sensitize nociceptors (pain-stimulating receptor), thereby resulting in a prolonged, post-stimulus feeling of pain (hyperpathia) and an increase response to a normally painful stimulus (hyperalgesia). Thermally induced

stresses due to non-uniform temperature distributions may also lead to the sensation of thermal pain, in addition to the pain generated by heating alone. Supporting evidence shows that, for the same level of nociceptor activity, a heat stimulus evokes more pain than a mechanical stimulus and that tissue deformation due to heating and cooling may explain the origins of pain^[4,5].

Although pain sensation has been studied for a long time over a range of scales, from molecular (such as ion channel) to the entire human neural system (a whole human), the understanding of the underlying mechanism is still far from clear. One reason is that pain is influenced by many factors, including physiological, such as stimulus intensity and duration, and psychological factors such as attention and empathy.

1.2.3 Schematic of skin biothermomechanics and thermal pain research

The study of skin biothermomechanics and thermal pain is a highly interdisciplinary area involving bioheat transfer, biomechanics and neurophysiology. The relationship between these areas is schematically shown in Figure 1.1. The skin tissue is characterized by its structure, such as its constituent components, blood flow, metabolism etc, and properties, such as thermal, mechanical, optical, dielectric properties. When thermal loading, such as contact heating, electromagnetic energy, or acoustic energy, and/or mechanical loading, such as force or deformation, are applied to skin tissue, then, according to different skin descriptions, there are different skin states, including temperature, thermal damage/inflammation, and stress/strain distributions. These states will then decide the level of pain sensation through neural system. Therefore, a better understanding of skin properties, skin bioheat transfer and kinetics of thermal damage, skin biomechanics and skin thermal pain sensation, promise to contribute to the continuing advancement of study of skin biothermomechanics and thermal pain.

1.2.4 Importance of skin thermomechanics and thermal pain

1) Medical applications

With advances in laser, microwave, radio-frequency, and similar technologies, a variety of thermal methods have been developed and applied to the treatment of disease/injury involving skin tissue. These thermal treatment methods normally involve either a raising or lowering of temperature in targeted skin area to kill or thermally denaturize the necrotic cells, in which the precise monitoring of the spatial and temporal distribution of temperature

and stress in the skin tissue is required. Meanwhile, to keep the rest healthy skin in a safe temperature level, selective cooling techniques on skin surface are adopted during these treatments.

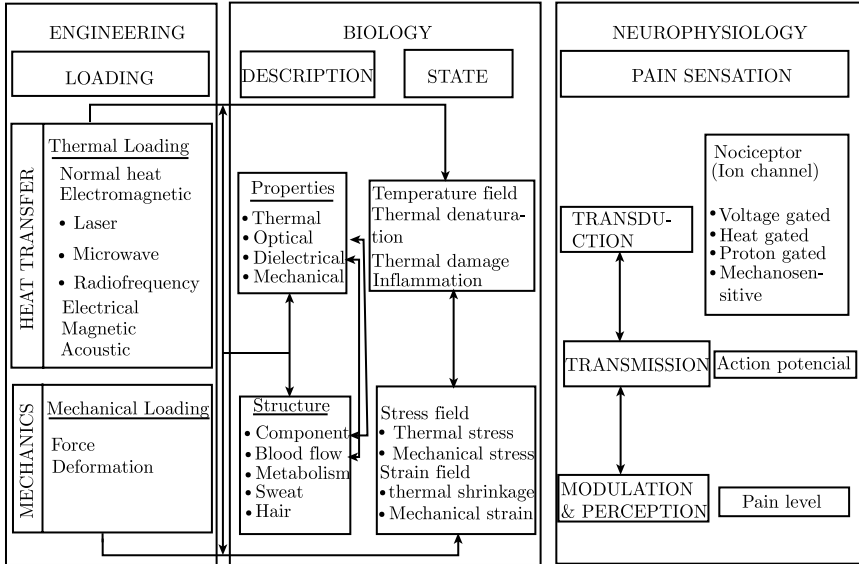


Figure 1.1 Schematic of skin Thermomechanics and thermal pain

In spite of these important and widely used medical applications, an understanding of the responsible thermal-mechanical-neurophysiological mechanism remains limited. Further refinement of current medical treatments and innovation in thermal treatments, requires a thorough understanding of this interdisciplinary area. Therefore, the proposed research is of great importance and can contribute to medical applications by understanding the macroscale tissue response to heat-induced micro-structural transformations in the areas of ① design and characterization of strategies for delivering thermal therapies; ② optimization of a thermal treatments by maximizing the therapeutic effect while minimizing unwanted side effects; ③ comparison of various treatment parameters by use of model instead of extensive parametric studies; ④ new treatment strategies proposing predictions and evaluation of their outcome by developing models and simulation tools.

2) Contribution to pain study and pain relief

A noxious thermal stimulus (heat or cold) applied to human skin is one of the three main causes of pain; solving how to relieve thermal pain implies further study and development of these thermal methods outlined above. Thermally induced damage plays an important role in causing pain (thermal

pain) and therefore, a better understanding of the temperature distribution, heat transfer process and related thermomechanics in skin will contribute to the study of pain causes and its relief.

3) Other applications

Besides biomedical applications, advances related to space and military missions may benefit from the proposed study. Extreme environments encountered in space travel and in some military activities make it necessary to provide astronauts and military personnel with sophisticated garments for protection from thermal extremes. As the “interface” between these outside materials and human inside body, skin certainly plays a significant role. Furthermore, challenges are also posed by the need to understand possible thermal effects on military personnel exposed to irradiation, such as incidental radio frequency radiation.

1.3 Outline of the Book

Biothermomechanical behavior of skin tissue is an interdisciplinary problem, involving the subjects of heat transfer, mechanics, biology and neurophysiology. According to the schematic relationship between the areas involved, as shown in Figure 1.1, the book is divided into four parts: PART I. Skin bioheat transfer and thermal damage; PART II. Skin biomechanics; PART III. Skin biothermomechanics; PART IV. Skin thermal pain.

References

- [1] Fung Y C. *Biomechanics: Motion, Flow, Stress, and Growth*. New York: Springer-Verlag, 1990.
- [2] Hömann H, Schlebusch H. Reversible and irreversible denaturation of collagen fibers. *Biochemistry*, 1971, 10(6): 932–937.
- [3] Chen S S, Wright N T, Humphrey J D. Phenomenological evolution equations for heat-induced shrinkage of a collagenous tissue. *IEEE Transactions on Biomedical Engineering*, 1998, 45(10): 1234–1240.
- [4] Van Hees J, Gybels J. C nociceptor activity in human nerve during painful and non painful skin stimulation. *Journal of Neurology, Neurosurgery, and Psychiatry*, 1981, 44(7): 600–607.
- [5] Reuck A V S, Knight J. *Touch, Heat and Pain*. London: Churchill, 1966.

Chapter 2

Skin Structure and Skin Blood Flow

2.1 Introduction

The skin is the largest organ of the body (makes up approximately 14%~16% of human adult body weight), and plays a variety of important roles ① sensory: it serves as a sense organ for cutaneous senses such as pain, heat, cold, pressure, touch; ② thermoregulation: it functions thermally as a heat generator, absorber, transmitter, radiator, conductor and vaporizer; ③ host defense: it prevents entrance of foreign bodies such as microorganisms and protects underlying tissues from different injuries such as mechanical, heat, cold, biological injuries; ④ skin works as a reservoir for food and water: adipose tissue and prevents excess water loss; ⑤ skin assist in the process of excretion such as H₂O, Salt, Urea, Lactic acid and it serves as a seat of origin for Vitamin D.

It is thus of great necessities to appreciate the structure, function and properties of the skin. The structure of human skin is different from site to site and at a particular area on the human body it depends on its functions^[1].

2.2 Skin Structure

2.2.1 Skin layers

There are three main kinds of human skin^[2]. Glabrous skin (hairless areas such as the palms of the hands) with its characteristic dermatoglyphics (the grooves on its surface), is found on the palms and the soles. It is characterized by a relatively thick epidermis and by lack of hair follicles. In hairy skin on the other hand, hair follicles are present. The third kind is mucocutaneous (skin areas that border the entrances to the interior of the body). For all three kinds, the skin generally consists of three layers: epidermis, dermis, and subcutaneous tissue. The thickness of these layers varies depending on the location of the skin. The general structure of human skin is shown in Figure 2.1. The macromolecular components of skin were presented in Figure 2.2^[3], which illustrates the primary macromolecular components of dermis including

collagens, proteoglycans (PGs), and hyaluronan.

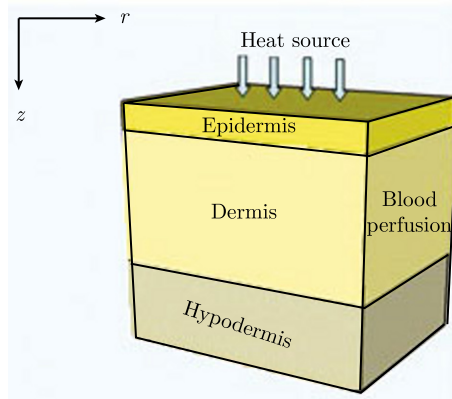


Figure 2.1 Structure of human skin

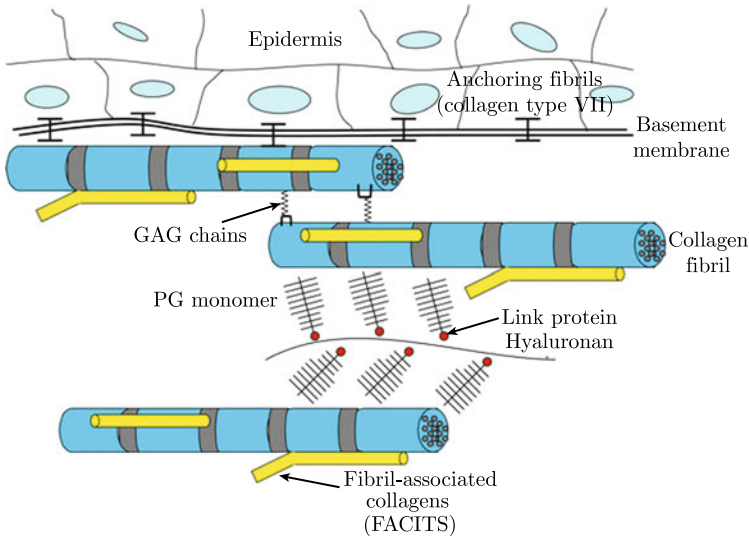


Figure 2.2 Macromolecular components of skin

2.2.2 Epidermis

The epidermis is the outer-layer of the skin containing both living and dead cells and is about $75\sim 150\ \mu\text{m}$ in thickness^[3,4]. The epidermis is composed of 95% of keratin-synthesizing epithelial cells (keratinocytes) and 5% of non-keratinocytes (cells that do not synthesize keratins). The keratinocytes change in cellular constituents as they move peripherally, which results in a clear distinction between the different cell layers in the epidermis. The well-defined layers are shown in Figure 2.1, where the outermost and thickest layer

is the stratum corneum consisting of dead cells, which plays a role as a barrier between environment and organism. The non-keratinocytes that can be found in the epidermis are melanocytes (pigment forming cells), Langerhans cells (which have immunological functions) and Merkel cells (which express immunoreactivity for several substances)^[5].

Inferior to the stratum corneum are stratum granulosum from two to three layers of dark cells filled with granules. Below the stratum granulosum is the stratum spinosum, a thicker layer of polyhedral cells. The deepest cell layer in the epidermis is the stratum basale or stratum germinativum, the cells of which contain brown melanin granules. The stratum basal is attached to a thin connective tissue basement membrane that separates the epidermis from the dermis. All the layers consist of viable cells except stratum corneum. In addition, in friction surfaces or in areas where the epidermis is very thick, there is a hyalin layer, the stratum lucidum, which lies between the stratum corneum and the stratum granulosum^[5,6].

2.2.3 Dermis

Human dermis makes up the bulk of the human skin and contributes to 15%~20% of the total body weight. The dermis is much thicker (1~4 mm^[4]) than the epidermis and is composed of three fibrin proteins: collagen, elastin and a little reticulin, group substance. In the dermis there are blood vessels, nerves, lymph vessels, and the skin appendages such as hair follicles and small hair muscles, sebaceous glands and sweat glands, which are held together by collagen. Dermis plays the important functions of thermoregulation and supports the vascular network to supply the non-vascularized epidermis with nutrients. The dermis is generally divided into two, poorly distinguishable layers, the papillary layer and lower reticular layer. The papillary dermis is the thinner outermost portion of the dermal connective tissue, constituting approximately 10% of the thickness of the dermis. It contains smaller and more loosely distributed elastic and collagen fibrils than the underlying reticular dermis and it has a greater amount of ground substance. The reticular dermis constitutes the greater bulk of the dermis. This dense collagenous and elastic connective tissue contains a relatively small amount of cells and veins.

1) Dermal-epidermal junction

The dermal-epidermal junction (DEJ) is an important interface of mechanical attachment between these two distinctly different layers of the skin: the epidermis and the dermis. It is composed of a basement membrane that

is way in shape with finger-like projections that extend into the dermis. The junction provides a physical barrier for cells and large molecules and a strong bandage between the dermis and the epidermis by macromolecular attachments. The firmness of the attachment is enhanced by parts of the epidermis penetrating the papillary dermis resulting in large cones and rete ridges, or papillae^[4,5].

2) Collagen fibres in dermis

Collagen is a rather stiff and hard protein which is a major constituent of the extracellular matrix of connective tissue and is the main load-carrying element in a wide variety of soft tissues where it provides structural integrity.

In dermis, collagen is the major constituent and accounts for approximately 60%~80% of dry weight of fat-free skin^[5,7~11] and 18%~30% of the volume of dermis^[5]. The collagen in human dermis are mainly the periodically banded, interstitial collagens¹⁾(types I, III and IV)^[12], where about 80%~90% is type I collagen and 8%~12% is type III collagen.

Collagen is a macromolecule with a diameter of about 1.5 nm and a length of about 280 nm^[13]. Figure 2.3 shows the structure of collagen. Three

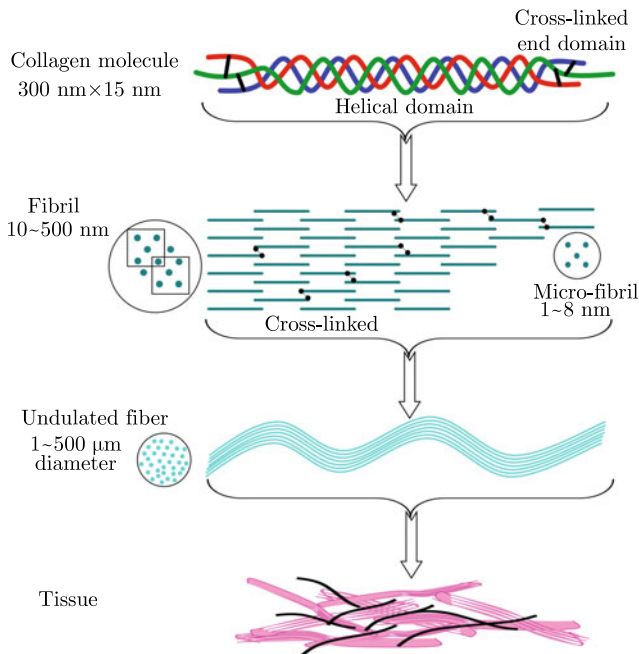


Figure 2.3 Molecular/fibrillar configuration of Type I collagen

1) Collagen occurs in many places throughout the body and there are 28 types of collagen reported in literature.

polypeptide chains make up the type I collagen molecule and are stabilized in a right-handed triple-helix arrangement (with a period of about 8.6 nm) by intramolecular cross-links, where each strand is a left-handed α helix with about 0.87 nm per turn and is made up of sequences of amino acids²⁾ [14] as shown in Figure 2.4. These collagen molecules are linked to each other, and in turn, aggregated into a parallel pattern to form collagen fibrils with diameter of about 50 nm, which is maintained by intermolecular crosslinks and provides the tissue with its tensile properties. The intramolecular cross-links are reducible covalent aldehyde bonds, which are progressively replaced by irreducible multivalent cross-links as the tissue ages^[15]. Each fibril has transverse striations, which are spaced approximately 67 nm apart (see Figure 2.5), due to the staggering of the individual collagen molecules. These fibrils form fibers, with diameter of 1 μm , which is mediated by proteoglycans. Fibers are bundles of fibrils with diameters between 0.2 μm and 12 μm . Type IV collagen co-distributes and assembles into fibrils with both types I and III collagen in which it assists in regulating fibril diameter.

The wavy and unaligned collagen fiber bundles form an irregular network in the dermis, which does not appear to extend randomly in three dimensions, but appears to have preferred directions parallel to the surface^[17,18]. This allows considerable deformation in all directions without requiring elongation of the individual fibers and thus provide both tensile strength and elasticity^[19,20]. However, in order to prevent out-of-plane shearing, some fiber orientations also have components out of plane.

Figure 2.6 shows the dermal collagen fiber weave in the skin of a child and Figure 2.3 gives the molecular/fibrillar configuration of Type I collagen.

3) Elastin fibres in dermis

Elastin is one of the most stable and insoluble proteins in the body. Elastin fibres are a minor structural component of the dermis structure, accounting for 4% of the dermis dry weight and 1% of the volume of

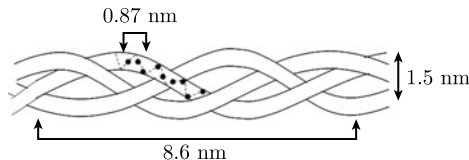


Figure 2.4 Triple helix structure of collagen: the dots shown in a strand represent glycine and different amino acids

2) Most of the collagen molecule consists of three amino acids: glycine (33%), which enhances the stability of the molecule, proline (15%), and hydroxyproline (15%).

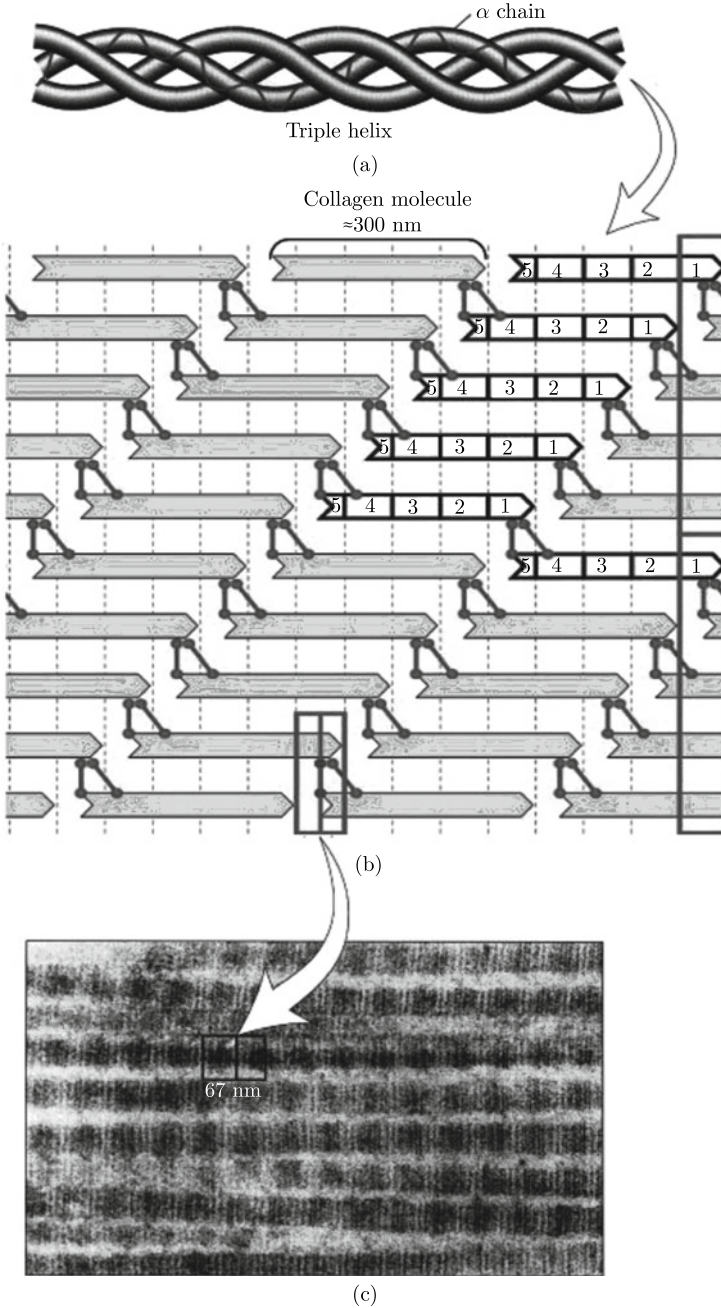


Figure 2.5 Collagen-composed triple helix, forming microfibrils which have 67 nm gaps: (a) general scheme; (b) representation of 300 nm segments with gaps and overlaps; (c) electron micrograph^[16] (by permission of Elsevier)



Figure 2.6 Dermal collagen fiber in the skin of a child^[21]
(by permission of IOP)

dermis^[5,10,22]. Elastin fibres are considerably thinner (ca. $\phi 100$ nm^[19]) and more convoluted than collagen fibres. The structure of elastin is shown in Figure 2.7^[23]. Each fibrous monomer is linked to many others and forms a three-dimensional network. Elastin is found in skin, walls of arteries and veins, and lung tissue. It is not yet understood how the elastin fibres are constructed from smaller elastin fibrils. However, it is known that the base unit of elastin is a long protein chain that is cross-linked by lysine molecules. Four elastin chains are joined at each cross-link by the covalent bonding of lysine molecules from each elastin chain. Although direct connections between elastin and collagen fibres have not been shown^[24], collagen fibres appear to wind around the elastin cores^[10].

The elastin is a fibrous protein in skin elastin fibres. These fibres possess extraordinary elasticity, which explains their name. They are elastomers according to their behaviour—they have small elastic module and restore their initial size even after significant stretching. The structures in the tissues, with elastin as their basic component, are called elastic and are interesting because of their specific biomechanical properties. The elastin has amorphous network structure with a small extent of arrangement. This structure explains the high elasticity of its fibres, which are built from long flexible disordered chains of molecules. The orientation of the molecules occurs when the fibres are stretched^[25].

4) Ground substance

The ground substance, which comprises about 20% of the dry weight of

skin and makes up between 70% and 90% of the skin's volume^[26], is a gel like substance containing a class of chemicals including glycosaminoglycans (GAG), proteoglycans and glycoproteins.

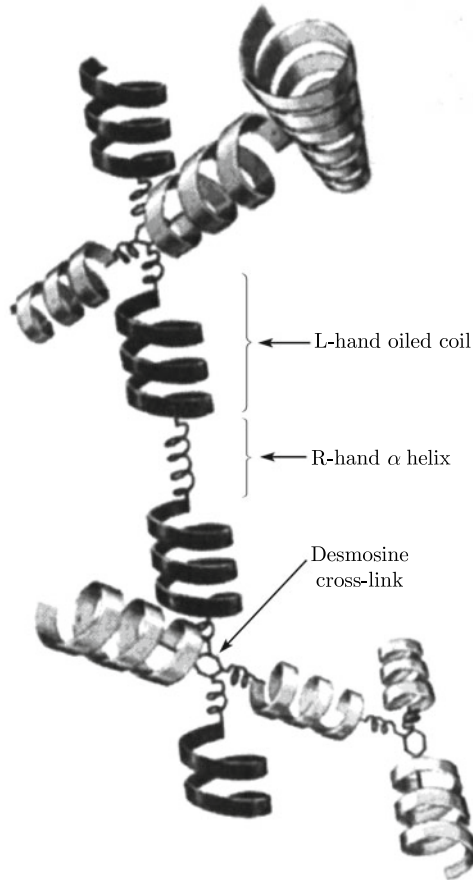


Figure 2.7 Molecular model for elastin^[23]
(by permission of Nature Publishing Group)

The amorphous ground substance can be characterized as a semi-fluid amorphous material and can be considered as a highly viscous, thixotropic liquid whose fluid properties are determined by a low concentration (0.05% wet weight of human dermis) of mucopolysaccharides, proteoglycans and glycoproteins^[26]. The most important mucopolysaccharides in ground substance is hyaluronic acid, a long unbranched, polysaccharide chain composed of repeating disaccharide units with a molecular weight ranging from 2×10^5 to 3×10^6 Daltons^[26]. Hyaluronic acid is analogous to the polymer molecules found within rubbers. The hyaluronic acid chain has proteoglycans side-

chain, which in turn are cross-linked by glycoproteins to additional structures within dermis, such as collagen or elastin fibrils. It is this cross-linking function that is responsible for forming fibres from the collagen fibrils and providing the dermis with its rubber-like constitutive behaviour.

Together they form a gel which does not leak out of the dermis, even under high pressure.

2.2.4 The hypodermis

The third layer is the hypodermis (also called subcutaneous fat or subcutis), which is composed of loose fatty connective tissue. It is not part of the skin but appears as a deep extension of the dermis. Hypodermis is composed of mainly fat and carries major blood vessels and nerves to the overlying skin. The thickness of the layers varies considerably over the surface of the body^[4], and also varies with age, sex, race, endocrine and nutritional status of the individual. It acts as an insulating layer and a protective cushion and constitutes about 10% of the bodyweight^[27].

2.2.5 Appendages in skin

Vertebrate appendages are significant thermoregulatory organs because of their high surface to mass ratio and their dense distribution of blood vessels. Since hair and sweat gland play important role in the thermoregulation, they are simply introduced here.

1) Hair

See Figure 2.1.

2) Sweat gland

The sweat gland is a simple, highly coiled, tubular gland, as shown in Figure 2.8. In general, it extends deep into the dermis and is composed of three regions: ① secretory portion, which is the coiled region of the sweat gland and located in the dermis; ② excretory duct, which leaves the secretory region of the sweat gland and straightens out to the epidermis; ③ the spiral course in the epidermis, which passes through the epidermal cells to the skin surface.

3) Receptors of the skin

The skin is a large sense organ of the external environment. Numerous encapsulated and free sensory nerve endings within the skin respond to stimuli for temperature (heat and cold), pressure, touch, and pain. These perceptions are a consequence of variable combinations of three types of sensory receptors: mechanoreceptors for touch, vibration, pressure; thermal recep-

tors for temperature; and nociceptors for pain. Receptor cells can be found both in epidermis and dermis: Figure 2.9 shows the free nerve endings (for pain) both in epidermis and dermis.

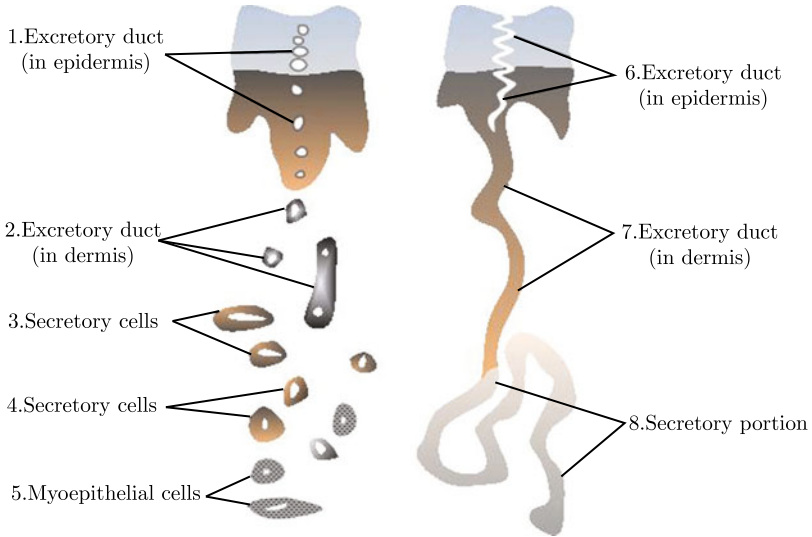


Figure 2.8 Sweat gland in skin

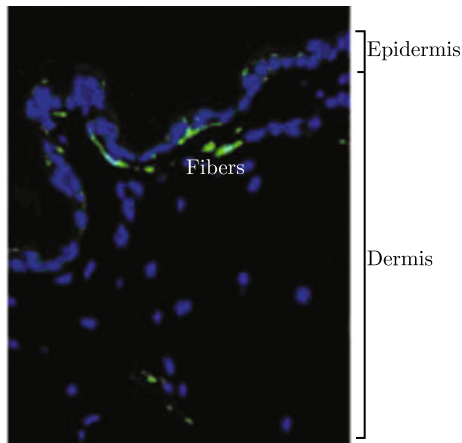


Figure 2.9 Histological section of free nerve endings in skin^[28]
(by permission of Nature Publishing Group)

Ivanov et al. ^[29] reported thermoreceptors in different layers of the skin. They proposed that these thermoreceptors might inform the central nervous system not only about the absolute temperature of the skin surface, but

also the value and direction of the heat flow through the skin. Morin & Bushnell^[30] suggested that although both the cold and warmth receptors are located within the dermis, cold receptors are located deeper than the warmth receptors. Both types of thermoreceptors are approximately 1mm in diameter and cold receptors are more abundant than warmth receptors with between 3 to 10 times more cold receptors being located across the body. Pain receptors are activated only at the extreme ranges of hot and cold, whereas cold and warmth receptors are stimulated at particular points within the boundary of this range.

2.3 Skin Blood Perfusion

The thermoregulation function of skin is realized mainly by modifying the blood flow, which is located in a microcirculatory bed composed of arterioles, arterial and vein capillaries, and venules. Most of the microvasculature is contained in the papillary dermis within 1 to 2 μm below the epidermal surface^[31]. The arterioles and venules form two important plexuses in the dermis: the deep dermal plexus is located just below the dermis and small vessels arise almost perpendicularly from it, pass through the dermis and form a more superficial plexus just below the epidermis^[32]. These two horizontal plexuses represent the physiologically important areas in the skin. The microvessels in the papillary dermis vary in diameter from 10 to 35 μm , but most are in the 17 to 22 μm range; in the mid and deep dermis, the microvascular diameters range from 40 to 50 μm , although rarely a vessel as large as 100 μm can be found^[31].

Besides the usual dermal plexuses, some areas of the body contain arteriovenous anastomoses (AVA), which are found most abundantly in the dermis of acral skin^[33]. AVA are located in the deep dermis close to the level of the sweat glands^[34] and play an important role in regulating the relative degree of skin blood perfusion by shunting directly from the arterial to the venous systems, bypassing the capillary network, and thus play an important role in temperature regulation^[35].

References

- [1] Parsons K C. Human Thermal Environments. London: Taylor and Francis, 1993.
- [2] Adams M J, Briscoeb B J, Johnson S A. Friction and lubrication of human skin. *Tribology Letters*, 2007, 26(3): 239–253.

- [3] Silver F H, Siperko L M, Seehra G P. Mechanobiology of force transduction in dermal tissue. *Skin Research and Technology*, 2003, 9(1): 3–23.
- [4] Odland G F. Structure of the skin// Goldsmith L A. *Physiology, Biochemistry, and Molecular Biology of the Skin*. Oxford: Oxford University Press, 1991.
- [5] Ebling F, Eady R, Leigh I. Anatomy and organization of human skin// Champion R H, Burrington J L, Ebling F J G. *Textbook of Dermatology*. New York: Blackwell Scientific Publications, 1992.
- [6] Montagna W, Parakkal P F. *The Structure and Function of Skin*. New York: Academic Press, 1974.
- [7] Bottoms E, Shuster S. Effect of ultra-violet light on skin collagen. *Nature*, 1963, 199(4889): 192–193.
- [8] Dombi G W, Haut R C. The tensile strength of skin and correlations with collagen content. *Advances in Bioengineering Presented at the Winter Annual Meeting of the American Society of Mechanical Engineers*. New York, 1985: 95–96.
- [9] Reihnsner R, Balogh B, Menzel E J. Two-dimensional elastic properties of human skin in terms of an incremental model at the in vivo configuration. *Medical Engineering and Physics*, 1995, 17(4): 304–313.
- [10] Brown I A. Scanning electron microscopy of human dermal fibrous tissue. *Journal of Anatomy*, 1972, 113(Pt2): 159–168.
- [11] Sanjeevi R. A viscoelastic model for the mechanical properties of biological materials. *Journal of Biomechanics*, 1982, 15(2): 107–109.
- [12] Douven L F A, Meijer R, Oomens C W J. Characterisation of mechanical behaviour of human skin in vivo. *The International Society for Optical Engineering*, 2000, 3914: 618–629.
- [13] Nimni M E, Harkness R D. Molecular structure and functions of collagen// Nimni M E. *Collagen*. Boca Raton: CRC Press, 1988: 3–35.
- [14] Ramachandran G N. Chemistry of collagen// Ramachandran G N. *Treatise on Collagen*. New York: Academic Press, 1967: 103–183.
- [15] Arnoczky S P, Aksan A. Thermal modification of connective tissues: Basic science considerations and clinical implications. *Journal of the American Academy of Orthopaedic Surgeons*, 2000, 8(5): 305–313.
- [16] Meyers M A, Chen P Y, Lin A Y M, et al. Biological materials: Structure and mechanical properties. *Progress in Materials Science*, 2008, 53(1): 1–206.
- [17] Millington P F, Gibson T, Evans J H, et al. Structural and mechanical properties of connective tissues// Kenedi R M. *Advances in Biomedical Engineering*. New York: Academic Press, 1971: 189–248.
- [18] Hunter J A A, Finlay B. Scanning electron microscopy of connective tissues in health and disease// Hall D A, Jackson D S. *Connective Tissue Research*. New York: Academic Press, 1973.
- [19] Finlay B. Scanning electron microscopy of the human dermis under uni-axial strain. *Bio-medical Engineering*, 1969, 4(7): 322–327.
- [20] Wegst U G K, Ashby M F. The mechanical efficiency of natural materials. *Philosophical Magazine*, 2004, 84(21): 2167–2181.

- [21] Kenedi R M, Gibson T, Evans J H, et al. Tissue mechanics. *Physics in Medicine and Biology*, 1975, 20(3): 699–717.
- [22] Hult A M, Goltz R W. The measurement of elastin in human skin and its quantity in relation to age. *Journal of Investigative Dermatology*, 1965, 44(6): 408–412.
- [23] Gray W R, Sandberg L B, Foster J A. Molecular model for elastin structure and function. *Nature*, 1973, 246(5434): 461–466.
- [24] Oxlund H, Manschot J, Viidik A. The role of elastin in the mechanical properties of skin. *Journal of Biomechanics*, 1988, 21(3): 213–218.
- [25] Partidge S. Physical chemistry of elastin. *Advances in Experimental Medicine and Biology*, 1977, 79: 603–606.
- [26] Tregear R T. *Physical Functions of the Skin*. New York: Academic Press, 1966.
- [27] Burton J L, Cunliffe W J. *Subcutaneous fat*// Champion R H, Burrington J L, Ebling F J G. *Textbook of Dermatology*. New York: Blackwell Scientific Publications, 1992.
- [28] Patapoutian A, Peier A M, Story G M, et al. Thermo TRP channels and beyond: Mechanisms of temperature sensation. *Nature Reviews Neuroscience*, 2003, 4(8): 529–539.
- [29] Ivanov K P, Konstantinov V A, Danilova N K. Thermoreceptor localization in the deep and surface skin layers. *Journal of Thermal Biology*, 1982, 7(2): 75–78.
- [30] Morin C, Bushnell M C. Temporal and qualitative properties of cold pain and heat pain: A psychophysical study. *Pain*, 1998, 74(1): 67–73.
- [31] Braverman I M. *Anatomy and physiology of the cutaneous microcirculation*// Berardesca E, Elsner P, Maibach H I. *Bioengineering of the Skin: Cutaneous Blood Flow and Erythema*. Boca Raton: CRC Press, 1995.
- [32] Sonksen J, Craggs J. Circulation of the skin. *Current Anaesthesia and Critical Care*, 1999, 10(2): 58–63.
- [33] Moschella S, Harley H J. *Dermatology*. London: WB Saunders, 1985.
- [34] Greenfield A D M. Circulation through the skin// Hamilton W F. *Handbook of Physiology*. Washington: American Physiological Society, 1963: 1325.
- [35] Fagrell B. *Microcirculation of the skin*// Fagrell B. *The physiology and pharmacology of the microcirculation*. London: Academic Press, 1984: 133–180.

PART I SKIN BIOHEAT TRANSFER

Chapter 3

Skin Bioheat Transfer and Skin Thermal Damage

3.1 Introduction

3.1.1 Skin bioheat transfer

All biological bodies live in a thermal environment of spatially heterogeneous temperatures. Even within a single organism, the temperatures of the organs and the tissues can not be uniform due to their spatial and temporal heat sources and sinks. The non-uniformity induces heat transfer both inside the organism and through the interface with its external environment. Heat transfer is thus a primary mechanism affecting temperature.

Living organisms involve a great number of hierarchy levels from bi-macromolecules up to total organisms functioning as a whole which are related to each other by energy and mass flow. Living tissue forms a basic level of this hierarchy which in turn contains its own complex hierarchical substructure and, from the stand point of heat and mass transfer, can be treated as a certain medium.

The transport of thermal energy in living tissue is a complex process involving multiple phenomenological mechanisms including conduction, convection, radiation, metabolism, evaporation, and phase change. Thermal behaviour, or, heat transfer, in skin is mainly a heat conduction process coupled to complicated physiological processes, including blood circulation, sweating, metabolic heat generation, and, sometimes, heat dissipation via hair or fur above the skin surface.

3.1.2 Thermal damage

When biological tissue is subjected to higher than physiological temperatures, protein and cell organelle structures can be altered resulting in cell death and subsequent tissue necrosis. Skin thermal damage or skin burns are the most commonly encountered type of trauma in civilian and military

communities^[1], resulting from many different causes such as contact with hot fluids and surfaces, flames, chemicals and electrical sources. For example, burn injuries are experienced by about 250,000 people in the UK each year, where about 175,000 people visit A&E Departments with burn injuries each year and some 13,000 of them are admitted to hospital where 6,400 are children (UK national report). The cost of skin thermal damage is also very huge, for example, the cost of hot drink scald on children is expected to be about £266,400 per year^[2]. The quantification of skin thermal damage has major physiologic significance in determining whether and how soon healing might occur, as well as the severity of the scarring process^[3], in arriving at a subsequent prognosis^[4] and in guiding the treatment^[3].

Besides, advances in electromagnetic technologies such as laser and microwave have led to recent developments of thermal treatments for different diseases and injuries involving skin tissue, such as the removal of port-wine stains^[5], pigmented and cutaneous lesions^[6] and tattoos^[7]. The objective is to induce thermal damage precisely within tissue structures located up to several millimeters below the surface but without affecting the surrounding, healthy tissue. The quantification of thermal damage distribution is helpful for the optimization of thermal treatments by maximizing the therapeutic effect while minimizing unwanted side effects.

Further, when the skin is heated to a temperature beyond a critical value ($\approx 43^\circ\text{C}$), thermal damage of skin tissue is accumulated. The thermal damage causes cells to break down and to release a number of tissue byproducts and mediators, which will activate and sensitize nociceptors^[8], special receptor for pain sensation. Burn damage induces severe pain that is difficult to manage^[9]. Moreover, thermal damage-induced pain may contribute to sensory problems, including cold allodynia and chronic pain^[10], as well as psychologic disorders, such as post-traumatic stress disorder^[11], all of which commonly reduce quality of life after burn damage. The quantification of thermal damage will help to better understand the pain sensation such as hyperpathia and finally contribute to pain relief.

3.1.3 Outline of this chapter

This chapter aims to provide a comprehensive description of the thermal behaviour in skin tissue and is outlined as follows. The bioheat transfer in skin tissue is first presented, which is then followed by the thermal damage in skin tissue, and a short summary is given in the end.

3.2 Skin Bioheat Transfer

3.2.1 Blood vessels classification based on their influence on heat propagation

1) Importance of blood perfusion in the heat transfer process in tissue

Blood perfusion has great effect on the heat transfer process in living tissues. The number of vessel levels in the vascular network of tissue is typically large^[12], and blood flow in vessels of different hierarchy levels (as shown in Figure 3.1) has different influences on heat transfer. Abramson^[13] suggested that heat transfer between flowing blood and surrounding tissue occurred predominantly in small capillary loops arising from the more superficial plexus, while Chato^[14] proposed the lower levels of the dermis. Weinbaum et al^[15] and Lemons et al^[16] experimentally found that all arteries of diameter less than 100 μm and all veins of diameter less than 400 μm can be considered fully equilibrated with the surrounding tissue in normothermic conditions.

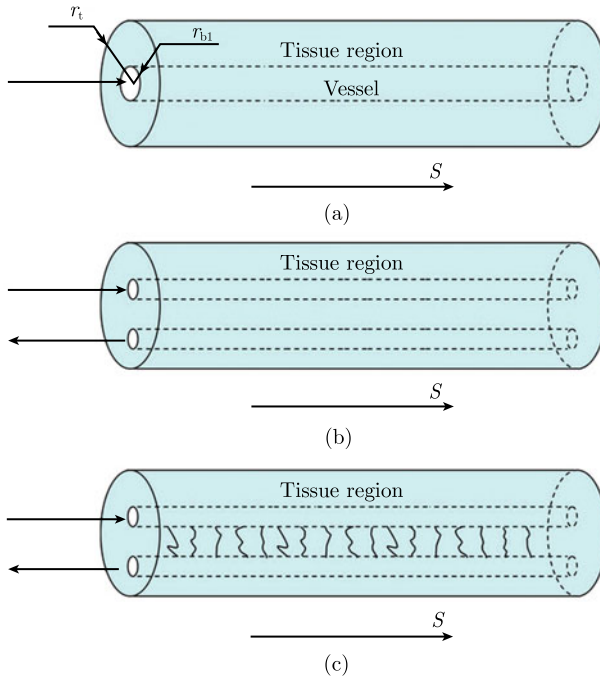


Figure 3.1 Vessel configurations of vascular models: (a) unidirectional vessel configuration; (b) countercurrent vessel configuration; (c) large/small/large vessel configuration

As for skin, there are about 20~25 of arteriovenous anastomoses¹⁾ (AVA) structures per square centimeter in the finger pad, and are located about 1~1.5 mm below the surface of the skin^[17]. Mescon et al.^[18] reported that when these specialized AVA are open, heat exchange occurs uniformly over the local area. Greenfield^[19], Sherman^[20] and Braverman^[21] found that heat transfer occurs close to the deep dermal plexus and is complete before reaching the smaller vessels of the arterial tree as most arterioles in the deep dermis have diameters around 50 μm while the arterial networks superficial to these are much smaller.

2) Classification of blood vessels

From the description above, it can be seen that the effect of blood vessels on heat transfer is strongly related to their sizes. Therefore, a thermal equilibration length of blood vessels, L_{eq} , is defined as the length at which the difference between the blood and tissue temperature decreases to $1/e$ of the initial value, where e is the exponent, 2.718. Similar equations for L_{eq} have been proposed by different researchers^[22], and a typical expression is as follows:

$$L_{\text{eq}} = \frac{\rho_b c_b}{8k_b} V D_v^2 \left(\frac{1}{2} + \frac{k_b}{k_{\text{eff}}} \ln \frac{D_c}{D_v} \right) \quad (3.1)$$

where k_{eff} is the effective thermal conductivity; ρ_b , c_b and k_b denote the density, specific heat and thermal conductivity of blood, respectively; D_c and D_v denote the mean tissue cylinder and vessel diameter; and V is the mean vessel flow velocity.

The ratio of L_{eq} to the actual vessel length demonstrates the distinction of thermal significance, ε

$$\varepsilon = L_{\text{eq}}/L \quad (3.2)$$

If $\varepsilon \ll 1$, i.e. L_{eq} is much shorter than the characteristic length of the blood vessel length L , the blood will exit the vessel at, essentially, the tissue temperature. Conversely, if $\varepsilon \gg 1$, the blood temperature will not decay and will leave the tissue at the same inflow temperature^[14].

In order to imagine the extent to which blood flow in vessels of different levels can affect heat transfer, some authors have examined characteristic properties of blood flow in various vessels as well as vessels themselves. The characteristic properties of blood flow in various vessels as well as vessels themselves are shown in Table 3.1 for a 13 kg dog and in Table 3.2 for human. From Table 3.1 and Table 3.2, we can see that the vessels where

1) Anastomoses occur normally in the body in the circulatory system, serving as backup routes for blood to flow if one link is blocked or otherwise compromised.

arterial blood attains thermal equilibrium with the surrounding cellular tissue for the first time are approximately of the length L_{eq} (≈ 2 cm). Typically, a regional vascular network contains vessels whose length is much larger and much smaller than L_{eq} . Thus, the bioheat transfer models should take into account that the vascular network can contain vessels significantly different in effect on heat transfer.

Table 3.1 Properties of different kinds of blood vessels of a 13 kg dog^[22] (by permission of IOP)

Vessel	Percentage of vascular volume	Average radius/mm	Average length /mm	Velocity /(mm/s)	L_{eq} /mm
Aorta	3.30	10	380	500	112,000
Large artery	6.59	3	200	130	2700
Arterial branch	5.49	1	90	80	180
Terminal artery Branch	0.55	0.6	8	80	65
Arteriole	2.75	0.02	2	3	0.0029
Capillary	6.59	0.008	1.2	0.7	0.0001
Venula	12.09	0.03	1.6	0.7	0.0014
Terminal vein	3.30	1.5	10	13	67
Venous branch	29.67	2.4	90	15	300
Large vein	24.18	6	200	36	2900
Vena cava	5.49	12.5	380	330	117,000

Table 3.2 A selection of vessel parameters for the human circulation^[23] (by permission of IOP)

Vessel	Average diameter /mm	Velocity /(mm/s)	Reynolds number	Entrance length /mm	L_{eq} /mm
Ascending aorta	25	220	1600	23,000	321,000
Ascending aorta	20~32	630 (peak)	3600~5800		
Descending aorta	16~20	270 (peak)	1200~1500		
	4	500	570	1300	19,000
Internal carotid artery	6.2	145	250	900	13,000
	6.2	360 (peak)	650		
			1200 (peak)		
Femoral artery	5	260	370	1100	
Renal artery	4	500	570	1300	15,000
Large arteries	2~6	200~500 (peak)	110~850		19,000
Capillaries	0.005 ~ 0.01	0.5~1		$2 \times 10^{-6} \sim 1.5 \times 10^{-5}$	$3 \times 10^{-5} \sim 2 \times 10^{-4}$
Large veins	5~10	150~200	210~570	600~3500	9000~ 47,000
Venae cavae	20	110~160	630~900	7500~10,000	100,000 ~ 150,000

3.2.2 Heat transfer models of soft tissues

For the theory of heat and mass transfer in living tissue one of the central issues is how to create good models that describe these transport phenomena in terms of certain physical fields and the corresponding governing equations accounting for interaction between different levels of the living tissue hierarchy.

Since the appearance of Pennes bioheat equation^[24] in 1947, a variety of models on heat transfer in different tissues of human body have been proposed, where the tissue may be represented as a homogeneous continuum material with an embedded hierarchical vascular network^[25]. But there is no general agreement on one more appropriate model, which is mainly due to the disagreement on the level at which heat exchange occurs between the blood and the tissues^[26]. There are several good reviews of the modeling of heat transfer in soft tissues: Charny^[27] gave a detailed chronological development of mathematical models of bioheat transfer; Arkin et al.^[28] compared and contrasted several bioheat transfer models, emphasizing the problematics of their experimental validation; Crezee et al.^[29] carried out comparison of four different bioheat models or combinations of models with both theoretical and experimental methods; Stanczyk & Telega^[30] compared the continuum models and vascular models and discussed the shortcomings of these popular bioheat equations; Khaled & Vafai^[31] discussed the progress in the development of bioheat equation and the associated applications while emphasis was put on the bioheat models based on the porous media theory.

According to the different ways in which the influence of blood flow in the vascular network may be considered, these models can be basically classified into four categories^[31]: ① continuum models, where the blood perfusion is accounted for by means of the effective conductivity of the tissue; ② vascular models, where real vascularity of the tissue is reproduced and all local heat transfer in the individual vessels are described, which requires the detailed knowledge of the vascular geometry; ③ hybrid model, where different continuum models and/or vascular models are used together; ④ models based on porous media theory, where the perfused tissue is treated as a porous media. The descriptions of each of the model are presented in the following, together with the assumptions used for the derivation of the models and their limitation.

In continuum models, the blood perfusion is accounted for by means of the effective conductivity of the tissue which is dependent on the blood flow rate or by means of other global parameters. The general form of bioheat

equation of continuum models is as following:

$$\rho c \frac{\partial T}{\partial t} = k \nabla^2 T + q_{\text{perf}} + q_{\text{met}} + q_{\text{ext}} \quad (3.3)$$

where ρ , c and k are the density, specific heat and thermal conductivity of skin tissue, respectively; T is the temperature of the tissue; q_{perf} is the heat generation caused by blood perfusion; q_{met} is the metabolic heat generation; q_{ext} is the heat generation from external heat source.

The first continuum model was introduced by Pennes to analyze heat transfer in a resting human forearm, which developed a quantitative basis for describing the thermal interaction between tissue and perfused blood^[24]. His work consisted of a series of experiments to measure temperature distribution as a function of radial position in the forearms of nine human subjects. Pennes proposed a model to describe the effects of metabolism and blood perfusion on the energy balance within tissue. These two effects were incorporated into the standard thermal diffusion equation. The Pennes bioheat model was the first major effort in quantifying the heat transfer contribution of perfusion. The model is unique in that the perfusion term is very simple. The equation was previously given as

$$\rho c \frac{\partial T}{\partial t} = k \nabla^2 T + \varpi_b \rho_b c_b (T_a - T) + q_{\text{met}} + q_{\text{ext}} \quad (3.4)$$

where ρ , c and k are the density, specific heat and thermal conductivity of skin tissue, respectively; ρ_b and c_b are the density and specific heat of blood as before; ϖ_b is the blood perfusion rate per unit volume; T_a and T are the temperatures of blood and skin tissue, respectively; q_{met} is the metabolic heat generation in the skin tissue and q_{ext} is the heat generation due to external heating sources. Note that the Pennes equation is based on the classic Fourier's law for heating, which assumes that the propagating speed of any temperature disturbance or thermal wave is infinite.

1) The main assumptions of Pennes model

(1) The blood perfusion effect is homogeneous and isotropic, and that thermal equilibration occurs in the microcirculatory capillary bed. In this case, the blood is supplied to the tissue at arterial temperature T_a , perfuses the tissue at rate ϖ_b , attains the thermal equilibrium with it and then is collected in the veins.

(2) There is no energy transfer either before or after the blood passes through the capillaries, so that the temperature at which it enters the venous circulation is that of the local tissue. The total energy exchange between blood and tissue is therefore $q_{\text{perf}} = \varpi_b c_b (T_a - T_v)$.

(3) Metabolic heat generation q_{met} is assumed to be homogeneously distributed throughout the tissue of interest as rate of energy deposition per unit volume.

A major advantage of the Pennes model is that the added term to account for perfusion heat transfer is linear in temperature, which facilitates the solution of Pennes equation. Pennes model is widely used for prediction of temperature elevation during hyperthermia as well as for predictions of temperature response in cryosurgical protocols. But common usage of the Pennes model is not always accompanied by careful examination of its limits of applicability.

2) The limitations of Pennes model

The limitations of Pennes model arise from the erroneous view of the heat transfer process and its anatomical location: neglecting the effects of thermally significant large vessels. The discussion of the shortcomings of Pennes equation was done by numerous authors and ranged from putting emphasis on the applicability limitations to complete negation of its validity. The main drawbacks of the Pennes model are:

(1) The Pennes model assumes that blood arrives at each point in the tissue at one temperature T_a regardless of the distance, which separates that point from the supplying vessel. No transport mechanism has been found to accomplish such a requirement. Furthermore, the local arterial temperature depends on the temperature gradient in the tissue resulting from environmental conditions^[32].

(2) The thermal equilibration length in the Pennes model is assumed to be infinite for all vessels except the capillaries and zero for capillaries. This is also a non-physical assumption. Chen & Holmes' analysis of blood vessel thermal equilibration lengths has proved this^[33]. They indicated that thermal equilibration occurs predominantly within the terminal arterioles and venules, and that blood is essentially equilibrated prior to the capillaries.

(3) The blood perfusion term fails to account for the specific vascular architecture such as directed character of the blood flow and counter-current arteries and veins, and it is unable to account for local temperature variations caused by large vessels, a feature inherent to all continuum models and unacceptable in certain applications like localised hyperthermia.

(4) The blood perfusion term has been obtained via the global energy balance for blood and is applied to describe local energy balance for tissue.

(5) The first-order differentiability condition of numerous physical entities in the equation like heat flux, physical properties and heat generation, is not

necessarily met in heterogeneous tissue structures.

Despite its erroneous concept, the perfusion term of Pennes model has been widely used, especially in analyses where a closed form analytical solution is sought, and found to be valid for situations other than the forearm. Its predictions are often superior to those of more elaborate formulations. This fact gives rise to the need for reconsidering the physical foundations of the approach.

Charny et al.^[34] compared Weinbaum-Jiji's counter-current model^[35] and Pennes model against the experimental results of Pennes. The simulations found that Pennes model is valid in the initial branchings of the largest microvessels from the counter-current vessels (diameter > 500 μm) in deep tissue. In this case, the microvessel blood temperature is close to arterial temperature. Charny suggested that the blood perfusion term in Pennes equation does not represent the isotropic thermal equilibration in capillaries but describes the small vessel bleed-off occurring in the regions of the largest counter-current vessels and supplying the capillary bed in tissue. In this manner the temperature of the blood entering these capillaries is the temperature of the blood in the largest vessels, but in the region dominated by smaller vessels this condition is not always satisfied and other models are preferred. Along with the observations in porcine kidney^[36], Pennes model appears to be applicable to regions where the vasculature comprises of numerous small thermally significant vessels ($\epsilon \approx 1$).

The limitations of Pennes model have motivated subsequent investigators to develop their own models.

3.2.3 Heat transfer in skin tissue

1) Studies on skin bioheat transfer

Skin bioheat transfer has been studied for many years. Most of the earlier studies considered the skin temperature around heat sources for diagnosing tumors^[37], which is based on observations of Lawson^[38] that the skin temperature over a malignant tumor is higher than that of surrounding skin due to the increased blood flow within the tumor (see Figure 3.2)^[39,40].

Later, attention was paid to the general heat transfer response of skin tissue in contact with hot or cold sources^[41], in order to quantify the relationship between the threshold of skin temperature for pain sensation and the thermal properties of contact source. Nowadays, because of laser, microwave and similar technologies, emphasis has been transferred to electromagnetic heating effects, including microwave^[42], radiofrequency^[43] and laser^[44]. However,

most of these works are theoretical due to the difficulty of performing heat transfer experiments on skin tissue *in vivo*.

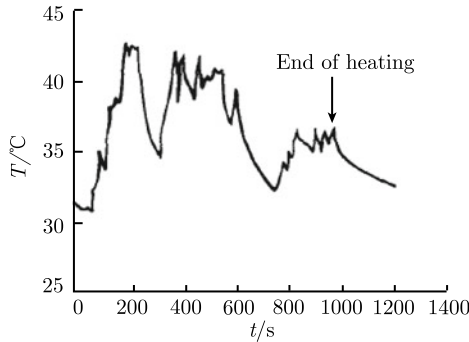


Figure 3.2 Temperature oscillation in tumor under microwave heating (by permission of Science Press)

As noted before, in general, the success of thermal therapies depends on the precise prediction and control of temperature, damage and stress distributions in the tissue. A mathematical model of heat transfer in skin tissue is thus very helpful for the present technology can only provide information of the tissue at discrete points. The model can be used for optimizing thermal treatments by maximizing therapeutic effect while minimizing unwanted side effects, for predicting the outcome of a treatment, for extensive parametric studies in order to characterize the stability of various treatment parameters, and for the development of new treatment strategies. During the development of the mathematical model, several factors need to be considered, such as the thermophysical properties of different layers of skin tissue, skin geometry, skin-electromagnetic wave interaction, metabolic heat generation, heat flow due to blood perfusion, thermoregulatory mechanisms, and thermal induced mechanical response.

2) Consideration of blood perfusion

Since L_{eq} for blood vessels in the skin tissue lies in the range of $3 \times 10^{-5} \sim 2 \times 10^{-4}$ ^[22], as can be seen from Table 3.1 and Table 3.2, the blood will exit the vessel at essentially the tissue temperature. Thus, the Pennes equation is good enough to describe skin heat transfer, which is taken directly from^[24] as given in Equation (3.4)

As for the effect of blood perfusion in theoretical analysis and numerical modeling, which is in most cases considered only for the dermis layer and neglected otherwise, several methods have been used to account for it, as given below.

Constant blood perfusion rate

The effect of blood perfusion is treated as a heat source or the effect is accounted for by use of effective thermal conductivity and thermal diffusivity, where the rate of blood perfusion is assumed to be a constant^[45]. This is the most used method, given as

$$\omega_b = \text{constant} \quad (3.5)$$

Temperature-dependent and/or spatially heterogeneous

The effect of blood perfusion is treated as a heat source and the rate of blood perfusion is considered to be temperature-dependent and/or spatially heterogeneous^[46]. For example, Sanyal & Majji^[47] found that in the middle layer of the skin, the blood mass flow, thermal conductivity and the metabolic heat generation are position dependent because the density of blood vessel varies within the skin. These researchers, therefore, applied depth dependent blood perfusion rate where the rate was assumed to increase linearly in the dermis layer. Since both *in vivo* and *in vitro* studies have shown that the tissue response to thermal loading is strongly temperature-dependent^[48], many researchers have adopted temperature dependent blood perfusion, where the coefficient of temperature dependence could be either a linear or non-linear function of temperature. The non-linear function is preferred since it reflects a decrease in perfusion above specific temperatures resulting from heat-induced damage to blood capillaries, given as

$$\omega_b(T) = \begin{cases} \omega_0 + \omega_1 (T - T_a), & T \leq T_{th} \\ \omega_{\max}, & T_{th} < T < T_{cg} \\ 0, & T \geq T_{cg} \end{cases} \quad (3.6)$$

where ω_0 is the blood perfusion rate under normal condition, and ω_1 increase rate of blood perfusion with temperature; ω_{\max} is the maximum blood perfusion rate; $T_{th} = 45^\circ\text{C}$ is the temperature when the blood perfusion achieve its maximum value; $T_{cg} = 60^\circ\text{C}$ is the temperature when coagulation occurs in the tissue. Similarly, Sekins et al.^[49] and Rai & Rai^[50] used the following equations:

$$\begin{aligned} \varpi_b &= \varpi_{b0}, & T &\leq T_{cr} \\ \varpi_b &= \varpi_{b0} \left(1 + \frac{\varpi_{\max} - \varpi_{b0}}{\varpi_{b0}} \frac{T - T_{cr}}{T_{\max} - T_{cr}} \right), & T_{cr} &\leq T \leq T_{\max} \\ \varpi_b &= \varpi_{\max}, & T_{cr} &\leq T \end{aligned} \quad (3.7)$$

where ϖ_{b0} and ϖ_{\max} are the basal and maximum perfusion rate respectively; T_{\max} is fixed at 45°C ; T_{cr} is the critical temperature (approximately 42.5°C).

Temperature and damage dependent

The effect of blood perfusion is treated as a heat source where the rate of blood perfusion is considered as temperature- and damage-dependent^[51], given as

$$\omega_b = \omega_{b0} f(T) \exp(-\Omega) \quad (3.8)$$

where ω_{b0} is the basal perfusion rate; $f(T)$ is a dimensionless function that accounts for vessel dilation at slightly elevated temperatures; Ω is the damage integral.

Heat-generating interface

The effect of blood perfusion has also been considered by introducing a heat-generating interface between epidermis and subdermal tissue representing the thermal effect of blood flow through the dermis, which could simplify the skin model but resulted in a discontinuity of heat flux^[52].

3) Heat loss/generation under normal conditions

Under normal conditions, heat loss occurs through radiation to environment (if lower than body temperature) and through sweating, while heat generation occurs through metabolic process.

Heat loss by radiation

Different methods have been proposed to calculate the heat loss by radiation from skin. Draper & Boag^[53] suggested the following equation:

$$Q_{\text{rad}} = 4\sigma\varepsilon T_m^3 \quad (3.9)$$

where σ is the Stefan constant; ε is the emissivity of skin surface and $T_m = (T_s + T_a)/2$, T_s is the skin surface temperature, and T_a is the surrounding air temperature.

Wilson & Spence^[54] and Deng & Liu^[55] suggested another equation

$$Q_{\text{rad}} = \sigma\varepsilon (T_s^4 - T_a^4) \quad (3.10)$$

Heat loss by sweat evaporation

As for the heat loss by sweat evaporation, Wilson & Spence^[54] suggested the following equation:

$$Q_{\text{rsw}} = 9.66 \times 10^{-8} (T_s - T_f) (10^{0.265} T_s - RH \times 10^{0.265} T_f) \quad (3.11)$$

Deng & Liu^[55] suggested another equation, given as

$$Q_s = Q_{\text{dif}} + Q_{\text{rsw}} \quad (3.12)$$

$$Q_{\text{dif}} = 3.054 (0.256 T_s - 3.37 - P_a) \quad (3.13)$$

$$Q_{\text{rsw}} = 16.7h_f W_{\text{rsw}} (0.256T_s - 3.37 - P_a) \tag{3.14}$$

where T_f is the temperature of ambient fluid; Q_{dif} is the heat loss by evaporation of implicit sweat secretion when the skin is dry; Q_{rsw} is the heat loss by evaporation of explicit sweat secretion; W_{rsw} is the skin humidity; P_a is the ambient vapor pressure in Pa; h_f is the convective heat transfer coefficient; RH is the relative humidity.

Metabolic heat generation

The effect of metabolic heat generation is in most cases assumed to be constant. In some studies, it is also assumed to be temperature dependent^[47], which is based on the reversible nature of chemical reactions involving adenosine tri-, di- and monophosphates liberating heat energy in the *in vivo* tissue^[56].

4) Source terms for different heating methods

Hitherto, skin heat transfer due to different kinds of heating methods have been studied, such as contact heating^[57], laser heating^[44], microwave^[42], electrical heating^[58] and radiofrequency heating^[43], and electromagnetic heating is now widely used in thermal therapies. The electromagnetic (EM) spectrum is composed of an array of electromagnetic waves increasing in frequency from extremely low frequency and very low frequency (ELF/VLF), through radio frequency (RF) and microwaves, to infrared (IR) light, visible light, ultraviolet (UV) light, X-rays, and gamma rays, as shown in Figure 3.3.

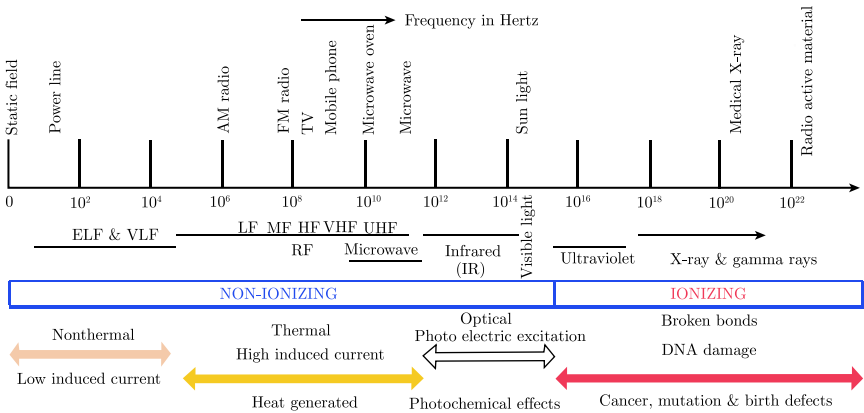


Figure 3.3 Electromagnetic spectrum^[59] (by permission of the author)

The ways for accounting for the heat generation due to different heating methods are discussed in this section.

(1) Normal heating.

Heating by contact with hot material such as hot plate and convective

hot fluid heating or by immersion in hot water are the most frequently encountered heating methods in skin thermal problems. When modeling, these heating methods can be accounted for by choosing the corresponding boundary conditions.

(2) Laser heating.

Lasers have been widely used in medical applications due to advantages such as directivity, ability used in pulsed mode, monochromaticity and so on. Typical lasers used in dermatology are summarized in Table 3.3. In general, there are three types of laser-skin tissue thermal interaction, depending on the degree and the duration of tissue heating: ① hyperthermia, where there is a moderate rise in temperature in the range of $41 \sim 44$ °C for some tens of minutes, resulting in cell death due to changes in enzymatic processes; ② coagulation, which refers to an irreversible necrosis without immediate tissue destruction with temperature in the range of $50 \sim 100$ °C for around seconds; ③ volatilization, which refers to a loss of material with temperature above 100 °C for a relatively short time of around one tenth of a second.

Table 3.3 Laser used in dermatology^[60] (by permission of Springer-Verlag London)

Laser	Wavelength/nm	Output	Skin chromophores
Excimer	193	Pulsed	Protein
Tripled Nd	355	Pulsed	Melanin
Argon ion	488	Continuous	Melanin, Hemoglobin
Argon ion, dye	514	Continuous	Melanin, Hemoglobin
Pigmented lesion dye	500~520	Pulsed	Melanin
Copper vapor	511	Quasi-continuous	Melanin
	578	Quasi-continuous	Hemoglobin
Krypton	530	Continuous	Melanin
	568	Continuous	Hemoglobin
Frequency-doubled Nd:YAG	532	Q-switched	Melanin, Hemoglobin
KTP	532	Quasi-continuous	
Pulsed dye	577, 585~600	Pulsed	Melanin, Hemoglobin
Argon dye	585, 630	Continuous	
Gold vapor	628	Quasi-continuous	
Ruby	694	Continuous, Q-switched	Melanin
Alexandrite	755	Pulsed, Q-switched	Melanin
Diode	795~830	Continuous	
Nd:YAG	1064	Continuous, Q-switched	Melanin, Hemoglobin
Holmium	2100		H ₂ O
Er:YAG	2940	Pulsed, Q-switched	H ₂ O
CO ₂	10,600	Continuous, Pulsed	H ₂ O

According to the wavelength of the light, there are three different methods for calculating the heat generation due to light-tissue interaction^[61].

Strong absorption

For wavelengths in the ultraviolet and IR region, where the absorption of the tissue is much larger than scattering, the fluence rate in the tissue, which is defined as the energy per unit area, decreases exponentially with increasing depth according to Beer's law. Therefore, the fluence rate in the tissue can be calculated using the following equation:

$$I_c(z, r) = I_L(r) (1 - r_{\text{sp}}) e^{-(\mu_a + \mu_s)z} \approx I_L(r) (1 - r_{\text{sp}}) e^{-\mu_a z} \quad (3.15)$$

where I_L is the radial profile of the incident laser beam; I_c is the fluence rate in the tissue; r_{sp} is the specular reflection coefficient; z (radius) and r (tissue depth) are the spatial coordinates; μ_a and μ_s are the absorption and scattering coefficients of the tissue, respectively.

Equation (3.15) was later modified by Welch et al.^[62], who took the scattering anisotropy into account, as follows:

$$I_c(z, r) = I_L(r) (1 - r_{\text{sp}}) e^{-[\mu_a + (1+g)\mu_s]z} \quad (3.16)$$

where g is the scattering anisotropy factor.

Strong scattering

When the wavelength is between about 300~1000 nm, the scattering of non-pigmented tissue dominates over absorption. The transport equation can be approximated by a diffusion equation in the diffuse light fluence rate $\phi_d(z, r)$, which is defined as the total amount of diffuse light power that passes through a small sphere at location of (z, r) divided by the cross-sectional area of that sphere. The diffusion equation is given as

$$\begin{aligned} & \frac{d^2 \phi_d(z, r)}{dz^2} + \frac{d^2 \phi_d(z, r)}{dr^2} + \frac{1}{r} \frac{d\phi_d(z, r)}{dr} - 3\mu_a [\mu_a + \mu_s (1 - g)] \phi_d(z, r) \\ & = -3\mu_s [\mu_s + \mu_a (1 - g)] I_c(z, r) \end{aligned} \quad (3.17)$$

here, the first term on the left side represents diffusion losses in the z and r directions; the right side term involves the collimated laser beam attenuated by absorption and scattering $I_c(z, r)$, which is the source for the diffuse light distribution.

The total fluence rate is the sum of the collimated and the diffuse components

$$\phi(z, r) = \phi_c(z, r) + \phi_d(z, r) \quad (3.18)$$

Scattering equal to absorption

When the scattering of the tissue is approximately equal to the absorption, there is no simplified solution to the transport equation, which means this

equation has to be completely solved to obtain the fluence rate distribution in the tissue

$$\frac{dL(r, s)}{ds} = -(\mu_a + \mu_s) L(r, s) + \frac{\mu_a + \mu_s}{4\pi} \int_{4\pi} p(s, s') L(r, s') d\varpi' \quad (3.19)$$

where p is the light power density; $L(r, s)$ is the radiance at tissue location (r, s) ; $L(r, s') d\varpi'$ is the amount of light power confined within solid angle $d\varpi$, moving in the direction s , which crosses an unit area located at r .

(3) Microwave heating.

The basic equations for the electromagnetic field are based on the well-known Maxwell relations. For the microwave thawing of dielectric materials, the governing equations can be written in terms of the electric and magnetic field intensities^[63] as

$$\frac{\partial H}{\partial x} + \varepsilon \frac{\partial E}{\partial t} + \sigma E = 0 \quad (3.20)$$

$$\frac{\partial E}{\partial x} + \mu_e \frac{\partial H}{\partial t} = 0 \quad (3.21)$$

where E is the electrical field; H is the magnetic field; μ_e is the magnetic permeability.

The microwave heat generation ($q_{\text{ext_MW}}$) can then be calculated as^[64]

$$q_{\text{ext_MW}} = \frac{r}{2} \left(|E_r|^2 + |E_z|^2 \right) \quad (3.22)$$

For one-dimensional skin model, the following equations can be used to calculate q_{MW} for different skin layers^[46]:

Epidermis layer : $q_{\text{ext_MW}} = P = \frac{1}{2} \sigma_e |E_z|^2 \quad (3.23)$

$$E_z(z, t) = \hat{x} E(0, t) T_{\text{sa}} \sum_{n=0}^{\infty} \left\{ \begin{array}{l} (\Gamma_{\text{sa}} \Gamma_{\text{df}})^n \exp \left[- \left(\frac{1}{\eta_e} + \frac{i2\pi}{\lambda_e} \right) (2nz_e + z) \right] \\ + (\Gamma_{\text{sa}} \Gamma_{\text{df}})^n \Gamma_{\text{df}} \exp \left[- \left(\frac{1}{\eta_e} + \frac{i2\pi}{\lambda_e} \right) (2nz_e - z) \right] \end{array} \right\} \quad (3.24)$$

$$E(0, t) = \sqrt{2P(0, t) Z_a} \quad (3.25)$$

Dermis layer : $q_{\text{ext_MW}} = P = \frac{1}{2} \sigma_d |E_z|^2 \quad (3.26)$

$$E_z(z, t) = \hat{x} E(0, t) T_{\text{sa}} \sum_{n=0}^{\infty} \left\{ \begin{array}{l} (\Gamma_{\text{sa}} \Gamma_{\text{df}})^n \exp \left[- \left(\frac{1}{\eta_d} + \frac{i2\pi}{\lambda_d} \right) (2nz_d + z) \right] \\ + (\Gamma_{\text{sa}} \Gamma_{\text{df}})^n \Gamma_{\text{df}} \exp \left[- \left(\frac{1}{\eta_d} + \frac{i2\pi}{\lambda_d} \right) (2nz_d - z) \right] \end{array} \right\} \quad (3.27)$$

$$E(0, t) = \sqrt{2P(0, t) Z_a} \quad (3.28)$$

$$\text{Fat layer :} \quad E(z, t) = \hat{x}E(z_d, t) T_{df} \exp \left[- \left(\frac{1}{\eta_f} + \frac{i2\pi}{\lambda_f} \right) (z - z_d) \right] \quad (3.29)$$

$$P = \frac{1}{2} \sigma_f |E_z|^2 \quad (3.30)$$

In the above equations, σ_d is the electrical conductivity; E_z is the propagating electric field; $P(0, t)$ is the power density incident on the skin surface at time t ; $E(0, t)$ is the corresponding electric field amplitude; $E(z, t)$ is the propagating electric field in the epidermis and dermis; $E(z_d, t)$ is the electric field at the dermis-subcutaneous fat interface; η_d and η_s are the penetration depths for dermis and subcutaneous fat; λ_d and λ_s are the wavelengths in dermis and subcutaneous fat; Z_a , Z_d and Z_f are the intrinsic impedances of air, dermis, and subcutaneous fat, respectively. Note that the incident power, $P(0, t)$, is expressed as an area density whereas the absorbed power density in the skin, $P(z, t)$, is expressed as a volume density. The reflection (Γ) and transmission (T) coefficients at the skin/air (sa) and dermis/fat (df) interfaces are given together with the intrinsic impedances, as^[65]

$$\begin{aligned} \Gamma_{sa} &= \frac{Z_a - Z_d}{Z_a + Z_d}, & \Gamma_{df} &= \frac{Z_d - Z_f}{Z_d + Z_f}, & T_{sa} &= \frac{2Z_d}{Z_a + Z_d}, & T_{df} &= \frac{2Z_f}{Z_f + Z_d}, \\ Z_a &= \sqrt{\mu_0/\varepsilon_0} = 377, & Z_d &= \sqrt{i2\pi f \mu_0 / (\sigma_d + i2\pi f \varepsilon_0 \varepsilon_d)}, & & & & (3.31) \\ Z_f &= \sqrt{i2\pi f \mu_0 / (\sigma_f + i2\pi f \varepsilon_0 \varepsilon_f)} \end{aligned}$$

where $i = \sqrt{-1}$; σ_d and σ_s are the conductivities of dermis and subcutaneous fat; ε_d and ε_s are the permittivities of dermis and fat; μ_0 is the permeability of free space [$1.256, 637, 06 \times 10^{-6} \text{Wb}/(\text{A} \cdot \text{m})$], and ε_0 is the permittivity of free space [$8.854, 187, 82 \times 10^{-12} \text{C}^2/(\text{N} \cdot \text{m}^2)$].

3.2.4 Non-Fourier thermal behaviour of skin tissue

In many situations, heat conduction has been treated according to the classic Fourier's law, which assumes that any thermal disturbance on a body is instantaneously felt throughout the body or, equivalently, the propagation speed of thermal disturbance is infinite. Although this assumption is reasonable in the majority of practical applications, it fails in particular thermal conditions or heat conduction media, where the heat conduction behaviour shows a non-Fourier feature such as thermal wave phenomenon, or hyperbolic heat conduction as defined mathematically.

Non-Fourier heat conduction behaviour has been experimentally observed in engineering materials or heat conduction media operating at low temperatures, such as liquid Helium II^[66] and Al_2O_3 crystal^[67] etc. Later, following

developments in laser technology, non-Fourier thermal behaviour was observed in short-pulse laser processing of thin-film engineering structures^[68]. A similar phenomenon has also been experimentally observed in materials with non-homogeneous inner structure^[69], such as H acid, NaHCO_3 , sand, glass ballontini, ion exchange, and sand with an irregular grain structure, which are similar in heterogeneity to biological tissues.

1) Non-Fourier heat conduction in non-homogeneous materials

Although non-Fourier heat conduction in materials having a non-homogeneous inner structure has been reported by various researchers, this claim was initially rebutted by Grassmann & Peters^[70] and Herwig & Beckers^[71], for they observed no evidence of hyperbolic conduction in skin tissue. Different investigators however have reported flaws in their experimental philosophy^[72], where one limitation was found to be the determination of thermal diffusivity and relaxation time. Accordingly, Roetzel et al.^[72] carried out an experiment to simultaneously determine these parameters from a single experiment and their results confirmed a hyperbolic behaviour of thermal propagation, but smaller in extent compared to that reported in the literature.

The non-homogeneous inner structure of biological tissue suggests the existence of non-Fourier heat conduction behaviour, as temperature oscillation¹⁾ and wave-like behaviour are commonly observed. Temperature oscillation in living tissue was first observed by Richardson et al.^[73] and later by Roemer et al.^[74], who subjected canine thigh muscle to an abrupt application of microwave heating at different power levels. Subsequently, Mitra et al.^[75] carried out four different experiments with processed meat for different boundary conditions and also observed the wave-like behaviour (temperature jumps which can be regarded as the wave front): ① tissue temperature rose monotonically with time to an elevated steady state value at low power levels; ② temperature rose above a “critical temperature” before an abrupt increase in blood perfusion was activated to reduce the temperature to a new steady state value; ③ temperature responded as damped or self-sustained large oscillations (jumps); ④ temperature increased continuously at a rapid rate at high power levels. On the other hand, Davydov et al.^[76] experimentally observed that heat transfer in a muscle tissue under local strong heating exhibits substantial anisotropy, which cannot be explained by the standard Fourier-theory based heat diffusion model. Banerjee et al. measured the

1) An unusual oscillation of tissue temperature with heating: the tissue temperature doesn't increase or decrease monotonically with the heating time or cooling time, but oscillates in a specific range.

thermal response of meat under laser irradiation, and found that the non-Fourier hyperbolic heat conduction equation is a better approximation than the classical parabolic Fourier heat conduction formulation.

As with engineering materials, there are different viewpoints on the non-Fourier behaviour of biological materials. For example, Tilahun et al.^[77] and Herwig & Beckert^[78] questioned the experimental results of Mitra et al.^[75]; the former tried to reproduce Mitra's experiment^[75] with processed meat but did not observe any non-Fourier behaviour. In turn, they cited several issues associated with the Mitra's experiments that might have caused the observed temperature jumps. Herwig & Beckert^[78] also found no evidence of non-Fourier heat conduction effects, and they pointed out that the thermal lag effect can be explained by the Fourier heat conduction rather than by the wave behaviour. Unfortunately, it was not possible to reconcile the conflicting measurements of Mitra with Tilahun and Herwig & Beckert, for the experiments were performed differently and there was no information in either study about the processed meats^[79].

Although a wave-like heat transfer behaviour in living tissue is intriguing, no ultimate conclusion can be drawn at present due to the complexity of biological systems^[80]. Theoretically, treating the non-homogeneous biological material as a porous medium under the same boundary conditions as in one of Mitra's experiments, Xu & Liu^[81] found that the wave-like thermal behaviour in the meat may be caused by the convection of water inside the tissue. This aspect was thought to be induced in the experiments of Mitra et al.^[75] by pressing the meat samples together at the start of each experiment and by the subsequent development of temperature gradients across the samples. The temperature jumps were attributed to the arrival of warm water at the measurement locations in the colder samples before the effect of "pure conduction" became noticeable at these locations. However, Xu & Liu^[81] did not directly compare their predictions with measurements. Davydov et al.^[76] also attributed their observation of anomalous heat transfer behaviour in muscle tissue to the flow of interstitial liquid as a result of non-uniform heating. Despite the resemblance between the findings of Mitra et al.^[75] and Xu & Liu^[81], to interpret the experiments of Mitra in the context of convection rather than "pure conduction" requires additional study.

Alternatively, the temperature oscillation phenomenon has been attributed to blood perfusion oscillation due to heating^[82]. However, this explanation was subsequently questioned by others^[80]. Using an artificially simulating construction similar to a bioheat transfer system, Liu et al.^[83] carried out a series of experiments and found that the temperature oscillations can be well fitted with the thermal wave analysis.

2) Importance in thermal therapies

Advances in laser, microwave and similar technologies have led to recent developments of thermal treatments for diseased and injured skin tissue, such as skin cancer and skin burn. The objective is to induce thermal injury precisely within tissue structures located several millimeters below the surface but without affecting the surrounding, healthy tissue. The success of these thermal therapies depends on the precise prediction and control of temperature, damage and stress distributions in the tissue.

From a therapeutic viewpoint, the high-intensity short duration heating scheme can efficiently produce an appropriate and precise dose of heat during thermal therapies. In addition, reducing the overall treatment time is important, especially when the treatment target volume is large. A rapid heating scheme with a good strategy is therefore essential for an effective thermal therapy. However, the possible non-Fourier nature of heat transfer in living tissue may play an important role during rapid heating, such as thermal ablation/thermal surgery, when a high-intensity thermal source such as focused laser, ultrasound or radiofrequency ablation is used. For example, it has been shown that the thermal relaxation of tissue (as given in Table 3.4) will delay the appearance of peak temperature during thermal treatments, leading to a lower thermal dose level^[84]. Furthermore, damage to human tissue from thermal agitation is an exponential function of temperature^[85], so even small improvements in the prediction of temperature can strongly influence the prediction of damage. Knowledge of temperature distribution is also essential for the understanding of the corresponding thermomechanical behaviour.

Table 3.4 Thermal relaxation times of important cutaneous structures

Structure	Melanosome cell			Blood vessel	
Size/ μm	0.5~1	10	50	100	200
Thermal relaxation time (approximate)/ms	0.001	0.3	1	5	20

3.3 Skin Thermal Damage

3.3.1 Burn classification

1) Different kinds of skin burn

In general, skin burns can be classified as thermal, electric, radiant and chemical burns according to the different agents that cause them. Skin thermal burns are evoked by interactions of skin tissue with different high temperature sources. Since electrical and radiant burns are also due to their thermal effect on skin tissue^[86], they are also regarded as thermal burns.

Thus thermal burn wounds can be classified in to five separate groups based on the different mechanisms of damage: ① scald burn injuries, which can be caused by liquids, grease, or steam where liquid scalds can be further divided into spill and immersion scalds^[87]; ② contact burns, which is often due to contact with a hot solid surface^[87]; ③ fire burn injuries, which can further be divided into flash and flame burns, both of which can be described as an incident heat flux boundary condition on the surface of the skin^[88]; ④ thermal irradiation damage from laser or other sources^[89]. Materials like skin can reflect a significant amount (50%~85%) of the incident energy when the radiation originates from a very high temperature source like a carbon arc lamp or nuclear explosion^[90]; Electrical burns, which generally consists of two mechanisms (thermal tissue damage^[91] and electroporation damage) and are considered as summative in action and have a variable degree of contribution to the ultimate damage produced^[86].

2) Burn degree

There are different classification systems used to categorize skin burns, which have been reviewed by Diller^[92] and Muir et al.^[93], and are summarized by Parsons^[94], as shown in Table 3.5. Briefly, burns generally are classified as first, second, third degree based on the extent of damage to the different layers of skin.

Table 3.5 Different classification systems for burns

A	B (Scotland)	C(USA)	Description
Partial thickness skin destruction	1 st degree	1 st degree	Characterized by redness in the burned region. Discomfort is temporary and healing is rather quick, with no permanent damage.
		2 nd degree	Also referred to as partial thickness burns. The epidermal layer is damaged and injury extends into the dermal layer as well. There is damage to sweat glands and hair follicles. Blisters, severe pain, reddening, and swelling characterize these burns.
Whole thickness skin destruction	2 nd degree	3 rd degree	Burns destroy all the epidermal and dermal layers. There is tissue damage below the hair follicles and sweat glands into the subcutaneous tissue. The burned area will appear charred or a dry white color. There is no possibility for spontaneous healing, so skin grafting is required.

3.3.2 Experimental study

1) Experimental study of skin burn

Although skin burn has been studied on human^[95], due to the ethical and immunological issues associated with testing human skin, many researchers

have used pig skin^[96] in view of the high degree of functional similarity of the structure of pigskin to human skin^[97]. However, since using of pigs pose practical problems such as more housing space and more maintaining expense^[98], many different smaller animals have also been used in burn research, such as rats and hamsters^[99].

Leach et al.^[100] and Sevitt^[101] applied a heated iron onto the skin surface and studied the correlation between the contact time and the resulting damage. Enalejev & Kachalkin^[96] carried out experimental and analytical study of skin burn resulting from contact with a heated material. Knabl et al.^[98] presented partial skin thickness burn lesions in rabbits by use of a round aluminum stamp. Stoll & Greene^[102] carried out experimental research to study the time required for the occurrence of second degree burn damage resulting from thermal radiation with given heat flux by use of a 1 kW projection lamp. Takata et al.^[103] performed experiments involved exposing porcine skin to flames generated by the controlled burning of fuel in a furnace. Ross & Diller^[104] experimentally studied the burn injury in hamster cheek pouch by using very precise temperature measurement and control technique. They fitted the data of burn time and temperature causing a specified degree of burn damage and high correlation was found between each other: $t = t_0 \exp [(T_0 - T) / T_0]$, where t_0 and T_0 were initial time and temperature, separately. Okumura & Reinhold^[105] inflated the rat subcutis with air and placed anaesthetized animals in a heated water bath with the upper part of this air pouch exposed to the hot water. De Camara et al.^[106] studied the sequential morphologic changes following untreated partial-thickness burns of Guinea pigs induced by 75°C water immersion for 10 seconds. Skin samples obtained at 2, 8, 24, and 96 hours after the burn were examined by light and electron microscopy. The results showed that there was a definite progression of the thermal injury with maximum tissue destruction occurring 8 hours after the burn; at 24 hours after the burn, some improvement in the burn wound was noted, especially in the dermal microvasculature; at 96 hours, the damaged epidermis sloughed, exposing a dermis that contained areas resembling microabscesses. By use of ultrasonic techniques, Cantrell^[107] measured the burn time-dependent depth of conductive cutaneous burns induced in anesthetized Yorkshire pigs in vivo by keeping the skin surface temperature at 100°C. The data were then used to solve the one-dimensional heat diffusion equation with time-dependent boundary conditions. The threshold temperature of 65.3°C was obtained and the energy associated with the transition of the tissue from the state of viability to the state of necrosis was found to be 408 J/g. Nanney^[108] studied the microvascular alterations characteristic

of thermal damage by using electron microscopy. The caudal 50 per cent of anaesthetized Guinea-pigs was scalded by immersion in 100 °C water for 3 seconds. Skin samples were obtained separately from 15 minutes to 24 hours after scalding. It was found that large intercellular gaps were present in venule endothelium by 15 minutes after injury and in capillary endothelium by 30 minutes after injury; and extensive destruction in peripheral nerves and endothelial cells was observed 15 minutes and 4 hours after scalding, respectively.

2) Comparison of different types of burns

Jelenko & Wheeler^[109] compared the effects of 15 methods of burning on the clipped abdomen of rabbit, including radiant heat, flame, branding, and scalding. Response of the surface to hyperthermic insult was observed with regard to thermotemporal alteration, change in thickness, and variation in water-retentive capacity of the challenge site. Branding with a 730°C Pyrex disc produced the greatest surface damage, but exposure to open flame and X-second immersion in 100°C or 90°C water were statistically comparable. Scalding at 70°C although followed by transient skin thickening, produced no significant alteration by 3 hours postburn.

Investigations on skin injury as a result of transfer of low to moderate amounts of heat or electrical energy are sparse and contradictory. Most authors claim that heat energy and electrical energy induce similar histological changes in the skin^[110] while others found that heat lesions and electrical lesions are characteristic and differ markedly from each other^[111]. Danielsen et al.^[111] and Nielsen et al.^[112] pointed out that some of the difference may be associated with differences in intensity of energy during exposure to heat and electricity, while Thomsen et al.^[113] argued it is probable that pH shifts in the cells due to electrolysis is the main cause of the specific morphology of electrical lesions in spite of the possibility of differences in distribution and intensity of energy.

Hoekstra et al.^[114] and Brans et al.^[115] investigated the similarities and differences between the levels of tissue damage caused by contact burns or scald burns by using two different burn models in pigs. Middelkoop et al.^[116] pointed out that different types of burns may lead to different levels of vascular damage while the vascular damage greatly influences the ultimate level of tissue damage. Mercer & Sidhu^[87] compared the three mechanisms for thermal burns due to an automotive airbag, namely, contact with the hot expelled gases from the airbag, contact with the hot airbag itself and melting of clothing from either of these contacts and found that direct contact with

high temperature exhaust gases venting from the airbag can indeed lead to burns and that burns from contacting the hot airbag material are possible but far less likely to occur.

3.3.3 Theoretical analysis and numerical modeling

With the development of various thermal therapeutic techniques, which rely on the application of elevated temperatures to degenerate tissue, the understating of thermal damage mechanisms become more and more necessary, and many investigators have discussed burn injuries under different situations. Comprehensive analysis of skin burns has been given^[92].

It would be very useful to have a computer program that could promptly predict the seriousness of different burns accurately since this would help to reduce on the chances of burn patients developing poisons in their vital organs due to toxic agents entering the bloodstream from their wounds. Doctors would know exactly how much dead tissue to debride to prevent this happening.

Henriques & Moritz were one of the first pioneers in the area of thermal injury and did the most extensive and influential studies^[85]. They proposed one of the first analytical models for thermal injury to skin. Their results showed that a burn injury of standard threshold severity could be produced by progressively decreasing temperatures as the thermal insult period was logarithmically increased. They computed the time-temperature relationship at the dermal-epidermal junction for two different cases involving boundary conditions of constant temperature and constant heat flux. The solution of the Fourier heat conduction was obtained. Damage was assumed to be caused by injury to the “basal cells” located just below the epidermis at a distance of about 80 μm below the skin surface. Most of later theoretical analyses are based on the study of Henriques & Moritz^[117].

Because the geometric of skin tissue is complex and their thermal properties are variable, numerical methods have been widely used to simulate the burn processes, including Finite Difference Method^[62], Finite Element Method^[87], and Boundary Element Method^[118].

3.3.4 Models of burn damage quantification

1) Critical thermal load approach

The Critical thermal load approach was often used during earlier times to quantify thermal damage in tissue, which assumes that the total damage was a function of only total cumulative dosage so that equal doses produced

equal injury.

$$\Omega = \int_0^t q dt \quad (3.32)$$

where Ω is measure of thermal damage; q is the heat flux.

However, this method has been criticized by several researchers, for example, Stoll^[119] has demonstrated that a large amount of energy delivered over an extended period of time may produce no damage whatever, where the same dose delivered nearly instantaneously may destroy the skin.

2) Arrhenius burn integration approach

Nowadays, the Arrhenius burn integration proposed by Henriques & Moritz^[120] is widely used. Henriques & Moritz were the first pioneers in the area of heat transfer and thermal injury of biological tissues. Their results showed that a burn injury of standard threshold severity can be produced by progressively decreasing temperatures as the thermal insult period is logarithmically increased. They conducted two different experiments, which involved boundary conditions of constant temperature and constant heat flux to compute the time-temperature relationship at the dermal-epidermal junction. They worked out the solution of the Fourier heat conduction equation for a semi-infinite body in order to model the transfer of heat through skin. Based on their observation, Moritz & Henriques^[85] proposed that skin damage could be represented as a chemical rate process, which is calculated by using a first order Arrhenius rate equation, whereby damage is related to the rate of protein denaturation (k) and exposure time (t) at a given absolute temperature (T). The measure of thermal damage Ω was introduced and its rate k was postulated to satisfy

$$k(T) = d\Omega/dt = A \exp(-E_a/RT) \quad (3.33)$$

or, equivalently

$$\Omega = \int_0^t A \exp(-E_a/RT) dt \quad (3.34)$$

where A is a material parameter (frequency factor); E_a is the activation energy; R is the universal gas constant. Equation (3.34) indicates that a reaction proceeds faster with larger values of T or A for the same E_a , or with smaller values of E_a for the same A . The constants A and E_a are usually obtained experimentally.

In the study of Moritz & Henriques^[85], the integration was carried out over the time range where the basal layer temperature was greater than or equal to 44°C, which was the threshold temperature for thermal damage

to skin. According to different levels of tissue damage and heating modes, Henriques^[121] proposed three different thresholds corresponding three different burn degrees ① Threshold I: the longest time at which constant predetermined surface temperature could be tolerated without causing irreversible transepidermal damage (denoted by $\Omega = 0.53$); ② Threshold II: the shortest time at which constant predetermined cutaneous surface temperature produces transepidermal necrosis (denoted by $\Omega = 1$); ③ Threshold III: the shortest time at which circumambient and circumradiant heat of measured intensity caused transepidermal necrosis (denoted by $\Omega = 10^4$).

After the pioneer work of Henriques & Moritz^[120], many researchers have also proposed some other models, but most of them have similar format. There are only differences in the coefficients used in the burn damage integral, which are mainly due to the different experimental databases used to define the models and the different emphasis when analysing the burn process. The available Arrhenius parameters (A , E_a) used to calculate thermal damage for skin tissue from the literature has been reviewed, as given in Table 3.6, and is fitted with the method used by Wright^[128], as shown in Figure 3.4.

Table 3.6 Review of activation energy and frequency factor for skin tissue

Temperature range/ $^{\circ}\text{C}$	Sample and assay	Site	Activation energy, $E_a/(\text{J/mol})$	E_a/R /K	Frequency factor/(1/s)	References
$44 \leq T \leq 70$	Necrosis	Epidermis	6.27×10^5	75,000	3.1×10^{98}	[121]
$T \leq 55$	Necrosis		6.27×10^5	75,000	3.1×10^{98}	[122]
$T > 55$	Necrosis		2.96×10^5	35,406.7	5.0×10^{45}	
$44 \leq T \leq 50$	Necrosis	Epidermis	7.82×10^5	93,540.7	$\frac{2.185 \times 10^{124}}{10^{124}}$	[102]
$T > 50$	Necrosis	Epidermis	3.27×10^5	39,114.8	$\frac{1.823 \times 10^{51}}{10^{51}}$	
	Necrosis	Bulk skin	5.5×10^8		7.6×10^{76}	[123]
Whole range	Necrosis	Epidermis	4.60×10^5	55,000	1.43×10^{72}	[124]
Whole range	Necrosis	Dermis	4.60×10^5	55,000	$\frac{2.86 \times 10^{69}}{10^{69}}$	
$44 \leq T < 50$	Necrosis	Dermis	4.18×10^5	50,000	$\frac{4.322 \times 10^{64}}{10^{64}}$	[103]
$50 \leq T \leq 60$	Necrosis	Dermis	6.69×10^5	80,000	$\frac{9.389 \times 10^{104}}{10^{104}}$	
$T \leq 50$	Necrosis		6.27×10^5	75,000	3.1×10^{98}	[125]
$T > 50$	Necrosis		$6.27 \times 10^5 \sim$ 5.10×10^2 $\times (T - 53)$		3.1×10^{98}	
$48 \leq T \leq 57$	Purpura formation	Porcine epidermis	3.39×10^5	40,550.2	$\frac{4.11 \times 10^{53}}{10^{53}}$	[126]
$40 \leq T \leq 60$	Birefringence loss	Rat skin collagen	3.06×10^5	36,602.9	$\frac{1.606 \times 10^{45}}{10^{45}}$	[127]

The results of Figure 3.4 clearly suggest a linear relationship between the Arrhenius parameters for skin tissue, given by (after a least-square fit)

$$E_a = 21,149.324 + 2688.367 \ln A \quad (3.35)$$

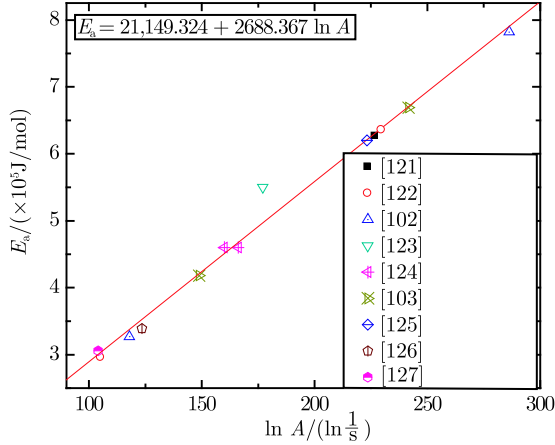


Figure 3.4 Cross-plot of Arrhenius parameters (A , E_a)

With the above relation, the reaction rate of the thermal damage process is given as

$$k(T) = \exp [(E_a - 21,149.324)/2688.367] \exp (-E_a/RT) \quad (3.36)$$

If the temperature is constant and E_a specified, the thermal damage can be calculated as

$$\Omega = \int_0^t k(T) dt = k(T)t \quad (3.37)$$

Assuming that $\Omega = 1.0$ denotes the beginning of irreversible damage, the time for the appearance of irreversible damage at temperature T as specified by threshold A can be calculated as

$$t_{\Omega=1} = 1/k(T) = 1/\{\exp [(E_a - 21,149.324)/2688.367] \exp (-E_a/RT)\} \quad (3.38)$$

The relation between reaction rate and E_a for constant temperature is given in Figure 3.5 (a) and the variation of the time for the irreversible damage with the E_a is shown in Figure 3.5 (b).

The Arrhenius burn damage model has been shown to be a useful tool by which the time-temperature history and damage accumulation are connected. However, it has several shortcomings^[30]: ① the models are mainly based on the burns created by surface heating; ② these models do not account

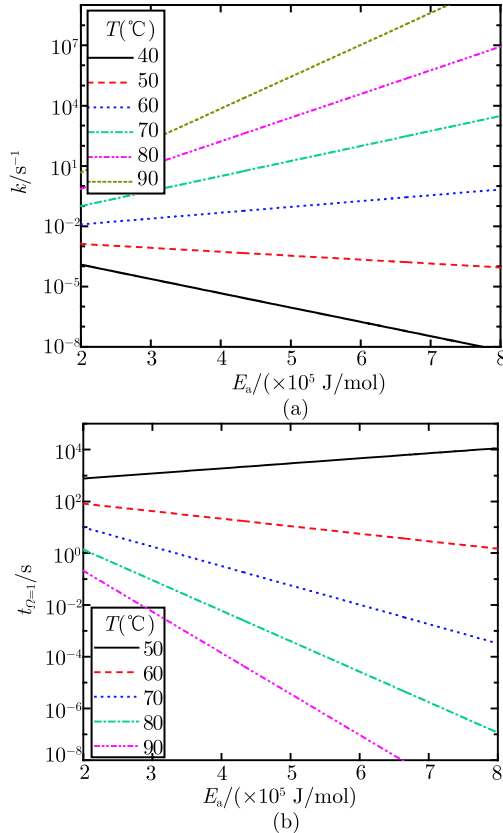


Figure 3.5 Effect of activation energy E_a on (a) thermal damage process rate and (b) the time for the irreversible damage

for the history of thermal insult; ③ these models do not consider many other factors besides temperature, such as pH variations, preheating, and mechanical loading etc; ④ these models are based on the Arrhenius chemical reaction rate equation, but often applied in a context not matched; ⑤ the experiments performed to derive A and E_a are only for rather long times of hyperthermic exposure covering tens to thousands of seconds.

3) Approach based on enzyme-catalyzed reactions

Based on the analysis of enzyme-catalyzed reactions in living tissue, Xu & Qian^[129] presented a thermal damage model where the thermal stability of the substrate-enzyme complex was taken into account. Based on the experimental results of Moritz & Henriques^[120], a new damage function was given, which better fitted the data

$$\Omega = \int_0^t \frac{Ae^{\alpha z}}{1 + Be^{-\beta z}} dt \quad (3.39)$$

where α and β are empirical constants. By fitting the data of Henriques & Moritz^[120], the constants were given as: $\alpha = 100$, $\beta = 195$, $A = 1.0 \times 10^{-4}$, $B = 8.0 \times 10^4$.

Many investigators have discussed burn injuries for different situations. Diller and Hayes presented a finite element model of burn injuries in blood-perfused skin^[130]. Torvi and Dale developed a finite element model of skin for a flash fire exposure and discussed the sensitivity of burn predictions to variations in thermal physical properties^[88]. Ng & Chua presented a mesh-independent model to predict skin burn injuries using the finite element method^[41]. Ng & Chua compared one- and two-dimensional program for predicting skin burns and showed that the temperature distributions predicted by the one- and two-dimensional programmes were similar^[131]. Diller proposed a one-dimensional model to calculate the transient temperature and injury distributions in skin using the finite difference method^[132]. Jiang developed a model which presents the transient temperature and damage function distributions variations for the variations of the initial temperature, blood perfusions and skin layer thicknesses^[133]. The results show that the epidermis and dermis thicknesses significantly affect the temperature and burn injury distributions.

Besides skin, it has also been shown that the dissipation of heat is different in cancerous and in healthy tissues and higher temperatures can be attained within tumours. High temperatures also have a sensitizing effect in the radiation therapy resulting in better response and longer tumour control with acceptable normal tissue effects^[134] and the references therein.

3.3.5 Experimental quantification

Successful use of the burn damage model depends on identifying a quantitative measure of burn damage and direct comparisons between numerical models and experiment^[135]. However, since typical damage end points have been qualitative tissue indicators, such as edema formation, vascular stasis, nuclear pyknosis, or hyalinization of collagen, till now, measurement of thermal damage of skin tissue is still very difficult and there are only few efficient methods.

Collagen is the major component of skin, and it accounts for approximately 75% of the skin's dry weight and 18%~30% of the dermis's volume^[136]. It is reasonable to take the state of collagen as a marker of thermal damage in skin. Quantitative histologic markers of thermal damage in collagen include changes of intensity, color shifts of birefringent images, phase retardation and hyalinization of collagen fibers^[137].

Under thermal loading, with the increase of skin temperature, the heat-labile intramolecular crosslinks in collagen are broken, and the collagen undergoes a transition from a highly organized crystalline structure to a random, gel-like state^[138]. This process is thermal denaturation, which appears accordingly as thermal shrinkage. It is pointed out that the dimensionless indicator of damage, Ω , is in fact the logarithm of relative concentration of “reactants” (undenatured collagen) in collagen denaturation process^[135]:

$$\Omega(t) = \ln \frac{C(0)}{C(t)} \quad (3.40)$$

where $C(0)$ is the initial concentration and $C(t)$ is the concentration of undenatured collagen remaining at time t .

The degree of thermal denaturation (percentage of denatured collagen) can then be calculated as

$$Deg(t) = \frac{C(0) - C(t)}{C(0)} = 1 - \exp[-\Omega(t)] \quad (3.41)$$

where Deg is the degree of thermal damage ($Deg = 0$ equals no damage while $Deg = 1$ equals fully damaged).

1) Thermal measurements

Differential scanning calorimetry (DSC) has been used extensively to characterize the thermal behaviour of collagenous tissues such as skin^[139]. DSC detects thermodynamic changes by measuring the flow of heat between a sample and a reference, whereby the effect of thermal history on the heat capacity of tissue can be determined and different parameters derived, including Arrhenius parameters (A , E_a).

In our previous study^[140], we have measured the thermal stability of collagen in pig skin scanning from 20 to 100°C at four different heating rates (2°C/min, 5°C/min, 10°C/min, 20°C/min). A typical DSC thermogram of a flank skin sample is shown in Figure 3.6. The measured specific heat of skin tissue falls in the reasonable range in comparison with existent data in literature^[120]. The result of Figure 3.6 demonstrates that, for a stress-free skin sample, within the temperature range of 30 to about 90°C, only broad endothermal peak appears in each sample. Denaturation is characterized by a sudden increase in the energy absorption endotherm, starting at about 60°C. With further heating, the endotherm reaches its maximum value at the denaturation temperature of 66.83°C and then decreases. It is known that the temperature of thermal denaturation strongly depends on the water content in collagen and its degree of cross-linking between the chains^[141].

The endothermal peak (see Figure 3.6) is connected with the transition of collagen structure from triple helix to a randomly coiled conformation, taking place in the domains between the cross-links.

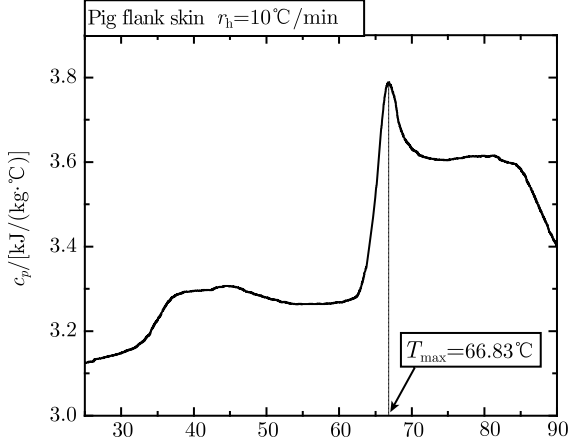


Figure 3.6 Characteristic DSC thermogram of a skin tissue sample

It is also observed that the denaturation endotherm characteristics are heating rate dependent (not shown here for brevity), where the maximum of the peak at higher heating rates is shifted towards higher temperatures. If a collagenous tissue is heated from an initial value at a constant heating rate (r), as in this study, the rate of decline in the number of native molecules with time follows the first order kinetics, given by^[142]

$$T = T_i + rt \quad (3.42)$$

$$\frac{dN}{dt} = -k(T) N \quad (3.43)$$

where T_i is the initial tissue temperature; N is the molecules of native (not denatured) collagen in the tissue; T is the current tissue temperature; $k(T)$ is the reaction rate.

Combining Equations (3.42) and (3.43) one obtains

$$\frac{1}{N} \frac{dN}{dT} = -\frac{k(T)}{r} \quad (3.44)$$

This equation predicts that the maximum of $-dN/dT$ can be obtained when

$$d^2N/dT^2 = 0 \Rightarrow \frac{d}{dT} \left[\frac{k(T)}{r} N \right] = 0 \quad (3.45)$$

$$\Rightarrow N \frac{dk(T)}{dT} + k(T) \frac{dN}{dT} = 0 \quad (3.46)$$

Together with the Arrhenius equation

$$k(T) = A \exp\left(-\frac{E_a}{RT}\right) \quad (3.47)$$

the relation between Arrhenius parameters (E_a , A) and the peak temperature of thermal denaturation (T_{\max}) can be obtained as

$$\frac{rE_a}{ART_{\max}^2} = \exp\left(-\frac{E_a}{RT_{\max}}\right) \quad (3.48)$$

Equation (3.48) can be rewritten as

$$\ln \frac{r}{T_{\max}^2} = -\frac{E_a}{R} \frac{1}{T_{\max}} - \ln \frac{E_a}{R} + \ln A \quad (3.49)$$

The activation energy E_a can be obtained from the slope (*Slope*) of the $\ln(r/T_{\max}^2)$ versus $1/T_{\max}$ curve, while A can be derived through the intercept (*Int*)

$$E_a = -\text{Slope} \times R \quad (3.50)$$

$$A = \exp(\text{Int}) \frac{E_a}{R} \quad (3.51)$$

A characteristic plot of $\ln(r/T_{\max}^2)$ versus $1/T_{\max}$ for flank skin sample is presented in Figure 3.7. Tests with belly, back, ear and face skin samples have also been performed and the results are shown in Figure 3.8. The results of derived Arrhenius parameters are presented in Table 3.7. As shown above,

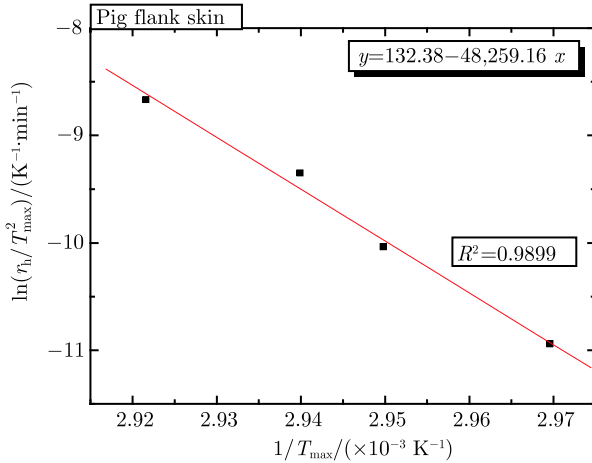


Figure 3.7 Characteristic plot of $\ln(r/T_{\max}^2)$ versus $1/T_{\max}$ for pig flank skin

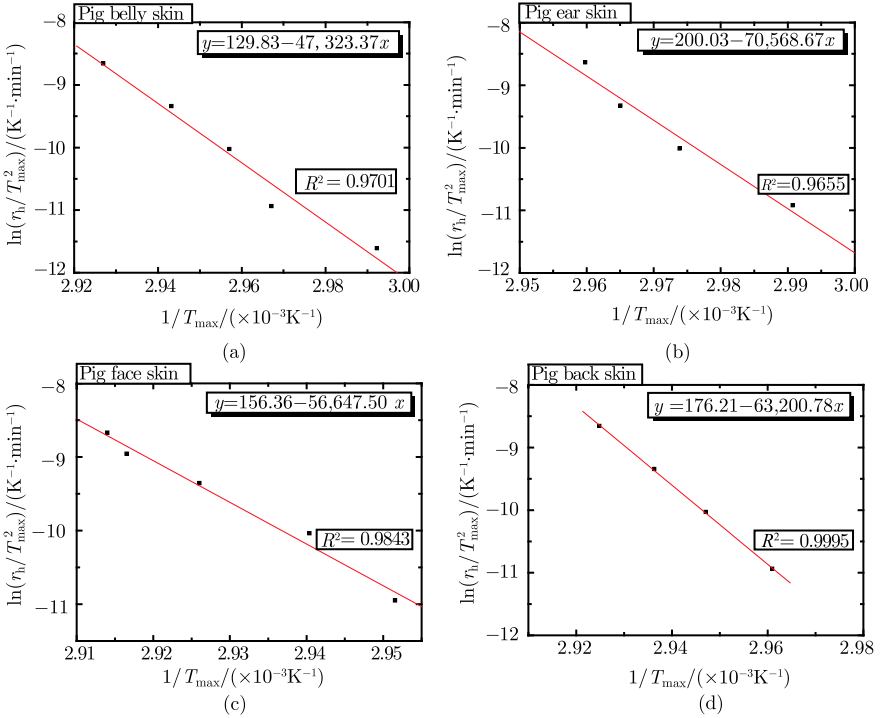


Figure 3.8 Plot of $\ln(r/T_{\max}^2)$ versus $1/T_{\max}$ for skin tissue from (a) belly, (b) ear, (c) face and (d) back

Table 3.7 Experimental results of Arrhenius parameters (E_a , A)

Sample	$E_a/(\times 10^5 \text{J/mol})$	A/s^{-1}
Back skin	5.255	2.126×10^{81}
Belly skin	3.935	1.151×10^{61}
Ear skin	5.867	5.240×10^{91}
Face skin	4.710	4.575×10^{72}
Flank skin	4.012	1.501×10^{61}

there is a linear relationship between the published experimental result of Arrhenius parameters $\ln A$ and E_a for skin tissue, as shown in Equation (3.51). The comparison of our results for different pig skin samples with results calculated from Equation (3.51) has been given in Figure 3.9. It can be seen that a very good agreement has been achieved. With these results, the thermal damage and the degree of thermal denaturation of skin collagen for a given heating history can be quantified with Equation (3.40) and Equation (3.41). It should be noted here that the thermal denaturation of a collagenous tissue depends on not only the temperature history but also the stress state during heating^[143], which is, however, very difficult to quantify due to the

lack of corresponding research. Therefore, in the following calculation of thermal damage the parameters obtained from load free DSC measurements were used.

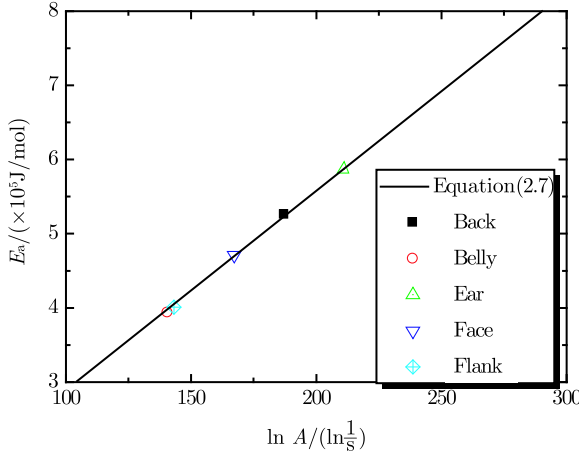


Figure 3.9 Comparison of our results of Arrhenius parameters with literature results

2) Birefringence measurement

It has long been accepted that birefringence is directly related to tissue structure. Collagenous tissue such as skin tissue in situ are birefringent: they act similarly to an optical quarter wave transformer in that polarized light will have its polarization rotated as it passes through the molecular array. In collagen, the array and spacing of the fibrous bundles is the origin of birefringence. The regularity of the array and birefringence is lost due to burn damage. Thus, when observed through an analyzer filter rotated 90° with respect to the polarizer, native-state birefringent tissue appears bright and damaged non-birefringent tissue dark. However, the natural variation in normal skin birefringence are influenced by several parameters, such as location, age, skin type, etc. Thus the absolute birefringence values cannot be directly related to burn severity^[135]. Instead, the relative birefringence intensity can be related to thermal damage

$$\Omega(\tau) = \ln \frac{I_B(0)}{I_B(\tau)} \quad (3.52)$$

where I_B is the relative birefringence intensity (in photometric units), which is normalized by dividing by the background light for that slide (I_0) and represents a measure of the volumetric number density of birefringent particles. I_B is defined as

$$I_B = \frac{I_S - I_D}{I_N - I_D} \quad (3.53)$$

where I_S , I_D and I_N are birefringence intensity for measured specimen, fully denatured specimen and native state specimen, respectively.

It has been shown that the polarimetric properties of collagenous samples can be used as marker to distinguish a healthy collagenous tissue from thermal damaged due to different heating methods such as laser^[144] and heated bath^[137], for different tissue such as skin^[137], myocardium^[144], urinary bladder^[145], tendon^[144].

Polarization-sensitive optical coherence tomography (PS-OCT) has been shown to be able to quantify collagen birefringence of skin tissue^[146]. Pearce et al.^[147] found that the loss of birefringence of skin tissue during thermal damage is a first-order kinetic reaction and thermal coagulation of collagen can be described as an end point of the rate process. According to the data of birefringence loss in rat skin collagen heated in vitro, they obtained the kinetic rate coefficients, $A = 1.606 \times 10^{45} \text{s}^{-1}$ and $E_a = 3.06 \times 10^5 \text{J/mol}$.

But it should be noted that interpreting the birefringence image requires great care. There are two phenomena that contribute to tissue birefringence, intrinsic birefringence and form birefringence^[148], where the former is due to the optical anisotropy and the latter is due to the different refractive index from the material between the fibers (the extrafibrillar matrix). Changes in either the collagen fibrils or in the extrafibrillar matrix can both, therefore, alter birefringence^[149]. For example, it has been observed that dehydration is also a possible origin for the retardation changes of collagenous tissue in response to hating besides the thermal denaturation of collagen^[150] and external load also changes the birefringence of collagen^[151]. Besides, significant area averaging is needed since the collagen fibers are moderately dispersed in the skin.

Quantitative histologic markers of thermal damage in collagen include changes of intensity, color shifts of birefringent images, phase retardation and hyalinization of collagen fibers^[137].

However, contradictory results have also been reported. Sankaran et al.^[152] measured the changes of rail tail tendon in collagen denaturation during laser heating on a millisecond timescale. The resulting kinetic analysis has shown that the rate coefficients for each denaturation process can fall into one of two regions. In the low radiant exposure region, thermal denaturation is rate-limited; no Arrhenius model predicts such behaviour. In the high radiant exposure region, denaturation is both thermally and mechanically induced; no Arrhenius model accounts for mechanical damage to tissue.

Beghuin et al.^[153] found that a strong reversible correlation exists between

rat tail tendon birefringence and temperature during very fast heating, which is totally different from the loss of birefringence that results from a denaturation process. Below the threshold temperature leading to denaturation, an increase in temperature is systematically accompanied by a reversible increase in birefringence, which means that there are only small modifications of the tissue structure at the fibril level.

3) Other methods

There are also several other potential methods, which can be used to quantify thermal damage. One of them is the intraoperative ultrasound, which is based on thermally induced changes in tissue intrinsic properties^[154]. However, the applicability of intraoperative ultrasound is hampered by its poor sensitivity. Other methods include enzyme deactivation^[155] and extravasation of fluorescent-tagged plasma proteins^[156].

3.4 Summary

Advances in laser, microwave and similar technologies have led to recent developments of thermal treatments for disease and injury involving skin tissue. In spite of the widespread use of heating therapies in dermatology, they do not draw upon the detailed understanding of the bio-thermo-mechanics of behaviour, for none exists to date, even though each behavioural facet is well established and understood. It is proposed that a detailed understanding of the coupled biological-mechanical response under thermal agitation will contribute to the design, characterization and optimization of strategies for delivering better treatment. For a comprehensive understanding on the underlying mechanisms of thermomechanical behaviour of skin tissue, recent progress on bioheat transfer, thermal damage, thermomechanics and thermal pain should be systematically reviewed. This article focuses on the transfer of heat through skin tissue. Experimental study, theoretical analysis and numerical modeling of skin thermal behaviour are reviewed, with theoretical analysis carried out and closed-form solutions obtained for simple one-layer Fourier theory based model. Non-Fourier bioheat transfer models for skin tissue are discussed, and various skin cooling technologies summarized. Finally, the predictive capacity of various heat transfer models is demonstrated with selected case studies.

The Arrhenius burn damage model is the most often used model for quantification of thermal damage in skin tissue and has been shown to be a useful tool by which the time-temperature history and damage accumulation are connected. However, it has several shortcomings^[30]. The models are mainly

based on the burns created by surface heating and the history of thermal insult is not considered. Besides, these models don't consider many other factors besides temperature, such as pH variations, preheating, and mechanical loading et al.

Experimental data indicate that multiple rate processes govern the manifestation of damage and that these processes may act over a broad spectrum of time domains, however, experimental observation of burn damage suggests that the burn damage process can be described as a function of a single kinetic process^[135]. As for this dilemma, Despa et al.^[157] pointed out that there are two possibilities include statistical arguments such as the "central limit theorem", which states that a process that depends on an infinite number of subordinate different processes behaves like a single Arrhenius process; and another hypothesis is that lethal burn damage is dominated by only a few molecular processes. More work is needed to check these two hypotheses. Besides, the experiments performed to derive A and E_a are only for rather long times of hyperthermic exposure covering tens to thousands of seconds.

While there has been considerable effort to characterize the time-temperature dependence of the injury, relatively little attention has been paid to the other important variable such as the thermal susceptibility of the tissue. The lipid bilayer components of the cells and membrane-bound ATPases have been shown to be most vulnerable to thermal damage because they are held together only by forces of hydration^[135]. Further work will be required to validate these predictions in an *in vivo* model.

References

- [1] Brigham P A, McLoughlin E. Burn incidence and medical care use in the United States: Estimates, trends, and data sources. *Journal of Burn Care and Research*, 1996, 17(2): 95–107.
- [2] Griffiths H R, Thornton K L, Clements C M, et al. The cost of a hot drink scald. *Burns*, 2006, 32(3): 372–374.
- [3] Waxman K, Lefcourt N, Achauer B. Heated laser Doppler flow measurements to determine depth of burn injury. *American Journal of Surgery*, 1989, 157(6): 541–543.
- [4] Sheridan R L. Burns. *Critical Care Medicine*, 2002, 30(11): S500–S514.
- [5] Kono T, Groff W F, Sakurai H, et al. Evaluation of fluence and pulse-duration on purpuric threshold using an extended pulse pulsed-dye laser in the treatment of port wine stains. *The Journal of Dermatology*, 2006, 33(7): 473–476.
- [6] Pustovalov V K, Jean B. Melanin granule models for the processes of laser-induced thermal damage in pigmented retinal tissues. I. Modeling of laser-

- induced heating of melanosomes and selective thermal processes in retinal tissues. *Bulletin of Mathematical Biology*, 2007, 69(1): 245–263.
- [7] Diette K M, Bronstein B R, Parrish J A. Histologic comparison of argon and tunable dye lasers in the treatment of tattoos. *Journal of Investigative Dermatology*, 1985, 85(4): 368–373.
 - [8] Junger H, Moore A C, Sorkin L S. Effects of full-thickness burns on nociceptor sensitization in anesthetized rats. *Burns*, 2002, 28(8): 772–777.
 - [9] Choinière M, Melzack R, Girard N, et al. Comparisons between patients' and nurses' assessment of pain and medication efficacy in severe burn injuries. *Pain*, 1990, 40(2): 143–152.
 - [10] Gallagher G, Rae C P, Kinsella J. Treatment of pain in severe burns. *American Journal of Clinical Dermatology*, 2000, 1(6): 329–335.
 - [11] Van Loey N E, van Son M J. Psychopathology and psychological problems in patients with burn scars: Epidemiology and management. *American Journal of Clinical Dermatology*, 2003, 4(4): 245–272.
 - [12] Song W J, Weinbaum S, Jiji L M, et al. A combined macro and microvascular model for whole limb heat transfer. *Journal of Biomechanical Engineering*, 1988, 110(4): 259–268.
 - [13] Abramson D I. *Circulation in the Extremities*. New York: Academic Press, 1967.
 - [14] Chato J C. Heat transfer to blood vessels. *Journal of Biomechanical Engineering*, 1980, 102(2): 110–118.
 - [15] Weinbaum S, Jiji L M, Lemons D E. Theory and experiment for the effect of vascular microstructure on surface tissue heat transfer, Part I: Anatomical foundation and model conceptualization. *Journal of Biomechanical Engineering*, 1984, 106(4): 321–330.
 - [16] Lemons D E, Chien S, Crawshaw L I, et al. Significance of vessel size and type in vascular heat transfer. *American Journal of Physiology*, 1987, 253(1-2): R128–R135.
 - [17] Sonksen J, Craggs J. Circulation of the skin. *Current Anaesthesia and Critical Care*, 1999, 10(3): 58–63.
 - [18] Mescon H, Hurley H J, Moretti G. The anatomy and histochemistry of the arteriovenous anastomoses in human digital skin. *Journal of Investigative Dermatology*, 1956, 27(3): 133–145.
 - [19] Greenfield A D M. Circulation through the skin//Hamilton W F. *Handbook of Physiology*. Washington: American Physiological Society, 1963:1325.
 - [20] Sherman J L. Normal arteriovenous anastomoses. *Medicine*, 1963, 42(4): 247–267.
 - [21] Braverman I M, Yen A. Ultrastructure of the human dermal microcirculation. II. The capillary loops of the dermal papillae. *Journal of Investigative Dermatology*, 1977, 68(1): 44–52.
 - [22] Crezee J, Lagendijk J J. Temperature uniformity during hyperthermia: The impact of large vessels. *Physics in Medicine and Biology*, 1992, 37(6): 1321–1337.

- [23] Crezee J, Lagendijk J J. Experimental verification of bioheat transfer theories: Measurement of temperature profiles around large artificial vessels in perfused tissue. *Physics in Medicine and Biology*, 1990, 35(7): 905–923.
- [24] Pennes H H. Analysis of tissue and arterial blood temperatures in the resting human forearm. *Journal of Applied Physiology*, 1948, 1(2): 93–122.
- [25] Lubashevsky I A, Gafiychuk V V. Mathematical description of the heat transfer in living tissue (Part I). *Adaptation, Noise, and Self-Organizing Systems*, 1999.
- [26] Chato J C, Lee R C. The future of biothermal engineering. *Annals of the New York Academy of Sciences*, 1998, 858(0): 1–17.
- [27] Charny C K. Mathematical models of bioheat transfer. *Advances in Heat Transfer*, 1992, 22: 19–155.
- [28] Arkin H, Xu L X, Holmes K R. Recent developments in modeling heat transfer in blood perfused tissues. *IEEE Transactions on Biomedical Engineering*, 1994, 41(2): 97–107.
- [29] Crezee J, Mooibroek J, Lagendijk J J, et al. The theoretical and experimental evaluation of the heat balance in perfused tissue. *Physics in Medicine and Biology*, 1994, 39(5): 813–832.
- [30] Stanczyk M, Telega J J. Modelling of heat transfer in biomechanics: A review. Part I. Soft tissues. *Acta of Bioengineering and Biomechanics*, 2002, 4(1): 31–61.
- [31] Khaled A R A, Vafai K. The role of porous media in modeling flow and heat transfer in biological tissues. *International Journal of Heat and Mass Transfer*, 2003, 46(26): 4989–5003.
- [32] Brinck H, Werner J. Efficiency function: Improvement of classical bioheat approach. *Journal of Applied Physiology*, 1994, 77(4): 1617–1622.
- [33] Chen M M, Holmes K R. Microvascular contributions in tissue heat transfer. *The New York Academy of Sciences*, 1980, 335(1): 137–150.
- [34] Charny C K, Weinbaum S, Levin R L. An evaluation of the Weinbaum-Jiji bioheat equation for normal and hyperthermic conditions. *Journal of Biomechanical Engineering*, 1990, 112(1): 80–87.
- [35] Weinbaum S, Jiji L M. A new simplified bioheat equation for the effect of blood flow on local average tissue temperature. *Journal of Biomechanical Engineering*, 1985, 107(2): 131–139.
- [36] Xu L X, Holmes K R, Chen M M, et al. Theoretical evaluation of the Pennes, the Chen-Holmes and the Weinbaum-Jiji bioheat transfer models in the pig renal cortex. *ASME Heat Transfer Division*, 1991, 189: 15–21.
- [37] Gustafsson S E, Nilsson S K, Torell L M. Analytical calculation of the skin temperature distribution due to subcutaneous heat production in a spherical heat source. *Physics in Medicine and Biology*, 1975, 20(2): 219–224.
- [38] Lawson R N. Implications of surface temperatures in the diagnosis of breast cancer. *Canadian Medical Association Journal*, 1956, 75(4): 309.
- [39] Ng E Y K, Sudharsan N M. Effect of blood flow, tumour and cold stress in a female breast: A novel time-accurate computer simulation. *International Journal of Engineering in Medicine*, 2001, 215(H4): 393–404.

- [40] Liu J, Wang C. *Bioheat Transfer*. Beijing: Science Press, 1997.
- [41] Ng E Y K, Chua L T. Mesh-independent prediction of skin burns injury. *Journal of Medical Engineering and Technology*, 2000, 24(6): 255–261.
- [42] Stewart D A, Gowrishankar T R, Weaver J C. Skin heating and injury by prolonged millimeter-wave exposure: Theory based on a skin model coupled to a whole body model and local biochemical release from cells at suprathreshold temperatures. *IEEE Transactions on Plasma Science*, 2006, 34(4 II): 1480–1493.
- [43] Weiss R A, Weiss M A, Munavalli G, et al. Monopolar radiofrequency facial tightening: A retrospective analysis of efficacy and safety in over 600 treatments. *Journal of Drugs in Dermatology*, 2006, 5(8): 707–712.
- [44] Goldberg D J. Laser- and light-based hair removal: An update. *Expert Review of Medical Devices*, 2007, 4(2): 253–260.
- [45] Li H, Zhang X, Liu J. Heat transfer analysis on laser-tissue thermal interaction using heterogeneous model. *Chinese Journal of Lasers*, 2002, A29(5): 465–470.
- [46] Gowrishankar T R, Stewart D A, Martin G T, et al. Transport lattice models of heat transport in skin with spatially heterogeneous, temperature-dependent perfusion. *BioMedical Engineering OnLine*, 2004, 3(1): 42.
- [47] Sanyal D C, Maji N K. Thermoregulation through skin under variable atmospheric and physiological conditions. *Journal of Theoretical Biology*, 2001, 208(4): 451–456.
- [48] Davies C R, Saidel G M, Harasaki H. Sensitivity analysis of one-dimensional heat transfer in tissue with temperature-dependent perfusion. *Journal of Biomechanical Engineering*, 1997, 119(1): 77–80.
- [49] Sekins K M, Lehmann J F, Esselmann P, et al. Local muscle blood flow and temperature responses to 915 MHz diathermy as simultaneously measured and numerically predicted. *Archives of Physical Medicine and Rehabilitation*, 1984, 65(1): 1–7.
- [50] Rai K N, Rai S K. Heat transfer inside the tissues with a supplying vessel for the case when metabolic heat generation and blood perfusion are temperature dependent. *Heat and Mass Transfer*, 1999, 35(4): 345–350.
- [51] Ma N, Gao X, Zhang X X. Two-layer simulation model of laser-induced interstitial thermo-therapy. *Lasers in Medical Science*, 2004, 18(4): 184–189.
- [52] Hodson D A, Eason G, Barbenel J C. Modeling transient heat transfer through the skin and superficial tissues: I. Surface insulation. *Journal of Biomechanical Engineering*, 1986, 108(2): 183–188.
- [53] Draper J W, Boag J W. The calculation of skin temperature distributions in thermography. *Physics in Medicine and Biology*, 1971, 16(2): 201–211.
- [54] Wilson S B, Spence V A. A tissue heat transfer model for relating dynamic skin temperature changes to physiological parameters. *Physics in Medicine and Biology*, 1988, 33(8): 895–912.
- [55] Deng Z S, Liu J. Mathematical modeling of temperature mapping over skin surface and its implementation in thermal disease diagnostics. *Computers in Biology and Medicine*, 2004, 34(6): 495–521.

- [56] Guyton A C. *Medical Physiology*. London: WB Saunders, 1976.
- [57] Timoshenko D A, Timoshenko D D, Golovushkin A A. Mathematical simulation of heat-induced effects on human skin surface. *BioMedical Engineering Online*, 2002, 36(1): 19–22.
- [58] Panescu D, Webster J G, Stratbucker R A. A nonlinear finite element model of the electrode-electrolyte-skin system. *IEEE Transactions on Biomedical Engineering*, 1994, 41(7): 681–687.
- [59] Zamanian A, Hardiman C. Electromagnetic radiation and human health: A review of sources and effects. *High Frequency Electronics*, 2005: 16–26.
- [60] Lanigan S W. *Lasers in Dermatology*. London: Springer-Verlag, 2000.
- [61] Van Gemert M J, Jacques S L, Sterenborg H J, et al. Skin optics. *IEEE Transactions on Biomedical Engineering*, 1989, 36(12): 1146–1154.
- [62] Welch A J, Pearce J A, Diller K R, et al. Heat generation in laser irradiated tissue. *Journal of Biomechanical Engineering*, 1989, 111(1): 62–68.
- [63] El-dabe N T M, Mohamed M A A, El-Sayed A F. Effects of microwave heating on the thermal states of biological tissues. *African Journal of Biotechnology*, 2003, 2(11): 453–459.
- [64] Tremblay B S. The effects of driving frequency and antenna length on power deposition within a microwave antenna array used for hyperthermia. *IEEE Transaction Biomedical Engineering*, 1985, 32(2): 152–157.
- [65] A Balanis C. *Advanced Engineering Electromagnetics*. New York: John Wiley and Sons, 1989.
- [66] Peshkov V. Second sound in helium II. *Journal of Physics*. VIII, 1944, 381.
- [67] Brown J B, Chung D Y, Matthews P W. Heat pulse at low temperature. *Physics Review Letter*, 1966, 21: 241
- [68] Banerjee A, Ogale A A, Das C, et al. Temperature distribution in different materials due to short pulse laser irradiation. *Heat Transfer Engineering*, 2005, 26(8): 41–49.
- [69] Kaminski W. Hyperbolic heat conduction equation for materials with a non-homogeneous inner structure. *Journal of Heat Transfer*, 1990, 112(3): 555–560.
- [70] Grassmann A, Peters F. Experimental investigation of heat conduction in wet sand. *Heat and Mass Transfer*, 1999, 35(4): 289–294.
- [71] Herwig H, Beckert K. Experimental evidence about the controversy concerning Fourier or non-Fourier heat conduction in materials with a nonhomogeneous inner structure. *Heat and Mass Transfer*, 2000, 36(5): 387–392.
- [72] Roetzel W, Putra N, Das S K. Experiment and analysis for non-Fourier conduction in materials with non-homogeneous inner structure. *International Journal of Thermal Sciences*, 2003, 42(6): 541–552.
- [73] Richardson A W, Imig C G, Feucht B L, et al. Relationship between deep tissue temperature and blood flow during electromagnetic irradiation. *Archives of Physical Medicine and Rehabilitation*, 1950, 31: 19–25.
- [74] Roemer R B, Oleson J R, Cetas T C. Oscillatory temperature response to constant power applied to canine muscle. *American Journal of Physiology*, 1985, 249(2): R153–R158.

- [75] Mitra K, Kumar S, Vedavarz A, et al. Experimental evidence of hyperbolic heat conduction in processed meat. *ASME Journal of Heat Transfer*, 1995, 117(3): 568–573.
- [76] Davydov E V, Lubashevsky I A, Milyaev V A, et al. Nondiffusive heat transfer in muscle tissue. Preliminary results. *Arxiv:cond-mat/0102006*, 2001, 1(1).
- [77] Tilahun M, Scott E P, Vick B. The question of thermal waves in heterogeneous and biological materials. *ASME Bioengineering Division (Publication) BED*, 1999, 44: 145–152.
- [78] Herwig H, Beckert K. Fourier versus non-Fourier heat conduction in materials with a nonhomogeneous inner structure. *ASME Journal of Heat Transfer*, 2000, 122(2): 363–365.
- [79] Antaki P J. New interpretation of non-Fourier heat conduction in processed meat. *Journal of Heat Transfer*, 2005, 127(2): 189–193.
- [80] Liu J, Chen X, Xu L X. New thermal wave aspects on burn evaluation of skin subjected to instantaneous heating. *IEEE Transactions on Biomedical Engineering*, 1999, 46(4): 420–428.
- [81] Xu L X, Liu J. Discussion of non-equilibrium heat transfer in biological systems. *Advances in Heat and Mass Transfer in Biotechnology, Proceedings of the 1998 ASME International Mechanical Engineering Congress and Exposition*. Fairfield, 1998: 13–17.
- [82] Chen C, Roemer R B. A thermo-pharmacokinetic model of tissue temperature oscillations during localized heating. *International Journal of Hyperthermia*, 2005, 21(2): 107–124.
- [83] Liu J, Wang C C, Ren Z P. Theory and experiments on temperature oscillations effects in living tissue. *Journal of Tsinghua University (Sci and Tech)*, 1997, 2: 91–95.
- [84] Shih T C, Kou H S, Liauh C T, et al. The impact of thermal wave characteristics on thermal dose distribution during thermal therapy: A numerical study. *Medical Physics*, 2005, 32(9): 3029–3036.
- [85] Moritz A R, Henriques F C. Study of thermal injuries II. The relative importance of time and source temperature in the causation of cutaneous burns. *American Journal of Pathology*, 1947, 23: 695–720.
- [86] Kalkan T, Demir M, Ahmed A S, et al. A dynamic study of the thermal components in electrical injury mechanism for better understanding and management of electric trauma: An animal model. *Burns*, 2004, 30(4): 334–340.
- [87] Mercer G N, Sidhu H S. Modeling thermal burns due to airbag deployment. *Burns*, 2005, 31(8): 977–980.
- [88] Torvi D A, Dale J D. A finite element model of skin subjected to a flash fire. *Journal of Biomechanical Engineering*, 1994, 116(3): 250–255.
- [89] Dai T, Pikkula B M, Wang L V, et al. Comparison of human skin optothermal response to near-infrared and visible laser irradiations: A theoretical investigation. *Physics in Medicine and Biology*, 2004, 49(21): 4861–4877.
- [90] Hardee H C, Lee D O, Benedick W B. Thermal hazard from LNG fireballs. *Combustion Science and Technology*, 1978, 17(5-6): 189–197.

- [91] Fish R. Electric shock, Part II: Nature and mechanisms of injury. *The Journal of Emergency Medicine*, 1993, 11(4): 457–462.
- [92] Diller K R. *Heat Transfer in Medicine and Biology: Analysis and Applications*. New York: Plenum, 1985: 85–134.
- [93] Muir I, Barclay T, Settle J. *Burns and their Treatment*. 3rd Edition. London: Butterworths, 1987.
- [94] Parsons K C. *Human Thermal Environments*. Hampshire: Taylor and Francis, 1993.
- [95] Stoll A M, Chianta M A, Piergallini J R. Thermal conduction effects in human skin. *Aviation Space and Environmental Medicine*, 1979, 50(8): 778–787.
- [96] Enalejev R S, Kachalkin W A. Mathematical simulation of heat transfer process in skin cover at burn injury. *Burn Injury*, 1998, 858: 30–35.
- [97] Meyer W, Schwarz R, Neurand K. The skin of domestic mammals as a model for the human skin, with special reference to the domestic pig. *Current Problems in Dermatology*, 1978, 7: 39–52.
- [98] Knabl J S, Bayer G S, Bauer W A, et al. Controlled partial skin thickness burns: An animal model for studies of burnwound progression. *Burns*, 1999, 25(3): 229–235.
- [99] DaCosta R, Aggarwal S J, Diller K R, et al. The effects of epinephrine, ibuprofen and tetrachlorodecaoxide on cutaneous microcirculation in thermally injured hamsters. *Journal of Burn Care and Rehabilitation*, 1992, 13(4): 396–402.
- [100] Leach E H, Peters R A, Rossiter R J. Experimental thermal burns, especially the moderate temperature burn. *Journal of Experimental Physiology and Cognate Medical Sciences*, 1943, 32: 67.
- [101] Sevitt S. Local blood flow changes in experimental burns. *Journal of Pathology and Bacteriology*, 1949, 61: 427–442.
- [102] Stoll A M, Greene L C. Relationship between pain and tissue damage due to thermal radiation. *Journal of Applied Physiology*, 1959, 14(3): 373–382.
- [103] Takata A N, Rouse J, Stanley T. Thermal Analysis Program, in I I T. Research Institute Report, 1973.
- [104] Ross D C, Diller K R. An experimental investigation of burn injury in living tissue. *ASME Journal of Heat Transfer*, 1976, 98(2): 292–296.
- [105] Okumura Y, Reinhold H S. Heat sensitivity of rat skin. *European Journal of Cancer*, 1978, 14(11): 1161–1166.
- [106] De Camara D L, Raine T J, Robson M C. Ultrastructural aspects of cooled thermal injury. *The Journal of Trauma*, 1981, 21(11): 911–919
- [107] Cantrell J H. Ultrasonic determination of thermodynamic threshold parameters for irreversible cutaneous burns. *Journal of the Acoustical Society of America*, 1982, 72(2): 337–339.
- [108] Nanney L B. Changes in the microvasculature of skin subjected to thermal injury. *Burns*, 1982, 8(5): 321–327.
- [109] Jelenko C, Wheeler M L. Production of the experimental burn: A critical technical evaluation. *Journal of Surgical Research*, 1969, 9(3): 159–165.

- [110] Pioch W. Histologisch-histokemische Untersuchung zur Identifizierung von Strommarken, *Deutsche Zeitschrift für die gesamte gerichtliche. Medizin*, 1966, 57: 165–169.
- [111] Danielsen L, Thomsen H K, Nielsen O, et al. Electrical and thermal injuries in pig skin: Evaluated and compared by light microscopy. *Forensic Science International*, 1978, 12(3): 211–225.
- [112] Nielsen K G, Nielsen O, Thomsen H K. Device and methods for the measurement of energy transfer in experiments involving thermal and electrical injuries of skin. *Forensic Science International*, 1981, 17(3): 203–209.
- [113] Thomsen H K, Danielsen L, Nielsen O, et al. Early epidermal changes in heat- and electrically injured pig skin. I. A light microscopic study. *Forensic Science International*, 1981, 17(2): 133–143.
- [114] Hoekstra M J, Hupkens P, Dutrieux R P, et al. A comparative burn wound model in the New Yorkshire pig for the histopathological evaluation of local therapeutic regimens: Silver sulfadiazine cream as a standard. *British Journal of Plastic Surgery*, 1993, 46(7): 585–589.
- [115] Brans T A, Durtieux R P, Hoekstra M J, et al. Histopathological evaluation of scalds and contact burns in the pig model. *Burns*, 1994, 20(1): 48–51.
- [116] Middelkoop E, van den Bogaerd A J, Lamme E N, et al. Porcine wound models for skin substitution and burn treatment. *Biomaterials*, 2004, 25(9): 1559–1567.
- [117] Wu Y C. Material properties criteria for thermal safety. *Journal of Materials*, 1972, 7(4): 573–579.
- [118] Majchrzak E, Jasinski M. Sensitivity analysis of burns integrals. *Computer Assisted Mechanics and Engineering Sciences*, 2004, 11(2-3): 125–135.
- [119] Stoll A M. Heat transfer in biotechnology//Hartnett J P, Irvine T F. *Advances in Heat Transfer*. New York: Academic Press, 1967: 65–141.
- [120] Henriques F C, Moritz A R. Studies of thermal injury, I. The conduction of heat to and through skin and the temperatures attained therein. A theoretical and an experimental investigation. *The Journal of Physiology*, 1947, 23(4): 531–549.
- [121] Henriques F C. Study of thermal injuries, V. The predictability and the significance of thermally induced rate processes leading to irreversible epidermal injury. *Archives of Pathology*, 1947, 43: 489–502.
- [122] Fugitt C E. A rate process of thermal injury. *Armed Forces Special Weapons Project*, 1955, AFSWP-606.
- [123] Weaver J A, Stoll A M. Mathematical model of skin exposed to thermal radiation. *Aerosp Med*, 1969, 40(1): 24–30.
- [124] Mehta A K, Wong F C. Measurement of Flammability and Burn Potential of Fabrics. Full Report from Rules Research Laboratory, 1973.
- [125] Wu Y C. A Modified Criterion for Predicting Thermal Injury. Washington: National Bureau of Standards, 1982.
- [126] Pearce J A, Cheong W F, Pandit K, et al. Kinetic models for coagulation processes: Determination of rate coefficients in vivo. *Lasers in Dermatology and Tissue Welding*, 1991: 27–33.

- [127] Pearce J A, Thomsen S, Vijverberg H, et al. Quantitative measurement of thermal damage: Birefringence changes in thermally coagulated collagen. *Advances in Bioheat and Mass Transfer, Microscale Analysis of Thermal Injury Processes, Instrumentation, Modeling, Clinical Applications*, 1993: 141–144.
- [128] Wright N T. On a relationship between the Arrhenius parameters from thermal damage studies. *Journal of Biomechanical Engineering*, 2003, 125(2): 300–304.
- [129] Xu Y, Qian R. Analysis of thermal injury process based on enzyme deactivation mechanism. *Journal of Biomechanical Engineering*, 1995, 117(4): 462–465.
- [130] Diller K R, Hayes L J. A finite element model of burn injury in blood-perfused skin. *Journal of Biomechanical Engineering*, 1983, 105(3): 300–307.
- [131] Ng E Y, Chua L T. Comparison of one- and two-dimensional programmes for predicting the state of skin burns. *Burns*, 2002, 28(1): 27–34.
- [132] Diller K R. Development and solution of finite difference equations for burn injury with spreadsheet software. *Journal of Burn Care and Rehabilitation*, 1999, 20(Pt1): 25–32.
- [133] Jiang S, Ma N, Li X, et al. Effects of thermal properties and geometrical dimensions on skin burn injuries. *Burns*, 2002, 28(8): 713–717.
- [134] Perez C A. Clinical hyperthermia: Mirage or reality? *International Journal of Radiation Oncology Biology, Physics*, 1984, 10(6): 935–937.
- [135] Diller K R, Pearce J A. Issues in modeling thermal alterations in tissues. *Annals New York Academy of Science*, 1999, 888(0): 153–164.
- [136] Ebling F, Eady R, Leigh I. *Anatomy and organization of human skin*//Champion R H, Burrington J L, Ebling F J G. *Textbook of Dermatology*. 5th Edition. New York: Blackwell Scientific Publications, 1992.
- [137] Srinivas S M, de Boer J F, Park H, et al. Determination of burn depth by polarization-sensitive optical coherence tomography. *Journal of Biomedical Optics*, 2004, 9(1): 207–212.
- [138] Flory P J, Garrett R R. Phase transition in collagen and gelatin systems. *Journal of the American Chemical Society*, 1958, 80(12): 4836–4845.
- [139] Schiller R, Funke A P, Gunther C. DSC measurements on full thickness mice skin: An additional tool to investigate permeation enhancement of highly lipophilic drugs. *Journal of Thermal Analysis and Calorimetry*, 2004, 77(2): 497–510.
- [140] Xu F, Wen T, Lu T J, Seffen K A. Skin biothermomechanics for medical treatments. *Journal of the Mechanical Behavior of Biomedical Materials*, 2008, 1(2): 172–187
- [141] Pietrucha K. Changes in denaturation and rheological properties of collagen-hyaluronic acid scaffolds as a result of temperature dependencies. *International Journal of Biological Macromolecules*, 2005, 36(5): 299–304.
- [142] Miles C A, Burjanadze T V, Bailey A J. The kinetics of the thermal denaturation of collagen in unrestrained rat tail tendon determined by differential scanning calorimetry. *Journal of Molecular Biology*, 1995, 245(4): 437–446.

- [143] Humphrey J D. Continuum thermomechanics and the clinical treatment of disease and injury. *Applied Mechanics Reviews*, 2003, 56(2): 231–260.
- [144] Schoenenberger K, Colston B W J, Maitland D J, et al. Mapping of birefringence and thermal damage in tissue by use of polarization-sensitive optical coherence tomography. *Applied Optics*, 1998, 37(25): 6026–6036.
- [145] Thomsen S, Pearce J A, Cheong W. Changes in birefringence as markers of thermal damage in tissues. *IEEE Transactions on Biomedical Engineering*, 1989, 36(12): 1174–1179.
- [146] Boulvert F, Boulbry B, Le Brun G, et al. Analysis of the depolarizing properties of irradiated pig skin. *Journal of Optics A: Pure and Applied Optics*, 2005, 7(1): 21–28.
- [147] Pearce J A, Thomsen S L M D, Vijverberg H, et al. Kinetics for birefringence changes in thermally coagulated rat skin collagen. *Society of Photo-Optical Instrumentation Engineers*, 1993, 1876: 180–186.
- [148] Yarker Y E, Aspden R M, Hukins D W. Birefringence of articular cartilage and the distribution on collagen fibril orientations. *Connective Tissue Research*, 1983, 11(2-3): 207–213.
- [149] Huang Y, Meek K M, Ho M W, et al. Analysis of birefringence during wound healing and remodeling following alkali burns in rabbit cornea. *Experimental Eye Research*, 2001, 73(4): 521–532.
- [150] Youn J I, Vargas G, Wong B J, et al. Depth-resolved phase retardation measurements for laser-assisted non-ablative cartilage reshaping. *Physics in Medicine and Biology*, 2005, 50(9): 1937–1950.
- [151] Komatsu K, Chiba M. Synchronous recording of load-deformation behaviour and polarized light-microscopic images of the rabbit incisor periodontal ligament during tensile loading. *Archives of Oral Biology*, 2001, 46(10): 929–937.
- [152] Sankaran V, Walsh J T. Birefringence measurement of rapid structural changes during collagen denaturation. *Photochemistry and Photobiology*, 1998, 68(6): 846–851.
- [153] Beghuin D, Schöenenberger K, Delacrétaz G, et al. Temperature-related reversible birefringence changes in rat tail tendon. *Applied Optics*, 2000, 19(1): 3388–3395.
- [154] Goldberg S N, Gazelle G S, Compton C C, et al. Treatment of intrahepatic malignancy with radiofrequency ablation: Radiologic-pathologic correlation. *Cancer Letter*, 2000, 88(11): 2452–2463.
- [155] Bhowmick S, Bischof J C. Supraphysiological thermal injury in dunning AT-1 prostate tumor cells. *Advances in Heat and Mass Transfer in Biotechnology*, 1998, ASME HTD-Vol. 362/BED-Vol. 40: 77–78.
- [156] Green D M, Diller K R. Measurement of burn induced leakage of macromolecules in living tissue. *Journal of Biomechanical Engineering*, 1978, 100: 153–158.
- [157] Despa F, Orgill D P, Neuwalder J, et al. The relative thermal stability of tissue macromolecules and cellular structure in burn injury. *Burns*, 2005, 31(5): 568–577.

Chapter 4

Analysis of Skin Bioheat Transfer

4.1 Introduction

Advances in laser, microwave and similar technologies have led to recent developments of thermal treatments for different diseases and injuries involving skin tissue^[1], such as the removal of port-wine stains^[2~4], pigmented and cutaneous lesions^[5~7] and tattoos^[8]. The objective is to induce thermal injury precisely within tissue structures located up to several millimeters below the surface but without affecting the surrounding healthy tissue, where the precise prediction of temperature distribution is essential. This chapter aims to provide a detailed theoretical analysis of the thermal behaviour in skin tissue. It is organised as follows. At first, theoretical analysis is carried out and closed-form solutions for simple one-layer Fourier theory based model are obtained using the Green function method. Furthermore, non-Fourier bioheat transfer models are developed for skin tissue. Finally, the models for considering sweating and hair effect are also developed.

4.2 Skin Bioheat Transfer Analysis with Fourier Model

In the present section, a one-layer model is proposed first for the theoretical analysis of heat transfer in skin, where the skin is treated as a homogenous medium with constant properties. One-dimensional case is studied, as shown in Figure 4.1, which is a good approximation when heat mainly propagates in the direction to the skin surface (e.g. the laser heating).

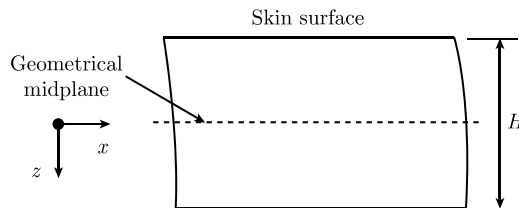


Figure 4.1 Schematic of the one-layer skin model

The skin tissue is considered as a crack-free infinite plate of thickness H , where the Cartesian coordinates are embedded at the centre of the plate, as shown in Figure 4.1, which is reasonable according to their anatomical structure. Initially, the skin tissue is at a temperature distribution $T_0(z)$, and at time $t = 0$ the skin surface (at $z = -H/2$) are suddenly exposed to different thermal shocks, hot plate, convective medium, constant heat flux or laser heating, whereas the bottom (at $z = H/2$) is kept at core temperature. The induced transient non-uniform temperature field will result in a stress field.

The classical and widely used Pennes equation, as given in Equation (4.1), is employed to describe the heat transfer process. It is rewritten as

$$\rho c \frac{\partial T}{\partial t} = k \frac{\partial^2 T}{\partial z^2} + \varpi_b \rho_b c_b (T_a - T) + q_{\text{met}} + q_{\text{ext}} \quad (4.1)$$

Through the following transformation^[9]:

$$T(z, t) = T_0(z) + W(z, t) e^{-\frac{\varpi_b \rho_b c_b}{\rho c} t} \quad (4.2)$$

Equation (3.1) can be changed to

$$\frac{\partial W}{\partial t} = \alpha \frac{\partial^2 W}{\partial z^2} + \frac{q_{\text{ext}}(z, t)}{\rho c} e^{-\frac{\varpi_b \rho_b c_b}{\rho c} t} \quad (4.3)$$

where $\alpha = k/(\rho c)$ is the thermal diffusivity of the skin tissue.

In this chapter, solutions of Equation (4.1) under six different kinds of boundary conditions have been obtained by using the Green function method^[10] and listed below, including those two solutions under boundary conditions II and III given by Deng & Liu^[9].

$$(1) \text{ Boundary condition I: } \begin{cases} T = T_\infty, & z = -H/2 \\ T = T_c, & z = H/2 \end{cases}$$

Green function:

$$G(z, t | z', \tau) = \frac{2}{H} \sum_{m=1}^{\infty} e^{-\alpha \beta_m^2 (t-\tau)} \sin(\beta_m z) \sin(\beta_m z') \quad (4.4)$$

Solution:

$$\begin{aligned} T(z, t) = & T_0(z) + \frac{2\alpha}{H} \left[T_\infty - k \frac{dT_0(z)}{dz} \Big|_{x=0} \right] \\ & \times \sum_{m=1}^{\infty} \beta_m \sin[\beta_m(z + H/2)] \frac{1}{\alpha \beta_m^2 + \frac{\varpi_b \rho_b c_b}{\rho c}} (1 - e^{-\alpha \beta_m^2 t - \frac{\varpi_b \rho_b c_b}{\rho c} t}) \end{aligned} \quad (4.5)$$

where $\beta_m = m\pi/H$, $m = 1, 2, 3, \dots$; T_∞ is the constant temperature boundary at skin surface.

$$(2) \text{ Boundary condition II: } \begin{cases} -k\partial T/\partial z = f_2(t), z = -H/2 \\ T = T_c, z = H/2 \end{cases}$$

Green function:

$$G_2(z, t|z', \tau) = \frac{2}{H} \sum_{m=1}^{\infty} e^{-\alpha\beta_m^2(t-\tau)} \cos(\beta_m z) \cos(\beta_m z') \quad (4.6)$$

Solution:

$$\begin{aligned} T(z, t) = & T_0(z) + \left[k \frac{dT_0(z)}{dz} \Big|_{x=0} + f_2(t) \right] \frac{\alpha}{k} \frac{2}{H} \\ & \times \sum_{m=1}^{\infty} \cos[\beta_m(z + H/2)] \frac{1}{\alpha\beta_m^2 + \frac{\varpi_b \rho_b c_b}{\rho c}} (1 - e^{-\alpha\beta_m^2 t - \frac{\varpi_b \rho_b c_b}{\rho c} t}) \end{aligned} \quad (4.7)$$

where $\beta_m = \pi(2m - 1)/(2H)$, $m = 1, 2, 3, \dots$; f_2 is the constant heat flux boundary at skin surface.

$$(3) \text{ Boundary condition III: } \begin{cases} -k\partial T/\partial z = h_1[f_3(t) - T], z = -H/2 \\ T = T_c, z = H/2 \end{cases}$$

Green function:

$$\begin{aligned} G_3(z, t|z', \tau) = & \frac{2[\beta_m^2 + (h_1/k)^2]}{H[\beta_m^2 + (h_1/k)^2] + h_1/k} \\ & \times \sum_{m=1}^{\infty} e^{-\alpha\beta_m^2(t-\tau)} \sin[\beta_m(H - z)] \sin[\beta_m(H - z')] \end{aligned} \quad (4.8)$$

Solution:

$$\begin{aligned} T(z, t) = & T_0(z) + \frac{\alpha}{k} h_f \left[\frac{k}{h_f} \frac{dT_0(z)}{dz} \Big|_{x=0} - T_0(z) \Big|_{x=0} + f_3(t) \right] \\ & \times \sum_{n=1}^{\infty} \left\{ \frac{2[\beta_n^2 + (h_f/k)^2]}{H[\beta_n^2 + (h_f/k)^2] + h_f/k} \sin[\beta_n(H/2 - z)] \sin(\beta_n H) \right\} \\ & \times \frac{1}{\alpha\beta_n^2 + \frac{\varpi_b \rho_b c_b}{\rho c}} \left(1 - e^{-\alpha\beta_n^2 t - \frac{\varpi_b \rho_b c_b}{\rho c} t} \right) \end{aligned} \quad (4.9)$$

where β_m is the positive roots of $\beta_m \cot(\beta_m H) = -h_1/k$, h_1 is the surface heat transfer coefficient; f_3 is the temperature of thermal stimulus.

$$(4) \text{ Boundary condition IV: } \begin{cases} T = T_\infty, z = -H/2 \\ \partial T/\partial z = 0, z = H/2 \end{cases}$$

Solution:

$$T(z, t) = T_0(z) + \frac{2\alpha}{H}(T_\infty - T_0) \sum_{m=1}^{\infty} \beta_m \sin(\beta_m z) \times \frac{1}{\alpha\beta_m^2 + \frac{\varpi_b \rho_b c_b}{\rho c}} \left(1 - e^{-\alpha\beta_m^2 t - \frac{\varpi_b \rho_b c_b}{\rho c} t}\right) \quad (4.10)$$

where $\beta_m = \pi(2m-1)/(2H)$, $m = 1, 2, 3, \dots$; T_∞ is the constant temperature boundary at skin surface.

$$(5) \text{ Boundary condition V: } \begin{cases} -k\partial T/\partial z = f_5(t), & z = -H/2 \\ \partial T/\partial z = 0, & z = H/2 \end{cases}$$

Solution:

$$T(z, t) = T_0(z) + \left[k \frac{dT_0(z)}{dz} \Big|_{x=0} + f_5(t) \right] \frac{\alpha}{k} \frac{2}{H} \times \left\{ \begin{aligned} & \frac{\rho c}{\varpi_b \rho_b c_b} \left(1 - e^{-\frac{\varpi_b \rho_b c_b}{\rho c} t}\right) \\ & + \sum_{m=2}^{\infty} \cos[\beta_m(z+H/2)] \frac{1}{\alpha\beta_m^2 + \frac{\varpi_b \rho_b c_b}{\rho c}} \left(1 - e^{-\alpha\beta_m^2 t - \frac{\varpi_b \rho_b c_b}{\rho c} t}\right) \end{aligned} \right\} \quad (4.11)$$

where $\beta_m = \pi(m-1)/H$, $m = 2, 3, 4, \dots$; f_5 is the constant heat flux boundary at skin surface

$$(6) \text{ Boundary condition VI: } \begin{cases} -k\partial T/\partial z = h_f[f_6(t) - T], & z = -H/2 \\ \partial T/\partial z = 0, & z = H/2 \end{cases}$$

Solution:

$$T(z, t) = T_0(z) + \frac{\alpha}{k} h_f \left[\frac{k}{h_f} \frac{dT_0(z)}{dz} \Big|_{x=0} - T_0(z) \Big|_{x=0} + f_6(t) \right] \times \sum_{n=1}^{\infty} \left\{ \frac{2[\beta_n^2 + (h_f/k)^2]}{H[\beta_n^2 + (h_f/k)^2] + h_f/k} \cos[\beta_n(H/2 - z)] \cos(\beta_n H) \right\} \times \frac{1}{\alpha\beta_n^2 + \frac{\varpi_b \rho_b c_b}{\rho c}} \left(1 - e^{-\alpha\beta_n^2 t - \frac{\varpi_b \rho_b c_b}{\rho c} t}\right) \quad (4.12)$$

where β_m is the positive roots of $\beta_m \tan(\beta_m H) = h_1/k$; h_f is the surface heat transfer coefficient; f_6 is the temperature of thermal stimulus.

4.3 Skin Bioheat Transfer Analysis with Non-Fourier Models

The success of thermal therapies depends on the precise prediction and control of temperature, damage and stress distributions in the tissue. From a therapeutic viewpoint, the high-intensity short duration heating scheme can efficiently produce an appropriate and precise dose of heat during thermal therapies. In addition, reducing the overall treatment time is important, especially when the treatment target volume is large. A rapid heating scheme with a good strategy is therefore essential for an effective thermal therapy. However, the possible non-Fourier nature of heat transfer in living tissue may play an important role during rapid heating, such as thermal ablation/thermal surgery, when a high-intensity thermal source such as focused laser, ultrasound or radiofrequency ablation is used. For example, it has been shown that the thermal relaxation of tissue will delay the appearance of peak temperature during thermal treatments, leading to a lower thermal dose level^[11]. Furthermore, damage to human tissue from thermal burns is an exponential function of temperature^[12], so even small improvements in the prediction of temperature can strongly influence the prediction of damage.

In this section, different non-Fourier heat conduction models are developed to describe the thermal behaviour of skin tissue.

4.3.1 Non-Fourier bioheat transfer models

1) Fourier heat equation

As is well known, the conduction term in the traditional Pennes bioheat transfer equation^[13] is based on the classical Fourier's law, which has been known since the publication of Fourier's studies concerning heat conduction (1807, 1812)

$$q(\mathbf{r}, t) = -k\nabla T(\mathbf{r}, t) \quad (4.13)$$

where \mathbf{r} stands for the position vector.

The bioheat transfer equation is given as

$$\rho c \frac{\partial T}{\partial t} = -\nabla q + \varpi_b \rho_b c_b (T_a - T) + q_{\text{met}} + q_{\text{ext}} \quad (4.14)$$

From above two equations, we can get the Pennes bioheat transfer equation (PBHTE)

$$\rho c \frac{\partial T}{\partial t} = k\nabla^2 T + \varpi_b \rho_b c_b (T_a - T) + q_{\text{met}} + q_{\text{ext}} \quad (4.15)$$

Although the law of Fourier has been used extensively and successfully, some doubts have been cast on its completeness^[14]. In the Fourier law, it is assumed that any temperature disturbance or thermal wave will propagate at an infinite speed through the medium. However, this assumption has been shown to be physically unrealizable^[15] since, in reality, any equilibrium state in thermodynamic transition needs time to establish^[16]. Fourier's law has been shown to fail during the short duration of an initial transient, or when the thermal propagation speed is not high^[17], such as the microscale laser heating of thin metal films and even laser surgery^[18~20]. Liu & Lu^[21] and Lu et al.^[22,23] reported that some thermal wave effects of changing power on bioheat transfer in tissue cannot be explained by the PBHTE.

2) Hyperbolic heat equation

Since the experimental observation of a finite thermal wave speed in liquid helium^[24], the wave behaviour in heat conduction has been argued from various physical points of view^[25~27]. The necessity of a finite heat propagation speed has also been demonstrated from a microscopic point of view^[28,29]. Applying the concept of finite heat propagation velocity, Vernott^[27] and Cattaneo^[26] formulated a modified unsteady heat conduction equation, which is a linear extension of the unsteady Fourier equation

$$q(r, t + \tau_q) = -k\nabla T(r, t) \quad (4.16)$$

The first order Taylor expansion of above equation gives

$$q(r, t) + \tau_q \partial q(r, t) / \partial t = -k\nabla T(r, t) \quad (4.17)$$

where $\tau_q = \alpha / C_t^2$ is defined as the thermal relaxation time; α is the thermal diffusivity; C_t is the speed of thermal wave in the medium^[30,31]. The reciprocal of the relaxation time, $f = 1/\tau$, is the critical frequency dictating the activation of thermal wave behaviour^[28]. Since both τ_q and α are intrinsic thermal properties of the medium, the resulting thermal wave speed C_t is also an intrinsic property^[32]. Due to its similarity with the acoustic wave, the proposed wave-like propagation of thermal signals is termed the "second sound wave"^[24,28].

A direct integration of Equation (4.17) leads to^[33]

$$\begin{aligned} \int_0^t [q(r, \xi) + \tau_q \partial q(r, \xi) / \partial \xi] d\xi &= \int_0^t [-k\nabla T(r, \xi)] d\xi \Rightarrow q(r, t) \\ &= -\frac{k}{\tau_q} \exp\left(-\frac{t}{\tau_q}\right) \int_0^t \exp\left(\frac{\xi}{\tau_q}\right) \nabla T(r, \xi) d\xi \end{aligned} \quad (4.18)$$

According to this equation, the heat flux $q(r, t)$ at certain time t depends on the entire history of the temperature gradient established from time 0 to t . In other words, the heat flux now has a memory that keeps track of the time-history of temperature gradient due to the appearance of τ_q ^[34]. The thermal wave theory presents a strong path dependency of temperature gradient rather than the point value (i.e., ∇T at t) depicted by Fourier's law^[33,35].

Physical meaning and experimental determination of the relaxation time

For the physical meaning of thermal relaxation time τ_q , various physical points of view have been proposed: ① τ_q results from the rate equation within the mainframe of the second law in non-equilibrium, irreversible thermodynamics; ② mechanically, τ_q arises due to the phase-lag between heat flux vector and temperature gradient in a high-rate response; ③ when considering diffusion behaviour and wave propagation, τ_q is the physical instant at which the intrinsic length scales merge together.

The value of relaxation time for homogeneous materials can be calculated theoretically^[36,37]. However, these equations are not suitable for materials having non-homogeneous inner structures such as skin tissue and, at present, no direct experimental method exists for the determination of τ_q . It has been suggested that τ_q can be determined by fitting experimental temperature data with theoretical predictions from the hyperbolic equation, by using τ_q as a variable parameter^[38~42]. By using the equation $\tau = \alpha/C_t^2$, τ_q for non-homogeneous materials could also be determined based on the measurement of penetration time - which is the period of temperature jump at a measurement point - the distance of this point to the heat source and the thermal diffusivity.

Kaminski^[34] proposed that τ_q represents the interaction of different inner structural elements of material during heat transfer. For homogeneous materials, this interaction is at the molecular or crystal lattice level and τ_q has a value ranging from $10^{-8} \sim 10^{-14}$ s. For non-homogeneous materials, the structural heat transfer interaction takes place at a different level and τ_q characterizes thermal inductance, defined as the time needed for accumulating the thermal energy required for propagative transfer to the nearest element of the inner structure. It may take a much larger value ($10^{-3} \sim 10^3$ s) in non-homogeneous substances^[43].

Most biological materials that contain cells, superstructures, liquids, and solid tissue are non-homogeneous, so that their thermal relaxation times are much larger compared to engineering materials. Vedavarz et al.^[19] found τ_q of biological materials and tissue has a value in the range of $10 \sim 1000$ s at

cryogenic temperature and 1~100 s at room temperature. For meat products, $\tau_q = 20 \sim 30$ s^[34,40]; Mitra et al.^[30] found that the value of τ_q in processed meat was about 15.5 s while Roetzel et al.^[44] found it to be 1.77 s.

As for skin tissue, no data about the thermal relaxation time has been reported, but those of some important cutaneous structures have been presented by Stratigos & Dover^[45], as given in Table 3.4.

Thermal wave model of bioheat transfer (TWMBT)

Applying the thermal wave theory Equation (4.17) to bioheat conduction Equation (4.14), we can get thermal wave model of bioheat transfer

$$\begin{aligned} \tau_q \rho c \frac{\partial^2 T}{\partial t^2} = k \nabla^2 T - \varpi_b \rho_b c_b T - (\tau_q \varpi_b \rho_b c_b + \rho c) \frac{\partial T}{\partial t} \\ + \varpi_b \rho_b c_b T_b + q_m + q_{\text{ext}} + \tau_q \frac{\partial q_m}{\partial t} + \tau \frac{\partial q_{\text{ext}}}{\partial t} \end{aligned} \quad (4.19)$$

the above equation is known as a hyperbolic heat equation because there appears a two double-derivative term (called the wave term) that modifies the parabolic Fourier heat equation^[46].

Application of the model

The above equation without blood perfusion terms was introduced by Luikov^[43] to chemical and process engineering. It was subsequently advanced to heat transfer processes that take place in dissipative and dispersive systems where Fourier's heat equation fails to predict accurate temperatures. More details on the development of thermal wave theory in heat conduction can be found in Ozisik & Tzou^[33].

For biological materials, Mitra et al.^[30] found that their experimental results can be well predicted by the hyperbolic heat conduction model. This model has also been applied to the measurement of blood perfusion rate^[47~49], the prediction of temperature transients and thermal stresses in skin cryopreservation^[50], the prediction of temperature/thermal dose distributions in living tissue during thermal therapies^[11], and the explanation of temperature oscillations^[51].

The wave-like behaviour of bioheat transfer, occurring in skin tissue under different heating conditions, was studied by Liu et al.^[52,53]. A comparison of the temperature and thermal damage distributions predicted separately with TWMBT and PBHTE models showed great deviation in all cases. Liu et al.^[52,53] found that, for heating with a high flux under an extremely short duration, the model accounting for finite thermal wave propagation provides more realistic predictions. Similar results have also been reported by Ma et al.^[54], who analyzed the non-Fourier effect of laser irradiation in human skin

and found that the rates of temperature rise at different depths of skin were comparatively slow due to the non-Fourier effect.

Problems with thermal wave model

Although the thermal wave model has led to many interesting phenomena^[35] and the relaxation behaviour has been shown to be admissible within the framework of the second law of extended irreversible thermodynamics, for a few reasons the hyperbolic heat equation is questionable: ① it is not based on the details of energy transport in the material; ② material properties may not be regarded as constant, e.g. the relaxation time τ_q is generally temperature-dependent; ③ although the thermal wave model can capture the microscale response in time^[31,33], the wave concept does not capture the microscale response in space^[55,56] and the thermal wave model introduces some unusual behaviours and physical solutions^[37,57,58]; ④ due to the assumption of a macroscopic behaviour averaged over many grains, the validity of the thermal wave model becomes debatable in view of the fast-transient response with microstructural interaction effects^[59].

3) Dual-phase-lag (DPL) model

In order to account for deviations from the classical approach involving Fourier conduction and, at the same time, to consider the effect of microstructural interactions in the fast transient process of heat transport (missing in the thermal wave model), a new phase lag τ_T of temperature gradient is introduced^[31,33,59]. Together with τ_q , the corresponding equation is called the DPL equation, given by

$$q(r, t + \tau_q) = -k\nabla T(r, t + \tau_T) \quad (4.20)$$

where τ_q and τ_T are interpreted as non-zero times accounting for the effects of “thermal inertia” and “microstructural interaction”, respectively^[60]: τ_q is the phase-lag in establishing heat flux and associated conduction through a medium; while τ_T accounts for the diffusion of heat ahead of sharp wave fronts that would be induced by τ_q , and is the phase-lag in establishing the temperature gradient across the medium during which conduction occurs through its small-scale structures. Thus, Equation (4.20) states that the gradient of temperature at a point in the material at time $t + \tau_T$ corresponds to the heat flux vector at the same point at time $t + \tau_q$ ^[61].

Through the first and second order Taylor expansions, the DPL model can represent several models, which cover a wide range of space and time for physical observations.

Type 1 DPL model of bioheat transfer (DPL1MBT)

The simplest example of DPL model is its first order expansions for both q and T , given as

$$q(r, t) + \tau_q \frac{\partial q(r, t)}{\partial t} = -k \left[\nabla T(r, t) + \tau_T \frac{\partial \nabla T(r, t)}{\partial t} \right] \quad (4.21)$$

Applying the equation to bioheat conduction equation. we can get type 1 DPL model of bioheat transfer

$$\begin{aligned} \tau_q \rho c \frac{\partial^2 T}{\partial t^2} = & k \nabla^2 T + \tau_T k \nabla^2 \frac{\partial T}{\partial t} - \varpi_b \rho_b c_b T - (\tau_q \varpi_b \rho_b c_b + \rho c) \frac{\partial T}{\partial t} \\ & + \varpi_b \rho_b c_b T_a + q_{\text{met}} + q_{\text{ext}} + \tau_q \frac{\partial q_{\text{met}}}{\partial t} + \tau_q \frac{\partial q_{\text{ext}}}{\partial t} \end{aligned} \quad (4.22)$$

The DPL1MBT reduces to the thermal wave model by setting $\tau_T = 0$ and reduces to Fourier's heat equation by setting $\tau_q = \tau_T = 0$.

The DPL1MBT model without blood perfusion terms has been shown to give good agreement with experiments across a wide range of length and time scales for engineering materials^[60,62]. Antaki^[63] pointed out that the DPL model combines the wave features of hyperbolic conduction with a diffusion-like feature not captured by the hyperbolic case. By fitting the experimental data of Mitra et al.^[30] to the prediction of DPL1MBT without blood perfusion terms, it was found that $\tau_q = 16\text{s}$, $\tau_T = 0.043\text{s}$ for experiment I and $\tau_q = 14\text{s}$, $\tau_T = 0.056\text{s}$ for experiment III.

Type 2 DPL model of bioheat transfer (DPL2MBT)

Apply first-order approximation for q and second-order approximation for T

$$\begin{aligned} q(r, t + \tau_q) = & -k \nabla T(r, t + \tau_T) \Rightarrow q + \tau_q \frac{\partial q}{\partial t} \\ = & -k \left(\nabla T + \tau_T \frac{\partial \nabla T}{\partial t} + \frac{\tau_T^2}{2} \frac{\partial^2 \nabla T}{\partial t^2} \right) \end{aligned} \quad (4.23)$$

Applying the equation to bioheat conduction equation, we can get type 2 DPL model of bioheat transfer

$$\begin{aligned} \tau_q \rho c \frac{\partial^2 T}{\partial t^2} = & k \nabla^2 T + \tau_T k \nabla^2 \frac{\partial T}{\partial t} + k \frac{\tau_T^2}{2} \frac{\partial^2}{\partial t^2} \nabla^2 T - \varpi_b \rho_b c_b T \\ & - (\tau_q \varpi_b \rho_b c_b + \rho c) \frac{\partial T}{\partial t} + \varpi_b \rho_b c_b T_a + q_{\text{met}} \\ & + q_{\text{ext}} + \tau_q \frac{\partial q_{\text{met}}}{\partial t} + \tau_q \frac{\partial q_{\text{ext}}}{\partial t} \end{aligned} \quad (4.24)$$

Type 3 DPL Model of Bioheat Transfer (DPL3MBT)

Apply both second-order approximation for q and T

$$\begin{aligned} q(r, t + \tau_q) &= -k\nabla T(r, t + \tau_T) \Rightarrow q + \tau_q \frac{\partial q}{\partial t} + \frac{\tau_q^2}{2} \frac{\partial^2 q}{\partial t^2} \\ &= -k \left(\nabla T + \tau_T \frac{\partial \nabla T}{\partial t} + \frac{\tau_T^2}{2} \frac{\partial^2 \nabla T}{\partial t^2} \right) \end{aligned} \quad (4.25)$$

Applying the equation to bioheat conduction equation we can get type 3 DPL model of bioheat transfer

$$\begin{aligned} \frac{\tau_q^2}{2} \rho c \frac{\partial^3 T}{\partial t^3} &= k\nabla^2 T + k\tau_T \frac{\partial}{\partial t} \nabla^2 T + k \frac{\tau_T^2}{2} \frac{\partial^2}{\partial t^2} \nabla^2 T + (-\varpi_b \rho_b c_b) T \\ &+ (-\tau_q \varpi_b \rho_b c_b - \rho c) \frac{\partial T}{\partial t} + \left(-\frac{\tau_q^2}{2} \varpi_b \rho_b c_b - \tau_q \rho c \right) \frac{\partial^2 T}{\partial t^2} \\ &+ \varpi_b \rho_b c_b T_b + q_m + q_{\text{ext}} + \tau_q \frac{\partial q_m}{\partial t} + \tau_q \frac{\partial q_{\text{ext}}}{\partial t} + \frac{\tau_q^2}{2} \frac{\partial^2 q_m}{\partial t^2} + \frac{\tau_q^2}{2} \frac{\partial^2 q_{\text{ext}}}{\partial t^2} \end{aligned} \quad (4.26)$$

4.3.2 Theoretical solutions

The analytical solution of TWMBT model under boundary condition

$\begin{cases} T = T_\infty, z = 0 \\ \partial T / \partial z = 0, z = H \end{cases}$ and initial condition $\begin{cases} T = T_i, t = 0 \\ \partial T / \partial t = 0, t = 0 \end{cases}$ has been given by Liu et al.^[52], which can be used to verify our numerical predictions.

4.4 Summary

In this chapter, models for describing heat transfer processes in skin tissue under different conditions have been developed. Theoretical analysis has been carried out for Pennes bioheat transfer equation and closed-form solutions for simple one-layer model have been obtained using the Green function method for six different boundary conditions. Different non-Fourier heat conduction models have been developed. Together with the thermal wave model of bioheat transfer, the DPL model is employed to study bioheat transfer in skin tissue for the first time, for it has the ability to characterize microstructural interactions in heat transport. Finally, the models for considering sweating and hair effect are also developed.

However, it should be pointed out that although the non-Fourier bioheat model can solve the paradox of infinite thermal propagation speed, it introduces some unusual behaviours and physically impossible solutions such as negative thermal energies^[64].

References

- [1] Arendt-Nielsen L, Chen A. Lasers and other thermal stimulators for activation of skin nociceptors in humans. *Clinical Neurophysiology*, 2003, 33(6): 259–268.
- [2] Kono T, Groff W F, Sakurai H, et al. Evaluation of fluence and pulse-duration on purpuric threshold using an extended pulse pulsed-dye laser in the treatment of port wine stains. *The Journal of Dermatology*, 2006, 33(7): 473–476.
- [3] Asahina A, Watanabe T, Kishi A, et al. Evaluation of the treatment of port-wine stains with the 595-nm long pulsed dye laser: A large prospective study in adult Japanese patients. *Journal of the American Academy of Dermatology*, 2006, 54(3): 487–493.
- [4] Shafirstein G, Baumler W, Lapidoth M, et al. Laser tissue interaction modeling for treatment planning of port-wine stain. *The 16th Annual Meeting IEEE Lasers and Electro-Optics Society*. Tucson, 2003: 313–315.
- [5] Pustovalov V K, Jean B. Melanin granule models for the processes of laser-induced thermal damage in pigmented retinal tissues. I. Modeling of laser-induced heating of melanosomes and selective thermal processes in retinal tissues. *Bulletin of Mathematical Biology*, 2007, 69(1): 245–263.
- [6] Kauvar A N, Rosen N, Khrom T. A newly modified 595-nm pulsed dye laser with compression handpiece for the treatment of photodamaged skin. *Lasers in Surgery and Medicine*, 2006, 38(9): 808–813.
- [7] Hamilton M M. Laser treatment of pigmented and vascular lesions in the office. *Facial Plastic Surgery*, 2004, 20(1): 63–69.
- [8] Diette K M, Bronstein B R, Parrish J A. Histologic comparison of argon and tunable dye lasers in the treatment of tattoos. *Journal of Investigative Dermatology*, 1985, 85(4): 368–373.
- [9] Deng Z S, Liu J. Analytical study on bioheat transfer problems with spatial or transient heating on skin surface or inside biological bodies. *Journal of Biomechanical Engineering*, 2002, 124(6): 638–649.
- [10] Ozisik M N. *Heat Conduction*. New York: John Wiley and Sons, 1993.
- [11] Shih T C, Kou H S, Liauh C T, et al. The impact of thermal wave characteristics on thermal dose distribution during thermal therapy: A numerical study. *Medical Physics*, 2005, 32(9): 3029–3036.
- [12] Moritz A R, Henriques F C. Study of thermal injuries II. The relative importance of time and source temperature in the causation of cutaneous burns. *American Journal of Pathology*, 1947, 23(5): 695–720.
- [13] Pennes H H. Analysis of tissue and arterial blood temperatures in the resting human forearm. *Journal of Applied Physiology*, 1948, 1(2): 93–122.
- [14] Herivel J. *Joseph Fourier: Face aux objections contre sa theorie de la chaleur*. Paris: Bibliotheque Nationale, 1980.
- [15] Herwig H, Beckert K. Fourier versus non-Fourier heat conduction in materials with a nonhomogeneous inner structure. *ASME Journal of Heat Transfer*, 2000, 122(2): 363–365.

- [16] Ozisik M N, Tzou D Y. On the wave theory in heat conduction. *ASME Journal of Heat Transfer*, 1994, 116(3): 526–535.
- [17] Glass D E, Ozisik M N, Vick B. Hyperbolic heat conduction with surface radiation. *International Journal of Heat and Mass Transfer*, 1985, 28(10): 1823–1830.
- [18] Qiu T Q, Tien C L. Short-pulse laser heating on metals. *International Journal of Heat and Mass Transfer*, 1992, 35(3): 719–726.
- [19] Vedavarz A, Kumar S, Moallemi M K. Significance of non-Fourier heat waves in conduction. *ASME Journal of Heat Transfer*, 1994, 116(1): 221–224.
- [20] Antaki P J. Importance of nonFourier heat conduction in solid-phase reactions. *Combustion and Flame*, 1998, 112(3): 329–341.
- [21] Liu J, Lu W Q. Dual Reciprocity boundary element method for solving thermal wave model of bioheat transfer. *Space Medicine and Medical Engineering*, 1997, 10(6): 391–395.
- [22] Lu W Q, Liu J, Zeng Y. Simulation of the thermal wave propagation in biological tissues by the dual reciprocity boundary element method. *Engineering Analysis with Boundary Elements*, 1998, 22(3): 167–174.
- [23] Lu W Q, Liu J, Zeng Y. Extension of the dual reciprocity boundary element method to simulate thermal wave propagation in biological tissue. *Journal of Engineering Thermophysics*, 1998, 19(6): 728–731.
- [24] Peshkov V. Second sound in helium II. *Journal Physics*. VIII, 1944, 8: 381.
- [25] Morse P M, Feshbach H. *Methods of Theoretical Physics*. New York: McGraw-Hill, 1953.
- [26] Cattaneo C. A form of heat conduction equation which eliminates the paradox of instantaneous propagation. *Compte Rendus*, 1958, 247: 431–433.
- [27] Vernotte P. Les paradoxes de la theorie continue de l'equation de la chaleur. *Compte Rendus*, 1958, 246: 3154–3155.
- [28] Chester M. Second sound in solid. *Physics Review*, 1963, 131(5): 2013–2015.
- [29] Weymann H D. Finite speed of propagation in heat conduction, diffusion and viscous shear motion. *American Journal of Physics*, 1967, 35(6): 488–496.
- [30] Mitra K, Kumar S, Vedavarz A, et al. Experimental evidence of hyperbolic heat conduction in processed meat. *ASME Journal of Heat Transfer*, 1995, 117(3): 568–573.
- [31] Tzou D Y. *Macro- to Micro-scale Heat Transfer: The Lagging Behavior*. Washington: Taylor and Francis, 1997.
- [32] Yu Tzou D. An engineering assessment to the relaxation time in thermal wave propagation. *International Journal of Heat and Mass Transfer*, 1993, 36(7): 1845–1851.
- [33] Ozisik M N, Tzou D Y. On the wave theory in heat conduction. *ASME Journal of Heat Transfer*, 1994, 116(3): 526–535.
- [34] Kaminski W. Hyperbolic heat conduction equation for materials with a non-homogeneous inner structure. *ASME Journal of Heat Transfer*, 1990, 112(3): 555–560.
- [35] Tzou D Y. Thermal shock phenomena under high-rate response in solids// Tien C L. *Annual Review of Heat Transfer*. Washington: Hemisphere, 1992:

- 111–185.
- [36] Sieniutycz S. The variational principles of classical type for non-coupled non-stationary irreversible transport processes with convective motion and relaxation. *International Journal of Heat and Mass Transfer*, 1977, 20(11): 1221–1231.
 - [37] Taitel Y. On the parabolic hyperbolic and discrete formulation of the heat conduction equation. *International Journal of Heat and Mass Transfer*, 1972, 15(2): 369–371.
 - [38] Antonishyn N V, Geller M A, Parnas A L. Hyperbolic heat conduction equation for disperse system. *Inzhenerno Fizicheskij Zhurnal*, 1974, 26(3): 503–508.
 - [39] Raspopov B M. Control of some transfer processes. *Inzhenerno Fizicheskij Zhurnal*, 1967, 12: 444.
 - [40] Brazhnikov A M, Karpychev V A, Luikova A V. One engineering method of calculating heat conduction processes. *Inzhenerno Fizicheskij Zhurnal*, 1975, 28(4): 677–680.
 - [41] Michalowski S, Mitura E, Kaminski W. The application of mathematical method to describe the kinetics of drying. *Hungarian Journal of Industrial Chemistry*, 1982, 10: 387.
 - [42] Mitura E, Michalowski S, Karnlnski W. A mathematical model of convection drying in falling drying rate period. *Drying Technology*, 1988, 6(1): 113–137.
 - [43] Luikov A V. Application of irreversible thermodynamics methods to investigation of heat and mass transfer. *International Journal of Heat and Mass Transfer*, 1966, 9(2): 139–152.
 - [44] Roetzel W, Putra N, Das S K. Experiment and analysis for non-Fourier conduction in materials with non-homogeneous inner structure. *International Journal of Thermal Sciences*, 2003, 42(6): 541–552.
 - [45] Stratigos A J, Dover J S. Overview of lasers and their properties. *Dermatologic Therapy*, 2000, 13(1): 2–16.
 - [46] Tang D W, Araki N. The wave characteristics of thermal conduction in metallic films irradiated by ultra-short laser pulses. *Journal of Physics D*, 1996, 29(10): 2527–2533.
 - [47] Liu J, Zhang X X, Wang C C, et al. Engineering investigation on medical application approaches for the thermal wave effects in living tissue. *Space Medicine and Medical Engineering*, 1997, 10(2): 135–139.
 - [48] Liu J, Zhang X X, Lu W Q, et al. The thermal pulse decay method for invasive measurement of blood perfusion of tissue in vivo. *Progress in Natural Science*, 1999, 9(2): 179–184.
 - [49] Zhu T C, Feng X Z. Numerical analysis of the relationship between blood flow coefficient and living tissue thermal behavior. *Chinese Journal of Hemorheology*, 2001, 11(3): 182–183.
 - [50] Deng Z S, Liu J. Non-Fourier heat conduction effect on prediction of temperature transients and thermal stress in skin cryopreservation. *Journal of Thermal Stresses*, 2003, 26(8): 779–798.

- [51] Chato J C, Lee R C. The future of biothermal engineering. *Annals of the New York Academy of Sciences*, 1998, 858: 1–17.
- [52] Liu J, Chen X, Xu L X. New thermal wave aspects on burn evaluation of skin subjected to instantaneous heating. *IEEE Transactions on Biomedical Engineering*, 1999, 46(4): 420–428.
- [53] Liu J. Preliminary survey on the mechanisms of the wave-like behaviors of heat transfer in living tissues. *Forschung im Ingenieurwesen*, 2000, 66(1): 1–10.
- [54] Ma N, Jiang S, Li H, et al. Analysis of non-Fourier effect and laser-induced thermal damage of laser-irradiated layered human skin tissue. *Space Medicine and Medical Engineering*, 2003, 16(2): 133–137.
- [55] Bayazitoglu Y, Peterson G P. Fundamental issues in hyperbolic heat conduction. *ASME Heat Transfer Division*, 1992: 227.
- [56] Tzou D Y, Ozisik M N, Chiffelle R J. The lattice temperature in the microscopic two-step model. *Journal of Heat Transfer*, 1994, 116(4): 1034–1038.
- [57] Koerner C, Bergmann H W. Physical defects of the hyperbolic heat conduction equation. *Applied Physics A: Materials Science and Processing*, 1998, 67(4): 397–401.
- [58] Godoy S, Garcia-Colin L S. Nonvalidity of the telegrapher's diffusion equation in two and three dimensions for crystalline solids. *Physics Review E*, 1997, 55(3): 2127–2131.
- [59] Tzou D Y. A unified field approach for heat conduction from macro- to micro-scales. *ASME Journal of Heat Transfer*, 1995, 117(1): 8–16.
- [60] Tzou D Y. Experimental support for the lagging behavior in heat propagation. *Journal of Thermophysics and Heat Transfer*, 1995, 9(4): 686–693.
- [61] Quintanilla R, Racke R. A note on stability in dual-phase-lag heat conduction. *International Journal of Heat and Mass Transfer*, 2006, 49(7-8): 1209–1213.
- [62] Tzou D Y, Chiu K S. Temperature-dependent thermal lagging in ultrafast laser heating. *International Journal of Heat and Mass Transfer*, 2001, 44(9): 1725–1734.
- [63] Antaki P J. New interpretation of non-Fourier heat conduction in processed meat. *Journal of Heat Transfer*, 2005, 127(2): 189–193.
- [64] Bai C, Lavine A S. On hyperbolic heat conduction and the second law of thermodynamics. *ASME Journal of Heat Transfer*, 1995, 117(2): 256–263.

PART II SKIN BIOMECHANICS

Chapter 5

Skin Mechanical Behaviour

5.1 Introduction

Soft organ tissues exhibit complex nonlinear, anisotropic, nonhomogeneous, time, and rate dependent behaviour. Fung has revealed that a nonlinear stress-strain relationship is common for soft tissues but the degrees are different for different tissues. Since soft organs are composed of different materials, like elastin and collagen, in different combinations, hence, soft tissue properties are both coordinate and direction dependent. Time and rate dependent behaviour is also common for soft tissues and explained by viscoelasticity.

Due to great importance in clinical and cosmetic applications, the mechanical properties of skin have been experimentally investigated *in vivo* and *in vitro* for a long time since the study of Langer in 1861. *In vitro* tests are often used in lieu of *in vivo* measurements, as the latter is affected by both skin tissue itself and other structures it is attached to, which means it is very difficult to obtain a uniform strain field in the sample and control boundary conditions when performing.

5.2 Skin Behaviour under Stretch

Tensile loading occurs when skin is pulled in the plane of its surface, e.g. closure of a wound with a suture induces tension across the wound. It can also be induced by other loadings such as swelling and shearing. For example, near adherent scar tissue or at the distal region of a residual limb as the prosthesis is donned.

The tensile behaviour of skin is the most studied and there exist several comprehensive reviews^[1~5]. Typical stress versus strain relationships under uniaxial and biaxial tension are schematically shown in Figure 5.1(a) and (b), respectively. From the figure, it can be seen the stress-strain curve of skin under tension shows a typical J shape and is nonlinear although the elastin and collagen fibres are considered linear elastic, which is mainly due to the non-uniformity of its structure. This form, representative for the

mechanical behaviour of many (collagenous) soft connective tissues, differs significantly from stress-strain curves of hard tissues or from other types of (engineering) materials. Three obviously different regions can be observed based on microscopic observations of skin samples fixed at various strain levels, e.g. light microscopy^[6~11] and electron microscopy^[12], as described below.

(1) Low modulus portion, which is caused by the gradual straightening of an increasing fraction of the wavy collagen fibres, where either the elastin and/or the proteoglycan matrix provides resistance to deformation. This region can be further divided into two Phases, where in phase I the collagen fibres are in relaxed conditions (appear wavy) and the elastin fibres are mainly responsible for the stretching mechanism, while in phase II, the crimped collagen fibres gradually elongate, tend to line up with the load direction and bear loads as the load is increased.

(2) Linear region, in which, at high tensile stresses, crimp patterns disappear and the collagen fibres become straighter primarily aligned with one another in the direction of stretching. The straightened collagen fibres resist the load strongly, which makes the skin stiffer and the stress-strain relation becomes linear due to the stretching and slippage of collagen molecules within crosslinked collagen fibres and collagen fibril slippage.

(3) Final yield region, during which the ultimate tensile strength is reached and fibres begin to break due to the loss of fibrillar structure resulting from the defibrillation of collagen fibrils.

Compared with uniaxial stretch, biaxial tensile loading results in the lateral compression of the stress-strain curve and the reduction in the strain before entry into the linear region occurs, which is due to the two-directional stretch of collagen fibres, as shown in Figure 5.1(b).

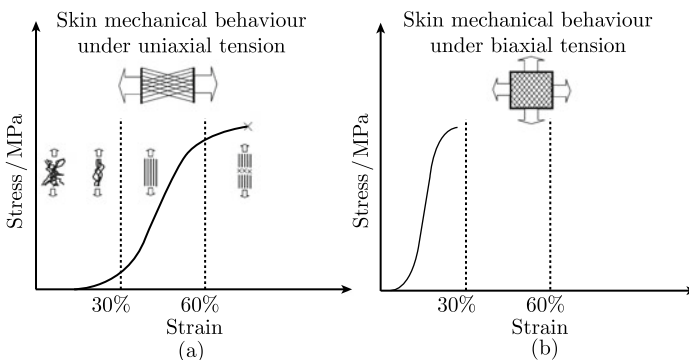


Figure 5.1 Schematic of skin mechanical behaviour under (a) uniaxial and (b) biaxial tension (by permission of Springer-Verlag)

5.3 Skin Behaviour under Compression

In vivo, skin is under compressive load from different media such as chairs, shoes and the sockets of prosthetic limbs. Although there are abundant published experimental data for skin in tension, the mechanical behaviour of skin in compression has been rarely studied. The pressure in the skin tissue is composed of solid tissue pressure and interstitial fluid pressure^[13], where the first one is carried mainly by the solid elements in the tissue and is the important factor and the main cause of the tends to occlude tile blood vessels and the second one determines the motion of tissue fluid and the diffusion coefficient of blood into the capillaries. This point has also bee proved by Oomens et al.^[14], who found a good agreement between experimental results of skin response under compression and finite element calculations with mixture elements (solid/fluid mixtures). The compressive response of skin is highly viscoelastic and also nonlinear^[15~28]. Both the viscous and the nonlinear aspects were found to diminish greatly by preload^[29] and depend on age, sex, site, hydration and obesity^[17]. Further, almost all previously published mechanical models of skin tissue are based on experimental data under tension and few are based on data under compression.

Further, in view of the problems accompanying biaxial tensile tests, an unconfined compression test through the thickness direction can be used as an approximation which gives an averaged in-plane tensile response^[22,30]. If the skin deforms with a constant volume, then the compression test will have a similar effect to a biaxial test in the plane of the skin (through thickness compression results in lateral in-plane expansions). For example, Shergold^[31] found that the Ogden model evaluated from his compression tests of pig skin provided a reasonable approximation to the tensile orthotropic constitutive behaviour measured by Ankerson et al.^[32]. However, there are also problems with this method, where the most important one is the friction between skin sample and compression plates, which will limit lateral expansion. Fortunately, several methods can be adopted to overcome this problem. In order to minimize the effects of friction on the experimental results, researchers have made many efforts to reduce the specimen/platen friction during unconfined compressions, such as covering the moving platen with a polytetrafluoroethylene (PTFE) sheet^[33], using platens of polished stainless steel^[34], removing the epidermis layer from skin sample^[30], coating smooth compression plates with lubricant or grease (margarine)^[22,30], and using lubricated squeezing flow^[35], etc.

A representative compressive stress versus strain response of pig back skin

from our previous test is presented in Figure 5.2 (dot). The stress/strain relationship exhibits a three-stage strain hardening: toe region with low stiffness at low strain levels, transition region from low to high stiffness, and high stiffness region at large strain levels. Compared with the mechanical characteristics of skin in tension^[32], the compressive stress/strain curves are similar in trend; however, the transition from low to high stiffness in tension occurs mostly at a strain level of 10%~20%^[36~38], which is much smaller than that in compression (about 20%~30% strain), as shown in Figure 5.2. Similar results have also been reported for pig back skin^[22].

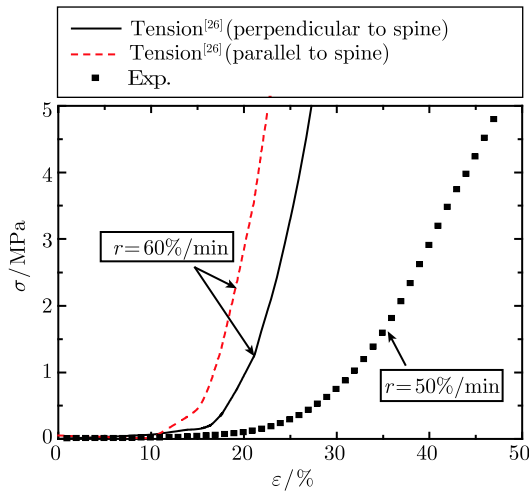


Figure 5.2 Representative stress-strain responses from a compressive test and comparison with published tensile behaviour in literature (by permission of Springer-Verlag)

5.4 Skin Failure

There are multiple types of soft tissue trauma, and the injuries can result in very complicated effects on physiological processes associated with the injured tissue. Understanding the factors that control the extent of tissue damage as a result of material failure in soft tissues may provide means to improve diagnosis and treatment of soft tissue injuries. Non-destructive testing can be carried out either *in vivo* or *in vitro* but failure properties must be obtained by destructive testing *in vitro*. The most common failure tests of skin are tensile failure tests^[32,39~52], piercing tests^[27,31,32,53~62] and tearing tests^[63~66]. In spite of these studies reported, the failure characteristics are still not clearly established yet. This is due to the difficulty in obtaining

reliable measurements on soft biological tissues. Further, there is almost no reported study of failure characteristics concerns dynamic loadings.

5.4.1 Tensile failure

Skin fails more often in a tensile manner than from a shear or cutting action, even when struck by relatively sharp metal edges or structures^[42,67,68]. For example, Gadd et al.^[42,68] studied the strength of skin and its ability to resist breakage under variable loading rates and argued that the predominant failure mode of skin is tensile fracture, rather than any shearing (cutting) action, when struck by sharp metal edges.

The tensile strength of skin primarily depends on the size and crosslinking of the collagen framework^[69]. However, the extension at which skin fails is independent of the degree to which the collagen crosslinks are broken. In other words when the skin is deformed by the application of the stress, the load is applied directly on the collagen fibre network^[70]. The failure of the skin may be result of the breakage of the fibre bundle or the slip of the fibre bundle, or both^[71].

The fracture pattern of fibres can be classified into three principal patterns depending on the nature of the resulting fractured fibre ends^[71]. These fracture patterns are: ① fracture occurring in a single plane perpendicular to the fibre axis, known as “smooth” fracture; ② fracture initiated in a plane perpendicular to the fibre axis and resulting in the splitting of the fibre along the axis known as “step” fracture; ③ fracture with the fracture end split open giving the appearance of the bristles of a brush, known as “fibrillation”^[71,72]. These patterns have been found to be extremely characteristic in both collagen^[73] and elastoidin fibres^[74] tested at different strain rates.

The failure mode occurred as a fracture of the epidermis and a coincident creeping failure of the laminated dermis. This behaviour has support from a structural viewpoint since the dermis is the more extensible of the two materials, and thus elongates to a greater degree than the cellular epidermis^[75].

Arumugam et al.^[71] studied the fracture behaviour of skin tissue by using scanning electron microscope at different strain rates. At lower strain rate the fibre bundles are thin and split, indicating that the fibre bundles have sufficient time to split into thinner ones and slip past one another during the application of the load. This is similar to the fracture behaviour of collagen fibres observed by Arumugam et al.^[73]. The wet collagen fibres exhibit fibrillation at low and high strain rates.

At higher strain rates the plastic set is very high and therefore there is a definite possibility of fibre slip at higher strain rates. At higher strain rates the frictional force is also high, resulting in higher stress. Owing to the lack of sufficient time for the fibre bundles to split up, the fractured ends of sample broken at higher strain rates tend to contain thicker fibre bundles.

The failure characteristics of soft biological tissue under dynamic loadings are not clearly established yet. Concerning planar soft tissue, the mechanical properties already studied exclusively concerning quasi-static loadings on rabbit skin^[38,76] and human skin^[77]. Moreover, only the most recent studies^[78,79] reported failure characteristics and only the first one^[79] concerns dynamic loadings. This lack of data is due to the difficulty in obtaining reliable measurements on soft biological tissue^[80]. This difficulty is amplified when the tests are carried out in dynamic loading conditions up to failure and in high strain conditions^[49].

5.4.2 Skin piercing

Knight^[55] recorded penetration forces by making incisions on cadavers using a simple, instrumented knife blade and showed the overriding factor to be the sharpness of the blade. He also noted that pretensioning of the skin reduced the force needed to cause penetration and so intercostal spaces were penetrated more easily than loose abdominal skin, whereas penetration was usually by the full length of the blade with the maximum force on the knife appearing just before initial penetration. The penetration force decreases with increasing sharpness of penetrator, which was also found by Green^[81] where cadavers were laid on top of a force table. However, Green^[81] tested clothed bodies and observed a tenfold increase in the force of penetration. Both workers noted that lower forces were required at higher impact velocities.

Brett et al.^[57] observed much higher penetration forces for pig skin than for human skin, while the penetration force through the underlying tissue is similar. However, the dependencies of the penetration force upon the strength of the skin and upon the level of pre-stretch are not straightforward. A larger penetration force for skin and muscle than that for fat was observed by O'Callaghan et al.^[58]. Ankersen et al.^[32] observed that the peak penetration force for knife incision of pig skin is similar to that for synthetic chamois, despite a large difference in tensile strengths. They found pigskin shows more tension stiffening towards the point of initial penetration (13 N) and a more gradual drop in force following penetration. Full penetration is reached

at a force approximately half of the peak value.

Frick et al.^[59] preloaded strips of sheep skin and reported that the force required to puncture the sample with a suture needle increased with increasing pre-tension in the skin. By contrast, Figge & Barnet^[60] performed tests on cadavers with a needle injector and demonstrated that less force is required to penetrate stretched skin than loose skin. This difference in behaviours may be attributed to the differences in constraint on the skin^[62]: when cadaver skin is loose, the needle injector compresses the skin against the underlying muscle fascia and the penetration load is high, while the skin remains unsupported by the underlying muscle fascia, and the penetration force is low when cadaver skin is pre-stretched and then subjected to a needle injector.

Contradictory evidence also exists for the relation between injector speed and force. Frick et al.^[59] found that the injector force did not change when the needle velocity was increased from 1 to 10 mm/s. However, Brett et al.^[57] found that the penetration force was speed dependent and it was found that the force decreased with increasing speed in the range 1~3 mm/s.

Davis et al.^[61] found that microneedle insertion force increases as a linear function of needle tip cross-sectional area and skin does not deform into the lumen of hollow needles during insertion. They proposed a theoretical model for the force of insertion

$$\bar{F}_i = \tau G_p A + \Theta \quad (5.1)$$

where G_p is the puncture fracture toughness; Θ is a pre-exponential constant; τ is an exponential constant; A is the cross-sectional area at the needle tip. By comparing the experimental results using needles of different thickness, they suggested that the full cross-sectional area of A should be used in the model.

Shergold & Fleck^[27] pointed out that the dependence of skin perforation upon the mechanical properties of skin, and the shape of the penetrator, is also relevant to the function and evolution of mammalian dentition: the successful predator must have sufficiently strong jaws and sharp teeth to cause skin perforation. They found that the penetration mechanism of a soft solid depends upon the punch tip geometry: a sharp tipped punch penetrates by the formation and wedging open of a mode I planar crack, while a flat-bottomed punch penetrates by the growth of a mode II ring crack. The average penetration pressure on the shank cross section of a flat-bottomed punch exceeds that for a sharp-tipped punch of the same diameter. In addition, the penetration pressure decreases as the diameter of the sharp-tipped punch increases. These findings are in broad agreement with the predictions

of Shergold & Fleck^[62].

5.4.3 Skin tearing

A tear test was found to be suitable for determining the fracture toughness of skin tissue^[63,82], which allows the mapping of toughness variations over an area of rat skin. However, tearing tests of skin is difficult to perform since the skin is not easily cut when excised and its low stiffness implies that it will deform under its own weight, causing errors in zero-strain measurement^[64].

The tear tests carried out by Purslow^[63] fractured specimens of rat skin. The samples were mounted in a tensiometer and extended at 50 mm/min. This tear test causes mode III fracture. The results of these tests to calculate the critical strain energy release rate (resistance to fracture or toughness), which showed that the toughness bears an inverse relationship to maximum stiffness parallel to the direction of crack propagation and increases slightly with increasing extension rate. Granot et al.^[66] investigated the skin tearing in broilers and found it was significantly influenced by strain and sex.

Periera et al.^[65] placed samples of human and rat skin between the blades of a scissor mounted in a universal testing machine. The samples were mounted unstretched on a wire mesh, the scissors closed by moving the crosshead of the machine, and the force required to cut the skin was measured. This configuration also causes similar fracture as that of Purslow^[63]. They attributed the high apparent fracture resistance of biological tissue to crack blunting, where the viscoelastic nature of biological tissue allows it to flow at the tip of the crack, blunting it and therefore requiring a much higher level of force to progress the crack further.

A method of measuring the fracture resistance of skin in opening mode (mode I) using this failure model was proposed by Doran et al.^[64]. It is assumed that until a certain level of strain is reached, there is no strain energy stored in the material. From this point on, the behaviour is linear elastic.

5.5 Skin Friction

Skin tissue is vitally important to our health and is also the outermost part of our sensitive system, where the friction between the skin and the solid surfaces reflects this double role^[83], limiting the tangential force transfer and reporting about the counter-surface texture, through pleasant and unpleasant feelings. The friction of skin clearly plays a major role in everyday life, for example, in the grip of sports equipment and the feel of a skin cream;

and it also has important medical consequences, for example, in the formation of bedsores and in the maintenance of eye comfort^[84]. The investigation of friction behaviour of the skin plays therefore an important role in both technical and health points of view^[85]: it provides valuable insight into how the skin interacts with other surfaces, and how it can change under various conditions, such as age and health, and chemical treatments, such as lotions and moisturizers^[86]; and offer convenient, non-invasive techniques to quantitatively assess skin health and hydration^[87]; studying the static friction properties of the hand-grabrail interface also provides an understanding of key mechanisms that contribute to a stable interface at the grabrail surface level^[88]. In spite of its importance, relatively few articles have dealt with the measurement of the skin's friction behaviour compared with, for example, the great number of studies concerning other biomechanical properties such as tension and compression.

Friction is a force acting parallel to the interface of two surfaces that are in contact during motion or impending motion of one surface moving over another. When friction exists between two surfaces, the magnitude of the frictional force (F_f) is directly proportional to the normal force (f_N) through the relationship

$$F_f = \mu f_N \quad (5.2)$$

where μ is the friction coefficient. The friction coefficient can be described in two ways: the static friction coefficient μ_s and the dynamic or kinetic friction coefficient μ_d , where the former refers to the ratio of the force required to initiate relative movement to the normal force between the surfaces; and the latter refers to the ratio of the friction force to the normal force when the two surfaces are moving relative to each other.

5.5.1 Measuring methods

A variety of methods have been used to determine friction properties of skin both *in vivo* and *in vitro*. The *in vitro* approach often uses specially developed equipment, which includes probes that apply a constant normal force against the skin under study, with a simultaneous sliding displacement. Various experimental designs have been devised in order to measure the dynamic friction on skin, as reviewed by Sivamani et al.^[86]; Comaish & Bottoms^[89] slid a cap over the skin while the test region of the skin remained stationary; other methods of determining skin friction have involved a moving probe^[90~94], a friction meter^[85,90,95,96], a moving belt^[97] and a gravity-based pinch test^[88,98,99]. All these fall into two categories despite the

different probe geometries and materials used^[100,101]: one using a probe or wheel rotating on the skin with a known normal force and the other using a probe sliding on the skin.

A perpendicular normal load varies from author to author and is poorly controlled with either static weights or spring^[86,87]. The major problems of these studies have been data repeatability from test to test and reproducibility from person to person, day to day, and apparatus to apparatus^[87].

5.5.2 Skin friction behaviour

Much of the research on skin friction behaviour has been focused on the dynamic friction coefficient wherein the two surfaces move at a relative constant velocity^[86]. There have been a number of reviews of the *in vivo* friction and lubrication of human skin such as those by Dowson^[102] and more recently by Sivamani et al.^[103,104] and Gitis & Sivamani^[87].

Although most of the skin research has focused on the dynamic friction coefficients, with the two surfaces moving at a relative constant velocity, some work has focused on static friction coefficients^[88,89,94,97,105~107], as common activities such as gripping handrails, gripping car steering wheels, or holding a cup involve the static friction coefficient more than the dynamic friction coefficient. The static friction properties of human skin have been shown to act differently from those of solid surfaces, which is due to the compliant, flexible nature of skin and the ability of skin to change its characteristics when hydrated. However, various studies have confirmed that the calculation of the coefficient of static friction can be applied to human skin when there is a normal force of sufficient magnitude.

A representative normal load—friction force of skin tissue is shown in Figure 5.3. Three distinct friction phases were distinguished^[108]: ① tangential force increases linearly to reach a maximum, which corresponds to the static limit friction force; ② the slope of the linear curve corresponds to the lateral



Figure 5.3 Representative normal load-friction force of skin tissue

contact stiffness; ③ the slope change in the transition regime between the static or partial slip and dynamic friction or gross slip corresponds to the second phase.

5.5.3 Origin of skin friction

Skin and polymers appear to behave similarly with respect to friction and do not follow the basic laws of friction that exist for solid materials^[97]. The assessment of the friction coefficient of skin is a highly complex problem, which involves: skin elasticity, the anisotropy of skin microtopography; nature of material employed, intersurface contact, skin physicochemical nature; variation in testing conditions and individual differences. Then, any change in the friction force of the skin is affected by its mechanical properties, its topographical intersurface contact and physicochemical properties^[109].

The coefficient of friction has been indicated to be due various combined effects of asperity deformation (μ_d), ploughing in the surface by wear particles (μ_p) and molecule adhesion between surfaces (μ_a)^[110]. The surface of the skin contributes to these different factors according to the following mechanisms^[97].

(1) μ_d : The friction due to asperity deformation. The deformation of the dermal ridges of the skin contributes to this factor during static and sliding conditions. Skin has visibly obvious topographical features that may be quantified by profilometry. The most pronounced feature of the texture is an intersecting network of *V* shaped grooves. There are also other features at smaller length scales. Thus it is reasonable to expect that skin in the dry state behaves as an extended multiple asperity surface with a coefficient of friction that is independent of the normal load for a spherical probe^[84].

(2) μ_p : The ploughing component is low when the soft surface of the skin slides against a hard surface.

(3) μ_a : The adhesion component depends on lubricants at the interface. Oil and lard have a reducing effect on this component of friction; there is also an unknown effect of proteins and an increasing effect of sweat on textured surfaces. The molecules on the skin surface are considered to affect the adhesion term greatly. According to Wolfram^[107], the phenomenon is driven mainly by the adhesion forces.

References

- [1] Larrabee W F. A finite element model of skin deformation. I. Biomechanics of skin and soft tissue: A review. *Laryngoscope*, 1986, 96(4): 399–405.

- [2] Edwards C, Marks R. Evaluation of biomechanical properties of human skin. *Clinical Dermatology*, 1995, 13(4): 375–380.
- [3] Vogel H G. Mechanical measurements of skin. *Acta Dermato-Venereologica Supplement (Stockh)*, 1994, 185: 39–43.
- [4] Pierard G E. EEMCO guidance to the in vivo assessment of tensile functional properties of the skin, Part 1: Relevance to the structures and ageing of the skin and subcutaneous tissues. *Skin Pharmacology and Applied Skin Physiology*, 1999, 12(6): 352–362.
- [5] Payne P A. Measurement of properties and function of skin. *Clinical Physics and Physiological Measurement*, 1991, 12(2): 105–129.
- [6] Gibson T, Kenedi R M, Craik J E. The mobile micro-architecture of dermal collagen. *British Journal of Surgery*, 1965, 52(10): 764–770.
- [7] Craik J E, McNeil I R R. Histological studies of stressed skin//Kenedi R M. *Biomechanics and Related Engineering Topics*. Oxford: Pergamon Press, 1965: 159–164.
- [8] Ridge M D, Wright V. The rheology of skin. A bio-engineering study of the mechanical properties of human skin in relation to its structure. *British Journal of Dermatology*, 1965, 77(12): 639–649.
- [9] Ridge M D, Wright V. A rheological study of skin//Kenedi R M. *Biomechanics and Related Bio-engineering Topics*. Oxford: Pergamon Press, 1965: 165–175.
- [10] Ridge M D, Wright V. Mechanical properties of skin: A bioengineering study of skin structure. *Journal of Applied Physiology*, 1966, 21(5): 1602–1606.
- [11] Ridge M D, Wright V. The directional effects of skin. A bio-engineering study of skin with particular reference to Langer’s lines. *Journal of Investigative Dermatology*, 1966, 46(4): 341–346.
- [12] Brown I A. A scanning electron microscope study of the effects of uniaxial tension on human skin. *British Journal of Dermatology*, 1973, 89(4): 383–393.
- [13] Dinnar U. A note on theory of deformation in compressed skin tissues. *Mathematical Biosciences*, 1970, 8(1-2): 71–82.
- [14] Oomens C W, van Campen D H, Grootenboer H J. In vitro compression of a soft tissue layer on a rigid foundation. *Journal of Biomechanics*, 1987, 20(10): 923–935.
- [15] Tregear R T, Dirnhuber P. Viscous flow in compressed human and rat skin. *Journal of Investigative Dermatology*, 1965, 45: 119–125.
- [16] Hickman K E, Lindan O, Reswick J B, et al. Deformation and flow in compressed skin tissues. *ASME Biomedical Fluid Mechanics Symposium*, 1966: 127–147.
- [17] Daly C H. Biomechanical properties of dermis. *Journal of Investigative Dermatology*, 1982,79 (Suppl. 1): 17s–20s.
- [18] Wilkins E S, Pinder K L. Rheological properties of skin components under compressive load. *Physiological Chemistry and Physics*, 1979, 11(1): 23–35.
- [19] Oomens C W J, Van Campen D H, Grootenboer H J, et al. Experimental and theoretical compression on porcine skin. *Proceedings of Meetings of*

- European Society of Biomechanics. Davos, 1984: 227–232.
- [20] Sakata K, Parfitt G, Pinder K L. Compressive behaviour of a physiological tissue. *Biorheology*, 1972, 9(3): 173–184.
- [21] Dikstein S, Hartzshtark A. In vivo measurement of some elastic properties of human skin// Marks R, Payne P A. *Bioengineering and the Skin*. Lancaster: MTP Press, 1981: 45–53.
- [22] Shergold O A, Fleck N A, Radford D. The uniaxial stress versus strain response of pig skin and silicone rubber at low and high strain rates. *International Journal of Impact Engineering*, 2006, 32(9): 1384–1402.
- [23] Bonilla C M A, Massanet A R F, Almodóvar N V. Mechanics of biomaterials: Skin repair and grafts. *Proceedings of Applications of Engineering Mechanics in Medicine*. Nanjing, 2005.
- [24] North J F. Influence of strain rate themechanical properties of human skin and subcutaneous tissue. *Journal of Biomechanics*, 1978, 28(4): 124–127.
- [25] North J F, Gibson F. Volume compressibility of human abdominal skin. *Journal of Biomechanics*, 1978, 11(4): 203–207.
- [26] Paillet-Mattei C, Zahouani H. Study of adhesion strengths and mechanical properties of human skin in vivo. *Journal of Adhesion Science and Technology*, 2004, 18: 1739–1758.
- [27] Shergold O A, Fleck N A. Experimental investigation into the deep penetration of soft solids by sharp and blunt punches, with application to the piercing of skin. *Journal of Biomechanics Engineering*, 2005, 127(5): 838–848.
- [28] Mofid Y, Ossant F, Kathyr F, et al. In-vivo human skin elastography: A preliminary study. 5th Proceedings of World Congress on Ultrasonics. Paris, 2003: 205–208.
- [29] Ziegert J C, Lewis J L. In vivo mechanical properties of soft tissue covering bony prominences. *Journal of Biomechanical Engineering*, 1978, 100: 194–201.
- [30] Hepworth D G, Steven-fountain A, Bruce D M, et al. Affine versus non-affine deformation in soft biological tissues, measured by the reorientation and stretching of collagen fibres through the thickness of compressed porcine skin. *Journal of Biomechanics*, 2001, 34(3): 341–346.
- [31] Shergold O A. *The Mechanics of Needle-Free Injection* [Ph. D. Thesis]. Cambridge: University of Cambridge, 2004.
- [32] Ankersen J, Birkbeck A E, Thomson R D, et al. Puncture resistance and tensile strength of skin simulants. *Journal of Engineering in Medicine*, 1999, 213(6): 493–501.
- [33] Miller K, Chinzei K. Constitutive modeling of brain tissue: Experiment and theory. *Journal of Biomechanics*, 1997, 30(11-12): 1115–1121.
- [34] Miller-Young J E, Duncan N A, Baroud G. Material properties of the human calcaneal fat pad in compression: Experiment and theory. *Journal of Biomechanics*, 2002, 35(12): 1523–1531.
- [35] Nasser S, Bilston L, Tanner R. Lubricating squeezing flow: A useful method for measuring the viscoelastic properties of soft tissues. *Biorheology*, 2003,

- 40(5): 545–551.
- [36] Dunn M G, Silver F H, Swann D A. Mechanical analysis of hypertrophic scar tissue: Structural basis for apparent increased rigidity. *Journal of Investigative Dermatology*, 1985, 84(1): 9–13.
- [37] Wan A W. Biaxial tension test of human skin in vivo. *Bio-Medical Materials and Engineering*, 1994, 4(7): 473–486.
- [38] Lanir Y, Fung Y C. Two-dimensional mechanical properties of rabbit skin. II. Experimental results. *Journal of Biomechanics*, 1974, 7(2): 171–182.
- [39] Sandblom P. Determination of the tensile strength of the healing wound as a clinical test. *J Int Chir*, 1953, 13(4): 1–4.
- [40] Sandblom P, Petersen P, Muren A. Determination of the tensile strength of the healing wound as a clinical test. *Acta chirurgica scandinavica*, 1953, 105(1-4): 252–257.
- [41] Beckwith T G, Brody G S, Glaser A A, et al. Standardization of methods for measuring mechanical properties of wounds. *ASME New York*, 1963: 7.
- [42] Gadd C W, Lange W A, Peterson F J. Strength of skin and its measurement. *ASME New York*, 1965: 5.
- [43] Vogel H G. Antagonistic effect of aminoacetonitrile and prednisolone on mechanical properties of rat skin. *Biochimica et Biophysica Acta*, 1971, 252(3): 580–585.
- [44] Wildnauer R H, Bothwell J W, Douglass A B. Stratum corneum biomechanical properties. I. Influence of relative humidity on normal and extracted human stratum corneum. *Journal of Investigative Dermatology*, 1971, 56(1): 72–78.
- [45] Haut R C. The effects of orientation and location on the strength of dorsal rat skin in high and low speed tensile failure experiments. *Journal of Biomechanical Engineering*, 1989, 111(2): 136–140.
- [46] Ozyazgan I, Liman N, Dursun N, et al. The effects of ovariectomy on the mechanical properties of skin in rats. *Maturitas*, 2002, 43(1): 65–74.
- [47] Zeng Y, Xu C Q, Yang J, et al. Biomechanical comparison between conventional and rapid expansion of skin. *The British Association of Plastic Surgeons*, 2003, 56(7): 660–666.
- [48] Zeng Y J, Liu Y H, Xu C Q, et al. Biomechanical properties of skin in vitro for different expansion methods. *Clinical Biomechanics*, 2004, 19(8): 853–857.
- [49] Jacquemoud C, Bruyere-Garnier K, Coret M. Methodology to determine failure characteristics of planar soft tissues using a dynamic tensile test. *Journal of Biomechanics*, 2007, 40(2): 468–475.
- [50] Howes E L, Sooy J W, Harvey S C. The healing of wounds as determined by their tensile strength. *Jama*, 1929, 92(1): 42–45.
- [51] Sandblom P. Tensile strength of healing wounds: An experimental study. *Acta chirurgica scandinavica*, 1944, Suppl. 89.
- [52] Greven H, Zanger K, Schwinger G. Mechanical properties of the skin of *Xenopus laevis* (Anura, Amphibia). *Journal of Morphology*, 1995, 224(1): 15–22.

- [53] Jansen L H, Rottier P B. Comparison of the mechanical properties of strips of human abdominal skin excised from below and from above the umbilic. *Dermatologica*, 1958, 117(4): 252–258.
- [54] Jansen L H, Rottier P B. Some mechanical properties of human abdominal skin measured on excised strips: A study of their dependence on age and how they are influenced by the presence of striae. *Dermatologica*, 1958, 117(2): 65–83.
- [55] Knight B. The dynamics of stab wounds. *Forensic Science*, 1975, 6(3): 249–255.
- [56] Green M A. Stab wound dynamics: A recording technique for use in medico legal investigations. *Journal Forensic Science Society*, 1978, 18(3-4): 161–163.
- [57] Brett P N, Parker T J, Harrison A J, et al. Simulation of resistance forces acting on surgical needles. *Journal of Engineering in Medicine*, 1997, 211(4): 335–347.
- [58] O' Callaghan P T, Jones M D, James D S, et al. Dynamics of stab wounds: Force required for penetration of various cadaveric human tissues. *Forensic Science International*, 1999, 104(2-3): 173–178.
- [59] Frick T B, Marucci D D, Cartmill J A, et al. Resistance forces acting on suture needles. *Journal of Biomechanics*, 2001, 34(10): 1335–1340.
- [60] Figge F H J, Barnet D J. Anatomic evaluation of a jet injection instrument designed to minimize pain and inconvenience of parenteral therapy. *American Practitioner and Digest of Treatment*, 1948, 3(4): 197–206.
- [61] Davis S P, Landis B J, Adams Z H, et al. Insertion of microneedles into skin: Measurement and prediction of insertion force and needle fracture force. *Journal of Biomechanics*, 2004, 37(8): 1155–1163.
- [62] Shergold O, Fleck N A. Mechanisms of deep penetration of soft solids, with application to the injection and wounding of skin. *Proceedings of the Royal London Society A*. London, 2004, 460: 3037–3058.
- [63] Purslow P P. Measurement of the fracture toughness of extensible connective tissues. *Journal of Materials Science*, 1983, 18(12): 3591–3598.
- [64] Doran C F, McCormack B A O, Macey A. A simplified model to determine the contribution of strain energy in the failure process of thin biological membranes during cutting. *Strain*, 2004, 40(4): 173–179.
- [65] Pereira B P, Lucas P W, Swee-Hin T. Ranking the fracture toughness of thin mammalian soft tissues using the scissors cutting test. *Journal of Biomechanics*, 1997, 30(1): 91–94.
- [66] Granot I, Bartov I, Plavnik I, et al. Increased skin tearing in broilers and reduced collagen synthesis in skin in vivo and in vitro in response to the coccidiostat halofuginone. *Poultry Science*, 1991, 70(7): 1559–1563.
- [67] Nickerson J L, Drazic M. Young's Modulus and Breaking Strength of Body Tissues. Report AMRL-TDR-64-23, 1964: 1–11.
- [68] Gadd C W, Lange W A, Peterson F J. Strength of skin and its measurement. *Biomechanics Mono*, 1967: 184.

- [69] Harkness R D. Functional aspects of connective tissues of skin//Balazes E A. *Chemistry and Molecular Biology of Inter-Cellular Matrix*. London: Academic Press, 1970: 1309–1340.
- [70] Wainwright S A, Biggs W D, Curry J D, et al. *Mechanical Designs in Organisms*. London: Edward Arnold, 1976.
- [71] Arumugam V, Naresh M D, Sanjeevi R. Effect of strain rate on the fracture behaviour of skin. *Journal of Biosciences*, 1994, 19(3): 307–313.
- [72] Kamath Y K, Weigmann H D. Fractography of human hair. *Journal of Applied Polymer Science*, 1982, 27(10): 3809–3823.
- [73] Arumugam V, Naresh M D, Somanathan N, et al. Effect of strain rate on the fracture behaviour of collagen. *Journal of Materials Science*, 1992, 27(10): 2649–2652.
- [74] Arumugam V, Sanjeevi R. Effect of strain rate on the mode of fracture in elastoidin. *Journal of Materials Science*, 1987, 22(8): 2691–2694.
- [75] Veronda D R, Westmann R A. Mechanical characterization of skin-finite deformations. *Journal of Biomechanics*, 1970, 3(1): 111–124.
- [76] Lanir Y, Fung Y C. Two-dimensional mechanical properties of rabbit skin. I. Experimental system. *Journal of Biomechanics*, 1974, 7(1): 29–34.
- [77] Marcellier H, Vescovo P, Varchon D, et al. Optical analysis of displacement and strain fields on human skin. *Skin Research and Technology*, 2008, 7(4): 246–253.
- [78] Stemper B D, Yoganandan N, Pintar F A. Mechanics of arterial subfailure with increasing loading rate. *Journal of Biomechanics*, 2007, 40(8): 1806–1812.
- [79] Snedeker J G, Niederer P, Schmidlin F R, et al. Strain-rate dependent material properties of the porcine and human kidney capsule. *Journal of Biomechanics*, 2005, 38(5): 1011–1021.
- [80] Sanghavi P, Bose D, Kerrigan J, et al. Non-contact strain measurement of biological tissue. *Biomedical Sciences Instrumentation*, 2004, 40: 51–56.
- [81] Green M A. Stab wound dynamics—a recording technique for use in medico-legal investigations. *Journal Forensic Science Society*, 1978, 18(3-4): 161–163.
- [82] Purslow P P. Positional variations in fracture toughness, stiffness and strength of descending thoracic pig aorta. *Journal of Biomechanics*, 1983, 16(11): 947–953.
- [83] Ramalho A, Silva C L, Pais A A C C, et al. In vivo friction study of human skin: Influence of moisturizers on different anatomical sites. *Wear*, 2007, 263(7-12): 1044–1049.
- [84] Adams M J, Briscoeb B J, Johnson S A. Friction and lubrication of human skin. *Tribology Letters*, 2007, 26(3): 239–253.
- [85] Nacht S, Close J A, Yeung D, et al. Skin friction coefficient: Changes induced by skin hydration and emollient application and correlation with perceived skin feel. *Journal of the Society of Cosmetic Chemists*, 1981, 32: 55–65.
- [86] Sivamani R K, Goodman J, Gitis N V, et al. Coefficient of friction: Tribological studies in man-an overview. *Skin Research and Technology*, 2003,

- 9(3): 227–234.
- [87] Gitis N V, Sivamani R K. Tribometry of skin. *Tribology Transactions*, 2004, 47(4): 461–469.
- [88] Buchholz B, Frederick L J, Armstrong T J. An investigation of human palmar skin friction and the effects of materials, pinch force and moisture. *Ergonomics*, 1988, 31(3): 317–325.
- [89] Comaish S, Bottoms E. The skin and friction: Deviations from Amonton's laws, and the effects of hydration and lubrication. *British Journal of Dermatology*, 1971, 84(1): 37–43.
- [90] Highley D R, Coomey M, DenBeste M, et al. Frictional properties of skin. *Journal of Investigative Dermatology*, 1977, 69: 303–305.
- [91] Comaish J S, Harborow P R, Hofman D A. A hand-held friction meter. *British Journal of Dermatology*, 1973, 89(1): 33–35.
- [92] Naylor P F. The skin surface and friction. *British Journal of Dermatology*, 1955, 67(7): 239–246.
- [93] Sulzberger M B, Cortese T A, Fishman L, et al. Studies on blisters produced by friction. I. Results of linear rubbing and twisting technics. *Journal of Investigative Dermatology*, 1966, 47: 456–465.
- [94] El-Shimi A F. In vivo skin friction measurements. *Journal of the Society of Cosmetic Chemists*, 1977, 28: 37–51.
- [95] Cua A B, Wilhelm K P, Maibach H I. Frictional properties of human skin: Relation to age, sex, and anatomical region, stratum corneum hydration and transepidermal water loss. *British Journal of Dermatology*, 1990, 123(4): 473–479.
- [96] Zhang M, Mak A F T. In vivo friction properties of human skin. *Prosthetics and Orthotics International*, 1999, 23(2): 135–141.
- [97] Bobjer O, Johansson S E, Piguet S. Friction between hand and handle. Effects of oil and lard on textured and non-textured surfaces; perception of discomfort. *Applied Ergonomics*, 1993, 24(3): 190–202.
- [98] Cadoret G, Smith A M. Friction, not texture, dictates grip forces used during object manipulation. *Journal of Neurophysiology*, 1996, 75: 1963–1969.
- [99] Smith A M, Cadoret G, St-Amour D. Scopolamine increases prehensile force during object manipulation by reducing palmar sweating and decreasing skin friction. *Experimental Brain Research*, 1997, 114(3): 578–583.
- [100] Akers W A. Measurements of friction injuries in man. *American Journal of Industrial Medicine*, 1985, 8(4-5): 473–481.
- [101] Sivamani R K, Maibach H I. Tribology of skin. *Journal Engineering Tribology*, 2006, 220(8): 729–737.
- [102] Dowson D. Tribology of the skin surface//Wilhelm K P. *Bioengineering of the Skin: Skin Surface Imaging and Analysis*. Boca Raton: CRC Press, 1997.
- [103] Sivamani R K, Goodman J, Gitis N V, et al. Friction coefficient of skin in real-time. *Skin Research and Technology*, 2003, 9(3): 235–239.
- [104] Sivamani R K, Stoeber B, Wu G C, et al. Clinical microneedle injection of methyl nicotinate: Stratum corneum penetration. *Skin Research and*

- Technology, 2005, 11(2): 152–156.
- [105] Sanders J E, Greve J M, Mitchell S B, et al. Material properties of commonly-used interface materials and their static coefficients of friction with skin and socks. *Journal of Rehabilitation Research and Development*, 1998, 35(2): 161–176.
- [106] O’Meara D M, Smith R M. Static friction properties between human palmar skin and five grabrail materials. *Ergonomics*, 2001, 44(11): 973–988.
- [107] Wolfram L J. Friction of skin. *Journal of the Society of Cosmetic Chemists*, 1983, 34: 465–476.
- [108] Elleuch K, Elleuch R, Zahouani H. Comparison of elastic and tactile behavior of human skin and elastomeric materials through tribological tests. *Polymer Engineering and Science*, 2006, 46(12): 1715–1720.
- [109] Asserin J, Zahouani H, Humbert P, et al. Measurement of the friction coefficient of the human skin in vivo. Quantification of the cutaneous smoothness. *Colloids and Surfaces B: Biointerfaces*, 2000, 19(1): 1–12.
- [110] Yamaguchi Y. *Tribology of Plastic Materials*. New York: Elsevier, 1990.

Chapter 6

Skin Biomechanics Experiments: Measurement and Influence of Different Factors

6.1 Introduction

Due to the importance in clinical and cosmetic applications, mechanical properties of the skin tissue have been studied *in vivo* and *in vitro* for a long time since the study of Langer, who punctured skin of human cadavers with a round instrument to study anisotropy in 1861.

In the earlier studies, many different instruments and measurement conditions are used, and although there is no consensus on the detailed constitutive properties of skin, much is known about its general response when subjected to a variety of quasi-static load conditions: human skin in general is under tension *in vivo* and its properties are heterogeneous, anisotropic, nonlinear and viscoelastic.

The tests skin mechanical behaviour can be generally divided into two categories, *in vitro* (*ex vivo*) and *in vivo*, where *in vitro* testing involves testing the skin tissue after removal from the living body, whereas *in vivo* tests examine the skin while it is still on the living body. The only truly reliable method to determine skin properties is through *in vivo* testing since the deformation may be strongly dependent on active processes while *in vitro* tests, the skin is away from its influential surroundings such as blood perfusion, lymphatic drainage, metabolism, nervous and hormonal controls^[1,2]. For example, during compressing, the resulting deformation is largely a function of fluid interchange with the surrounding unstressed skin^[3]. The epidermal tissue used for *in vitro* experiments was not perfused and thus lacked restorative fluidic pressures, which could potentially have aided in reducing the visible compression of the tissue after application of pressure^[4]. Besides, there is the absence of surrounding skin and underlying tissue *in vitro* where the skin strip can freely contract in width, this contraction being limited by the sur-

rounding skin *in vivo*^[5]. Further, the epidermis and dermis primarily consist of living cells, from which it can be expected that the properties of these layers will change during *in vitro* studies^[6]. *In vitro* test samples cannot also be kept for an extended amount of time, usually shrink once removed, and cannot be further modified *in vivo*^[7]. Thus results obtained from *in vitro* measurements can be misleading.

However, *in vivo* measurements are affected by both skin tissue itself and other structures it is attached to, which means it is technically very difficult to obtain a uniform strain field in the sample and control boundary conditions when performing, thus *in vitro* tests are also often used.

Some researchers have studied the difference between *in vivo* and *in vitro* results. Cook et al.^[8] found that *in vivo* tension is higher than *in vitro* tension for the same strain level in rat skin, while Vogel & Denkel^[9] and Vogel^[10] showed that there is little difference if the same gripping method is used. Marangoni et al.^[11] observed gross difference in mechanical properties of specimens *in vivo* and *in vitro*, and proposed a fast-freezing/thawing technique to reduce differences in specimens tested some time after excision. Jacquet et al.^[12] pointed out that the shape of the stress-strain curve depends on whether the test is performed *in vivo* or *ex vivo*. The stress-strain curve of *in vivo* test is shifted compared with the *ex vivo* test where the shift is related to the initial stress of the skin.

Most of the *in vitro* experiments of skin mechanical properties use tensile method, where it is now accepted that biaxial mechanical test can better mimic the sorts of deformation that *in vivo* skin experiences for the following reasons: ① *in vivo*, skin is subjected to biaxial tensions; ② as the fibers in skin are arranged in a multidirectional way, the orientation of the fibers with respect to the load axis must be taken into account; ③ for incompressible or nearly incompressible materials such as skin tissue, biaxial mechanical testing can be used to obtain the material parameters for three dimensional constitutive models; ④ multiaxial analysis is of obvious clinical importance to surgeons: if the orientation of maximum extensibility is known, the excision can be planned to optimize wound closure.

However, there exist many difficulties to perform tensile experiments on soft biological tissues^[13,14]: ① small specimen sizes, structural and compositional heterogeneity, and difficulty in precisely identifying material axes; ② influence of different gripping techniques and difficulty in gripping without causing damage; ③ difficulty in assuring constant forces along specimen edges; ④ large variability between specimens, and time-dependent changes

due to biological degradation; ⑤ homogeneity of deformation within the specimen. Additionally, compared with uniaxial test, the biaxial test has one more axis to be controlled; and more requirements appear, which include: ① the edges must be able to expand freely in the lateral direction, and in the central target region the stress and strain states should be uniform so that data analysis can be performed simply; ② the target region must be small and located far away enough from the outer edges to avoid the effects of specimen grips or tethers.

6.1.1 Contributions of different layers to skin mechanics

The overall mechanical behaviour of the skin is a combination of the mechanical behaviour of the different layers. So knowledge of the mechanical behaviour of the different skin layers is of great importance for the comprehension of the overall mechanical behaviour of the skin. The relation between the constitutive behaviour of skin and its microstructure is complex due to the various structures found within skin.

Most studies have ignored the contribution of the different top layers of the skin, especially the stratum corneum and assume that the behaviour of the skin is dominated by the collagen-rich dermis, e.g. Reference [6]. It seems reasonable that biomechanical properties determined from testing whole skin are mainly due to the dermal collagen, since similar results are obtained from collagen tests^[15]. In mammalian skins the dermis is typically twenty times thicker than the epidermis and dominates the overall constitutive behaviour^[16]. Dikstein & Hartzshtark^[17] observed no difference between mechanical behaviour of skin with and without SC. The epidermis contributes little to the skin's resistance to stretch^[18]. Silver et al.^[19] also found removal of the epidermis does not change the viscoelastic properties of skin. The histological examination also shows that the viscoelastic properties of the fetal rat skin was mainly caused by the dermis, and not the epidermis in nature^[20]. Although the epidermis is stiffer than the dermis, usually the contribution of the epidermis to the mechanical properties of full thickness skin is neglected^[21]. However, during *in vivo* tests, it is virtually impossible to isolate the dermis from the epidermis, thus the tests performed are also tests of properties of epidermis, stratum corneum, and hypodermis. It can be therefore expected that epidermis and stratum corneum have behaviour distinct from the dermis, because these layers have a completely different composition. However, there exists intimate connections between the various skin layers, which makes it difficult to isolate the contribution of the

dermis to the mechanical behaviour from that of the epidermis and the subcutaneous tissue^[22]. Till now, little progress has been made in examining the mechanical properties of the outer layer of skin, the stratum corneum, despite its importance in wound healing, medicine and cosmetics. This is due to the facts that: its thickness is very small (20~40 μm) and thus difficult to distinguish the response of the stratum corneum to the stimulus from that of the underlying tissue to which it is closely connected; stratum corneum properties are highly influenced by environmental properties such as temperature and relative humidity, both *in vivo* and *in vitro*. The available studies that focus on SC layer mechanics can be broadly divided into two categories^[23~26]: investigations of mechanical properties in plane^[27] and out of plane^[28]. Most investigations have concentrated on in plane properties where the extensional properties of *in vitro* SC has been measured using techniques such as the linear extensometer^[27] and dynamic mechanical spectroscopy^[29]. Recent investigations by Wu et al.^[30] have, instead, measured the fracture properties of SC in the direction normal to the skin surface. Wu et al.^[28] presented an *in vitro* mechanics approach to quantify the mechanical behaviour of isolated human SC in a direction perpendicular to the skin surface.

However, it can be expected that epidermis and stratum corneum have behaviour distinct from the dermis, because these layers have a completely different composition. The epidermis has been found to play a significant role in determining the mechanical properties of human skin^[31] and play a predominant role in skin frictional resistance^[32,33]. Other authors do recognize the influence of the stratum corneum on the overall mechanical properties of the skin. For example, Yuan & Verma^[23] measured the elastic and viscoelastic properties of stratum corneum at the micron level. The elastic moduli values obtained are on the order of 100 MPa and 10 MPa for dry and wet SC, respectively, which are about three orders larger than that of dermis. Moreover, it can be expected that these surface layers are more sensitive with respect to environmental changes like temperature and humidity^[6]. Guibara et al.^[34] found that the skin with no stratum corneum had a different response from the intact specimen under compression. De Rigal & Leveque^[35] measured the mechanical behaviour of stratum corneum by extending their torsional technique as described by de Rigal et al.^[36] and Agache et al.^[37]. The inner disc (18 mm) and the guard ring were glued to the skin, leaving a gap for the skin of 1 mm, 3 mm or 5 mm. They conclude that the contribution of the stratum corneum on the mechanical response of the entire

skin increases with a decreasing gap size, where the contribution of the stratum corneum is approximately 80% using a 1 mm gap. Park & Baddiel^[24,25] showed that the contribution of stratum corneum depends on the relative humidity: the Young's modulus of stratum corneum decreases a 100 fold with increasing relative humidity from 60% to 100%, and as the Young's modulus of totally hydrated stratum corneum differs only slightly from that of total skin. It has been shown that the stratum corneum layer could have a strong effect on the wave propagation due to its high stiffness relative to the dermis^[38]. Pereira^[14] indicated that thickening of the stratum corneum in some human skin diseases such as ichthyotic and xerotic disorders is responsible for a marked decrease in the flexibility of that layer. All these studies still probe SC mechanical properties on a macroscopic length scale. Wang & Hayward^[39] found that the glabrous skin in the small deformation range appears to be much stiffer than the hairy skin, the stiffest skin being about 10 times stiffer than the softest skin. They attributed the large difference to the different thickness of the stratum corneum layer.

6.1.2 Contributions of different constituents

Biomechanical testing of skin tissue is usually done on whole tissue. Studies of the mechanical properties of each component of the tissue, however, are important for elucidating the connection between the functional properties and the molecular structure. From the skin structure introduced in Chapter 2, we know that skin consists of two important mechanical components, namely, collagen fibers and elastin fibers, which are supported by a matrix or ground substance where polysaccharides and protein are linked to form macromolecules with a remarkable capacity for holding water in their domain.

The mechanical properties of skin are governed by the geometry and interaction of collagen and elastin networks in the dermis^[40], which involves both a viscous component associated with energy dissipation by molecular and viscous sliding of collagen fibrils during alignment with the force direction^[41,42] and an elastic component associated with energy storage as a result of stretching of flexible regions in the collagen triple helix^[43]. For example, Viidik et al.^[44] found that tissues composed of three-dimensional network of collagen with identical fibers but different geometrical configurations showed different mechanical behaviours. In skin tissue, there is also a third type of the fiber protein, reticulin, however, it is in small amount in the derma (only 0.4 % of the fat-free dry weight) and does not play important role in the skin

mechanical properties.^[45]

It is generally accepted that during the initial, low-stiffness region where energy and shape recovery are critical, the behaviour of the elastic fiber networks dominates and/or the proteoglycan matrix provides resistance to deformation while the collagen fibers align themselves parallel to the maximum stretch direction while either the elastin^[46,47]. Once the collagen fibers are sufficiently aligned, collagen dominates the high strain response and further extension of the skin requires extension of the collagen fibers, resulting in a significant increase in skin stiffness^[46].

1) Role of collagen

The results of enzymatic treatment of tissue lead to an assessment of the relative contribution of each structural component to the mechanical behaviour. Experimental research shows that the constitutive response of skin is correlated to the collagen contents within the dermis.

Selective removal of the elastin fibers in dermis by elastase^[48,49] does not impair the ability of the remaining components (almost overwhelmingly collagen fibers) to support and recover from stresses and elongations about as large as those supported by the intact dermis; while enzymatic degradation of the collagen fibers in a specimen of dermis leads to complete loss of its mechanical integrity^[50]. Oxlund & Andreassen^[51] found that collagen is mainly responsible for the tensile strength of skin. Osborn et al.^[52] found that tight-skin mice, whose skin is stiffer than controls, have increased collagen in skin. Several studies on animal skins have shown that the ultimate tensile strength is higher when collagen matrix is denser^[53]. Vogel^[54] demonstrated that a denser collagen matrix in human skin leads to an increase in the tangent modulus at high strain rate and he also attributed the stiffness decreases in old subjects to the degradation of the skin collagen network. However, Corcuff et al.^[55] pointed out that the change in skin thickness with aging is due to a flattening of the collagen bundles, rather than a reduction in collagen content, which was confirmed by the experimental results of Smith^[56] and Hall et al.^[57].

The skin stiffness calculated according to volume fraction of collagen was found different to the measured values, and Manschof & Brakkee^[58,59] explained this as only a part of all fibers were involved in the straining process in one direction; the angular distribution of the fibers, which results also in a difference in stiffness between “along” and “across”; and the non-uniform fiber geometry, by which only a part of all the fibers were straightened and stretched as observed by Brown^[60]. An increase in collagen crosslinking was

found to increase the viscoelastic storage and loss moduli of guinea pig skin under dynamic loading^[61]. It is the reorientation of the collagen fibers within these networks that allows large extensions of the tissues and is responsible for their non-linear stress–strain curves^[62]. Reorientation of collagen fibers due to finite extension gives rise to the nonlinear load extension curve of skin^[63]. The long-range extensibility of skin tissues is accommodated by significant reorientation of their collagen fiber networks^[64]. The constitutive behaviour of skin depends upon the structure and density of the collagen fibers found within the dermal layer^[54]. Besides experimental studies, models taking into account separate roles of collagen (in tension) has also been shown to be able to describe the stress relaxation behaviour^[65].

However, the constitutive response of skin can't be explained solely in terms of the constitutive properties of an individual collagen fibre. The collagen fibres can be considered as elastic-plastic rods with Young's modulus from about 100 MPa^[66] to even 1 GPa^[67] in the linear region which yield at 10% engineering strain and fail at 20% engineering strain^[68]. It has been shown that the Young's modulus of skin is only in the order of 1 MPa at low strains, and engineering strain in excess 1.0 maybe achieved before a specimen of skin fails in a uniaxial tensile test. The greater flexibility of skin compared to an individual collagen fibre is attributed to the capacity of the network of fibres to align and straighten in the direction of an applied strain^[69,70]. Consequently, at low engineering strains (< 0.3 ^[71]) the constitutive response of skin is dominated by the bending stiffness of the collagen fibres and the viscous shear between the fibres and the ground substance^[42,72], whilst at a higher engineering strains (> 0.4) the constitutive response of skin is dominated by tensile elastic response of the collagen fibres^[41]. At high engineering strains (> 0.6 ^[73]) this assumption appears reasonable: the tangent modulus of skin (ca. 20~70 MPa^[54,74]) is approximately 3%~10 % of the Young's modulus of a collagen fibre, is comparable to the 10% volume fraction of the hydrated collagen within skin^[75] and the proportion of fibres that likely to be aligned in the direction of the applied strain.

Contradictory results have also been reported. Del Prete et al.^[76] studied the correlation of skin mechanical properties with collagen content by using three types of mice known to differ with regard to content of type I collagen and found no obvious correspondence, which was attributed to the large number of changes, including alterations in the composition and structure of the skin, caused by genetic defects.

2) Role of elastin

Elastin fibers are the second main component of the dermis (see Chapter 2). They appear to be a highly compliant material (much less stiff than collagen) and exhibit elastic behaviour over a large strain range^[77], showing reversible strains of more than 100%^[22].

With mechano-enzymatic and mechano-histological methods, it has been observed that the elastin fibers are the first to be stretched when the skin tissue is strained^[41]. Their effect on the response of whole skin is thus significant at low level of strain when the collagen fibrils are still crimped. For example, the stress-strain curve of elastin-free human skin^[49] shows that elastin supports the entire load up to strains of about 50%, at about this strain level the slope begins to increase rapidly as collagen fibers presumably carry the major part of the load to higher strain levels up to fracture. The similar results has also been obtained by Lanir & Fung^[78] who found that at low strain level skin has a negative thermal expansion coefficient (as in elastin) while at higher strain level it is positive (as in collagen). The elastic modulus of elastin has been found to be approximately 1 MPa^[79], which agrees well with the Young's modulus of skin at low strain level. Elastin and proteoglycans dominate the low and intermediate strain responses, and are affected by preconditioning and PG depletion^[46]. Silver et al.^[19] also pointed out that the initial portion of the stress-strain curve involves stretching of the elastic fibers, which have an elastic constant of about 4.0 MPa and during this portion, the collagen fibrils and fibers are presumably folded so that deformation involves little collagen molecular stretching and slippage. Reihnsner et al.^[80] pointed out that while collagen is the main source of strength and stiffness of skin, elastin fibers forming a scattered delicate network between the collagen fibers are thought to be especially responsible for the recoiling mechanism after a stress or deformation has been applied. Oxlund et al.^[71] showed that degradation of elastin in skin by use of elastase plus soybean trypsin inhibitor significantly increases the strain, at a given tensile load, more than would be expected if elastin and collagen form separate interpenetrating networks that deform in an affine way, indicating disappearance of load bearing properties of the elastin fibers of the skin at small stress values.

However, some other researchers gave contradictory arguments. Manschot^[66] found that there was a significant correlation between the ultimate skin stiffness and the initial skin stiffness, which showed elastin was not relevant for the (initial) stiffness. Manschof & Brakkee^[58,59] and Belkoff & Haut^[81] pointed out that the elastin fibres can only make a minor contribu-

tion to the constitutive response due to its small proportion in the dry weight of the dermis (less than 1% of the dry weight^[82]) and low modulus^[83]. The results of their model without considering elastin agreed well with their experimental results, which further confirmed their argument. Oxlund et al.^[71] argued that enzymatical treatment with buffered elastase for elastin extraction caused the skin to become more lax, to exhibit larger deformation and loss of elastic behaviour at small stress levels, to show an increase in the high strain stiffness, but not to affect the time scale of viscoelastic relaxation, based on which they suggested that Daly's conclusion may have been misguided.

3) Role of ground substance

The ground substance is a gel like substance containing a class of chemicals including glycosaminoglycans (GAG), proteoglycans and glycoproteins.

The mechanical properties of a connective tissue are strongly correlated with the type and amount of glycosaminoglycans^[84]. This positive correlation exists in comparing skins from different sites within an animal, in comparing different species, and in comparing skins at various stages of development^[85]. For example, in altricial animals, there is a greater content of hyaluronic acid, a proteoglycan functionally designed for its hydrophilic properties but not particularly strong. In precocial animals, their more mature skins at birth contain a greater proportion of sulfated proteoglycans (keratin sulfate), glycosaminoglycans designed to withstand greater mechanical forces.

The ground substance has been shown to contribute mainly to the viscoelastic behaviour of skin^[40], which slows down the mechanical processes in the skin; this can be regarded as manifest of viscosity^[45]. For example, Oxlund & Andreassen^[51] found that treatment with hyaluronidase or with α -amylase to remove free macromolecules including hyaluronan, had no effect on the stress-strain curve of rat skin. Kronick & Sacks^[86] used salt extraction or treatment with hyaluronidase and found no influence on the viscoelasticity of bovine reticular dermis, while using both chondroitinase ABC together with hyaluronidase reduced the dynamic modulus of calf skin at low strains. Vogel^[87] suggested that a correlation exists between the course of changes in the coefficients of relaxation and the content of GAG in skin. Gillard et al.^[88] noted a difference in the GAG composition of loaded and unloaded areas of skin, where they observed increased hexuronic acid in the loaded dermis. Based on this, they speculated that dermatan sulphate may be more associated with tensile mechanisms whereas hyaluronic acid may relate to hydroelastic systems. Haut^[68] further showed that the sensitivity

of tensile strength to strain rate and the GAG content of dorsal rat skin decrease with age during maturation of the animal. It has been indicated that the ground substance probably plays a major role when the tissue is under compression^[89]. Veronda & Westmann^[63] observed both increase and decrease in volume of skin tissue during uniaxial tensile loading: at a certain stress level, the strained fibers collapse the oil glands of the dermis and cause exuding of oil. The ground substance then occupies the voids which were previously filled oil ducts, which causes the dermal fibers to return to a new neutral position upon unloading and induces the inelastic character of skin.

The similar results have also been reported for other collagenous tissues: the viscoelastic behaviour of soft tissues has been associated with the shear interaction of collagen with the matrix of proteoglycans^[90] and it has been shown that the removal of ground substance in tendon, aorta and ligamentum nuchae induced a decrease in stress level, stiffness, relaxation hysteresis and other time-dependent effects^[91].

6.2 *In Vivo* Measurements

6.2.1 Measuring methods

The most frequently used techniques in the *in vivo* characterization of skin mechanical properties are tensile, indentation, torsion, suction tests and wave propagation, each of which tests makes use of a specific approach related to the type of stress applied^[92].

1) Tensile

In vivo tensile test of skin mechanical properties is the most often used method where load parallel to the skin surface is applied. The most popular instrument using this method is extensometer. The tensile test has been the subject of numerous studies^[93,94], and from it, different models based on empirical formulations have been proposed to account for the mechanical behaviour of human skin^[95,96]. For example, through the use of *in vivo* tensile creep test, Jamison et al.^[97] shown that skin tissue (guinea pig skin and chamois skin) can be considered as viscoelastic materials. They measured the deformation of the soft tissues by the combination of a scaled grid attached to a fixed grip and a pointer fastened to the movable grip, while time was recorded by photographing a stop watch and the two grips with a movie camera. From the results, they developed a viscoelastic model.

2) Compression

Which use the most often testing method is mechanics to investigate the mechanical behaviour of skin under compression. Plenty of works have been

done by former researchers^[98].

The most important thing that needs to pay attention here is the friction between the clasper and the sample. Sometimes it is so big that the data is greatly influenced. What researchers do most frequently to this problem is smearing some lubrication on the interface of the sample and clasper. The choice of the lubricate shall be: first, lubricity enough so that the friction there is small enough, which will show little influence on the data. Second, the lubricate can not have any influence on the morphology and functionality stability of skin. John et al.^[99] did a lot of work at this. He used the universal micro-mechanical testing machine (model match-I, biosyntech, Montreal, Canada) with a high resolution of displacement and load cell. A traditional composite material mechanics was used to draw the mechanical behaviour of different layer of skin.

The dynamic compressive performance of skin is also performed by^[100] to see the energy absorption ability with focusing on the disasters that happens during the cars crash or other accidents happens in the operation. A SHPB method is used here to investigate the rate dependence of the dynamic response of skin.

However another method is also used here which glue the sample to the platen of the machine. Esra Roan et al.^[101] performed an experiment called no-slip method who first ignore the friction and later a comparison was given with the one without friction with a maximum error of 50%.

3) Indentation

Indentation uses the application of a negative trust through a disc or point (for example a plane ended cylinder, a cone shaped tip or a sphere) glued to the skin and apply a specific force or deformation to the skin^[102~105]. This method is one of the simplest and easiest to perform, and has been used in clinical medicine as a diagnostic tool to test for changes in mechanical response seen in many skin diseases.

Dikstein & Hartzstark^[17] used *in vivo* low-pressure indentometry (100~1000 Pa) on 0.2 cm² human forehead skin to evaluate the influence of the stratum corneum on the measured amount of indentation deformation. They measured on moisturized skin, on skin after removal of stratum corneum by stripping, on control samples, and on skin treated with enzyme injections, which effect the dermis composition. Bader & Bowker^[102] used a plane-ended indenter to study mechanical behaviour of skin and underlying tissue, where a constant load was applied for two minutes, then the load was removed and the tissue was allowed to recover for two minutes. 11.7 kPa was applied

through a 20 mm diameter indenter at the forearm, and 7.0 kPa was applied through a 40 mm indenter to the thigh. Like in the torsion experiment, skin shows immediate deformation after load application, creep, partial immediate recovery and a long term recovery. At reapplication of load, a similar pattern is found, but all deformations are smaller. Zheng & Mak^[104] developed an ultrasound indentation system to study mechanical properties of soft tissues. They combined a load cell (10 N ranges) and an ultrasound transducer (0.25-inch diameter, 5 MHz), which was simultaneously used as an indenter, in a pen-size, hand-held probe. Several ultrasound probes could be combined with the load cell. With this apparatus deformations of different tissue layers could be measured in real time with an accuracy of 0.02 mm and 10 ns. The system was validated by combining the results of test on porcine tissue using the newly developed probe and a Hounsfield material testing machine. A quasi-linear viscoelastic model was employed to characterize porcine tissue.

But it is hard to get an exact model to describe the mechanical behaviour of skin. Besides in the indentation test of skin, the postulate is skin is regard as a membrane which regardless of the influence of soft tissue under skin. And the use of the parameter that derive from the model still need some improvement.

4) Suction

Suction applies a negative pressure to the skin (usually in the range of 50~500 mbar) via a circular aperture in a measuring probe and measure the corresponding skin elevation with an optical or ultrasound methods^[106~109]. Alexander et al.^[106] reported results on the mechanical properties of skin *in vivo* using a racetrack-shaped suction cup, where a one-dimensional pretension device consisting of two pads with strain gauges mounted on cantilever legs to determine the natural tension in the skin and the anisotropy. With the pretension device still in place, removing the natural tension from the skin, the suction cup was deployed between the two pads, where the pressure inside the cup was decreased at a constant rate down to a typical value (7.5 kPa). The pressure and the central deflection of the skin were continuously measured. Their results demonstrated that a uniform strain field on the skin in the central part of the cup (between the parallel sides) can be achieved. With the suction method, two different commercial instruments have been developed, the Dermaflex and the Cutometer, both using an optical system.

5) Torsion

Torsion applies a torque to the skin by attaching a guard ring and an

intermediary disc to skin surface^[110~113], which has two advantages^[113]: hypodermis and underlying tissues have not effect the measurements and the anisotropic character of the skin is minimized. For example, Agache et al.^[37] applied a torque of 28.6×10^{-3} N·m for 2 minutes to the dorsal forearm skin by using a 25 mm diameter disc surrounded by a 35 mm diameter guard ring fixed to the skin by double adhesive tape, where a pressure of 12.6 kPa is applied to the disc to assure constant skin contact. The applied torque resulted in a rotation of $2^\circ \sim 6^\circ$ and Young's moduli are evaluated for the linear part of the stress-strain curve. They claim that the resistance of the hypodermal connections is practically negligible, as the skin is readily movable over underlying muscle. Using a guard ring with inner diameter 24 mm and central disc with diameter 18 mm, Escoffier et al.^[113] applied different torques in the range of $2.3 \times 10^{-3} \sim 10.4 \times 10^{-3}$ N·m for 60 seconds on the ventral forearm, which resulted in an immediate deformation, followed by a time dependent increase (the viscous part). Release of the torque leads to an immediate decrease in deformation (immediate recovery) followed by a very slow recovery to the initial state. Grebenyuk & Uten'kin^[114] applied a constant torque to various anatomical sites on 12 year old children for several seconds, resulting in $7^\circ \sim 10^\circ$ rotation, causing no wrinkles.

6) Wave propagation

Wave propagation is a method where a low frequency elastic surface wave is applied and the surface wave speed is measured^[115]. Vexler et al.^[116] pointed out most of the above methods deform transiently the fibers network of the skin and therefore affect the readings; those based on suction are limited in the range of viscoelasticity that they can evaluate; and they cannot evaluate anisotropy of the skin. The principles of wave study lies on the dynamic mechanics of viscous solid. With a periodic force with a constant frequency of force or displacement, there will be a consequent reaction of displacement or stress of the skin. A difference between the force/displacement and the resultant displacement/force will be figure out. According to the difference, the existing model of skin can be tested and tell which one is the most proper one that fit the result best.

6.2.2 *In vivo* skin testing devices

Till now, many different types of devices have been developed and used to perform the above-mentioned *in vivo* test of skin mechanical behaviour. The measurement systems differ in the type of deformation and how stress is applied to skin, such as tension, torsion, suction, indentation, elastog-

raphy, wave propagation, etc. Some of the devices are even commercially available, where some of the basic devices used to study skin *in vivo* properties include the Cutometer[®], the Dermaflex A[®], the “echorheometer,” Gas-bearing electrodyneometer and linear skin rheometer, the extensometers, the Durometer[®], the microindentometer, and the Dermal Torque Meter[®], and the ballistometer. There are several extended overview^[4,125,194,195] on this topic.

6.3 *In Vitro* Measurements

In vitro tests typically involve removing animal or dead human skin. The most obvious advantage of *in vitro* testing on the skin is the relatively easiness in setting the cross-section of the sample, boundary conditions, and direction of loading in advance, where classical testing methods can be used (i.e. tension or compression tests using Instron testing machine). Another advantage of *in vitro* testing on the skin is the possibility to separate the skin layers. However, it is not clear what the effect is of this disruption on the mechanical properties of the individual skin layers. A third advantage is the possibility to perform tests for strength, time-dependent values, and non-time-dependent values.

Most tissue experiments conducted in the past have been *in vitro* studies and the experimental data has been collected from the excised and shaped tissue samples. In this section, *in vitro* methodology for experimentally characterizing the skin mechanical properties is presents.

6.3.1 Measuring methods

Numerous *in vitro* experiments have been performed to characterize the mechanical behaviour of skin tissue in the past. Several devices for uniaxial and biaxial mechanical properties evaluation of skin tissue under nonsterile conditions have been described. An overview can be found in Lanir^[117], Marks^[15] and Wilkes et al.^[21].

1) Uniaxial tests

The uniaxial test^[118~120] has probably been the most commonly used technique in research on the mechanical properties of skin. These are simple to use and are well suited for measurements of directional mechanical effects. Many of the uniaxial tests use Instron testing machine^[120]. Besides commercial equipments, custom designed devices have also been used. For example, Vogel & Papanicolaou^[121] presented a system for constant creep testing and

Arbogast et al.^[122] presented a high-frequency shear device for testing soft biological tissue.

Uniaxial tests are relatively easy to perform and interpret, and have also provided a lot results for the understating of skin mechanical behaviour, however, it cannot provide a unique description of the tissue's three-dimensional constitutive properties. While the general three-dimensional constitutive properties also cannot be deduced from biaxial data alone, in some cases they can be inferred when biaxial data are combined with those from another type of test such as torsion or shear. Thus, biaxial tests are a step towards a full description of the constitutive properties of tissue.

2) Biaxial Tests

Compared with uniaxial testing, biaxial mechanical testing has several advantages: ① *in vivo*, skin tissue is loaded biaxially; ② as the fibers in skin tissue are multi-directional, the orientation of the fibers with respect to the load axis must be taken into account; ③ for incompressible or nearly incompressible materials, biaxial mechanical testing can be used to obtain the material parameters for 3-D constitutive models; ④ pursuit of a multiaxial analysis is of clinical importance to surgeons for if the orientation of maximum extensibility is known, the excision can be planned to optimize wound closure; ⑤ uniaxial test can also be performed with a biaxial testing system by loading in only one direction.

Several devices to apply in-plane loads in two orthogonal directions have been developed^[123~125], where Lanir & Fung^[123] were the first to apply biaxial testing to skin. Lanir & Fung^[123] developed a biaxial rig set-up that could measure several mechanical properties in a square shaped soft tissues, as shown in Figure 6.1. The sample was placed in a chemical bath, each side connected with hooks to several silk threads, which were then connected to a force transducer, a pulley system and a displacement motor at the other end. With this set-up, a variety of different loadings to the tissue sample have been achieved: the stress-strain relationship was measured by changing the displacement on one axis while maintaining a constant displacement on the other, or by dynamically changing the displacement on both axes simultaneously; stress relaxation was measured as the rate of change in force after a rapid increase in displacement, while creep was measured as the rate of change in displacement when a constant force was applied. In this rig, a loading speed up to 6.0 mm/s can be achieved and effect of the temperature can also be measured. Lanir & Fung^[123] performed a number of experiments on *in vitro* rabbit skin, from which Tong & Fung's model^[126] was derived.

Schneider et al.^[127] used the biaxial rig developed by Lanir & Fung to perform a study on *in vitro* human skin.

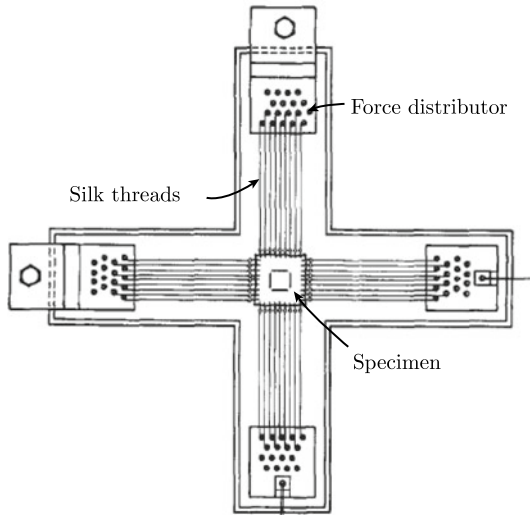


Figure 6.1 The biaxial rig setup of Lanir & Fung^[123] (by permission of Elsevier)

Most of later biaxial systems are based on the system of Lanir & Fung^[123]. For example, Thubrikar & Eppink^[128] presented a system for biaxial bending and shearing method. Hung & Williams^[129] presented a system where equibiaxial and uniform strains can be achieved. Mitchell et al.^[130] presented a biaxial device which can be used to apply user-specified strains to soft tissue such as skin. Sanders et al.^[131] presented a system which can be used to applied controlled compressive and shear load to skin surface.

More recently, multiaxial systems have also been developed. Reihnsner & Menzel^[124] presented a similar system with that of Lanir & Fung^[123] but for circular sample with 12 axes, where twelve step motors with strain gauges are in a circular arrangement and loadings can be imposed on the tissue sample along six different axes, as shown in Figure 6.2. With this system, Reihnsner & Menzel^[124] investigated the mechanical properties of *in vitro* human skin at sixteen different locations on five human cadavers of different ages. Kvistedal^[132] extended this design to a multiaxial testing rig with sixteen displacement actuators, each equipped with a force transducer, arranged in a circular array. This allowed a variety of strain states to be imposed on the tissue along eight different axes^[133].

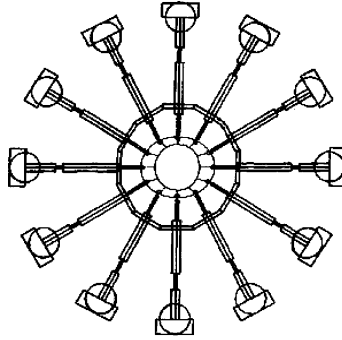


Figure 6.2 The multi-axial rig setup^[80] (by permission of Elsevier)

6.3.2 Mechanical measurement

1) Force measurement

Square samples with multiple attachments on each edge is generally connected to motor arm and loading is applied by using electric motors with gears^[125] or stepper motors^[134]. Besides the generally used measurement by load cell, other advanced methods have also been used to measure force, such as atomic force microscope^[23].

2) Displacement and strain measurement

As for the measurement of strain, two fundamental approaches have been used in previous biomechanical studies on isolated soft biological tissue: direct contact systems and optical systems^[135]. Direct contact systems involve attaching a transducer to the tissue during a mechanical test. Commonly used displacement transducers include extensometers, liquid metal strain gauges, and Hall effect strain gauges^[136].

Saint-Venant effect, stating that strain measurements based on the grip-to-grip displacement may grossly overestimate the specimen, has been observed in uniaxial connective tissue samples^[137,138], which suggests measurement of strains should be made at the local of sample centre. For example, for a tissue sample with aspect ratio of 8 : 1, Saint Venant's principle implies that end effects fall to 1% of their values at the grips within one strip width distance from the grip edges along the sample axis and so the strain field in the center of these samples should be uniform. However, Wright et al.^[139] pointed out that for soft tissues Saint Venant's principle is not strictly applicable and end effects may extend further into the sample and so the strain field at the center may in fact have been less uniform than intended. Since Saint-Venant effect depends significantly on the material axes orientation^[140] and skin tissue is of high anisotropy, optical measurement of strain is pre-

ferred. Another advantage of optical systems is that the loading response of the specimen is virtually unaffected because, except for the markers, nothing comes in contact with the specimen.

Direct contact systems (displacement transducers)

Direct contact systems involve attaching a transducer to the tissue during a mechanical test. Commonly used displacement transducers include extensometers, liquid metal strain gauges, and Hall effect strain gauges^[136]. But this kind of measuring method has an instinct flaw: additional stiffness will be appended to the result, which makes skin seem a little stiffer.

Optical strain measurement systems

Because of the non-contact convenience of optical measurement method more and more test rig use this method to perform the experiment. Basically there are two methods to perform the optical test: one is based on the markers movement analysis, where markers with a small radius are arranged in a square grid that has a regular shape. Another method is based on the comparison of two figures that recorded before and after the deformation, say image correlation method (ICM).

Optical strain measurement systems in various forms have been used by many investigators, where markers are affixed on the tissue surface and the strains are inferred by comparing the displacements of the marker directly measured using a camera with the initial reference image. Till now, many different kinds of optical methods have been used and one of the most used is the video dimensional analyzer (VDA)^[141]. Although VDA has been widely used due to its simplicity and easiness to apply, it has many drawbacks^[142], such as only one dimensional strains can be measured, strains are averaged over the distance between the parallel markers, and the frequency response is low. Other methods include stereomicroscope-dial indicator method^[143], low speed photography^[137], light board^[144], high-speed, high-resolution video digitizing system^[145].

Derwin et al.^[135] pointed out that most of above methods have drawbacks due to the radial distortion and a geometrically decentered optical center. They advised to utilize a higher lensf-stop by adjusting lighting and thus increase the depth of field for non-idealized experimental tests where the surface of the tissue is not perfectly smooth. Finite element method is then used to calculate the plane strain tensor at any point inside the element.

The effect of marker size has been studied by Smutz et al.^[136], who found that both the static and dynamic errors were independent of marker size for loading rates smaller than 50% of the camera field of view (CFV) per second

while the marker size did have an effect on the dynamic error for loading rates greater than 50% of CFV per second.

6.3.3 Effect of different factors on measurements

1) Effect of boundary conditions

In the biaxial testing the edges must be able to expand freely in the lateral direction, and in the central target region the stress and strain states should be uniform so that data analysis can be performed simply; the target region must be small and located far away enough from the outer edges to avoid the effects of specimen grips or tethers^[13]. Besides, the high compliance of skin made it difficult to mount samples in the testing machine without taking special precautions^[146]. It is thus imaginable that the sample geometry of soft connective tissue and the method of gripping the sample edges have profound effects on any measured mechanical properties since they directly influence how the load is transferred to the underlying fibrous network^[147~150]. The most used gripping methods are clamp gripping and suture gripping, as shown in Figure 6.3.

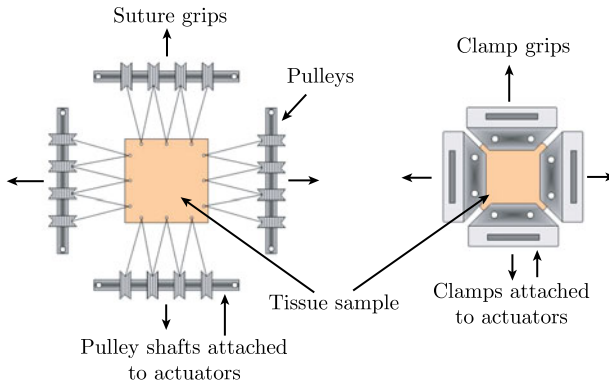


Figure 6.3 Different holding methods

Clamp

Numerous designs of pure mechanical clamps have been developed, such as flat-surfaced clamps, where the free ends of tissue were air-dried before fastening^[68], jaws with high-friction surfaces^[151~153], sand paper^[154], glue the skin end to two plexiglass plate^[155], and more recently cryogenic holder^[147]. Clamping methodology can be improved by methods such as increasing the clamped area of the connective tissue^[156], using two concentric cones^[157], using a layer of Neoprene rubber or glue^[158].

However, classical grips which apply a pressure on the sample ends lead to a slippage of the sample if the pressure is too low, or damage of the sample near the grips if the pressure is too high^[147]. Gluing the samples to the grip can be successfully done for very thin samples. However, if samples are too thick there is shear between the fixed sample sides and the sample core, giving a complex pattern of strain in this region^[159] and the inner fibers of the sample are less strained than the fibers at the surface. Despite the reduced slippage or failure of connective tissue at the clamping site, a non-uniform loading pattern may occur, with uneven fiber recruitment of the tissue under tension^[160] and the constraint on the extracellular fibers at the bounds of the sample is induced^[149], which will result in low measurement precision and non-repeatability^[146].

Suture

Due to the drawbacks of clamping described above, many researches have used suture^[161], where a specimen is attached to loading assemblies by several continuous loops of medical suture per edge since using thin threads allows the free expanding of sample edges in the lateral direction^[13], as shown in Figure 6.3. However, suturing sample edges might result in a discontinuous load transfer to the underlying fibrous network since only discrete groups of fibers within the vicinity of the suture attachment point are loaded^[149].

Waldman & Lee^[149] compared the dynamic biaxial mechanical response of soft biological tissue samples under suturing and clamping under the same conditions. It was found that the tissue samples appeared to be stiffer and less extensible when mechanically tested with clamped sample edges, as opposed to when tested with sutured sample edges; and suture attachment methods demonstrated minimal boundary effects where four suture attachments are sufficient to obtain uniform stress field in biaxial testing. The same results have also been obtained by Sun et al.^[140], who found that there were strong boundary effects with the clamped methods, which resulted in the fact that the inner region was not fully loaded and therefore not fully stretched and makes the tissue appear to be substantially stiffer.

2) Effect of sample size and geometry

Nilsson^[153] studied the influence of sample size of abdominal wall tissue from rabbits on its mechanical behaviour and found that the mechanical characteristics of specimens, when the width was kept constant, depended upon the fiber orientation in the specimens and the length of the specimens while width has no effects. The difference between the mechanical characteristics of short and long specimens was explained as that the short specimens contain

relatively more fibers running all the way through the specimen from clamp to clamp than do the long specimens. The similar sample length effect has also been observed in other soft tissue such as tendon^[162].

As for biaxial testing, different sample geometries have been adopted, such as square specimen^[123], circular specimen^[163], cruciform specimen^[164]. Waldman & Lee^[148] studied the effect of the sample arms length for cruciform specimen, and found that as the length of the sample arms are reduced, an apparent increase in stiffness and decrease in extensibility of the material sample will occur presumably due to an increasing proportion of collagen fibers that fully extend between the grips. They then pointed out that samples should be created to ensure that the majority of the extracellular reinforcing fibers are effectively contained with the grips.

3) Effect of preconditioning

Viscoelasticity is readily evident in many soft tissues, where there is energy dissipation, or hysteresis, between the loading and unloading of the tissue during mechanical tests. It has also been shown that in the initial cycles of a cyclic test on soft tissue, the stress strain curve forms hysteresis loops, which continually decrease and then stabilize. This period, leading to repeatability of the stress-strain curve, is called preconditioning. Generally, the natural state of soft tissue is difficult to obtain, which can be used as a reference state. Thus the soft tissue has to be preconditioned in order to obtain repeatable measurements. Preconditioning has been observed in skin tissue both *in vitro* and *in vivo*^[165~169].

If skin has uniaxial tension applied *in vitro*, there may be a progressive decrease in the total volume of the stretched specimen when fluid is physically extruded from the specimen^[166]. Initially, as tension is applied to skin, a small load results in extension, but this phase is followed by a phase in which much greater loads are required for similar extensions^[170]. *In vitro*, preconditioning was found to be recoverable upon rest, with time constant of the order of several hours. Fung^[167] found that successive cyclic uniaxial tests of tissue yield unequal results which converge as the number of cycle increases and one way to ensure repeatability of results is to precondition the tissue by carrying out a test procedure several times until the results converge. Lanir & Fung^[123] found that the descending curve of biaxial tests does not terminate in the origin and a preconditioned specimen will return to the original dimensions only after a long period of relaxation. Lanir & Fung^[78] found that the effects of preconditioning are reversible if no damage has been caused. Recovery of both initial configuration and initial response

will occur provided the specimen has not contracted in any planar direction. Vogel & Denkel^[168] studied the mechanical behaviour of rat skin in repeated straining and found that only the skin *in vivo* reached a full recovery after cyclic straining; the skin *in vitro* could not recover to its “natural” state after being strained. This finding further supported Fung’s preconditioning theory. Lanir^[17] found that the preconditioning caused a parallel increase of gauge length in uniaxial tests and configurational changes in biaxial tests. Nicolopoulos et al.^[119] found that preconditioning significantly reduced the fracture energy of stratum corneum. Edsberg et al.^[169] found that static pressure alone altered the tissue’s mechanical properties more than dynamic pressure cycles. Tissue subjected to pressure prior to uniaxial tensile testing always was less stiff than control tissue, which was maybe due to the damage to the initially randomly oriented tissue collagen fiber bundles in the fibrous matrix caused by sustained compression. Eshel & Lanir^[46] studied the effects of the preconditioning on the stress/strain relationship using rat dorsal skin and found that the maximum stress at each cycle decreases with cycle number up to a steady state after several cycles and the preconditioning is strain specific, which means a new process of preconditioning is needed if the strain level is different from that for the previous preconditioning.

Most of these studies have been conducted in tension^[169] and few studies have been conducted for the effect of preconditioning behaviour of skin in compression. Compared to the preconditioning of the skin in tension, in which the samples are typically preconditioned by loading/unloading for more than 20 cycles skin samples in compression need fewer loading/unloading cycles for preconditioning^[171]; Wu et al.^[172] found that skin samples should also be preconditioned in compressive tests to achieve repeatable mechanical behaviour and skin samples reach a repeatable “steady-state” after 3-4 cycles of compressive loading, despite of the loading rate and loading configurations (confined or unconfined).

Although preconditioning has been routinely applied in soft tissue tests, the exact mechanism that is responsible for the improved replicability remains unclear^[171]. This can be indicated by the fact that there is no a consistent preconditioning protocol for mechanical testing of skin tissue, even for soft tissues^[166]: published studies report a wide range of cycles of loading depending on the particular tissue type and mode of deformation. From a microstructural point-of-view, tensile preconditioning serves to orient the originally randomly distributed collagen fibers to a more straight and uniform pattern such that their mechanical properties become more repeatable^[173],

which can be indicated by the fact that there is a qualitative consistence on the effects of preconditioning of stretch controlled uniaxial tension tests where the stress-strain response is shifted to the right^[173]; in compression, preconditioning does not significantly affect the orientation of the collagen fibers, rather, it improves the contact conditions between the sample and the compression platens or chamber walls^[172].

However, preconditioning is frequently not used for *in vivo* analysis, in order to represent the biomechanical properties of the tissue as would be experienced during injury or clinical intervention; for example, *in vivo* tests on skin are frequently performed in the absence of preconditioning^[174]. *In vitro* tests have also been performed in the absence of cyclic preconditioning, allowing for full relaxation between tests or quasi-static loading^[175], or for when the noncyclic, viscoelastic response is desired^[176].

6.4 Influence of Different Factors

6.4.1 Directional effects of skin

It is well-recognised that the collagen fibers in skin have a preferred orientation, known as Langer lines¹⁾^[177~179], due to pre-tension in the skin. Previous works have addressed the directional effects of skin and found the orientation of the fibers plays a dominant role and therefore the strength is different in different directions. In general, the strength is greater in the direction parallel to the backbone than in the direction perpendicular to it. Some of these effects are strongly correlated with the Langer's lines^[179] while some others are related to the body geometry.

Kenedi et al.^[178] showed that the mechanical properties of skin are largely dependent on the spatial arrangement of collagen and elastin fibers in the dermis. Gibson et al.^[94] observed a directional variation in the extensibility of human skin is found on uniaxial loading in the plane of the skin, where the direction of maximum extensibility of the skin is at right angles to Langer's Lines, substantiating the hypothesis that Langer's Lines represent a preferred orientation of the fibers within the dermis. Daly^[3] reported that a skin

1) Langer's lines, sometimes called cleavage lines, is a term used to define the direction within the human skin along which the skin has the least flexibility. These lines correspond to the alignment of collagen fibers within the dermis. They were first given detailed attention in 1861 by Austrian anatomist Karl Langer (1819~1887) in his study "On the Anatomy and Physiology of the Skin". Langer argued that the physiological basis for his lines was the directional orientation of the collagen fibres in the dermis. Later studies have proved that both collagen and elastin fibres are predominantly arranged in the direction of the Langer lines.

specimen taken from the abdomen along to the cranio-caudal axis could be stretched longer than one taken perpendicularly. Manschot & Brakkee^[58,59] and others^[123] report higher stiffness in the lateral direction than in the longitudinal direction. It was found that stiffness for the lateral specimens is greater compared with that for longitudinal specimens^[81].

It was found tensile failure tended to be slightly greater for circumferential specimens than longitudinal ones and the ultimate tensile strength of skin is higher when the stress is applied in the direction of maximum fibres alignment^[180]. However, Vogel & Hilgner^[181] found the ultimate load, tensile strength and ultimate modulus of elasticity of rat skin *in vitro* were identical regardless of whether the samples were taken perpendicularly or longitudinally to the body axis. In contrast to this, ultimate strain showed a significant difference, being 35% higher for specimens oriented transversely versus longitudinally to the spine. Aging process had more influence on the failure strain perpendicular to the body axis than those parallel to body axis^[182]. Pereira et al.^[183] also found no significant differences of toughness between the human dorsal skin in the longitudinal and circumferential directions, neither between the palmar skin across creases and parallel to the creases.

However, most of early measurement of skin mechanics does not capture the orthotropic constitutive response of skin arising from the preferential alignment of the collagen fibers in the dermal layer^[184], although experimental investigations have revealed the orthotropic constitutive response of skin tissue^[185]. These collagen fibers are aligned in the direction of maximum skin tension, thereby defining the Langer's lines. Consequently, the onset of strain hardening begins at lower strains when the skin is stretched *in vivo* parallel to the direction of maximum skin tension, compared with stretching perpendicular to the direction of maximum skin tension^[186]. When a skin sample is excised from the body, the sample contracts, but the preferential alignment of the fibers is retained, and the skin's constitutive response remains orthotropic^[80].

6.4.2 Influence of aging

The aging of the skin is the consequence of the way of life and many factors influence skin aging, including solar radiation, infective micro-organisms, gravitational forces, electromagnetic fields, psychological stressors, cigarette smoke, etc^[187]. A typical change of skin structure with ageing is its thickness, where the thickness of skin has been found to decrease with age^[188,189], although no correlation between skin thickness and age have also been observed in other studies^[113].

Changes in the mechanical properties of skin versus age have been extensively studied by scientists with physical methods in the last decade^[190]. With the increase of age, it has been experimentally observed that there was increase of stiffness and decrease of elasticity of skin tissue^[191~195]. For example, Vogel^[87] reported an increase in lateral tangent modulus of rat skin from 17 MPa at 1 month to 38 MPa at 4 months whereas the tangent moduli of lateral specimens increased from 14 MPa at 1 month to 36 MPa at 4 months. Silver et al.^[191] found that the initial slope of the elastic stress-strain curve for young dermis (23-year-old) and old dermis (87-year-old) decreases from 2.10 to 0.60 at strain rate of 10%/min and from 4.30 to 1.08 MPa at strain rate of 1000%/min while at high strains the elastic slope increases from 41.0 to 45.0 MPa for young dermis and decreases from 15.0 to 7.31 MPa for old dermis. The same result of increase of stiffness with age has also been obtained by the lateral stiffness parameter in the model of Belkoff & Haut^[81], who found a similar correlation for lateral specimens, however, for longitudinal specimens, a correlation between tangent modulus and model stiffness and insoluble collagen content was not as strong.

However, it was also reported that aging has no influence on the mechanical response of skin tissue at high strain state^[106], while Vogel^[182] found stress and moduli of elasticity at low strain were decreased by maturation and increased by senescence, exactly the opposite of the changes at high strain. The stiffness of the final region is more or less independent of age^[165]. Hashmi & Malone-Lee^[195] found that the elastic behaviour of the skin from the plantar aspect of the third metatarsophalangeal joint did not alter with age^[195], and similar results have also been reported for plantar and palmar skin^[196]. Hashmi & Malone-Lee^[195] pointed out that it is possible that the external mechanical stresses may affect the nature of the skin, such that any age-related changes become masked.

Besides, decrease in the stiffness of skin with age was also reported^[197], which is in contradiction to other work. Sanders^[112] found that the elastic component of the extensibility of the human skin *in vivo* under torsional conditions increases with age between 6 and 61 years. Pugliese & Potts^[197] observed a decrease in stiffness with age until the 50 years, after which stiffness began to increase. This contradiction may be due to the non-delimited area of skin undergoing torsion which results in more influence from the mobility of the underlying tissue^[108].

The viscoelastic properties of skin also varied with age. Sanders^[112] the viscoelastic and plastic components of the extensibility of the human skin

in vivo under torsional conditions are constant up to an age of forty and then increase a little at higher ages. Relaxation was shown to decrease during both maturation and aging^[87]. There was a diminished elasticity and stretchability after the age of 30 in the range of 3 to 89 years old, associated with an increase in the viscoelastic component whereas the Young's modulus doubled with age^[37]. Vogel^[198] found viscoelastic properties were barely influenced by the aging process. The viscous part of the deformation was constant through life, whereas the creep relaxation time decreased linearly with age^[113]. Vexler et al.^[116] found no significant age-dependent changes in both viscoelasticity and anisotropy of the forearm skin for both males and females, but the viscoelasticity of the breasts skin was found to decrease with age when this parameter was measured horizontally but not vertically. It has also reported that there is no variation of plasticity of skin tissue with ageing^[192]. Silver et al.^[191] reported a decrease of the initial slope of the viscous stress-strain curve with age.

The tensile strength also varies with age^[199], and this may well be due to variation in the collagen component of the skin^[200]. For example, Fry et al.^[201] found the tensile strength calculated per unit cross-sectional area of collagen increased with age in rat of 3~85 weeks old, with the maximal value in the oldest group being about three times that in the youngest. The quantity present per unit area of surface also increased with age. The total "surface mechanical resistance" obtained by multiplying collagen per unit area of skin and tensile strength rose continuously about twenty-fold between the youngest to oldest of the groups. Extensibility was found to fall with age, the range being about eighty fold. Vogel & Hilgner^[202] found that the first and second moduli of elasticity of rat skin showed a minimum at an age of 2 months, whereas the ultimate elasticity modules increased with maturation up to a maximum at 12 months followed by a decrease similar to that observed in tensile strength at an age of 24 months. Vogel^[182] found that the time for break of rat skin under constant load rose continuously with aging, whereas ultimate extension rate showed a sharp fall during maturation and a slow decrease during senescence. Haut^[203] found that failure strain increased slightly with age in the orientation perpendicularly to the spine, which reflected that of individual bundles of collagen fibrils; and decreased continually with age in longitudinal direction, which reflected more the changes in dimension or compactness of the collagen fiber network and/or properties of the ground substance matrix. The tensile strength of skin tissue increased during maturation and started decreasing above an optimum level^[87].

It has been reported that skin fatiguability increased with ageing^[192].

Natural stress was found to increase until maturity and then rapidly decrease^[108]. Aging has been found to be an important factor affecting the pressure-duration relationship.

The age-related dependence of skin biomechanical behaviour have been generally attributed to three factors^[80], as described below.

(1) The first factor is the increased crosslinking of collagen fibers. Vogel^[182] pointed out that the change of most of the mechanical parameters at high strain during maturation may be explained by an increase of cross-linking of collagen. Grahame & Holt^[74] found a slight increase in the modulus of elasticity at higher ages, which was attributed to the increase of cross-linkages between peptide chains of the collagenous network by the authors mention. The model of Bischoff et al.^[204] indicated that collagen network density increases and fiber free length decreases as rat skin ages. Collagen fibers are observed to be more compact with increased age and appear to unravel^[188].

(2) The second factor is the degradation of the elastin and collagen network of the dermis and subcutaneous tissue^[205]. For example, Daly & Odland^[1] attributed the lost of skin elasticity at low stress level to a gradual destruction of the elastin network with age. Silver et al.^[191] attributed the decrease in the elastic spring constant with increased age observed to the disruption of the elastic fibers and loss of α -helical structure. Fibers in the upper dermis are markedly modified, thinned and/or fractionated with age^[206]. Elastic fibers from skin from older individuals appear to fray and contain holes^[188]. Sanders^[112] ascribed their observed loss of skin elasticity to the fraying and fragmentation of elastic fibers at advancing age. By dividing the moduli found by the volume fraction (0.01) of the elastic fibers in human skin^[75], Sanders^[112] found the moduli of elasticity of the elastic fibers in the living skin were between about 2 MPa and 10 MPa, which was found to agree well with the value 5 MPa for pure elastic tissue^[75]. The less elastic and less extensible properties in aged skin may be related to the existence of a region in the upper dermis of aged persons, where collagen and elastin are less dense and only present under thinner layers, compared to the upper dermis of a young person^[194]. Collagen concentration in the skin of rats increases up to 6 months of age, after which it decreases whereas the type III collagen content decreases from 33% (2 weeks) to 18.6% at 1 year^[207]. Collagen volume fractions of skin decreased from 16.6% and 9.6% from young skin to old skin^[191]. Reihnsner et al.^[80] pointed out that the biomechanical effect is due to a gradual destruction of the elastin network with age and not

necessarily to a destruction of the elastin itself.

(3) The third factor is age-dependent changes in the ground substance, where proteoglycan, and water content, as well as blood supply, have all been shown to decrease with age, which alter mainly the viscoelastic properties^[55]. The GAG content is reported to decrease with respect to the amount of protein with increased age^[208]. Aged skin has a lower water content than the skin of younger men^[209].

6.4.3 Regional variations

Since skin in different parts of body play different roles, thus it can be imaged that there exist large difference in structure, which will results in the difference of mechanical behaviours. Malm^[210] and Pierard-Franchimont et al.^[193] pointed out that regional variations in tensile functions reveal a vertically orientated gradient of skin distensibility¹⁾ on the body which seems to be determinant in resisting both hydrostatic pressure and gravitation, particularly in the lower limb in the upright position. The difference has been observed by many researchers^[107,153,183]. For example, Nilsson^[153] pointed out influence of the original position on skin mechanical properties was not only due to different quantities and qualities of tissue, but also might be due to differences in fiber direction. Pereira et al.^[183] found that the toughness value of the human palmar skin was significantly greater than the dorsal skin, which was attributed to the difference in the quantity of collagen present. Diridollou et al.^[107] found that the skin is thicker, stiffer and less tense and elastic on the forehead than on the ventral forearm: Young's modulus is on the volar forearm is only about half of that on forehead while the initial stress on the volar forearm is double that on forehead. The difference was explained as due to the greater skin thickness for the forehead than for the ventral forearm. The explanation of different thickness seems more likely in view that the properties of isolated fibers from these locations did not differ significantly, in a single animal^[211], although the mechanical properties of skin samples vary significantly with location and direction of cutting.

6.4.4 Influence of hydration and relative humidity²⁾

Hydration is a complex phenomenon influenced by both intrinsic (age, anatomical site) and extrinsic (ambient humidity, chemical exposure) fac-

1) Distensibility (stiffness), i.e., resistance to change of shape.

2) Humidity or relative humidity is a term used to describe the amount of water vapor that exists in a gaseous mixture of air and water, which is defined as the ratio of the partial pressure of water vapor in the mixture to the saturated vapor pressure of water at a given temperature.

tors. These factors can affect the mechanical properties of skin and research has been performed in order to correlate hydration levels with the skin's mechanical properties.

It has long been recognized that hydration affects the mechanical properties of skin^[55], including elasticity^[212], viscoelasticity^[213,214] and shear wave propagation^[192] and to a large extent these changes are reversible^[215]. For example, Hendley et al.^[103] found that the indentation force decreased with increasing hydration, while Rigal & Leveque^[35] observed increase in immediate deformation of stratum corneum after applying water to the skin (direct hydration) or applying occlusion (covering of the skin with plastic for a certain time, indirect hydration).

Jemec et al.^[31] and Overgaard & Jemec^[213] observed significant increases in distensibility and resilient distensibility after applying tap water to the skin. Auriol et al.^[212] found that elasticity of *in vivo* human skin increased with increasing hydration. It has been found that the stratum corneum become brittle with increasing hydration both *in vivo* and *in vitro*^[215].

Besides elastic properties, hydration has also been found to influence skin's viscoelastic properties. Jemec et al.^[31] and Overgaard & Jemec^[213] observed significant increases in hysteresis after applying tap water. The storage and loss modulus of guinea pig skin increased when bathed in a ribose solution^[61]. Auriol et al.^[212] found that the viscosity and hysteresis of *in vivo* human skin were unmodified with increasing hydration. Bert & Reed^[214] found that rat back skin becomes progressively stiffer in dehydration and more compliance in over hydration under compression. Fracture energies and peak separation stresses of stratum corneum were also found to decrease with increasing hydration^[30].

The friction properties of skin have also been found to be dependent on the amount of moisture at the skin surface. A small amount of water on the skin surface increases the frictional force compared with a dry surface, while a large amount of water on the surface decreases the frictional force compared with a dry surface^[33].

Since humidity greatly affect the skin hydration, several studies have been conducted to investigate the effect of humidity on the mechanical properties of skin tissue, especially its surface layer, stratum corneum^[216]. Wildnauer et al.^[197] examined the effect of relative humidity (*RH*) on the total force-elongation curve of human stratum corneum and found that the strength of untreated SC decreased 85%, tensile strain increased from 20 to 190% while the fracture work increased 600% with the increasing *RH* in the range of

0%~100%. Ether extraction increased the tensile strength while has little effect on the tensile strain. Sequential ether-water extraction significantly decreased the tensile strain at the higher *RH* while tensile strength was less dependent on *RH* than untreated. The results suggested the role of water soluble materials being responsible for the water binding necessary for membrane flexibility. Park & Baddiel^[24,25] studied the effect of the relative humidity on the elastic modulus of pig's ear stratum corneum, which differs only slightly from human stratum corneum, and found that the Young's modulus of SC for 30% relative humidity (2 GPa) is three orders larger than that for 100% relative humidity (6 MPa), and as the Young's modulus of totally hydrated stratum corneum differs only slightly from that of total skin. The strain at yield point increased from 1% at 30% *RH* to 20% at 100% *RH*. Papir et al.^[26] studied the effect of water on the tensile properties of newborn rat stratum corneum with relative humidities varying from 26%~100% *RH* at 25°C and observed a brittle to ductile transition once the relative humidity exceeded 70% and the presence of a molecular relaxation process which migrated from 42°C at 40% relative humidity to -18°C at 95% relative humidity. Yuan & Verma^[23] found the elastic modulus of dry stratum corneum is one order larger than that of wet one. Complementary nanoindentation results on excised (porcine) stratum corneum show a smaller, but still considerable, reduction in the Young's modulus from 100 to 10 MPa with increasing *RH*^[23]. Nicolopoulos et al.^[119] found that both the crack propagation and fracture energy of stratum corneum increased with *RH*.

The changes of skin mechanical behaviour with increasing humidity and hydration has been attributed many to the corresponding structural changes.

The equilibrium water content of (excised) SC is typically about 10% on a dry weight basis at 50% *RH*^[217], which increases to 30% at 90% *RH* and 70% at 100% *RH* or when immersed in water^[218]. Ultrastructural studies of the SC have suggested that it was elevated desmosome degradation and disruption of intercellular lipid structures due to increased water content that affect mechanical properties^[219]. Water is believed to act as a plasticizer causing a transition of a polymer from a glassy state to a rubbery state. At low *RH*, large chain movements are restricted and extension takes place by stretching of bonds; while at higher *RH*, the hydrogen bonds are hydrated (and thus weakened) but the disulphide bonds remain intact, resulting in a lightly cross-linked network^[24]. Park & Baddiel^[25] found that aqueous extraction removes the hygroscopic materials in stratum corneum, which causes the protein network to collapse resulting in more protein-protein bonds in the

cell and a higher elastic modulus. Luscher et al.^[220] investigated collagen hydration with X-ray diffraction and reported that the adsorption of water by the helical structure of the collagen molecule becomes saturated at a water content of 26% (at 60% *RH*). Above this water content water is adsorbed within the intermolecular space^[221]. Besides, a pronounced swelling is associated with water immersion^[222] and a considerable reduction in the Young's modulus.

6.4.5 Influence of radiation

Since radiation has great influence in the structure of collagen and elastin network in the skin, for example, sun exposure habits are related to known dermal collagen and elastin changes due to ultraviolet radiation, it is thus imaginable that mechanical behaviour of skin is influence by the radiation, depending on both the dose and the time, as observed in many studies^[5,69,106,151,152,211,223].

Ranu et al.^[152] found that elasticity of rat skin is little changed by irradiation, but the stiffness of the collagen itself decreased with increasing dose which was explained as the appearance of extensive cracks within the collagen structure of irradiated samples. The stiffness of normal rat skin increased from 12.1 to 16.2 MPa at 50 and 120 days after irradiation. Burlin et al.^[224] studied the long term effects of irradiation on the mechanical properties of mouse skin is presented and found that the strain and stress at rupture decrease monotonically with exposure, while the skin stiffness exhibits a shoulder on the response curve. Alexander & Cook^[106] observed a increase of strain-stress slope low strain level and significantly decrease at high strain level with sun exposure. Gunner et al.^[5] found that the treatments of X-irradiation have most effect on the second part of the stress-strain curve of skin tissue, associated with extension of the collagen fibers, which was shown due to weakening of the fibers of their crosslinks, while photochemotherapy with long wavelength ultraviolet light treatments have not been shown to induce any marked change in the skin's mechanical properties. Ranu^[69] observed that after radiation the rupture occurs at lower stress levels. Baker et al.^[223] studied the changes in the mechanical properties of pig skin after X-irradiation with a single dose. They found that there was no significant change in the stiffness of irradiated skin, until 9 weeks after irradiation when the irradiated skin was significantly stiffer; a significant increase in the unrelaxed elastic modulus of irradiated skin was only observed 12 weeks after irradiation; and there were no significant changes in stress relaxation. The reduction in skin stiffness and the elastic modulus after irradiation were also

found to be dose related. Ranu^[151] studied the effect of irradiation on skin mechanical properties both *in vivo* and *in vitro*. *In vivo*, with increasing dose, there is an initial decline in the skin elasticity, reaching a minimum, followed by an increase to a peak response, following which the elasticity falls again but remains, apparently at a plateau, above the initial value. *In vitro*, at low doses, the stress at rupture is relatively constant, while the stress at rupture decreases with increasing dose. The variation of the stiffness of the skin shows a marked dependence on dose. Dobrev^[225] found that sun-exposed skin of the dorsal forearm showed a significantly lower distensibility and elasticity than the unexposed volar forearm skin.

The radiation induced changes in mechanical properties of skin tissue are mainly explained as due to the corresponding changes in skin structure. Radiation causes the formation of visible wrinkles, change of skin texture, and skin discoloration^[226,227]. For example, ultraviolet irradiation has been found to provoke the sagging of skin^[228]. Below the skin surface, increased skin thickness, marked accumulation of denatured elastin, degradation of the stereo structure of elastic fibers, and increased total glycosaminoglycan content have been reported^[229,230]. The destruction and degradation of collagen structures have been reported after radiation, such as narrowing of collagen fibers and blurring of fiber contours^[231]. Nishimori et al.^[226] reported marked ultrastructural degeneration of dermal collagen fiber bundles in sun exposed human forearm skin, but not in unexposed skin of the inner upper arm. Fourtanier & Berrebi^[229] observed the ultra-structural details of the continuous exposure of mini-pig skin to ultraviolet radiation and found that after 24 months of exposure, the fibers of collagen are no longer oriented, they are entangled, instead, and this might explain the loss of elasticity, the loss of resilience and the sagging of photo-aged skin.

The marked three-dimensional structural changes in the dermis can then explain the changes in the mechanical properties of the skin^[227]. Ranu^[69] observed that after radiation the normal fibrous structure of collagen in rat dermis is replaced by a solid mat which is ill adapted to support stress, so that rupture at low stress levels is inevitable. Alexander & Cook^[106] explained that the increase of strain-stress slope low strain level was attributed to the increased of elastin-like protein in chronically sun-damaged skin, as observed by Smith et al.^[232]; while the significantly decrease at high strain level was attributed to the degradation of the collagen molecular into smaller molecular fragments and the change in the insoluble collagen caused by ultraviolet radiation, as observed by Cooper & Davidson^[233] and Smith et al.^[232].

Dobrev^[225] pointed out that the changes of mechanical properties of sun-exposed skin are related to the massive increase and disorganization of the elastic tissue, which are accompanied by lost of functional elastic fibers. The later plays an important role in maintaining the collagen fiber network, in controlling the movements of this network within the ground substance and in restoring the initial position of the skin after deformation. Irradiation with gamma-rays caused severe destruction of the fibrillar structure at the X-ray and electronmicroscopic levels and non-hydrolytic scission of the polypeptide chains seemed to be responsible for the changes observed^[211].

6.4.6 Influence of loading rate

Soft tissue is known to be a viscoelastic material. During cyclic deformation, soft tissue demonstrates hysteresis that is rate independent over several decades of strain rate^[173]. As strain rate increases in displacement controlled tests, the overall stiffness of the fully preconditioned response increases in soft tissues, such as skin^[166], ligament^[234], myocardium^[235], collagen fibers^[236].

The sensitivity of skin mechanical behaviour to strain rate has been observed early by Jamison et al.^[96] when they attempted to characterize skin tissue as a linear viscoelastic material. Haut^[205] and Dombi et al.^[237] conducted uniaxial tensile tests on rat skin at strain rates of 0.3~60 s⁻¹ and found a 50%~100% increase in the ultimate tensile strength with increased strain rate, although the failure strain was unchanged. Finlay^[111] used a rotational device applied to the skin to apply a torque to the surface and found that the skin showed a reduced viscosity with increased strain rate, characteristic of thixotropic behaviour. Vogel & Hilgner^[181] also reported an increase in stiffness when strain rate was increased, but his research was done with rat skin (0.5 mm/min, 5 mm/min, 50 mm/min, 500 mm/min with sample size 30 mm). Potts et al.^[238] studied the attenuation of shear waves in human skin at frequencies between 0 and 1000 Hz and found that the viscosity of wet skin decreased from about 22.5 to about 4Pa·s at frequencies between 0Hz and 500 Hz. Edsberg et al.^[169] found that with the increasing uniaxial tensile strain rate (10.6 mm/min, 21.2 mm/min, 31.8 mm/min, 42.3 mm/min with sample average size 27.5 mm), the stiffness has little change at lower deformation rates and but decreased at greater deformation rates. The same phenomenon was also observed for extra high strain rate. Xu et al.^[120] studied the uniaxial compressive responses of pig skin over a wide range of strain rates (0.004~4000 s⁻¹) and a greater strain rate sensitivity was observed: pig skin stiffens and strengthens with increasing strain rate over the full range explored. The same results are also reported for biaxial

test. The biaxial tensile tests of Lanir & Fung^[78] showed that the stress for the same strain increases with increasing strain rates (0.02 mm/s, 0.2 mm/s, 2 mm/s with sample size 35 mm×35 mm) although not significantly.

The tensile strength of skin also depends on the rate of tensile strain. Vogel^[239] observed that the tensile strength of rat skin increased with the logarithm of strain rate. Gadd et al.^[240] showed that the tensile strength of aged human skin increased approximately 150% over three orders of magnitude in strain rate. Much of the sensitivity to strain rate has been attributed to uncoiling and aligning movement of collagen^[40], while Daly^[3] believed that the rate sensitivity of skin occurred at all structure levels of collagen and are due in part to bonds between fibrils and fibers. The movement of fluid in the hydrated matrix may also play an important role^[241]. Haut^[203] found that the tensile strength of rat dorsal skin depended on strain rate while failure strain didn't. The sensitivity of strain rate decreased with age during maturation. Silver et al.^[191] found that the elastic and viscous slopes at low strain and only the viscous slope at high strain were observed to be strain rate dependent, all of which increase with the increase of strain rate.

As described in Chapter 2, collagen fibers comprise bundles of collagen fibrils aligned parallel to a hyaluronic acid chain, and linked to the hyaluronic acid by proteoglycan side-chains. It is hence probably that the strain rate sensitivity is attributable to viscous losses from the interaction of the ground substance with the collagen fibres at the macroscopic scale^[72], and with the collagen fibres at the microscopic scale^[68]. From the model results of Xu et al.^[120], we can also get the same explanation: the strain rate sensitivities are well modeled by Xu et al.^[120] by increasing in the shear modulus with increasing strain rate, with no attendant change in the strain hardening exponent. However some other explanations are also given. For example, Edsberg et al.^[169] attributed the decrease in stiffness seen with an increase in strain rate to the Mullins effect.

It should be noted that almost all the above studies are under displacement controlled tests, however, under load controlled conditions, the tissues exhibited an increase in nonlinear stiffness with a decrease in loading rate^[166]: the faster the test was performed, the more compliant was the preconditioned material behaviour. Giles et al.^[166] explained this dilemma as due to the interplay of nonlinear effects and creep behaviour within the context of cyclic load controlled deformations. For a given tissue, the relationship between loading rate and the preconditioned material stiffness is not monotonic; rather, there is a well-defined loading rate at which the amount of creep during preconditioning is maximized, resulting in the stiffest tissue

response^[166].

However, strain-rate insensitivity has also been reported. Fung^[167] suggested that for soft tissue in a wide range of strain rates the stress-strain relationship is insensitive to the strain rate in a constant strain-rate test. The small variation in the storage and loss modulus over the frequency range that was examined indicated that the viscoelastic properties are relatively insensitive to strain rate^[47]. The strain rate insensitivity has also been observed by Fung^[77] and is the basis for his pseudoelastic model of skin. Results in the frequency range up to 1000 Hz produced a loss tangent of roughly 0.6. Zhang et al.^[242] found that the effective Young's modulus was roughly rate-insensitive for the rates imposed in the indentation test of forearm skin *in vivo*. Vogel^[239] reported for rat skin that the strain to failure was independent of strain rate. It has been found^[126] that the stress-strain loop of skin tissue in cyclic loading and unloading is unique after preconditioning, and is insensitive to strain rate, although it is an inelastic material.

6.5 Summary

Problem with all of the testing techniques however, is that they are associated with a non-uniform strain field. Their value as research tools on the constituent stress-strain relationship in human skin is thus limited. Again, if the obtained experimental data is to be used in a geometrical model of the skin, then the experimental technique must be able to account for the skin's nonlinear and anisotropic properties. To date the only experimental techniques reported to do so are the suction test with a racetrack-shaped cup^[8], the biaxial test^[127] and the multiaxial test^[132].

In vitro soft tissue measurements are performed in a laboratory environment using tissue samples of known geometries and standard mechanical tests. The characterization of material properties using the measurement data is relatively easy since cross-section of the sample, boundary conditions, direction of loading and other factors mentioned above shall be set in advance compared with experiment *in vivo*. However, this is not the case with *in vivo* or *in situ* studies. For this reason, an inverse solution is formulated to determine the unknown material properties from measured system response. An optimization routine is typically combined with a finite element method to match experimental data with the numerical solution through iterations.

References

- [1] Daly C H, Odland G F. Age-related changes in the mechanical properties of human skin. *Journal of Investigative Dermatology*, 1979, 73(1): 84–87.

- [2] Gambarotta L, Massabo R, Morbiducci R, et al. In vivo experimental testing and model identification of human scalp skin. *Journal of Biomechanics*, 2005, 38(11): 2237–2247.
- [3] Daly C H. Biomechanical properties of dermis. *Journal of Investigative Dermatology*, 1982, 79 (Suppl. 1): 17s–20s.
- [4] Bonilla C M A, Massanet A R F, Almodóvar N V. Mechanics of biomaterials: Skin repair and grafts. *Proceedings of Applications of Engineering Mechanics in Medicine*. Puerto Rico, 2005: D1–D24.
- [5] Gunner C W, Hutton W C, Burlin T E, et al. Effects of some clinical treatments on the mechanics of skin. *Engineering in Medicine*, 1979, 8(2): 58–62.
- [6] Hendriks F M, Brokken D, Oomens C W, et al. Influence of hydration and experimental length scale on the mechanical response of human skin in vivo, using optical coherence tomography. *Skin Research and Technology*, 2004, 10(4): 231–241.
- [7] Edwards C, Marks R. Evaluation of biomechanical properties of human skin. *Clinical Dermatology*, 1995, 13(4): 375–380.
- [8] Cook T, Alexander H, Cohen M. Experimental method for determining the 2-dimensional mechanical properties of living human skin. *Medical and Biological Engineering and Computing*, 1977, 15(4): 381–390.
- [9] Vogel H G, Denkel K. Methodological studies on biomechanics of rat skin comparing in vivo and in vitro results. *Bioengineering Skin*, 1982, 4: 71–79.
- [10] Vogel H G. Mechanical properties of rat skin as compared by in vivo and in vitro measurement. *Bioengineering Skin*, 1982, 3: 198–209.
- [11] Marangoni R D, Glaser A A, Must J S, et al. Effect of storage and handling techniques on skin tissue properties. *Annals of the New York Academy of Sciences*, 1966, 136(16): 439–454.
- [12] Jacquet E, Gwendal J, Khatyr F, et al. A new experimental method for measuring skin's natural tension. *Skin Research and Technology*, 2008, 14(1): 1–7.
- [13] Sacks M S, Sun W. Multiaxial mechanical behavior of biological materials. *Annual Reviews Biomedical Engineering*, 2003, 5: 251–284.
- [14] Pierard G E. EEMCO guidance to the in vivo assessment of tensile functional properties of the skin, Part 1: Relevance to the structures and ageing of the skin and subcutaneous tissues. *Skin Pharmacology and Applied Skin Physiology*, 1999, 12(6): 352–362.
- [15] Marks R. Mechanical properties of the skin//Goldsmith L A. *Physiology, Biochemistry, and Molecular Biology of the Skin*. Oxford: Oxford University Press, 1991.
- [16] Shergold O A. *The Mechanics of Needle-Free Injection* [Ph. D. Thesis]. Cambridge: University of Cambridge, 2004.
- [17] Dikstein S, Hartzshtark A. What does low-pressure indentometry measure. *Arzt Kosmetol*, 1983, 16: 327–328.
- [18] Daly C H. *The Biomechanical Characteristics of Human Skin* [Ph. D. Thesis]. Glasgow: University of Strathclyde, 1966.

- [19] Silver F H, Freeman J W, DeVore D. Viscoelastic properties of human skin and processed dermis. *Skin Research and Technology*, 2001, 7(1): 18–23.
- [20] Tsubouchi K, Enosawa S, Harada K, et al. Evaluation of the relationship between the viscoelastic stress and strain of fetal rat skin as a guide for designing the structure and dynamic performance of a manipulator for fetal surgery. *Surgery Today*, 2006, 36(8): 701–706.
- [21] Wilkes G L, Brown I A, Wildnauer R H. The biomechanical properties of skin. *CRC Critical Reviews in Bioengineering*, 1973, 1(4): 453–495.
- [22] Hendricks F M. Mechanical Behaviour of Human Skin in Vivo a Literature Review. National Laboratory Unclassified Report 820, 2001.
- [23] Yuan Y, Verma R. Measuring microelastic properties of stratum corneum. *Colloids and Surfaces B: Biointerfaces*, 2006, 48(1): 6–12.
- [24] Park A C, Baddiel C B. Rheology of stratum corneum I. A molecular interpretation of the stress-strain curve. *Journal of the Society of Cosmetic Chemists*, 1972, 23(1): 3–12.
- [25] Park A C, Baddiel C B. Rheology of stratum corneum II. A physio-chemical investigation of factors influencing the water content of the corneum. *Journal of the Society of Cosmetic Chemists*, 1972, 23: 13–21.
- [26] Papir Y S, Hsu K H, Wildnauer R H. The mechanical properties of stratum corneum. I. The effect of water and ambient temperature on the tensile properties of newborn rat stratum corneum. *Biochimica et Biophysica Acta*, 1975, 399(1): 170–180.
- [27] Rawlings A V, Watkinson A, Harding C R, et al. Changes in stratum corneum lipid and desmosome structure together with water barrier function during mechanical stress. *Journal of the Society of Cosmetic Chemists*, 1995, 46(3): 141–151.
- [28] Wilkes G L, Nguyen A, Wildnauer R. Structure property relations of human and neo-model rat stratum corneum. I. Thermal stability of the crystalline lipid structure as studied by X-ray diffraction and differential thermal analysis. *Biochimica et Biophysica Acta*, 1973, 304(2): 267–275.
- [29] Wu K S, Van Osdol W W, Dauskardt R H. Mechanical and microstructural properties of stratum corneum. *Biological and Biomimetic Materials—Properties to Function*. San Francisco, 2002: 27–33.
- [30] Wu K S, van Osdol W W, Dauskardt R H. Mechanical properties of human stratum corneum: Effects of temperature, hydration, and chemical treatment. *Biomaterials*, 2006, 27(5): 785–795.
- [31] Jemec G B, Jemec B, Jemec B I, et al. The effect of superficial hydration on the mechanical properties of human skin in vivo: Implications for plastic surgery. *Plastic and Reconstructive Surgery*, 1990, 85(1): 100–103.
- [32] Highley D R, Coomey M, DenBeste M, et al. Frictional properties of skin. *Journal of Investigative Dermatology*, 1977, 69: 303–305.
- [33] Naylor P F. The skin surface and friction. *British Journal of Dermatology*, 1955, 67(7): 239–246.
- [34] Guibara E, Nicholls S, Marks R. Measurement of force required for point indentation of stratum corneum: The effect of hydration. *Bioengineering of*

- the Skin, 1979, 2: 29–30.
- [35] De Rigal J, Leveque J. In vivo measurement of the stratum corneum elasticity. *Bioengineering and the Skin*, 1985, 1: 13–23.
- [36] De Rigal J, Leveque J L, Agache P G, et al. Influence of ageing on the in vivo extensibility of human skin at low stress. *Archives of Dermatological Research*, 1980, 269(2): 127–135.
- [37] Agache P G, Monneur C, Leveque J L, et al. Mechanical properties and Young's modulus of human skin in vivo. *Archives of Dermatological Research*, 1980, 269(3): 221–232.
- [38] Pereira J M, Mansour J M, Davis B R. Effects of layer properties on shear disturbance propagation in skin. *Journal of Biomechanical Engineering*, 1991, 113(1): 30–35.
- [39] Wang Q, Hayward V. In vivo biomechanics of the fingerpad skin under local tangential traction. *Journal of Biomechanics*, 2006, 40(4): 851–860.
- [40] Lanir Y. The rheological behavior of the skin: Experimental results and a structural model. *Biorheology*, 1979, 16(3): 191–202.
- [41] Silver F H, Kato Y P, Ohno M, et al. Analysis of mammalian connective tissue: Relationship between hierarchical structures and mechanical properties. *Journal of Long-Term Effects of Medical Implants*, 1992, 2(2-3): 165–198.
- [42] Silver F H, Christiansen D L, Snowhill P B, et al. Role of storage on changes in the mechanical properties of tendon and self-assembled collagen fibers. *Connective Tissue Research*, 2000, 41(2): 155–164.
- [43] Silver F H, Horvath I, Foran D J. Viscoelasticity of the vessel wall: The role of collagen and elastic fibers. *Critical Reviews in Biomedical Engineering*, 2001, 29(3): 279–301.
- [44] Viidik A, Danielsen C C, Oxlund H C. On fundamental and phenomenological models, structure and mechanical properties of collagen, elastin and glycosaminoglycan complexes. *Biorheology*, 1982, 19(3): 437–451.
- [45] Dulgerova P. Biophysical modeling of viscoelastic deformations of cattle skin in vivo. *Trakia Journal of Sciences*, 2004, 2(4): 1–3.
- [46] Eshel H, Lanir Y. Effects of strain level and proteoglycan depletion on preconditioning and viscoelastic responses of rat dorsal skin. *Annals of Biomedical Engineering*, 2001, 29(2): 164–172.
- [47] Pereira J M, Mansour J M, Davis B R. Dynamic measurement of the viscoelastic properties of skin. *Journal of Biomechanics*, 1991, 24(2): 157–162.
- [48] Pailler-Mattei C, Bec S, Zahouani H. In vivo measurements of the elastic mechanical properties of human skin by indentation tests. *Medical Engineering and Physics*, 2008, 30(5): 599–606.
- [49] Oxlund H, Manschot J, Viidik A. The role of elastin in the mechanical properties of skin. *Journal of Biomechanics*, 1988, 21(3): 213–218.
- [50] Hoffman A S, Grande L A, Gibson P, et al. Preliminary studies on mechanochemical structure relationships in connective tissues using enzymolysis techniques//Kenedi R. *Perspectives in Biomedical Engineering*. State College, Pa: University Park Press, 1973: 173–176.
- [51] Oxlund H, Andreassen T T. The roles of hyaluronic acid, collagen and elastin

- in the mechanical properties of connective tissues. *Journal of Anatomy*, 1980, 131(Pt4): 611–620.
- [52] Osborn T G, Bauer N E, Ross S C, et al. The tight-skin mouse: physical and biochemical properties of the skin. *Journal of Rheumatology*, 1983, 10(5): 793–796.
- [53] Wang Y L, Attenburrow G E. Strength of Brazilian goatskin leathers in relation to skin and animal characteristics. *Journal of the Society of Leather Technologists and Chemists*, 1994, 78(2): 55–60.
- [54] Vogel H G. Age dependence of mechanical and biochemical properties of human skin. Part I. Stress-strain experiments, skin thickness and biochemical analysis. *Bioengineering of Skin*, 1987, 3(1): 67–91.
- [55] Corcuff P, De Rigal J, Leveque J, et al. Skin relief and aging. *Journal of the Society of Cosmetic Chemists*, 1983, 34: 177–190.
- [56] Smith L. Histopathologic characteristics and ultrastructure of aging skin. *Cutis*, 1989, 43(5): 414–424.
- [57] Hall C W, Cox P A, McFarland S R, et al. Some factors that influence prolonged interfacial continuity. *Journal of Biomedical Materials Research*, 1981, 18(4): 383–393.
- [58] Manschot J F, Brakkee A J. The measurement and modeling of the mechanical properties of human skin in vivo-II. The model. *Journal of Biomechanics*, 1986, 19(7): 517–521.
- [59] Manschot J F, Brakkee A J. The measurement and modeling of the mechanical properties of human skin in vivo-I. The measurement. *Journal of Biomechanics*, 1986, 19(7): 511–515.
- [60] Brown I A. A scanning electron microscope study of the effects of uniaxial tension on human skin. *British Journal of Dermatology*, 1973, 89(4): 383–393.
- [61] Mansour J M, Davis B R, Srour M, et al. Effects of ribose on the tensile behavior of skin: Application to a theory of aging. *ASME Proceedings 1991 Biomechanics Symposium*, 1991: 299–302.
- [62] Wainwright S A, Biggs W D, Currey J D, et al. *Mechanical Design in Organisms*. London: Edward Arnold, 1976.
- [63] Veronda D R, Westmann R A. Mechanical characterization of skin-finite deformations. *Journal of Biomechanics*, 1970, 3(1): 111–124.
- [64] Purslow P P. Strain-induced reorientation of an intramuscular connective tissue network: Implications for passive muscle elasticity. *Journal of Biomechanics*, 1989, 22(1): 21–31.
- [65] Fortin M, Soulhat J, Shirazi-Adl A, et al. Unconfined compression of articular cartilage: Nonlinear behavior and comparison with a fibril-reinforced biphasic model. *Journal of Biomechanical Engineering*, 2000, 122(2): 189–195.
- [66] Manschot J F M. *The Mechanical Properties of Human Skin in Vivo* [Ph.D. Thesis]. Nijmegen: Catholic University of Nijmegen, 1985.
- [67] Maurel W, Wu Y, Magneat Thalmann N, et al. *Biomechanical models for soft tissue simulation*. ESPRIT Basic Research Series. Berlin: Springer-Verlag, 1998.

- [68] Haut R C. The sensitivity of skin to strain rate of loading. 7th Annual Meeting of the American Society of Biomechanics. Rochester, 1983.
- [69] Ranu H S. Mechanical and structural response of skin to irradiation. *Journal of Biomechanics*, 1979, 12(8): 601–608.
- [70] Millington P, Wilkinson R. Mechanical, thermal and electrical properties. *Skin*. Cambridge: Cambridge University Press, 1983.
- [71] Oxlund H, Manschot J, Viidik A. The role of elastin in the mechanical properties of skin. *Journal of Biomechanics*, 1988, 21(3): 213–218.
- [72] Cohen R E, Hooley C J, McCrum N G. Viscoelastic creep of collagenous tissue. *Journal of Biomechanics*, 1976, 9(4): 175–184.
- [73] Silver F H. *Biological Materials: Structure, Mechanical Properties, and Modeling of Soft Tissues*. New York: New York University Press, 1987.
- [74] Grahame R, Holt P J L. The influence of aging on the in vivo elasticity of human skin. *Gerontologia*, 1969, 15(2): 121–139.
- [75] Tregear R T. *Physical Functions of the Skin*. New York: Academic Press, 1966.
- [76] Del Prete Z, Antoniucci S, Hoffman A H, et al. Viscoelastic properties of skin in Mov-13 and Tsk mice. *Journal of Biomechanics*, 2004, 37(10): 1491–1497.
- [77] Fung Y C. *Biomechanics: Mechanical Properties of Living Tissue*. New York: Springer-Verlag, 1993.
- [78] Lanir Y, Fung Y C. Two-dimensional mechanical properties of rabbit skin. II. Experimental results. *Journal of Biomechanics*, 1974, 7(2): 171–182.
- [79] Sanjeevi R. A viscoelastic model for the mechanical properties of biological materials. *Journal of Biomechanics*, 1982, 15(2): 107–109.
- [80] Reihnsner R, Balogh B, Menzel E J. Two-dimensional elastic properties of human skin in terms of an incremental model at the in vivo configuration. *Medical Engineering and Physics*, 1995, 17(4): 304–313.
- [81] Belkoff S M, Haut R C. A structural model used to evaluate the changing microstructure of maturing rat skin. *Journal of Biomechanics*, 1991, 24(8): 711–720.
- [82] Ryhanen L, Uitto J. Elastic fibers of the connective tissue//Goldsmith L A. *Biochemistry and Physiology of the Skin*. New York: Oxford University Press, 1983.
- [83] Jenkins R B, Little R W. A constitutive equation for parallel-fibered elastic tissue. *Journal of Biomechanics*, 1974, 7(5): 397–402.
- [84] Flint M H, Craig A S, Reilly H C, et al. Collagen fibril diameters and glycosaminoglycan content of skins—indices of tissue maturity and function. *Connective Tissue Research*, 1984, 13(1): 69–81.
- [85] Flint M H, Gillard G C, Merrilies M J. The effects of local physical environmental factors on connective tissue organisation and glycosaminoglycan synthesis//Parry D, Creamer L K. *Fibrous Proteins: Scientific, Industrial and Medical Aspects*. London: Academic Press, 1980: 107–119.
- [86] Kronick P L, Sacks M S. Matrix macromolecules that affect the viscoelasticity of calfskin. *Journal of Biomechanical Engineering*, 1994, 116(2): 140–145.

- [87] Vogel H G. Tensile strength, relaxation and mechanical recovery in rat skin as influenced by maturation and age. *Journal of Medicine*, 1976, 7(2): 177–188.
- [88] Gillard G C, Reilly H C, Bell-Booth P G, et al. The influence of mechanical forces on the glycosaminoglycan content of the rabbit flexor digitorum profundus tendon. *Connective Tissue Research*, 1979, 7(1): 37–46.
- [89] Oomens C W, van Campen D H, Grootenboer H J. In vitro compression of a soft tissue layer on a rigid foundation. *Journal of Biomechanics*, 1987, 20(10): 923–935.
- [90] Minns R J, Soden P D, Jackson D S. The role of the fibrous components and the ground substance in the mechanical properties of biological tissues: A preliminary investigation. *Journal of Biomechanics*, 1973, 6(2): 153–165.
- [91] Egan J M. A constitutive model for the mechanical behaviour of soft connective tissues. *Journal of Biomechanics*, 1987, 20(7): 681–692.
- [92] Rodrigues L, Group E. EEMCO guidance to the in vivo assessment of tensile functional properties of the skin, Part II. Instrumentation and test methods. *Skin Pharmacol. Applied Skin Physiology*, 2001, 14(1): 52–67.
- [93] Retel V, Vescovo P, Jacquet E, et al. Nonlinear model of skin mechanical behaviour analysis with finite element method. *Skin Research and Technology*, 2001, 7(3): 152–158.
- [94] Gibson T, Stark H, Evans J H. Directional variation in extensibility of human skin in vivo. *Journal of Biomechanics*, 1969, 2(2): 201–204.
- [95] Zhou B, Xu F, Chen C Q, et al. Strain rate sensitivity of skin tissue under thermomechanical loading. *Philosophical Transactions. Series A. Mathematical, Physical, and Engineering Sciences*. 2010, 368(1912): 679–690.
- [96] Wijn P. The Alinear Viscoelastic Properties of Human Skin in Vivo for Small Deformations [Ph. D. Thesis]. Nijmegen: University of Nijmegen, 1980.
- [97] Jamison C E, Marangoni R D, Glaser A A. Viscoelastic properties of soft tissue by discrete model characterization. *Journal of Biomechanics*, 1968, 1(1): 33–36.
- [98] William R, Ledoux J J B. The compressive material properties of the plantar soft tissue. *Journal of biomechanics*, 2007, 40(13): 7.
- [99] John Z, Wu R G C, Andrew M E, et al. Simultaneous determination of the nonlinear-elastic properties of skin and subcutaneous tissue in unconfined compression tests. *Skin Research and Technology*, 2007, 13(1): 9.
- [100] Oliver A, Shergold N A F, Darren R. The uniaxial stress versus strain response of pig skin and silicone rubber at low and high strain rates. *International Journal of Impact Engineering*, 2006, 32(9): 1384–1402.
- [101] Esra Roan K V. The nonlinear material properties of liver tissue determined from no-slip uniaxial compression experiments. *Journal of Biomechanical Engineering*, 2007, 129(3): 7.
- [102] Bader D L, Bowker P. Mechanical characteristics of skin and underlying tissues in vivo. *Biomaterials*, 1983, 4(4): 305–308.
- [103] Hendley A, Marks R, Payne P. Measurement of forces for point indentation of the stratum corneum in vivo: The influences of age, sex, site delipidisation

- and hydration. *Bioengineering and the Skin*, 1982, 3: 234–240.
- [104] Zheng Y P, Mak A F T. An ultrasound indentation system for biomechanical properties assessment of soft tissues in-vivo. *IEEE Transactions on Biomedical Engineering*, 1996, 43(9): 912–918.
- [105] Yuan Y, Verma R. Mechanical properties of stratum corneum studied by nano-indentation. *Spatially Resolved Characterization of Local Phenomena in Materials and Nanostructures*, 2002: 265–272.
- [106] Alexander H, Cook T H. Accounting for natural tension in the mechanical testing of human skin. *Journal of Investigative Dermatology*, 1977, 69(3): 310–314.
- [107] Diridollou S, Patat F, Gens F, et al. In vivo model of the mechanical properties of the human skin under suction. *Skin Research and Technology*, 2000, 6(4): 214–221.
- [108] Diridollou S. Mechanical properties of the skin under suction. *Skin Research and Technology*, 2001, 7(2): 127.
- [109] Hendriks F M, Brokken D, Oomens C W, et al. The relative contributions of different skin layers to the mechanical behavior of human skin in vivo using suction experiments. *Medical Engineering and Physics*, 2006, 28(3): 259–266.
- [110] Agache P G. Twistometry measurement of skin elasticity//Serup J, Jemec G B E. *Handbook of Non-Invasive Methods and the Skin*. Boca Raton: CRC Press, 1995: 319–328.
- [111] Finlay J B. Thixotropy in human skin. *Journal of Biomechanics*, 1978, 11(6-7): 333–342.
- [112] Sanders R. Torsional elasticity of human skin in vivo. *Pflügers Archiv European Journal of Physiology*, 1973, 342(3): 255–260.
- [113] Escoffier C, Rochefort A, et al. Age-related mechanical properties of human skin: An in vivo study. *Journal of Investigative Dermatology*, 1989, 93(3): 353–357.
- [114] Grebenyuk L A, Uten'kin A A. Mechanical properties of the human skin: Communication. *Human Physiology*, 1994, 20(2): 157–162.
- [115] Gennisson J L, Baldeweck T, Tanter M, et al. Assessment of elastic parameters of human skin using dynamic elastography. *IEEE Transactions on Ultrasonics, Ferroelectrics, and Frequency Control*, 2004, 51(8): 980–989.
- [116] Vexler A, Polyansky I, Gorodetsky R. Evaluation of skin viscoelasticity and anisotropy by measurement of speed of shear wave propagation with viscoelasticity skin analyzer. *Journal of Investigative Dermatology*, 1999, 113: 732–739.
- [117] Lanir Y. *Skin mechanics*//Skalak R, Chien S. *Handbook of Bioengineering*. New York: McGraw-Hill, 1987: 11.11–11.25.
- [118] Gunner C W, Hutton W C, Burlin T E. The mechanical properties of skin in vivo: A portable hand-held extensometer. *British Journal of Dermatology*, 1979, 100(2): 161–163.
- [119] Nicolopoulos C S, Giannoudis P V, Glaros K D, et al. In vitro study of the failure of skin surface after influence of hydration and preconditioning.

- Archives logical Research, 1998, 290(11): 638–640.
- [120] Xu F, Lu T, Seffen K. Biothermomechanical behavior of skin tissue. *Acta Mechanica Sinica*, 2008, 24(1): 1–23.
- [121] Vogel S, Papanicolaou M N. A constant stress creep testing machine. *Journal of Biomechanics*, 1983, 16(2): 153–156.
- [122] Arbogast K B, Thibault K L, Scott Pinheiro B, et al. A high-frequency shear device for testing soft biological tissues. *Journal of Biomechanics*, 1997, 30(7): 757–759.
- [123] Lanir Y, Fung Y C. Two-dimensional mechanical properties of rabbit skin. I. Experimental system. *Journal of Biomechanics*, 1974, 7(1): 29–34.
- [124] Reihnsner R, Menzel E J. Two-dimensional stress-relaxation behavior of human skin as influenced by non-enzymatic glycation and the inhibitory agent aminoguanidine. *Journal of Biomechanics*, 1998, 31(11): 985–993.
- [125] Vito R P. The mechanical properties of soft tissues, I: A mechanical system for bi-axial testing. *Journal of Biomechanics*, 1980, 13(11): 947–950.
- [126] Tong P, Fung Y C. Stress-strain relationship for the skin. *Journal of Biomechanics*, 1976, 9(10): 649–657.
- [127] Schneider D C, Davidson T M, Nahum A M. In vitro biaxial stress-strain response of human skin. *Archives of Otolaryngology–Head and Neck Surgery*, 1984, 110(5): 329–333.
- [128] Thubrikar M, Eppink R T. A method for analysis of bending and shearing deformations in biological tissue. *Journal of Biomechanics*, 1982, 15(7): 529–535.
- [129] Hung C T, Williams J L. A method for inducing equibiaxial and uniform strains in elastomeric membranes used as cell substrates. *Journal of Biomechanics*, 1994, 27(2): 227–232.
- [130] Mitchell S B, Sanders J E, Garbini J L, et al. A device to apply user-specified strains to biomaterials in culture. *IEEE Transactions on Biomedical Engineering*, 2001, 48(2): 268–273.
- [131] Sanders J E, Mitchell S B, Wang Y N, et al. An explant model for the investigation of skin adaptation to mechanical stress. *IEEE Transactions on Biomedical Engineering*, 2002, 49: 1626–1631.
- [132] Kvistedal Y A. *Multiaxial in-Vivo Testing of Human Skin* [M. S. Thesis]. Auckland: University of Auckland, 2003.
- [133] Kvistedal Y A, Nielsen P M F. Investigating stress-strain properties of in-vivo human skin using multiaxial loading experiments and finite element modeling. 26th Annual International Conference of the IEEE Engineering in Medicine and Biology Society. Piscataway, 2004: 5096–5099.
- [134] Sacks M S, Chuong C J. Biaxial mechanical properties of passive right ventricular free wall myocardium. *Journal of Biomechanical Engineering*, 1993, 115(2): 202–205.
- [135] Derwin K A, Soslowsky L J, Green W D K, et al. A new optical system for the determination of deformations and strains: Calibration characteristics and experimental results. *Journal of Biomechanics*, 1994, 27(10): 1277–1285.

- [136] Smutz W P, Drexler M, Berglund L J, et al. Accuracy of a video strain measurement system. *Journal of Biomechanics*, 1996, 29(6): 813–817.
- [137] Butler D L, Grood E S, Noyes F R, et al. Effects of structure and strain measurement technique on the material properties of young human tendons and fascia. *Journal of Biomechanics*, 1984, 17(8): 579–596.
- [138] Zernicke R F, Butler D L, Grood E S, et al. Strain topography of human tendon and fascia. *Journal of Biomechanical Engineering*, 1984, 106(2): 177–180.
- [139] Wright D M, Wiig H, Winlove C P, et al. Simultaneous measurement of interstitial fluid pressure and load in rat skin after strain application in vitro. *Annals of Biomedical Engineering*, 2003, 31(10): 1246–1254.
- [140] Sun W, Sacks M S, Scott M J. Effects of boundry conditions on the estimation of the planar biaxial mechanical properties of soft tissues. *Journal of Biomechanical Engineering*, 2005, 127(4): 709–715.
- [141] Yin P, Tompkins W R, Peterson K L, et al. A video dimension analyzer. *IEEE Transactions on Biomedical Engineering*, 1972, BME-19: 376–381.
- [142] Downs J, Halperin H R, Humphrey J D, et al. An improved video-based computer tracking system for soft-biomaterialstesting. *IEEE Transactions on Biomedical Engineering*, 1990, 37: 903–907.
- [143] Roth V, Mow V C. The intrinsic tensile behavior of the matrix of bovine articular cartilage and its variation with age. *Journal of Bone and Joint Surgery*, 1980, 62(7): 1102–1117.
- [144] Amadio P C, Berglund L J, An K N. Biochemically discrete zones of canine flexor tendon: Evaluation of properties with a new photographic method. *Journal of Orthopaedic Surgery and Research*, 1992, 10(2): 198–204.
- [145] Mofid Y, Ossant F, Kathyr F, et al. In-vivo human skin elastography: A preliminary study. *Proceedings of World Congress on Ultrasonics*. Paris, 2003: 205–208.
- [146] Mansour J M, Davis B R, Srour M, et al. A method for obtaining repeatable measurements of the tensile properties of skin at low strain. *Journal of Biomechanics*, 1993, 26(2): 211–216.
- [147] Lepetit J, Favier R, Grajales A, et al. A simple cryogenic holder for tensile testing of soft biological tissues. *Journal of Biomechanics*, 2004, 37(4): 557–562.
- [148] Waldman S D, Lee J M. Effect of sample geometry on the apparent biaxial mechanical behaviour of planar connective tissues. *Biomaterials*, 2005, 26(35): 7504–7513.
- [149] Waldman S D, Michael Lee J. Boundary conditions during biaxial testing of planar connective tissues. Part I: Dynamic behavior. *Journal of Materials Science: Materials in Medicine*, 2002, 13(10): 933–938.
- [150] Waldman S D, Sacks M S, Lee J M. Boundary conditions during biaxial testing of planar connective tissues. Part II: Fiber orientation. *Journal of Materials Science Letters*, 2002, 21(15): 1215–1221.
- [151] Ranu H S. Effects of radiotherapy on the mechanical properties of human skin. *IEEE Engineering in Medicine and Biology*, 1991, 10(2): 55–57.

- [152] Ranu H S, Burlin T E, Hutton W C. The effects of X-irradiation on the mechanical properties of skin. *Physics in Medicine and Biology*, 1975, 20(1): 96–105.
- [153] Nilsson T. Biomechanical studies of rabbit abdominal wall - 2. The mechanical properties of specimens in relation to length, width and fiber orientation. *Journal of Biomechanics*, 1982, 15(2): 131–135.
- [154] Komatsu K, Sanctuary C, Shibata T, et al. Stress-relaxation and microscopic dynamics of rabbit periodontal ligament. *Journal of Biomechanics*, 2007, 40(3): 634–644.
- [155] Purslow P P, Wess T J, Hukins D W L. Collagen orientation and molecular spacing during creep and stress-relaxation in soft connective tissues. *Journal of Experimental Biology*, 1998, 201(1): 135–142.
- [156] Woo S L, Gomez M A, Woo Y K, et al. Mechanical properties of tendon and ligaments. The relationship of immobilization and exercise on tissue remodeling. *Biorheol*, 1982, 19(3): 397–408.
- [157] Svendsen K H, Thomson G. A new clamping and stretching procedure for determination of collagen fiber stiffness and strength relations upon maturation. *Journal of Biomechanics*, 1984, 17(3): 225–229.
- [158] Iatridis J C, Wu J R, Yandow J A, et al. Subcutaneous tissue mechanical behavior is linear and viscoelastic under uniaxial tension. *Connective Tissue Research*, 2003, 44(5): 208–217.
- [159] Riemersma D J, Schamhardt H C. The Cryo-jaw, a clamp designed for in vitro rheology studies of horse digital flexor tendons. *Journal of Biomechanics*, 1982, 15(8): 619–620.
- [160] Mommersteeg T J, Blankevoort L, Huiskes R, et al. Characterization of the mechanical behaviour of human knee ligaments: A numerical-experimental approach // Mommersteeg T J. *Human Knee Ligaments: Structure, Function and Mechanical Properties*. Wageningen: Ponsen and Looijen BV, 1994: 73–89.
- [161] Humphrey J D, Yin F C P. A new approach for describing soft tissue behavior. *Proceedings of the 13th Northeast Bioengineering Conference*. Philadelphia, 1987: 24–25.
- [162] Haut R C. The influence of specimen length on the tensile failure properties of tendon collagen. *Journal of Biomechanics*, 1986, 19(11): 951–955.
- [163] Reihnsner R, Melling M, Pfeiler W, et al. Alterations of biochemical and two-dimensional biomechanical properties of human skin in diabetes mellitus as compared to effects of in vitro non-enzymatic glycation. *Clinical Biomechanics*, 2000, 15(5): 379–386.
- [164] Flynn D M, Peura G D, Grigg P, et al. A finite element based method to determine the properties of planar soft tissue. *Journal of Biomechanical Engineering*, 1998, 120(2): 202–210.
- [165] Giles J M, Black A E, Bischoff J E. Anomalous rate dependence of the preconditioned response of soft tissue during load controlled deformation. *Journal of Biomechanics*, 2007, 40(4): 777–785.

- [166] Gibson T, Kenedi R M, Craik J E. The mobile micro-architecture of dermal collagen. *British Journal of Surgery*, 1965, 52: 764–770.
- [167] Fung Y C. Stress-strain history relations of soft tissues in simple elongation//Fung Y C, Perrone N, Anliker M. *Biomechanics: Its Foundations and Objectives*. Englewood Cliffs: Prentice-Hall, 1971: 181–208.
- [168] Vogel H G, Denkel K. In vivo recovery of mechanical properties in rat skin after repeated strain. *Archives of Dermatology Research*, 1985, 277(6): 484–488.
- [169] Edsberg L E, Mates R E, Baier R E, et al. Mechanical characteristics of human skin subjected to static versus cyclic normal pressures. *Journal of Rehabilitation Research and Development*, 1999, 36(2): 133–143.
- [170] Stark H L. Directional variations in the extensibility of human skin. *British Journal of Plastic Surgery*, 1977, 30(2): 105–114.
- [171] Xu F, Seffen K, Lu T. Temperature-dependent mechanical behaviors of skin tissue. *IAENG International Journal of Computer Science*, 2008, 35(1): 92–101.
- [172] Wu J Z, Dong R G, Smutz W P, et al. Non-linear and viscoelastic characteristics of skin under compression: Experiment and analysis. *Bio-Medical Materials and Engineering*, 2003, 13(4): 373–385.
- [173] Fung Y C. *Biomechanics: Mechanical Properties of Living Tissues*. New York: Springer-Verlag, 1993.
- [174] Meijer R, Douven L F A, Oomens C W J. Characterization of anisotropic and non-linear behaviour of human skin in vivo. *Computer Methods in Biomechanics and Biomedical Engineering*, 1999, 2(1): 13–27.
- [175] Belkoff S M, Naylor E C, Walshaw R, et al. Effects of subcutaneous expansion on the mechanical properties of porcine skin. *Journal of Surgical Research*, 1995, 58(2): 117–123.
- [176] Lanir Y, Manny V, Zlotogorski A, et al. Influence of ageing on the in vivo mechanics of the skin. *Skin Pharmacology and Applied Skin Physiology*, 1993, 6(3): 223–230.
- [177] Langer K. On the anatomy and physiology of the skin:IV. The swelling capabilities of skin. *British Journal of Plastic Surgery*, 1978, 31(4): 273–276.
- [178] Kenedi R M, Gibson T, Daly C H. Bio-engineering studies of the human skin: II//Kenedi R M. *Biomechanics and Related Bio-Engineering Topics*. Oxford: Pergamon Press, 1965: 147–158.
- [179] Ridge M D, Wright V. Mechanical properties of skin: A bioengineering study of skin structure. *Journal of Applied Physiology*, 1966, 21(5): 1602–1606.
- [180] Looney M, Kyrtziz L, Truong Y, et al. Enhancing the unique properties of kangaroo leather. RIRDC Publication No. 02/105, 2002.
- [181] Vogel H G, Hilgner W. The “step phenomenon” as observed in animal skin. *Journal of Biomechanics*, 1979, 12(1): 75–81.
- [182] Vogel H G. Directional variations of mechanical parameters in rat skin depending on maturation and age. *Journal of Investigative Dermatology*, 1981, 76(6): 493–497.

- [183] Pereira B P, Lucas P W, Swee-Hin T. Ranking the fracture toughness of thin mammalian soft tissues using the scissors cutting test. *Journal of Biomechanics*, 1997, 30(1): 91–94.
- [184] Shergold O A, Fleck N A. Experimental investigation into the deep penetration of soft solids by sharp and blunt punches, with application to the piercing of skin. *Journal of Biomechanical Engineering*, 2005, 127(5): 838–848.
- [185] Ankersen J, Birkbeck A E, Thomson R D, et al. Puncture resistance and tensile strength of skin simulants. *Journal of Engineering in Medicine*, 1999, 213(6): 493–501.
- [186] Manschot J F M, Brakkee A J M. Characterisation of in vivo mechanical skin properties independent of measuring configuration. *Bioengineering of the Skin*, 1987, 3: 1–10.
- [187] Giacomoni P U, Rein G. A mechanistic model for the aging of human skin. *Micron*, 2004, 35(3): 179–184.
- [188] Lavker R M, Zheng P, Dong G. Aged skin: A study by light, transmission electron, and scanning electron microscopy. *Journal of Investigative Dermatology*, 1987, 88(3Suppl.): 44s–51s.
- [189] De Rigal J, Escoffier C, Querleux B, et al. Assessment of aging of the human skin by in vivo ultrasonic imaging. *Journal of Investigative Dermatology*, 1989, 93: 621–625.
- [190] Hermanns-Le T, Uhoda I, Smitz S, et al. Skin tensile properties revisited during ageing. Where now, where next? *Journal of Cosmetic Dermatology*, 2004, 3(1): 35–40.
- [191] Silver F H, Seehra G P, Freeman J W, et al. Viscoelastic properties of young and old human dermis: A proposed molecular mechanism for elastic energy storage in collagen and elastin. *Journal of Applied Polymer Science*, 2002, 86(8): 1978–1985.
- [192] Couturaud V, Coutable J, Khaiat A. Skin biomechanical properties: In vivo evaluation of influence of age and body site by a non-invasive method. *Skin Research and Technology*, 1995, 1(2): 68–73.
- [193] Piérard-Franchimont C, Castelli D, van Cromphaut I, et al. Tensile properties and contours of aging facial skin, a controlled double-blind comparative study of the effects of retinol, melibiose-lactose and their association. *Skin Research and Technology*, 1998, 4(4): 237–243.
- [194] Bonilla C M A, Massanet A R F, Almodóvar N V. Mechanics of biomaterials: Skin repair and grafts. *Proceedings of Applications of Engineering Mechanics in Medicine*. Mayaguez, 2005.
- [195] Hashmi F, Malone-Lee J. Measurement of skin elasticity on the foot. *Skin Research and Technology*, 2007, 13(3): 252–258.
- [196] Ishikawa T, Ishikawa O, Miyachi Y. Measurement of skin elastic properties with a new suction device. I: Relationship with age, sex and the degree of obesity in normal individuals. *Journal of Dermatology*, 1995, 22(10): 713–717.

- [197] Pugliese P T, Potts J R. Hardware and measuring principles: The ballistometer//Elsner P, Berardesca E, Wilhelm K P, et al. *Bioengineering of the Skin: Skin Biomechanics*. Boca Raton: CRC Press, 2002: 147–159.
- [198] Vogel H. Directional variations of mechanical parameter in rat skin depending on maturation and age. *Journal of Investigative Dermatology*, 1981, 76(6): 493–497.
- [199] Elden H R. *Biophysical ageing of skin*//Elden H R. *Biophysical properties of skin*. New York: John Wiley and Sons, 1976: 1–62.
- [200] Nimini M E, de Guia E, Bavetta L A. Collagen, hexosamine and tensile strength of rabbit skin during aging. *Journal of Investigative Dermatology*, 1966, 47(2): 156–158.
- [201] Fry P, Harkness M L, Harkness R D. Mechanical properties of the collagenous framework of skin in rats of different ages. *American Journal of Physiology*, 1964, 206: 1425–1429.
- [202] Vogel H G, Hilgner W. Analysis of the low part of stress-strain curves in rat skin. Influence of age and desmotropic drugs. *Archives logical Research*, 1977, 258(2): 141–150.
- [203] Haut R C. The effects of orientation and location on the strength of dorsal rat skin in high and low speed tensile failure experiments. *Journal of Biomechanical Engineering*, 1989, 111(2): 136–140.
- [204] Bischoff J E, Arruda E M, Grosh K. Finite element modeling of human skin using an isotropic, nonlinear elastic constitutive model. *Journal of Biomechanics*, 2000, 33(6): 645–652.
- [205] Dinnar U. A note on theory of deformation in compressed skin tissues. *Mathematical Biosciences*, 1970, 8(1-2): 71–82.
- [206] Bernstein E F, Gasparro F P, Brown D B, et al. 8-methoxypsoralen and UV-A radiation activate the human elastin promoter in transgenic mice: In vivo and in vitro evidence for gene induction. *Photochem Photobiol*, 1996, 64(2): 369–374.
- [207] Mays P K, Bishop J E, Laurent G J. Age-related changes in the proportion of types I and III collagen. *Mechanisms of Ageing and Development*, 1988, 45(3): 203–212.
- [208] Clausen B. Influence of age on connective tissue. Uronic acid and uronic acid-hydroxyproline ratio in human aorta, myocardium, and skin. *Laboratory Investigation*, 1962, 11: 1340.
- [209] Potts R O, Buras E M, Chrisman D A. Changes with age in the moisture content of human skin. *Journal of Investigative Dermatology*, 1984, 82: 97–100.
- [210] Malm M, Samman M, Serup J. In vivo skin elasticity of 22 anatomical sites. *Skin Research and Technology*, 1995, 1(2): 61–67.
- [211] Mohanaradhakrishnan V, Muthiah P L, Hadhanyi A. A few factors contributing to the mechanical strength of collagen fibres. *Arzneimittelforschung*, 1975, 25(5): 726–735.
- [212] Auriol F, Vaillant L, Machet L, et al. Effects of short-time hydration on skin extensibility. *Acta Dermato-Venereologica*, 1993, 73(5): 344–347.

- [213] Overgaard O L, Jemec G B. The influence of water, glycerin paraffin oil and ethanol on skin mechanics. *Acta Dermato-Venereologica*, 1993, 73(6): 404–406.
- [214] Bert J L, Reed R K. Pressure-volume relationship for rat dermis: Compression studies. *Acta Physiologica Scandinavica*, 1997, 160(1): 89–94.
- [215] Hoffman A H, Robichaud D R, Grigg P. The effect of hydration upon the compliance properties of rat skin. 2003 Summer Bioengineering Conference. Key Biscayne, 2003: 633–634.
- [216] Dobrev H. Use of cutometer to assess epidermal hydration. *Skin Research and Technology*, 2000, 6(4): 239–244.
- [217] Potts R O. Stratum corneum hydration: Experimental techniques and interpretations of results. *International Journal of Cosmetic Science*, 1986, 37(1): 9–33.
- [218] Kasting G B, Barai N D. Equilibrium water sorption in human stratum corneum. *Journal of Pharmaceutical Sciences*, 2003, 92(8): 1624–1631.
- [219] Simon M, Bernard D, Minondo A M, et al. Persistence of both peripheral and non-peripheral corneodesmosomes in the upper stratum corneum of winter xerosis skin versus only peripheral in normal skin. *Journal of Investigative Dermatology*, 2001, 116: 23–30.
- [220] Luscher M, GIOvANou R, Hirter P. Untersuchungen der Hydratation von Collagen Sorptionsmessungen und Rbntgenweitwinkeldiffraktion an Tropocolagen. *Chimia*, 1973, 27: 112.
- [221] Katz E P, La S T. The intermolecular space of reconstituted collagen fibrils. *Journal of Molecular Biology*, 1973, 73(3): 351.
- [222] Ananthapadmanabhan K P, Lips A, Vincent C, et al. Ph-induced alterations in stratum corneum properties. *Journal of Cosmetic Sciences*, 2003, 25(3): 103–112.
- [223] Baker M R, Bader D, Hopewell J W. The effects of single doses of X rays on the mechanical properties of pig skin in vivo. *The British Journal of Radiology*, 1989, 62(741): 830–837.
- [224] Burlin T E, Challoner A V, Hutton W C, et al. Effects of radiation on the visual appearance and mechanical properties of mouse skin. *The British Journal of Radiology*, 1977, 50(590): 123–128.
- [225] Dobrev H. Research reports of the union of scientists in bulgaria—plovdiv. *Annual, Series B. Natural Sciences and Humanities*, 2000, 1: 117–120.
- [226] Nishimori Y, Edwards C, Pearse A, et al. Degenerative alterations of dermal collagen fiber bundles in photodamaged human skin and UV-irradiated hairless mouse skin: Possible effect on decreasing skin mechanical properties and appearance of wrinkles. *Journal of Investigative Dermatology*, 2001, 117(6): 1458–1463.
- [227] Oba A, Edwards C. Relationships between changes in mechanical properties of the skin, wrinkling, and destruction of dermal collagen fiber bundles caused by photoaging. *Skin Research and Technology*, 2006, 12(4): 283–288.
- [228] Bissett R, Hannon D P, Orr T V. Wavelength dependence of histological, physical, and visible changes in chronically UV-irradiated hairless mouse

- skin. *Photochemistry and Photobiology*, 1989, 50(6): 763–769.
- [229] Fournatier A, Berrebi C. Miniature pig as animal model to study photoaging. *Photochemistry and Photobiology*, 1989, 50(6): 771–784.
- [230] Margelin D, Medaisko C, Lombard D, et al. Hyaluronic acid and dermatan sulfate are selectively stimulated by retinoic acid in irradiated and nonirradiated hairless mouse skin. *Journal of Investigative Dermatology*, 1996, 106: 505–509.
- [231] Zheng P, Kligman L H. UVA-induced ultrastructural changes in hairless mouse skin: A comparison to UVB-induced damage. *Journal of Investigative Dermatology*, 1993, 100: 194–199.
- [232] Smith J G, Davidson E A, Sams W M, et al. Alternations in human dermal connective tissue with age and chronic sun damage. *Journal of Investigative Dermatology*, 1962, 39: 347–350.
- [233] Cooper D R, Davidson R J. The effect of ultraviolet radiation on soluble collagen. *Biochemical Journal*, 1965, 97(1): 139–147.
- [234] Pioletti D P, Rakotomanana L R. On the independence of time and strain effects in the stress relaxation of ligaments and tendons. *Journal of Biomechanics*, 2000, 33(12): 1729–1732.
- [235] Demer L L, Yin F C P. Passive biaxial mechanical properties of isolated canine myocardium. *Journal of Physiology (London)*, 1983, 339: 615–630.
- [236] Haut R C, Little R W. A constitutive equation for collagen fibers. *Journal of Biomechanics*, 1972, 5(5): 423–430.
- [237] Dombi G W, Haut R C, Sullivan W G. Correlation of high-speed tensile strength with collagen content in control and lathyrotic rat skin. *Journal of Surgical Research*, 1993, 54(1): 21–28.
- [238] Potts R O, Chrisman D A, Buras E M. The dynamic mechanical properties of human skin in vivo. *Journal of Biomechanics*, 1983, 16(6): 365–372.
- [239] Vogel H G. Influence of age, treatment with corticosteroids and strain rate on mechanical properties of rat skin. *Biochimica et Biophysica Acta*, 1972, 286(1): 79–83.
- [240] Gadd C W, Lange W A, Peterson F J. *Strength of skin and its measurement*. ASME New York, 1965: 5.
- [241] Li J T, Armstrong C G, Mow V C. The effect of strain rate on mechanical properties of articular cartilage in tension. *ASME Biomechanics Symposium*, 1983: 117–120.
- [242] Zhang M, Zheng Y P, Mak A F. Estimating the effective Young's modulus of soft tissues from indentation tests: Nonlinear finite element analysis of effects of friction and large deformation. *Medical Engineering and Physics*, 1997, 19(6): 512–517.

Chapter 7

Skin Biomechanics Modeling

7.1 Introduction

Besides the experimental studies, accurate, quantitative simulations of the biomechanics of living systems and their surrounding environment have the potential to facilitate advancements in nearly every aspect of medicine and biology, since computational models can yield estimates of stress and strain data over the entire continuum of interest, which becomes especially advantageous for locations where it may be difficult or impossible to obtain from experimental measurements^[1]. Specially, with the advances in imaging techniques and computing hardware, it is now possible to develop and non-invasively analyze patient-specific models, which may revolutionize the way clinicians diagnose and treat certain pathologies^[2].

7.1.1 Finite element models

In some cases, closed-form mathematical solutions to problems with relatively simple geometry and boundary conditions can be obtained by combining the equations of motion and appropriate constitutive law. Unfortunately, most problems of interest in biomechanics are too complex to obtain closed-form solutions, due to inhomogeneous material properties, complex three-dimensional geometry, and unique boundary/initial conditions such as *in vivo* stress. In these cases, numerical solution techniques must be utilized, where the finite element (FE) method appears to be ideal for the complex geometries often encountered in biomechanical systems: it provides a systematic method for assembling the response of a complex system from individual contributions of elements and provides a consistent way to address material inhomogeneities and differences in constitutive models between disjoint or continuous parts of a model.

Finite element models (FEMs), more recently, are used to simulate the mechanical behaviour of the skin and to determine the mechanical parameters with experiments. For example, DeHoff & Key^[3] used the finite element

technique to estimate the stresses in a closing wound following a Z-plasty. This is an incision technique commonly used by surgeons and is named after its characteristic shape. In their model they used a generalised uniaxial constitutive equation assuming isotropic behaviour. Despite this simplification they were able to successfully estimate stresses in different variations of the Z-plasty. Meijer et al.^[4] combined uniaxial extension experiments and a FEM with Lanir's structural skin model^[5] as a constitutive equation to characterize the anisotropic non-linear behaviour of human skin *in vivo*. Larrabee & Sutton^[6] and Larrabee & Galt^[7] used the finite element technique to model wound closures and skin deformations. They modeled the skin as an isotropic two-dimensional system connected to a rigid plane with linear springs, representing the subcutaneous attachment. The skin is modeled with a linear stress-strain relationship. Time dependence and skin pretension are ignored. To account for large deformations and large strains, Kirby et al.^[8] extended the model by Larrabee to a non-linear, isotropic FEM, where they modeled skin deformations in three-dimensional space. In their study, they successfully estimated the forces needed to close specific types of wounds. Bischoff et al.^[9] used the eight-chain model by Arruda and Boyce^[10] as an elastic constitutive equation for his FEM. They obtained the data of three different experiments from literature to determine the unknowns in the constitutive equations. Although a lot of assumptions had to be made to be able to use those data, they were quite successful in simulating the experiments. Manios et al.^[11] and Retel et al.^[12] used non-linear finite element methods, assuming isotropy and elastic behaviour, to model large stresses and displacements in incisions and sutures that can occur during wound closure. These models used incremental displacements with linear regions, rather than a continuous constituent equation, to describe the non-linear behaviour of the skin.

For the successful application of the FE method to studies of skin mechanics, a detailed mathematical description of the material behaviour of the skin is necessary.

7.1.2 Importance of biomechanics modeling

Mathematical models of soft tissue mechanical properties may find applications, for example, in a surgical robot control system, where the prediction of deformation is needed^[13], surgical operation planning and surgeon training systems based on the virtual reality techniques, where force feedback is needed, and registration^[14], where knowledge of local deformation is required. Such systems for rigid tissues already exist. Their development for “very” soft

tissues is very much dependent on the knowledge of these tissues' mechanical properties and the existence of the appropriate mathematical models. Such models can also help to identify modes of injury, and improve injury prevention techniques^[15]. These models can help to further the understanding of the contribution of different tissue components to the material behaviour of the overall tissue for both the normal tissues and for tissues affected by injury, healing, immobilization, exercise, and other conditions that alter the homeostatic state of the tissue.

A detailed and accurate mathematical modeling of the mechanical properties of skin is especially important for several reasons^[16~18]: ① the skin contributes an important part to the total mechanical behaviour of various body parts and should be included in corresponding mathematical models since it is a continuous membrane covering almost the entire body; ② mechanical behaviour of skin as an isolated organ is also important in relation to surgery, where a good constitutive law could be used to simulate deformations relating to different types of incisions and closing techniques.

Unfortunately, accurate mathematical descriptions of the mechanical behaviour of soft tissues remain the limiting factor in the advancement of realistic medical simulations and noninvasive diagnostic tools, which is due to the complex nonlinear, anisotropic, inhomogeneous, viscoelastic material properties of soft tissues when they undergo large mechanical deformations during minimally invasive procedures and diagnostic palpations^[13,17].

7.1.3 Classification of mechanical models of soft tissues

A material model is referred to in continuum mechanics terminology as a constitutive model/equation, which is used to describe the mechanical behaviour of ideal materials through specification of the dependence of stress on kinematic variables such as the deformation gradient, rate of deformation, temperature, and pressure. The development of constitutive relations for a material generally follows specific steps^[17]: ① the material is first classified according to its behaviour and composition, e.g. elastic or viscoelastic, isotropic or anisotropic, linear or nonlinear, and homogeneous or heterogeneous; ② an appropriate theoretical framework is then chosen to develop the relationship between kinematic quantities and stress, where hyperelasticity is often used for biomechanics; ③ a specific constitutive equation is identified based on microstructural observations or experimental data; ④ experiments are performed in the last step to determine values for the material parameters, which can be used to validate the model's predictive ability.

Till now, a variety of constitutive models have been proposed to describe the mechanical behaviour of skin tissue (see References [5,19,20] for a review on earlier models). Three predominant approaches have been adopted in the characterization of mechanical behaviour of skin tissue and the proposed models can be generally classified as three kinds^[5,20]: continuum models, in which general material theories are specialized for tissues, phenomenological models, which consists of fitting mathematical equations to experimental tensile curves, and structural models, which are based on the assumed behaviour of the structural components of the tissue and are thus formulated in terms of structural parameters. The various specific skin models may be further distinguished with respect to several criterions, whether they are elastic or viscoelastic, uniaxial or multi-dimensional, isotropic or orthotropic, incompressible or compressible.

In this chapter, an overview of the development of skin material models is presented, with the purpose not to point at the model to apply, but rather to outline as far as possible the different forms they can take. The reader will find complete details in the given references.

7.2 Continuum Models and Phenomenological Models

The continuum models use general material theories to demonstrate the multiaxial behaviour of skin^[21~25]. The phenomenological models apply mathematical formulas, such as using a mathematical formation^[26~29] or a strain energy density function^[23,30], to imitate skin's response to various types of mechanical response based on the data from mechanical experiments, without detailed internal structural consideration.

7.2.1 Elastic model

Based on the observations of early researchers that the material behaviour of skin is relatively insensitive to strain rate over several decades of variation and it reaches a “preconditioned” state after repeated loadings, many investigators have neglected the time- and rate-dependent components of tissue behaviour and concentrate on modeling the nonlinear elastic response, where most models have been one-dimensional or have assumed that the three-dimensional behaviour is isotropic. Hence, the stress-strain relationship is derived from a strain energy function which is in turn a function of the strain invariants. Although there are different stress-strain relationships during loading and unloading and a complete description should take into account the both phases, almost all the studies considered the loading phase

only. Fung et al.^[31] proposed that the strain-energy function derived in this manner should be called a “pseudo strain energy function” since it is, strictly speaking, incomplete.

Two functional forms seem to predominate in the elastic models for the stress-strain relationship, the power form^[24,27,32~34] as well as exponential and logarithmic equations^[21,23,35~39]. Following are models that have been developed to characterize the elastic behaviour of skin.

1) Ridge & Wright^[40]

$$\varepsilon = Ck\sigma^b \quad (7.1)$$

where σ and ε denote stress and strain, and attempted to relate the constants k and b to the physical state of the fibre network. No attempt was made to validate these expressions for three-dimension.

2) Veronda & Westmann^[21]

Development by Veronda & Westmann, for the case in which $\partial W/\partial I_1$ and $\partial W/\partial I_2$ are constant, gave time independent stress-strain relations valid for the large deformations appropriate to physiological strains in skin tissue. This analysis, however, presupposes isotropy, which is clearly invalid, and does not take into account the non-linear viscoelastic nature of skin tissues.

Veronda & Westmann^[21] developed a nonlinear isotropic, rate-independent model of cat skin tissue by applying finite deformation theory. The existence of a strain-energy function was assumed, and a compressible isotropic approximation and an exact solution to the incompressible isotropic case were presented, although the anisotropic nature was observed in their experiments where the lateral extension ratios were found to be significantly different. The strain-energy function was given as

For assumption of being compressible:

$$W = C_1 \{\exp[\beta(I_1 - 3)] - 1\} + C_2 [(I_2 - 3) + f(I_3 - 1)] \quad (7.2)$$

For assumption of being incompressible:

$$W = C_1 \{\exp[\beta(I_1 - 3)] - 1\} + C_2 (I_2 - 3) + g(I_3) \quad (7.3)$$

where C_1 , C_2 and β are material constants; $g(I_3)$ and $f(I_3)$ are unknown functions of invariant I_3 with $g(1) = 0$. Based on the uniaxial tensile data of cat skin *in vitro*, the following parameters are obtained

Compressible:

$$C_1 = 0.003, 91, C_2 = -0.019, 85, \beta = 5.03$$

Incompressible:

$$C_1 = 0.013, 4, C_2 = -0.029, \beta = 4.4$$

Both these approaches were found to yield good correlation with experimental results for a static uniaxial test. However, the authors made no effort to examine the rate effects, irreversible behaviour of the material, or applicability of these results to multiaxial situations.

3) Danielson^[37]

Based on the theory of nonlinear deformation of an arbitrarily-shaped membrane, Danielson's^[37] theoretically proposed two models for skin tensile behaviour, where the human skin is described as an elastic membrane. He modeled the mechanical behaviour under two different scenarios.

For relatively small deformations, where it is assumed that the skin is elastic and the strain energy is preserved, the constitutive equation is given as

$$N^{\alpha\beta} = \partial W / \partial \gamma_{\alpha\beta} \quad (7.4)$$

where $N^{\alpha\beta}$ are the stress tensors and W is the strain energy function given by

$$W = A^{\alpha\beta\lambda\mu} \gamma_{\alpha\beta} \gamma_{\lambda\mu} \exp(B^{K\delta} \gamma_{K\delta} + C \gamma^{\rho\phi} \gamma_{\rho\phi})$$

where A and B are material constants (tensors of elastic constants); C is a scalar and γ is the strain components.

For relatively large deformation, where it is assumed that skin is viscoelastic and there would be no conservation of strain energy, the constitutive equation is given as

$$N^{\alpha\beta} = A^{\alpha\beta\lambda\mu} \gamma_{\lambda\mu} \exp(B^{\kappa\delta} \gamma_{\kappa\delta} + C \gamma^{\rho\phi} \gamma_{\rho\phi}) \quad (7.5)$$

The two models contain seven and eight material constants, respectively, which need to be determined experimentally.

Danielson's equations are the first attempt to apply the well-established mechanics of membranes to human skin. They can be used to solve several simple two-dimensional problems. Danielson argued himself that several modifications to the theory would probably be required in order to give a more realistic description of human skin. It should be noted that in the models skin is assumed to be orthotropic, which needs the coordinate system to coincide with the axes of orthotropy, or in practice, means that the coordinate system has to be chosen to coincide with the Langer lines. The existence of symmetry across the Langer lines is however an assumption that may not be valid in all situations.

4) Danielson & Natarajan^[41]

Tension field theory is generalized to membranes undergoing arbitrarily large deformations, where it is assumed that the tension rays¹⁾^[41] extend all the way to the outer boundaries of the skin, skin is isotropic membrane where one principal stress is large and positive and the others are negligible, the initial stresses present naturally in the skin is ignored. The theory is used to model operations on the human skin performed by plastic surgeons.

The total strain energy of membrane is given as

$$U = \int_{\alpha_a}^{\pi/2} S d\alpha \quad (7.6)$$

where α is the angle tension ray makes with x -axis with α_a being value of α at

$x = a$. $S = \frac{C\Delta^3}{12(\sqrt{\eta_1} - \sqrt{\eta_2})^2}$ where C is the elastic constant in stress-strain

relationship $\sigma = C\varepsilon^2$; η is the distance measured along a tension ray with η_1 and η_2 being values of η at outer and inner boundaries; Δ is the change in length of line of particles which becomes a tension ray.

5) Snyder & Lee^[39]

For an isotropic, incompressible material, the constitutive equation can be written in the form of energy function

$$W = \frac{k}{\alpha^2} \exp[\alpha(\beta - 1)] - \frac{k}{\alpha}\beta \quad (7.7)$$

where $\beta = \frac{I_1 + (I_1^2 - 3I_2)^{1/2}}{I_2}$ with I_1 and I_2 being the first and second

invariants of the reciprocal Cauchy's deformation tensor^[42]

For tensile loading:

$$I_1 = \lambda_1^2 + \frac{2}{\lambda_1}, \quad I_2 = \frac{1}{\lambda_1^2} \quad (7.8)$$

The stress-strain relationship is

$$T^{11} = \left(\lambda_1 - \frac{1}{\lambda_1^2} \right) \left(2 \frac{\partial W}{\partial I_1} + \frac{2}{\lambda_1} \frac{\partial W}{\partial I_2} \right) \quad (7.9)$$

For pure shear loading:

$$I_1 = \lambda_1^2 + \lambda_2^2 + \frac{1}{\lambda_1^2 \lambda_2^2}, \quad I_2 = \frac{1}{\lambda_1^2} + \frac{1}{\lambda_2^2} + \lambda_1^2 \lambda_2^2 \quad (7.10)$$

1) The tension rays can be easily seen by grasping a pinch of skin on the back of the hand; note how the force is carried by straight rays of stretched skin. (In other problems, the tension rays may exist but not be so easily seen.)

The stress-strain relationship is

$$T^{22} = \left(\lambda_2 - \frac{1}{\lambda_2^3 \lambda_1^2} \right) \left(2 \frac{\partial W}{\partial I_1} + 2 \lambda_1^2 \frac{\partial W}{\partial I_2} \right) \quad (7.11)$$

where T^{11} and T^{22} is the Lagrangian stress (force per unit undeformed area); λ is the stretch (length/initial length).

The data derived from these tests show the same type of exponential stress-deformation curve which has been previously determined for tensile and torsional types of loading. However the potential function, which yields stress-deformation curves that are identical to experimentally determined curves for tension and torsion loads, does not yield as good a match for a pure shear load. The computed curves are in the neighborhood of the data, but appear to have the incorrect stiffness. It is of interest to note that the stress-extension curve in several cases is not as stiff as computed while the reverse is true of the third case.

The model used was derived for an incompressible isotropic material. Both of these assumptions are subject to question. If the material is not incompressible then one would expect it to appear less stiff than the incompressible model, which is true for two cases. Thus a change in the degree of compressibility in either direction would not explain the relative change between the model values and experimental values for the third case.

6) Tong & Fung^[23]

Fung^[30,43] proposed a generalized constitutive equation for the biological materials in the form of a strain potential function which can be written in tensor notation as follows:

$$W = 0.5 \alpha_{ijkl} \varepsilon_{ij} \varepsilon_{kl} + \beta_0 \beta_{mnpq} \varepsilon_{mn} \varepsilon_{pq} \exp(\nu_{ij} \varepsilon_{ij} + 0.5 \gamma_{ijkl} \varepsilon_{ij} \varepsilon_{kl} + \dots) \quad (7.12)$$

where α_{ijkl} , β_0 , β_{mnpq} , ν_{ij} , γ_{ijkl} are constants to be determined experimentally, and the Latin indices i, j, k, \dots range over 1, 2, 3. According to the rules of tensor notation, repetition of an index means summation over the index; thus, $\alpha_i \varepsilon_i$ means $\alpha_1 \varepsilon_1 + \alpha_2 \varepsilon_2 + \alpha_3 \varepsilon_3$, etc. The first term in above equation is not logically needed; but it is introduced because the experimental data appear to be “biphasic”. In practice, the second term is used to express the behaviour of the material at a high stress level, while the first term is used to remedy the situation at a lower stress level.

Based on an extensive collection of *in vitro* biaxial stretching data from experiments on rabbit skin^[22,44], Tong & Fung^[23] derived a model that gave the best fit to the observed behaviour. Their model was also based on the

preservation of strain energy, but their strain energy function different to that of Danielson. The stress-strain relationship is given by

$$S_{ij} = \partial W / \partial \varepsilon_{ij} \quad (7.13)$$

where S_{ij} are the Kirchhoff stress tensors; ε_{ij} are the Green strain tensor and the indexes i, j range over 1, 2, 3.

The strain energy function W is given by

$$W = 0.5 (\alpha_1 \varepsilon_1^2 + \alpha_2 \varepsilon_2^2 + \alpha_3 \varepsilon_{12}^2 + 2\alpha_4 \varepsilon_1 \varepsilon_2) + 0.5C \exp(a_1 \varepsilon_1^2 + a_2 \varepsilon_2^2 + a_3 \varepsilon_{12}^2 + 2a_4 \varepsilon_1 \varepsilon_2 + \gamma_1 \varepsilon_1^3 + \gamma_2 \varepsilon_2^3 + \gamma_4 \varepsilon_1^2 \varepsilon_2 + \gamma_5 \varepsilon_1 \varepsilon_2^2) \quad (7.14)$$

where α, a, γ and C are material constants. A series of parameters have been obtained based on the rabbit skin^[22,44], see Tables 1 and 2 in Reference [23].

It should be noted that in this model, the skin is assumed and to be in a state of generalized plane stress and orthotropic, which means that the coordinate system has to be chosen to coincide with the Langer lines. The existence of symmetry across the Langer lines is however an assumption that may not be valid in all situations. Tong & Fung^[23] pointed out that the pseudo strain potential, however, do not have the thermodynamic meaning of the “strain energy function”, because they depend not only on preconditioning, but also on whether the process is loading or unloading. The model could not predict experiments with slightly different boundary conditions, which is indicated by the fact that the parameters derived change considerably in a single specimen from one to another^[23].

Yin et al.^[45] found that even though this function fitted the observed data well, it was over-parameterized; the parameters a_i ($i = 1, 2, 3, 4$) are highly correlated. A slightly modified function was giving in the following form:

$$W = B_1 (E_x^2 + E_y^2) + B_2 E_x E_y + 0.5C \exp [(A_x E_x^2 + A_y E_y^2) - 1] \quad (7.15)$$

Examination of the correlation matrix for this model indicated that there was still some correlation for C, A_x and A_y coefficients but it was not sufficient to cause any numerical instabilities. Any further reduction in numbers of parameters, furthermore, would not enable us to obtain good fits to the data.

Chaudhry et al.^[46] argued that the material constants (α, a, γ and C) in model of Tong & Fung^[23] are obtained by referring to the unloaded i.e. undeformed state without its natural stress. They extended the model of Tong & Fung^[23] by taking the residual stress into account.

$$\frac{dT^1}{de^1} = \frac{1}{k_1} \frac{dT_1}{de_1}, \quad \frac{dT^2}{de^2} = \frac{1}{k_2} \frac{dT_2}{de_2} \quad (7.16)$$

where T_{ij} is Lagrangian stress tensor and is related to the Kirchhoff stress tensor S_{ij} as $T_1 = T_{11} = \lambda_1 S_1$, $T_2 = T_{22} = \lambda_2 S_2$; $T^1 = T_1 A_x / A^x$ with A_x being the area of cross-section normal to the x -axis in state 0, A^x being that for state 1¹⁾[46], T_1 being the Lagrangian stress referred to state 0, and T^1 being the stress referred to state 1.

Gambarotta et al.^[47] modified the model of Tong & Fung^[23] and applied it to the analysis of short-term reconstructive procedures of human scalp skin where the skin is typically stretched to large strains and stresses without preconditioning. In the model, skin is assumed to be a time independent, isotropic and hyperelastic material. The strain energy function is given as

$$W = A [\varepsilon_{11}^2 + \varepsilon_{22}^2 + 2\alpha\varepsilon_{11}\varepsilon_{22} + 2(1 - \alpha)\varepsilon_{12}\varepsilon_{21}] + c \exp \{ B [\varepsilon_{11}^2 + \varepsilon_{22}^2 + 2\beta\varepsilon_{11}\varepsilon_{22} + 2(1 - \beta)\varepsilon_{12}\varepsilon_{21}] \} \quad (7.17)$$

where the parameters A , B , α and β are related to γ_1 , γ_2 , μ_1 and μ_2 through $A = \mu_1 \frac{\gamma_1}{2}$, $B = \mu_2 + \frac{\gamma_2}{2}$, $\alpha = \frac{\gamma_1}{\gamma_1 + 2\mu_1}$, $\beta = \frac{\gamma_2}{\gamma_2 + 2\mu_2}$. γ_1 , γ_2 , μ_1 and μ_2 are constants to be determined experimentally.

7) Alexander & Cook^[36,48]

This theory considers the mechanical resistance of the skin to be mainly attributable to the dermis which in the strain range of interest has been shown to be an isotropic, homogeneous, incompressible material. A strain energy function of the form

$$W = G(I_1 - 3) + F(I_2 - 3)$$

where I_1 and I_2 being the first and second invariants of the reciprocal Cauchy's deformation tensor.

Comparing the results of tests performed on young subjects in a number of directions relative to the natural stress principal axes, Alexander & Cook developed a form for this strain energy function where G is quadratic in I_1 and $\partial F / \partial I_2$ is expressed as a hyperbola in I_2 . It has been subsequently found that for all age groups this function of I_1 is not general enough. Additionally, the hyperbolic function in I_2 quickly approaches zero with increasing I_2 making $F = 0$ a reasonable approximation. A revised stress-strain theory is given as

$$N = \frac{C}{\lambda} \left(\lambda^2 - \frac{1}{\lambda^2 \lambda_p^2} \right) \exp \left[k(I_1 - 3)^2 \right] \quad (7.18)$$

1) State 1 refers to the natural stress free state; State 1 refers to state under no external load or the undeformed state (with residual stresses).

where N is the skin tension in the test direction; λ is the extension ratio in the test direction, λ_p (transvers λ) is the extension ratio in the direction perpendicular to test and C and K are material constants. The constants C and K provide a rational basis for comparing curves obtained from different individuals.

The constant C is associated with the low-tension part of the curve which is mainly determined by the ground substance and elastic fiber components of the skin while the constant K is associated with the high-tension part of the curve which is determined by the mechanical characteristics of the collagen fiber network. Typical values are $C = 10^4$ Pa, $K = 100$.

Alexander & Cook^[36] used a phenomenological nonlinear strain energy function to model skin, but their results did not speak to the histologic basis for the observed behaviour. The data from suction test on human skin *in vivo* have been used to develop a new multidimensional stress-strain theory in terms of two material constants that are related to basic material characteristics of the dermis and are uniquely determinable regardless of the natural state stress field.

8) Reihnsner et al.^[49]

Materials with two-dimensional anisotropic linear stress-strain relationship require the determination of six independent elastic constants C_{ijkl}

$$\begin{bmatrix} \sigma_{11} \\ \sigma_{12} \\ \sigma_{22} \end{bmatrix} = \begin{bmatrix} C_{1111} & 2C_{1112} & C_{1122} \\ C_{1112} & 2C_{1212} & C_{1222} \\ C_{1122} & 2C_{1222} & C_{2222} \end{bmatrix} \begin{bmatrix} \varepsilon_{11} \\ \varepsilon_{12} \\ \varepsilon_{22} \end{bmatrix} \quad (7.19)$$

Skin is known to exhibit nonlinear anisotropic viscoelastic behaviour and therefore Equation (7.19) can be applied only under certain restrictions. In order to determine the two-dimensional pure elastic behaviour we performed relaxation tests at a certain set of strains. The equilibrium loads were plotted as a function of strain. The resulting stress-strain relationship can be considered as the typical behaviour of a nonlinear-elastic material.

The quality “orthotropic” or “completely anisotropic material” cannot be derived directly from non-zero values of C_{1112} and C_{1222} . For orthotropic tissues, however, these coefficients disappear after a specific rotation of the coordinate system. The rotation angle is determined from the solutions of the following equations:

$$p_1(t) = C_{1111}t + C_{1112}(3t^2 - 1) + 2C_{1212}(t^3 - t) + C_{1222}(t^4 - 3t^2) - C_{2222}t^3 = 0 \quad (7.20)$$

$$p_2(t) = C_{1111}t^3 + C_{1112}(t^4 - 3t^2) + 2C_{1212}(t - t^3) + C_{1222}(3t^2 - 1) - C_{2222}t = 0 \quad (7.21)$$

where $t = \tan \theta$ with θ being the rotation angle.

9) Diridollou et al.^[50]

Skin is assumed to be an isotropic elastic membrane with an initial tension and the following equation relating stress with strain is established:

$$\sigma = \frac{E\varepsilon}{1-\nu} + \sigma_0 \quad (7.22)$$

where E is the Young's modulus; ν is the Poisson's ratio; σ_0 is the initial stress.

The geometry of deformation under suction is assumed to be a portion of a sphere. The model is used to obtain a set of parameters intrinsic to the skin with suction testing.

$$P_{\text{ext}}(t) = \frac{4\delta(t)e}{\delta^2(t) + r_0^2} \left[\frac{E}{1-\nu} \left(\frac{\delta^2(t) + r_0^2}{2r_0\delta(t)} \arcsin \frac{2r_0\delta(t)}{\delta^2(t) + r_0^2} - 1 \right) + \sigma_0 \right] \quad (7.23)$$

where e is the thickness of the combined dermis and epidermis; r_0 is aperture radius that delineates the measurement area of the skin; $\delta(t)$ is the vertical displacement of the surface of the skin; $P_{\text{ext}}(t)$ is the applied suction.

10) Hendriks et al.^[51,52]

Extended Mooney material behaviour was modeled to account for the non-linear stress-strain relationship of the skin.

$$W = C_{10}(I_1 - 3) + C_{11}(I_1 - 3)(I_2 - 3) \quad (7.24)$$

where C_{10} and C_{11} are material parameters (as presented in Table 7.1). For small strains the contribution of the second part of the equation is negligible and C_{10} can be converted into a Young's modulus using $E = 6C_{10}$.

Table 7.1 Model constants obtained

	C_{10}/kPa	C_{11}/kPa
6 mm aperture diameter	29.6±21.1	493±613
2 mm aperture diameter	11.5±8.7	18.3±12.6
1 mm aperture diameter	10.8±9.5	9.3±7.7
For human dermis <i>in vivo</i>	9.4±3.6	82±60
For fat	0.02	

11) Shergold et al.^[53,54]

Shergold et al.^[53,54] proposed the Ogden model for an incompressible, isotropic, hyper-elastic solid to describe the constitutive behaviour of skin.

$$W = \frac{2\mu}{\alpha^2} (\lambda_1^\alpha + \lambda_2^\alpha + \lambda_3^\alpha - 3) \quad (7.25)$$

where W is the strain energy density; λ is the principal stretch ratios; α is a strain hardening exponent; μ has the interpretation of the shear modulus under infinitesimal straining. Model constants α and μ evaluated at different compressive strain rates for skin tissue *in vitro* are shown in Table 7.2. Pig skin stiffens and strengthens with increasing strain rate over the full range of $0.004 \sim 4000 \text{ s}^{-1}$. The strain rate sensitivities of the pig skin is quantified by an increase in the shear modulus with increasing strain rate, with no attendant change in the strain hardening exponent.

Table 7.2 Model constants α and μ (MPa) evaluated at different compressive strain rates for skin tissue *in vitro*

Strain rate/ s^{-1}	0.004	0.4	40	4000
Pig skin ($\alpha = 12$)/MPa	0.4	1.2	2.2	7.5
Human skin ($\alpha = 9$)/MPa	0.11			

7.2.2 Viscoelastic model

Generally the soft tissues testing in laboratory have demonstrated the following common biomechanical features.

(1) Stress relaxation: under a constant strain the stress is decreased with time.

(2) Creep: under a constant stress the deformation is continuous.

(3) Hysteresis: under a cyclic loading, the stress-strain relationship in the loading process is usually different from that in the unloading process due to the dissipation of internal energy.

(4) Pseudo-elasticity: after repeated cyclic loading enough times, the stress-strain loop becomes repeatable. For the loading and unloading branch separately, the stress-strain relationship is unique. These can be treated as one elastic material in loading, and another elastic material in unloading. The stress relaxation, strain creep and hysteresis are called the features of viscoelasticity.

In literature, many researchers have performed a lot of model to investigate the time- and stimulus frequency- dependent mechanical behaviour. Following are some of their typical models.

1) Viscoelastic models for the skin under stretch

(1) Jamison et al.^[55,56].

From the creep tests, Jamison et al.^[55,56] developed a discrete mechanical model (three element viscous type, as shown in Figure 7.1) to represent the viscoelastic nature of guinea pig skin. It is assumed that the material is

homogeneous, isotropic, and independent of the past straining history. Based on the uniaxial creep and constant rate tests with guinea pig skin *in vitro*, the parameters obtained are given in Table 7.3. However, Jamison et al.^[55,56] found E_2 , η_1 , η_2 depend on stress level and direction of stress.

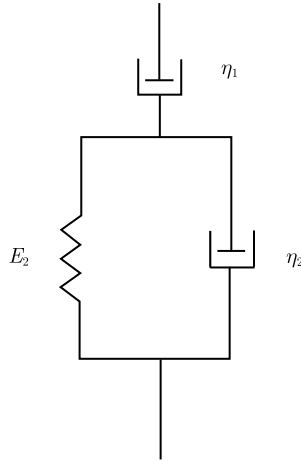


Figure 7.1 Three-element viscous model for skin. The upper viscous element η_1 , represents unrecoverable creep. The Voigt element (spring E_2 and dashpot η_2 in parallel with each other) represent the recoverable creep. Numerical values of these parameters are shown in Table 7.3

Table 7.3 Parameters used in model of Jamison et al.

Skin	$E_2/(\text{psi}^1)$	$\eta_1/(\text{lb} \cdot \text{s}/\text{in}^2)^2)$	$\eta_2/(\text{lb} \cdot \text{s}/\text{in}^2)$
Chamois skin (wet)	1.49×10^{-3}	2.73×10^{-3}	0.36×10^{-3}
Chamois skin (dry)	1.95×10^{-3}	0.70×10^{-3}	1.11×10^{-3}
Guinea pig skin (overall)	5.00×10^{-3}	12.22×10^{-3}	0.94×10^{-3}
Guinea pig skin (parallel to the longitudinal axis)	5.13×10^{-3}	11.31×10^{-3}	1.17×10^{-3}
Guinea pig skin (perpendicular to the longitudinal axis)	4.83×10^{-3}	13.42×10^{-3}	0.63×10^{-3}
Guinea pig skin (perpendicular to the longitudinal axis) $\sigma/\sigma_f < 0.1$	3.20×10^{-3}	4.74×10^{-3}	0.43×10^{-3}
Guinea pig skin (perpendicular to the longitudinal axis) where σ/σ_f is the ratio of creep stress to failure stress	4.70×10^{-3}	13.66×10^{-3}	0.31×10^{-3}

1) 1psi=6.895kPa.

2) $1\text{lb} \cdot \text{s}/\text{in}^2=23.26\text{N}/\text{m}^2$.

(2) Barbenel et al.^[57,58].

Barbenel^[57] developed a one-dimensional linear viscoelastic model, to account for the time-dependent behaviour of the model. Considering the

disagreement between the time dependent behaviour and the frequency behaviour of skin exist in many models, an alternative approach is used to characterize the viscoelastic behaviour. The torque relaxation behaviour is described by

$$T(t) = T(\infty) + T(0) \int_0^{\infty} A(\tau) \exp(-t/\tau) d\tau \quad (7.26)$$

or by the analogous logarithmic spectrum

$$T(t) = T(\infty) + T(0) \int_{-\infty}^{\infty} H(\tau) \exp(-t/\tau) d \ln \tau \quad (7.27)$$

where $T(t)$ is the torque at time t ; $T(0)$ is the torque at the start of the relaxation and $T(\infty)$ is the equilibrium torque; $A(\tau)$ and $H(\tau)$ are the relaxation spectra.

The validity of the proposed model has been proved by comparisons between predictions and experimental results of the torsion stress relaxation data and the dynamic response of human skin *in vivo*. For torsion test under constant torque, the relaxation spectra $H(\tau)$ was given as

$$H(\tau) = \begin{cases} 8 \times 10^{-2} \text{ mN} \cdot \text{m}, & 0 < \tau < 35 \text{ s} \\ 0, & \tau > 35 \text{ s} \end{cases} \quad (7.28)$$

one problem yet to be solved is the incorporation of nonlinear behaviour.

(3) Vogel & Hilgner^[59].

Vogel & Hilgner^[59] observed the step phenomenon as observed in rat skin. A mechanical model was proposed, as given in Figure 7.2, where one spring in the Kelvin element is replaced by a few springs in parallel with different constants. A step in the measured curve then can be attributed to the breakdown of one of these springs. It should be noted that this model does not fully describe all mechanical properties of skin like hysteresis, relaxation and recovery.

(4) Ward et al.^[60].

Real time compression of skinfolds was measured at three sites (triceps, abdominal medial calf), using a slim guide skinfold caliper adapted by the addition of a potentiometer. An average of eight trials for each subject at each site was used in modeling the compression curves. A mechanical model was developed, comprised of two parallel spring and viscous components in series with each other, as shown in Figure 7.3.

$$T_t = T_{\text{initial}} + F \left[\frac{1}{k_1} - \frac{\exp(-k_1 t/b_1)}{k_1} \right] + F \left[\frac{1}{k_2} - \frac{\exp(-k_2 t/b_2)}{k_2} \right] \quad (7.29)$$

where T_t is the thickness at time t ; T_{initial} is the initial skinfold thickness; F is the force exerted by caliper; k_1 and k_2 are coefficients of elasticity; b_1 and b_2 are coefficients of viscosity.

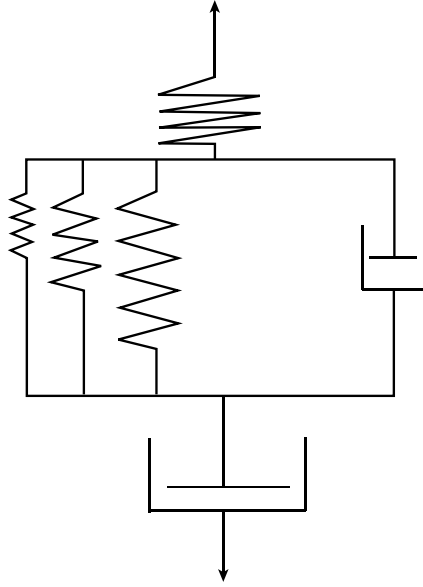


Figure 7.2 Schematic of model of Vogel & Hilgner

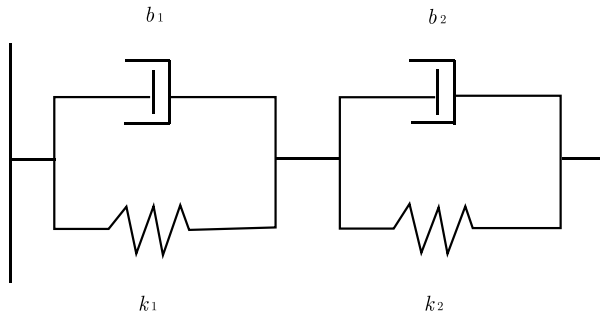


Figure 7.3 Representation of mechanical model of skinfold compression. b_1 and b_2 are coefficients of viscosity and k_1 and k_2 are spring constants

The hypothesized model provides a series of two damped springs. The first damped spring represents the response of the skin to initial compression, being influence by skin elasticity, original tension, and hydration. In series is a second damped spring representing the response of the skin plus adipose tissue to compression in the second slower phase of the displacement

curve. Based on the experimental data on human skin *in vivo*, the following parameters are obtained

For women:

$$b_1 = -0.077, b_2 = -7.738, k_1 = -1.275, k_2 = -6.276$$

For men:

$$b_1 = -0.135, b_2 = -14.59, k_1 = -2.499, k_2 = -11.362$$

(5) Sculari et al.^[61].

Sculari et al.^[61] use a standard linear solid, comprising a Maxwell solid in parallel with a spring, to describe human's skin.

$$F + \tau_\varepsilon \dot{F} = E_R (u + \tau_\sigma \dot{u}) \quad (7.30)$$

$$\tau_\varepsilon F(0) = E_R \tau_\sigma u(0) \quad (7.31)$$

where F is the load and u is the corresponding deformation; E_R , τ_σ , τ_ε are constant values related by the following equation.

The creep function:

$$c(t) = \frac{1}{E_R} \left[1 - \left(1 - \frac{\tau_\varepsilon}{\tau_\sigma} \right) e^{-t/\tau_\sigma} \right] \text{ valid at } t = 0$$

The relaxation function:

$$k(t) = E_R \left[1 - \left(1 - \frac{\tau_\varepsilon}{\tau_\sigma} \right) e^{-t/\tau_\sigma} \right] \text{ valid for } t > 0$$

(6) Wu et al.^[62~65].

The skin was assumed to experience large deformation, isotropic. The mechanical behaviour of skin tissue is considered to be nonlinear and viscoelastic. Assuming that the material is compressible and the stress-relaxation behaviour in volumetric compression is different from that in pure shear, the current tissue stress, $\sigma(t)$, can be characterized using a time-integration to account for the effects of the loading history.

$$\sigma_{ij}(t) = \int_0^t \left[g(t-\tau) \dot{S}_{ij}^0(\tau) + \frac{1}{3} k(t-\tau) \dot{\sigma}_{kk}^0(\tau) \delta_{ij} \right] d\tau, \quad i, j = 1, 2, 3 \quad (7.32)$$

where $g(t)$ and $k(t)$ are the shear and bulk stress-relaxation functions, respectively; σ_{ij}^0 is the elastic stress tensor and S_{ij}^0 is the elastic stress deviator which is defined as $S_{ij}^0 = \sigma_{ij}^0 - (1/3) \sigma_{kk}^0(\tau) \delta_{ij}$ with δ_{ij} being the Kronecker delta.

The total tissue stress (Cauchy stress), $\sigma(t)$, is to be decomposed into an elastic stress [$\sigma^0(t)$], representing instantaneous tissue response, and a viscous stress [$\sigma^v(t)$], representing delayed tissue response.

$$\sigma(t) = \sigma^0(t) + \sigma^v(t) \quad (7.33)$$

with

$$\sigma^v(t) = \sigma^0(t) + \int_0^t \dot{g}(t) \sigma^0(t - \tau) d\tau$$

where $g(t)$ and $k(t)$ are approximated using the Prony series.

$$g(t) = \frac{G(t)}{G_0} = 1 - \sum_{i=1}^{N_G} g_i \left[1 - e^{-(t/\tau_i)} \right], \quad k(t) = 1 - \sum_{i=1}^{N_G} k_i \left[1 - e^{-(t/\tau_i)} \right] \quad (7.34)$$

where G_0 and $G(t)$ are the instantaneous and time dependent moduli, respectively; g_i and τ_i are stress relaxation parameters; N_G is the number of terms used in the stress relaxation function.

The elastic part was assumed to be nonlinear and a function of strain energy density per unit volume was used to describe the elastic behaviour of the tissue

$$U = \sum_{i=1}^N \frac{2\mu_i}{\alpha_i^2} \left[\lambda_1^{\alpha_i} + \lambda_2^{\alpha_i} + \lambda_3^{\alpha_i} - 3 + \frac{1}{D_i} (J - 1)^{2i} \right] \quad (7.35)$$

where $J = \lambda_1 \lambda_2 \lambda_3$ is the volume ratio, λ_i are the principal stretch ratios; D_i , α_i and μ_i are the material parameters.

(7) Hoffman & Grigg^[66] and Richards et al.^[67].

Develop the uniaxial constitutive equations by using the calculation of Volterra–Wiener kernels and pseudorandom Gaussian white noise (PGN) stress

Wiener series:

$$\varepsilon(n) = h_0 + \sum_{j=0}^{R-1} h_1(j) \sigma(n-j) + \sum_{j_1=0}^{R-1} \sum_{j_2=0}^{R-1} h_2(j_1, j_2) \sigma(n-j_1) \sigma(n-j_2) \quad (7.36)$$

where $\varepsilon(n)$ is the strain at time increment n ; h_0 , $h_1(j)$ and $h_2(j_1, j_2)$ are the system kernels; R is the memory length and a uniform sampling rate is assumed. The memory length in units of time is the product of $(R - 1)$ and the time interval between data points. The kernels of the functional series depend upon the chosen reference level (i.e., the average level of the stimulus h_0). At second order, the Volterra kernels are equal to the Wiener kernels.

Volterra series:

$$\begin{aligned} \varepsilon(t) = & k_0 + \int_0^\infty k_1(\tau) \sigma(t - \tau) d\tau \\ & + \int_0^\infty \int_0^\infty k_2(\tau_1, \tau_2) \sigma(t - \tau_1) \sigma(t - \tau_2) d\tau_1 d\tau_2 \end{aligned} \quad (7.37)$$

where $\varepsilon(t)$ is the system output (strain); $\sigma(t)$ is the system input (stress); k_0 , $k_1(\tau)$ and $k_2(\tau_1, \tau_2)$ are the system kernels. The zeroth order kernel k_0 is the mean value of the response. The first order term involving $k_1(\tau)$ represents the convolution integral that appears in linear viscoelasticity. The second order kernels $k_2(\tau_1, \tau_2)$ describe the nonlinear response characteristics.

These kernels were used to predict the strain response to a variety of sinusoidal stress inputs. These predicted strains were compared with the measured strain response.

Overall, the method provides a means to develop soft tissue constitutive equations that can predict both nonlinear and viscoelastic behaviour over a wide range of stress inputs.

(8) Khatyr et al.^[68].

According to observation of Agache et al.^[69] that if a scale of stress is imposed upon the skin, the curve obtained can be decomposed into three parts: the first phase corresponds to a purely elastic deformation ε_e , the second phase of variable creep corresponds to the viscoelastic phase ε_{ve} and the third phase corresponds to the constant creep phase ε_s , Khatyr et al.^[68] proposed a four-parameter viscoelastic model, as shown in Figure 7.4, based on the analogical Kelvin–Voigt model in association with a spectral formulation.

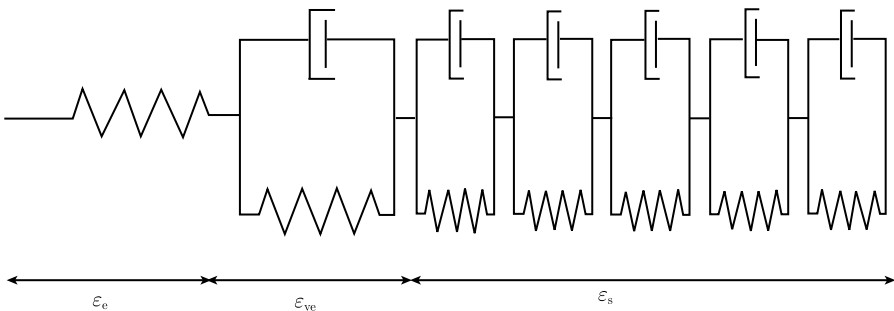


Figure 7.4 Model of Khatyr et al.

The model is composed of only three parts: ① a spring representing the elastic part of the skin; ② a simple spring-and-dashpot system that accounts for the short-term viscous part; ③ a spectrum that comes into play for longterm effects.

The total deformation e is then defined by the following differential equations:

$$\varepsilon = \varepsilon_e + \varepsilon_{ve} + \varepsilon_s \quad (7.38)$$

where (the elastic deformation) $\varepsilon_e = \sigma/E_e$ and the viscoelastic deformation is the solution of the differential equation

$$\varepsilon_{ve} = \frac{\sigma}{E_{ve}} [1 - \exp(-t/\tau)] \quad (7.39)$$

where $\tau = \eta/E_{ve}$.

The spectral deformation is given as

$$\varepsilon_s = A\sigma \left[1 - \sum_{i=1}^5 a_i \exp\left(-\frac{t}{b_i}\right) \right] \quad (7.40)$$

with $\sum_{i=1}^5 a_i = 1$. The a_i and b_i are chosen as: $a_1 = 0.1$, $a_2 = 0.1$, $a_3 = 0.1$, $a_4 = 0.3$, $a_5 = 0.4$, $b_1 = 20$, $b_2 = 120$, $b_3 = 250$, $b_4 = 310$, $b_5 = 610$.

The viscoelastic model proposed has only four intrinsic parameters: elasticity parameters E_e and E_{ve} and viscosity parameters ε_{ve} and the spectrum amplitude A . Skin being considered as orthotropic.

Based on the single-axis extension test on human skin *in vivo*, the following parameters are obtained from Table 7.4:

Table 7.4 The parameters used in the model of Khatyr

	$E_e/(\times 10^5 \text{ Pa})$	$E_{ve}/(\times 10^5 \text{ Pa})$	$\varepsilon_{ve}/(\times 10^5 \text{ Pa} \cdot \text{s})$	$A/(\times 10^5 \text{ Pa} \cdot \text{s})$
0 °	5.22 ± 1.34	8.05 ± 2.41	7.53 ± 2.27	2.05 ± 0.56
45 °	3.89 ± 1.03	6.09 ± 1.85	5.72 ± 1.77	2.76 ± 0.95
90 °	1.32 ± 0.60	2.16 ± 1.06	1.95 ± 1.01	8.31 ± 3.59
135 °	2.92 ± 1.20	4.32 ± 2.07	4.07 ± 1.94	4.24 ± 1.81

The orthotropic model enables the simulation of anisotropy in 80% of the patients. The parameters obtained with the viscoelastic model are independent of the type of load, the same coefficients enable a correct representation in creep and relaxation tests. The main directions vary from one person to another, Young's modulus in these directions could be an indicator for dermatologists and cosmeticians.

(9) Tsubouchi et al.^[70].

The skin of fetal Wistar rat was set on a rheometer and the relationship between stress and strain was examined *in vitro*. Based on the time-course curve of strain, Tsubouchi et al.^[70] proposed a mechanical-dynamical model,

which is composed of springs (elasticity) and dampers (viscosity) connected serially and in parallel, as given in Figure 7.5.

(10) Wang & Hayward^[71].

For viscoelasticity, Wang & Hayward^[71] tested the skin for small deformations and identified a five-parameter model for relaxation and another for creeping. The model is given as Figure 7.6. The model has been validated by comparison with experimental data on small patches of fingerpad glabrous skin in human subjects tested *in vivo* under tangential loading. The parameters used in the model of Wang & Hayward are given in Table 7.5.

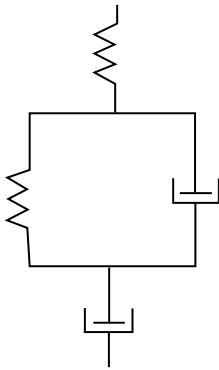


Figure 7.5 Model of Tsubouchi et al.

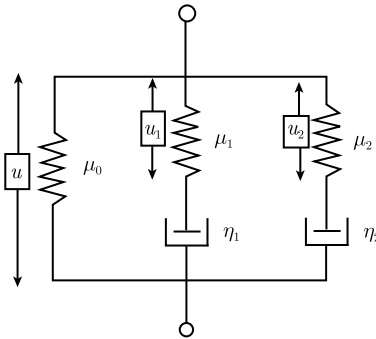


Figure 7.6 Second order linear viscoelastic model of Wang & Hayward

Table 7.5 The parameters used in the model of Wang & Hayward

	μ_0	μ_1	η_1	μ_2	η_2
Along ridges (relaxation)	1.05 ± 0.816	0.745 ± 0.308	0.681 ± 0.569	7.27 ± 5.66	0.0665 ± 0.0515
Cross ridges (relaxation)	0.769 ± 0.253	0.830 ± 0.561	0.800 ± 0.556	5.78 ± 4.41	0.0763 ± 0.0540
Along ridges (creep)	0.916 ± 0.801	3.70 ± 3.10	4.06 ± 5.14	17.1 ± 13.1	0.948 ± 0.867
Cross ridges (creep)	0.394 ± 0.319	3.14 ± 1.95	14.9 ± 19.5	21.2 ± 16.1	1.77 ± 1.11

(11) Giles et al.^[72].

Giles et al.^[72] proposed a quasi-linear viscoelastic model for skin tissue. The general form of the stress response (in terms of the second Piola–Kirchhoff stress S) is the hereditary integral equation:

$$S(t) = \int_0^t G(t - \tau) \frac{dS^e}{dE} \frac{dE}{d\tau} d\tau \tag{7.41}$$

where S^e is the elastic stress function; E is the Lagrangian strain; $G(t)$ is the reduced relaxation function. The following form for predicting the rate independent hysteretic behaviour of soft tissue is used^[73]:

$$G(t) = \frac{1 + C[E_1/(t/\tau_2) - E_1(t/\tau_1)]}{1 + C \ln(\tau_2/\tau_1)} \quad (7.42)$$

where C is a material parameter that reflects the amount of viscoelastic content of the tissue; τ_1 and τ_2 are time constants that regulate the short and long term material responses, respectively; $E_1(\cdot)$ is the exponential integral function. In their modeling, the parameter obtained for ligament^[74] were used for skin tissue: $C = 0.129$, $t_1 = 0.096$ s, and $t_1 = 2.09 \times 10^5$ s.

The elastic stresses are calculated from the strain energy function

$$W^e = \frac{c}{2} \{ \exp [b_1 E_{11}^2 + b_2 (E_{22}^2 + E_{33}^2)] - 1 \}$$

where c , b_1 , and b_2 are material parameters and E_{11} , E_{22} and E_{33} are Lagrangian strains along directions i_1 , i_2 , and i_3 , respectively. The material parameters with values of $c = 0.876$ kPa, $b_1 = 18.48$, and $b_2 = 3.58$ obtained for myocardium^[75] were used for skin tissue.

For simulations of planar biaxial deformation assuming incompressibility, the governing Cauchy stress versus strain equations are

$$\begin{aligned} T_{11} &= \lambda_1^2 S_{11} - \lambda_3^2 S_{33} \\ &= \lambda_1^2 \int_0^t G(t-\tau) \frac{dS_{11}^e}{d\tau} d\tau - \lambda_3^2 \int_0^t G(t-\tau) \frac{dS_{33}^e}{d\tau} d\tau \end{aligned} \quad (7.43)$$

$$\begin{aligned} T_{22} &= \lambda_2^2 S_{22} - \lambda_3^2 S_{33} \\ &= \lambda_2^2 \int_0^t G(t-\tau) \frac{dS_{22}^e}{d\tau} d\tau - \lambda_3^2 \int_0^t G(t-\tau) \frac{dS_{33}^e}{d\tau} d\tau \end{aligned} \quad (7.44)$$

2) Viscoelastic models for the skin under compression

(1) Dinnar^[76].

Dinnar^[76] gives the following relaxation function expression assuming that skin is linear elasticity:

$$J_{T1}(t_1) = \left\{ \frac{J_T(\infty)}{J_T(0)} + \frac{t_1}{J_T(0) \omega_0 Q_1} + \exp\left(-\frac{\lambda}{\omega_0} t_1\right) \left[1 - \frac{J_T(\infty)}{J_T(0)}\right] \right\} H(t_1) \quad (7.45)$$

from fit to data of Hickman et al. found: $k_1 = 2.5$, $k_2 = 10$, $C_2 = 1.8 \times 10^4$, $C_3 = 10^4$.

(2) Duchemin et al.^[77].

Many works have been done to model the skin behaviour in the pressure direction. However in most cases, the *in vivo* tests run to identify the parameters imply that not only the skin is modeled but also the underlying tissues. In Reference [78], a linear model has been used. D'Aulignac et al.^[79] have suggested a finite element mesh composed of two spring layers: a surface mesh model based on masses, linear dashpots and springs, then a second set of nonlinear springs orthogonal to the surface to model volumic effects. The nonlinear relationship between pressure force and penetration depth is given by

$$f_z(z) = k_z(z) z, \text{ with } k_z(z) = \frac{k_z^0}{1 - z/h} \text{ for } z < h \quad (7.46)$$

where k_z^0 and can h be interpreted respectively as the surface stiffness and the tissue thickness (maximum penetration depth).

However, D'Aulignac did not exploit the physical meaning of these parameters to validate it. Once again, for small deformations, a linear elastic behaviour can be deduced.

The first model describes skin behaviour along the pressure direction: since velocity is almost equal to zero in this direction once the desired force has been reached, this model does not include any damping parameter. It is based on a nonlinear stiffness relation whose parameters are an equivalent stiffness and an estimated thickness of the skin. Force control compression (FCC) (respectively, position control compression (PCC) tests have been performed and correlated with creep tests for different applied forces (respectively, relaxation tests for different penetration depths). Resulting responses of creep and relaxation tests have been modeled by a Kelvin–Boltzmann body. Moreover, reproducibility has been shown, as well as reciprocity, during FCC or PCC tests.

Pressure direction:

$$z(f_z) = f_z / (k_z^0 + f_z/h) \quad (7.47)$$

where z is the penetration depth; f_z is the applied force; k_z^0 and can h be interpreted respectively as the surface stiffness and the tissue thickness (maximum penetration depth).

The second model relates the applied force and the friction force in function of the displacement on the skin surface. It takes into account lubrication influence, as well as velocity of the tool, thanks to the friction coefficient of the skin.

Shear direction:

$$f_x^c(\Delta x^d, f_z^d) = \mu(\dot{x}^d) f_z^d \left(1 - e^{-\Delta x^d/L}\right) \quad (7.48)$$

where f_x^c is the friction force; $\Delta x^d = x^d - x_{\text{ref}}$ is the relative displacement; $\mu(\dot{x}^d)$ is the dynamic friction coefficient; f_z^d is the normal force.

(3) Quasi linear viscoelastic model (QLV theory)

Fung^[80,81] introduced a viscoelasticity theory that has become the most widely used theory in soft tissue biomechanics and is found both useful for compressive and tension behaviour of tissue. This theory is referred to as QLV. The basis of this theory is that ① the stress at a given time can be described by a convolution integral representation, separating the elastic response and the relaxation function; ② the relaxation function has a specific continuous spectrum.

The formulation of QLV theory is similar to finite linear viscoelasticity. It is assumed that the stress relaxation function can be expressed as a convolution of a relaxation function with an elastic response

$$\sigma(t) = \int_0^t G(t-\tau, \varepsilon) \dot{\varepsilon}(\tau) d\tau \quad (7.49)$$

$$\varepsilon(t) = \int_0^t J(t-\tau, \sigma) \dot{\sigma}(\tau) d\tau \quad (7.50)$$

where t is time; τ is the dummy variable for time; $\sigma(t)$ and $\varepsilon(t)$ are stress and strain; $J(t, \sigma)$ and $G(t, \varepsilon)$ are creep and relaxation moduli, respectively.

For the quasi-linear response of tissue, the relaxation functions $J(t, \sigma)$ and $G(t, \varepsilon)$ can be further separated into a strain-dependent part and a time-dependent part^[82]

$$G(t) = g(t) \sigma_e(\varepsilon) \quad (7.51)$$

$$J(t, \sigma) = j(t) \varepsilon_e(\sigma) \quad (7.52)$$

where $g(t)$ and $j(t)$ are normalized creep and relaxation functions that only depend on time; $\sigma_e(\varepsilon)$ is the instantaneous elastic response, i.e., the maximum stress in response to an instantaneous step input of strain, while $\varepsilon_e(\sigma)$ is the elastic strain response. This form is also called QLV theory^[80], which was formulated by Fung^[82] and has been proven useful for describing the viscoelastic behaviour of different soft tissues such as skin^[64,83,84], ligament^[85~87], cartilage^[88,89] and tendon^[86,90,91].

Insertion of Equations (7.51) and (7.52) into Equations (7.49) and (7.50), respectively, leads to the following nonlinear separable integral formulations:

$$\sigma(t) = \int_0^t g(t-\tau) \frac{d\sigma_e[\varepsilon(\tau)]}{d\varepsilon} \frac{d\varepsilon(\tau)}{d\tau} d\tau \quad (7.53)$$

$$\varepsilon(t) = \int_0^t j(t-\tau) \frac{d\varepsilon_e[\sigma(\tau)]}{d\sigma} \frac{d\sigma(\tau)}{d\tau} d\tau \quad (7.54)$$

where $\varepsilon_e(\tau)$ and $\sigma_e(\tau)$ are the elastic strain and stress response, respectively.

For biological soft tissues, Fung proposed a continuous relaxation representation for $G(t)$. It was assumed that the relaxation function was the same in all directions which reduced $G(t)$ to a scalar

$$G(t) = \frac{1 + c[E_1(t/\tau_2) - E_2(t/\tau_1)]}{1 + c \ln(\tau_2/\tau_1)} \quad (7.55)$$

where $E_1(t)$ was the exponential integral function.

$$E_1 = \int_z^\infty \frac{\exp(-t)}{t} dt \quad (7.56)$$

This relaxation function provides a smooth, linear decrease from short to long relaxation times. The stiffness (real part of complex modulus) increases with increasing frequency, whereas the damping (imaginary part) is relatively constant over a wide range of frequencies. This yields a hysteresis loop that is relatively insensitive to strain rate over several decades of change, a feature often observed for soft tissues. The three viscoelastic material coefficients, t_1 , t_2 , and c , can be determined from the analysis of a stress relaxation experiment. t_1 and t_2 represent time constants that bind the lower and upper limits of the constant damping range of the relaxation function and c is a dimensionless constant that scales the degree to which viscous effects are present. Complete details and history of the QLV theory can be found in Fung^[80].

7.3 Structural Models

The continuum and phenomenological models are useful in describing the macromechanical response of skin, but they have some drawbacks, where the main drawback of these approaches is that the various parameters generally do not have a direct physical or biological meaning since this method provide little insight into how the constitutive properties of the skin affect its mechanical behaviour^[17,77,92].

In view of the problems with continuum and phenomenological models, the structural models have been proposed, which describe gross mechani-

cal behaviour of skin by combining and analyzing the behaviour of its individual components on the basis of microstructural geometry and properties with the alignment and straightening of the fiber network taken into consideration^[5,84,92~96]. The structural model is based on the assumption that the tissue's response is the sum of the responses of its constituents and the overall tissue's response can be evaluated if the constituents' structure, their mechanics and interactions are known. The structural models have several merits^[5,17,97~99]: ① it is physical in the sense that all material functions are physical quantities and thus the microstructure of the tissues is more appropriately related to their mechanical behaviour since the responses of the individual constituents of a tissue are combined to determine an overall description of its material behaviour; ② the resulting models facilitate our understanding of the tissue's function and provide an insight into the tissue's response to a given deformation by building the relationship between tissue microstructure and mechanical properties; ③ structural models have a distinct advantage in tissue characterization since the structure is often known or can be investigated by available morphometric techniques and the mechanical properties of some of the tissue components can be determined independently by isolating them from the tissue.

Structural models have been used to describe the behaviour, under uniaxial tension, of parallel-fibered collagenous tissues such as tendons and ligaments^[97,100] or of a fibril assembly within a single collagen fiber^[101~103].

7.3.1 Elastic model

There are two general approaches that have been used in forming microstructural models according to how they model the low modulus "toe" region response based on collagen structure. One general approach used numerous elastic elements that were sequentially recruited causing nonlinear, elastic behaviour, while the other approach has been used to describe toe region behaviour by directly modeling collagen fiber geometry.

The "toe" region is probably caused by a gradual straightening of fibers, as suggested previously^[104~106]. The elastic response of skin was represented by numerous individual linearly elastic components, each of which represented a collagen fibril of different initial length in its unloaded and crimped form. As the skin was loaded, additional fibrils were recruited yielding the nonlinear behaviour characteristic of the toe region. At higher loads, all the fibrils were loaded and the skin stress-strain curve became linear. Several investigators^[5,93,95,107] have adopted this approach to develop models

attributing the mechanical response to this sequential straightening of the fibers.

1) Markenscoff & Yannas^[95]

The uniaxial behaviour of skin has also been described by directly modeling collagen fibril geometry. Markenscoff & Yannas^[95] proposed a simple structural model of the collagen fiber network in the dermis to describe the process of orienting collagen fibers in stretched skin in an effort and to calculate the strain level at which the stiffness of skin abruptly increases. The model was shown in Figure 7.7.

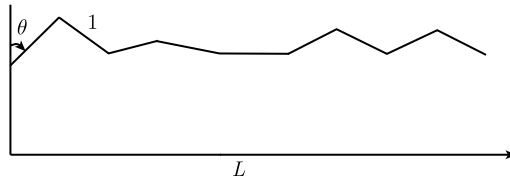


Figure 7.7 Model of a sequence of collagen fibers in the dermis: the fibers are assumed to have unit length, to be interconnected at their end and to advance monotonically forward as bound sequences, so that $0 < \theta < 180^\circ$

In the model, it is assumed that ① the overwhelming majority of collagen fibers lie in the plane of the dermis and that fibers crossing that plane contribute negligibly to the deformation of this tissue; ② the collagen fibers in the dermis are equal in length, interconnected at their end, and bound sequences of fibers are always monotonically advancing forward (there is efficient load transfer between ends of fibers).

The angle θ at each joint is considered as a random variable distributed with equal probability between 0° and 180° . The expected value of the length of this chain, consisting of n fibers is

$$E(L) = nE(\sin \theta \cdot 1) = \frac{n}{\pi} \int_0^\pi \sin \theta d\theta = \frac{2n}{\pi} \quad (7.57)$$

where $E(L)$ denotes the expected value of L .

The calculated critical strain level (57%) agrees roughly with experimental values. It is suggested that entry into the high-modulus region of the stress-strain curve of skin is simply a geometric effect, corresponding to thorough alignment, along the stress direction, of the fibers in the collagen network. The model finds use in systematizing data on the effect of age on the long-range extensibility of skin and on the morphological basis of skin extensibility along and across Langer's lines.

Although in the model only collagen fibres are considered, Markenscoff & Yannas^[95] pointed out that the contribution of elastin and of the matrix must

be accounted for in a more complex model in order to explain the mechanical behaviour of the dermis at low strain level.

2) Decraemer et al.^[107]

Decraemer et al.^[107] proposed a model consisting of a large number of purely elastic fibers embedded in a gelatin-like liquid. Schematic of Decraemer model was shown in Figure 7.8. It is assumed that: ① a large number (N) of purely elastic fibres, with identical Young's modulus (k), same cross-sectional area (S) but different initial length (l_i), embedded in a gelatin like liquid; ② the fibers were with a normal distribution spread about an assumed mean (μ) with a standard deviation (s).

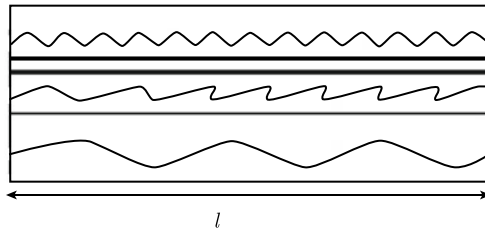


Figure 7.8 Schematic representation of the model containing fibers of different initial lengths l_i

According to their initial length l_i , the fibres are more or less stretched when the total specimen (initial length l_0) is extended up to a length l . The force needed to hold the specimen at length l is given by

$$K(l) = \int_{l_0}^l Sk \frac{l - l_i}{l_i} \frac{N}{\sqrt{2\pi}s} \exp \left[-\frac{(\mu - l_i)^2}{2s^2} \right] dl_i \quad (7.58)$$

or in terms of the Lagrangian stress ($\sigma = K/A_0$ with A_0 being the cross-section of the strip at rest) and the relative length ($\lambda = l/l_0$, $\lambda_i = l_i/l_0$)

$$\sigma(\lambda) = b \frac{l}{\sqrt{2\pi}s'} \int_{l_0}^l \frac{\lambda - \lambda_i}{\lambda_i} \exp \left[-(\mu' - l_i)/(2\varepsilon'^2) \right] dl_i \quad (7.59)$$

where $b = (NS/A_0)k$ is the effective Young's modulus; $\mu' = \mu/l_0$ and $s' = s/l_0$ are the normalized parameters for a strip of unit length and unit cross section.

Liao & Belkoff^[108] extended the model of sequential recruitment to include failure of ligament, where individual fibers, once recruited, behaved linear elastically until exceeding a limit strain at which point brittle failure occurred.

3) Manschot & Brakkee^[96]

The stress-strain relationship for human skin *in vitro* has a characteristic non linear shape even for low loads. Considerations are given on the basis of which a structural model has been selected, in which the mechanical properties of corrugated collagen fibrils are involved. It is found that such a model (shown in Figure 7.9) can describe the experimental stress-strain relationship surprisingly well with only three free parameters. These parameters are related to basic collagen fibril properties such as stiffness, diameter and waviness. The role of elastin is likely to be negligible for the purely elastic properties of human skin *in vivo*.

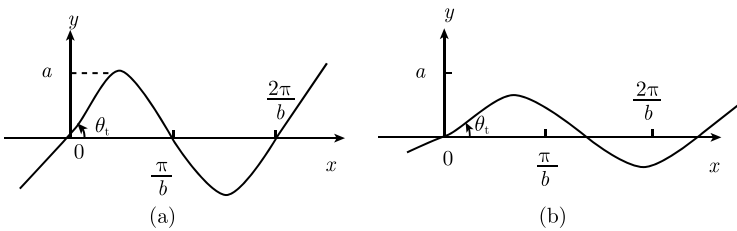


Figure 7.9 Geometry of a model collagen fibril in (a) a relaxed state and (b) a deformed state

In the preceding paper^[109] it was described how the mechanical properties of human skin *in vivo* can be determined by the use of high uniaxial loads. Furthermore it was presented how to obtain a stress-strain relationship which is independent of the *in vivo* measuring configuration. In the same paper the viscoelasticity of skin was discussed. A procedure was given by which the experimental data could be split into time dependent and time independent data.

These time independent properties are reflected in the purely elastic stress-strain relationship, which will be studied in the present paper. Such a relationship can be quantified by a mechanical structural model.

A model has been adopted which is based on the assumption that for unwinding each of the originally undulated collagen fibrils an increasing stress is needed (like a corrugated metal wire).

Therefore, the assumption has been made that after the preconditioning of the skin with a high uniaxial load the skin may be represented by a number of parallel aligned collagen fibres. Hence the straightening and the stretching of the skin fibres in such a situation is similar to that of the tendon fibres.

The collagen fibrils in the skin are considered to behave like elastic springs with a periodic corrugation. The corrugation is given by a planar sinusoidal

waveform and the material of the spring (i.e. collagen) is assumed to be linear elastic.

The stress-strain relationship of the skin is given as

$$\varepsilon = \frac{1 + \mu(1 + \sigma/E_c)}{1 + \mu\gamma^2} - 1 \quad (7.60)$$

where $\sigma = F/A_f$ is the stress with F being the force in the x -direction at the ends of the fibril and A_f being the cross-section of the fibril; ε is the strain defined as the relative increase in length along the x -axis; E_c determines the slope of the stress-strain curve for high stress values and represents the stiffness of the collagen fraction; μ indicates the strain value at which the mean corrugated fibril has become almost straight and is related to the max angle of the related wave form; $\gamma = 1 / \left[CF \frac{\sigma}{E_c} \left(\frac{\sigma}{E_c} + 1 \right) + 1 \right]$ with CF being the measure of the corrugation of the fibril and independent of the total number of fibrils.

Fitting to the data from tensile testing of leg skin *in vivo*^[109], the following parameters are obtained.

Along the main axis of leg:

$$E_c = 22 \text{ MPa}, \quad CF = 220, \quad \mu = 8\%$$

Cross the main axis of leg:

$$E_c = 6 \text{ MPa}, \quad CF = 100, \quad \mu = 20\%$$

4) Shoemaker et al.^[110]

The constitutive model described relies loosely upon considerations of irreversible thermodynamics and tissue ultrastructure.

Deformation of a network of fibres and its contribution of macroscopic stresses was considered by Shoemaker^[111] in a treatment similar to Lanir's, as a preliminary to development of the constitutive relation described herein. However, the final relation is ultimately empirical, of a form suggested by but not strictly based upon an ultrastructural model.

A constitutive relation proposed by Shoemaker^[111] to model the mechanical behaviour of membrane or two-dimensional soft tissues is described. Experiments by Schneider^[112] on human skin and the application of the constitutive model to biaxial stress-strain data from these experiments, are discussed. Some experimental data and predictions of the model obtained by curvefitting are presented for comparison. Values of material parameters are

also presented. It is concluded that the constitutive model is well able to fit results of individual tests, and that its generality (judged by consistency of parameters from test to test of the same specimen), though not complete, does compare favorably with some other results presented in the literature.

We assume that each component of the Kirchhoff stress tensor may be approximated by the sum of two terms, one due to the compliant component of the tissue, and the other due to its stiff, fibrous components

$$S_{ij} = S_{ij}^c + S_{ij}^f \quad (7.61)$$

where S_{ij} is the Kirchhoff stress tensor; S_{ij}^c are the “compliant” stresses; S_{ij}^f are the “stiff” fiber stresses. The “compliant” stresses S_{ij}^c , are assumed to depend on the Green strain components by a linear viscoelastic law, written as follows:

$$S_{ij}^c = C_{ijkl} \int_{-\infty}^t g(t - \tau) \dot{E}_{kl}(\tau) d\tau \quad (7.62)$$

where C_{ijkl} is a tensor of material constants; $g(t)$ is the reduced relaxation function; \dot{E}_{kl} are the rates of the components of the Green’s strain tensor. The stress components S_{ij}^f , take the following form:

$$S_{ij}^f = \int_{-\pi/2}^{\pi/2} d(\theta) S_f \frac{\partial E_f}{\partial E_{ij}} d\theta \quad (7.63)$$

where θ is the angle of orientation in $x_1 x_2$ plane, with respect to x_1 axis, where x_i ($i = 1, 2$) is the coordinates in a rectangular Cartesian system; the function $d\theta$ will be referred to as a distribution function for the stiff fibrous component; S_f and E_f will be referred to as fiber stress and strain measures, respectively, which depend upon θ , as well as the deformation history.

We suppose that the fiber strain measure in our model, E_f is dependent upon the line strain E , as well as another strain measure E^- , when the fiber stress measure S_f is tensile (> 0)

$$E_f = [(1 - b)E + bE^- - E_0]/\lambda_0^2, \quad E_f > 0 \quad (7.64)$$

where b is a constant between 0 and 1; E_0 is called the effective straightening strain and is supposed to depend upon θ and $\lambda_0 = \sqrt{2E_0 + 1}$ is called the perpendicular line strain and simply represents the line strain along a path perpendicular to the line element with reference orientation θ . It may be written

$$E^- = E_{11} \sin^2 \theta + E_{22} \cos^2 \theta - (E_{12} + E_{21}) \sin \theta \cos \theta \quad (7.65)$$

The fiber stress measure S_f is supposed to depend upon E_f according to a viscoelastic law

$$S_f = \int_{-\infty}^t G(t - \tau) E_f(\tau) d\tau \quad (7.66)$$

where G is a relaxation function. Just as in the example of the single fiber, which bent rather than accept compressive stress, it is assumed that the fiber stress measure S_f cannot be compressive (< 0).

The functions are chosen by Shoemaker et al.^[110] as

$$g(t) = \left[1 + 2a\sqrt{t/p}K_1(2\sqrt{pt}) \right] / (1 + a/p) \quad (7.67)$$

The effective straightening strain $E(\theta)$ is assigned the form

$$\begin{aligned} E_0 &= E\varepsilon_1 / (\cos\theta + E_2 \sin\theta), & 0 \leq \theta \leq \pi/2 \\ &= E_1 / (\cos\theta - E_2 \sin\theta), & -\pi/2 \leq \theta \leq 0 \end{aligned} \quad (7.68)$$

where E_1 , E_2 , a , p are material parameters; K_1 is the modified Bessel function of second kind, order one.

With condition of orthotropy and thermodynamic assumptions, the model is characterized by the constants C_{1111} , C_{2222} , C_{1122} as well as k , b , E_1 , E_2 , a , p . Based on the experimental data on human skin^[112], the following parameters are obtained:

$$C_{1111} = (30.7 \pm 6.3) \text{ N/m}, \quad C_{2222} = (83.1 \pm 17.9) \text{ N/m}, \quad C_{1212} = (24.9 \pm 5.4) \text{ N/m},$$

$$k = (121 \pm 69.2) \text{ kN/m}, \quad b = 0.244 \pm 0.062, \quad \varepsilon_1 = (0.848 \pm 0.036) \text{ rad}^{-1},$$

$$\varepsilon_2 = (1.55 \pm 0.121) \text{ rad}^{-1}, \quad a = (4.67 \pm 2.51) \text{ s}^{-1}, \quad p = (1.83 \pm 0.63) \text{ s}^{-1}$$

5) Oomens et al.^[113~115]

Oomens et al.^[115] proposed a structural model to describe the nonlinear elastic and time-dependent behaviour of the skin and subcutis, where skin is assumed to consist of a porous solid (representing the fibre network embedded in the colloid-rich part of the ground substance) and a freely movable fluid (the colloid-poor part of the ground substance). The model is based on the hypothesis that skin behaves as a sponge-like material, consisting of a porous solid with a fluid in it. This mixture approach is especially valuable for tissues under compression.

When the sponge is compressed the fluid will be pressed away. The time dependent behaviour can be explained as due to the resistance against this flow induced by the viscosity of the fluid; and nonlinear time dependent

behaviour can be explained as due to the decrease of the pores size of the sponge induced by the increase of the resistance to flow under compressing loading. Non-linear elastic behaviour can originate from the fibre reinforced solid.

The model is given as

$$\nabla \cdot (\mathbf{T}_{\text{eff}} - p\mathbf{I}) = 0 \quad (7.69)$$

$$\nabla \cdot \boldsymbol{\nu}^s - \nabla \cdot (\mathbf{K} \cdot \nabla p) = 0 \quad (7.70)$$

where ∇ represents the gradient operator with regard to the coordinates in the deformed configuration; \mathbf{T} is the Cauchy stress tensor with \mathbf{T}_{eff} being the effective stress in soil mechanics; \mathbf{K} is called the permeability tensor; $\boldsymbol{\nu}$ is the velocity tensor; the Lagrange multiplier p is a hydrodynamic pressure arising from the condition of incompressibility.

For solid phase

A simplified form of Fung's exponential strain energy function^[43] was used to represent the solid matrix

$$A^s = C \exp(a_1 E_{11}^2 + a_2 E_2^2 + a_3 E_{12}^2 + a_4 E_1 E_2) \quad (7.71)$$

where A^s is the Helmholtz free energy for the solid; E_{ij} is the components of the Green-Lagrange strain tensor according to a base along the symmetry planes of an orthotropic material; a_i ($i = 1, 2, 3, 4$) and C are material constants.

For liquid phase

A empirical relation for articular cartilage used by Mow et al.^[116] was used for the permeability the to large strains as follows

$$K = K_0 \exp M (J_3 - 1)$$

where K is the permeability before deformation; M is a nondimensional parameter; J_3 is the third invariant of the deformation tensor for the solid.

Based on the data, the following parameters are used: $C = 100$ kPa, $a_1 = 1$, $a_2 = 1$, $a_3 = 0.32$, $a_4 = 0.35$, $K = 1.4 \times 10^{-14} \text{m}^4/(\text{N} \cdot \text{s})$, $M = 6$.

6) Belkoff & Haut^[92]

Belkoff & Haut^[92] pointed out that previous structural models were not experimentally verified and have not verified alterations induced by different factors (location, direction of specimens on the body, age, and other influences), which are observed biochemically or microscopically and are reportedly caused by alterations in the organization and content of collagen fibers.

In view of this, they formulated a structural model to describe the nonlinear response of skin under uniaxial tension based on earlier models^[5,93,107], in order to investigate the ability of a microstructurally based model to identify changes in the collagenous microstructural network of skin which occur with age and specimen direction.

The model assumed that the collagen fibrils had a normally distributed slack length that caused a gradual disappearance of the crimp pattern as the individual fibers became straight and began to carry a load.

Assumptions: ① for the uniaxial specimen that all of the fibers are aligned in the direction of elongation; ② do not include any contribution from elastin; ③ the model does not include any viscous components; ④ only the collagen fiber network is included in the model. The fibers are assumed to be linear elastic and organized in a wavy fashion in the relaxed state.

The force generated, f , is correlated to the tissue length, x , as

$$f = k \int_{x_1}^x \int_{x_1}^{\eta} R(\zeta) / (l_0 + \zeta) d\zeta d\eta \quad (7.72)$$

where k is the net “stiffness” of the fibers, which is analogous to the tangent stiffness; x_1 is the tissue length at stress free state; l_0 is the gauge length (letting $x_1 = 0$); $R(x) = \exp[-(x - \mu)^2 / 2\sigma^2] / (\sigma\sqrt{2\pi})$ is a recruitment function of the fibers being straightened, which is a normal Gaussian distribution. The distribution is centered about a mean, μ , and has a standard deviation, σ , where μ is the deformation state for which half the fibers will have been recruited and σ determines how quickly the fibers are recruited with respect to the mean, μ .

Belkoff & Haut^[92] discussed with respect to uniaxial testing data and biochemical and morphological data. Quasi-static uniaxial tensile tests were conducted on dorsal skin of rats aged 1~4 months. Specimens were taken longitudinally and transversely (laterally) to the spine and tested at 1.5%. The model showed fiber stiffness to increase laterally during maturation and to be greater laterally than longitudinally. It also indicated the migration of the ‘heel’ portion of the response curve toward the origin during maturation to be due to less crimping in the fibers. These results were qualitatively supported by microscopical observations.

7) Bischoff et al.^[9,117~119]

Motivated by the statistical mechanics models of DNA stretching^[120] and by hypothesizing that the mechanical behaviour of skin at large stretches is dominated by the macromolecular collagen network, Bischoff et al.^[9,117~119] developed a constitutive model based on the entropy change upon stretch-

ing of long-chain molecules using physiologically meaningful parameters to represent the collagen network in skin to model the elastic behaviour of skin.

The model is initially isotropic rubbery elastic constitutive law developed by Arruda & Boyce^[10]. This was based on the microstructure of the skin and modeled the nonlinearity as stretching of long-chain molecules, these being the collagen fibres. This model accounted for anisotropy in the way that the initially isotropic constitutive law is transformed when the tissue is subjected to an anisotropic stress state. The strain energy function in this model is expressed as

$$W = W_0 + \frac{nk\Theta}{4} \left\{ N \sum_{i=1}^4 \left[\frac{\rho^{(i)}}{N} \beta_{\rho}^{(i)} + \ln \frac{\beta_{\rho}^{(i)}}{\sin \beta_{\rho}^{(i)}} \right] - \frac{\beta_{\rho}}{\sqrt{N}} \ln \left(\lambda_a^{a^2} \lambda_b^{a^2} \lambda_c^{a^2} \right) \right\} + B [\cosh(J - 1) - 1] \quad (7.73)$$

where W_0 is a constant; n is network collagen chain density; k is Boltzmann's constant; $\Theta = 298$ K is the absolute temperature; N is the fibre-free length; ρ is the deformed length of the molecule chains; β is the Langevin function and $B [\cosh(J - 1) - 1]$ is the compressible component of the strain energy; λ_c is the chain stretch defined as $\lambda_c = \sqrt{(\lambda_1^2 + \lambda_2^2 + \lambda_3^2)/3}$.

The true stress-stretch relation for the model is given by

$$\sigma_i = \frac{nk\Theta}{3} \frac{\sqrt{N}}{I_3} \left[L^{-1} \left(\frac{\lambda_c}{\sqrt{N}} \right) \frac{\lambda_i^2}{\lambda_c} - L^{-1} \left(\frac{1}{\sqrt{N}} \right) \frac{1}{I_3} \right] + \frac{k(1 - \ln I_3)}{I_3} \quad (7.74)$$

where σ_i and λ_i are principal stresses and stretches, respectively; L^{-1} is the inverse Langevin function with $L(x) = \coth x - 1/x$.

Bischoff et al.^[9] incorporated this constitutive law into a finite element simulation to verify the model in situations where the solution was known through experimental data. The model has been shown to have predictive capabilities by the good agreement between model predictions and experimental results obtained both *in vivo*^[121] and *in vitro*^[92,122].

From finite element simulations, this modeling approach predicts that the collagen network in hypertrophic scars is denser and the constituent collagen fibers have shorter free lengths than in healthy skin. Additionally, the model is shown to predict that as rat skin ages, collagen network density increases and fiber free length decreases.

It should be noted that in this model skin is assumed to be an orthotropic, hyperelastic material, which means anisotropic mechanical behaviour and viscoelastic properties of skin cannot be modeled. Besides, it can't model

any effects of the proteoglycan ground substance on the mechanical response since the model is based on the statistical mechanics of long-chain molecules.

8) Vesentini et al.^[123,124]

In order to investigate the optimal design for suturing, i.e., the spacing between two consecutive points able to minimize skin damage given the force needed to close the wound, Vesentini et al.^[123,124] developed a bi-dimensional nanostructural model, which is differently from Lanir's model and allows the application of concentrate loads within the skin sheet. This 2-dimensional recruitment model for a planar soft tissue is able to compute the local collagen fibers displacement caused by the application of a concentrated force and to evaluate the damage of the elastin matrix and on the fibrous component.

Assumptions

(1) The collagen fibers oppose to the force by means of geometrical modification and the generation of traction forces; the scratching of elastin would be driven by the orientation changes of the collagen fibers.

(2) Accordingly, in the model the reticular dermis is assumed to consist of a number of two-dimensional layers of collagen I fibrils and amorphous elastin. The contribution of epidermis, subcutis, and papillary dermis is neglected as well as the contribution of those collagen types different from type I, elastin-associated microfibrils, and ground substance.

(3) The tissue response is the sum of the responses of its constituents.

(4) This feature determines the tissue nonlinear stress-strain relationship, which is due to fibril recruitment and realignment toward load direction, although the component mechanical properties are linear (bilinear) elastic.

(5) the stress-strain behaviour of the collagen fibrils is assumed to be bilinear. In the first region, (uncrimping region) fibrils can elongate with zero stress, and collagen fibrils are not able to react to strains lower than 57%; when initially loaded, the collagen fibrils align in the direction of tension and straighten.

(6) It is assumed that collagen fibers are not able to react to strains lower than 57%^[95]; when initially loaded, the collagen fibers align in the direction of tension and straighten. For strains larger than 57%, the fibers are assumed to have a linear elastic behaviour with an elastic modulus $E = 1000$ MPa and ultimate stress and strain (σ_c^* , ε_c^*) equal to 50 MPa and 63%^[6,30]. Concerning the other constituent, the elastin matrix, a linear elastic behaviour has been considered with $E = 0.6$ MPa and ultimate stress and strain (σ_e^* , ε_e^*) equal to 1 MPa and 167%^[6,30].

(7) The reticular dennis is assumed to consist of two-dimensional layers

of collagen I fibers and amorphous elastin. For collagen I the following assumptions have been adopted: ① the fibril radius (R_c) is equal to 25 nm; ② the fibers have different orientation angles α ; ③ collagen fibrils group in fibril families, and each family is defined by one orientation.

A distribution function $p(\alpha)$, proposed by Lanir^[5], is used to set the collagen fiber orientation

$$\int_{\alpha_{\min}}^{\alpha_{\max}} p(\alpha) d\alpha = 1, \quad -\frac{\pi}{2} < \alpha \leq \frac{\pi}{2} \quad (7.75)$$

According to this definition a constant value of $p(\alpha)$ equal to $1/\pi$ corresponds to an isotropic fiber distribution.

As an initial estimate, the fibers are supposed to be perturbed within the range $\pm\Delta x$. The resultant modification in fiber orientation depends on whether the left (α_{1L}) or right (α_{1R}) hand side is considered. For instance, for the right side, the local strain of the fiber is $\varepsilon = (L_1 - L_0)/L_0$ with $L_0 = L_{DR}/\cos \alpha$ and $L_1 = L_{DR}/\cos \alpha_{1R}$.

The deformation stresses the collagen fiber and the force acting on it is $F_c = E_c \varepsilon_c \pi R_c^2$ with R_c and E_c being the collagen fibril radius and elastic modulus, respectively and ε_c being the strain of collagen. This force is distinguished within perpendicular and parallel component (F_- and F_\perp) with respect to the unstressed-condition. F_- loads the elastin matrix while F_\perp loads the collagen fibers.

The perpendicular component is calculated as

$$F_\perp = 2E_c \varepsilon_c \pi R_c^2 \sin\left(\frac{\alpha_{1R} - \alpha}{2}\right) \quad (7.76)$$

The force F applied by the collagen fibril transfers on the elastin matrix where the elastin stress (σ_e)-distance (r) relation is $\sigma_e = \sigma_{e\max} R_c^2 / r^2$.

The force transferred on the surrounding elastin matrix in this condition is given by

$$F_{\text{lim}} = 2 \int_{R_c}^{\infty} dr = 2\sigma_e l R_c \quad (7.77)$$

where l is the part of the fibril which stresses the elastin matrix by changing its curvature.

$$\varepsilon_{\text{clim}} = 2l\sigma_e^* / [R_c E_c \pi (\alpha_R - \alpha)] \quad (7.78)$$

where $\varepsilon_{\text{clim}}$ is the strain value at which the elastin matrix begins to rupture; $2l$ is the fibril segment working as force transfer to the neighbouring elastin matrix; the α is the fibril orientation angle.

Four different cases may result from the local strain of the fibril ε_c .

(1) $\varepsilon_c < \varepsilon_{\text{clim}}$ and $\varepsilon_c < \varepsilon_c^*$: in this case, the elastin matrix does not break and is still able to react to fibril drag. Consequently, this configuration is stable, the force is then successively moved down. The elastin matrix, and fibril strain is lower than its ultimate value.

(2) $\varepsilon_c^* < \varepsilon_c < \varepsilon_{\text{clim}}$: in this case, the collagen fibril breaks. The disrupted collagen fibers, when present, are no longer able to sustain the load and are consequently eliminated from the calculation.

(3) $\varepsilon_{\text{clim}} < \varepsilon_c < \varepsilon_c^*$: in this case, the elastin matrix disrupts and the damaged zone enlarges.

(4) $\varepsilon_c > \varepsilon_{\text{clim}}$ and $\varepsilon_c > \varepsilon_c^*$: in this case, both the elastin matrix and the collagen fibril disrupt; however, since the enlargement of the elastin matrix damaged area causes a decrease of the collagen fibril strain, the collagen fibril is not eliminated from the calculations, the damaged area is enlarged by in the direction, and calculation of the new strain value ($\varepsilon_{\text{clim}}$) is performed until case 1 or case 2 is achieved.

Vesentini et al.^[123,124] applied this model to investigate the collagen fibril and elastin matrix damage mechanics following suture point application. Results indicate that the force displacement caused by the suture point application curve initially stiffens and subsequently softens. Softening occurs due at first to the enlargement of the elastin matrix damaged area and second to the collagen fibril disruption. Accordingly, by properly choosing the number of suture points, it is possible to define the optimal suture points number for a given wound closure force.

7.3.2 Viscoelastic model

Microstructural viscoelastic models have been formulated with a similar basis as some of the previously discussed microstructural elastic models.

1) Decraemer et al.^[84]

Decraemer et al.^[84] refined their previous structural model for skin elastic behaviour^[107] to describe as well viscoelastic phenomena under different loading histories by adding damping to the model and assuming that the fibres all have identical linear viscoelastic properties described by the relaxation function $G(t)$.

A viscoelastic model based on the material structure of soft biological tissue is proposed and a corresponding nonlinear viscoelastic constitutive equation is derived. It is shown how the relaxation spectrum $H(r)$ may be derived using only the fundamental Fourier term of the stress corresponding

with harmonic strain oscillation.

$$F(t) = N \int_{-\infty}^t G(t-\tau) \frac{dl(\tau)}{d\tau} \times \int_{l_0}^{l(\tau)} \frac{1}{\sqrt{2\pi}sl_i} \exp\left[-(\mu - l_i)^2/(2s^2)\right] dl_i d\tau \quad (7.79)$$

where $F(t)$ is the force at any time t ($t \geq \tau$); N is the number of purely elastic fibres (modulus k) embedded in a gelatin like liquid, all having the same cross-sectional area S but different initial length l_i , normally distributed around a mean μ with a standard deviation s .

The above constitutive equation has been written in a particular way to show that it is similar to the linear viscoelastic constitutive equation, in which ε has been replaced by a function of ε , namely $\sigma^\varepsilon(\varepsilon)$

$$\sigma(t) = \int_{-\infty}^t G_r(t-\tau) \frac{d\sigma^\varepsilon[\varepsilon(\tau)]}{d\tau} d\tau \quad (7.80)$$

where the time function $G_r(t-\tau) = G(t-\tau)/G(0)$ [$G_r(0) = 1$] is called the “reduced relaxation function”, which describes the relative variation of the stress following a step variation in strain; the function $\sigma^\varepsilon (\equiv F^\varepsilon/A_0)$ describes the immediate stress response, which is a purely elastic relation (index ε) between stress and strain.

2) Lanir^[5,93,94,125]

One precedent for the use of ultrastructural considerations in formulation of constitutive laws is found in the work of Lanir^[5,93,94,125] on flat, collagenous tissues.

To the best of the authors’ knowledge, the only bidimensional nanostructural model has been developed by Lanir^[93] and concerns skin. With respect to a rectangular skin sheet and assuming an initially isotropic collagen fibril two-dimensional distribution and a collagen fibril wavy arrangement caused by elastin, Lanir investigated the anisotropy and stiffening effects under increasing shear strain level by applying a distributed shear load to one boundary.

Lanir’s^[93,94] proposed a conceptual model consisted of two networks of fibers (elastin and collagen) and uses a physically significant per fiber strain energy function which is incorporated into a continuum formulation. The fiber’s configurational alteration during deformation, and its resulting stretch and load were determined first. A statistical mechanical approach was then used to obtain the macroscopic constitutive relation. Thermodynamic considerations are introduced in their subsequent work^[5] for modeling the general three-dimensional viscoelastic behaviour.

Assumptions

(1) Skin is considered as an incompressible composite of undulating fibers embedded in a fluid matrix.

(2) The fibres are linear elastic under stretch.

(3) The mechanical behaviour of skin is assumed to be dominated by the dermis and the influence of the epidermis and hypodermis is neglected. The tissue's response is the sum of the responses of its constituents. The interaction between the fibres and the ground substance is ignored.

(4) All of the fibers are arranged spatially according to a distribution function.

(5) Each fibre is thin and perfectly flexible. It has no compressive stiffness and will buckle under a compressive load. The fibres that are undulated do not carry load until they are completely straightened. The collagen fibers and the unfolding and rotating of the fibers during deformation squeezed the matrix, resulting in an internal hydrostatic pressure.

(6) If a fibre is stretched, it is subjected to a uniaxial strain which is the tensorial transformation of the overall strain in the fibre's direction (affine deformation).

(7) Upon stretching, the fraction of fibres that are straightened and stretched rises, causing increased resistance against stretch and providing nonlinear behaviour.

The structure is defined in terms of the orientation of fibres. In order to reduce the computing effort, a two-dimensional (plane stress) model is considered. In flat tissues, the orientation distribution of each fibre type, k , can be described by a density distribution function $R(k)$ where the argument is the polar angle. In this study two fibre types are considered: collagen ($k = c$), and elastin ($k = e$).

The stress-strain relation is described with

$$\boldsymbol{\sigma} = \boldsymbol{\tau} - p\mathbf{I} \quad (7.81)$$

where $\boldsymbol{\sigma}$ is the Cauchy stress tensor; $\boldsymbol{\tau}$ is the so-called extra stress tensor, p is a hydrostatic pressure and \mathbf{I} is the second order unit tensor. The mechanical behaviour of the fibres is accounted for in $\boldsymbol{\tau}$, the contribution of the groundsubstance is accounted for in p . The stress-strain relation defined by Lanir^[5] for an in-plane continuous fibre distribution is given by:

$$\boldsymbol{\sigma} = \mathbf{J}^{-1} \sum_k S_k \int_0^\pi R_k(\theta) f_k^*[\lambda(\mathbf{r}_0)] \mathbf{F} \cdot \frac{\partial \lambda(\mathbf{r}_0)}{\partial \mathbf{E}} \cdot \mathbf{F}^c d\theta - p\mathbf{I} \quad (7.82)$$

where \mathbf{F} is the deformation tensor; $\mathbf{J} = \det(\mathbf{F})$ is a measure for the volume strain; \mathbf{r}_0 is a unit vector tangent to the fibre in reference configuration; $\lambda(\mathbf{r}_0)$ is the elongation ratio of the fibres oriented in the direction \mathbf{r}_0 in the reference state; S_k is the volumetric fraction (out of the total volume) of fibres of type k in the unstrained state; $R_k(\theta) d\theta$ the fraction of all fibres of type k oriented in direction between θ and $\theta + d\theta$ in the reference state, which should hold that $\int_0^\pi R_k(\theta) d\theta = 1$; $E = 1/2(\mathbf{F}^c \cdot \mathbf{F} - \mathbf{I})$ is the Green-Lagrange tensor (note that the term $\partial\lambda(\mathbf{r}_0)/\partial E$ can be expressed as $\lambda^{-1}(\mathbf{r}_0)\mathbf{r}_0\mathbf{r}_0$); $f_k^*[\lambda(\mathbf{r}_0)]$ is the load per unit undeformed cross-sectional area, which also accounts for the undulation of the fibres.

Fibre orientation distribution functions $R_k(\theta)$ for collagen fibres is given as by Lanir^[5] as

$$R_c(\theta) = A \cos^4(\theta - C_2) + B, \quad 0 \leq \theta \leq \pi \quad (7.83)$$

where A and B are constants. By requiring that the function is symmetric, cyclic, smooth and should satisfy the normalisation condition for density distribution functions, $R_c(\theta)$ attains the following form:

$$R_c(\theta) = 1/\pi + C_1[\cos^4(\theta - C_2) - 0.375] \quad (7.84)$$

The restriction $R_k(\theta) > 0$ for all θ imposes limits on C_1 , namely $0 \leq C_1 \leq 0.894$. The orientation associated with the angle C_2 ($0 \leq C_2 \leq \pi$) is the direction of physical symmetry of the fibrous structure or the preferred fibre orientation. The parameter C_1 is a measure for the anisotropy. The orientation distribution of elastin is assumed to be isotropic and can thus be defined by

$$R_c(\theta) = 1/\pi \quad (7.85)$$

The assumptions that fibres are perfectly thin and flexible, have no compressive strength, and if stretched are linear elastic, lead to the following stress-elongation relation for straightened fibres:

$$f_k(\lambda) = \begin{cases} 0 & \text{for } 0 < \lambda \leq 1 \\ K_k(\lambda - 1) & \text{for } \lambda > 1 \end{cases} \quad (7.86)$$

with K_k the stiffness of fibre type k . The elastin fibres are assumed to be already strained in reference configuration. In order to incorporate the undulation behaviour of the collagen fibres, the stress-elongation relation is adjusted. The undulation of collagen fibres is assumed to be normally distributed and expressed in the undulation density distribution function given

by

$$D_{c,r_0}(x) = \frac{1}{\sigma_{c,r_0} (2\pi)^{1/2}} \exp \left[\frac{-(x - \mu_{c,r_0})^2}{2\sigma_{c,r_0}^2} \right] \quad (7.87)$$

where x is the elongation ratio of the collagen fibres in the deformed state, the mean elongation ratio defined as the length at which the collagen fibres become straightened divided by the fibre length along in the undulated, unstrained state and its standard deviation.

Suppose is the fraction of collagen fibres orientated in direction i that is already straightened in reference configuration. Then, the total load per unit unstrained cross-sectional area contributed by all collagen fibres in direction i , with different straightening strain, can be formulated as

$$f_c^* [\lambda(\mathbf{r}_0)] = a_{c,r_0} f_k(\lambda) + \int_{x=1}^{\lambda} D_{c,r_0} f_c \frac{\lambda}{x} dx \quad (7.88)$$

$$N^{\alpha\beta} = \int_0^\pi U(\theta, t) (\partial\varepsilon/\partial\varepsilon_{\alpha\beta}) d\theta + N_p A^{\alpha\beta} \quad (7.89)$$

$$U(\theta, t) = \sum_{i=1}^2 S_i F_i \left[\varepsilon \left(\frac{t}{T} \right), t \right] R_i(\theta) \quad (7.90)$$

$$\varepsilon(t) = \varepsilon_{11}(t) \cos^2 \theta + 2\varepsilon_{12}(t) \sin \theta \cos \theta + \varepsilon_{22}(t) \sin^2 \theta \quad (7.91)$$

where F_i is rheological law for elastin ($I = 1$) and collagen ($I = 2$) fibers; $N_p A^{\alpha\beta}$ is time dependent pressure term; H_0 is initial thickness; ε is the fiber strain; S is the fiber density.

A good qualitative agreement was found with results from experiments on rabbit skin.

Applications

This model is implemented^[126] in the finite element code MARC^[127] and uses 8-node, isoparametric trilinear brick elements. Douven et al.^[128] applied Lanir's model^[5] to describe the uniaxial tensile behaviour of human skin *in vivo*.

7.4 Summary

The complex material properties of skin make the accurate modeling of their material behaviour a challenge. In this chapter, we have provided a critical review of the constitutive models that have been developed to represent skin tissues. The simplifying assumptions of each modeling approach have been discussed as well as their relative strengths and weaknesses.

Till now, a variety of constitutive models have been proposed to describe the mechanical behaviour of skin tissue. In spite of the huge number of models proposed, there is not a common constitutive model, which was capable of capturing all of the properties of native skin tissue, mainly due to the complexity of composition, microstructure, deformation mechanisms as well as the specific nature and conditions of the experiments the models were based on.

Phenomenological versus structural

Models based on continuum mechanics allow simulating two-dimensional behaviour of skin through the assignment of constitutive parameters calculated from experimental tests. In turn, they are not suited to approach the substructural mechanics of collagen fibrils, due to the continuum hypothesis.

A problem is the wide variability in the material parameters of continuum and phenomenological models for ① different experimental protocols for a given specimen, and ② slight cycle-to-cycle variations within a single protocol^[129]. Consequently, it is difficult to make reliable interpretations of a tissue's behaviour^[45]. The strain energy density functions that have been proposed to represent the orthotropic behaviour of skin^[30] require a large number of constants. Moreover, orthotropic strain energy density functions are not readily available in commercial finite element codes, which are often used in the analysis of non-linear, large deformation problems^[54].

Clearly, nearly all tissues are comprised of integrated collagen and elastin fiber networks, which are characterized by nonlinear elastic responses at medium and large deformations. Although nonlinear elastic responses have long been described by phenomenological approaches^[80], "structural" models have been introduced that reflect tissue architecture^[130], with each structural component described by a simple phenomenological model, such as a two-parameter Fung's model. Thus, while these newer schemes attempt to reflect microscale tissue architecture, molecular scale structure continues to be largely treated in a phenomenological fashion^[131]. To address this limitation, a physics-based polymer chain model has been recently used to describe nonlinear elasticity of biological tissues^[132]. Significantly, polymer chain models possess a number of advantages over phenomenological models, including enhanced capacity to capture the equilibrium response under different loading conditions and the potential to relate fitted constitutive parameters to biopolymer molecular structure.

Although structural models have physically significant parameters, which provide an insight into how the structure of the solids affects its constitutive

behaviour^[92], they are mathematically complex requiring precise quantification of the tissue architecture including constituent interactions. For example, structural models often contain a large number of parameters, making the model rather complex; this can result in an increase of computing effort. Thus far, however, these microstructural relations have not described the data better than phenomenological relations^[129].

One dimensional versus three dimensional

Many of these are models derived from fitting of uniaxial experimental data^[21,39,56,133,134], which have relatively simple mathematical expressions and have been successful at describing the uniaxial behaviour. Their value however, is restricted, as they are incapable of describing and predicting complex three-dimensional, anisotropic behaviour, and shear or transverse loading^[16,17]. Several of the proposed models were derived to solve more complex two-dimensional problems, but are still restricted to specific problem scenarios^[5,23,36~38,41,93,118,119].

Future

The ultimate goal of skin biomechanics modeling is to improve the clinical diagnosis and treatment of skin injuries, e.g. the models may identify means by which to prevent injuries. Despite the significant advances in recent years in both the complexity and accuracy of computational models of skin, current models are still incapable of completely describing and predicting skin behaviour. Improvement in future models will be achieved through research in a number of different areas^[17]: ① experimental methods need to be improved to allow inhomogeneities in material properties and *in situ* strain to be more accurately quantified; ② more data are also needed to quantify the multiaxial material properties of skin; ③ better material models will allow elastic and viscoelastic behaviour of skin to be more accurately represented. These models need to be capable of representing healing and diseased skin as well as healthy tissue.

References

- [1] Anderson A E, Ellis B J, weiss J A. Verification, validation and sensitivity studies in computational biomechanics. *Computer Methods in Biomechanics and Biomedical Engineering*, 2007, 10(3): 171–184.
- [2] Auer E, Luther W. *Numerical Validation in Current Hardware Architectures*. Berlin: Springer-Verlag, 2009: 145–160.
- [3] DeHoff P H, Key J E. Application of the finite element analysis to determine forces and stresses in wound closing. *Journal of Biomechanics*, 1981, 14(8): 549–554.

- [4] Meijer R, Douven L F A, Oomens C W J. Characterization of anisotropic and non-linear behaviour of human skin in vivo. *Computer Methods in Biomechanics and Biomedical Engineering*, 1999, 1(1): 13–27.
- [5] Lanir Y. Constitutive equations for fibrous connective tissues. *Journal of Biomechanics*, 1983, 16(1): 1–12.
- [6] Larrabee W F, Sutton D. A finite element model of skin deformation. II. An experimental model of skin deformation. *Laryngoscope*, 1986, 96(4): 406–412.
- [7] Larrabee W F, Galt J A. A finite element model of skin deformation. III. The finite element model. *Laryngoscope*, 1986, 96(4): 413–419.
- [8] Kirby S D, Wang B, To C W, et al. Nonlinear, three-dimensional finite-element model of skin biomechanics. *Journal of Otolaryngology*, 1998, 27(3): 153–160.
- [9] Bischoff J E, Arruda E M, Gresh K. Finite element modeling of human skin using an isotropic, nonlinear elastic constitutive model. *Journal of Biomechanics*, 2000, 33(6): 645–652.
- [10] Arruda E M, Boyce M C. A three-dimensional constitutive model for the large stretch behavior of rubber elastic materials. *Journal of the Mechanics and Physics of Solids*, 1993, 41(2): 389–412.
- [11] Manios A, Katsantonis J, Tosca A, et al. The finite element method as a research and teaching tool in the analysis of local skin flaps. *Dermatologic Surgery*, 1996, 22(12): 1029–1033.
- [12] Retel V, Vescovo P, Jacquet E, et al. Nonlinear model of skin mechanical behaviour analysis with finite element method. *Skin Research and Technology*, 2001, 7(3): 152–158.
- [13] Miller K, Chinzei K. Modeling of soft tissues deformation. *Journal of Computer Aided Surgery*, 1995, Suppl.1: 62–63.
- [14] Lavallée S. Registration for Computer Integrated Surgery: Methodology, State of the Art. *Computer-Integrated Surgery*. Cambridge: MIT Press, 1995: 77–97.
- [15] Huelke D F, Melvin J W. Anatomy, injury frequency, biomechanics, and human tolerances. *SAE Transactions*, 1980: 633–651.
- [16] Kvistedal Y A. Multiaxial in-Vivo Testing of Human Skin [Ph. D. Thesis]. Auckland: University of Auckland, 2003.
- [17] Weiss J A, Gardiner J C. Computational modeling of ligament mechanics. *Critical ReviewsTM in Biomedical Engineering*, 2001, 29(3): 303–371.
- [18] North J F. Impact Characteristics of Human Skin and Subcutaneous Tissue [Ph. D. Thesis]. Glasgow: University of Strathclyde, 1972.
- [19] Barbenel J C, Time dependent mechanical properties of skin [Ph. D. Thesis]. Glasgow: University of Strathclyde, 1978.
- [20] Lanir Y. Skin mechanics//Skalak R, Chien S. *Handbook of Bioengineering*. New York: McGraw-Hill, 1987: 11.11–11.25.
- [21] Veronda D R , Westmann R A. Mechanical characterization of skin-finite deformations. *Journal of Biomechanics*, 1970, 3(1): 111–124.

- [22] Lanir Y, Fung Y C. Two-dimensional mechanical properties of rabbit skin. II. Experimental results. *Journal of Biomechanics*, 1974, 7(2): 171–182.
- [23] Tong P, Fung Y C. Stress-strain relationship for the skin. *Journal of Biomechanics*, 1976, 9(10): 649–657.
- [24] Allaire P E, Thacker J G, Edlich R F, et al. Finite deformation theory for in-vivo human skin. *Journal of Bioengineering*, 1977, 1(3): 239–249.
- [25] Crisp J D C. Properties of tendon and skin//Fung Y C, Perrone N, Anliker M. *Biomechanics: Its Foundation and Objectives*. Englewood: Prentice-Hall, 1972: 141–179.
- [26] Ridge M D, Wright V. The rheology of skin. A bio-engineering study of the mechanical properties of human skin in relation to its structure. *British Journal of Dermatology*, 1965, 77(12): 639–649.
- [27] Ridge M D, Wright V. A rheological study of skin//Kenedi R M. *Biomechanics and Related Bio-engineering Topics*. Oxford: Pergamon Press, 1965: 165–175.
- [28] Ridge M D, Wright V. Mechanical properties of skin: A bioengineering study of skin structure. *Journal of Applied Physiology*, 1966, 21(5): 1602–1606.
- [29] Ridge M D, Wright V. A Rheological Study of the Skin//Kenedi R. *Biomechanics and Related Topics*. Oxford: Pergamon Press, 1967.
- [30] Fung Y C. *Biomechanics: Mechanical Properties of Living Tissue*. New York: Springer-Verlag, 1981.
- [31] Fung Y C, Fronek K, Patitucci P. Pseudoelasticity of arteries and the choice of its mathematical expression. *American Journal of Physiology*, 1979, 237: H620–H631.
- [32] Glaser A A, Marangoni R D, Must J S, et al. Refinements in the methods for the measurement of the mechanical properties of unwounded and wounded skin. *Medical Electronics and Biological Engineering*, 1965, 3(4): 411–419.
- [33] Kenedi R M, Gibson T, Daly C H. Bio-engineering studies of the human skin: II//Kenedi R M. *Biomechanics and Related Bio-engineering Topics*. Oxford: Pergamon Press, 1965: 147–158.
- [34] Peng S T J, Landel R F, Brody G S. In-vitro study of human rheology. The VI New England Bio-Medical Conference. Oxford: Pergamon Press, 1978: 350–354.
- [35] Fung Y C. Elasticity of soft tissues in simple elongation. *American Journal of Physiology*, 1967, 213(6): 1532–1544.
- [36] Alexander H, Cook T H. Accounting for natural tension in the mechanical testing of human skin. *Journal of Investigative Dermatology*, 1977, 69(3): 310–314.
- [37] Danielson D A. Human skin as an elastic membrane. *Journal of Biomechanics*, 1973, 6(5): 539–546.
- [38] Gou P F. Strain-energy functions for biological tissues. *Journal of Biomechanical Engineering*, 1970, 3(6): 547–550.
- [39] Snyder R W, Lee L H. Experimental study of biological tissue subjected to pure shear. *Journal of Biomechanics*, 1975, 8(6): 415–419.

- [40] Ridge M D, Wright V. The directional effects of skin. A bio-engineering study of skin with particular reference to Langer's lines. *Journal of Investigative Dermatology*, 1966, 46(4): 341–346.
- [41] Danielson D A, Natarajan S. Tension field theory and the stress in stretched skin. *Journal of Biomechanics*, 1975, 8(2): 135–142.
- [42] Snyder R W. Large deformation of isotropic biological tissues. *Journal of Biomechanics*, 1972, 5(6): 601–606.
- [43] Fung Y C. Biorheology of soft tissues. *Biorheology*, 1973, 10(2): 139–155.
- [44] Lanir Y, Fung Y C. Two-dimensional mechanical properties of rabbit skin. I. Experimental system. *Journal of Biomechanics*, 1974, 7(1): 29–34.
- [45] Yin F C P, Chew P H, Zeger S L. An approach to quantification of biaxial tissue stress-strain data. *Journal of Biomechanics*, 1986, 19(1): 27–37.
- [46] Chaudhry H R, Bukiet B, Findley T, et al. Evaluation of residual stress in rabbit skin and the relevant material constants. *Journal of Theoretical Biology*, 1998, 192(2): 191–195.
- [47] Gambarotta L, Massabo R, Morbiducci R, et al. In vivo experimental testing and model identification of human scalp skin. *Journal of Biomechanics*, 2005, 38(11): 2237–2247.
- [48] Alexander H, Cook T H. Variations with age in the mechanical properties of human skin in vivo//Kennedy R M. *Bedsore Biomechanics*. Bath: McMillan Press, 1976: 109–118.
- [49] Reihnsner R, Balogh B, Menzel E J. Two-dimensional elastic properties of human skin in terms of an incremental model at the in vivo configuration. *Medical Engineering and Physics*, 1995, 17(4): 304–313.
- [50] Diridollou S, Patat F, Gens F, et al. In vivo model of the mechanical properties of the human skin under suction. *Skin Research and Technology*, 2000, 6(4): 214–221.
- [51] Hendriks F M, Brokken D, Oomens C W, et al. Influence of hydration and experimental length scale on the mechanical response of human skin in vivo using optical coherence tomography. *Skin Research and Technology*, 2004, 10(4): 231–241.
- [52] Hendriks F M, Brokken D, Oomens C W, et al. The relative contributions of different skin layers to the mechanical behavior of human skin in vivo using suction experiments. *Medical Engineering and Physics*, 2006, 28(3): 259–266.
- [53] Shergold O A, Fleck N A. Experimental investigation into the deep penetration of soft solids by sharp and blunt punches, with application to the piercing of skin. *Journal of Biomechanical Engineering*, 2005, 127(5): 838–848.
- [54] Shergold O A, Fleck N A, Radford D. The uniaxial stress versus strain response of pig skin and silicone rubber at low and high strain rates. *International Journal of Impact Engineering*, 2006, 32(9): 1384–1402.
- [55] Jamison C E, Marangoni R D, Glaser A A. *Viscoelastic properties of soft tissue by discrete model characterization*. ASME New York, 1967: 9.

- [56] Jamison C E, Marangoni R D, Glaser A A. Viscoelastic properties of soft tissue by discrete model characterization. *Journal of Biomechanics*, 1968, 1(1): 33–36.
- [57] Barbenel J C, Evans J H. The time-dependent mechanical properties of skin. *Journal of Investigative Dermatology*, 1977, 69(3): 318–320.
- [58] Barbenel J C, Evans J H, Finlay J B. Stress-strain-time relations for soft connective tissue//Kenedi R M. *Perspective in Biomedical Engineering*. London: Macmillan, 1973: 165–172.
- [59] Vogel H G, Hilgner W. The “step phenomenon” as observed in animal skin. *Journal of Biomechanics*, 1979, 12(1): 75–81.
- [60] Ward R, Rempel R, Anderson G S. Modeling dynamic skinfold compression. *American Journal of Human Biology*, 1999, 11(4): 531–537.
- [61] Scalari G, Eisinberg A, Menciasci A, et al. Micro instrumentation for non-invasive measurement of mechanical properties of tissues. *Proceedings of the 1st Annual International IEEE-EMBS Special Topic Conference on Microtechnologies in Medicine and Biology*. Lyon, 2000: 199–202.
- [62] Wu J Z, Dong R G, Rakheja S, et al. Simulation of mechanical responses of fingertip to dynamic loading. *Medical Engineering and Physics*, 2002, 24(4): 253–264.
- [63] Wu J Z, Dong R G, Smutz W P, et al. Non-linear and viscoelastic characteristics of skin under compression: Experiment and analysis. *Bio-Medical Materials and Engineering*, 2003, 13(4): 373–385.
- [64] Wu J Z, Cutlip R G, Welcome D, et al. Estimation of the viscous properties of skin and subcutaneous tissue in uniaxial stress relaxation tests. *Bio-Medical Materials and Engineering*, 2006, 16(1): 53–66.
- [65] Wu J Z, Krajnak K, Welcome D E, et al. Analysis of the dynamic strains in a fingertip exposed to vibrations: Correlation to the mechanical stimuli on mechanoreceptors. *Journal of Biomechanics*, 2006, 39(13): 2445–2456.
- [66] Hoffman A H, Grigg P. Using pseudorandom stress stimuli to develop soft tissue constitutive equations. *Annals of Biomedical Engineering*, 2002, 30(1): 44–53.
- [67] Richards C L, Grigg P, Hoffman A H. Using pseudorandom stress stimuli to compare the properties of normal and diabetic rat skin. *Proceedings of the 2001 Bioengineering Conference*. Snowbird, 2001: 417–418.
- [68] Khatyr F, Imberdis C, Vescovo P, et al. Model of the viscoelastic behaviour of skin in vivo and study of anisotropy. *Skin Research and Technology*, 2004, 10(2): 96–103.
- [69] Agache P. *Physiologie de la peau et explorations fonctionnelles cutanées*. Cachan: Editions Médicales Internationales, 2000: 664.
- [70] Tsubouchi K, Enosawa S, Harada K, et al. Evaluation of the relationship between the viscoelastic stress and strain of fetal rat skin as a guide for designing the structure and dynamic performance of a manipulator for fetal surgery. *Surg Today*, 2006, 36(8): 701–706.
- [71] Wang Q, Hayward V. In vivo biomechanics of the fingerpad skin under local tangential traction. *Journal of Biomechanics*, 2007, 40(4): 851–860.

- [72] Giles J M, Black A E, Bischoff J E. Anomalous rate dependence of the preconditioned response of soft tissue during load controlled deformation. *Journal of Biomechanics*, 2007, 40(4): 777–785.
- [73] Fung Y C. Stress-strain-history relations of soft tissues in simple elongation//Fung Y C, Perrone N, Anliker M. *Biomechanics: Its Foundations and Objectives*. Englewood Cliffs: Prentice-Hall, 1972.
- [74] Kwan M K, Lin T H, Woo S L. On the viscoelastic properties of the antero-medial bundle of the anterior cruciate ligament. *Journal of Biomechanics*, 1993, 26(4-5): 447–452.
- [75] Guccione J M, McCulloch A D, Waldman L K. Passive material properties of intact ventricular myocardium determined from a cylindrical model. *Journal of Biomechanical Engineering*, 1991, 113(1): 42–55.
- [76] Dinnar U. A note on theory of deformation in compressed skin tissues. *Mathematical Biosciences*, 1970, 8(1-2): 71–82.
- [77] Duchemin G, Maillet P, Poinet P, et al. A hybrid position/force control approach for identification of deformation models of skin and underlying tissues. *IEEE Transactions on Biomedical Engineering*, 2005, 52(2): 160–170.
- [78] DiMaio S P, Salcudean S E. Needle insertion modeling and simulation. *IEEE Transactions on Automation Science and Engineering*, 2003, 19(5): 864–875.
- [79] D’Aulignac D, Laugier C, Cavusoglu M C. Toward a realistic echographic simulator with force feedback. *IEEE/RSJ International Conference on Intelligent Robots and Systems*. Kyongju, 1999: 727–732.
- [80] Fung Y C. *Biomechanics: Mechanical Properties of Living Tissues*. New York: Springer-Verlag, 1993.
- [81] Fung Y C. *Biomechanics, its scope, history and some problems of continuum mechanics in physiology*. *Applied Mechanics Reviews*, 1968, 21(1): 1–20.
- [82] Fung Y C. Stress-strain history relations of soft tissues in simple elongation//Fung Y C, Perrone N, Anliker M. *Biomechanics: Its Foundations and Objectives*. Englewood Cliffs: Prentice-Hall, 1971: 181–208.
- [83] Ledoux W R, Blevins J J. The compressive material properties of the plantar soft tissue. *Journal of Biomechanics*, 2007, 40(13): 2975–2981.
- [84] Decraemer W F, Maes M A, Vanhuyse V J, et al. A non-linear viscoelastic constitutive equation for soft biological tissues based upon a structural model. *Journal of Biomechanics*, 1980, 13: 559–564.
- [85] Moon D K, Woo S L, Takakura Y, et al. The effects of refreezing on the viscoelastic and tensile properties of ligaments. *Journal of Biomechanics*, 2006, 39(6): 1153–1157.
- [86] Defrate L E, Li G. The prediction of stress-relaxation of ligaments and tendons using the quasi-linear viscoelastic model. *Biomechanics and Modeling in Mechanobiology*, 2006, 6(4): 245–251.
- [87] Funk J R, Hall G W, Crandall J R, et al. Linear and quasi-linear viscoelastic characterization of ankle ligaments. *Journal of Biomechanical Engineering*, 2000, 122(1): 15–22.

- [88] Woo S L Y, Simon B R, Kuei S C, et al. Quasi-linear viscoelastic properties of normal articular cartilage. *Journal of Biomechanical Engineering*, 1980, 102(2): 85–90.
- [89] Simon B R, Coats R S, Woo S L Y. Relaxation and creep quasilinear viscoelastic models for normal articular cartilage. *Journal of Biomechanical Engineering*, 1984, 106(2): 159–164.
- [90] Sarver J J, Robinson P S, Elliott D M. Methods for quasi-linear viscoelastic modeling of soft tissue: Application to incremental stress-relaxation experiments. *Journal of Biomechanical Engineering*, 2003, 125(5): 754–758.
- [91] Johnson G A, Tramaglini D M, Levine R E, et al. Tensile and viscoelastic properties of human patellar tendon. *Journal of Orthopaedic Research*, 1994, 12(6): 796–803.
- [92] Belkoff S M, Haut R C. A structural model used to evaluate the changing microstructure of maturing rat skin. *Journal of Biomechanics*, 1991, 24(8): 711–720.
- [93] Lanir Y. A structural theory for the homogeneous biaxial stress-strain relationships in flat collagenous tissues. *Journal of Biomechanics*, 1979, 12(6): 423–436.
- [94] Lanir Y. The rheological behavior of the skin: Experimental results and a structural model. *Biorheology*, 1979, 16(3): 191–202.
- [95] Markenscoff X, Yannas I V. On the stress-strain relation for skin. *Journal of Biomechanics*, 1979, 12(2): 127–129.
- [96] Manschot J F, Brakkee A J. The measurement and modeling of the mechanical properties of human skin in vivo. II. The model. *Journal of Biomechanics*, 1986, 19(7): 517–521.
- [97] Woo S L, Johnson G A, Smith B A. Mathematical modeling of ligaments and tendons. *Journal of Biomechanical Engineering*, 1993, 115(4B): 468–473.
- [98] Maurel W, Wu Y, Magneat Thalmann N, et al. Biomechanical models for soft tissue simulation. *ESPRIT Basic Research Series*. Berlin: Springer-Verlag, 1998.
- [99] Van der Voorden W K L. Characterization of the in-Plane Mechanical Behaviour of Human Skin [Ph. D. Thesis]. Eindhoven: Eindhoven University of Technology, 1996.
- [100] Jenkins R B, Little R W. A constitutive equation for parallel-fibered elastic tissue. *Journal of Biomechanics*, 1974, 7(5): 397–402.
- [101] Haut R C, Little R W. A constitutive equation for collagen fibers. *Journal of Biomechanics*, 1972, 5(5): 423–430.
- [102] Comninou M, Yannas I V. Dependence of stress-strain nonlinearity of connective tissues on the geometry of collagen fibers. *Journal of Biomechanics*, 1976, 9(7): 427–433.
- [103] Lovell C R, Smolenski K A, Duance V C, et al. Type I and III collagen content and fiber distribution in normal human skin during ageing. *British Journal of Dermatology*, 1987, 117(4): 419–428.
- [104] Craik J E, McNeil I R R. Histological studies of stressed skin//Kenedi R M. *Biomechanics and Related Engineering Topics*. Oxford: Pergamon Press,

- 1965: 159–164.
- [105] Daly C H. Biomechanical properties of dermis. *Journal of Investigative Dermatology*, 1982, 79 (Suppl. 1): 17s–20s.
- [106] Brown I A. A scanning electron microscope study of the effects of uniaxial tension on human skin. *British Journal of Dermatology*, 1973, 89(4): 383–393.
- [107] Decraemer W F, Maes M A, Vanhuysse V J. An elastic stress-strain relation for soft biological tissues based on a structural model. *Journal of Biomechanics*, 1980, 13(6): 463–468.
- [108] Liao H, Belkoff S M. A failure model for ligaments. *Journal of Biomechanics*, 1999, 32(2): 183–188.
- [109] Manschot J F, Brakkee A J. The measurement and modeling of the mechanical properties of human skin in vivo. I. The measurement. *Journal of Biomechanics*, 1986, 19(7): 511–515.
- [110] Shoemaker P A, Schneider D, Lee M C, et al. A constitutive model for two-dimensional soft tissues and its application to experimental data. *Journal of Biomechanics*, 1986, 19(9): 695–702.
- [111] Shoemaker P A, Irreversible Thermodynamics, the Constitutive Law, and a Constitutive Model for Two-Dimensional Soft Tissues [Ph. D. Thesis]. San Diego: University of California, 1984.
- [112] Schneider D. Viscoelasticity and Tearing Strength of the Human Skin [Ph. D. Thesis]. San Diego: University of California, 1982.
- [113] Oomens C W J, Grootenboer H J, et al. Experimental and theoretical compression studies on porcine skin//Perren S M, Schneider E. *Biomechanics: Current Interdisciplinary Research*. Martinus Nijhoff: The Hague, 1985: 227–232.
- [114] Oomens C W, van Campen D H, Grootenboer H J. In vitro compression of a soft tissue layer on a rigid foundation. *Journal of Biomechanics*, 1987, 20(10): 923–935.
- [115] Oomens C W, van Campen D H, Grootenboer H J. A mixture approach to the mechanics of skin. *Journal of Biomechanics*, 1987, 20(9): 877–885.
- [116] Mow V C, Kuei S C, Lai W M, et al. Biphasic creep and stress relaxation of articular cartilage in compression: Theory and experiments. *Journal of Biomechanical Engineering*, 1980, 102(1): 73–84.
- [117] Bischoff J E, Arruda E M, Grosh K. Constitutive modeling of human skin allowing for anisotropy and growth. 21st Annual Conference and the 1999 Annual Fall Meeting of the Biomedical Engineering Society. Blacksburg, 1999: 130.
- [118] Bischoff J E, Arruda E M, Grosh K. A microstructurally based orthotropic hyperelastic constitutive law. *Journal of Applied Mechanics*, 2002, 69(5): 570–579.
- [119] Bischoff J E, Arruda E M, Grosh K. Finite element simulations of the orthotropic hyperelasticity. *Finite Elements in Analysis and Design*, 2002, 38(10): 983–998.

- [120] Marko J F, Siggia E D. Stretching DNA. *Macromolecules*, 1995, 28(26): 8759–8770.
- [121] Gunner C W, Hutton W C, Burlin T E. The mechanical properties of skin in vivo: A portable hand-held extensometer. *British Journal of Dermatology*, 1979, 100(2): 161–163.
- [122] Dunn M G, Silver F H, Swann D A. Mechanical analysis of hypertrophic scar tissue: Structural basis for apparent increased rigidity. *Journal of Investigative Dermatology*, 1985, 84(1): 9–13.
- [123] Vesentini S, Redaelli A, Montevecchi F M. A two-dimensional recruitment model for the skin. *Proceedings of the IEEE-EMBS Special Topic Conference on Molecular, Cellular and Tissue Engineering*. Genoa, 2002: 168–170.
- [124] Vesentini S, Redaelli A, Montevecchi F M. Skin nanostructural features determine suture biomechanics. *IEEE Transactions on Nanobioscience*, 2003, 2(2): 79–88.
- [125] Lanir Y. The fibrous structure of the skin and its relation to mechanical behaviour//Marks R, Payne P A. *Bioengineering and the Skin*. San Francisco: MTS Press, 1981: 93–95.
- [126] Feron R P M J. A 3 D Structural Skin Model: Development and Implementation [M. S. Thesis]. Eindhoven: Eindhoven University of Technology, 1993.
- [127] MARC Analysis Research Corporation. Volumes A-E of the MARC Reference Library Manuals. Revision K.5. Palo Alto, 1994.
- [128] Douven L F A, Meijer R, Oomens C W J. Characterisation of mechanical behaviour of human skin in vivo. *The International Society for Optical Engineering*, 2000, 3914: 618–629.
- [129] Humphrey J D, Yin F C P. A new approach for describing soft tissue behavior. *Proceedings of the 13th Northeast Bioengineering Conference*. Philadelphia, 1987: 24–25.
- [130] Sacks M S. Incorporation of experimentally-derived fiber orientation into a structural constitutive model for planar-collagenous tissues. *Journal of Biomechanical Engineering*, 2003, 125: 280–287.
- [131] Wu X Y, Levenston M E, Chaikof E L. A constitutive model for protein-based materials. *Biomaterials*, 2006, 27(30): 5315–5325.
- [132] Bergstrom J S, Boyce M C. Constitutive modeling of the timedependent and cyclic loading of elastomers and application to soft biological tissues. *Mechanics of Materials*, 2001, 33(9): 523–530.
- [133] Demiray H. A note on the elasticity of soft biological tissues. *Journal of Biomechanical Engineering*, 1972, 5(3): 309–311.
- [134] Galford J E, McElhaney J H. A viscoelastic study of scalp, brain and dura. *Journal of Biomechanical Engineering*, 1970, 3(2): 211–221.

PART III
SKIN BIOTHERMOMECHANICS

Chapter 8

Introduction of Skin Biothermomechanics

8.1 Introduction

Skin biothermomechanics here is defined as the response of skin under thermomechanical loading, which leads to damage—the thermal denaturation of collagen. Since the thermal mechanical interaction is related to the thermal damage of tissue, which is mainly due to the denaturation of collagen (the main component of the dermis, see Chapter 2), the thermal denaturation (thermal shrinkage) is first reviewed here. Due to the clinical importance, the thermal denaturation of collagen and collagenous tissues has been studied a lot, and there are several good reviews on this subject (e.g. References [1, 2]).

In this chapter, the mechanism of thermal denaturation of collagen is first presented; then collagen thermal denaturation in skin tissue are reviewed, followed by talks on the influence of thermal denaturation of collagenous tissue on their properties; a simple model development for skin biothermomechanics is last presented.

8.2 Mechanism of Thermal Denaturation (Shrinkage) of Collagen

The collagen in human dermis are mainly the periodically banded, interstitial collagens (types I, III and IV), where about 80%~90% is type I collagen and 8%~12% is type III collagen (see Chapter 2). As noted, skin tissue also contains a small amount of elastin but which is very thermally stable [3]. For example, elastin can survive boiling for several hours with no apparent change, and does not need attention here.

Type I collagen has a domain within the triple helix that is completely devoid of hydroxyproline¹⁾. Since hydroxyproline readily forms hydrogen

1) Hydroxyproline ($C_5H_9O_3N$) is an uncommon amino acid.

bonds¹⁾[4] that stabilize the molecule, its absence makes this domain particularly susceptible to thermal damage^[5]. There are two levels of organization where breakdown is thermodynamically significant^[6]: one is the collagen molecule itself, in which three peptide chains are twisted around each other to form a helical, rod-shaped molecule; the other is the semi-crystalline fibril in which collagen molecules are assembled side-by-side in a staggered manner with the long axis of each molecule aligned with axial orientation of the fibril. When collagen is heated, the heat-labile intramolecular crosslinks are broken, as shown in Figure 8.1, and the collagen undergoes a transition from a highly organized crystalline structure to a random, gel-like state, which is the denaturation process^[7]. Collagen shrinkage occurs through the cumulative effect of the unwinding of the triple helix, due to the destruction of the heat-labile intramolecular crosslinks, and the residual tension of the heat-stable intermolecular crosslinks^[1,7,8].

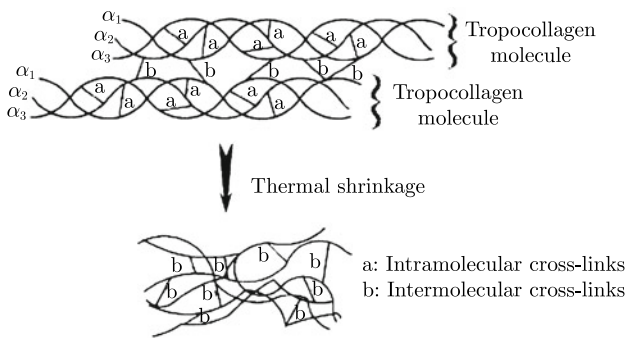


Figure 8.1 Schematic of thermal denaturation of collagen^[1] (by permission of AAOS)

The effects of heating on collagen can be reversible or irreversible and the precise heat-induced behaviour of collagenous tissue and shrinkage depend on several factors, including the collagen content^[9], the maximum temperature reached and exposure time^[8], the mechanical stress applied to the tissue during heating^[10,11], and aging^[9,12]. As for different heating methods, Arnoczky & Aksan^[1] pointed out that in spite of the different heat generation mechanisms within a tissue such as radio-frequency devices and lasers, once critical temperatures are reached (45°C), cells will die, and collagen will become denatured (about 65°C).

1) A hydrogen bond is a special type of dipole-dipole bond that exists between an electronegative atom and a hydrogen atom bonded to another electronegative atom. These bonds can occur between molecules (intermolecularly), or within different parts of a single molecule (intramolecularly).

Different metrics have been used to characterize the thermal denaturation and heat-induced damage of collagen and collagenous tissues, including biological metrics such as enzyme deactivation^[13] and extravasation of fluorescent-tagged plasma proteins^[14], thermal metrics such as changes in enthalpy^[15,16], mechanical metrics such as thermal shrinkage^[10,17~19], and optical metrics such as thermally-induced loss of birefringence (see Figure 8.2)^[20~23]. Although the shrinkage of collagen due to thermal denaturation has been widely used and has been suggested as a convenient continuum metric of thermal damage^[24,25], Wells et al.^[26] pointed out that shrinkage may not be a universal metric to measure thermal damage. Rather, there is a need to identify an independent metric by which one can determine the extent of thermal damage^[27]. Diller & Pearce^[25] pointed out that the dimensionless indicator of damage, Ω , is, in fact, the logarithm of the relative concentration of “reactants”, or undenatured collagen, in the collagen denaturation process, where Ω can be alternatively considered as

$$\Omega(t) = \ln \frac{C(0)}{C(t)} \quad (8.1)$$

where $C(0)$ and $C(t)$ are the initial concentration and the concentration remaining at time t of undenatured collagen, respectively. The degree of thermal denaturation, defined as the fraction of denatured collagen, and denoted by $Deg(t)$, can be calculated by

$$Deg(t) = \frac{C(0) - C(t)}{C(0)} = 1 - \exp[-\Omega(t)] \quad (8.2)$$

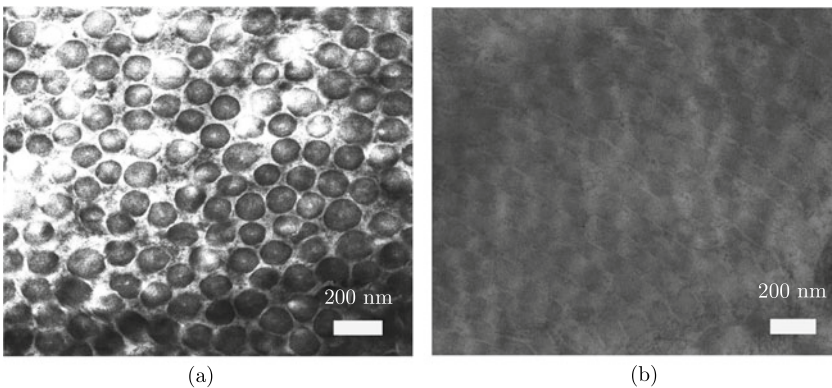


Figure 8.2 Scanning electron micrographs of dermal collagen fibres in untreated (a) or humid heat-treated (b) sections of a formalin fixed paraffin-embedded skin specimen. Note that the collagen fibres in the heat-treated section have lost their ultrastructural features and appear gelatinized

8.3 Properties Variations due to Thermal Denaturation of Collagen

Denaturation of collagen occurs as the temperature of the tissue increases. As well as structural changes, the hydration level of collagen also changes, which may involve an initial liberation and subsequent absorption of water^[28]. Not surprisingly, thermal denaturation of a collagenous tissue, can result in marked changes in the thermal^[29], mechanical^[10,19,30~35] and optical properties^[36~41]. For example, increased extensibility of soft tissues due to thermal treatment has been observed in both uniaxial^[30,42,43] and biaxial studies^[26,44]. However, none of these studies are for skin tissue and there are only few studies focused on the thermal denaturation process of skin tissue^[11,45~49], despite skin dermis being mainly composed of collagen.

8.3.1 Thermal properties changes due to thermal damage

There are few papers on thermal variations of tissue properties induced by thermal denaturation of collagen. So far, the properties that have been studied mainly include the specific heat and thermal diffusivity. The specific heat is often measured by DSC as a function of the temperature, from which the temperature of thermal denaturation can be obtained. The typical variation of specific heat with temperature (damage) is given in Figure 8.3.

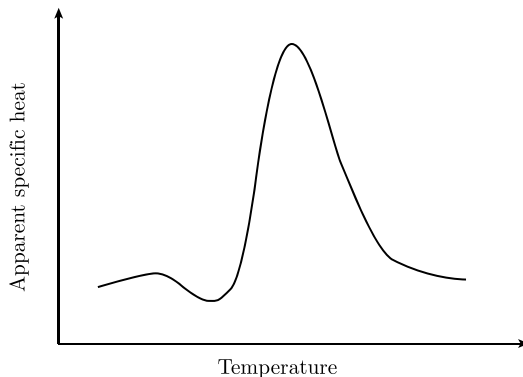


Figure 8.3 Variation of rabbit patellar tendon collagen apparent specific heat with temperature at a stress-free state (ramp heating at $2^{\circ}\text{C}/\text{min}$ between $35\sim 95^{\circ}\text{C}$)

By using the flash method, Davis et al.^[29] measured the through-wall component of thermal diffusivity, of bovine aorta before and after the tissue undergoing two hours of heating at 75°C and found that there was a 10.1% increase in the thermal diffusivity of the tissue post-heating.

8.3.2 Mechanical properties changes due to thermal denaturation

The influence of thermal damage has been observed in many collagenous tissues such as tendon and cartilage, which is also composed of type I collagen as skin. Chen et al.^[10,30,31] performed a series of thermal shrinkage tests on bovine chordae tendineae. The experimental results showed that scaling the actual heating time via the characteristic time, $\tau_2 = ce^{m/T}$ for free shrinkage and $\tau_2 = ce^{\alpha+\beta P} e^{m/T}$ for isotonic-shrinkage, resulted in a single correlation between free shrinkage and the duration of heating, which suggested a time-temperature-load equivalence.

Based on experimental data, Chen et al.^[19] proposed two phenomenological equations to quantify time-dependent thermal damage in a uniaxial collagenous tissue. Using the mixture rule suggested by Danielsen^[50], they showed that an empirical model could describe well the heat-induced axial shrinkage induced by a spectrum of thermo-mechanical loading histories. An exponential decay model was also shown to describe well the partial recovery when returned to body temperature following heating.

For the shrinkage region:

$$\xi = [1 - f(\nu)] (A_0 + A_1\nu) + f(\nu) (a_0 + a_1\nu), \forall \nu \quad (8.3)$$

here, $\nu = \ln(\tau/\tau_2)$, $\tau_2 = e^{\alpha+\beta P} e^{m/T}$; A_0 , A_1 , a_0 and a_1 are material constants; $f \in [0, 1]$ is the distribution fraction of the linear behaviours, defined as

$$f(\nu) = 1 - e^{-\Omega} = \frac{e^{a(\nu-\nu_m)}}{1 + e^{a(\nu-\nu_m)}}, \forall \nu \in (\ln(\tau_a/\tau_2), \ln(\tau_b/\tau_2)) \quad (8.4)$$

For the recovery region:

$$\xi(t) = B_0 - B_1(1 - e^{-t/t_c}) \quad (8.5)$$

where $B_0 = \xi_0$ is the shrinkage at $t = 0$, $B_0 - B_1 = \xi_e$ is the equilibrium shrinkage after recovery, and t_c is a material constant.

Diaz et al.^[32] carried out an experimental study on the mechanical response of porcine cartilage during laser heating, and found that with heating there were significant variations in internal stress and the corresponding stain rate, which were thermally mediated and strongly dependent on tissue orientation.

Chao et al.^[33] measured the dynamic variations of elastic modulus of rabbit nasal septal cartilage during laser radiation. Assuming linear elastic behaviour, they calculated the elastic modulus and found that: the modulus

in native tissue was 6.08 MPa, which decreased during and after each successive laser exposure for the first (5.41MPa, 4.94MPa), second (5.05MPa, 4.17MPa), and third (4.23MPa, 3.71MPa) laser exposures, respectively. Following rehydration, the modulus returned to near-baseline values (5.33MPa).

Using a dynamic thermo-mechanical analyzer and frequency multiplexing techniques, Serge et al.^[51] experimentally measured the time-temperature dependent flexural storage moduli and mechanical relaxation in transversely and longitudinally oriented specimens of porcine nasal septal cartilage. The results showed that: ① the storage moduli of porcine cartilage decreased with increasing temperature, and a critical change in mechanical properties (reduction in the storage modulus by 85%~90%) occurred between 58°C and 60°C; ② The shift of stress relaxation behaviour from viscoelastic solid to viscoelastic liquid was observed between 50°C and 57°C, which corresponded to the transition temperature region of structural changes.

Aksan & McGrath^[35] experimentally studied and quantified the heat-induced thermo-mechanical response characteristics of New Zealand white rabbit patellar tendon. They found that for all of the specimens tested, irrespective of the thermal and mechanical history of the specimen, during tensile testing the mechanical stress, σ , varied exponentially with the applied strain, ε , as

$$\sigma = C_1 + C_2 e^{C_3 \varepsilon} \quad (8.6)$$

$$\frac{d\sigma}{d\varepsilon} = C_3 \sigma - C_1 C_3 \quad (8.7)$$

where C_1 , C_2 , C_3 are functions of thermal damage Ω accumulated before the onset of tensile test, defined as

$$C_3 = 7.738 + 95.79e^{-0.102 \sum e_2} \quad (8.8)$$

$$\frac{\sum e_2}{e_{2,\max}} = 1 - e^{-0.6489\Omega/\Omega_m} \quad (8.9)$$

$$e_{2,\max} = 23.77 + \frac{12.41}{1 + e^{T-0.364/0.025,58}} \quad (8.10)$$

$$\Omega_m = 15.796e^{7.857T} \quad (8.11)$$

Here, Ω_m represents the thermal damage accumulated in tendon specimens where 50% of the maximum equilibrium shrinkage is reached.

Dahan et al.^[52] observed a dramatic increase of initial stress of the forehead skin (firmness) from 7.62 before treatment to 16.68 three months after the fifth treatment of neck line with a non-ablative laser.

8.3.3 Optical properties changes due to thermal damage

Since collagen fibers are the main scatters in collagenous tissue^[53,54], it is obvious that thermal denaturation will have great influence on the optical properties of these tissue.

Bosman^[36] studied the ultrastructure changes in heated bovine myocardium and their relation with the corresponding changes in optical properties. The tissue samples were pre-damaged by immersed in a water bath for 1000s at different temperatures (25~75°C). The results showed that the scattering anisotropy factor began to decrease gradually from 45°C, which corresponded to the beginning of the collagen denaturation.

Thomsen & Vijverberg^[55] experimentally measured the changes in optical properties of in vitro rat skin during thermal coagulation and their results showed that thermal coagulation of albino rat skin results in prominent changes of light scattering but relatively little in light absorption. The reduced scattering coefficients gradually increased with the increasing temperatures from room temperature to 55°C then rapidly decreased to plateau after 70°C. The differences among the reduced scattering coefficients values for the different wavelengths were greater at the lower temperatures than those at higher temperatures. The absorption coefficient changed very little over the test temperature range (room temperature to 90°C).

Nilsson et al.^[56] simultaneously measured the total transmittance, diffuse reflectance and surface temperature of fresh and thermally damaged human skin during laser heating. They found that thermally induced changes in the optical properties of tissue caused a decrease in the total transmittance and an increase in the diffuse reflectance of both fresh and pre-damaged skin samples. For fresh tissue, these changes were primarily reversible until photocoagulation occurred, then both the reversible and the irreversible changes were observed. But for pre-damaged tissue, the reversible changes in the optical properties were dominant, while the irreversible changes were insignificant.

Agah et al.^[39] experimentally studied the variation of optical properties of bovine myocardial tissue due to collagen denaturation and the results showed that the optical properties could be well fitted by exponential forms that exhibit temperature-dependent time constant as predicted by Arrhenius thermal damage theory, which suggested that the optical properties change could also be parameterized using a single measure of the prior thermal damage. The calculated optical coefficients of the samples were fitted to the

functional form

$$m = m_1 - m_2 \exp[-(t - t_0)/\tau] \quad (8.12)$$

where m_1 is the initial properties and m_2 is the final properties; t_0 is the initial starting time, and τ is the previously defined time constant of the denaturation process, defined as

$$\ln(\tau) = -\ln(A) + \Delta E/(RT) \quad (8.13)$$

Schwarzmaier et al.^[40] studied the changes in the optical properties of fully damaged bovine myocardium caused by laser and hot bath heating. The experimental data showed that the changes due to different heating methods were comparable and in both cases, the absorption coefficient and scattering coefficient were increased by a factor of 2 and 4, respectively, while the scattering anisotropy factor was not changed significantly.

Chin et al.^[57] experimentally measured the dynamic changes in internal light fluence during interstitial laser heating of tissue phantoms and *ex vivo* bovine liver. The results showed that, during irradiation at 810 nm, dynamic changes in optical properties result in three important trends: ① an increase in light fluence; ② a decrease in light fluence due to coagulation of tissue; ③ a sharp second drop in light fluence due to the onset of tissue charring.

Ritz et al.^[58] measured the optical properties of native and coagulated porcine liver tissue by using of a double integrating sphere system in the wavelength range of 400~2400 nm. The results showed that the optical parameters had great fluctuations in the examined wavelength range mainly due to the water and hemoglobin content in the tissue and the greatest optical penetration depth of 7.46 mm was achieved at 1070 nm. The scattering coefficient had a clear increase due to thermal coagulation, while there was only a slight decrease in absorption coefficient. Ritz et al.^[59] examined porcine liver tissue samples in a native state (35°C) and after exposure to different temperatures (45~80°C). They found that with the increase of temperature there was a decrease in the absorption coefficient and anisotropy factor and an increase in the scattering coefficient. These changes were only significant in the temperature range of 50~65°C and above 65°C, there was no significant change in the tissue optical properties.

Jun et al.^[41] measured the effect of thermal damage and biaxial loading on the optical properties of bovine epicardium. Results showed that the scattering coefficient increased with increasing mechanical load but decreased as the degree of thermal damage increased, and there was no significant

change in the absorption coefficient due to thermal damage over the ranges studied.

References

- [1] Arnoczky S P, Aksan A. Thermal modification of connective tissues: Basic science considerations and clinical implications. *Journal of the American Academy of Orthopaedic Surgeons*, 2000, 8(5): 305–313.
- [2] Wright N T, Humphrey J D. Denaturation of collagen via heating: An irreversible rate process. *Annual Review of Biomedical Engineering*, 2002, 4: 109–128.
- [3] Davidson J M, Giro M, Sutclie M, et al. Regulation of elastin synthesis//Tamburro A M, Davidson J M. *Elastin: Chemical and Biological Aspects*. Galatina: Congedo Editore, 1990.
- [4] Bunthawin S, Wanichapichart P. An RC-model for dielectrophoresis of ellipsoidal cells: A method for determination of dielectric properties. 2nd IEEE International Conference on Nano/Micro Engineered and Molecular Systems. Bangkok, 2007, 1-3: 186–191.
- [5] Miles C A, Bailey A J. Thermally labile domains in the collagen molecule. *Micron*, 2001, 32(3): 325–332.
- [6] Young G S. Thermodynamic characterization of skin, hide and similar materials composed of fibrous collagen. *Studies in Conservation*, 1998, 43(2): 65–79.
- [7] Flory P J, Garrett R R. Phase transition in collagen and gelatin systems. *Journal of the American Chemical Society*, 1958, 80(18): 4836–4845.
- [8] Allain J C, Le Lous M, Cohen-Solal L, et al. Isometric tensions developed during the hydrothermal swelling of rat skin. *Connective Tissue Research*, 1980, 7(3): 127–133.
- [9] Chvapil M, Jensovsky L. The shrinkage temperature of collagen fibres isolated from the tail tendons of rats of various ages and from different places of the same tendon. *Gerontologia*, 1963, 1: 18–29.
- [10] Chen S S, Wright N T, Humphrey J D. Heat-induced changes in the mechanics of a collagenous tissue: Isothermal, isotonic shrinkage. *Journal of Biomechanics Engineering*, 1998, 120(3): 382–388.
- [11] Antunes L, Montagne K, Weinbreck N, et al. Possible role of tissue shrinkage in high-temperature antigen retrieval. *Histopathology*, 2005, 48(4): 471–473.
- [12] Le Lous M, Cohen-Solal L, Allain J C, et al. Age related evolution of stable collagen reticulation in human skin. *Connect Tissue Research*, 1985, 13(2): 145–155.
- [13] Bhowmick S, Bischof J C. Supraphysiological thermal injury in dunning AT-1 prostate tumor cells. *Advances in Heat and Mass Transfer in Biotechnology*. 1998, 40: 77–78.
- [14] Green D M, Diller K R. Measurement of burn induced leakage of macromolecules in living tissue. *Journal of Biomechanical Engineering*, 1978, 100: 153–158.

- [15] Jacques S L. Ratio of entropy to enthalpy in thermal transitions in biological tissues. *Journal of Biomedical Optics*, 2006, 11(4): 041108.
- [16] Miles C A. Kinetics of collagen denaturation in mammalian lens capsules studied by differential scanning calorimetry. *International Journal of Biological Macromolecules*, 1993, 15(5): 265–271.
- [17] Lin S J, Lo W, Tan H Y, et al. Prediction of heat-induced collagen shrinkage by use of second harmonic generation microscopy. *Journal of Biomedical Optics*, 2006, 11(3): 34020.
- [18] Kondo E, Yasuda K, Kitamura N, et al. The effect of electrothermal shrinkage on the biomechanical properties of the anterior cruciate ligament: An experimental study. *Arthroscopy*, 2005, 21(4): 448–456.
- [19] Chen S S, Wright N T, Humphrey J D. Phenomenological evolution equations for heat-induced shrinkage of a collagenous tissue. *IEEE Transactions on Biomedical Engineering*, 1998, 45(10): 1234–1240.
- [20] Thomsen S. Pathologic analysis of photothermal and photomechanical effects of laser-tissue interactions. *Photochem Photobiol*, 1991, 53(6): 825–835.
- [21] Pearce J, Thomsen S, Vijverberg H, et al. Kinetics of birefringence changes in thermally coagulated rat skin collagen. *Lasers in Otolaryngology, Dermatology, and Tissue Welding*, 1993: 180–186.
- [22] De Boer J F, Srinivas S M, Malekafzali A, et al. Imaging thermally damaged tissue by polarization sensitive optical coherence tomography. *Optics Express*, 1998, 3(6): 212–218.
- [23] Srinivas S M, de Boer J F, Park H, et al. Determination of burn depth by polarization-sensitive optical coherence tomography. *Journal of Biomedical Optics*, 2004, 9(1): 207–212.
- [24] Fung Y C. *Biomechanics: Motion, Flow, Stress, and Growth*. New York: Springer–Verlag, 1990.
- [25] Diller K R, Pearce J A. Issues in modeling thermal alterations in tissues. *Annals New York Academy of Science*, 1999, 888: 153–164.
- [26] Wells P B, Harris J L, Humphrey J D. Altered mechanical behavior of epicardium under isothermal biaxial loading. *Journal of Biomechanical Engineering*, 2004, 126(4): 492–497.
- [27] Baek S, Wells P B, Rajagopal K R, et al. Heat-induced changes in the finite strain viscoelastic behavior of a collagenous tissue. *Journal of Biomechanical Engineering*, 2005, 127(4): 580–586.
- [28] Humphrey J D. Continuum thermomechanics and the clinical treatment of disease and injury. *Applied Mechanics Reviews*, 2003, 56(2): 231–260.
- [29] Davis E D, Doss D J, Humphrey J D, et al. Effects of heat-induced damage on the radial component of thermal diffusivity of bovine aorta. *Journal of Biomechanical Engineering*, 2000, 122(3): 283–286.
- [30] Chen S S, Humphrey J D. Heat-induced changes in the mechanics of a collagenous tissue: Pseudoelastic behavior at 37 degrees C. *Journal of Biomechanics*, 1998, 31(3): 211–216.
- [31] Chen S S, Wright N T, Humphrey J D. Heat-induced changes in the mechanics of a collagenous tissue: Isothermal free shrinkage. *Journal of Biome-*

- chanical Engineering, 1997, 119(4): 372–378.
- [32] Diaz S, Lavemia E, Wong B J F. Mechanical behavior of cartilage during laser irradiation. Society of Photo-Optical Instrumentation Engineers, 2001: 192–197.
- [33] Chao K K H, Burden M A, Wong B J F. Dynamic changes in the elastic modulus of lagomorph nasal septal cartilage during Nd : YAG ($\lambda=1.32$) laser irradiation. Society of Photo-Optical Instrumentation Engineers, 2001: 247–254.
- [34] Chae Y, Aguilar G, Lavernia E J, et al. Characterization of temperature dependent mechanical behavior of cartilage. Lasers in Surgery and Medicine, 2003, 32(4): 271–278.
- [35] Aksan A, McGrath J J. Thermomechanical analysis of soft-tissue thermotherapy. Journal of Biomechanical Engineering, 2003, 125(5):700–708.
- [36] Bosman S. Heat-induced structural alterations in myocardium in relation to changing optical properties. Applied Optics, 1993, 32(4):461–463.
- [37] Thomsen S, Vijverberg H. Changes in optical properties of rat skin during thermal coagulation. SPIE Proceedings of Laser-Tissue Interaction, 1993: 230–236.
- [38] Lin W, Motamedi M M, Welch A J. Dynamics of tissue optics during laser heating of turbid media. Applied Optics, 1996, 35(19): 3413–3420.
- [39] Agah R, Gandjbakhche A H, Motamedi M, et al. Dynamics of temperature dependent optical properties of tissue: Dependence on thermally induced alteration. IEEE Transactions on Biomedical Engineering, 1996, 43(8):839–846.
- [40] Schwarzmaier H J, Yaroslavsky A N, Terenji A, et al. Changes in the optical properties of laser-coagulated and thermally coagulated bovine myocardium. Laser-Tissue Interaction IX, 1998: 361–365.
- [41] Jun J H, Harris J L, Humphrey J D, et al. Effect of thermal damage and biaxial loading on the optical properties of a collagenous tissue. Journal of Biomechanical Engineering, 2003, 125(4): 540–548.
- [42] Lennox F G. Shrinkage of collagen. Biochimica et Biophysica Acta, 1949, 3: 170–187.
- [43] Chachra D, Gratzner P F, Pereira C A, et al. Effect of applied uniaxial stress on rate and mechanical effects of cross-linking in tissue-derived biomaterials. Biomaterials, 1996, 17(19): 1865–1875.
- [44] Harris J L, Wells P B, Humphrey J D. Altered mechanical behavior of epicardium due to isothermal heating under biaxial isotonic loads. Journal of Biomechanical Engineering, 2003, 125(3): 381–388.
- [45] Melling M, Pfeiler W, Karimian-Teherani D, et al. Differential scanning calorimetry, biochemical, and biomechanical analysis of human skin from individuals with diabetes mellitus. The Anatomical Record, 2000, 259(3): 327–333.
- [46] Reihnsner R, Melling M, Pfeiler W, et al. Alterations of biochemical and two-dimensional biomechanical properties of human skin in diabetes mellitus as compared to effects of in vitro non-enzymatic glycation. Clinical

- Biomechanics, 2000, 15(5): 379–386.
- [47] Pierce M C, Sheridan R L, Park B H, et al. Collagen denaturation can be quantified in burned human skin using polarization-sensitive optical coherence tomography. *Burns*, 2004, 30(6): 511–517.
- [48] Le Lous M, Flandin F, Herbage D, et al. Influence of collagen denaturation on the chemorheological properties of skin, assessed by differential scanning calorimetry and hydrothermal isometric tension measurement. *Biochimica et Biophysica Acta—General Subjects*, 1982, 717(2): 295–300.
- [49] McHugh A A, Fowlkes B J, Maevsky E I, et al. Biomechanical alterations in normal skin and hypertrophic scar after thermal injury. *Journal of Burn Care and Rehabilitation*, 1997, 18(2): 104–108.
- [50] Danielsen C C. Thermal stability of reconstituted collagen fibrils: Shrinkage characteristics upon in vitro maturation. *Mechanisms of Ageing and Development*, 1981, 15(3): 269–278.
- [51] Serge M, Tao W, Laurence F, et al. Laser cartilage reshaping in an in vivo rabbit model using a 1.54 μm Er : Glass laser. *Lasers in Surgery and Medicine*, 2004, 34(4): 315–322.
- [52] Dahan S, Lagarde J M, Turlier V, et al. Treatment of neck lines and forehead rhytids with a nonablative 1540-nm Er: Glass laser: A controlled clinical study combined with the measurement of the thickness and the mechanical properties of the skin. *Dermatologic Surgery*, 2004, 30(6): 872–880.
- [53] Saidi I S, Jacques S L, Tittel F K. Mie and Rayleigh modeling of visible-light scattering in neonatal skin. *Applied Optics*, 1995, 34(31): 7410–7418.
- [54] Jacques S L. Origins of tissue optical properties in the UVA visible and NIR regions. *OSA TOPS on Advances in Optical Imaging and Photon Migration*, 1996, 2: 364–369.
- [55] Thomsen S L M D, Vijverberg H, Huang R, et al. Changes in optical properties of rat skin during thermal coagulation. *Society of Photo-Optical Instrumentation Engineers*, 1993: 230–236.
- [56] Nilsson A M K, Stuesson C, Liu D L, et al. Changes in spectral shape of tissue optical properties in conjunction with laser-induced thermotherapy. *Applied Optics*, 1998, 37(7): 1256–1267.
- [57] Chin L C L, Whelan W M, Sherar M D, et al. Changes in relative light fluence measured during laser heating implications for optical monitoring and modeling of interstitial laser photocoagulation. *Physics in Medicine and Biology*, 2001, 46(9): 2407–2420.
- [58] Ritz J P, Roggan A, Germer C T, et al. Continuous changes in the optical properties of liver tissue during laser-induced interstitial thermotherapy. *Lasers in Surgery and Medicine*, 2001, 28(4): 307–312.
- [59] Ritz J P, Roggan A, Isbert C, et al. Optical properties of native and coagulated porcine liver tissue between 400 and 2400 nm. *Lasers in Surgery and Medicine*, 2001, 29(3): 205–212.

Chapter 9

Analysis of Skin Biothermomechanics

9.1 Introduction

In Part I of this book, an in-depth description of thermal behaviour of skin tissue has been presented where different heat transfer models for skin tissue have been developed based on both Fourier and non-Fourier theories. Associated issues of thermal stresses and thermal damage are addressed in this chapter. The aim is to develop a computational approach to examine the heat transfer process, thermal damage and the heat-induced mechanical response, so that the underlying mechanism of clinically applied thermal therapies can be understood and that the differences among these thermal therapies can be quantified.

Depending on how skin structure is considered, both one-layer and multi-layer models are developed in this chapter. For one-layer model, exact solutions for temperature, thermal damage and thermal stress are derived for different boundary conditions. For multi-layer models, numerical simulations using the finite element method are explored to determine the temperature, thermal damage and thermal stress distributions in the skin tissue. Based on these models, the influences of different parameters on the thermomechanical response will be discussed, and their relative contributions will be assessed.

This chapter is laid out as follows. In Section 9.2, a scheme for characterizing the skin thermomechanical behaviour is proposed, where a general closed-form solution of thermal stress for one-dimensional, multi-layer skin model is obtained. Depending on which type of model is used for deriving the temperature distributions, two types of analysis are then carried out, one with Fourier model and the other with non-Fourier model. In Section 9.3, analysis of the thermomechanical behaviour of skin tissue is performed with Fourier bioheat transfer model. Exact solutions of thermal stress are derived for one-dimensional, one-layer skin model under different boundary conditions based on the exact solutions of temperature obtained in Chapter 3, while numerical method is employed for more complicated cases, where the

skin tissue is regarded as a multi-layered material. In Section 9.4, analysis is performed with different non-Fourier heat transfer models developed in Chapter 3, including thermal wave and dual-phase-lag models, to investigate the relationship between the thermal relaxation time and the thermomechanical response of skin tissue. Finally, a summary is given in Section 9.5.

9.2 Theoretical Analysis of Thermal Stress

As previously discussed, skin tissue has a complicated multi-layer structure (see Figure 9.1).

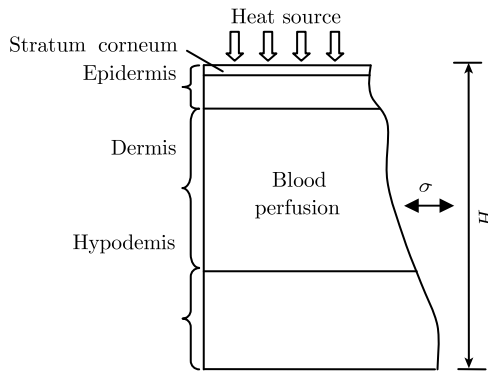


Figure 9.1 Idealized skin model (by permission of Elsevier)

The thermal properties of different layers have the same order of magnitude (see Table 9.1), but the mechanical properties vary greatly by up to three orders of magnitude from one layer to another. A one-layer continuum model for heat transfer may be assumed; while, in order to obtain the distribution of heat-induced stresses, the skin tissue must be treated as a laminated composite structure, with each layer assumed to be uniform with linear, orthotropic thermoelastic properties, as shown in Figure 9.2.

Table 9.1 Thermophysical properties of skin tissue for four-layer model

Parameters		Value	References
Thermal expansion coefficient/ $(\times 10^{-4}/\text{K})$	Stratum corneum	1	Assumption
	Epidermis	1	Assumption
	Dermis	1	Assumption
	Subcutaneous fat	1	Assumption
Poisson's ratio	Stratum corneum	0.48	[1]
	Epidermis	0.48	[1]
	Dermis	0.48	[1]
	Subcutaneous fat	0.48	[1]

continued

Parameters		Value	References
Young's modulus/MPa	Stratum corneum	1998.0	[2]
	Epidermis	102	[2]
	Dermis	10.2	[2]
	Subcutaneous fat	0.0102	[2]
Skin density/(kg/m ³)	Stratum corneum	1500.0	[3]
	Epidermis	1190.0	[3]
	Dermis	1116.0	[3]
	Subcutaneous fat	971.0	[3]
Skin thermal conductivity/[W/(m · K)]	Stratum corneum	0.235	
	Epidermis	0.235	[4]
	Dermis	0.445	[4]
	Subcutaneous fat	0.185	[5]
Skin specific heat/[J/(kg · K)]	Stratum corneum	3600.0	
	Epidermis	3600.0	[5]
	Dermis	3300.0	[5]
	Subcutaneous fat	2700.0	[5]
Metabolic heat generation/(W/m ³)	Stratum corneum	368.1	
	Epidermis	368.1	[6]
	Dermis	368.1	[6]
	Subcutaneous fat	368.3	[6]
Thickness/mm	Stratum corneum	0.02	Assumption
	Epidermis	0.08	Assumption
	Dermis	1.5	[7]
	Subcutaneous fat	4.4	Assumption

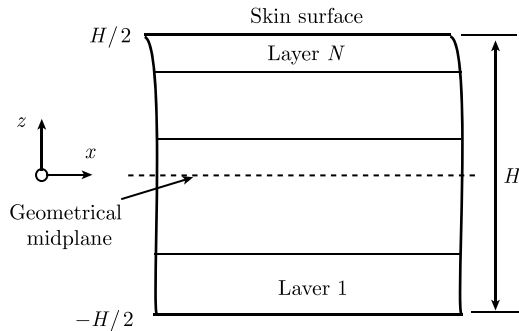


Figure 9.2 Schematic of the multi-layer skin tissue (by permission of Elsevier)

The thermomechanical behaviour of skin tissue is simplified to be a “sequentially-coupled” problem, in other words, the mechanical behaviour has no influence on thermal behaviour. The temperature field in skin tissue is first obtained from solving the governing equations of bioheat transfer, which is then used as the input of the thermomechanical model, from which the corresponding thermal stress field is obtained.

In multi-layer models, skin is regarded as a multi-layer structure, each having a thickness, t_k , and material properties of Young's modulus, E_k , and Poisson's ratio, ν_k , where $k = 1, 2, \dots, N$ with N being total number of layers, the in-plane extensional ($[A]$), bending ($[B]$) and coupling ($[D]$) stiffnesses of the overall laminate of structure are given by respectively^[8]

$$\begin{aligned} A_{ij} &= \sum_{k=1}^N (\bar{Q}_{ij})_k (z_k - z_{k-1}), & B_{ij} &= \frac{1}{2} \sum_{k=1}^N (\bar{Q}_{ij})_k (z_k^2 - z_{k-1}^2), \\ D_{ij} &= \frac{1}{3} \sum_{k=1}^N (\bar{Q}_{ij})_k (z_k^3 - z_{k-1}^3) \end{aligned} \quad (9.1)$$

where A_{ij} , B_{ij} and D_{ij} ($i, j = 1, 2, 6$) are separately assembled into the elements of 3×3 stiffness matrices $[A]$, $[B]$ and $[D]$; $[\bar{Q}]$ is the stiffness matrix of the layered skin structure, defined by

$$[\bar{Q}] = \begin{bmatrix} \bar{Q}_{11} & \bar{Q}_{12} & \bar{Q}_{16} \\ \bar{Q}_{12} & \bar{Q}_{22} & \bar{Q}_{26} \\ \bar{Q}_{16} & \bar{Q}_{26} & \bar{Q}_{66} \end{bmatrix}, \quad \begin{cases} (\bar{Q}_{11})_k = (\bar{Q}_{22})_k = \frac{E_k}{1 - \nu_k^2}, & (\bar{Q}_{16})_k = (\bar{Q}_{26})_k = 0 \\ (\bar{Q}_{12})_k = \frac{\nu_k E_k}{1 - \nu_k^2}, & (\bar{Q}_{66})_k = \frac{E_k}{2(1 + \nu_k)} \end{cases} \quad (9.2)$$

Due to the combined thermal and mechanical loading, the vector of strains, $\{\varepsilon\}_k$, at a point in each layer under plane-strain conditions are

$$\{\varepsilon\}_k = [\bar{S}]_k \{\sigma\}_k + \{\lambda\}_k \Delta T \quad (9.3)$$

where ΔT is the temperature difference at a point relative to a reference temperature; $\{\lambda\}_k$ is the vector of the thermal expansion coefficient and $[\bar{S}]_k$ is the stiffness matrix. It should be noted here that the vectors of stress, $\{\sigma\}_k$, and strain, $\{\varepsilon\}_k$, refer to in-plane strain and stress. By inverting the above equation, the vector of stresses, $\{\sigma\}_k$, can be obtained as

$$\{\sigma\}_k = [\bar{Q}]_k [\{\varepsilon\}_k - \{\lambda\}_k \Delta T] \quad (9.4)$$

In a lamina, the total strains over the whole depth generally do not vanish, but are given as

$$\{\varepsilon\}_k = \{\varepsilon^0\} + z \{\kappa\} \quad (9.5)$$

The resulting stresses are

$$\{\sigma\}_k = [\bar{Q}]_k (\{\varepsilon^0\} + z \{\kappa\} - \{\lambda\}_k \Delta T) \quad (9.6)$$

where $\{\varepsilon^0\}$ and $\{\kappa\}$ are the strain and curvature at the geometrical midplane. The resultant in-plane laminate forces per unit length, $\{N\}$, are found by

integrating through the thickness of the laminate

$$\begin{aligned} \{N\} &= \int \{\sigma\}_k dz \\ &= \int [\bar{Q}]_k (\{\varepsilon^0\} + z\{\kappa\} - \{\lambda\}_k \Delta T) dz \\ &= [A]\{\varepsilon^0\} + [B]\{\kappa\} - \{N^T\} \end{aligned} \tag{9.7}$$

where $[A] = \begin{bmatrix} A_{11} & A_{12} & A_{16} \\ A_{12} & A_{22} & A_{26} \\ A_{16} & A_{26} & A_{66} \end{bmatrix}$, $[B] = \begin{bmatrix} B_{11} & B_{12} & B_{16} \\ B_{12} & B_{22} & B_{26} \\ B_{16} & B_{26} & B_{66} \end{bmatrix}$, and

$$\{N^T\} = \int [\bar{Q}]_k \{\lambda\}_k \Delta T dz.$$

Similarly, the resultant in-plane moments per unit length are found to be

$$\begin{aligned} \{M\} &= \int \{\sigma\}_k z dz \\ &= \int [\bar{Q}]_k (\{\varepsilon^0\} + z\{\kappa\} - \{\lambda\}_k \Delta T) z dz \\ &= [B]\{\varepsilon^0\} + [D]\{\kappa\} - \{M^T\} \end{aligned} \tag{9.8}$$

where $[D] = \begin{bmatrix} D_{11} & D_{12} & D_{16} \\ D_{12} & D_{22} & D_{26} \\ D_{16} & D_{26} & D_{66} \end{bmatrix}$ and $\{M^T\} = \int [\bar{Q}]_k \{\lambda\}_k \Delta T dz$.

From Equations (9.7) and (9.8) and by defining $\begin{cases} \{N^E\} = \{N\} + \{N^T\} \\ \{M^E\} = \{M\} + \{M^T\} \end{cases}$, it is found

$$\begin{aligned} \begin{cases} \{N\} + \{N^T\} = [A]\{\varepsilon^0\} + [B]\{\kappa\} \\ \{M\} + \{M^T\} = [B]\{\varepsilon^0\} + [D]\{\kappa\} \end{cases} \\ \Rightarrow \begin{Bmatrix} \varepsilon^0 \\ \kappa \end{Bmatrix} = \begin{Bmatrix} A' & B' \\ B' & D' \end{Bmatrix} \begin{Bmatrix} N^E \\ M^E \end{Bmatrix} \Rightarrow \begin{cases} \varepsilon^0 = A'N^E + B'M^E \\ \kappa = B'N^E + D'M^E \end{cases} \end{aligned} \tag{9.9}$$

where

$$[A'] = [A^*] - [B^*][D^*]^{-1}[C^*] = \begin{bmatrix} a'_{11} & a'_{12} & 0 \\ a'_{12} & a'_{11} & 0 \\ 0 & 0 & a'_{66} \end{bmatrix}, [C'] = [B'] = \begin{bmatrix} c'_{11} & c'_{12} & 0 \\ c'_{12} & c'_{11} & 0 \\ 0 & 0 & c'_{66} \end{bmatrix},$$

$$[B'] = [B^*][D^*]^{-1} = \begin{bmatrix} b'_{11} & b'_{12} & 0 \\ b'_{12} & b'_{11} & 0 \\ 0 & 0 & b'_{66} \end{bmatrix}, [D'] = [D^*]^{-1} = \begin{bmatrix} d'_{11} & d'_{12} & 0 \\ d'_{12} & d'_{11} & 0 \\ 0 & 0 & d'_{66} \end{bmatrix},$$

$$[A^*] = [A]^{-1}, [B^*] = -[A]^{-1}[B], [C^*] = [B][A]^{-1}, [D^*] = [D] - [B][A]^{-1}[B].$$

Thus, the in-plane stresses parallel to the skin surface, σ_{xx} , in each layer (see Figure 9.2) can be obtained as

$$\{\sigma_{xx}\}_k = \bar{E}_k \left\{ \begin{array}{l} -\bar{\lambda}_k \Delta T + \left[\begin{array}{l} (a'_{11} + a'_{12})(1 + \nu_k) \sum_{i=1}^N \int_{z_{i-1}}^{z_i} \bar{E}_i \bar{\lambda}_i \Delta T dz \\ + (b'_{11} + b'_{12})(1 + \nu_k) \sum_{i=1}^N \int_{z_{i-1}}^{z_i} \bar{E}_i \bar{\lambda}_i \Delta T z dz \end{array} \right] \\ + z(1 + \nu_k) \left[\begin{array}{l} (b'_{11} + b'_{12}) \sum_{i=1}^N \int_{z_{i-1}}^{z_i} \bar{E}_i \bar{\lambda}_i \Delta T dz \\ + (d'_{11} + d'_{12})(1 + \nu_k) \sum_{i=1}^N \int_{z_{i-1}}^{z_i} \bar{E}_i \bar{\lambda}_i \Delta T z dz \end{array} \right] \end{array} \right\} \quad (9.10)$$

where $\bar{E} = E/(1 - \nu^2)$, $\bar{\lambda} = (1 + \nu)\lambda$ and N is the total number of skin layers.

Equation (9.10) has been applied to one-, two-, three-, and four-layer skin models and the detailed results are given in Section 9.6. Since the in-plane stress is the only stress studied in this chapter, σ_{xx} is reduced to σ .

9.3 Analysis with Fourier Bioheat Transfer Models

9.3.1 One-layer model

For one-layer model, using the exact solutions of temperature profile obtained in Chapter 3, the closed-form solutions of thermal stress can be obtained by substituting the temperature solutions into Equation (9.25) in Section 9.6. For illustration, the temperature distribution obtained with the one-layer model for six different kinds of boundary conditions and uniform initial temperature is used to calculate the thermal stress in the skin tissue, as given below. Please refer to Chapter 4 for the descriptions of the different boundary conditions.

1) Case 1: $T = T_\infty|_{z=-H/2}$ and $T = T_c|_{z=H/2}$

Substituting the closed-form solution of temperature, Equation (4.9), into Equation (9.25), the exact solution of thermal stress under this boundary condition can be obtained as

$$\sigma = \bar{E} \bar{\lambda} \frac{2\alpha}{H} (T_\infty - T_0) \sum_{m=1}^{\infty} \left\{ \frac{\beta_m}{\alpha\beta_m^2 + \frac{\varpi_b \rho_b c_b}{\rho c}} \left(1 - e^{-\alpha\beta_m^2 t - \frac{\varpi_b \rho_b c_b}{\rho c} t} \right) \times \right.$$

$$\left\{ \begin{array}{l} \frac{12z}{H^3} \frac{\sin(\beta_m H) - \frac{H}{2}\beta_m - \frac{H}{2}\beta_m \cos(\beta_m H)}{\beta_m^2} \\ + \frac{1 - \cos(\beta_m H)}{\beta_m H} - \sin[\beta_m(z + H/2)] \end{array} \right\} \quad (9.11)$$

where $\beta_m = m\pi/H, m = 1, 2, 3, \dots$

2) Case 2: $-k\partial T/\partial z = f_2(t)|_{z=-H/2}$ and $T = T_c|_{z=H/2}$

Substituting the closed-form solution of temperature, Equation (4.11), into Equation (9.25), the exact solution of thermal stress under this boundary condition can be obtained as

$$\sigma = \bar{E} \bar{\lambda} f_2 \frac{\alpha}{k} \frac{2}{H} \sum_{m=1}^{\infty} \left(\frac{1}{\alpha\beta_m^2 + \frac{\varpi_b \rho_b c_b}{\rho c}} \left(1 - e^{-\alpha\beta_m^2 t - \frac{\varpi_b \rho_b c_b}{\rho c} t} \right) \times \right. \\ \left. \left\{ \frac{12z}{H^3} \frac{\frac{H}{2}\beta_m \sin(\beta_m H) + \cos(\beta_m H) - 1}{\beta_m^2} + \frac{\sin(\beta_m H)}{\beta_m H} - \cos[\beta_m(z + H/2)] \right\} \right) \quad (9.12)$$

where $\beta_m = (2m - 1)\pi/(2H), m = 1, 2, 3, \dots$

3) Case 3: $-k\partial T/\partial z = h_3(f_3 - T)|_{z=-H/2}$ and $T = T_c|_{z=H/2}$

Substituting the closed-form solution of temperature, Equation (4.12), into Equation (9.25), the exact solution of thermal stress under this boundary condition can be obtained as

$$\sigma = \bar{E} \bar{\lambda} \frac{\alpha h_3 (f_3 - T_0)}{k} \sum_{m=1}^{\infty} \left(\frac{2 \left[\beta_m^2 + (h_3/k)^2 \right]}{H \left[\beta_m^2 + (h_3/k)^2 \right] + h_3/k} \sin(\beta_m H) \times \right. \\ \left. \frac{1 - e^{-\alpha\beta_m^2 t - \frac{\varpi_b \rho_b c_b}{\rho c} t}}{\alpha\beta_m^2 + \frac{\varpi_b \rho_b c_b}{\rho c}} \left\{ \frac{12z}{H^3} \frac{\frac{H}{2}\beta_m + \frac{H}{2}\beta_m \cos(\beta_m H) - \sin(\beta_m H)}{\beta_m^2} \right. \right. \\ \left. \left. + \frac{1 - \cos(\beta_m H)}{\beta_m H} - \sin[\beta_m(H/2 - z)] \right\} \right) \quad (9.13)$$

where β_m is the positive roots of $\beta_m \cot(\beta_m H) = -h_1/k, m = 1, 2, 3, \dots$

The above closed-form solutions for one-layer model [Equations (9.11)~(9.13)], although much simplified, provide an essential calibration tool for more complex numerical analysis. For more complicated cases, the complex structure of skin tissue limits the accessibility needed for a detailed experimental investigation and theoretical solution of the thermomechanical behaviour. This reason has motivated the use of numerical simulation to understand the thermomechanics of skin tissue.

9.3.2 Multi-layer model

This section describes the numerical method employed in the multi-layer models, and four case studies with multi-layer models, as shown in Figure 9.1. A commercial finite element package, ABAQUSTM, is employed since the finite element method is an approximation for continuum mechanics.

1) Numerical methods

Developing a finite element model involves first generating a mesh for the given object or domain space. The level of approximation error of the finite element method is heavily dependent on the quality of the mesh used: the more regular the mesh, the higher the quality of the simulation. For example, for an axisymmetrical case as shown in Figure 9.3, the corresponding mesh is shown in Figure 9.4. Since there is a stress concentration at the corner of contact where the compressive load is applied, for example, the mesh is refined in this region.

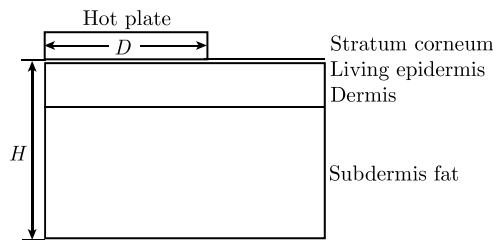


Figure 9.3 Axisymmetrical (two-dimensional) geometry of skin tissue in cylindrical coordinates (by permission of Elsevier)

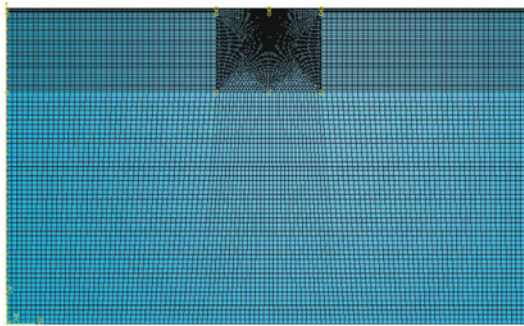


Figure 9.4 Mesh of the skin model in Figure 9.3 (by permission of Elsevier)

A sensitivity analysis is performed to assess the related numerical error¹⁾. For example, the influence of different parameters are considered: the ratio of

1) See the case study 2 for the initial and boundary conditions in Section 9.3.2.

length to thickness of the skin tissue, r/H , the length of time steps, Δt , and grid density, N , as shown in Figure 9.5(a)~(c), respectively. According to these results, in the following computation of this case, the above parameters are chosen as $r/H = 20$, $\Delta t = 0.1$, and $N = 19,420$. During the simulation, the calculation terminates when the maximum residuals¹⁾ for variables become smaller than the convergence criteria.

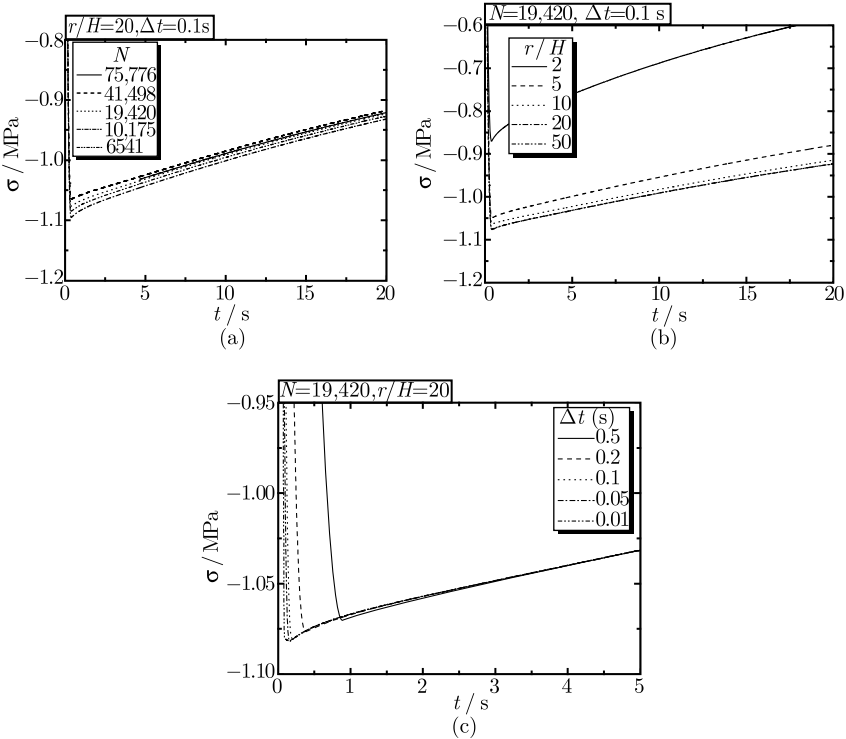


Figure 9.5 Sensitivity analysis: (a) influence of mesh size, N ; (b) influence of the ratio of skin radius, r , to skin thickness, H ; (c) influence of time step, Δt

To validate the numerical simulation, the temperature and corresponding stress fields obtained with the one-layer skin model for three different thermal boundary conditions, as given in Table 9.2, are compared with closed-form solutions obtained in Section 9.3.1, as shown Figure 9.6(a) and (b), which demonstrate excellent agreement.

Four more cases are considered below, including one-dimensional surface heating, two-dimensional surface heating, one-dimensional microwave heating, and one-dimensional laser heating, where the first two cases are problems

1) A residual is an observable estimate of the unobservable error.

often occurring in daily life, e.g. hand in contact with a hot pan during cooking, while the last two cases are used to simulate clinical thermal treatments.

Table 9.2 Boundary conditions used for model verification

Case 1:	$\begin{cases} T = T_\infty _{z=-H/2} \\ T = T_c _{z=H/2} \end{cases}$	$T_\infty = 90^\circ\text{C}, T_c = 37^\circ\text{C}$
Case 2:	$\begin{cases} -k\partial T/\partial z = f_2 _{z=-H/2} \\ T = T_c _{z=H/2} \end{cases}$	$f_2 = 2500 \text{ W/m}^2$ $T_c = 37^\circ\text{C}$
Case 3:	$\begin{cases} -k\partial T/\partial z = h_f(T_f - T) _{z=-H/2} \\ T = T_c _{z=H/2} \end{cases}$	$T_f = 90^\circ\text{C}, h_f = 2500 \text{ W}/(\text{m}^2 \cdot ^\circ\text{C})$ $T_c = 37^\circ\text{C}$

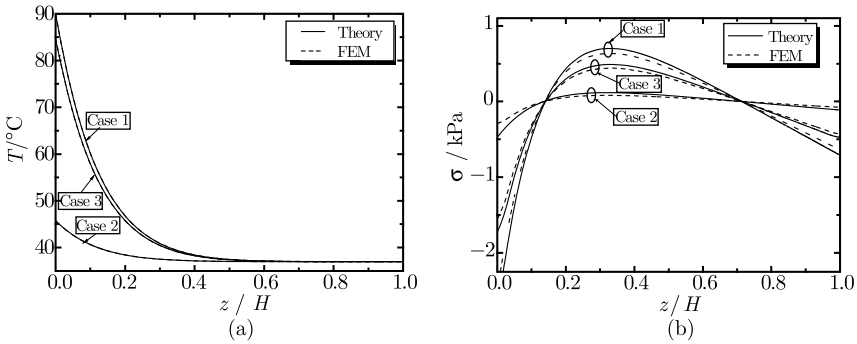


Figure 9.6 (a) Temperature and (b) stress fields obtained with analytical and numerical models of skin tissue for three different boundary conditions as given in Table 9.2. Note that $z/H = 0.0167, 0.267$ indicate epidermis-dermis (ED) and dermis-fat (DF) interfaces, respectively

2) Case study 1: one-dimensional surface heating

The skin tissue is initially at a steady state with the surface cooled by natural convection of environmental air [$T_e = 25^\circ\text{C}, h = 7 \text{ W}/(\text{m}^2 \cdot \text{K})$]. At $t = 0$, the skin surface is suddenly taken into contact with a hot source having a constant temperature 90°C ; after contacting for 15 s, the hot source is removed and the skin tissue is cooled by natural convection of environmental air for 30 s. The temperature fields are obtained by using the finite element method, and subsequently used to calculate the corresponding thermal stress field by using the exact solution [see Equation (9.10)].

A four-layer skin model is used, which is composed of stratum corneum, epidermis, dermis, and fat. Effect of blood perfusion on skin thermal response is considered only in the dermis layer while metabolic heat generation is considered in all four layers. The parameters used for both heat transfer and thermal stress analyses are summarized in Tables 9.1 and 9.3.

The skin thermal damage is calculated by Equation (3.34), with $A = 3.1 \times 10^{98}$ and $E_a/R = 75,000$. Following definition for burn degrees is now

widely accepted in medicine: $\Omega = 0.53$, first degree burn; $\Omega = 1.0$, second degree burn; $\Omega = 10^4$, third degree burn.

Table 9.3 Thermophysical properties of blood

Parameters	Value	References
Blood density/(kg/m ³)	1060.0	[3]
Blood specific heat/[J/(kg · K)]	3770.0	[9]
Arterial blood temperature/°C	37	
Core temperature/°C	37	

Influence of dermis blood perfusion

The temperature distributions in the skin tissue at the end of heating ($t = 15$ s) and cooling ($t = 45$ s) are respectively shown in Figure 9.7(a) and (b) for selected blood perfusion rates, with the skin surface heat transfer coefficient fixed at $h = 7$ W/(m² · K). Figure 9.8(a) and (b) and Figure 9.9(a) and (b) respectively plot the corresponding levels of temperature and thermal damage at the skin surface and epidermis-dermis (ED) interface as functions of time, and Figure 9.10(a) and (b) present the temporal and spatial distributions of stress respectively.

It is found that the effect of blood perfusion rate in skin tissue has a significantly larger influence on temperature distribution during cooling than that during heating. In general, the skin temperature decreases with increasing blood perfusion rate. When the thermal damage is incurred during heating, the blood perfusion rate has little effect on the thermal damage on skin surface, as shown in Figure 9.8(b), and a weak influence on that at the ED interface, as shown in Figure 9.9(b).

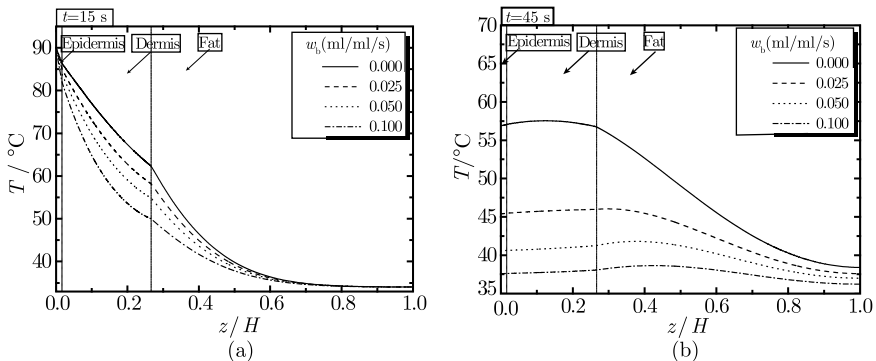


Figure 9.7 Temperature distribution in skin tissue at the end of (a) heating, $t = 15$ s, and (b) cooling, $t = 45$ s, for selected blood perfusion rates. Note that $z/H = 0.0167, 0.267$ indicate ED and DF interfaces, respectively (by permission of Elsevier)

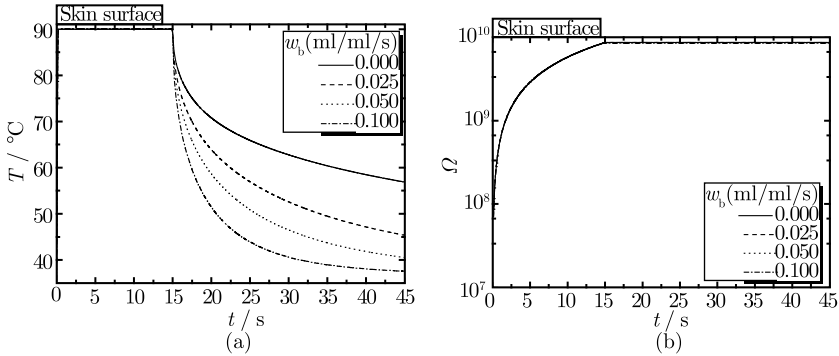


Figure 9.8 (a) Temperature and (b) thermal damage, Ω [see Equation (3.34)], at the surface of epidermis for selected blood perfusion rates (by permission of Elsevier)

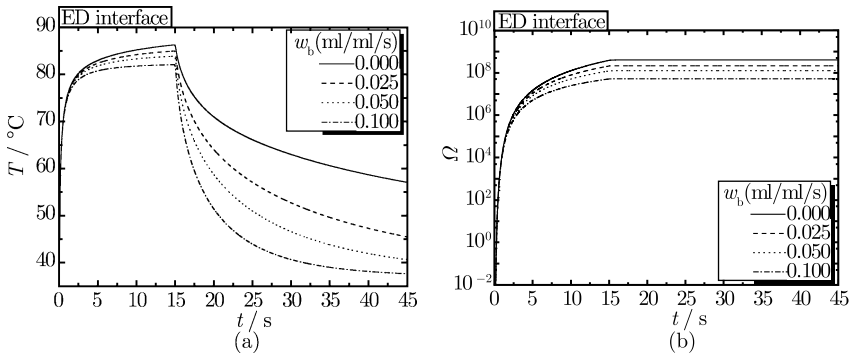


Figure 9.9 (a) Temperature and (b) thermal damage, Ω , at ED interface for selected blood perfusion rates (by permission of Elsevier)

Both the skin surface and ED interface are subjected to large tensile stresses, typically larger than 10 MPa, as shown in Figure 9.10(a) and (b), especially during heating, indicating severe thermal damage, which is consistent with the results of Figure 9.8(b) and Figure 9.9(b). The large tensile stresses at skin surface and ED interface predicted by the four-layer skin model are in sharp contrast with those obtained with the one-layer model shown in Figure 9.6(a). Overall, the skin tissue has endured severe damage, as evinced by absolute values of Ω being four orders of magnitude beyond the threshold for third degree burns ($\Omega = 10^4$). This is not unexpected given the boundary conditions.

Influence of cooling heat transfer coefficient

For selected values of surface cooling heat transfer coefficient, h , and with the blood perfusion rate in the dermis fixed at $\varpi_b = 0.025$ ml blood/ml tissue/s, Figure 9.11 plots the temperature distribution at the end of cooling ($t = 45$ s).

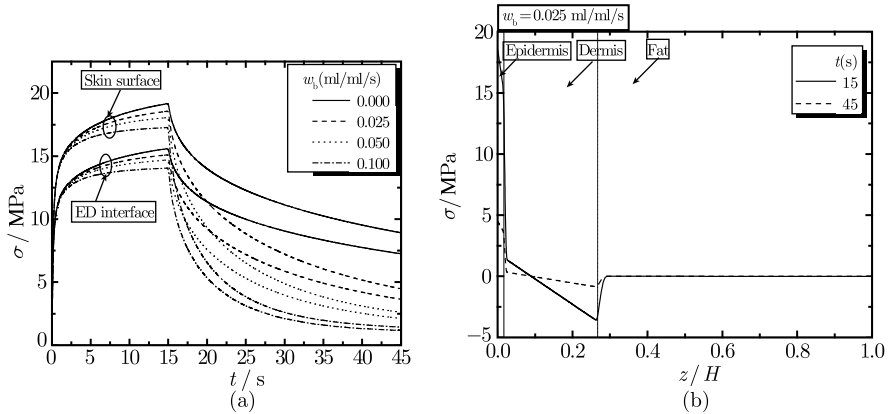


Figure 9.10 In-plane thermal stress (a) at the skin surface and ED interface for selected blood perfusion rates, and (b) distribution in skin tissue at the end of heating, $t = 15$ s, and cooling, $t = 45$ s. Note that $z/H = 0.0167, 0.267$ indicate ED and DF interfaces, respectively (by permission of Elsevier)

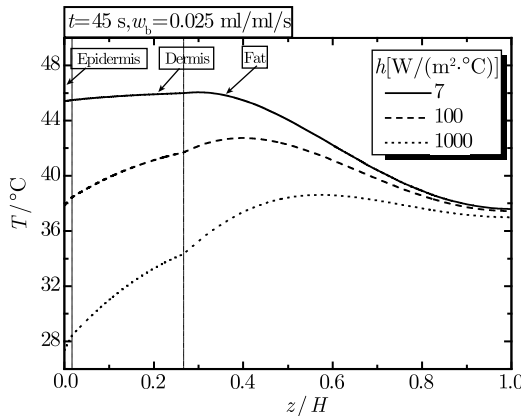


Figure 9.11 Temperature distribution in skin tissue at the end of cooling, $t = 45$ s, for selected heat transfer coefficient at the skin surface. Note that $z/H = 0.0167, 0.267$ indicate ED and DF interfaces, respectively (by permission of Elsevier)

Note that, the results of Figure 9.11 are similar to those shown in Figure 9.7(b), suggesting that increasing the surface heat transfer coefficient, h , with blood perfusion rate, ϖ_b , being fixed, has a similar effect as increasing ϖ_b with h being fixed. Correspondingly, the variations of temperature and damage integration with the time at the ED interface have similar trends as those exhibited in Figure 9.9(a) and (b) and hence are omitted from display here.

3) Case study 2: two-dimensional surface heating

In some cases, the lateral heat transfer¹⁾ in the skin tissue cannot be neglected and needs to be considered. For this purpose, an axisymmetrical (two-dimensional) physical model, shown in Figure 9.3, which is similar to those used by Diller & Hayes^[10] and Ng & Chua^[11], is employed in this case study. Initially, the skin tissue of thickness H and radius R_0 is at a steady state with the surface cooled by natural convection of environmental air. At time $t = 0$, the skin surface is suddenly in contact with a hot plate (90°C) of radius D (assumed $D = H$) while the bottom of the skin tissue is kept at constant temperature. The boundary at $r = R_0$ is set isothermally as normal skin temperature. Effect of blood perfusion is considered only in the dermis layer while metabolic heat generation is considered in all four layers, as before. The skin tissue is free to expand except at the bottom where it is fixed due to connection with the body core.

So far, there is no experimental data or closed-form solution for stresses available to make a comparison, and hence only the temperature field is verified here. The calculated temperature distribution accounting for the influence of blood perfusion is compared with that obtained by Ng & Chua^[11] in Figure 9.12.

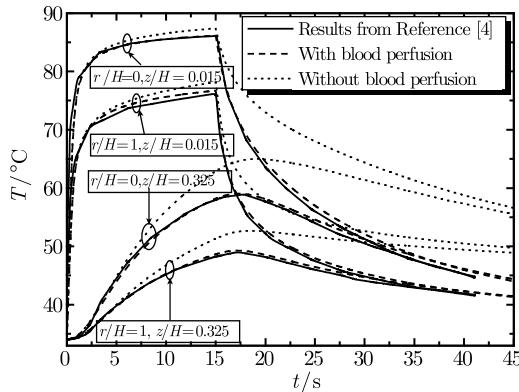


Figure 9.12 Verification of the two-dimensional skin model (by permission of Elsevier)

Good agreement is observed, demonstrating the feasibility of the present approach. Also plotted is the temperature obtained without considering the effect of blood perfusion, which is significantly higher than that with this effect considered.

Influence of the number of layers in skin model

1) Heat transfer in the direction parallel to the skin surface.

The stratum corneum layer has been shown to play an important role in the thermal and mechanical behaviours of skin tissue^[12,13], however, its effect is often neglected in most studies due to its small thickness (about 0.02 mm in thickness, see Table 9.1). Here, in order to study its effect, results predicted from three different axisymmetrical skin models are compared: ① a one-layer model, where the skin tissue is treated as a homogeneous medium with constant properties; ② a three-layer model, where the skin tissue is consisted of epidermis, dermis and subcutaneous fat layers; ③ a four-layer model, where the skin tissue is composed of stratum corneum, epidermis, dermis and subcutaneous fat layers. The Young's modulus varies by approximately an order of magnitude as each layer is crossed, being 2 GPa for the stratum corneum and 0.01 MPa for the subcutaneous fat layer. It is remarkable that this dramatic change in elastic modulus occurs over a distance less than 2 mm, see Table 9.1.

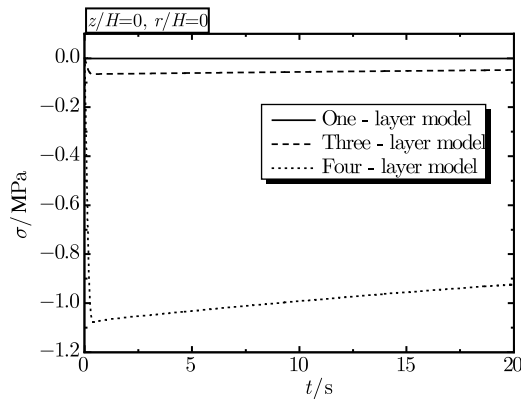


Figure 9.13 Thermal stress at the center of skin surface ($r/H = 0$, $z/H = 0$) plotted as a function of time for one-, three- and four-layer skin models (by permission of Elsevier)

Figure 9.13 plots the radial stress at the center of skin surface ($r/H = 0$, $z/H = 0$) as a function of time predicted respectively from the one-, three- and four-layer skin models. It is shown that there exist very large discrepancies between the different models, highlighting the important role of stratum corneum layer in thermomechanical modelling of skin tissue. In particular, with the stratum corneum layer considered, a large compressive stress is developed on the skin surface as a result of sudden heating (see Figure 9.13): this feature is not captured by the one- or three-layer skin model. The mean mechanical threshold of nociceptors in the skin tissue lies in the range of about $0 \sim 0.6$ MPa and mainly between $0.1 \sim 0.2$ MPa^[14], which suggests

that, in addition to heating, thermal stress may also contribute to thermal pain. Other supporting evidence shows that, for the same level of nociceptor activity, a heat stimulus evokes more pain than a mechanical stimulus and that tissue deformation due to heating and cooling may explain the origins of pain^[15,16].

Spatial and temporal distributions of temperatur and stress

Figure 9.14(a) and (b) show the temperature and stress distributions at different skin depths at $t = 20$ s, and Figure 9.15(a) and (b) show the variations of temperature and stress distributions with time at different skin locations. It is found that, although the heat penetrates deep into the skin tissue, the results of Figure 9.14 and Figure 9.15 show that the thermal stress is only limited to the top layers of the skin tissue, specifically, in the stratum corneum and the epidermis.

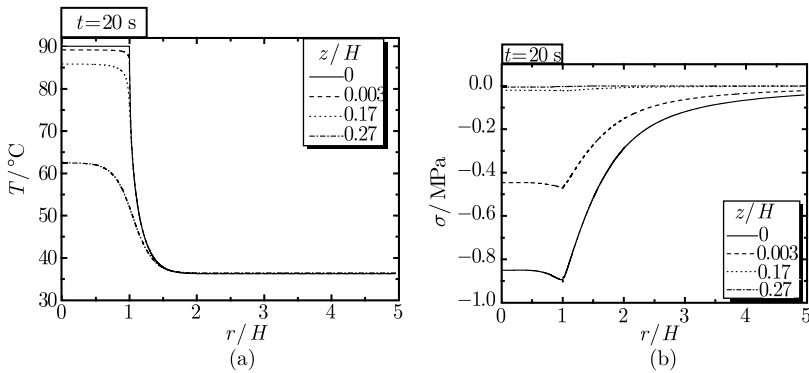


Figure 9.14 (a) Temperature and (b) stress distributions at time $t = 20$ s (by permission of Elsevier)

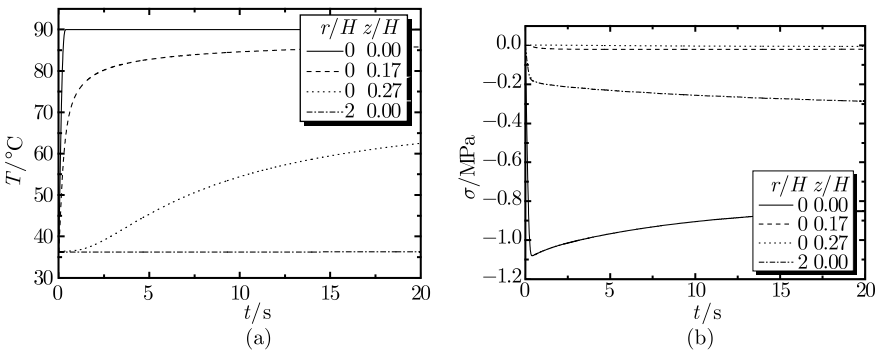


Figure 9.15 Variations of (a) temperature and (b) stress with time (by permission of Elsevier)

In the previous two case studies, the thermomechanical behaviour of skin

tissue is obtained for surface heating, from which some important results are obtained. However, surface heating cases are very different from the currently-used medical heating methods, which are the emphasis of the next two case studies.

4) Case study 3: microwave heating

The skin tissue-microwave interactions are governed by the well-known Maxwell relations, which enable the heat flux to be calculated. For the microwave heating of dielectric materials, the governing equations can be written in terms of the electric and magnetic field intensities

$$\nabla H + c_\epsilon \frac{\partial E}{\partial t} + c_\sigma E = 0 \tag{9.14}$$

$$\nabla E + c_\mu \frac{\partial H}{\partial t} = 0 \tag{9.15}$$

where E and H are the electrical and magnetic fields, respectively; c_ϵ , c_σ and c_μ are the electric permittivity, electrical conductivity and magnetic permeability of skin tissue, respectively.

The heat generation in skin tissue due to microwave heating ($q_{\text{ext_MW}}$) can then be calculated as^[17]

$$q_{\text{ext_MW}} = \frac{r}{2} \left(|E_r|^2 + |E_z|^2 \right) \tag{9.16}$$

where E_r and E_z are the electric fields in the along the skin depth and normal to the skin depth directions, respectively. In particular, for a one-dimensional skin model, the analytical solutions for calculating the $q_{\text{ext_MW}}$ in different skin layers have can be obtained by Gowrishankar et al.^[18], as presented in Table 9.4 and are used here. The dielectric properties of each layer are listed in Table 9.5.

Table 9.4 Calculation of heat generations due to microwave heating in different layers of one-dimensional skin model^[18,19]

Epidermis	
$q_{\text{ext_MW}} = P = \frac{1}{2} c_{\sigma-e} E_z ^2$	
$E_z(z, t) = \hat{x} E(0, t) T_{\text{sa}} \sum_{n=0}^{\infty} \left\{ \begin{array}{l} (\Gamma_{\text{sa}} \Gamma_{\text{df}})^n \exp \left[- \left(\frac{1}{c_{\eta-e}} + \frac{i2\pi}{c_{\lambda-e}} \right) (2nz_e + z) \right] + \\ (\Gamma_{\text{sa}} \Gamma_{\text{df}})^n \Gamma_{\text{df}} \exp \left[- \left(\frac{1}{c_{\eta-e}} + \frac{i2\pi}{c_{\lambda-e}} \right) (2nz_e - z) \right] \end{array} \right\}$	
$E(0, t) = \sqrt{2P(0, t) Z_a}$	

continued

Dermis		
$q_{\text{ext-MW}} = P = \frac{1}{2} c_{\sigma-d} E_z ^2$		
$E_z(z, t) = \hat{x} E(0, t) T_{\text{sa}} \sum_{n=0}^{\infty} \left\{ \begin{array}{l} (\Gamma_{\text{sa}} \Gamma_{\text{df}})^n \exp \left[- \left(\frac{1}{c_{\eta-d}} + \frac{i2\pi}{c_{\lambda-d}} \right) (2nz_d + z) \right] + \\ (\Gamma_{\text{sa}} \Gamma_{\text{df}})^n \Gamma_{\text{df}} \exp \left[- \left(\frac{1}{c_{\eta-d}} + \frac{i2\pi}{c_{\lambda-d}} \right) (2nz_d - z) \right] \end{array} \right\}$		
$E(0, t) = \sqrt{2P(0, t) Z_a}$		
Fat layer		
$E(z, t) = \hat{x} E(z_d, t) T_{\text{df}} \exp \left[- \left(\frac{1}{c_{\eta-f}} + \frac{i2\pi}{c_{\lambda-f}} \right) (z - z_d) \right]$		
$P = \frac{1}{2} c_{\sigma-f} E_z ^2$		
where		
$\Gamma_{\text{sa}} = \frac{Z_a - Z_d}{Z_a + Z_d}, \quad \Gamma_{\text{df}} = \frac{Z_d - Z_f}{Z_d + Z_f}, \quad T_{\text{sa}} = \frac{2Z_d}{Z_a + Z_d}, \quad T_{\text{df}} = \frac{2Z_f}{Z_f + Z_d},$		
$Z_a = \sqrt{c_{\mu_0}/c_{\epsilon_0}} = 377\Omega, \quad Z_d = \sqrt{i2\pi f c_{\mu_0} / (c_{\sigma-d} + i2\pi f c_{\epsilon_0} c_{\epsilon-d})},$		
$Z_f = \sqrt{i2\pi f c_{\mu_0} / (\sigma_f + i2\pi f c_{\epsilon_0} c_{\epsilon-f})}$		
E_z	Electric field	$c_{\eta-e}$ Penetration depth for epidermis
$E(0, t)$	Electric field amplitude on the skin surface at time t	$c_{\eta-d}$ Penetration depth for dermis
$\bar{E}(z, t)$	Electric field in the epidermis and dermis	$c_{\eta-f}$ Penetration depth for fat
$\bar{E}(z_d, t)$	Electric field at the dermis-fat (DF) interface	$c_{\lambda-e}$ Wavelength in dermis
Z_a	Intrinsic impedances of air	$c_{\lambda-d}$ Wavelength in dermis
Z_d	Intrinsic impedances of dermis	$c_{\lambda-f}$ Wavelength in dermis fat
Z_f	Intrinsic impedances of fat	$c_{\sigma-e}$ Conductivity of epidermis
$P(0, t)$	Power density incident on the skin surface at time t	$c_{\sigma-d}$ Conductivity of dermis
$P(0, t)$	Incident power, expressed as an area density	$c_{\sigma-f}$ Conductivity of fat
$P(z, t)$	Incident power, expressed as a volume density	c_{μ_0} Permeability of free space, $1.26 \times 10^{-6} \text{Wb}/(\text{A} \cdot \text{m})$
Γ	Reflection coefficient	c_{ϵ_0} Permittivity of free space, $8.85 \times 10^{-12} \text{C}^2/(\text{N} \cdot \text{m}^2)$
T	Transmission coefficient	$c_{\epsilon-d}$ Permittivity of dermis
sa	Skin/air interface	$c_{\epsilon-f}$ Permittivity of fat
df	Dermis/fat interface	$i \quad \sqrt{-1}$

The problem is described as follows. The skin tissue is initially cooled by natural convection of environment air. At $t = 0$, a microwave radiation with frequency $f = 10^{10}$ Hz is applied to skin surface for a duration of 3 s; at the same time, the skin surface is continually cooled by natural convection. These parameters are chosen in accordance with those used in clinical treatments^[20,21].

Table 9.5 Dielectrical properties of skin tissue^[18]

Skin layer	Electrical conductivity c_{σ} /(S/m)	Relative permittivity c_{ϵ}	Penetration length c_{η} /mm	Wavelength c_{λ} /mm
Epidermis	8.01	31.3	3.8	5.2
Dermis	8.01	31.3	3.8	5.2
Subcutaneous	0.585	4.60	19.6	13.9

The Maxwell equations are first used to obtain the heat generation in skin tissue due to microwave heating, then the temperature, thermal damage and thermal stress are calculated using the thermomechanical model. The calculated heat generation distribution in skin tissue is plotted in Figure 9.16, which shows that the heat generation decreases along skin depth, with a sudden decrease at the DF interface due to the large difference between the absorption coefficients of dermis and fat.

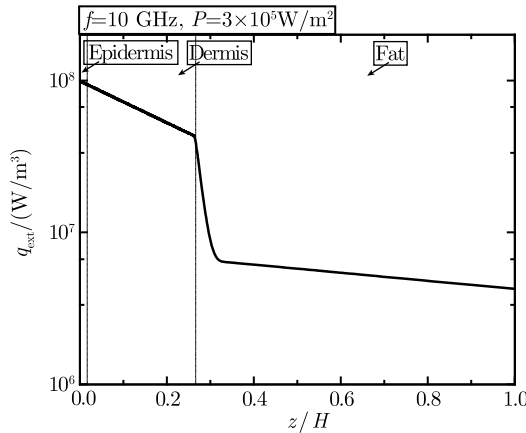


Figure 9.16 Heat generation, $q_{\text{ext_MW}}$, in skin tissue due to microwave heating. Note that $z/H = 0.0167, 0.267$ indicate ED and DF interfaces, respectively (by permission of Elsevier)

The temperature histories at the ED interface and DF interface are shown in Figure 9.17(a), whilst Figure 9.17(b) presents the temperature distributions along skin depth. The temperatures, T_{ED} , at the ED interface and, T_{DF} , at DF interface increase quickly after the application of microwave radiation. Upon end of the heating, T_{ED} begins to decrease immediately whereas T_{DF} rises further for about 5 s before decreasing.

The thermal damage at both ED and DF interfaces increases during heating, but the rate is higher for the ED interface, as shown in Figure 9.18(a). Once the microwave heating is stopped, the thermal damage changes little, for thermal damage is a process of accumulation. The thermal damage distribution across the skin depth is similar to that of temperature, as shown in

Figure 9.18(b).

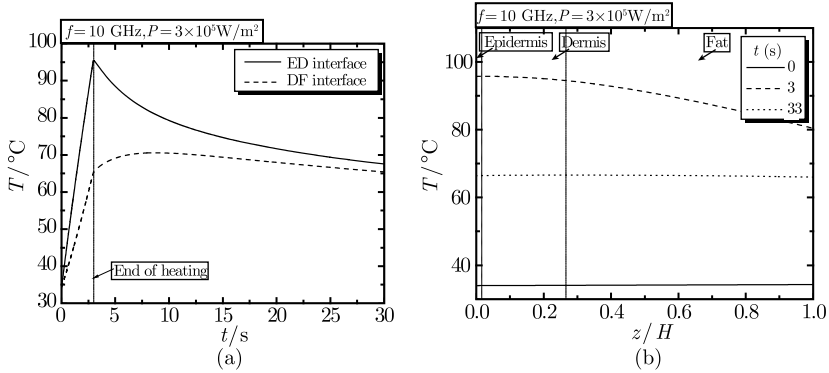


Figure 9.17 (a) Temperature history at ED interface and DF interface, and (b) temperature distribution in skin tissue at the end of heating, $t = 3$ s, and cooling, $t = 33$ s. Note that $z/H = 0.0167, 0.267$ indicate ED and DF interfaces, respectively (by permission of Elsevier)

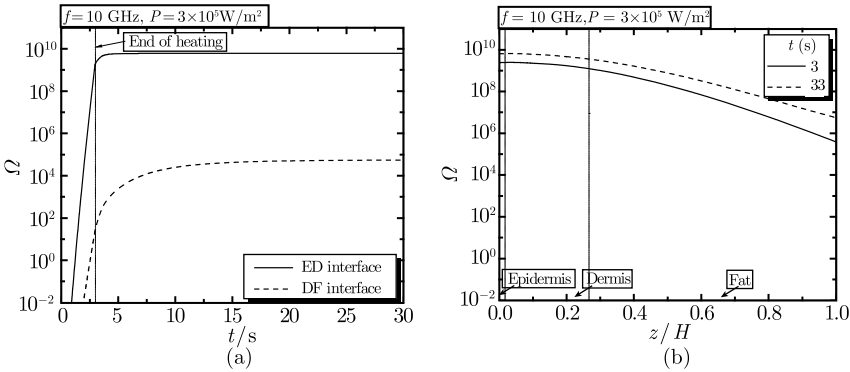


Figure 9.18 (a) Thermal damage history at ED interface and DF interface, and (b) thermal damage distribution in skin tissue at the end of heating, $t = 3$ s and cooling, $t = 33$ s. Note that $z/H = 0.0167, 0.267$ indicate ED and DF interfaces, respectively (by permission of Elsevier)

5) Case study 4: laser heating

Lasers have been widely used for medical applications mainly due to its control in delivering a precise form of heating. The absorption of laser light in the tissue has been modelled using the Monte Carlo method^[22], which traces a large number of single photons and thus predicts the distribution of absorbed photons in the tissue. The light absorption in tissues with a layered structure, each layer with different optical properties, can be modelled straightforwardly. For the present case, the computer code developed by Wang & Jacques^[23] is used for simulating the absorption of laser light in the

skin tissue.

A one-dimensional, four-layer skin model is used here. In order to capture the very different optical properties of blood compared to the surrounding tissue, additional blood layer inside the dermis is added to the four-layer skin model. With the assumption of a Henyey-Greenstein scattering phase function, the input parameters for the Monte Carlo simulations are the absorption coefficient μ_a , the scattering coefficient μ_s , the anisotropy factor g (dimensionless), and the refractive index of tissue n (dimensionless) that is equal to 1.38^[24]. The optical properties of each skin layer used in this case study are given in Figure 9.19, where the stratum corneum is assumed to have the same properties as epidermis.

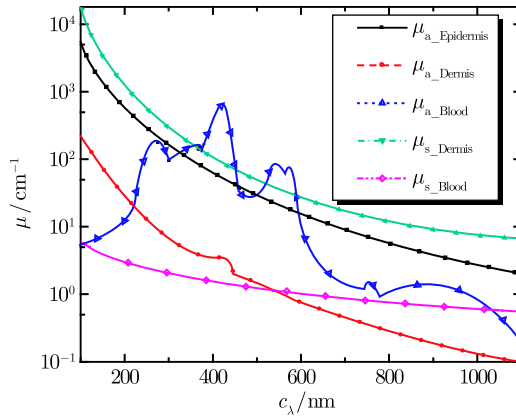


Figure 9.19 Optical properties of different skin layers (by permission of Elsevier)

The problem for this case study is described as follows. The skin tissue is initially cooled by natural convection of environment air. At $t = 0$, a laser pulse with power of $P = 150\text{W}/\text{cm}^2$ and is applied to its surface for a duration of 0.1 s; at the same time, the skin surface is cooled by ice-water mixture at 0°C . These parameters are chosen in accordance with those adopted in clinical treatments, specifically, lasers of two different wavelength ($c_\lambda = 532\text{ nm}, 1064\text{ nm}$) are used, which are wavelengths of Q-switched Nd:YAG laser widely used in laser-skin treatments in medicine^[25~28].

By irradiating the skin surface at normal incidence, the distribution of absorbed photons is obtained from the Monte Carlo simulations. From this distribution, the heat generation in skin tissue due to laser heating is derived, as shown in Figure 9.20. With the same power density, the amount of heat generated is higher for smaller wavelength, but more limited to a region near

the skin surface. Heat generation, $q_{ext,laser}$, in skin tissue is slightly higher than that in the surrounding tissue due to its higher absorption coefficient.

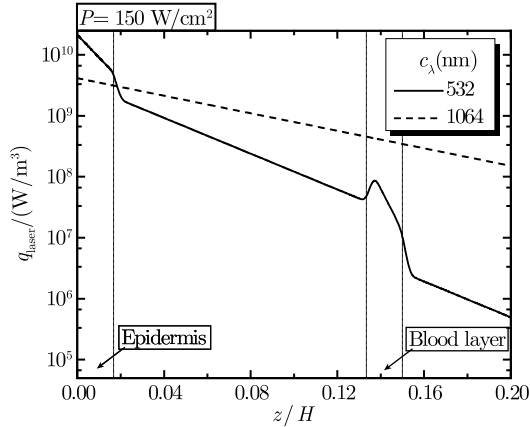


Figure 9.20 Heat generation, $q_{ext,laser}$, in skin tissue due to laser heating. Note that $z/H = 0.0167, 0.267$ indicate ED and DF interfaces, respectively (by permission of Elsevier)

The temperature history at the ED interface is presented in Figure 9.21(a), while Figure 9.21(b) gives the temperature distribution across the skin depth at the end of the laser pulse. The temperature rises abruptly after the application of laser, where the peak value is higher for laser heating with the shorter wavelength, and located closer to the skin surface. After laser heating is stopped, the temperature decreases continually due to the cooling at the skin surface.

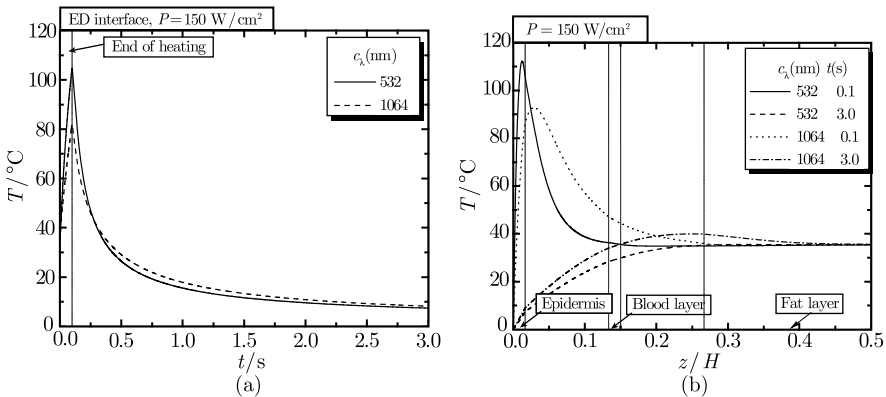


Figure 9.21 (a) Temperature history at ED interface, and (b) temperature distribution in skin tissue at the end of heating, $t = 0.1$ s, and cooling, $t = 3$ s. Note that $z/H = 0.0167, 0.267$ indicate ED and DF interfaces, respectively (by permission of Elsevier)

Thermal damage at the ED interface increases almost linearly during the laser pulse, but the rate is higher for the shorter wavelength laser, as shown in Figure 9.22(a). The thermal damage changes very little after heating is stopped. The distribution of thermal damage along skin depth is similar to that of the temperature profile, as shown in Figure 9.22(b). This again suggests that, in skin thermotherapy, laser with different wavelengths can be selected according to the depth of target tissue.

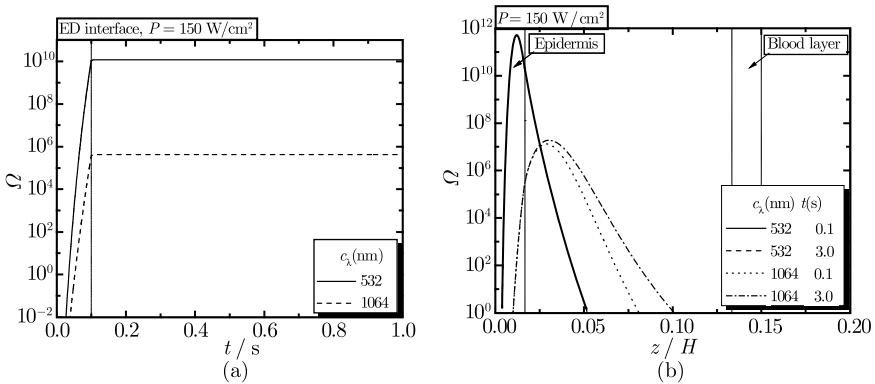


Figure 9.22 (a) Thermal damage history at ED interface, and (b) thermal damage distribution in skin tissue at the end of heating, $t = 0.1 \text{ s}$, and cooling, $t = 3 \text{ s}$. Note that $z/H = 0.0167, 0.267$ indicate ED and DF interfaces, respectively (by permission of Elsevier)

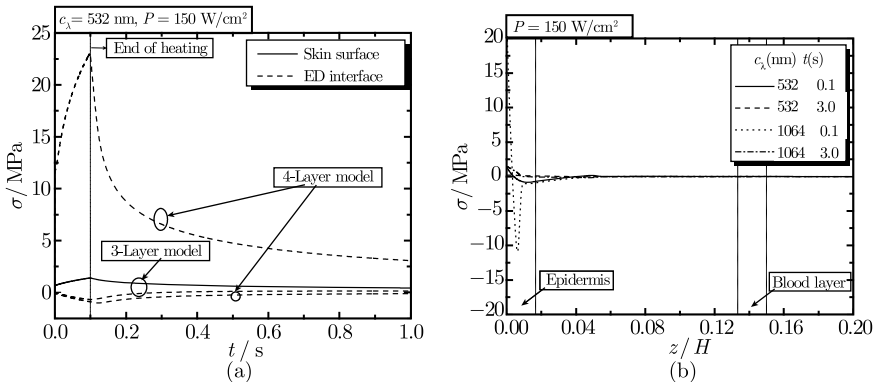


Figure 9.23 (a) Thermal stress history at the skin surface and ED interface, and (b) thermal stress distribution in skin tissue at the end of heating, $t = 0.1 \text{ s}$, and cooling, $t = 3 \text{ s}$. Note that $z/H = 0.0167, 0.267$ indicate ED and DF interfaces, respectively (by permission of Elsevier)

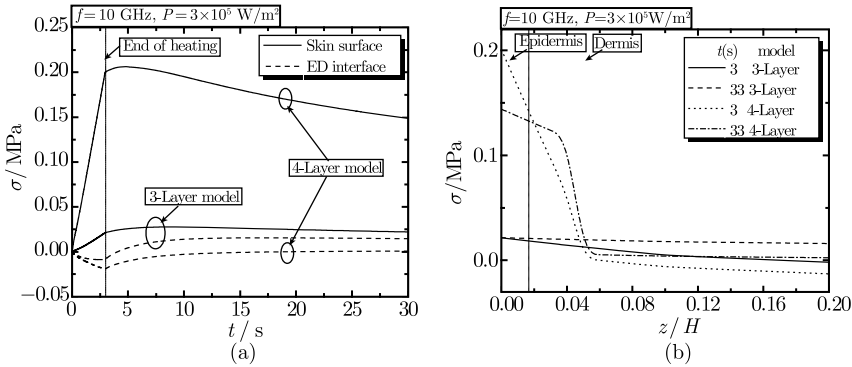


Figure 9.24 (a) Thermal stress history at the skin surface and ED interface, and (b) thermal stress distribution in skin tissue at the end of heating, $t = 3$ s, and cooling, $t = 33$ s. Note that $z/H = 0.0167$, 0.267 indicate ED and DF interfaces, respectively (by permission of Elsevier)

In order to study the effect of stratum corneum during microwave and laser heating, the results from the three- and four-layer models are compared. The stress fields are shown in Figure 9.24 for microwave heating and in Figure 9.23 for laser heating. For both heating methods, substantial discrepancies exist, suggesting that the contribution of stratum corneum layer is important and must be considered in these heating methods. By comparing Figure 9.24(a) and Figure 9.23(a), it can be seen that thermal stress due to laser heating is about 100 times larger than that due to microwave heating, which is mainly due to the different heat generation as shown in Figure 9.17 and Figure 9.21. Also, during cooling, the thermal stress decreases much quicker for laser heating, which is attributed to the different cooling methods used in medical treatments, where active cooling is often applied in laser heating^[29].

9.4 Analysis with Non-Fourier Bioheat Transfer Models

In this section, different non-Fourier heat transfer models are employed in both one-layer and multi-layer models to investigate the relationship between thermal relaxation times and the thermomechanical response in skin tissue. The work in this section does not seek to prove that onemodel is better (or not) than another; rather, it attempts to address whether non-Fourier models merit additional study.

9.4.1 One-layer model

For one-layer skin model, the closed-form solution of temperature for the thermal wave model has been obtained by Liu et al.^[30] under the follow-

ing conditions: $T = T_\infty|_{z=0}$, $\partial T/\partial z = 0|_{z=H}$ (boundary conditions); and $T = T_i|_{t=0}$, $\partial T/\partial t = 0|_{t=0}$ (initial condition). Submitting the temperature solution into Equation (9.25) in Section 9.6, the closed-form solution of thermal stress can be obtained as follows.

$$\sigma_{xx}(z, t) = \text{term1} \times \text{term2} + \text{term3} \tag{9.17}$$

where

$$\text{term1} = \overline{E\lambda} \left(T_\infty - T_i - \frac{Q_r}{\rho_b \omega_b c_b} \right) / \cosh \left(\sqrt{\frac{\rho_b \omega_b c_b}{k}} H \right) \tag{9.18}$$

$$\begin{aligned} \text{term2} = & -\cosh \left[\sqrt{\frac{\rho_b \omega_b c_b}{k}} (z - H) \right] + \left(\frac{\sqrt{\frac{k}{\rho_b \omega_b c_b}} \sinh \left(\sqrt{\frac{\rho_b \omega_b c_b}{k}} H \right)}{H} \right) \\ & \times \frac{12(H/2-z)}{H} \left\{ \begin{aligned} & \sqrt{\frac{k}{\rho_b \omega_b c_b}} \frac{H}{2} \sinh \left(\sqrt{\frac{\rho_b \omega_b c_b}{k}} H \right) + \\ & \frac{k}{\rho_b \omega_b c_b} \left[1 - \cosh \left(\sqrt{\frac{\rho_b \omega_b c_b}{k}} H \right) \right] \end{aligned} \right\} \end{aligned} \tag{9.19}$$

$$\text{term3} = \overline{E} \bar{\lambda} e^{-(\alpha'/2)t} \sum_{n=1}^{\infty} \left[\begin{aligned} & \left(-\sin \left[\frac{\left(n - \frac{1}{2} \right) \pi}{H} z \right] + \frac{1}{(n - 0.5) \pi} \right) \\ & + \frac{12(H/2-z)}{H} \left\{ \frac{H^2}{\left[\frac{(2n-1)\pi}{(n-0.5)\pi} \right]^2} \sin(n\pi - 0.5\pi) \right\} \end{aligned} \right] \tag{9.20}$$

The term4 in Equation (9.20) is calculated as

$$\text{term4} = \begin{cases} A_n \cos \varpi_n t + B_n \sin \varpi_n t & \text{when } \left| 1 - \frac{\tau_q \rho_b \omega_b c_b}{\rho c} \right| < \frac{(2n-1)\pi \sqrt{\alpha \tau_q}}{H} \\ C_n \exp(\gamma_n t) + D_n \exp(-\gamma_n t) & \text{when } \left| 1 - \frac{\tau_q \rho_b \omega_b c_b}{\rho c} \right| > \frac{(2n-1)\pi \sqrt{\alpha \tau_q}}{H} \end{cases} \tag{9.21}$$

The skin surface, in this case, is defined to be at $z = 0$.

These closed-form solutions of temperature and thermal stress can be used to check the accuracy of numerical modelling using finite element method for multi-layer skin model in the next section.

9.4.2 Multi-layer model

In this section, case studies are conducted on thermomechanical analysis of skin tissue by use of a multi-layer model with different non-Fourier bio-heat transfer models including the thermal wave model and three types of dual-phase-lag models (DPL1MBT, DPL2MBT and DPL3MBT). A similar problem as proposed in case study 1 in Section 9.3.2 is revisited here, except that the temperature of the hot source in this case is 100°C, the heating is lasted for 15 s, and the skin tissue is cooled by water-ice mixture of 0°C afterwards. A four-layer skin model is used and the skin properties used are given in Tables 9.1 and 9.3. Once again, the problem is solved numerically by using finite element method.

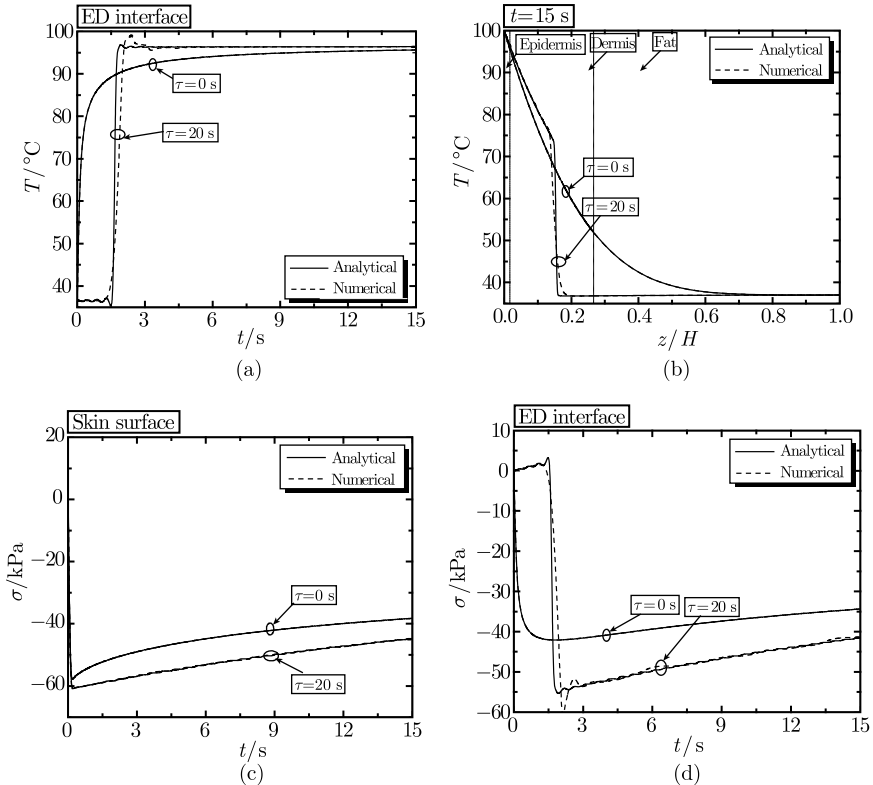


Figure 9.25 Verification of numerical method (finite element method) used for multi-layer skin model in non-Fourier analysis: (a) variation of temperature with time at ED interface, (b) distribution of temperature along skin depth at $t = 15\text{ s}$, (c) variation of stress with time at skin surface, and (d) variation of stress with time at ED interface. Note that $z/H = 0.0167, 0.267$ indicate ED and DF interfaces, respectively (by permission of Elsevier)

A quick check of the feasibility of numerical models is firstly conducted by assuming the same properties for each layer in the four-layer model (in this way, the four-layer model is simplified to the one-layer model) and by comparing the predictions with those obtained from closed-form solutions obtained in Section 9.4.1, as shown in Figure 9.25(a)~(d). Excellent agreement for both temperature and stress fields has been achieved.

1) Comparison of different models

Predictions from different bioheat transfer models, both Fourier (which is the Pennes model) and non-Fourier, are shown in Figure 9.26 for temperature, in Figure 9.27 for thermal damage, and in Figure 9.28 for thermal stress. The temperature, thermal damage and thermal stress distributions in the skin tissue at the end of heating ($t = 15$ s) and cooling ($t = 45$ s) are shown separately in Figure 9.26(c) and (d), Figure 9.27(c) and (d) and Figure 9.28(c) and (d), whilst Figure 9.26(a) and (b) and Figure 9.27(a) and (b) plot the corresponding temperature and burn damage at the ED interface and DF interface as functions of time, respectively. Since the nociceptors emerge from superficial dermis running into epidermis^[31] as low as $50 \mu\text{m}$ from the skin surface^[32], attention is focused on thermal stress at the skin surface and ED interface, as shown in Figure 9.28(a) and (b).

Figure 9.26(a)~(d) demonstrate that the tissue temperature calculated from different models deviate substantially under constant surface temperature heating. With the thermal wave model, the tissue temperature inside the body is undisturbed during the initial stage of heating, which is attributed to the nonthermally consumption related biological activities¹⁾^[30]; followed by a instantaneous jump, which may be viewed as the wave-front emerging from the finite propagation of the thermal wave or the existence of the relaxation time τ_q . The results from three DPL models exhibit similar behaviours, but differ from the results of both the Pennes model and the thermal wave model. Unlike the thermal wave model, no wave behaviour is observed in the DPL models as expected, but a non-Fourier diffusion-like behaviour exists due to the second thermal relaxation time, τ_T , whose effect is to weaken the thermal wave effect, thereby to destroy the sharp wave-front. Additionally, a sudden temperature drop for heating or a step for cooling at the skin surface is associated with the DPL models, as shown in Figure 9.26(c) and (d).

In DPL models, various orders of τ_T and τ_q may yield close results. The underlying mathematical reason can be explained as follows:

1) Activities like driving a water particle or an ion, changing electrical potentials of cell membranes, or triggering a biochemical process.

$$\sum_{n=0}^{\infty} \frac{\tau_q^n}{n!} \frac{\partial q^n(\mathbf{r}, t)}{\partial t^n} = -k \sum_{m=0}^{\infty} \frac{\tau_T^m}{m!} \frac{\partial \nabla T^m(\mathbf{r}, t)}{\partial t^m} \tag{9.22}$$

$$\Rightarrow \sum_{n=0}^{\infty} \frac{\partial q^n(\mathbf{r}, t)}{\partial [(n!)^{1/n} t / \tau_q]^n} = -k \frac{\partial q^m(\mathbf{r}, t)}{\partial [(m!)^{1/m} t / \tau_T]^m}$$

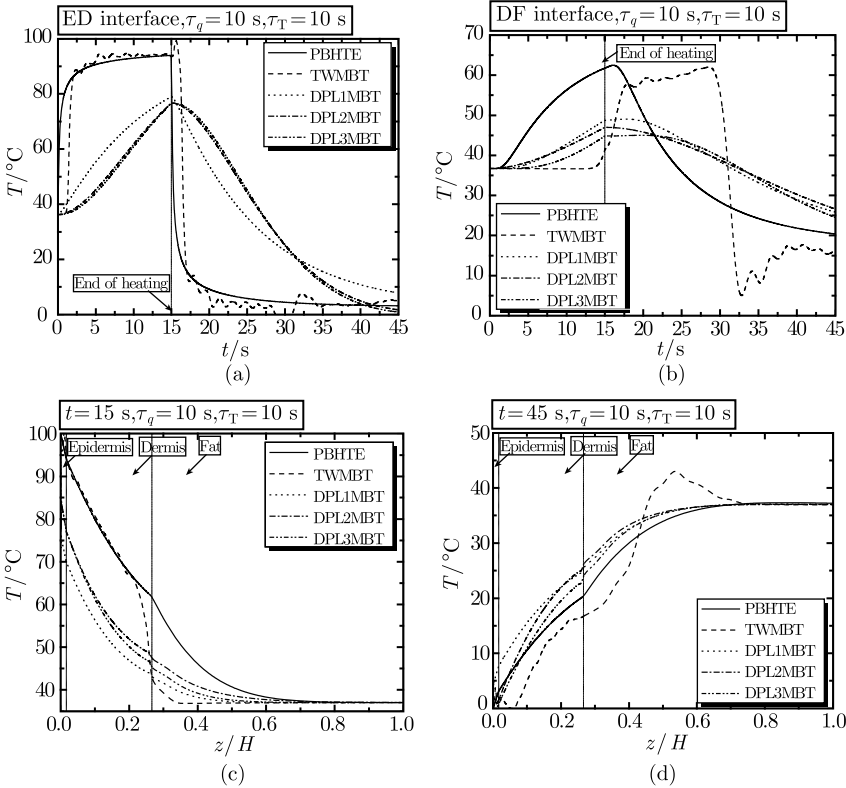


Figure 9.26 Comparison of predictions of temperature from different models for the case of surface contact heating in non-Fourier analysis: (a) variation with time at ED interface, (b) variation with time at DF interface, (c) distribution along skin depth at $t = 15$ s, and (d) distribution along skin depth at $t = 45$ s. (PBHTE: Pennes model; TWMBT: thermal wave model; DPL: dual-phase-lag model). Note that $z/H = 0.0167, 0.267$ indicate ED and DF interfaces, respectively (by permission of Elsevier)

In view of the finite-difference approximations, the effect of τ_T becomes important if t is much smaller than τ_T and the effect of τ_T^m becomes important if $[(m!)^{1/m} t]^m$ is much smaller than τ_T^m . Depending on the value of τ_T and the accuracy demanded, the former condition may or may not imply the latter. This can be exemplified by the last two terms on the right-hand-side of

Equation (4.26) with constant τ_T and τ_q

$$q + \frac{\partial q}{\partial(t/\tau_q)} + \frac{\partial^2 q}{\partial(\sqrt{2}t/\tau_q)^2} = -k \left[\nabla T + \frac{\partial \nabla T}{\partial(t/\tau_T)} + \frac{\partial^2 \nabla T}{\partial(\sqrt{2}t/\tau_T)^2} \right] \quad (9.23)$$

The large differences amongst the predicted temperatures of different models cause significant deviations in thermal damage evaluations. For example, the thermal damage predicted by the thermal wave model at the end of heating for the ED interface is the largest, about three orders larger in magnitude than that from the Pennes model, and about seven orders larger

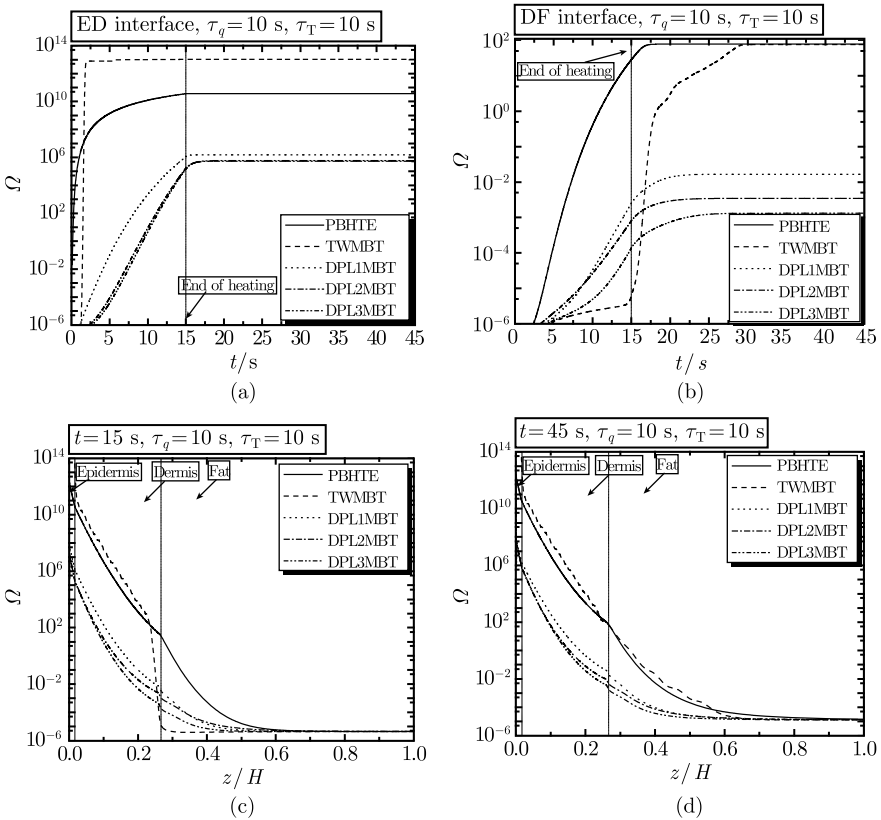


Figure 9.27 Comparison of predictions of thermal damage from different models for the case of surface contact heating in non-Fourier analysis: (a) variation with time at ED interface, (b) variation with time at DF interface, (c) distribution along skin depth at $t = 15$ s, and (d) distribution along skin depth at $t = 45$ s. (PBHTE: Pennes model; TWMBT: thermal wave model; DPL: dual-phase-lag model). Note that $z/H = 0.0167, 0.267$ indicate ED and DF interfaces, respectively (by permission of Elsevier)

than those from the DPL models. A wave-front for thermal damage is also observed for the thermal wave model, which appears in Figure 9.27(b) as a steep profile. As for the thermal damage distribution along the skin depth, the Pennes and the thermal wave models give similar results, which are much larger in magnitude than the DPL models.

The thermal stresses developed due to nonuniform temperature distributions are confined near the skin surface, see Figure 9.28(c) and (d) and both the skin surface and ED interface are subjected to large tensile stresses (> 10 MPa), see Figure 9.28(a) and (b), during both heating and cooling processes. This implies higher thermal damage occurring in these locations, consistent with the results of Figure 9.27(a) and (b). Note that the large

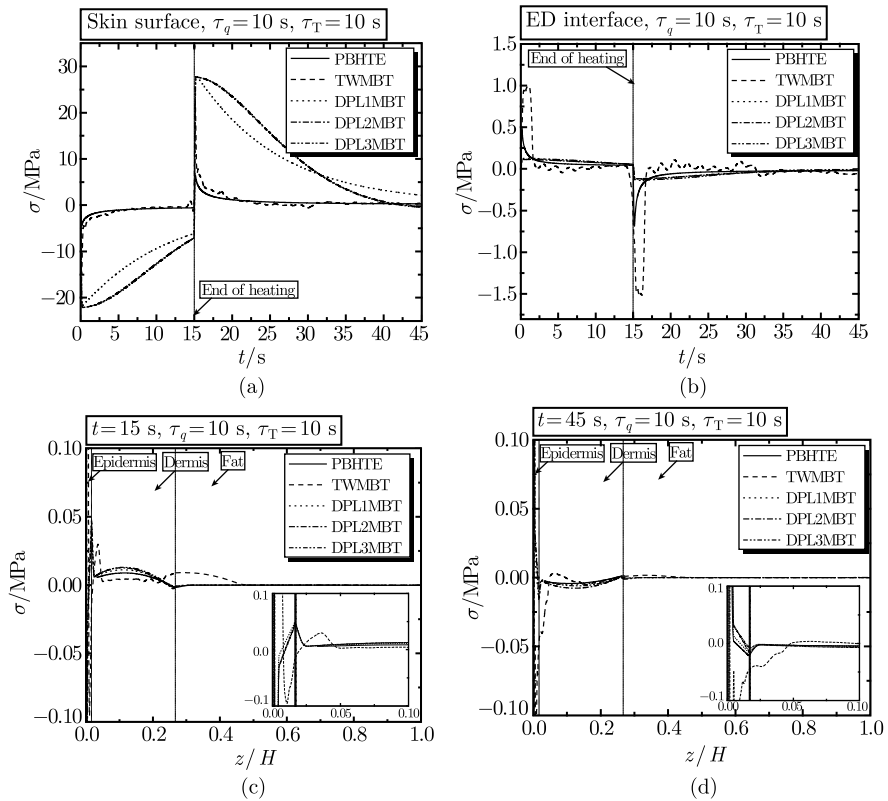


Figure 9.28 Comparison of predictions of thermal stress from different models for the case of surface contact heating in non-Fourier analysis: (a) variation with time at skin surface, (b) variation with time at ED interface, (c) distribution along skin depth at $t = 15$ s, and (d) distribution along skin depth at $t = 45$ s. (PBHTE: Pennes model; TWMBT: thermal wave model; DPL: dual-phase-lag model). Note that $z/H = 0.0167, 0.267$ indicate ED and DF interfaces, respectively (by permission of Elsevier)

tensile stresses predicted by the multi-layer skin model are in sharp contrast with those obtained with the one-layer model, see Figure 9.25. Furthermore, the magnitude of stress at the skin surface obtained with the DPL models is much larger than that with other models, although the same boundary condition is applied. This is caused by the sudden temperature drop at skin surface, see Figure 9.26(c).

2) Thermal wave model

The calculation with the thermal wave model are carried out for four different cases, where $\tau_q = 0.0, 0.1, 1.0,$ and 10.0 s, with $\tau_q = 0$ corresponding to the Pennes model. The skin temperature distributions at the end of heating ($t = 15$ s) and cooling ($t = 45$ s), are respectively shown in Figure 9.29(a) and (b), and the corresponding temperature profiles at the ED and

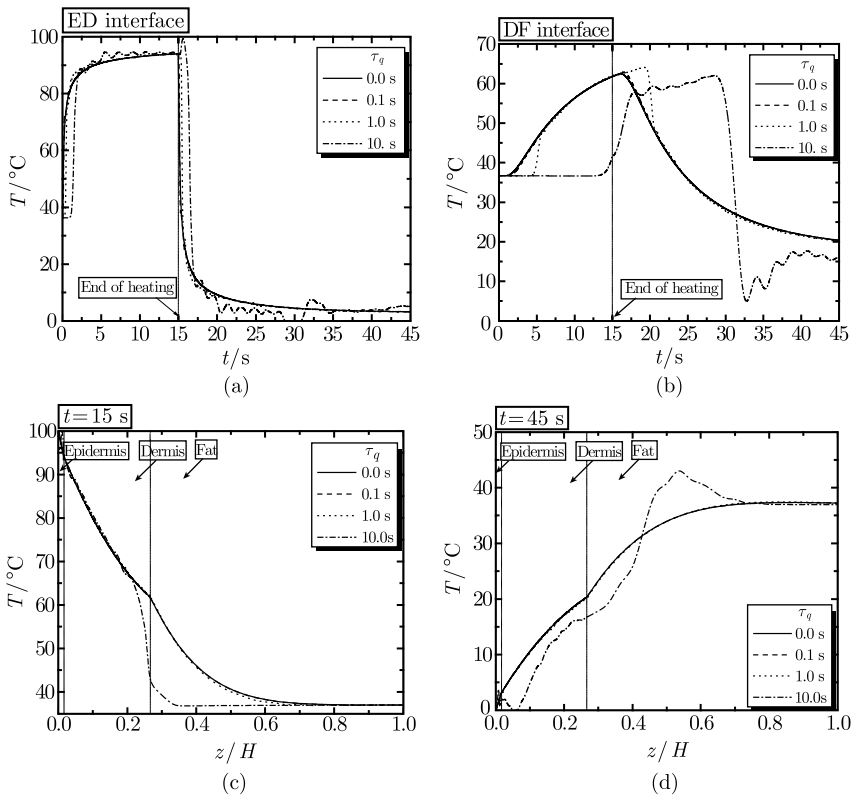


Figure 9.29 Influence of thermal relaxation time τ_q on temperature from the thermal wave model: (a) variation with time at ED interface, (b) variation with time at DF interface, (c) distribution along skin depth at $t = 15$ s, and (d) distribution along skin depth at $t = 45$ s. Note that $z/H = 0.0167, 0.267$ indicate ED and DF interfaces, respectively (by permission of Elsevier)

DF interfaces are respectively plotted in Figure 9.29(c) and (d). Skin thermal damage and thermal stress are plotted in Figure 9.30(a)~(d) and Figure 9.31(a)~(d), respectively.

Figure 9.29(a) and (b) show that the thermal relaxation time τ_q tends to induce an abrupt step in the temperature, introducing a wave-front, which separates the heated surface area from the unheated inner area. As it appears, when $\tau_q > 1.0$ s, the magnitude of τ_q has an important effect on temperature prediction and, thus, on thermal damage and thermal stress evaluations; conversely it makes little difference when $\tau_q \leq 0.1$ s. This can be easily observed from the temperature history at the DF interface, as shown in Figure 9.29(b). The appearance of the wave-front for $\tau_q = 1.0$ s occurs at $t \approx 5$ s, while for

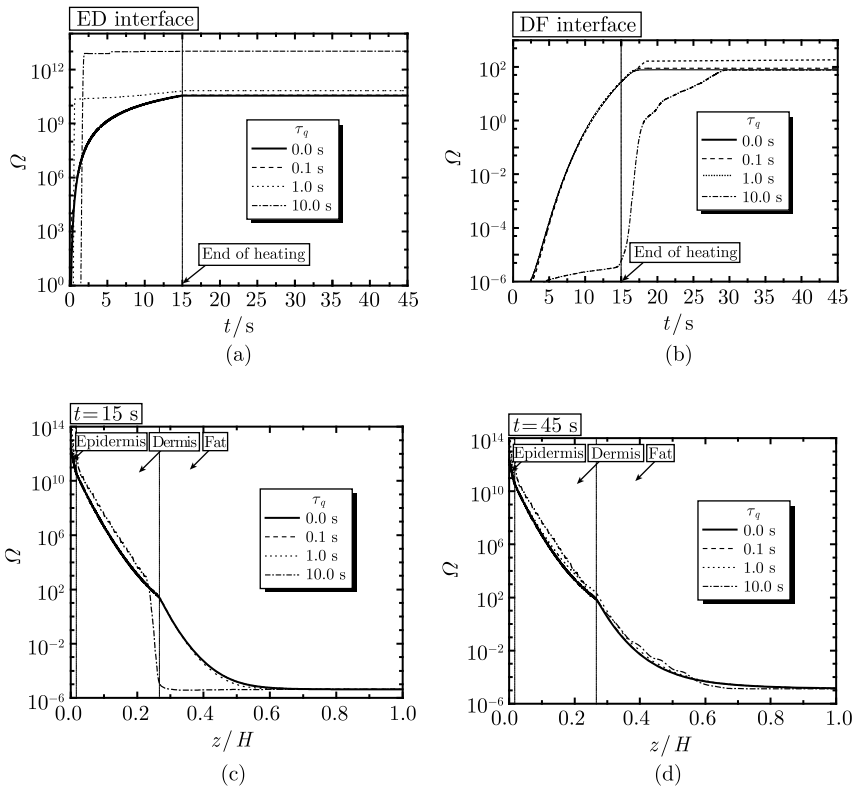


Figure 9.30 Influence of τ_q on thermal damage results from the thermal wave model: (a) variation with time at ED interface, (b) variation with time at DF interface, (c) distribution along skin depth at $t = 15$ s, and (d) distribution along skin depth at $t = 45$ s. Note that $z/H = 0.0167, 0.267$ indicate ED and DF interfaces, respectively (by permission of Elsevier)

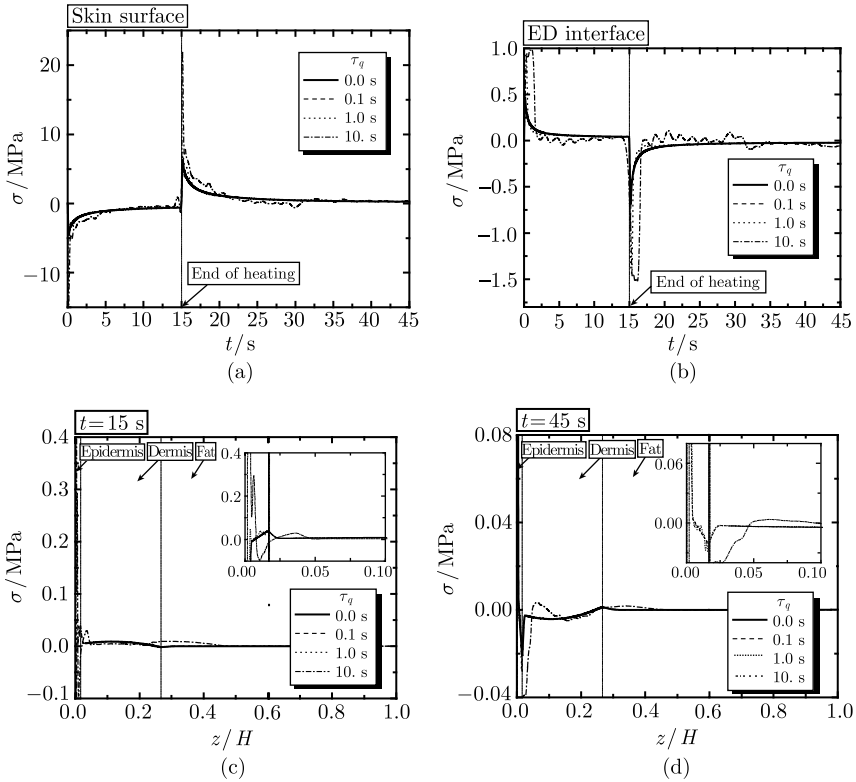


Figure 9.31 Influence of τ_q on thermal stress results from the thermal wave model: (a) variation with time at skin surface, (b) variation with time at ED interface, (c) distribution along skin depth at $t = 15$ s, and (d) distribution along skin depth at $t = 45$ s. Note that $z/H = 0.0167, 0.267$ indicate ED and DF interfaces, respectively (by permission of Elsevier)

$\tau_q = 10$ s it occurs much later at $t \approx 14$ s. Since the thermal wave speed C_t is correlated with τ_q from $C_t = \sqrt{\alpha/\tau_q}$, a smaller τ_q leads to a larger C_t for a fixed thermal diffusivity (recall, known as α).

A wave-like behaviour can also be observed in the results of thermal damage. For example, at the ED interface, little or no damage appears before $t \approx 3$ s for $\tau_q = 10$ s, whilst a sudden jump occurs thereafter and the resulting damage is about three orders larger than the cases when τ_q is smaller. However, there is almost no thermal damage at the DF interface during the entire heating process.

The thermal stress output shows a similar behaviour except for the peak values, where a larger τ_q results in a higher peak. Once again, the value is larger than the threshold of nociceptors.

3) Dual-phase-lag model

Since different DPL models give similar results, as shown above, only the type 1 DPL model, DPL1MBT, is discussed here. The calculation is carried out for nine cases: $\tau_q = 0.1s, 1.0s, 10.0 s$ and $\tau_T = 0.1s, 1.0s, 10.0 s$; for comparison, the results corresponding to the case $\tau_q = \tau_T = 0$ are also included. The results for temperature distributions are presented in Figures 9.32~9.35. The trends of thermal damage and thermal stresses are similar to those exhibited by temperature and hence, for brevity, are not included below.

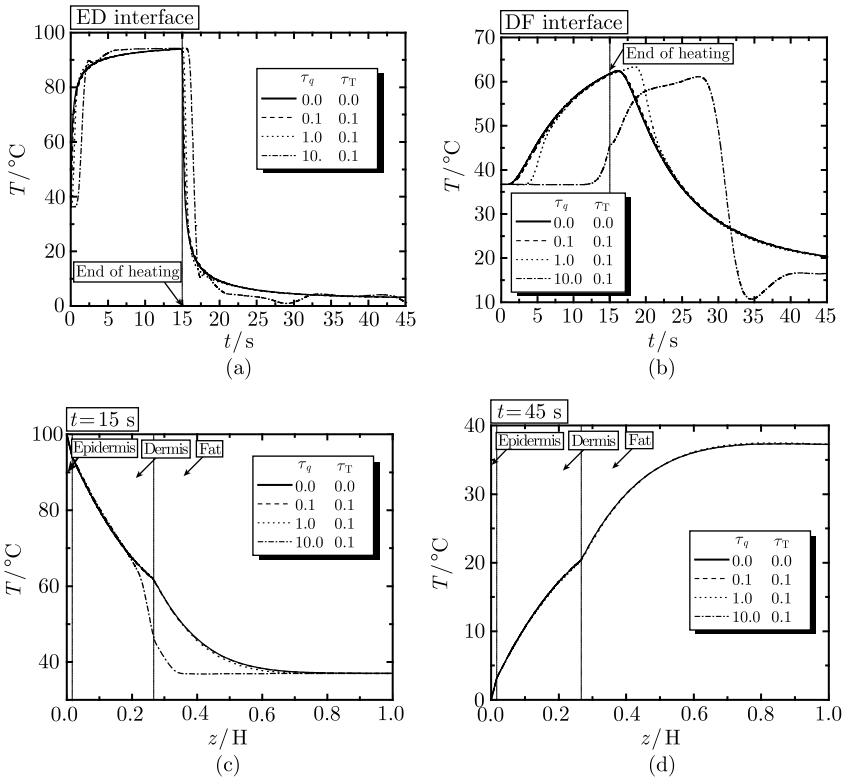


Figure 9.32 Influence of τ_q on temperature results from the type I dual-phase-lag model (DPL1MBH) at $\tau_T = 0.1$ s: (a) variation with time at ED interface, (b) variation with time at DF interface, (c) distribution along skin depth at $t = 15$ s, and (d) distribution along skin depth at $t = 45$ s. Note that $z/H = 0.0167, 0.267$ indicate ED and DF interfaces, respectively (by permission of Elsevier)

Effect of τ_q

The effect of τ_q on temperature evolution at $\tau_T = 0.1$ s is shown in Figure 9.32. Note that the results are similar to those of the thermal wave

model, especially for smaller τ_q : obvious wave-fronts are observed, and the wave-front at the same place appears earlier for a smaller value of τ_q . With increasing τ_q , the temperature is generally lower during initial heating but higher during cooling.

Effect of τ_T

The effects of τ_T on temperature profile are given in Figure 9.33 for $\tau_q = 0.1$ s and in Figure 9.34 for $\tau_q = 10$ s. As can be seen from Figure 9.33, no obvious wave-fronts can be found, which is attributable to the stronger dissipation from the mixed derivative term ($\tau_T k \nabla^2 \partial T / \partial t$), as shown in Equation (4.23). The results are almost the same for different values of τ_T , except for $\tau_T = 10.0$ s, where the temperature is lower during initial heating but higher under cooling.

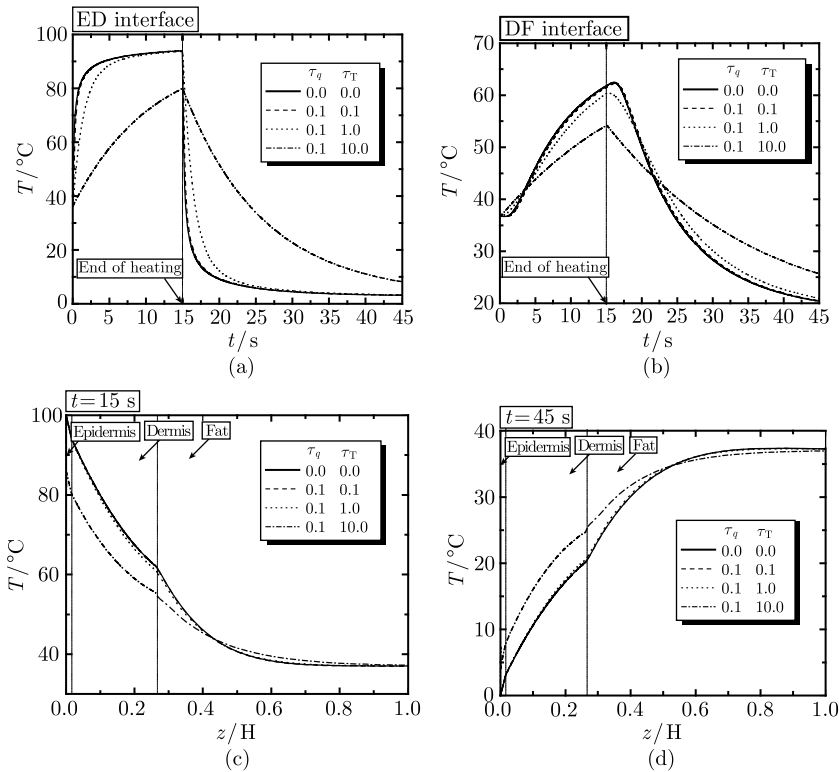


Figure 9.33 Influence of τ_T on temperature results from the type I dual-phase-lag model (DPL1MBH) at $\tau_q = 0.1$ s: (a) variation with time at ED interface, (b) variation with time at DF interface, (c) distribution along skin depth at $t = 15$ s, and (d) distribution along skin depth at $t = 45$ s. Note that $z/H = 0.0167, 0.267$ indicate ED and DF interfaces, respectively (by permission of Elsevier)

When $\tau_q = 10.0$ s, as shown in Figure 9.34, a wave behaviour is observed for all cases in spite of the different values of τ_T , which demonstrates that τ_q , rather than τ_T , dominates the mechanism of thermal wave propagation in skin tissue. However, the sharp wave-fronts due to τ_q are smoothed by the promoting conduction of τ_T , and the effect is more noticeable with increasing values of τ_T , leading to the non-Fourier, diffusion-like conduction. This result agrees well with the non-Fourier behaviour observed for engineering materials^[33~35]. However, despite different values of τ_q , the absolute value of thermal stress for $\tau_T = 10.0$ s is much larger at the skin surface but much lower at the ED interface (not shown here for brevity). This arises because the thermal stress is influenced by temperature change along the whole skin depth, as shown in Equation (9.10).

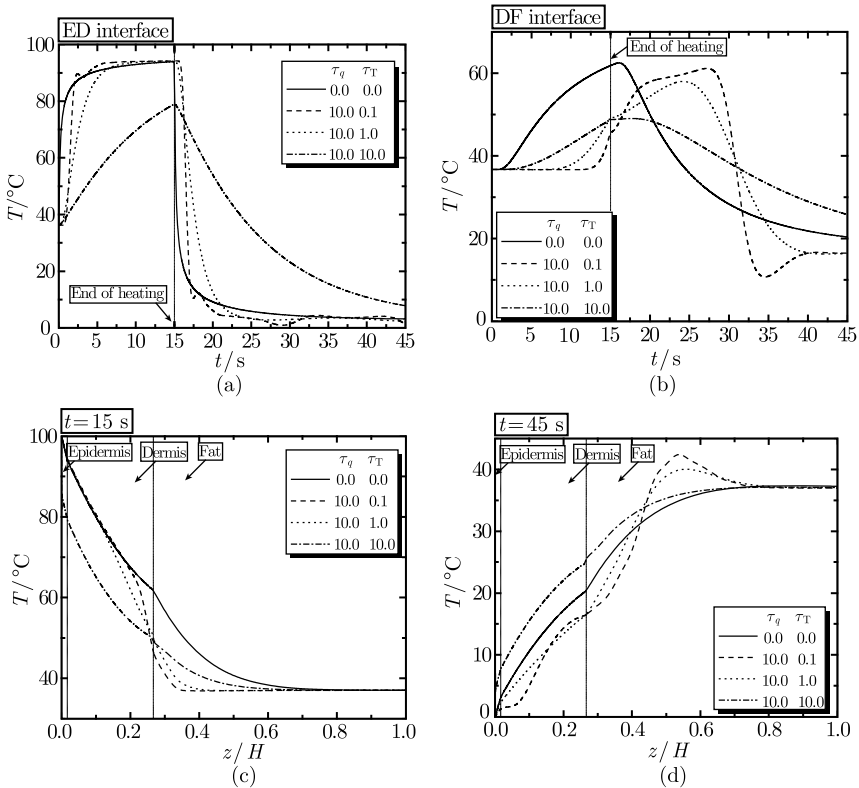


Figure 9.34 Influence of τ_T on temperature results from the type I dual-phase-lag model (DPL1MBH) at $\tau_q = 10.0$ s: (a) variation with time at ED interface, (b) variation with time at DF interface, (c) distribution along skin depth at $t = 15$ s, and (d) distribution along skin depth at $t = 45$ s. Note that $z/H = 0.0167$, 0.267 indicate ED and DF interfaces, respectively (by permission of Elsevier)

Effect of τ_q/τ_T

Tzou^[34] has suggested that the ratio of τ_q/τ_T dominates the lagging behaviour of heat transfer, i.e. the thermal responses are identical for a specified value of τ_q/τ_T . To check the suitability of this assertion in the cases here, comparisons of temperature distributions under the same τ_q/τ_T ratio are performed for three different cases, $\tau_q/\tau_T = 0.1, 1.0, 10$, as shown in Figure 9.35. It is clear, from these results that there is no concurrency of behaviour for temperature, as well as thermal damage and thermal stress, in the three cases studied, which implies that the lagging thermomechanical behaviour in skin tissue depends on the absolute magnitudes of τ_T and τ_q , in addition to the ratio of τ_q/τ_T . A similar conclusion has been obtained for engineering

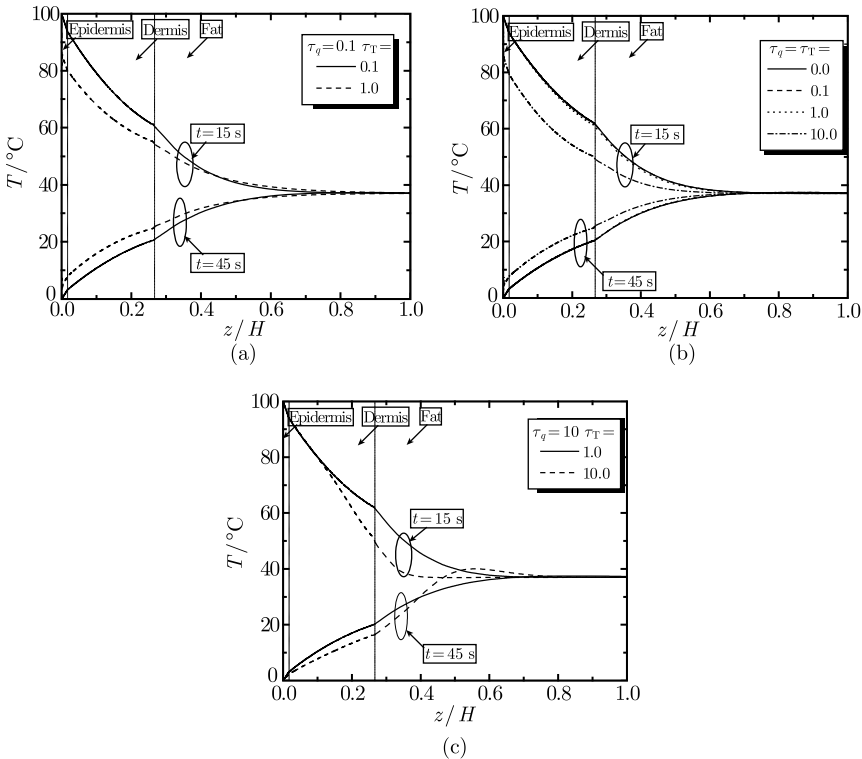


Figure 9.35 Influence of ratios of τ_T/τ_q on predictions of temperature for the type I dual-phase-lag model (DPLIMBH): (a) variation with time at ED interface and DF interface for $\tau_T/\tau_q = 0.1$, (b) variation with time at ED interface and DF interface for $\tau_T/\tau_q = 1.0$, and (c) variation with time at ED interface and DF interface for $\tau_T/\tau_q = 10.0$. Note that $z/H = 0.0167, 0.267$ indicate ED and DF interfaces, respectively (by permission of Elsevier)

materials^[36]. The difference between the results in this study and Tzou's observations are due to the different problems tackled. Tzou^[34] derived analytically the thermal lagging behaviour in a semi-infinite solid without instantaneous surface heating, which is different from the problems tackled in this work. The tangling behaviour of the real and apparent heat sources in this study, as shown in Equation (4.23), for example, may very well yield a lagging temperature that depends on the individual values of τ_T and τ_q rather than their ratio.

It is interesting to note that the temperature computed with $\tau_T = \tau_q$ differs from that computed with the Pennes' bioheat conduction equation. This is in contrast to the traditional DPL heat conduction model for industry materials, for which it approaches the Fourier heat conduction equation when $\tau_T = \tau_q$ (not necessarily equal to zero)^[37]. The discrepancy can be attributed to the blood perfusion in the bioheat model. The presence of blood perfusion leads to an extra term involving with τ_q in the temperature formulation and two extra terms involving with τ_T in the heat flux formulation. These make the intrinsic characteristic of the DPL bioheat conduction model different from that of the traditional DPL heat conduction model.

9.5 Summary

In this chapter, a mathematical approach has been developed to examine the heat transfer process, thermal damage and the heat-induced mechanical response. Analyses have been performed with both Fourier and non-Fourier heat transfer models. Exact solutions for temperature, thermal damage and thermal stress for one-layer skin model are derived for different boundary conditions. For multi-layer models, numerical simulations using the finite element method have been used to determine the temperature, thermal damage and thermal stress distributions in the skin tissue. Accordingly, the influences of different parameters on the thermomechanical response have been investigated, in order to assess their relative contributions, with the following interesting results.

From the analysis with Fourier heat transfer model, a simple one-dimensional solution predicts very high stresses compared to an axisymmetrical (two-dimensional) solution, but the stresses from the latter remain above the pain threshold in view of the high surface temperatures specified in these examples. The blood perfusion has a great influence on thermal stress under thermal agitation due to its large cooling effect on the skin temperature distribution. With laser heating, the peak temperature is higher for shorter wavelength laser, with the peak temperature being located closer to the skin surface. As

a result of the exponential decrease of heat generation along skin depth, thermal stress due to laser and microwave heating is mainly limited to the top epidermis layer. The stratum corneum layer, although very thin, dominates the thermomechanical response; more importantly, it is found that internal stress alone, induced by heating, can lead to the sensation of thermal pain, in addition to the pain generated by heating alone.

The thermal relaxation time for biological tissue is typically large, leading to the need for considering the non-Fourier nature in the skin biothermomechanics. Using the thermal wave model and dual-phase-lag models, the non-Fourier thermomechanical behaviour of skin tissue has been studied for surface heating. It is found that substantial discrepancies exist among the predictions by the Pennes model, the thermal wave model and the dual-phase-lag models whilst different dual-phase-lag models give similar results. Both types of relaxation time, τ_T and τ_q , have a significant influence on the temperature, thermal damage and thermal stress fields. τ_q dominates the thermal wave propagation in stead of τ_T ; τ_q induces a sharp wave-front that is smoothed by τ_T . The absolute magnitudes of τ_T and τ_q , not the ratio τ_q/τ_T , govern the general trends in the thermomechanical behaviour of skin tissue.

9.6 Appendix

Equation (9.10) has been solved for one-, two-, three-, and four-layer skin models and the detailed results are given in this section.

1) For one-layer model

$$\sigma_{xx}(x, t) = -\bar{E}\bar{\lambda}(T - T_0) + \frac{\bar{E}\bar{\lambda}}{H} \int_{-H/2}^{H/2} (T - T_0) dz + \bar{E}\bar{\lambda} \frac{12x}{H} \int_{-H/2}^{H/2} (T - T_0) z dz \tag{9.24}$$

2) For two-layer model (epidermis and dermis)

$$\sigma_{xx} = \bar{E}_d (1 + \nu_d) \left\{ \begin{array}{l} \left[(a'_{11} + a'_{12}) \left(\int_{z_0}^{z_1} \bar{E}_d \bar{\lambda}_d \Delta T dz + \int_{z_1}^{z_2} \bar{E}_e \bar{\lambda}_e \Delta T dz \right) + \right. \\ \left. (b'_{11} + b'_{12}) \left(\int_{z_0}^{z_1} \bar{E}_d \bar{\lambda}_d \Delta T z dz + \int_{z_1}^{z_2} \bar{E}_e \bar{\lambda}_e \Delta T z dz \right) \right] + \\ z \left[(b'_{11} + b'_{12}) \left(\int_{z_0}^{z_1} \bar{E}_d \bar{\lambda}_d \Delta T dz + \int_{z_1}^{z_2} \bar{E}_e \bar{\lambda}_e \Delta T dz \right) + \right. \\ \left. (d'_{11} + d'_{12}) \left(\int_{z_0}^{z_1} \bar{E}_d \bar{\lambda}_d \Delta T z dz + \int_{z_1}^{z_2} \bar{E}_e \bar{\lambda}_e \Delta T z dz \right) \right] \\ \left. - \lambda_d \Delta T \right\} \tag{9.25}$$

$z_0 \leq z < z_1$, epidermis layer

$$\sigma_{xx} = \bar{E}_e (1 + \nu_e) \left\{ \begin{array}{l} \left[\begin{array}{l} (a'_{11} + a'_{12}) \left(\int_{z_0}^{z_1} \bar{E}_d \bar{\lambda}_d \Delta T dz + \int_{z_1}^{z_2} \bar{E}_e \bar{\lambda}_e \Delta T dz \right) + \\ (b'_{11} + b'_{12}) \left(\int_{z_0}^{z_1} \bar{E}_d \bar{\lambda}_d \Delta T z dz + \int_{z_1}^{z_2} \bar{E}_e \bar{\lambda}_e \Delta T z dz \right) \end{array} \right] + \\ z \left[\begin{array}{l} (b'_{11} + b'_{12}) \left(\int_{z_0}^{z_1} \bar{E}_d \bar{\lambda}_d \Delta T dz + \int_{z_1}^{z_2} \bar{E}_e \bar{\lambda}_e \Delta T dz \right) + \\ (d'_{11} + d'_{12}) \left(\int_{z_0}^{z_1} \bar{E}_d \bar{\lambda}_d \Delta T z dz + \int_{z_1}^{z_2} \bar{E}_e \bar{\lambda}_e \Delta T z dz \right) \end{array} \right] \\ -\lambda_e \Delta T \end{array} \right\} \quad \begin{array}{l} z_1 \leq z < z_2, \text{ dermis layer} \\ (9.26) \end{array}$$

3) For three-layer model (epidermis, dermis, and fat)

$$\sigma_{xx} = (1 + \nu_f) \bar{E}_f \left\{ \begin{array}{l} \left[\begin{array}{l} (a'_{11} + a'_{12}) \left(\int_{z_0}^{z_1} \bar{E}_f \bar{\lambda}_f \Delta T dz + \int_{z_1}^{z_2} \bar{E}_d \bar{\lambda}_d \Delta T dz \right. \right. \\ \left. \left. + \int_{z_2}^{z_3} \bar{E}_e \bar{\lambda}_e \Delta T dz \right) \right. \\ \left. + (b'_{11} + b'_{12}) \left(\int_{z_0}^{z_1} \bar{E}_f \bar{\lambda}_f \Delta T z dz + \int_{z_1}^{z_2} \bar{E}_d \bar{\lambda}_d \Delta T z dz \right. \right. \\ \left. \left. + \int_{z_2}^{z_3} \bar{E}_e \bar{\lambda}_e \Delta T z dz \right) \right] + \\ z \left[\begin{array}{l} (b'_{11} + b'_{12}) \left(\int_{z_0}^{z_1} \bar{E}_f \bar{\lambda}_f \Delta T dz + \int_{z_1}^{z_2} \bar{E}_d \bar{\lambda}_d \Delta T dz \right. \right. \\ \left. \left. + \int_{z_2}^{z_3} \bar{E}_e \bar{\lambda}_e \Delta T dz \right) \right. \\ \left. + (d'_{11} + d'_{12}) \left(\int_{z_0}^{z_1} \bar{E}_f \bar{\lambda}_f \Delta T z dz + \int_{z_1}^{z_2} \bar{E}_d \bar{\lambda}_d \Delta T z dz \right. \right. \\ \left. \left. + \int_{z_2}^{z_3} \bar{E}_e \bar{\lambda}_e \Delta T z dz \right) \right] \\ -\lambda_f \Delta T \end{array} \right\} \quad \begin{array}{l} z_0 \leq z < z_1, \text{ fat layer} \\ (9.27) \end{array}$$

$$\sigma_{xx} = (1 + \nu_d) \bar{E}_d \left\{ \begin{array}{l} \left[\begin{array}{l} (a'_{11} + a'_{12}) \left(\int_{z_0}^{z_1} \bar{E}_f \bar{\lambda}_f \Delta T dz + \int_{z_1}^{z_2} \bar{E}_d \bar{\lambda}_d \Delta T dz \right. \\ \left. + \int_{z_2}^{z_3} \bar{E}_e \bar{\lambda}_e \Delta T dz \right) \\ + (b'_{11} + b'_{12}) \left(\int_{z_0}^{z_1} \bar{E}_f \bar{\lambda}_f \Delta T z dz + \int_{z_1}^{z_2} \bar{E}_d \bar{\lambda}_d \Delta T z dz \right. \\ \left. + \int_{z_2}^{z_3} \bar{E}_e \bar{\lambda}_e \Delta T z dz \right) \end{array} \right] + \\ z \left[\begin{array}{l} (b'_{11} + b'_{12}) \left(\int_{z_0}^{z_1} \bar{E}_f \bar{\lambda}_f \Delta T dz + \int_{z_1}^{z_2} \bar{E}_d \bar{\lambda}_d \Delta T dz \right. \\ \left. + \int_{z_2}^{z_3} \bar{E}_e \bar{\lambda}_e \Delta T dz \right) \\ + (d'_{11} + d'_{12}) \left(\int_{z_0}^{z_1} \bar{E}_f \bar{\lambda}_f \Delta T z dz + \int_{z_1}^{z_2} \bar{E}_d \bar{\lambda}_d \Delta T z dz \right. \\ \left. + \int_{z_2}^{z_3} \bar{E}_e \bar{\lambda}_e \Delta T z dz \right) \end{array} \right] \\ -\lambda_d \Delta T \end{array} \right\} \\ z_1 \leq z < z_2, \text{ dermis layer} \tag{9.28}$$

$$\sigma_{xx} = (1 + \nu_e) \bar{E}_e \left\{ \begin{array}{l} \left[\begin{array}{l} (a'_{11} + a'_{12}) \left(\int_{z_0}^{z_1} \bar{E}_f \bar{\lambda}_f \Delta T dz + \int_{z_1}^{z_2} \bar{E}_d \bar{\lambda}_d \Delta T dz \right. \\ \left. + \int_{z_2}^{z_3} \bar{E}_e \bar{\lambda}_e \Delta T dz \right) \\ + (b'_{11} + b'_{12}) \left(\int_{z_0}^{z_1} \bar{E}_f \bar{\lambda}_f \Delta T z dz + \int_{z_1}^{z_2} \bar{E}_d \bar{\lambda}_d \Delta T z dz \right. \\ \left. + \int_{z_2}^{z_3} \bar{E}_e \bar{\lambda}_e \Delta T z dz \right) \end{array} \right] + \\ z \left[\begin{array}{l} (b'_{11} + b'_{12}) \left(\int_{z_0}^{z_1} \bar{E}_f \bar{\lambda}_f \Delta T dz + \int_{z_1}^{z_2} \bar{E}_d \bar{\lambda}_d \Delta T dz \right. \\ \left. + \int_{z_2}^{z_3} \bar{E}_e \bar{\lambda}_e \Delta T dz \right) \\ + (d'_{11} + d'_{12}) \left(\int_{z_0}^{z_1} \bar{E}_f \bar{\lambda}_f \Delta T z dz + \int_{z_1}^{z_2} \bar{E}_d \bar{\lambda}_d \Delta T z dz \right. \\ \left. + \int_{z_2}^{z_3} \bar{E}_e \bar{\lambda}_e \Delta T z dz \right) \end{array} \right] \\ -\lambda_e \Delta T \end{array} \right\} \\ z_2 \leq z < z_3, \text{ epidermis layer} \tag{9.29}$$

4) For four-layer model (stratum corneum, living epidermis, dermis, and

fat)

$$\sigma_{xx} = (1 + \nu_f) \bar{E}_f \left\{ \begin{array}{l} \left[\begin{array}{l} (a'_{11} + a'_{12}) \left(\int_{z_0}^{z_1} \bar{E}_f \bar{\lambda}_f \Delta T dz + \int_{z_1}^{z_2} \bar{E}_d \bar{\lambda}_d \Delta T dz \right. \\ \left. + \int_{z_2}^{z_3} \bar{E}_e \bar{\lambda}_e \Delta T dz + \int_{z_3}^{z_4} \bar{E}_{sc} \bar{\lambda}_{sc} \Delta T dz \right) \\ + (b'_{11} + b'_{12}) \left(\int_{z_0}^{z_1} \bar{E}_f \bar{\lambda}_f \Delta T z dz + \int_{z_1}^{z_2} \bar{E}_d \bar{\lambda}_d \Delta T z dz \right. \\ \left. + \int_{z_2}^{z_3} \bar{E}_e \bar{\lambda}_e \Delta T z dz + \int_{z_3}^{z_4} \bar{E}_{sc} \bar{\lambda}_{sc} \Delta T z dz \right) \end{array} \right] + \\ z \left[\begin{array}{l} (b'_{11} + b'_{12}) \left(\int_{z_0}^{z_1} \bar{E}_f \bar{\lambda}_f \Delta T dz + \int_{z_1}^{z_2} \bar{E}_d \bar{\lambda}_d \Delta T dz \right. \\ \left. + \int_{z_2}^{z_3} \bar{E}_e \bar{\lambda}_e \Delta T dz + \int_{z_3}^{z_4} \bar{E}_{sc} \bar{\lambda}_{sc} \Delta T dz \right) \\ + (d'_{11} + d'_{12}) \left(\int_{z_0}^{z_1} \bar{E}_f \bar{\lambda}_f \Delta T z dz + \int_{z_1}^{z_2} \bar{E}_d \bar{\lambda}_d \Delta T z dz \right. \\ \left. + \int_{z_2}^{z_3} \bar{E}_e \bar{\lambda}_e \Delta T z dz + \int_{z_3}^{z_4} \bar{E}_{sc} \bar{\lambda}_{sc} \Delta T z dz \right) \end{array} \right] \\ -\lambda_f \Delta T \end{array} \right\} \\ z_0 \leq z < z_1, \text{ fat layer} \quad (9.30)$$

$$\sigma_{xx} = (1 + \nu_d) \bar{E}_d \left\{ \begin{array}{l} \left[\begin{array}{l} (a'_{11} + a'_{12}) \left(\int_{z_0}^{z_1} \bar{E}_f \bar{\lambda}_f \Delta T dz + \int_{z_1}^{z_2} \bar{E}_d \bar{\lambda}_d \Delta T dz \right. \\ \left. + \int_{z_2}^{z_3} \bar{E}_e \bar{\lambda}_e \Delta T dz + \int_{z_3}^{z_4} \bar{E}_{sc} \bar{\lambda}_{sc} \Delta T dz \right) \\ + (b'_{11} + b'_{12}) \left(\int_{z_0}^{z_1} \bar{E}_f \bar{\lambda}_f \Delta T z dz + \int_{z_1}^{z_2} \bar{E}_d \bar{\lambda}_d \Delta T z dz \right. \\ \left. + \int_{z_2}^{z_3} \bar{E}_e \bar{\lambda}_e \Delta T z dz + \int_{z_3}^{z_4} \bar{E}_{sc} \bar{\lambda}_{sc} \Delta T z dz \right) \end{array} \right] + \\ z \left[\begin{array}{l} (b'_{11} + b'_{12}) \left(\int_{z_0}^{z_1} \bar{E}_f \bar{\lambda}_f \Delta T dz + \int_{z_1}^{z_2} \bar{E}_d \bar{\lambda}_d \Delta T dz \right. \\ \left. + \int_{z_2}^{z_3} \bar{E}_e \bar{\lambda}_e \Delta T dz + \int_{z_3}^{z_4} \bar{E}_{sc} \bar{\lambda}_{sc} \Delta T dz \right) \\ + (d'_{11} + d'_{12}) \left(\int_{z_0}^{z_1} \bar{E}_f \bar{\lambda}_f \Delta T z dz + \int_{z_1}^{z_2} \bar{E}_d \bar{\lambda}_d \Delta T z dz \right. \\ \left. + \int_{z_2}^{z_3} \bar{E}_e \bar{\lambda}_e \Delta T z dz + \int_{z_3}^{z_4} \bar{E}_{sc} \bar{\lambda}_{sc} \Delta T z dz \right) \end{array} \right] \\ -\lambda_d \Delta T \end{array} \right\} \\ z_1 \leq z < z_2, \text{ dermis layer} \quad (9.31)$$

$$\sigma_{xx} = (1 + \nu_e) \bar{E}_e \left\{ \begin{array}{l} \left[\begin{array}{l} (a'_{11} + a'_{12}) \left(\int_{z_0}^{z_1} \bar{E}_f \bar{\lambda}_f \Delta T dz + \int_{z_1}^{z_2} \bar{E}_d \bar{\lambda}_d \Delta T dz \right. \\ \left. + \int_{z_2}^{z_3} \bar{E}_e \bar{\lambda}_e \Delta T dz + \int_{z_3}^{z_4} \bar{E}_{sc} \bar{\lambda}_{sc} \Delta T dz \right) \\ + (b'_{11} + b'_{12}) \left(\int_{z_0}^{z_1} \bar{E}_f \bar{\lambda}_f \Delta T z dz + \int_{z_1}^{z_2} \bar{E}_d \bar{\lambda}_d \Delta T z dz \right. \\ \left. + \int_{z_2}^{z_3} \bar{E}_e \bar{\lambda}_e \Delta T z dz + \int_{z_3}^{z_4} \bar{E}_{sc} \bar{\lambda}_{sc} \Delta T z dz \right) \end{array} \right] + \\ z \left[\begin{array}{l} (b'_{11} + b'_{12}) \left(\int_{z_0}^{z_1} \bar{E}_f \bar{\lambda}_f \Delta T dz + \int_{z_1}^{z_2} \bar{E}_d \bar{\lambda}_d \Delta T dz \right. \\ \left. + \int_{z_2}^{z_3} \bar{E}_e \bar{\lambda}_e \Delta T dz + \int_{z_3}^{z_4} \bar{E}_{sc} \bar{\lambda}_{sc} \Delta T dz \right) \\ + (d'_{11} + d'_{12}) \left(\int_{z_0}^{z_1} \bar{E}_f \bar{\lambda}_f \Delta T z dz \right. \\ \left. + \int_{z_1}^{z_2} \bar{E}_d \bar{\lambda}_d \Delta T z dz + \int_{z_2}^{z_3} \bar{E}_e \bar{\lambda}_e \Delta T z dz \right. \\ \left. + \int_{z_3}^{z_4} \bar{E}_{sc} \bar{\lambda}_{sc} \Delta T z dz \right) \end{array} \right] \\ -\lambda_e \Delta T \end{array} \right\} \\ z_2 \leq z < z_3, \text{ epidermis layer} \quad (9.32)$$

$$\sigma_{xx} = (1 + \nu_{sc}) \bar{E}_{sc} \left\{ \begin{array}{l} \left[\begin{array}{l} (a'_{11} + a'_{12}) \left(\int_{z_0}^{z_1} \bar{E}_f \bar{\lambda}_f \Delta T dz + \int_{z_1}^{z_2} \bar{E}_d \bar{\lambda}_d \Delta T dz \right. \\ \left. + \int_{z_2}^{z_3} \bar{E}_e \bar{\lambda}_e \Delta T dz + \int_{z_3}^{z_4} \bar{E}_{sc} \bar{\lambda}_{sc} \Delta T dz \right) \\ + (b'_{11} + b'_{12}) \left(\int_{z_0}^{z_1} \bar{E}_f \bar{\lambda}_f \Delta T z dz + \int_{z_1}^{z_2} \bar{E}_d \bar{\lambda}_d \Delta T z dz \right. \\ \left. + \int_{z_2}^{z_3} \bar{E}_e \bar{\lambda}_e \Delta T z dz + \int_{z_3}^{z_4} \bar{E}_{sc} \bar{\lambda}_{sc} \Delta T z dz \right) \end{array} \right] + \\ z \left[\begin{array}{l} (b'_{11} + b'_{12}) \left(\int_{z_0}^{z_1} \bar{E}_f \bar{\lambda}_f \Delta T dz + \int_{z_1}^{z_2} \bar{E}_d \bar{\lambda}_d \Delta T dz \right. \\ \left. + \int_{z_2}^{z_3} \bar{E}_e \bar{\lambda}_e \Delta T dz + \int_{z_3}^{z_4} \bar{E}_{sc} \bar{\lambda}_{sc} \Delta T dz \right) \\ + (d'_{11} + d'_{12}) \left(\int_{z_0}^{z_1} \bar{E}_f \bar{\lambda}_f \Delta T z dz + \int_{z_1}^{z_2} \bar{E}_d \bar{\lambda}_d \Delta T z dz \right. \\ \left. + \int_{z_2}^{z_3} \bar{E}_e \bar{\lambda}_e \Delta T z dz + \int_{z_3}^{z_4} \bar{E}_{sc} \bar{\lambda}_{sc} \Delta T z dz \right) \end{array} \right] \\ -\lambda_{sc} \Delta T \end{array} \right\} \\ z_3 \leq z < z_4, \text{ stratum corneum layer} \quad (9.33)$$

References

- [1] Delalleau A, Josse G, Lagarde J M, et al. Characterization of the mechanical properties of skin by inverse analysis combined with the indentation test. *Journal of Biomechanics*, 2006, 39(9): 1603–1610.
- [2] Hendriks F M, Brokken D, Oomens C W, et al. The relative contributions of different skin layers to the mechanical behavior of human skin in vivo using suction experiments. *Medical Engineering and Physics*, 2006, 28(3): 259–266.
- [3] Duck F A. *Physical Properties of Tissue: A Comprehensive Reference Book*. New York: Academic Press, 1990.
- [4] Elkins W, Thomson J G. Instrumented Thermal Manikin. Acurex Corporation, Aerotherm Division Report AD-781, 1973: 176.
- [5] Henriques F C, Moritz A R. Studies of thermal injury, I. The conduction of heat to and through skin and the temperatures attained therein. A theoretical and an experimental investigation. *American Journal of Pathology*, 1947, 23(4): 531–549.
- [6] Roetzel W, Xuan Y. Transient response of the human limb to an external stimulus. *International Journal of Heat and Mass Transfer*, 1998, 41(1): 229–239.
- [7] Dahan S, Lagarde J M, Turlier V, et al. Treatment of neck lines and forehead rhytids with a nonablative 1540-nm Er: glass laser: A controlled clinical study combined with the measurement of the thickness and the mechanical properties of the skin. *Dermatologic Surgery*, 2004, 30(6): 872–879.
- [8] Kollar L P, Springer G S. *Mechanics of Composite Structure*. Cambridge: Cambridge University Press, 2003.
- [9] Torvi D A, Dale J D. A finite element model of skin subjected to a flash fire. *Journal of Biomechanical Engineering*, 1994, 116(3): 250–255.
- [10] Diller K R, Hayes L J. A finite element model of burn injury in blood-perfused skin. *Journal of Biomechanical Engineering*, 1983, 105(3): 300–307.
- [11] Ng E Y, Chua L T. Mesh-independent prediction of skin burns injury. *Journal of Medical Engineering and Technology*, 2000, 24(6): 255–261.
- [12] Rigal J D, Leveque J. In vivo measurement of the stratum corneum elasticity. *Bioengineering and the Skin*, 1985, 1: 13–23.
- [13] Magnenat-Thalmann N, Kalra P, Leveque J L, et al. A computational skin model: Fold and wrinkle formation. *IEEE transactions on information technology in biomedicine*, 2002, 6(4): 317–323.
- [14] James N C, Richard A M. *Cutaneous nociceptors*//Belmonte C, Cervero F. *Neurobiology of Nociceptors*. Oxford: Oxford University Press, 1996: 117–145.
- [15] Van Hees J, Gybels J. C nociceptor activity in human nerve during painful and non painful skin stimulation. *Journal of Neurology, Neurosurgery and Psychiatry*, 1981, 44(7): 600–607.
- [16] Reuck A V S, Knight J. *Touch, Heat and Pain*. London: Churchill, 1966.
- [17] Trembly B S. The effects of driving frequency and antenna length on power deposition within a microwave antenna array used for hyperthermia. *IEEE*

- Transactions on Biomedical Engineering, 1985, 32(2): 152–157.
- [18] Gowrishankar T R, Stewart D A, Martin G T, et al. Transport lattice models of heat transport in skin with spatially heterogeneous, temperature-dependent perfusion. *BioMedical Engineering OnLine*, 2004, 3(1): 42.
- [19] ABalanis C. *Advanced Engineering Electromagnetics*. New York: John Wiley and Sons, 1989.
- [20] Özen S, Çerezci O, Çömlekçi S, et al. Heat effect analysis o microwave exposed skin by using a multilayer human skin model. *Bioeffects of EMFS*, 2nd International Workshop. Rhobes, 2002.
- [21] Lofland S E, Mazzatenta J D, Croman J, et al. Multimode near-field microwave monitoring of free water content of skin and imaging of tissue. *Physics in Medicine and Biology*, 2007, 52(5): 1295–1301.
- [22] Wilson B C, Adam G. A Monte Carlo model for the absorption and flux distributions of light in tissue. *Medical Physics*, 1983, 10(6): 824–830.
- [23] Wang L, Jacques S, Monte Carlo Modeling of Light Transport in MultiLayered Tissues in Standard C. Houston: University of Texas, 1992.
- [24] Jacques S L, Prahl S A. Modeling optical and thermal distributions in tissue during laser irradiation. *Lasers in Surgery and Medicine*, 1987, 6(6): 494–503.
- [25] Goldberg D J. Laser treatment of pigmented lesions. *Dermatology: Clinical*, 1997, 15(3): 397–407.
- [26] Lee M W. Combination 532-nm and 1064-nm lasers for noninvasive skin rejuvenation and toning. *Archives of Dermatology*, 2003, 139(10): 1265–1276.
- [27] Prinz B M, Vavricka S R, Graf P, et al. Efficacy of laser treatment of tattoos using lasers emitting wavelengths of 532 nm, 755 nm and 1064 nm. *British Journal of Dermatology*, 2004, 150(2): 245–251.
- [28] Spigulis J, Gailite L, Lihachev A, et al. Simultaneous recording of skin blood pulsations at different vascular depths by multiwavelength photoplethysmography. *Applied Optics*, 2007, 46(10): 1754–1759.
- [29] Sturesson C, Andersson-Engels S. Mathematical modelling of dynamic cooling and pre-heating, used to increase the depth of selective damage to blood vessels in laser treatment of port wine stains. *Physics in Medicine and Biology*, 1996, 41(3): 413–428.
- [30] Liu J, Chen X, Xu L X. New thermal wave aspects on burn evaluation of skin subjected to instantaneous heating. *IEEE Transactions on Biomedical Engineering*, 1999, 46(4): 420–428.
- [31] Patapoutian A, Peier A M, Story G M, et al. Thermo TRP channels and beyond: Mechanisms of temperature sensation. *Nature Reviews Neuroscience*, 2003, 4(8): 529–539.
- [32] Kruger L, Perl E R, Sedivec M J. Fine structure of myelinated mechanical nociceptor endings in cat hairy skin. *The Journal of Comparative Neurology*, 1981, 198(1): 137–154.
- [33] Tzou D Y, Ozisik M N, Chiffelle R J. The lattice temperature in the microscopic two-step model. *Journal of Heat Transfer*, 1994, 116(4): 1034–1038.
- [34] Tzou D Y, *Macro- to Micro-Scale Heat Transfer: The Lagging Behavior*. Washington: Taylor and Francis, 1997.

- [35] Antaki P J. Importance of nonFourier heat conduction in solid-phase reactions. *Combustion and Flame*, 1998, 112(3): 329–341.
- [36] Liu K C. Analysis of dual-phase-lag thermal behaviour in layered films with temperature dependent interface thermal resistance. *Journal of Physics D: Applied Physics*, 2005, 38(19): 3722–3732.
- [37] Tzou D Y. A unified field approach for heat conduction from macro- to micro-scales. *ASME Journal of Heat Transfer*, 1995, 117(1): 8–16.

Chapter 10

Experimental Characterization of Skin Biothermomechanics

10.1 Introduction

In the previous chapter, a mathematical approach has been introduced for determining the thermomechanical response in skin tissue, e.g. that induced by electromagnetic heating whereby simulating medical treatments. Whilst insightful, there are, nonetheless, some limitations, where the main deficiency is that the skin tissue is assumed to have constant properties due to the comparatively few relative studies. More experiments are thus needed to better understand the variation in properties with temperature and the corresponding collagen denaturation, so that these properties can be reliably used in future, more sophisticated models.

The experimental characterization of thermomechanical behaviour of skin tissue is presented in this chapter. The objective is to test the hypothesis that collagen is a significant determinant of the thermally-induced change in the mechanical properties of skin tissue. For this purpose, differential scanning calorimetry analysis is used to detect the denaturation of collagen in skin tissue and to measure its thermal stability. The integrity of the collagen network is analyzed using the thermal damage integration [see Equation (3.34) in Chapter 3]. Hydrothermal tensile and compressive experiments are then performed to assess the thermal dependency of skin mechanical behaviour. In order to characterize viscoelastic properties of skin tissue as a function of temperature and collagen denaturation, stress relaxation tests under tension and dynamic mechanical analysis versus temperature are also performed.

10.2 Experimental Methodology

10.2.1 Sample preparation techniques

1) Selection of samples

The ethical and immunological issues associated with human skin tissue

testing request us to find a substitute tissue. Pig skin tissue is chosen due to its structural and functional efficacy compared to human skin tissue^[1~5], including the histology, morphology, cell kinetics, density of hair, etc. Furthermore, repetitive tests can be realized for the same animal because of its large size, reducing the variation in results^[6].

Pig skin tissue varies in thickness by site; however, there appears to be a good concordance in thickness among age-matched donors. Therefore, skin samples from the cheek, ear, back, belly, and flank areas are used. Specifically, pig ear skin tissue taken from the center auricle is used for tensile tests, which has been shown to be very similar to human skin tissue^[7], while skin tissue from the back of pig is chosen for compression tests in consideration of its large thickness and low anisotropy^[8]. In this series of experiments, skin samples from domestic British breeds of pigs are used, which are obtained from a local slaughter house near Cambridge, at Dalehead Foods in Linton.

2) Sample procurement

Samples of pig skin tissue to a depth of the subcutaneous fat at different body sites are procured daily, ten minutes post mortem by block dissection. The skin sample is excised with sharp scissors and a single-edged razor blade, taking care to minimize the mechanical strain applied to the tissue. They are then fast-chilled following the standard tissue procurement protocol to 4°C in a pre-gassed Krebs-Henseleit Ringer¹⁾ (KHR, pH 7.4). The components of the KHR solution are given in Table 10.1. Samples are transported to the laboratory immediately afterwards, where the samples are separated from subcutaneous fat by wet/fast-dissection in KHR at 4°C and the epidermal layers are not removed to prevent the death of cells caused by mechanical trauma. The skin samples are tested within a few hours of slaughter, in order to minimize degradation of the tissue structure. In all, efforts have been placed on keeping the cellular component of the samples viable. Any storage of test samples at room temperature has been avoided, and only samples that have been stored at 4°C are used in this study. This routine has been shown to best preserve the samples^[7,9] and fibroblasts remain viable for long periods^[10].

3) Sample preparation

Sample cutting

Before cutting, any hair on the skin tissue is closely clipped with electric

1) A physiological solution that meets the metabolic requirements of skin tissue and prevents sample degradation, which is supplied on a daily basis by the Pharmacology Department, Cambridge University.

clippers. The outline geometry of the sample is marked on the skin tissue with surgical skin marker prior to excision. Skin samples of different shapes are prepared in KHR at 4°C by use of tissue punches immediately prior to mounting in the experimental apparatus.

Table 10.1 Component of Krebs-Henselite ringer (KHR)^[11]

NaCl	118 mmol	MgSO ₄	1.2 mmol
KCl	4.7 mmol	KH ₂ PO ₄	1.2 mmol
NaHCO ₃	25 mmol	Glucose (C ₆ H ₁₂ O ₆)	5.6 mmol
CaCl ₂ · 2H ₂ O	0.94 mmol		
Gassed using 95% O ₂ , 5% CO ₂ by diffuser			

For tensile and relaxation tests, a rectangular specimen, approximately 20 mm by 20 mm for biaxial tests (20 mm by 2.5 mm for uniaxial tests), is cut from the excised skin tissue with a press-knife constructed from disposable razor blades held in a block of perspex. A dumbbell shape is not selected due to technical difficulty and potential tissue damage, although it may have been preferable to use on strictly mechanical grounds due to the uniform distribution of load in the central region of sample and the avoidance of end effects^[10].

For compression tests, cylindrical specimens¹⁾ are cut from pig skin tissue, using a 10 mm diameter leather die punch²⁾ mounted on a hand press in KHR at 4°C The punch is straight internally and tapered externally, and has a sharp edge.

Sample measurements

For tensile tests, the thickness of each rectangular strip is measured using a micrometer after stretching the samples to their original size as measured before excision³⁾, accurate to 0.01 mm, and its width is measured using digital slide calipers, accurate to 0.01 mm. Five sets of measurements are performed at different locations and the average set is taken for the size of sample. Any errors due to penetration of the micrometer probe into the skin tissue are observed to be less than 0.1 mm by comparing with direct measurements using a microscope. Precise measurement of the length of sample in tensile tests is not performed since an optical method is used for the displacement/strain measurement, as described in Section 10.4, where the length can be optically recorded instead.

1) Compression of the specimen during the cutting process produces a curved rather than straight edge to specimen. The curved shape is induced due to the tissue expansion resulted from compression during cutting.

2) Supplied by RS components.

3) This is aimed to remove the effect of shrinkage induced during cutting.

For compressive tests, both the thickness (height) and diameter of each sample are measured using a micrometer, accurate to 0.01 mm, after placing the sample between glass slides in the undeformed state.

Predamage of samples

In order to study the influence of thermal denaturation/damage on skin properties, some skin samples are thermally denatured before testing by wrapping them in water-tight aluminum foil packets and submerging in a KHR bath with prescribed heating histories^[12,13]. Care is taken during this process to minimize dehydration.

Mechanical preconditioning of samples

In this study, mechanical preconditioning of skin samples in KHR solution at 37°C is applied before each test, in order to obtain reproducible responses. The skin sample is subjected to a displacement controlled sinusoidal excitation at a specific frequency (0.05 Hz), and the loading/unloading curves are examined to determine if repeatable stress-strain curves are achieved. The test data are discarded if the loading/unloading curves fail to converge to a repeatable stress-strain relationship. After preconditioning, the samples are preloaded to a stress state of 10 kPa, which is a reasonable initial stress *in vivo*^[14], to mimic its *in vivo* condition. Enough time is allowed, prior to starting the test, for the skin sample to get to the equilibrium state, which is chosen as the reference configuration.

Identification of material axis

The thermal and mechanical behaviours of skin tissue are anisotropic; therefore, the samples' material axis¹⁾ should be first identified. Generally, identification of the material axis is based on observations of the gross specimen shape or the fiber architecture. However, in skin tissue, the fibers are too small to be observed visually. The equal-load method^[15] is therefore used in this study where the material axis is identified by determining which direction, when loaded to the same stress, demonstrates the greatest and least strain values. A circular skin specimen has opposing pairs of small clamps placed on its perimeter: each pair is separately preloaded, and two markers are made, and aligned to the stretch axes. For several positions on the perimeter, the markers produce an ellipsoidal pattern whose semi-axes are aligned to the material axes.

For uniaxial tensile tests, the sample is cut along the minor semi-axes, while for biaxial tests, the square sample is cut with adjacent sides parallel to the semi-axes, respectively.

1) Direction of collagen fiber orientation in skin tissue.

10.2.2 Differential scanning calorimetry tests

Thermal metric is used in this study to characterize the thermal denaturation and heat-induced damage of skin tissue by using differential scanning calorimetry (DSC), which has been used extensively to characterize the thermal behaviour of collagenous tissues including skin tissue^[16,17]. DSC detects thermodynamic changes by measuring the flow of heat between a sample and a reference, whereby the variation of enthalpy or apparent specific heat¹⁾ of skin samples with temperature is recorded during the heating and the parameters for describing thermal denaturation process are then calculated based on the assumed reaction model of first-order kinetics [see Equation (3.33) in Section 3.34].

In this study, the thermal stability of collagen in pig skin sample is assessed with a TA Instruments DSC of type Q1000 T_{zero}²⁾, scanning from 20 to 100°C at four different heating rates ($r_h = 2^\circ\text{C}/\text{min}, 5^\circ\text{C}/\text{min}, 10^\circ\text{C}/\text{min}, 20^\circ\text{C}/\text{min}$). The skin sample, of about 8 mg in weight, is put inside a hermetically sealed pan, which is kept away from all contamination. The pan is then placed in a differential scanning calorimetric cell and heating is applied at a constant rate, r_h . The controlled heating-rate protocol is chosen for it needs comparatively much fewer specimens than temperature-jump tests^[18].

10.2.3 Hydrothermal tensile tests

1) System design

A hydrothermal tensile system has been designed and built, which can be either force or displacement controlled, and which enables a variety of uniaxial and biaxial tensile tests under hydrothermal conditions, such as hydrothermal isometric tension tests and hydrothermal isotonic tests.

Biaxial mechanical testing is chosen in the present system for the following reasons: ① *in vivo*, skin tissue is loaded biaxially; ② as the fibers in skin tissue are multi-directional, the orientation of the fibers with respect to the load axis must be taken into account; ③ for incompressible or nearly incompressible materials, biaxial mechanical testing can be used to obtain the material parameters for three dimensional constitutive models; ④ pursuit of a multiaxial analysis is of clinical importance to surgeons for if the orientation of maximum extensibility is known, the excision can be planned to optimize wound closure; ⑤ uniaxial test can also be performed with a

1) Representing the combined effects of specific and latent heats.

2) In the Polymer Characterization Laboratory, in the Department of Materials Science and Metallurgy, Cambridge University.

biaxial testing system by loading in only one direction.

In order to perform accurate tensile experiments on soft biological tissues, the following should be considered. Small specimen sizes should be considered for it becomes difficult to precisely identify material axes. The correct gripping technique is needed to avoid causing damage and to assure a uniform distribution of forces along the specimen edges. Biological degradation can be avoided by testing quickly, and testing should aim for homogeneous deformation within the specimen. Compared to the uniaxial test, biaxial testing should account for additional requirements: the edges must be able to expand freely in the lateral direction, and in the central target region, the stress and strain states should be uniform so that data analysis can be performed simply; and the target region must be small and located far away enough from the outer edges to avoid the effects of specimen grips or tethers.

Based on the above requirements, the designed experimental system composes of four main subsystems, as schematically shown in Figure 10.1, which are now described.

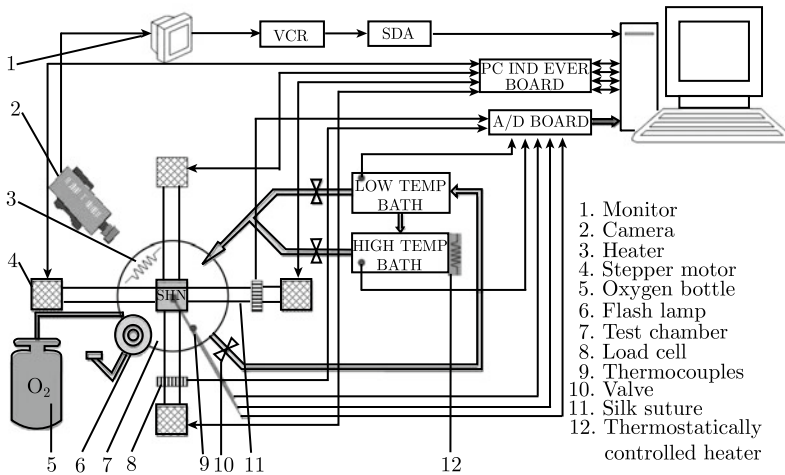


Figure 10.1 Schematic design of the hydrothermal tensile experimental system (by permission of ASME)

Environmental chamber

The environmental chamber applies a specific thermal boundary condition to the specimen, and allows testing of the sample in air or liquid under user-defined thermal conditions, e.g. nearly constant temperatures (a temperature-jump test) or constant heating rates. The top plate of the chamber has a central port that allows the optical strain measurement with a charge-coupled device (CCD) camera. The bottom plate has drains to remove liquid from the chamber. The temperature of the fluid in the test

bath is controlled by means of fluid exchange via a pump with thermally-controlled reservoirs and maintained at a prescribed level using a heat insulation method¹⁾: there are two reservoirs, one with a high temperature, which is controlled by a thermostatic immersion heater up to temperatures of 100°C and the other has a low temperature.

The temperatures of both reservoirs are monitored by a T-type thermocouples²⁾ (thermocouple 1). Another T-type thermocouple (thermocouple 2) is immersed into the KHR solution and placed very near the tissue³⁾ to monitor the temperature of the KHR solution.

Loading system

The loading system applies either a uniaxial or a biaxial set-of-forces or deformations to the specimen, and is shown in Figure 10.2. It is mounted on a square, custom machined, aluminum plate. A circular watertight specimen chamber is mounted centrally on the top plate and the loading assemblies are aligned at the four ends of the chamber with two perpendicular loading axes.

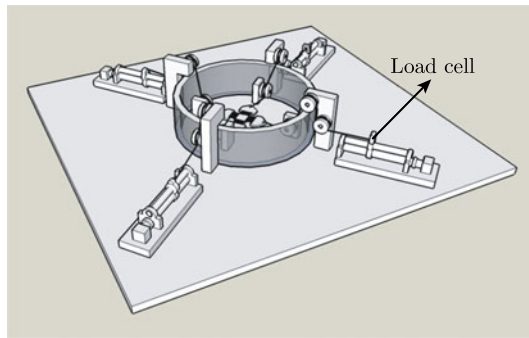


Figure 10.2 Loading subsystem of the hydrothermal tensile testing system: user-defined loading, such as isometric tension tests and isotonic tension tests, can be achieved through the pulley system

Nearly uniformly distributed in-plane biaxial forces/deformations are applied to the square specimen through four load carriers. The load can be applied in each of the four carriage assemblies independently by use of a pul-

1) Minimization of heat loss by use of heat insulation material around the testing chamber.

2) Copper-constantan thermocouple with a temperature range of $-200 \sim 400^\circ\text{C}$.

3) Approximately 0.5 mm from the surface of the sample.

ley system. Part of the pulley system is connected to stepper motors¹⁾, which impose deformations on the skin being tested and allows computer-controlled loading in orthogonal directions. The stepper motors are individually controlled using custom-designed motor controller, which is modified from a four-axis indexer card²⁾. Each motor is connected to a gearbox with ratio of 500:1 in order to make the velocity in the range needed, which gives a resolution of 1.571 μm and a maximum velocity of 6.283 mm/s ³⁾. A pair of motors is used to stretch the specimen in opposing directions to keep the specimen located nearly at center of test chamber in order to improve video strain resolution. The other part of the pulley/weight system is to apply isotonic loads (equal loading): pairs of identical weights are placed at the ends of the pulley system so that equal forces are applied along each axis.

One of the major challenges in the project is the design of the holding system of connecting the tissue to the load cell: there is a slot of wideness of 0.12 mm and length of 18 mm in each clamp, and the skin sample is fixed in the clamp by putting five pins with diameter of about 0.1 mm through the slot. In this way, the sample can be able to expand freely in the lateral direction during tensile test. The clamp is connected to the pulley system by using inextensible string.

Another problem is that the density of skin tissue ($\approx 1200 \text{ kg/m}^3$) is larger than that of the liquid ($\approx 1000 \text{ kg/m}^3$), which results in the sinking of tissue sample in the liquid during the test. In order to solve this, small pieces of polystyrene foam are placed on the underside of the tissue to render it nearly neutrally buoyant, as used by other researchers^[19].

Strain/displacement and stress/force measurement system

Two force transducers (load cells⁴⁾), which are watertight and temperature compensated, are mounted outside of the specimen chamber⁵⁾ on two orthogonal load carriages, as shown in Figure 10.2. In-plane finite strains and deformations in the tissue are measured optically by tracking the position histories of contrasting markers on the surface of the specimen, based on the method of Downs et al.^[20]: the strain and deformation are traced

1) McLennan 1.8 degree hybrid stepper motor, with holding torque 14 N·cm and rotor initial 0.018 $\text{kg}\cdot\text{cm}^2$.

2) Trinamic quadpack 4 axis controller/driver.

3) This equals a strain rate of 62.83%/s for a sample with length of 20 mm.

4) Entran[®] ELPM-T2. Two load cells are used instead of four in view that the strain rate is not very high and the behaviour can be treated as a quasi-equilibrium one. Two load cells, instead of four, are used here, which is because the testing is performed at a comparatively low speed and the process can be treated as being quasi-static.

5) This is in order to reduce the error induced by the large temperature variation inside the chamber.

between different deformation states by performing a two-dimensional cross-correlation on subsets of the images^[21], which are recorded with a CCD camera at 30 Hz. The image is captured to video file for detailed off-line analysis, although in time analysis can also be achieved via a video frame grabber board. The accuracy of the cross-correlation relies on high-contrast, high-frequency information within the images, which is provided by staining the tissue sample with a surgical marker pen before each experiment and by self-holding surface feature¹⁾ of skin tissue. The deformation field is obtained by comparing current marker positions, given by pixel coordinates, to the reference positions. It should be noted here that the bidirectional tissue strain is measured only in a central region so that the effects of local stress concentrations of the gripping attachments are avoided. In order to keep the interested region within the field of view of the CCD, the two motors are set to the same speed. Force measurements are synchronized with CCD images by a LED in-shot²⁾ at the beginning of each sequence.

Temperature measurement system

The temperatures of both reservoirs are recorded by T-type thermocouples³⁾. Another T-type thermocouple is immersed³⁾ into the KHR solution and placed approximately 0.5 mm from the surface of the sample to measure the temperature of the KHR solution.

Data acquisition system

The current system uses two computers to acquire the data: one for recording the video and the other for recording the force and temperature. Analog signals from the load cells and thermocouples are transmitted to a custom-made amplifier⁴⁾, and later to an A/D converter⁵⁾. The A/D conversion board employed has eight signal channels, where two channels are reserved for analog signals from the thermocouples and another two are occupied by analog signals from the load cells, which are connected to a signal conditioner⁶⁾. The data acquisition from the load cells and thermocouples and the motor control are all performed using an integrated software system developed with

1) Some natural feature of skin surface can also be used as marker, such as wrinkle.

2) A light-emitting diode (LED), which is connected to an analogue voltage output channel of the force data logging board, is lit-up at the start of data force measurement. This process is recorded by CCD camera and in the video it can be seen in which frame the loading starts. Therefore the strain data to the load data can be aligned and synchronization is achieved.

3) Copper-constantan thermocouple with a temperature range of $-200 \sim 400^{\circ}\text{C}$.

4) The signals are transformed into a scaled $\pm 10\text{ V}$ voltage.

5) NI PCI6220, which has 16 analogue input channels with 16-bit resolution, 24 digital input/output channels, and a maximum sampling frequency of 1 MHz.

6) Entran[®] IMV-15-WW.

LabVIEW (National Instruments) by the author, which allows the user to operate the rig and perform experiments through a single graphical user interface. This software supports motor control in either position or force feedback modes, allowing deformation states to be specified in terms of stress or strain.

2) Calibration and validation of the system

The system was made in Engineering Department, Cambridge University, and is shown in Figure 10.3.



Figure 10.3 Practical implementation of Figure 10.1

Before being used to test skin samples, the system is calibrated and validated. The two components of the experimental system requiring calibration are the loaded cells and the thermocouples. The details of the calibration and validation procedures are given below.

(1) Calibrations.

Calibration of thermocouples

The two thermocouples used in the system are of type T. A constant temperature bath with max temperature 180°C and precision 0.1°C is used for the calibration according to the following procedure: ① the temperature in the constant temperature bath is first set to a desired level, against which the thermocouple is to be calibrated; ② the thermocouple is then dipped into the thermo-bath liquid and wait for a few minutes for it to reach the steady state; ③ the output voltage of the thermocouple is recorded using the data acquisition system, as described above. Change the temperature of the thermo-bath liquid in the range of $0 \sim 100^{\circ}\text{C}$ and repeat the steps ② and ③.

The voltage from the thermocouple can be converted to temperature by fitting a line to the calibration data. Figure 10.4 shows the calibration data from the two thermocouples. Linear lines have been fit to the data and found

to have slopes of 11.998,35 and 11.833,64°C/V, and R^2 values of 0.999,81 and 0.999,95 for thermocouples 1 and 2, respectively.

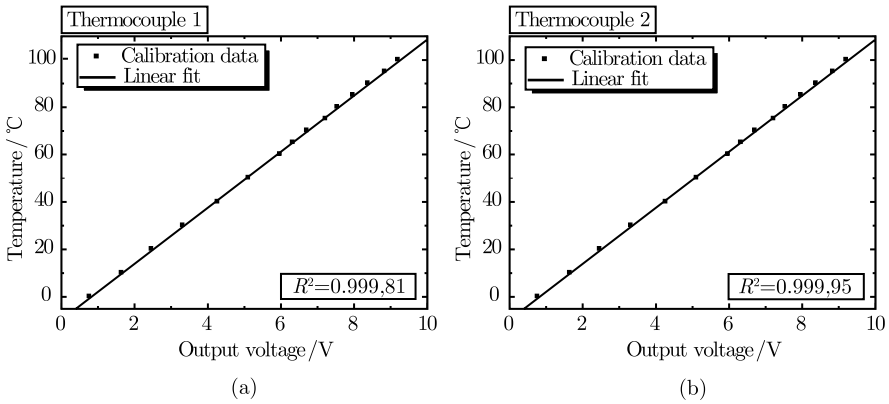


Figure 10.4 Calibration of (a) thermocouple 1 and (b) thermocouple 2. Note the obvious linear relationship between the temperature and output voltage

Calibration load cells

The output of the load cell to the PC is in volts, and calibration of the load cells is thus needed in order to convert the load cell output of voltage to force. To calibrate the load cells, a method using weights is used by mounting known weights with an effectively inextensible string to the pulley connected with the load cell. Different known weights¹⁾ are hung from the pulley, and readings are recorded from the data acquisition system. Linear lines have been fit to the data using a linear least square regression, as shown in Figure 10.5, and found to have slopes of 5.241,66 and 5.166,54 N/V, and R^2 values of 0.999,99 and 0.999,58 for load cell 1 and load cell 2, respectively.

(2) System validation

Heat transfer analysis

The system is aimed at testing the mechanical behaviour of skin samples under different heating conditions. It is thus important to analyze the heat transfer in the sample during the tests. The Pennes equation [see Equation (3.4)] without blood perfusion term²⁾ is used here for the heat transfer analysis, where the skin sample is assumed to be thin and flat, and to experience on its two surfaces a step change in temperature from a uniform room temperature to an immersion fluid temperature up to 100°C. The unloaded

1) Ten different loads were used for calibration to decrease the standard deviation of the calibration parameters, and thus increase the accuracy of the force measurements. Increasing the sampling rate also helped to decrease the errors associated with noise.

2) In view that the samples are tested *in vitro*.

thickness of skin sample is in the range of 1.6 ~ 2.4 mm and the maximum value of 2.4 mm is used to estimate the maximum time required for the samples to reach the target temperature. Thermal properties are obtained from published data in the literature as given in Table 9.1. Using the closed-form solution obtained in Chapter 4, the centerline temperature history of the skin sample under heating of different temperatures can be obtained, as shown in Figure 10.6.

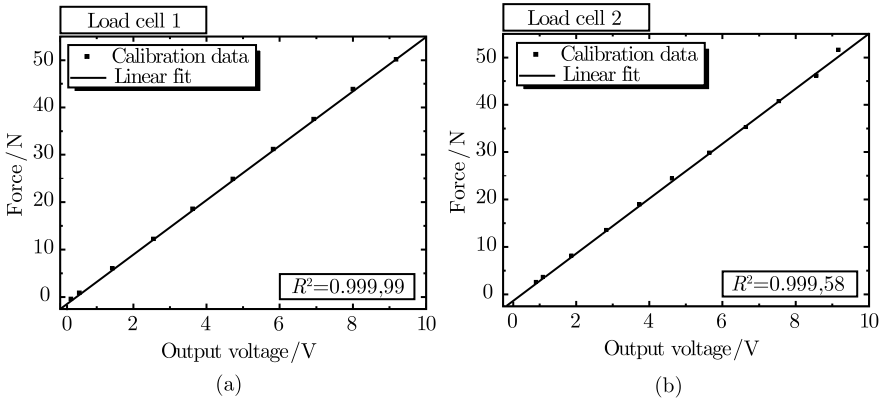


Figure 10.5 Calibration of the (a) load cell 1 and (b) load cell 2. Note the obvious linear relationship between the force and output voltage

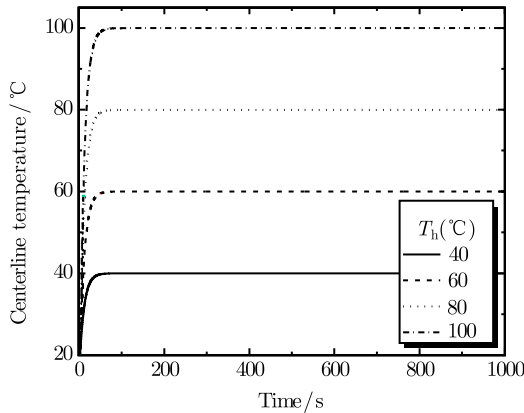


Figure 10.6 Validation of the heating condition of the current system: centerline temperature of the skin sample reaches the targeted temperature very quickly as compared to the duration of the tests (by permission of ASME)

For example, with heating of 100°C, the centerline temperature of the skin sample gets to 90°C within 10 s, which is very short compared to the whole duration of the test (10 minutes). Analyses for other temperatures reveal

similar maximum values, see Figure 10.6. These values are conservative in view that the maximum thickness of 2.4 mm is used in the analysis, and the samples get thinned due to mechanical loading during testing. Hence, it can be assumed that an approximately isothermal condition during testing can be achieved almost instantly.

Tissue-like phantom experiment for system validation

Since the constitutive response and strain rate sensitivity of silicone rubber is close to that of skin^[22], it is considered as an in-vitro model for skin. Silicon rubber Sil8800¹⁾ is used here to validate the current system in view that a model for its constitutive response has been obtained by the previous study in our lab^[1]. The system can thus be validated by comparing the measured results from the current system with the predictions of the constitutive model. Square specimens of similar dimensions with skin samples to be tested (approximately 20 mm by 20 mm and thickness 2.0 mm) are cut from silicone rubber sheets using a leather die punch mounted onto a hand press. The biaxial tensile stress versus strain responses are measured at two strain rates of 1%/s and 10%/s. Three tests are conducted for each silicone rubber sample and the average response is calculated. The measured tensile stress versus strain responses of Sil8800 silicone rubber are shown in Figure 10.7 and a good agreement has been achieved between the measurement and model prediction, which indicates the validity of the current system.

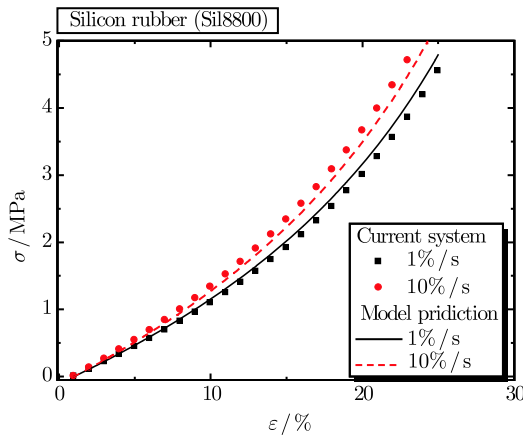


Figure 10.7 Validation of the current system: comparison of biaxial tensile results with the prediction of model from Shergold et al.^[1]

3) Hydrothermal tensile test procedure

In biaxial testing, a square specimen (rectangular for uniaxial tests) is

1) Sil8800 (Red, 80 IRHD) is supplied by Superior Seals (Wimborne, Dorset).

attached to each of the four loading assemblies (two for uniaxial test) by a self-designed holding system, as described in Section 10.4, across two perpendicular axes to allow physiological movement. A valve in the test chamber is opened to allow the hot KHR liquid or cold KHR liquid to fill the experimental tank, and the sample is fully immersed in the liquid. The thermocouple near the sample is used to inform the PC software of the exact time at which experiment begins. To minimize the temperature gradient at sample surface, the liquid is circulated continuously. A load is applied to the skin sample either by the pulley/weight system or by the motor/drive system. The applied displacement and loads are recorded, along with the time of measurement, relative to the start of the experiment. Each test is repeated three times with three different samples and the averaged values are used.

4) Hydrothermal relaxation test procedure

Skin is a viscoelastic material. Previous studies of the viscoelasticity (time/frequency dependence) of skin tissue reveal that its stress-strain relationship depends on the strain rate, the period of loading and on the preconditioning stress history, or, in other words, the stress at any instant of time depends not only on the strain at that time, but also on the history of deformation. Skin tissue exhibits considerable stress relaxation under constant strain, creep under constant stress, as well as hysteresis in cyclic tests^[23~37]. Stress relaxation implies that when the tissue is suddenly extended and maintained at its new length, the stress required to keep it gradually decreases slowly against time. Creep means that when the tissue is suddenly submitted to a constant tension, it continues to stretch as long as the stretching force is applied (within safe limits of circulation and tissue tearing). Hysteresis implies that, under cyclic loading, the stress-strain curve of skin shows two distinct paths corresponding separately to the loading and unloading trajectories.

As for viscoelasticity, although other collagenous tissues such as cartilage^[23~37] and bone^[38,39] have been studied in detail, however, there are comparatively few studies of the thermal denaturation of skin tissue and to the author's knowledge, there is no published study on temperature dependency of skin viscoelasticity, despite skin dermis being mainly composed of collagen.

The viscoelastic properties of skin tissue are usually characterized by two classic experimental tests, either a stress relaxation test or a creep test. These are static methods: stress relaxation test involves stretching/compressing a sample to a constant strain level and then allowing the stress to vary with

time, while a creep test involves subjecting a sample to a constant stress suddenly while the length gradually increases with time. A uniaxial stress-relaxation test is adopted in this study, where the stress relaxation test is conducted with two protocols. First, the stress relaxation is performed for different strain levels (10%, 30% and 50%) with a high loading speed ($\dot{\gamma} = 50\%/s$) in order to study the effect of strain level on relaxation and to check the validity of the assumptions of QLV for the skin samples tested here: at low levels of strain, the mechanical behaviour is mainly due to the role of elastin^[40,41] which has been shown to be temperature-stable^[42,43]; but the loads are too small relative to the noise level^[44], and high strain levels are adopted. In the second protocol, the tissue samples are stretched to 1.5 times their initial length (a strain of 50%) at a low loading speed of 1%/s, and the displacements of the samples are then kept constant while the time histories of the force are recorded for a time period of 500 s. As before, each test is repeated three times with three different samples and the averaged values are used.

10.2.4 Hydrothermal compressive tests

1) System design

A hydrothermal compressive system has been designed and built to study the thermomechanical behaviour of skin tissue under compression, and is schematically shown in Figure 10.8.

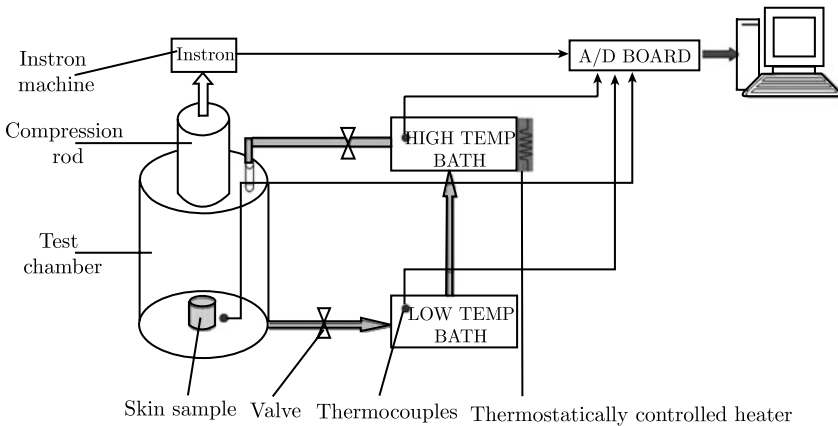


Figure 10.8 Schematic of the hydrothermal compressive experimental system (by permission of World Scientific Publishing Co.)

The cylindrical skin sample is placed at the bottom of a cylindrical test chamber filled with KHR solution. The chamber temperature is controlled by a circulation system similar to the hydrothermal tensile system. The temper-

ature of the KHR solution in the test chamber is measured by a T-type thermocouple, which is placed approximately 0.5 mm away from the skin sample surface. An axial compressive load is applied to the sample through a compression indenter that is connected to an InstronTM materials testing machine (5500R), operating under the MerlinTM software. Longitudinal strain measurements are made with a linear variable displacement transducer (LVDT) and an Electronic Instrument Research Ltd laser extensometer (LE-05) using two strips of retroreflective material glued in the compression platens. All load cells, thermocouples and laser extensometer signals are logged by a PC using an ADC board, as before.

2) Hydrothermal compressive test procedure

Only when friction is negligible, can one assume that the sample expands uniformly during compression and, that the state of deformation within the sample is orthogonal. Therefore a lubricant¹⁾ is applied to the faces of the specimen before loading to reduce friction between the specimen and the compression platens.

In the unconfined compression tests, the cylindrically-shaped samples, of diameter 10 mm and thickness 2 ~ 5 mm, are compressed between two impermeable, smooth platens, allowing the samples' freedom to expand laterally during compression. The top platen is driven down until it just touched the top surface of the specimen. Similar to tensile testing, the liquid in the high temperature reservoir is heated to a chosen temperature, while the low temperature reservoir contained cold liquid. A valve in the test chamber is opened to allow the hot or cold liquid to fill the test chamber until the sample is fully immersed in the liquid, while a thermocouple near the sample is used to inform the software of the exact time at which the experiment started. A force is applied to the skin sample by the compression indenter and the applied displacement, strain, and loads are recorded. As before, each test is repeated three times with three different samples and the averaged values are used.

10.3 Thermal Denaturation of Collagen in Skin Tissue

10.3.1 DSC test procedure

In this study, the thermal stability of collagen in pig skin sample is assessed with a TA Instruments DSC of type Q1000 T_{zero}²⁾, scanning from 20 to 100°C

1) Vaseline by Johnson.

2) In the Polymer Characterization Laboratory, in the Department of Materials Science and Metallurgy, Cambridge University.

at four different heating rates ($r_h = 2^\circ\text{C}/\text{min}, 5^\circ\text{C}/\text{min}, 10^\circ\text{C}/\text{min}, 20^\circ\text{C}/\text{min}$). The skin sample, of about 8 mg in weight, is put inside a hermetically sealed pan, which is kept away from all contamination. The pan is then placed in a differential scanning calorimetric cell and heating is applied at a constant rate, r_h . The controlled heating-rate protocol is chosen for it needs comparatively much fewer specimens than temperature-jump tests^[45,46].

10.3.2 DSC test results

A typical DSC thermogram¹⁾ of a skin sample from pig flank is shown in Figure 10.9.

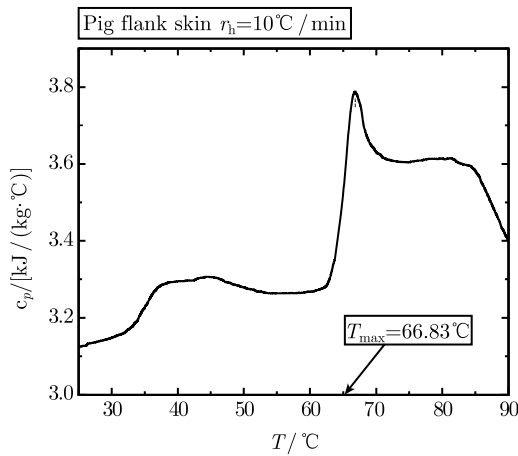


Figure 10.9 Characteristic DSC thermogram, i.e., variation of specific heat with temperature, of a skin tissue sample: the temperature corresponding to the peak is 66.83°C

The measured specific heat capacity falls in a range comparable to current data in the literature^[18]. The result of Figure 10.9 demonstrates that, for a stress-free skin sample subjected to temperatures in the range of $30 \sim 90^\circ\text{C}$, a broad endothermal²⁾ peak appears: denaturation is characterized by a sudden increase in the energy absorption, which immediately precedes this peak, starting at about 60°C . With further heating, the endotherm reaches its maximum value at the denaturation temperature of 66.83°C and then decreases. It is known that the temperature of thermal denaturation strongly depends on the water content in collagen (e.g., it has been found that there is an

1) Data of DSC test are plotted as specific heat against temperature, which is called a thermogram.

2) In thermodynamics, endothermal describes a process or reaction that absorbs energy in the form of heat.

increase of the rate of shrinkage, and hence denaturation, with increased hydration at a given temperature^[16,47], and on the degree of crosslinking between the chains^[48]. The peak in Figure 10.9 is connected with the transition of collagen structure from the ordered triple helix form to a randomly coiled conformation in the domains between crosslinks.

It has also been observed that the characteristics of denaturation are heating-rate dependent (not shown here for brevity), where the maximum value of the peak at higher heating rates moves towards higher temperatures. If a collagenous tissue is heated from an initial value at a constant heating rate, r_h , the rate of the decline in the number of native molecules with time follows the first order kinetics¹⁾, given by^[49]

$$T = T_i + r_h t \quad (10.1)$$

$$dN/dt = -k(T)N \quad (10.2)$$

where T_i is the initial tissue temperature; N is the molecules of native, or undenatured, collagen in the tissue; T is the current tissue temperature; $k(T)$ is the usual reaction rate. Combining Equations (10.1) and (10.2) results in

$$\frac{1}{N} \frac{dN}{dT} = -\frac{k(T)}{r_h} \quad (10.3)$$

This equation predicts that the maximum of $-dN/dT$ can be obtained when

$$\frac{d^2 N}{dT^2} = 0 \Rightarrow \frac{d}{dT} \left[\frac{k(T)}{r_h} N \right] = 0 \Rightarrow N \frac{dk(T)}{dT} + k(T) \frac{dN}{dT} = 0 \quad (10.4)$$

When combined with the Arrhenius equation [see Equation (3.35) from Chapter 3]

$$k(T) = A \exp \left(-\frac{E_a}{RT} \right) \quad (10.5)$$

the relation between Arrhenius parameters (E_a , A) and the peak temperature of thermal denaturation (T_{\max}) can be obtained as

$$\frac{r_h E_a}{A R T_{\max}^2} = \exp \left(-\frac{E_a}{R T_{\max}} \right) \quad (10.6)$$

Equation (10.6) can be rewritten as

$$\ln \frac{r_h}{T_{\max}^2} = -\frac{E_a}{R} \frac{1}{T_{\max}} - \ln \frac{E_a}{R} + \ln A \quad (10.7)$$

1) A term describing the reaction rate of a chemical reaction in which the rate is proportional to the concentration (in moles) of only one of the reactants.

The activation energy E_a can be obtained from a ln-ln plot of $\ln(r_h/T_{\max}^2)$ versus $1/T_{\max}$, while A can be derived through the intercept. With these results, the thermal damage and the degree of thermal denaturation of skin collagen for a given heating history can be quantified with Equation (3.34), respectively. It should be noted here that the thermal denaturation of a collagenous tissue depends not only on the temperature history but also on the stress state during heating^[50~52], which is, however, very difficult to quantify due to the lack of corresponding research. Therefore, in the following calculation of thermal damage the parameters obtained from DSC measurements in the absence of mechanical loading are used.

A characteristic plot of $\ln(r_h/T_{\max}^2)$ versus $1/T_{\max}$ for pig flank skin sample is presented in Figure 10.10. Tests with belly, back, ear and face skin samples have also been performed and the results of derived Arrhenius parameters are presented in Table 10.2. As shown in Chapter 3, there is a linear relationship between the published experimental result of Arrhenius parameters $\ln A$ and E_a for skin tissue, as given by Equation (10.7). The comparison

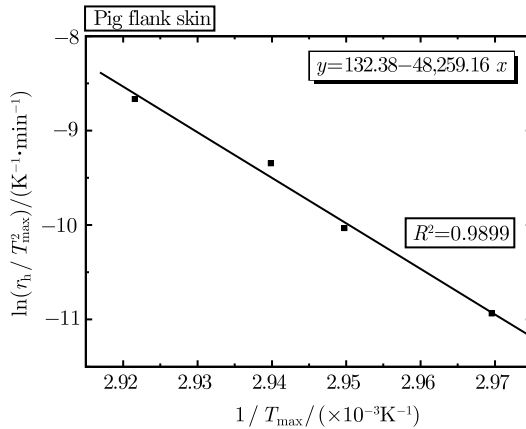


Figure 10.10 Characteristic plot of $\ln(r_h/T_{\max}^2)$ versus $1/T_{\max}$ for pig flank skin tissue: dots are experimental data; line is the best fit line by least squares; also indicated is the equation of fitted line with x for $1/T_{\max}$ and y for $\ln(r_h/T_{\max}^2)$.

R^2 value represents the scatter of data along the line of best fit

Table 10.2 Experimental results of Arrhenius parameters (E_a, A)

Sample	$E_a / (\times 10^5 \text{J/mol})$	A / s^{-1}
Back skin	5.255	2.126×10^{81}
Belly skin	3.935	1.151×10^{61}
Ear skin	5.867	5.240×10^{91}
Face skin	4.710	4.575×10^{72}
Flank skin	4.012	1.501×10^{61}

of the results here for different pig skin samples with results calculated from Equation (10.7) has been presented in Figure 10.11, where it can be seen that a very good agreement has been achieved.

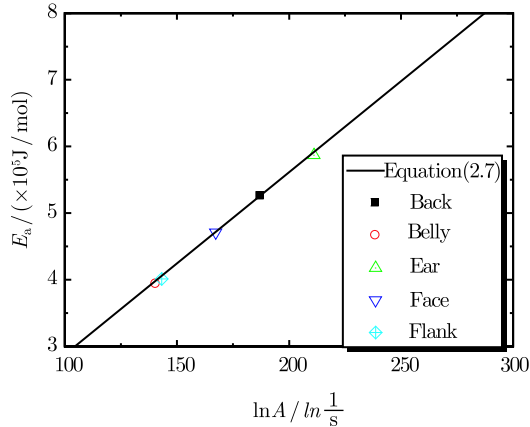


Figure 10.11 Comparison of the results of Arrhenius parameters of this study with literature results.

10.4 Hydrothermal Tensile Tests

The hydrothermal tensile tests, which enable the variation of temperature to be applied during mechanical tests, are performed to quantify the effects of temperature and corresponding thermal denaturation on the tensile behaviour of skin tissue.

10.4.1 Uniaxial tests

A typical uniaxial tensile behaviour of pig ear skin sample measured at $T = 37^\circ\text{C}$ is shown in Figure 10.12 (black dots).

Note that skin has a low stiffness at low strains but undergoes significant strain hardening at high strain level. This J-shaped stress-strain curve is typical for mammalian skin, although the strain hardening characteristic varies from specie to specie. In the Figure 10.12, the uniaxial tensile stress-strain responses of human chest skin^[55] and cat back skin^[54] are also shown for comparison. It is interesting to find that the uniaxial tensile behaviour of pig ear skin obtained in this study agree well with that of human skin. This is, however, not unexpected in view that pig ear skin is selected purposely for tensile tests due to its high similarity with human skin tissue^[55] as described in Section 10.2.1. Compared with pig ear skin and human chest skin, cat back skin strain hardens at a faster rate.

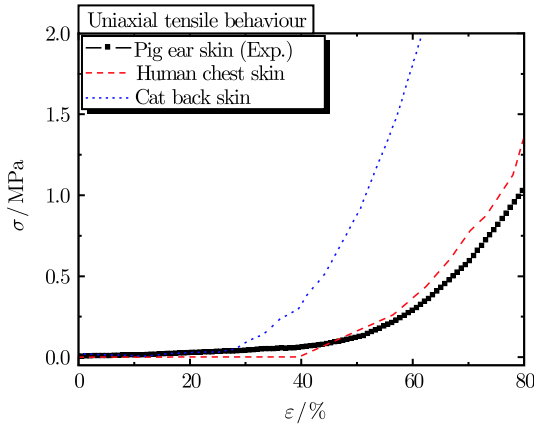


Figure 10.12 Comparison of the uniaxial tensile behaviour of pig ear skin measured at $T = 37^{\circ}\text{C}$ with reported data on human chest skin^[53] and cat back skin^[54] (by permission of ASME)

Uniaxial tensile tests of pig ear skin samples under different temperatures have been performed and the stress-strain relationships are given in Figure 10.13: a good repeatability has been noted for three same tests and a single averaged response is shown.

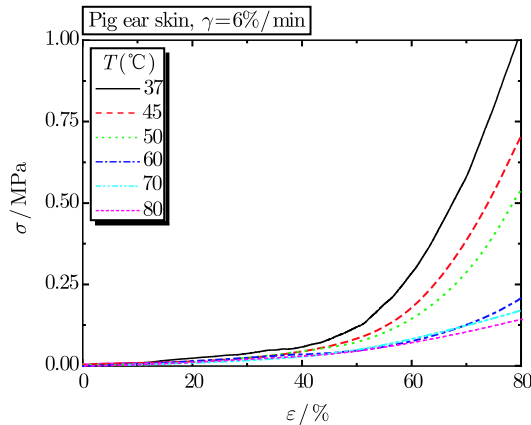


Figure 10.13 Stress-strain relation of uniaxial hydrothermal tensile tests under different temperatures: γ is the strain rate at which tests are performed

As described above, there are also two behaviour regimes for all the curves. First, when $\varepsilon < 50\%$, the curves almost overlap although the data set is swamped by larger values. This low modulus region is very thermally stable due to the dominance of elastin in the skin behaviour and there is gradual straightening of an increasing fraction of the wavy collagen fibers and

stretching of elastic fibers. When $\varepsilon > 50\%$, the stress increases almost linearly with strain; and the slopes under different temperatures are different, and reduce with increasing temperature. This effect is due to the stretching and slippage of collagen molecules within crosslinked collagen fibers and to collagen fibril slippage: with an increase in temperature, the highly organized crystalline structure of collagen changes to a random, gel-like state, which results in the corresponding decrease in stiffness. Furthermore, the hydration change with temperature may also make a contribution. Water plays a significant role in governing the gross properties of skin tissue^[7], which consist primarily of water. However, due to heating, the level of hydration may vary, e.g., Luescher et al.^[56] suggested that primary hydration water is set free during the process of thermal denaturation. It should be noted that when $T \geq 60^\circ\text{C}$, there is relatively little change in the modulus with temperature, which can be explained by the thermal damage process: when the strain rate and temperature are given, the relationship between the strain and thermal denaturation degree (Deg) calculated according to the heating history can be obtained, as shown in Figure 10.14.

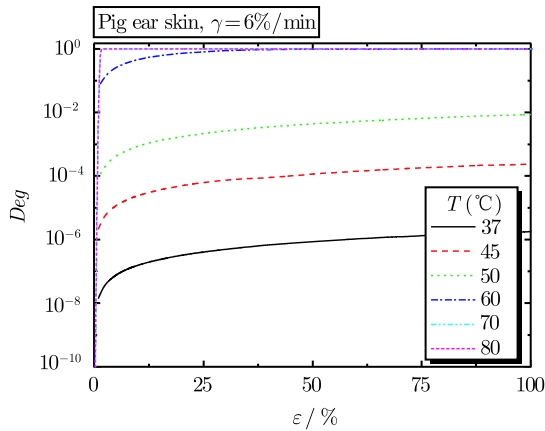


Figure 10.14 Strain-thermal damage degree (Deg) relation of hydrothermal tensile tests under different temperatures: Deg is obtained from Equation (3.41) with given heating condition and strain rate. Figure 10.14 shows that when $T \geq 60^\circ\text{C}$, the collagen is fully denaturated, while at $T = 45^\circ\text{C}$ and 50°C , denaturation is much slower

10.4.2 Biaxial tests

The biaxial tensile behaviours of the skin samples are tested at 37°C and 60°C . The stress-strain relationships measured for samples from different

body sites are given in Figure 10.15.

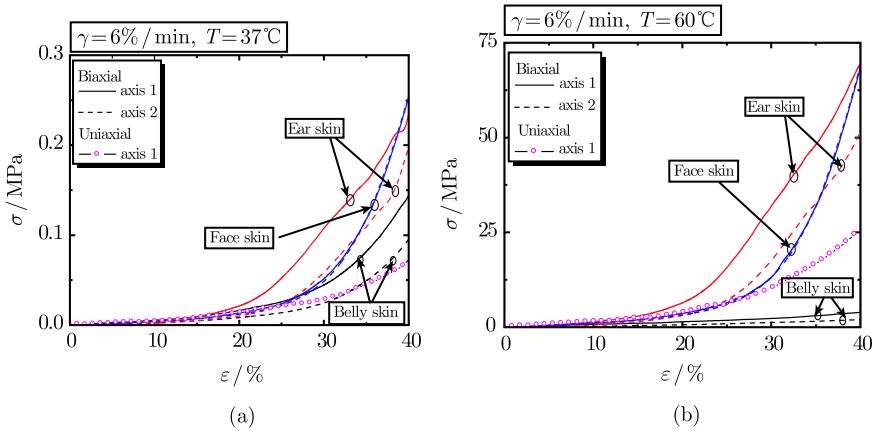


Figure 10.15 Stress-strain relation of biaxial hydrothermal tensile tests for samples from different sites at (a) $T = 37^\circ\text{C}$ and (b) $T = 60^\circ\text{C}$: axis 1 (solid lines) and axis 2 (dashed lines) are material axes identified with the equal-load method as described in Section 10.2.3; scattered points are experimental results from uniaxial tests

An interesting result can be observed from the figure: only the skin tissue from porcine cheek appears to be abnormal in the fact that the curves for the two different axes overlap each other. This means that it has an equal distribution of collagen/elastin fibres across both axes of a square, independent of the cutting angle. This discovery may allow the series of experiments on skin tissue to come to fruition since a uniform stress distribution in the tissue can be easily achieved even in biaxial tests. However, this observation is abnormal since it is well known that clear Langer's lines¹⁾[57] have been observed for face skin tissue^[56]. Compared with that under body temperature, skin's stiffness under hyperthermal temperature decreases a lot. This feature is due to the similar reasons as those in uniaxial results described above.

In Figure 10.15, the uniaxial tensile behaviours of pig ear skin samples (dots) obtained under the same strain rate and heating conditions have also been given for comparison. Agreed with the observation in the literature, as described in Section 10.4.1, biaxial tensile loading, compared with uniaxial stretch, results in the lateral compression of the stress-strain curve and the reduction in the strain before entry into the linear region occurs, which is

1) Langer's lines, sometimes called cleavage lines, is a term used to define the direction within the human skin along which the skin has the least flexibility. These lines correspond to the alignment of collagen fibers within the dermis.

due to the two-directional stretch of collagen fibers.

10.5 Hydrothermal Compressive Tests

Almost all of the previously published mechanical models of skin tissue are based on experimental data under tension, although *in vivo*, skin tissue is often subjected to compressive loading by different agents. The goal of the present section is to study the relationship between temperature, thermal damage and the corresponding change in the compressive behaviour of skin tissue.

10.5.1 Model of skin compressive behaviour

It has been assumed that the compressibility is negligible in the constitutive models of skin tissue^[57], which is considered reasonable in view of its similar behaviour to other natural polymers, such as rubber. Von Gierke^[58] found that human skin tissue had a volume compressibility of $0.38 \text{ m}^2/\text{GN}$ and North & Gilbson^[59] obtained a similar value of $0.30 \text{ m}^2/\text{GN}$, which is less compressible than water^{1)[60]}. These results suggest that skin tissue is extremely difficult to compress in a constrained condition and thus the assumption of incompressibility is valid and Poisson's ratio is equal to 0.5. Based on the experimental results of North & Gilbson, Vossoughi & Vaishnav^[59,61] calculated the shear modulus as well as the bulk modulus of skin tissue. They found that the latter is $2 \sim 3$ orders of magnitude higher than the shear modulus, and thus argued that in analytical and experimental investigations of skin mechanics, the skin tissue can be safely considered as incompressible. More recently, Wu et al.^[62] found that pig skin tissue under compression is compressible but only marginally.

Skin tissue is also anisotropic even when relaxed^[62]. However, observations of anisotropy are generally based on tensile behaviour where anisotropy refers to plane parallel to skin surface, while the compression is through thickness and the assumption of isotropy is reasonable. Besides, the anisotropy is found to be also site dependent, where in back skin tissue, as used in this study, the anisotropy has been found to be low; Ankersen et al.^[63] even found that the anisotropy of pig back skin tissue was negligible. In the following, the compressibility of skin tissue is ignored and skin tissue is assumed to be isotropic.

1) The compressibility of water is a function of pressure and temperature: at 25°C in the limit of zero pressure the compressibility is $0.46 \text{ m}^2/\text{GN}$.

Based on previous observation of isotropy in the planar directions with anisotropy in the thickness direction^[63].

1) Ogden model

Under assumptions of incompressibility and isotropy, it is reasonable to simulate the elastic behaviour of skin tissue under compression using a hyper-elastic model for rubber-like materials. This model is traditionally formulated using a strain energy function based on invariant quantities. In this study, the Ogden strain energy density function is adopted, which is more accurate in fitting experimental results when multiple experimental tests data are available, and which has been used satisfactorily to describe the mechanical behaviour of skin tissue^[64~67]. The Ogden strain energy potential function, U , is expressed in the form

$$U = \sum_{i=1}^N \frac{2\mu_i}{\alpha_i^2} [\bar{\lambda}_1^{\alpha_i} + \bar{\lambda}_2^{\alpha_i} + \bar{\lambda}_3^{\alpha_i} - 3] + \sum_{i=1}^N \frac{1}{D_i} (J - 1)^{2i} \quad (10.8)$$

where $J = \lambda_1 \lambda_2 \lambda_3$ is the volumetric ratio, $\lambda_i (i = 1, 2, 3)$ are the principal stretch ratios equal to the current length/initial length in a given direction; $\bar{\lambda}_i = J^{-1/3} \lambda_i$ are the deviatoric principal stretches; α_i are the exponential parameters; μ_i are shear parameters; D_i are the bulk parameters; N is the number of terms needed to fit to the experimental data satisfactorily.

2) Identification of material constants

The principal nominal engineering stresses, $\sigma_i (i = 1, 2, 3)$, are work-conjugate to the principal stretch ratios $\lambda_i (i = 1, 2, 3)$. With the assumption of skin incompressibility, σ_i can be obtained from the given strain energy density function $U(\lambda_i)$, as

$$\sigma_i = \frac{dU}{d\lambda_i} - p \quad (10.9)$$

where p is a hydrostatic pressure.

In this study, the skin sample is considered to be in a state of plane stress during uniaxial unconfined compression. For a Cartesian coordinate system, with the z -axis aligned with the loading direction, the stresses in the x and y directions are zero ($\sigma_x = \sigma_y = 0$), and thus one can find p in terms of λ_i and σ_z . Furthermore, incompressibility demands that $J = 1$ and that the principal stretch ratios are related by

$$\lambda_x = \lambda_y = \frac{1}{\sqrt{\lambda_z}} \quad (10.10)$$

Substitution of Equations (10.9) and (10.10) into the Ogden strain energy density function of Equation (10.8) leads to the following stress-stretch rela-

tionship:

$$\sigma_z = \sum_{i=1}^N \frac{2\mu_i}{\alpha_i} (\lambda_z^{\alpha_i-1} - \lambda_z^{-1-\alpha_i/2}) \quad (10.11)$$

The identification of material parameters (α_i, μ_i) is achieved by minimizing the function, ϕ , of the difference between the experimentally obtained data, σ_z , and the model prediction, $\hat{\sigma}_z$, using a nonlinear optimization algorithm in MATLAB¹⁾, where ϕ is given by

$$\phi = \sum \left(\frac{\sigma_z - \hat{\sigma}_z}{\sigma_z} \right)^2 \quad (10.12)$$

10.5.2 Typical example of compressive test and fitting with Ogden model

A representative compressive stress-strain response at a strain rate $\gamma = 24\%/min$ ²⁾ is presented in Figure 10.16(a). The relationship exhibits a consistent three-stage hardening of a toe region with low stiffness at low strain levels, a transition region from low to high stiffness, and a high stiffness region at large strain levels. The results are comparable to the published compressive behaviour of pig back skin tissue obtained at similar strain rate ($\gamma = 25\%/min$)^[1,5,28,62,68], as shown in Figure 10.16 (a).

Compared with the mechanical characteristics of skin tissue in uniaxial tension, the compressive stress/strain curves are similar in trend; however, the transition from low to high stiffness in uniaxial tension occurs mostly at a strain level of 40% ~ 60%^[70], which is much larger than that in compression (20% ~ 30%) as observed in the results here [see Figure 10.16(b)]. Similar results have also been reported elsewhere for pig back skin tissue^[54,57,69]. Wu et al.^[70] observed a transition at an even lower strain level of 4% ~ 5% for confined compression and 6% ~ 7% for unconfined compression: the difference is because the fat layer is removed in this study. However, compared with biaxial tensile behaviour of pig back skin obtained by Ankersen et al.^[63], the compressive behaviour obtained in this study shows a slower rate of strain hardening, as shown in Figure 10.16(b). This is mainly due to the different testing environments adopted: in current study all the tests were performed in liquid (KHR), while the tests of Ankersen et al. were performed in air environment. Testing in the air will induce the decrease of the hydration and humidity of the samples, which have been shown to increase the stiffness of skin tissue^[63].

1) Version 6.5.1, The Mathworks, Natick, MA, USA.

2) This strain rate is chosen for a better comparison with data reported in the literature.

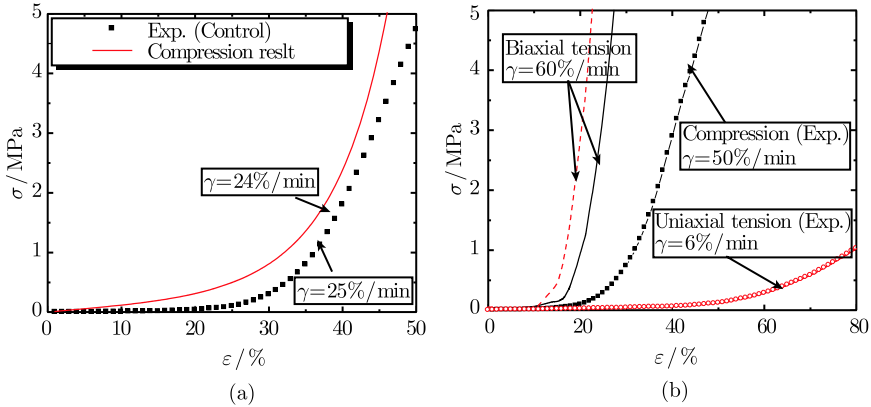


Figure 10.16 Representative stress-strain responses from a compressive test (solid dots) and comparison between the compression results (a) with published compressive behaviour^[1], and (b) with uniaxial tensile behaviour (circle dots) obtained in this study and published biaxial tensile behaviour of pig back skin tissue^[1] (by permission of World Scientific Publishing Co.)

Figure 10.17(a) and (b) present the fitting of the measured constitutive response of skin samples from control groups¹⁾ in compression under body temperature to the Ogden model of Section 10.4.2. Shergold et al.^[1,5,22] showed that the one-term Ogden model is good enough for describing the compressive behaviour of skin tissue in a large strain rate range of $4 \times 10^{-3} \sim 4 \times 10^3 s^{-1}$, whereas Wu et al.^[70] used a three-term Ogden model to achieve

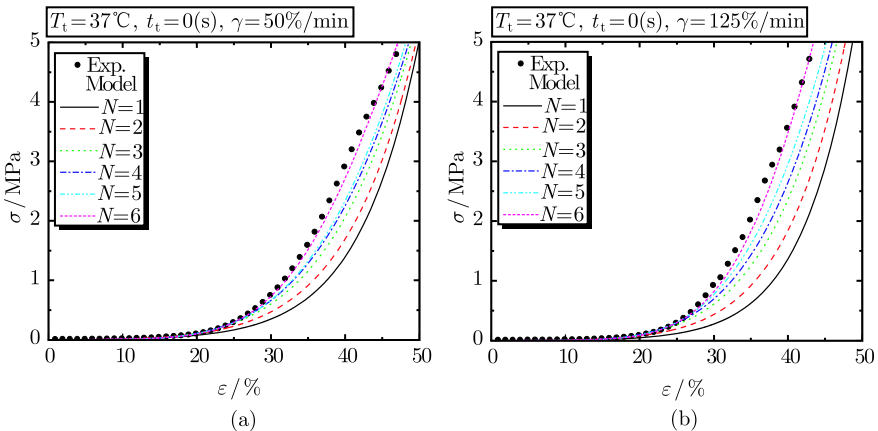


Figure 10.17 Typical Ogden fits to the measured constitutive response in compression of control skin tissue under strain rates of (a) $\gamma = 50\%/min$ and (b) $\gamma = 125\%/min$

1) Skin samples with no predamage as described in Chapter 3.

the best fit to their test data. However, it can be seen from the results here, a satisfying fit can only be achieved through an Odgen model with six terms, although Odgen models having less terms give a similar trend.

10.5.3 Temperature dependent compressive behaviour

The hydrothermal compressive tests of back skin tissue under different temperatures have been performed and results are given in Figure 10.18.

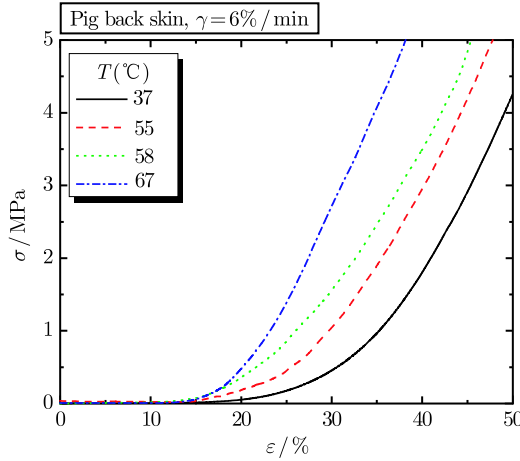


Figure 10.18 Stress-strain relation of hydrothermal compressive tests under different temperatures

It is interesting that, contrary to the tensile tests of Section 10.3.2, the compressive stiffness increases with increasing temperature although the thermal damage degree also increases, as shown in Figure 10.19.

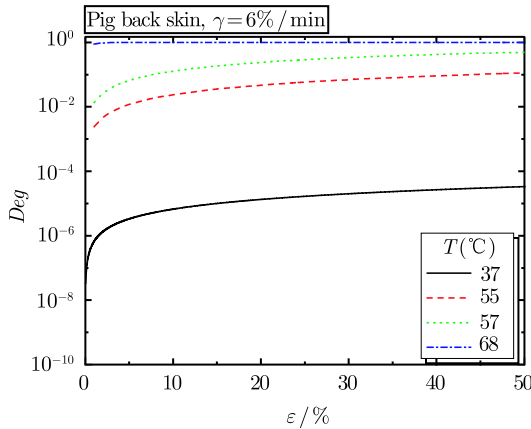


Figure 10.19 Strain-thermal damage degree relation of hydrothermal compressive tests under different temperatures

One key difference is that the compressive tests are performed in a direction normal to the principal orientation of collagen and elastin fibers. Even though there exists denaturation of collagen, which appears in the tensile tests, the compressive behaviour is governed by the mechanical properties of the gel-like ground substance, inside which the fibers are located^[62]. Very little is known about the mechanical properties of this substance; it can only be speculated that its stiffness increases with increasing temperatures.

In order to characterize the temperature effect on skin mechanical behaviour and compare their characteristics under different testing methods, a procedure is proposed here to obtain the modulus of skin sample at low (E_l) and high (E_h) strain levels, as shown in Figure 10.20: the strain-stress curve is treated as a bi-linear line, the tangents at low and high strain levels are then obtained, and E_l and E_h are defined as the slope of the two tangents. The variations of E_l and E_h with temperatures for tensile and compressive behaviours are given in Figure 10.21(a) and (b), respectively. While E_l for tensile behaviour of skin tissue doesn't change much with temperature, E_h decreases almost linearly with increasing temperature until about 60°C, after which it decreases little. E_h for tensile behaviour obtained here (0.3 ~ 4.5MPa) also agrees well with the published *in vitro* measurements of Young's modulus for animal skin tissue, e.g., cat skin (0.5MPa)^[71,72], rat skin (1.18 ~ 4.62MPa)^[55]. Compared with that for tensile behaviour, E_h for compressive behaviour increases with temperature and is much higher (28 ~ 54MPa). This is due to: ① the different mechanism of tensile and compressive behaviours as discussed above; ② different skin samples used for tensile (pig ear skin) and compressive (pig back skin) testing, where regional difference of skin mechanical behaviour has been observed by many researchers^[73,74].

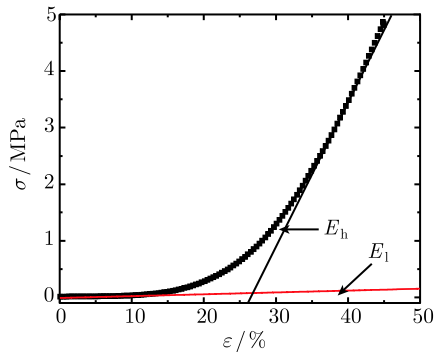


Figure 10.20 Method for calculating the moduli at low (E_l) and high (E_h) strain levels

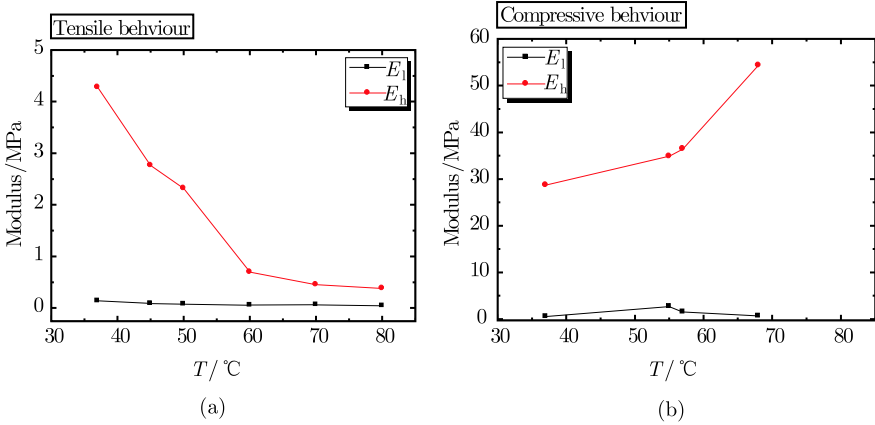


Figure 10.21 Variations of the moduli at low (E_l) and high (E_h) strain levels with temperatures for (a) tensile behaviour and (b) compressive behaviour

10.5.4 Thermal damage-induced changes in compressive behaviour

In order to separate reversible changes from irreversible ones and to study the influence of thermal denaturation on skin properties, some skin samples are thermally denatured before testing (predamaged). Using the Arrhenius parameters (E_a , A) of pig skin tissue from the DSC analysis, different heating temperatures, T_h , and durations, t_h , are chosen to induce damage in skin sample to a specified degree. In all, 22 groups of samples are prepared, with groups 1 ~ 4 having no predamage and used as control groups. Details of each group are given in Table 10.3.

Table 10.3 Details of pre-damaged samples

Sample Group No.	$T_h/^\circ\text{C}$	t_h/s	Ω	Deg	$r/(\%/min)$
1	37	0	0	0	25
2	37	0	0	0	50
3	37	0	0	0	125
4	37	0	0	0	250
5	55	12	0.0579	0.0563	25
6	55	12	0.0579	0.0563	50
7	55	12	0.0579	0.0563	125
8	55	12	0.0579	0.0563	250
9	65	1	1.44	0.762	25
10	65	1	1.44	0.762	50
11	65	1	1.44	0.762	125
12	65	3	4.31	0.987	25
13	65	3	4.31	0.987	50
14	65	3	4.31	0.987	125
15	65	30	86.2	1	25
16	65	30	86.2	1	50

						Continued
Sample Group No.	$T_h/^\circ\text{C}$	t_h/s	Ω	Deg	$r/(\%/min)$	
17	70	10	219	1	25	
18	70	10	219	1	50	
19	70	5	109	1	25	
20	70	5	109	1	50	
21	70	18.5	405	1	25	
22	75	10	3081	1	25	

Figure 10.22(a)~(c) presents the thermal-damage-induced changes in skin compressive behaviour at three different strain rates ($\gamma = 25\%/min, 50\%/min,$

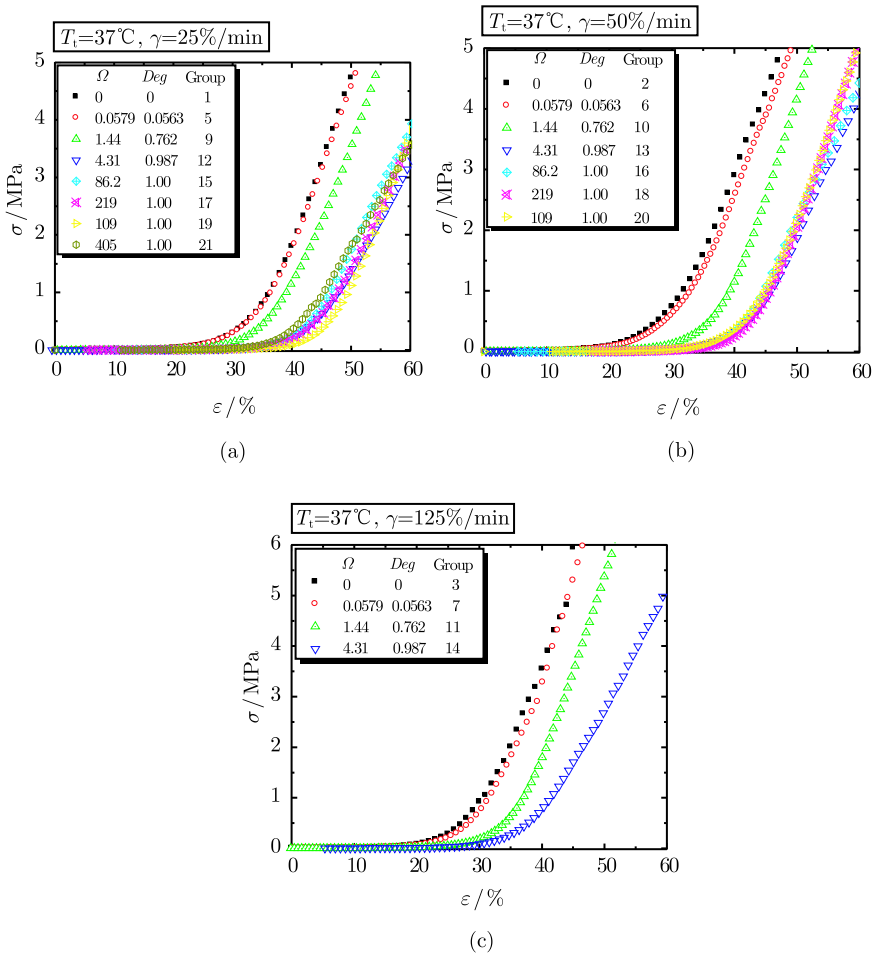


Figure 10.22 Effect of thermal denaturation on skin compressive behaviour at different strain rates of (a) $\gamma = 25\%/min$, (b) $\gamma = 50\%/min$, and (c) $\gamma = 125\%/min$ (by permission of World Scientific Publishing Co.)

125%/min). The results at all three strain rates exhibit a clear trend of curve shifting towards the right with increasing damage. When the damage degree (*Deg*) has a value near unity, implying that the collagen is fully denaturated, there is little difference between curves: the stiffness of skin tissue decreases with increasing degree of thermal damage, which is reasonable; and increased extensibility of soft tissues due to thermal treatment has been observed in both uniaxial^[24,75~79] and biaxial tensile testing^[80~82] of skin tissue.

There are several possible mechanisms for explaining why the thermal damage changes the compressive behaviour of skin tissue. The first one is the hyperthermal-temperature-induced thermal denaturation of dermal collagen. It has been suggested that collagen may play an important role in determining the overall mechanical properties of skin tissue^[83,84], and thus it seems reasonable to assume that collagen would play a major role in the compressive behaviour of skin tissue. However, this cannot be the principal reason since the compressive tests are performed normal to the principal orientation of collagen. Another possible mechanism is the dehydration change accompanying thermal damage as well as rehydration during thermal recovery process after heating. It is known that there can be an inward or outward flux of interstitial fluid due to the heating of a soft tissue^[85], and the compressive behaviour is governed by the mechanical properties of the gel-like ground substance, inside which the fibers are located^[53]. Luescher et al.^[56] and Hörmann & Schlebusch^[86] suggested renaturation, or reformation of some of the triple-helix structures, occurs after heating, which involves the slow rebounding of primary hydration water to the amorphous protein and the formation of additional water bridges within the more disorganized molecule. A third possible mechanism is the viability of cells in the skin tissue, where specifically, Yip et al.^[87] found that the in situ fibroblast viability has great influence on the mechanical properties of rate back skin tissue.

It is interesting to note that Figure 10.22, compared to Figure 10.18, exhibits contradictory results: the compressive stiffness increases with increasing temperature even though the thermal damage and the degree of thermal denaturation also increase. It has been shown by others that the stiffness of skin tissue increases progressively in dehydration and decreases in over hydration under compression^[87]. In Figure 10.22, all the tests are performed with fresh samples at hyperthermal temperatures where only heat-induced dehydration occurs, whilst tests in Figure 10.18 are performed with predamaged samples at body temperature where the samples are rehydrated during the thermal recovery process of predamage procedure.

Test data from each specimen at different temperatures are fitted with the Ogden model and it has been established that a good agreement is achieved for all the data, but are not shown here for brevity. The material constants, α_i and μ_i , are instead plotted in Figure 10.23(a) and (b). For the one-term Ogden model, μ has the interpretation of shear modulus under infinitesimal straining while α serves as the strain hardening exponent. It is also expected that there is quantitative relationship between temperature and the constants in the multi-term Ogden model. However, no clear trend can be found from the results of Figure 10.23. This may be because there is no exact physical meaning for each constant appearing in the six-term Ogden model used in this study.

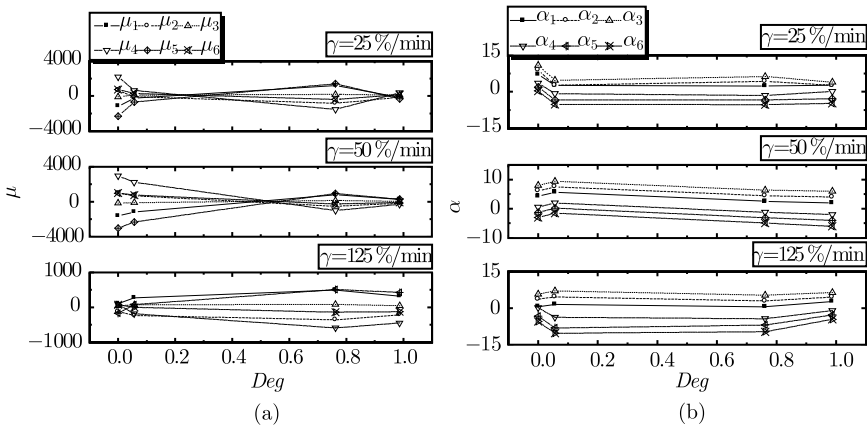


Figure 10.23 Effect of thermal damage degree on the constants of (a) μ_i and (b) α_i under three deterrent strain rates in the six-term Ogden model as described by Equation (6.11) (by permission of World Scientific Publishing Co.)

10.5.5 Strain rate sensitivity at different damage levels

The strain-rate sensitivity of pig skin tissue at four different damage levels is presented in Figure 10.24(a)~(d) for uniaxial compressive loads. A clear sensitivity emerges for all damage levels, where the skin tissue stiffens and strengthens with increasing strain rates. This feature mirrors results in the literature. For example, it has been observed by others that, under stretch-controlled tests, the overall stiffness of skin tissue decreases with decreasing strain rates^[70].

Since collagen fibers comprise bundles of collagen fibrils aligned parallel to a hyaluronic acid chain, and linked to the hyaluronic acid by proteoglycan side-chains, it is likely that the strain-rate sensitivity of skin tissue is

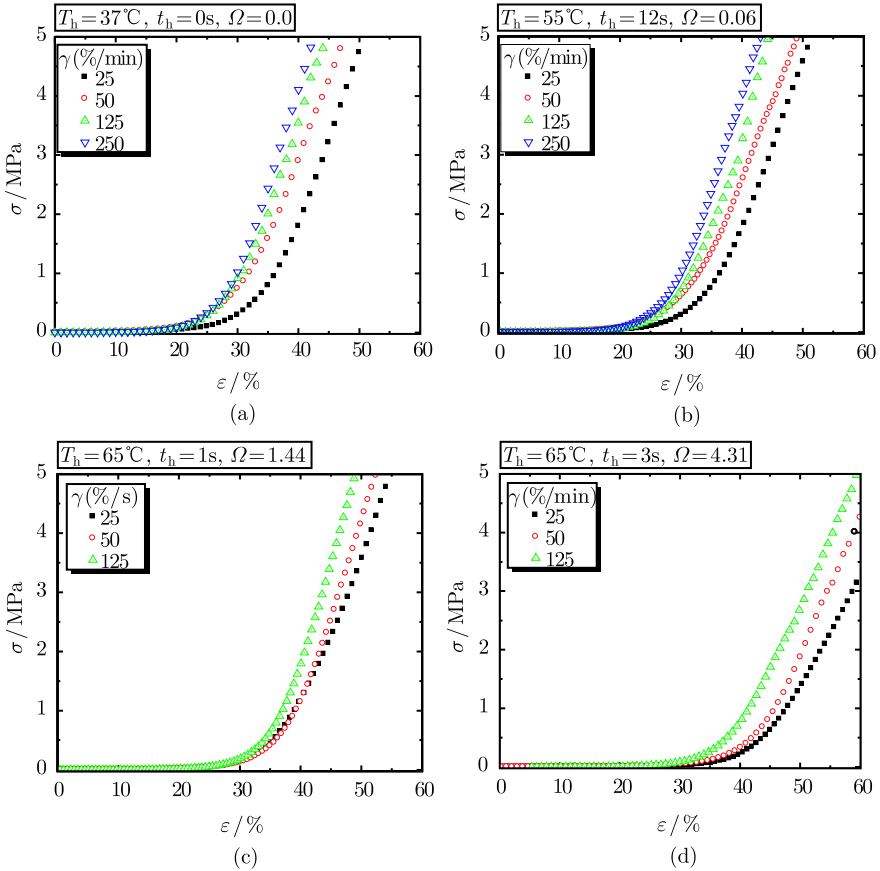


Figure 10.24 Stain-rate sensitivity at damage levels of (a) $\Omega = 0$, (b) $\Omega = 0.06$, (c) $\Omega = 1.44$, and (d) $\Omega = 4.31$. T_h and t_h are heating temperature and duration, respectively (by permission of World Scientific Publishing Co.)

attributable to viscous losses due to the interaction of ground substance with collagen fibers at the macroscopic scale^[1,57,88~92] as well as with collagen fibers at the microscopic scale^[93]. For example, much of the sensitivity to strain rate has been attributed to the uncoiling and aligning movement of collagen^[94], and Daly^[95] suggested that the strain-rate sensitivity of skin tissue occurred at all structure levels of collagen and was due in part to bonds between fibrils and fibers. However, the uncoiling and aligning movement of collagen should not be the main mechanism for the case here, since the compressive tests are performed through the skin thickness direction and a similar strain sensitivity has been observed at all damage levels. Thus the strain-rate sensitivity may be attributed to the variation of viscous interaction between collagen fibers and ground substance induced by hydration

change accompanying thermal damage. For example, the strain-rate sensitivity was well modeled by Shergold et al.^[1,5] by increasing the shear modulus with increasing strain rate, with no attendant change in the strain hardening exponent. Arurnugam et al.^[30] also attributed the higher stress to higher frictional force at higher strain rates. The movement of fluid in the hydrated matrix may also play an important role^[90].

10.6 Characterization of Skin Viscoelasticity with Static Tests

Skin tissue is a viscoelastic material. However, to the author's knowledge, there is no published study on the temperature dependency of skin viscoelasticity, although other collagenous tissues such as cartilage^[96] and bone^[38,39] have been studied in detail. The aim of the present section is to characterize the temperature-dependent relaxation behaviour of skin tissue. The hydrothermal relaxation test procedure using the system described in Section 10.4 is first described. A viscoelastic model for skin tissue is then developed based on quasi-linear viscoelastic (QLV) theory. Stress relaxation tests under different temperatures are performed, and results and discussion are presented.

10.6.1 Modeling

1) QLV theory

The time-dependent mechanical behaviours of soft tissues can be formulated using Boltzmann hereditary integrals^[40,41]. The nonlinear separable integral formulations are given as follows:

$$\sigma(t) = \int_0^t g(t - \tau) \frac{d\sigma_e[\varepsilon(\tau)]}{d\varepsilon} \frac{d\varepsilon(\tau)}{d\tau} d\tau \quad (10.13)$$

$$\varepsilon(t) = \int_0^t j(t - \tau) \frac{d\varepsilon_e[\sigma(\tau)]}{d\sigma} \frac{d\sigma(\tau)}{d\tau} d\tau \quad (10.14)$$

where t is time; τ is the dummy variable for time; $\sigma(t)$ and $\varepsilon(t)$ are stress and strain, respectively; $\varepsilon_e(\tau)$ and $\sigma_e(\tau)$ are the elastic strain and stress response, respectively; $g(t)$ and $j(t)$ are normalized creep and relaxation functions that only depend on time; $\sigma_e(\varepsilon)$ is the instantaneous elastic response, i.e., the maximum stress in response to an instantaneous step input of strain, while $\varepsilon_e(\sigma)$ is the elastic strain response. This form is also called QLV theory^[25,97], which was formulated by Fung^[25] and has been proven useful for describing the viscoelastic behaviour of different soft tissues such as skin^[98], ligament^[28,99,100], cartilage^[101~103] and tendon^[104,105].

The QLV theory was developed on the basis that the reduced relaxation function describes the normalized stress response of a sample in response to a step increase in strain such that the tissue has no time to relax during this loading process. This, however, is experimentally impossible. In order to isolate the nonlinear elastic properties of tissue from its viscous properties, relatively high rates have been used. However, with a high strain rate, it is technically difficult to obtain reliable instantaneous material parameters due to inertial effects and, thus, greater technical challenges must be overcome in the design of the testing machine and data acquisition system, especially for small tissue samples^[102,106,107]. Although several methods have been proposed to modify the analysis where finite ramp times are considered in order to better approximate solutions^[70], these methods are still dependent on fast ramp rates, and therefore, may be affected by the associated errors. One of the main problems is overshoot, followed by a rebound back to the target strain under high rates due to limitations in the mechanical testing equipment. This has been shown to have a considerable effect on the measured forces^[108,113] and to introduce an unwanted bias into the estimation of QLV parameters^[111]. For example, during stress relaxation of tendon, Gimbel et al.^[114] found that there was an average overshoot magnitude of 7.5% of the intended strain, causing an error as large as 30% of the estimation of QLV parameters when the overshoot is not accounted for in the data fitting process.

It has been recommended that a slow strain rate should be used in stress-relaxation tests^[114], since at low strain rate the actual strain history (variation of strain with time) can be well approximated by a linear ramp followed by holding at constant strain. Thus, the errors associated with fast strain rates (e.g., overshoot, vibration, poorly approximated strain histories) can be reduced or avoided^[114,115]. For instance, recent studies have shown that a slow ramp rate (0.15%/s) in conjunction with a direct fit for the ramp and stress-relaxation portions can provide an accurate estimation of parameters avoiding thus the errors associated with fast strain rates^[114,115]. In view of these, comparatively low strain rates have been used in the tests performed in this study.

2) Skin model development of based on QLV theory

An exponential approximation has been often chosen to describe the nonlinear elastic behaviour of skin tissue. Here, the following expression is used to describe the instantaneous elastic response:

$$\sigma_e(\varepsilon) = A(e^{B\varepsilon} - 1) \quad (10.15)$$

where A is a linear factor having the same dimension as stress; B is a non-dimensional parameter representing the nonlinearity of elastic response (rate of stress stiffening). The product of A and B represents the initial slope of the elastic stress-strain curve.

The combination of exponentials has been shown to provide a good fit to viscoelastic behaviour of soft tissues with efficient computational implementation^[115] and has been used satisfactorily to describe the viscoelastic behaviour of skin tissue^[116], given as

$$g(t) = k_0 + \sum_{i=1}^n k_i e^{-t/\tau_i} \quad (10.16)$$

where k_0 represents the percentage of stress at the equilibrium state of relaxation process, and $\sum_{i=0}^n k_i = 1$. The preliminary investigation demonstrates that the sum of three exponentials is sufficient to correlate well with the experimental data in this study

$$g(t) = k_0 + k_1 e^{-t/\tau_1} + k_2 e^{-t/\tau_2} \quad (10.17)$$

where τ_i ($i = 1, 2$) are the long- and short-term time constants.

With the elastic and viscous components described above, a model based on the QLV theory is developed. For a linear ramp in strain followed by holding at constant strain, the strain history of this “ramp-and-hold” relaxation can be described as

$$\varepsilon(t) = \gamma(t - t_0), \quad \text{for } t_0 \leq t \leq t_R (\text{ramp}) \quad (10.18)$$

$$\varepsilon(t) = \gamma(t_R - t_0) = \varepsilon_{\max}, \quad \text{for } t_R \leq t \leq t_\infty (\text{hold}) \quad (10.19)$$

where γ is the strain rate; ε_{\max} is the maximum strain; t_0 , t_R and t_∞ denote moments in time at the start of ramp, the end of ramp, and the end of relaxation, respectively.

The stress resulting from a ramp phase over time period $t_0 \leq t \leq t_R$ can be expressed by substituting Equations (10.16)~(10.18) into Equation (10.15) as

$$\sigma(t, \theta) = Ak_0 [e^{B\gamma(t-t_0)} - 1] + \sum_{i=1}^2 \frac{AB\gamma k_i}{B\gamma + 1/\tau_i} [e^{B\gamma(t-t_0)} - e^{-(t-t_0)/\tau_i}] \quad (10.20)$$

where $\theta = \theta(A, B, k_0, k_1, k_2)$ is a dummy function.

Similarly, the stress resulting from subsequent stress relaxation phase can be described as

$$\sigma(t, \theta) = Ak_0 [e^{B\gamma(t_R-t_0)} - 1]$$

$$+ \sum_{i=1}^2 \frac{AB\gamma k_i}{B\gamma + 1/\tau_i} [e^{B\gamma(t_R - t_0)} - e^{-(t_R - t_0)/\tau_i}] e^{-(t - t_0)/\tau_i} \quad (10.21)$$

For the case of $t_0 = 0$, these expressions simplify to

$$\sigma(t, \theta) = Ak_0(e^{B\gamma t} - 1) + \sum_{i=1}^2 \frac{AB\gamma k_i}{B\gamma + 1/\tau_i} (e^{B\gamma t} - e^{-t/\tau_i}), \quad 0 \leq t \leq t_R(\text{ramp}) \quad (10.22)$$

$$\sigma(t, \theta) = Ak_0(e^{B\gamma t_R} - 1) + \sum_{i=1}^2 \frac{AB\gamma k_i}{B\gamma + 1/\tau_i} (e^{B\gamma t_R} - e^{-t_R/\tau_i}) e^{-t/\tau_i}, \quad t_R \leq t \leq t_\infty(\text{hold}) \quad (10.23)$$

From Equation (10.23) the stress during relaxation can be considered as the sum of three components, an equilibrium stress at t_R and the other two are long- and short-term decay components, respectively.

10.6.2 Results

The proposed procedure for determining the temperature- and collagen denaturation- dependent viscoelastic properties of skin tissue is carried out as: perform stress relaxation tests under different temperatures, and convert the stress relaxation results to the corresponding creep results using the previously described mathematical method. The results and discussion are given in this section.

1) Relaxation behaviour

In this study, stress relaxation tests at three different strains levels were performed, which were then used to validate the separation of variables in QLV theory. Once verified, the QLV model was used to fit the stress-time data during both the ramp and relaxation phases obtained with a slow strain ramp rate.

Typical example of stress-relaxation tests

A representative uniaxial stress-time response from a relaxation test performed at body temperature ($T = 37^\circ\text{C}$), is presented in Figure 10.25, which shows the response of pig ear skin tissue during both the ramp and relaxation phases of the test. In the ramp region ($0 \leq t \leq 50\text{s}$), the response is concave due to the nonlinearity caused by an increasing recruitment of collagen fibers with increasing strain. In the relaxation region, the stress-relaxation curve is characterized by a sharp decrease in stress, followed by a gradual reduction up to 550 s. The uniaxial tensile relaxation results of pig ear skin tissue obtained here are comparable with those of human skin tissue^[28,117] and rat

skin tissue^[128] under tension, and pig foot skin tissue under compression^[119] both qualitatively and quantitatively.

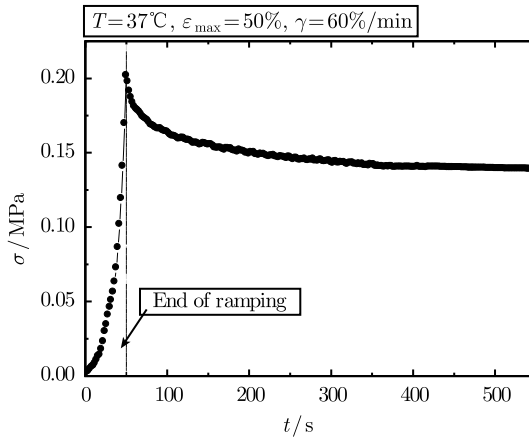


Figure 10.25 Representative uniaxial tensile stress-relaxation response of pig ear skin tissue (by permission of ASME)

Verification of the QLV theory

The model developed in Section 10.5.2 is based on the QLV theory, which is built upon the assumption that the stress relaxation function can be separated into one time-dependent and one strain-dependent portion. In other words, the normalized stress relaxation function, $g(t)$, should be independent of the strain/stress level. Different trends in viscous-elastic separability have been seen in soft biological tissues. For example, the validity of the assumption has been justified for relaxation behaviour of different soft tissues including ligament, tendon and esophagi, both qualitatively^[28] and quantitatively^[120,121], and has been argued to be reasonable for other soft tissues composed mainly of collagen^[122,123]. But in some other studies, it has been also shown that the relaxation behaviour of collagenous tissues was dependent on strain level^[122], which demonstrates the limits of Fung's quasi-linear viscoelastic approach.

In order to verify the hypothesis of variables separation in QLV theory for skin tissue, stress relaxation tests of skin samples at three different strain levels ($\varepsilon_{\max} = 10\%, 30\%, 50\%$ with rate $\gamma = 50\%/s$) at $T = 37^\circ\text{C}$ are performed. The normalized relaxation response, calculated as $g(t) = \sigma_t / \sigma_{t_R}$, from different values of ε_{\max} is plotted in Figure 10.26. The results show that the normalized relaxation of skin tissue is significant at all strain levels. According to the QLV model, the normalized responses, $g(t)$, should have an identical shape, regardless of ε_{\max} , which is a direct result of the

strain–relaxation function separability [Equation (10.14)]. However, experimental results in Figure 10.26 show that $g(t)$ depends strongly on the ε_{\max} , which are inconsistent with the QLV modelling approach. This inconsistency can also be shown by the strong dependence of the elastic (equilibrium) stress fraction, $Frac_E = \sigma_\infty/\sigma_{t_R}$, as proposed by Oyen et al.^[124], on ε_{\max} : $Frac_E = 0.69, 0.65, 0.57$ for $\varepsilon_{\max} = 50\%, 30\%, 10\%$, respectively. The similar results with an increasing elastic fraction at larger strain levels have also been observed elsewhere for skin tissue^[124] and human amnion^[125].

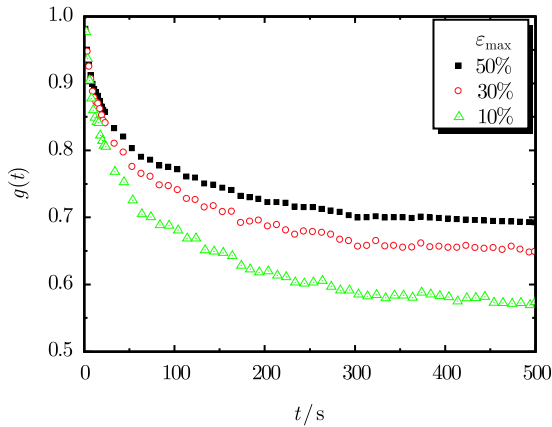


Figure 10.26 Normalized relaxation responses, $g(t) = \sigma_t/\sigma_{t_R}$, from three experimental uniaxial relaxation tests demonstrate differences in shape for the time-dependent responses

The QLV approach is applicable only to tissues for which the separation of viscous and elastic energy is independent of strain level. All the results here show that this model is therefore not applicable to skin tissue tested in this study.

2) Relaxation behaviour of skin tissue under different temperatures

Relaxation behaviour under hypothermic temperatures

Uniaxial tensile tests of pig ear skin tissue at four different hypothermic temperatures¹⁾ ($T = 5^\circ\text{C}, 10^\circ\text{C}, 20^\circ\text{C}, 30^\circ\text{C}$) have been performed. Together with the result obtained at body temperature, the normalized function of $g(t) = \sigma_t/\sigma_{t_R}$ is presented in Figure 10.27.

From the figure, it can be seen that skin tissue tested at higher temperature relaxes faster and reaches the equilibrium state much sooner than a tissue tested at temperatures further from body temperature: a similar behaviour

¹⁾ A condition in which an organism's temperature drops below that required for normal metabolism and bodily functions.

has been observed by other researchers for collagenous tissues. For example, Cohen et al.^[93] found that there was a significant increase in the relaxation rate of ligament with increasing temperature, in the range of $2 \sim 37^\circ\text{C}$. It was reported that the cyclic load relaxation of medial collateral ligament was greater at 37°C than at 22°C in dogs^[93] and greater at 35°C than at 25°C in rabbits^[126]. However, Rigby et al.^[127] found no measurable change in the stress relaxation between 0°C and 37°C , but a rapid drop in the rate of stress relaxation between 32°C and 40°C .

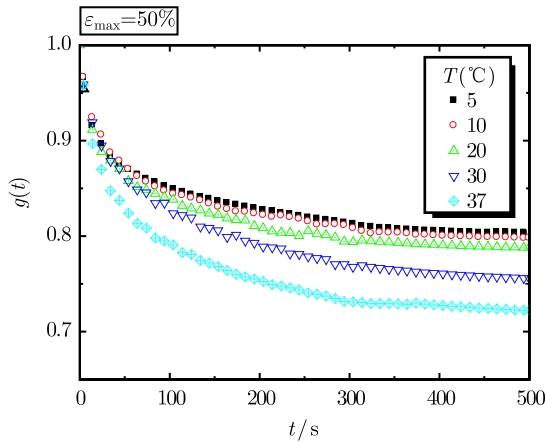


Figure 10.27 The normalized relaxation function, $g(t) = \sigma_t/\sigma_{t_R}$, under different hypothermic temperatures

Relaxation behaviours under hyperthermal temperatures

The uniaxial tensile tests of pig ear skin tissue under four hyperthermal temperatures ($T = 50^\circ\text{C}, 60^\circ\text{C}, 70^\circ\text{C}, 80^\circ\text{C}$) have been performed. Together with the result obtained at body temperature, the normalized function of $g(t) = \sigma_t/\sigma_{t_R}$ is given in Figure 10.28.

Within physiological temperature ranges, it has been shown that the viscoelastic behaviour of collagenous tissues is independent of temperature history^[127]. However, in the hyperthermal range, the stress-relaxation responses of skin tissue at a lower temperature relax faster and reach an equilibrium state much sooner than those at temperatures closer to body temperature, as shown in Figure 10.28. This observation is in agreement with those reported in the open literature. For example, the stress in thermally treated collagenous tissue was found to relax faster and to a larger degree for a similar loading^[93,127]. The acceleration of stress relaxation due to thermal heating in mechanically deformed tissue was also observed in the laser reshaping of cartilage^[45], and laser thermokeratoplasty of corneal^[128~133].

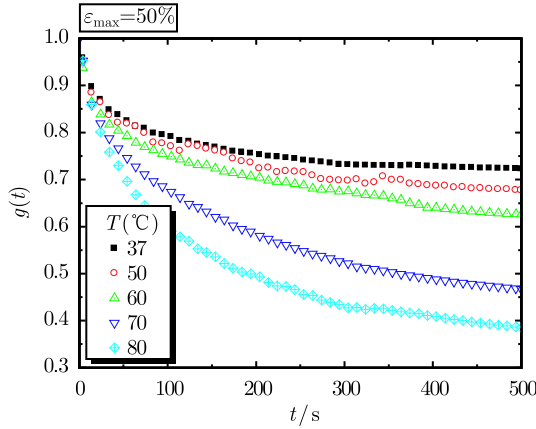


Figure 10.28 The normalized relaxation function, $g(t) = \sigma(t)/\sigma_{t_R}$, under different hyperthermal temperatures

Variation of elastic fraction with temperature

The elastic (equilibrium) stress fraction, $Frac_E = \sigma_\infty/\sigma_{t_R}$, under different temperatures has been obtained from Figure 10.27 and 10.28, as shown in Figure 10.29.

It can be seen $Frac_E$ depends strongly on the temperature: it decreases with increasing temperature over the whole temperature range, but decreases much faster in the hyperthermal range ($T = 50 \sim 80^\circ\text{C}$). In other words, as the temperature decreases, the energy dissipation decreases and the mechanical energy is increasingly elastic.

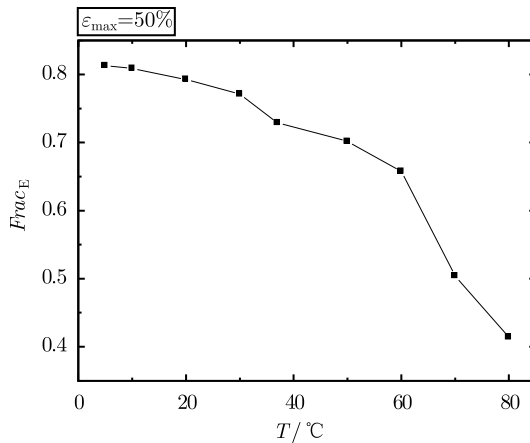


Figure 10.29 The effect of temperature on the elastic fraction, $Frac_E = \sigma_\infty/\sigma_{t_R}$, for skin tissue (by permission of ASME)

10.6.3 Discussion

In this section, the possible roles played by different tissue components in skin viscoelasticity and the thermally-induced changes in these factors are discussed.

1) Effect of different components

Histological examination reveals that the viscoelastic response was mainly caused by the dermis, and not the epidermis in nature^[134]; Silver et al.^[43] also found the removal of epidermis does not change the viscoelastic properties of skin tissue. Therefore, the following discussion is relative to the role of different components of skin dermis.

Skin tissue is composed of cellular and extracellular compartments. The extracellular compartment consists of dominant collagen fibers embedded in ground substance. The mechanical response of skin tissue to applied loads involves two components as noted previously: a viscous component associated with energy dissipation by molecular and viscous sliding of collagen fibrils during alignment with the force direction^[135]; an elastic component associated with energy storage as a result of stretching of flexible regions in the collagen triple helix^[43]. The viscous nature of collagenous tissues arises from both the inherent viscoelasticity of the solid phase as well as fluid movement, resulting in viscous drag between the solid and fluid phases during loading^[135~137].

Effect of elastic components

The extent to which a tissue exhibits stress relaxation has been shown to be directly related to the elastic content (elastin and collagen)^[138]. However, in the study here of pig ear skin tissue, the elastin should not play an important role in the temperature-induced variation of viscoelastic behaviour, for a high strain level ($\varepsilon_{\max} = 50\%$) has been chosen. At this level, the mechanical behaviour of skin tissue is dominated by the response of collagen fibers^[139].

The collagen fiber component plays a major role in the stress-strain response of skin tissue, especially at high strain levels ($\varepsilon \geq 30\%$)^[43]. Collagen is intrinsically viscoelastic^[136,137,140], implying that collagen viscoelasticity may be the source leading to the viscoelastic behaviour of skin tissue^[141]. For example, a correlation between collagen content and the viscoelastic behaviour of rat skin has been established^[119]. An increase in collagen crosslinking was found to increase both the viscoelastic storage and loss moduli of guinea pig skin tissue under dynamic loading^[142]. Furthermore, upon loading the initially crimped collagen fibers in dermis undergo reorientation, suggesting that the time-dependent reorientation of collagen fibers may be responsi-

ble for skin viscoelasticity. It is commonly assumed that the time-dependent reorientation of collagen fibres within a viscous matrix explains the viscoelastic behaviour of connective tissues^[143]. For example, the increase of elastic fraction¹⁾ with increasing strain in the skin stress-relaxation response was attributed to the rearrangement of individual collagen fiber orientations, resulting in an aligned collagen network at high strain levels^[144]. Structural reorganization was also recognized to be important in tendon viscoelasticity^[125]. However, Purslow et al.^[119] found no involvement of collagen fiber rotation in skin viscoelastic stress relaxation.

Role of ground substance

The ground substance is a gel like substance containing a class of chemicals including glycosaminoglycans (GAG), proteoglycans (PG) and glycoproteins. The ground substance is found to play an important role in the viscoelastic behaviour of dermis. According to Wilkes et al.^[145], the time dependent behaviour of dermis can be related to the viscous resistance that fibers experience while moving through the ground substance. Minns et al.^[146] showed that the removal of ground substance in tendon, aorta and ligamentum nuchae induced a decrease in relaxation hysteresis and other time-dependent effects. Vogel^[142] found a correlation between the relaxation and the content of GAG in skin tissue. Purslow et al.^[119] also suggested that the viscoelastic effects of skin tissue arise from molecular relaxations within the proteoglycan matrix surrounding the collagen fibers or within the collagen fibers themselves. Eshel & Lanir^[46] found that the absence of proteoglycans influenced the low strain relaxation patterns and deteriorated viscoelastic mechanisms.

In summary, the skin viscoelasticity at high strain level is decided by the collagen and ground substance tissue while the elastic component should not play an important role. The temperature effect is discussed below.

2) Effect of temperature and thermal denaturation

Results from thermomechanical tests on collagenous tissues can be difficult to interpret due to the simultaneous occurrence of thermal damage, thermoelastic and thermoviscoelastic processes, the least understood being the altered viscoelastic behaviours during and after heating^[46].

As discussed in Sections 10.3 and 10.4, three possible mechanisms exist for why temperature effects change the viscoelastic behaviour of skin tissue. The first one is the thermal denaturation of dermis collagen and it seems reasonable to assume that collagen would play a major role in the viscoelastic

1) Equivalent to the ratio of equilibrium force to initial force.

nature of skin tissue subjected to thermal loading. For example, the acceleration of stress relaxation in laser reshaping of cartilage was partly attributed to temperature-dependent, bound-free water transition in the cartilage matrix and selective collagen denaturation^[45]. Wells et al.^[19] found a correlation between the relaxation rate of ovine aortic collagen and the concentration of thermally stable collagen crosslinks: if more crosslinking is present, the slippage of adjacent chain fragments will be inhibited, and the observed load relaxation will be slower. To check the role of collagen denaturation, the heat-induced thermal damage degree (*Deg*) of pig ear skin tissue under hyperthermal temperatures has been plotted as functions of time, as shown in Figure 10.30. These results clearly show that collagen in skin tissue is damaged to a higher degree with increasing time and temperature.

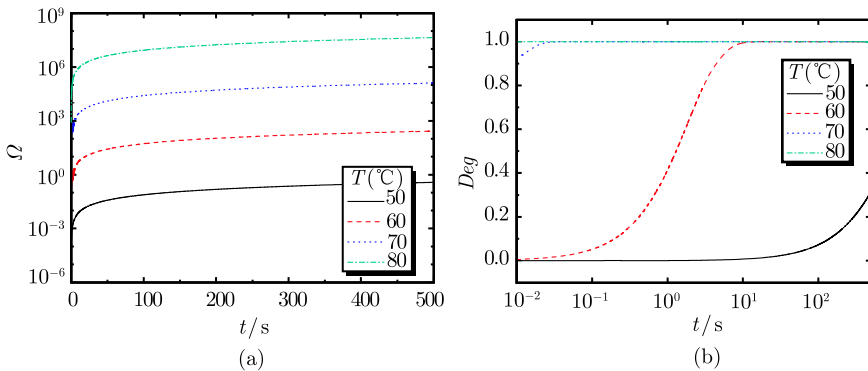


Figure 10.30 (a) Thermal damage and (b) damage degree due to temperature increase during the relaxation tests

Another possible mechanism is the temperature-induced change in hydration. It has been shown that the viscoelastic behaviour of soft tissues are related to the interactions amongst collagen, proteoglycans, and water molecules^[147]. There can be an inward or outward flux of interstitial fluid due to heating a soft tissue^[148,149] and the viscoelastic properties of a tissue can be changed by altering its water content^[53]. Baek et al.^[45] speculated that a loss of water causes the stress to relax, and the faster relaxation in thermally treated tissues is caused by the faster and greater water loss.

The third possible mechanism is the temperature-changed cell viability in skin tissue. From Figure 10.30, it can be seen that collagen in skin tissue is almost fully damaged (Deg is near unity), indicating that fibroblast viability decreases with heating duration and temperature. Using poison (2-deoxy-D-glucose), Yip et al.^[45] studied the effect of in situ fibroblast viability on the mechanical properties of rate back skin tissue. They found that there

is greater stress relaxation in skin tissue strained in normal Krebs's solution than that in Krebs's solution with poison, and that there exists a correlation between the amount of stress relaxation and the number of viable fibroblasts in the tissue: tissues with more viable fibroblasts have lower stress relaxation.

In summary, temperature has significant effect on the viscoelastic behaviour of skin tissue; in the hyperthermal temperature range, the effect is caused by thermal denaturation of collagen as well as heating induced hydration and cell viability changes.

10.7 Summary and Limitations

This chapter has presented the experimental methodology adopted to quantify the thermal denaturation and mechanical behaviour of skin tissue under thermal agitations. In particular, it has described the methodology for obtaining and preparing the skin samples; the methodology of thermal analysis with the differential scanning calorimetry; the design and manufacture of the hydrothermal tensile system and the hydrothermal compressive system; and the thermodynamic analysis of skin viscoelasticity with dynamic mechanical analyzer. The results of these experimental measurements are presented in Chapter 6.

10.7.1 Summary

This chapter has examined the tensile, compressive and viscoelastic behaviours of skin tissue under different temperatures and thermal damage levels, in order to characterize the effect of temperature and corresponding collagen denaturation on the mechanical properties of skin tissue. The results have been discussed together with the corresponding thermal damage process. Comparisons of the experimental results with reported results in literature have been performed, and a good agreement has been achieved. Internal comparisons of results obtained from different methods have also been made. More detailedly, the following conclusions can be made.

DSC results show that the transition temperature of collagen in the pig flank skin samples is about 66.8°C, and from the DSC results the Arrhenius parameters are obtained for skin samples from different locations. Under tensile loading, the modulus at high strain level of the tested skin samples decreases with increasing temperature due to the thermal denaturation of skin collagen: compressive loading, however, showed quite the opposite due to the different underlying mechanisms between tensile and compressive behaviours of skin tissue. Biaxial tests at 37°C and 60°C show that the skin

tissue from porcine cheek appears to be abnormal in the fact that it has an equal tensile response across both axes of a square independent of cutting angle. This discovery has allowed the series of experiments on skin tissue to come to fruition since a uniform stress distribution in the tissue can be easily achieved even in biaxial tests. Compared with uniaxial stretch, biaxial tensile loading results in the lateral compression of the stress-strain curve and the reduction in the strain before entry into the linear region occurs under all temperatures tested, which is due to the two-directional stretch of collagen fibers. Under compression, the stiffness of skin tissue decreases with increasing thermal damage degree. A strain-rate sensitivity is observed at different damage levels, and stiffness decreases with thermal damage. Temperature has a significant effect on the static viscoelasticity of skin tissue, where the QLV approach has been shown not to be applicable for skin tissue due to the strain level dependence of the viscous and elastic energy separation; and quantitative relationship has been found between temperature and the elastic fraction.

In Chapter 5, a mathematical approach has been developed for determining the thermomechanical response in skin tissue, where temperature/damage independent linear elastic mechanical properties of skin tissue have been used. The assumptions used are reasonable in view that: ① the strain level considered in Chapter 5 is purely thermal induced and is thus comparatively small ($< 1\%$); ② the results in this chapter have shown that temperature/damage has little effect at this low strain level. However, in medical applications, deformation of skin at high strain level also occurs, e.g. skin indentation during laser-skin treatment^[87]. For these cases, it can be expected that the incorporation of the temperature/damage dependent mechanical properties in the thermomechanical model will have a great effect on the thermomechanical behaviour of skin tissue. This will be done in our future work.

10.7.2 Limitations

There are several limitations to the present experimental study, as described below.

(1) The thermal denaturation of a collagenous tissue depends on not only the temperature history but also the stress state during heating^[150,151]. However, in the calculation of thermal damage we used parameters obtained from load free DSC measurements.

(2) It is well known that the mechanical properties of skin tissue are typically nonlinearly elastic and viscoelastic. In the tensile and compressive test-

ing of present study, however, we concentrated only on the nonlinear-elasticity of the tissue. The data of compressive behaviour was fit with the Odgen model with the assumption of incompressivity. However, it was found that pigskin under compression is compressible; even in unconfined compression, the volume of specimens varies with increasing compressive deformation^[53].

(3) The viscoelastic behaviour of skin was only tested for uniaxial loading and biaxial loading needs to be studied for skin in vivo experiences multi-axial natural tension. The strain applied in the present relaxation test was 50%, but a previous study found that after 20% strain the fibroblasts were apoptotic or necrotic^[67].

References

- [1] Shergold O A, Fleck N A, Radford D. The uniaxial stress versus strain response of pig skin and silicone rubber at low and high strain rates. *International Journal of Impact Engineering*, 2006, 32(9): 1384–1402.
- [2] Douglas W R. Of pigs and men and research: A review of applications and analogies of the pig, *sus scrofa*, in human medical research. *Space and Life Sciences*, 1972, 3(3): 226–234.
- [3] Johnson T E, Mitchell M A, Rico P J, et al. Corneal and skin laser exposures from 1540 nm laser pulses. *Laser-Tissue Interactions XI: Photochemical, Photothermal, and Photomechanical*. SPIE, 2001: 222–229.
- [4] Meyer W, Schwarz R, Neurand K. The skin of domestic mammals as a model for the human skin, with special reference to the domestic pig. *Current Problems in Dermatology*, 1978, 7: 39–52.
- [5] Shergold O A, Fleck N A. Experimental investigation into the deep penetration of soft solids by sharp and blunt punches, with application to the piercing of skin. *Journal of Biomechanical Engineering*, 2005, 127(5): 838–848.
- [6] Middelkoop E, van den Bogaerd A J, Lamme E N, et al. Porcine wound models for skin substitution and burn treatment. *Biomaterials*, 2004, 25(9): 1559–1567.
- [7] Meyer W, Kacza J, Zschemisch N H, et al. Observations on the actual structural conditions in the stratum superficiale dermidis of porcine ear skin, with special reference to its use as model for human skin. *Annals of Anatomy*, 2007, 189(2): 143–156.
- [8] Ankerson J. Puncture resistance and tensile strength of skin stimulants. *Proceedings of the Institution of Mechanical Engineers*, 1999, 213(Part H): 493–501.
- [9] Meyer W, Zschemisch N H, Godynicki S. The porcine ear skin as a model system for the human integument: Influences of storage conditions on basic features of epidermis structure and function—a histological and histochemical study. *Polish Journal of Veterinary Sciences*, 2003, 6(1): 17–28.
- [10] Wright D M, Wiig H, Winlove C P, et al. Simultaneous measurement of

- interstitial fluid pressure and load in rat skin after strain application in vitro. *Annals of Biomedical Engineering*, 2003, 31(10): 1246–1254.
- [11] Holtzhauer M. *Basic Methods for the Biochemical Lab*. New York: Springer-Verlag, 2006.
- [12] Essenpreis M. *Thermally Induced Changes in Optical Properties of Biological Tissues* [Ph. D. Thesis]. London: University College London, 1992.
- [13] Lin W, Motamedi M M, Welch A J. Dynamics of tissue optics during laser heating of turbid media. *Applied Optics*, 1996, 35(19): 3413–3420.
- [14] Diridollou S, Vabre V, Berson M, et al. Skin ageing: Changes of physical properties of human skin in vivo. *International Journal of Cosmetic Science*, 2001, 23(6): 353–362.
- [15] Choi H S, Vito R P. Two-dimensional stress-strain relationship for canine pericardium. *Journal of Biomechanical Engineering*, 1990, 112(2): 153–159.
- [16] Young G S. Thermodynamic characterization of skin, hide and similar materials composed of fibrous collagen. *Studies in Conservation*, 1998, 43(2): 65–79.
- [17] Schiller R, Funke A P, Gunther C. DSC measurements on full thickness mice skin: An additional tool to investigate permeation enhancement of highly lipophilic drugs. *Journal of Thermal Analysis and Calorimetry*, 2004, 77(2): 497–510.
- [18] Wright N T, Humphrey J D. Denaturation of collagen via heating: An irreversible rate process. *Annual Review of Biomedical Engineering*, 2002, 4: 109–128.
- [19] Wells P B. *Thermal Alteration of Collagenous Tissue Subjected to Biaxial Isometric Constraints* [Ph. D. Thesis]. Texas: Texas A & M University, 2005.
- [20] Downs J, Halperin H R, Humphrey J D, et al. An improved video-based computer tracking system for soft-biomaterials testing. *IEEE Transactions on Biomedical Engineering*, 1990, 37(9): 903–907.
- [21] Malcolm D T K, Nielsen P M F, Hunter P J, et al. Strain measurement in biaxially loaded inhomogeneous, anisotropic elastic membranes. *Biomechanics and Modeling in Mechanobiology*, 2002, 1(3): 197–210.
- [22] Shergold O A, *The Mechanics of Needle-Free Injection* [Ph. D. Thesis]. Cambridge: University of Cambridge, 2004.
- [23] Reihnsner R, Menzel E. Two-dimensional stress-relaxation behavior of human skin as influenced by non-enzymatic glycation and the inhibitory agent aminoguanidine. *Journal of Biomechanics*, 1998, 31(11): 985–993.
- [24] Elsner P, Wilhelm D, Maibach H I. Mechanical properties of human forearm and vulvar skin. *British Journal of Dermatology*, 1990, 122(5): 607–614.
- [25] Fung Y C. *Biomechanics: Mechanical Properties of Living Tissues*. New York: Springer-Verlag, 1993.
- [26] Pan L, Zan L, Foster F S. Ultrasonic and viscoelastic properties of skin under transverse mechanical stress in vitro. *Ultrasound in Medicine and Biology*, 1998, 24(7): 995–1007.
- [27] Hermanns-Le T, Uhoda I, Smitz S, et al. Skin tensile properties revisited during ageing. Where now, where next? *Journal of Cosmetic Dermatology*,

- 2004, 3(1): 35–40.
- [28] Paillet-Mattei C, Zahouani H. Study of adhesion forces and mechanical properties of human skin in vivo. *Journal of Adhesion Science and Technology*, 2004, 15(16): 1739–1758.
- [29] Lanir Y. Biaxial stress relaxation in skin. *Annals of Biomedical Engineering*, 1976, 4(3): 250–270.
- [30] Arumugam V, Naresh M, Sanjeevi R. Effect of strain rate on the fracture behaviour of skin. *Journal of Biosciences*, 1994, 19(3): 307–313.
- [31] Wu J Z, Cutlip R G, Welcome D, et al. Estimation of the viscous properties of skin and subcutaneous tissue in uniaxial stress relaxation tests. *Bio-Medical Materials and Engineering*, 2006, 16(1): 53–66.
- [32] Battaglia T C. GDF-5 deficiency alters stress-relaxation properties in mouse skin. *Journal of Dermatological Science*, 2005, 39(3): 192–195.
- [33] Reihnsner R, Menzel E J. Two-dimensional stress-relaxation behavior of human skin as influenced by non-enzymatic glycation and the inhibitory agent aminoguanidine. *Journal of Biomechanics*, 1998, 31(11): 985–993.
- [34] Vogel H G. Tensile strength, relaxation and mechanical recovery in rat skin as influenced by maturation and age. *Journal of Medicine*, 1976, 7(2): 177–188.
- [35] Vogel H G. Stress relaxation in rat skin after treatment with hormones. *Journal of Medicine*, 1973, 4(1): 19–27.
- [36] Lange L, Echt M, Kirsch K, et al. Studies in stress-relaxation and distensibility characteristics of small skin veins in vivo by a combined photoelectric-photographic and plethysmographic technique. *European Journal of Physiology*, 1972, 337(4): 311–322.
- [37] Pierard G E. EEMCO guidance to the in vivo assessment of tensile functional properties of the skin, Part 1: Relevance to the structures and ageing of the skin and subcutaneous tissues. *Skin Pharmacology and Applied Skin Physiology*, 1999, 12(6): 352–362.
- [38] Chae Y, Aguilar G, Lavernia E J, et al. Characterization of temperature dependent mechanical behavior of cartilage. *Lasers in Surgery and Medicine*, 2003, 32(4): 271–278.
- [39] Chao K K H, Burden M A, Wong B J F. Dynamic changes in the elastic modulus of lagomorph nasal septal cartilage during Nd:YAG laser irradiation. *Society of Photo-Optical Instrumentation Engineers*, 2001, 4257: 247–254.
- [40] Yamashita J, Li X, Furman B R, et al. Collagen and bone viscoelasticity: A dynamic mechanical analysis. *Journal of Biomedical Materials*, 2002, 63(1): 31–36.
- [41] Mano J F. Viscoelastic properties of bone: Mechanical spectroscopy studies on a chicken model. *Materials Science and Engineering C*, 2005, 25(2): 145–152.
- [42] Alexander H, Cook T H. Variations with age in the mechanical properties of human skin in vivo // Kennedy R M. *Bedsore Biomechanics*. Bath: McMillan Press, 1976, 16: 109–118.
- [43] Silver F H, Kato Y P, Ohno M, et al. Analysis of mammalian connective tissue: Relationship between hierarchical structures and mechanical properties.

- Journal of Long-Term Effects of Medical Implants, 1992, 2(2-3): 165–198.
- [44] Davidson J M, Giro M, Sutclie M, et al. Regulation of elastin synthesis//Tamburro A M, Davidson J M. Elastin: Chemical and Biological Aspects. Galatina: Congedo Editore, 1990.
- [45] Baek S, Wells P B, Rajagopal K R, et al. Heat-induced changes in the finite strain viscoelastic behavior of a collagenous tissue. *Journal of Biomechanical Engineering*, 2005, 127(4): 580–586.
- [46] Eshel H, Lanir Y. Effects of strain level and proteoglycan depletion on preconditioning and viscoelastic responses of rat dorsal skin. *Annals of Biomedical Engineering*, 2001, 29(2): 164–172.
- [47] Henriques F C, Moritz A R. Studies of thermal injury, I. The conduction of heat to and through skin and the temperatures attained therein. A theoretical and an experimental investigation. *The Journal of Pathology*, 1947, 23(4): 531–549.
- [48] Weir C E. Rate of shrinkage of tendon collagen-heat, entropy, and free energy of activation of the shrinkage of untreated tendon. Effect of acid, salt, pickle, and tannage on the activation of tendon collagen. *Journal of the American Leather Chemists Association*, 1949, 44: 108–140.
- [49] Pietrucha K. Changes in denaturation and rheological properties of collagen-hyaluronic acid scaffolds as a result of temperature dependencies. *International Journal of Biological Macromolecules*, 2005, 36(5): 299–304.
- [50] Ozawa T. Kinetic analysis of derivatives curves in thermal analysis. *Journal of Thermal Analysis and Calorimetry*, 1970, 2: 301–324.
- [51] Miles C A. Kinetics of collagen denaturation in mammalian lens capsules studied by differential scanning calorimetry. *International Journal of Biological Macromolecules*, 1993, 15(5): 265–271.
- [52] Miles C A, Burjanadze T V, Bailey A J. The kinetics of the thermal denaturation of collagen in unrestrained rat tail tendon determined by differential scanning calorimetry. *Journal of Molecular Biology*, 1995, 245(4): 437–446.
- [53] Humphrey J D. Continuum thermomechanics and the clinical treatment of disease and injury. *Applied Mechanics Reviews*, 2003, 56(2): 231–260.
- [54] Dunn M G, Silver F H, Swann D A. Mechanical analysis of hypertrophic scar tissue: Structural basis for apparent increased rigidity. *Journal of Investigative Dermatology*, 1985, 84(1): 9–13.
- [55] Veronda D R, Westmann R A. Mechanical characterization of skin-finite deformations. *Journal of Biomechanics*, 1970, 3(1): 111–124.
- [56] Luescher M, Ruegg M, Schindler P. Effect of hydration upon the thermal stability of tropocollagen and its dependence on the presence of neutral salts. *Biopolymers*, 1974, 13(12): 2489–2503.
- [57] Rubin L R. Langer's lines and facial scars. *Plastic and Reconstructive Surgery*, 1948, 3: 147–155.
- [58] Von Gierke H E. Biomechanics of impact injury. *Proceedings of the Impact Acceleration Stress Symposium*, National Academy of Sciences, 1962, Publication No. 977.

- [59] North J F, Gibson F. Volume compressibility of human abdominal skin. *Journal of Biomechanics*, 1978, 11(4): 203–207.
- [60] Cox H. The cleavage lines of the skin. *British Journal of Surgery*, 1941, 29: 234.
- [61] Vossoughi J, Vaishnav R N. Comments on the paper “Volume compressibility of human abdominal skin”. *Journal of Biomechanics*, 1979, 12(6): 481.
- [62] Wu J Z, Dong R G, Smutz W P, et al. Non-linear and viscoelastic characteristics of skin under compression: Experiment and analysis. *Bio-Medical Materials and Engineering*, 2003, 13(4): 373–385.
- [63] Ankersen J, Birkbeck A E, Thomson R D, et al. Puncture resistance and tensile strength of skin simulants. *Journal of Engineering in Medicine*, 1999, 213(6): 493–501.
- [64] Glaser A A, Marangoni R D, Must J S, et al. Refinements in the methods for the measurement of the mechanical properties of unwounded and wounded skin. *Medical Electronics and Biological Engineering*, 1965, 3(4): 411–419.
- [65] Ridge M D, Wright V. The directional effects of skin. A bio-engineering study of skin with particular reference to Langer’s lines. *Journal of Investigative Dermatology*, 1966, 46(4): 341–346.
- [66] Jamison C E, Marangoni R D, Glaser A A. Viscoelastic properties of soft tissue by discrete model characterization. ASME New York, 1967: 9.
- [67] Fung Y C. Biomechanics, its scope, history and some problems of continuum mechanics in physiology. *Applied Mechanics Reviews*, 1968, 21(1): 1–20.
- [68] Wu J Z, Dong R G, Rakheja S, et al. Simulation of mechanical responses of fingertip to dynamic loading. *Medical Engineering and Physics*, 2002, 24(4): 253–264.
- [69] Wan A W. Biaxial tension test of human skin in vivo. *Bio-Medical Materials and Engineering*, 1994, 4: 473–486.
- [70] Wu J Z, Cutlip R G, Andrew M E, et al. Simultaneous determination of the nonlinear-elastic properties of skin and subcutaneous tissue in unconfined compression tests. *Skin Research and Technology*, 2007, 13(1): 34–42.
- [71] Tregear R T, Dirnhuber P. Viscous flow in compressed human and rat skin. *Journal of Investigative Dermatology*, 1965, 45: 119–125.
- [72] Dikstein S, Hartzshtark A. What does low-pressure indentometry measure. *Arzt Kosmetol*, 1983, 16: 327–328.
- [73] Vogel H G. Antagonistic effect of aminoacetonitrile and prednisolone on mechanical properties of rat skin. *Biochimica et Biophysica Acta*, 1971, 252(3): 580–585.
- [74] Ranu H S, Burlin T E, Hutton W C. The effects of X-irradiation on the mechanical properties of skin. *Physics in Medicine and Biology*, 1975, 20(1): 96–105.
- [75] Jansen L H, Rottier P B. Comparison of the mechanical properties of strips of human abdominal skin excised from below and from above the umbilic. *Dermatologica*, 1958, 117(4): 252–258.
- [76] Jansen L H, Rottier P B. Some mechanical properties of human abdominal skin measured on excised strips: A study of their dependence on age and how

- they are influenced by the presence of striae. *Dermatologica*, 1958, 117(2): 65–83.
- [77] Smalls L K, Wickett R R, Visscher M O. Effect of dermal thickness, tissue composition, and body site on skin biomechanical properties. *Skin Research and Technology*, 2006, 12(1): 43–49.
- [78] Pierard G E, Letawe C, Dowlati A, et al. Effect of hormone replacement therapy for menopause on the mechanical properties of skin. *Journal of the American Geriatrics Society*, 1995, 43(6): 662–665.
- [79] Pierard G E, Nikkels-Tassoudji N, Pierard-Franchimont C. Influence of the test area on the mechanical properties of skin. *Dermatology*, 1995, 191(1): 9–15.
- [80] Lennox F G. Shrinkage of collagen. *Biochimica et Biophysica Acta*, 1949, 3: 170–187.
- [81] Chachra D, Gratzner P F, Pereira C A, et al. Effect of applied uniaxial stress on rate and mechanical effects of cross-linking in tissue-derived biomaterials. *Biomaterials*, 1996, 17(19): 1865–1875.
- [82] Chen S S, Humphrey J D. Heat-induced changes in the mechanics of a collagenous tissue: Pseudoelastic behavior at 37 degrees C. *Journal of Biomechanics*, 1998, 31(3): 211–216.
- [83] Harris J L, Wells P B, Humphrey J D. Altered mechanical behavior of epicardium due to isothermal heating under biaxial isotonic loads. *Journal of Biomechanical Engineering*, 2003, 125(3): 381–388.
- [84] Wells P B, Harris J L, Humphrey J D. Altered mechanical behavior of epicardium under isothermal biaxial loading. *Journal of Biomechanical Engineering*, 2004, 126(4): 492–497.
- [85] Lanir Y. *Skin mechanics*//Skalak R, Chien S. *Handbook of Bioengineering*. New York: McGraw-Hill, 1987: 11.11–11.25.
- [86] Hormann H, Schlebusch H. Reversible and irreversible denaturation of collagen fibers. *Biochemistry*, 1971, 10(6): 932–937.
- [87] Yip C P, Walker D, Fernlund G, et al. Role of dermal fibroblasts in rat skin tissue biomechanics. *Bio-Medical Materials and Engineering*, 2007, 17(2): 109–117.
- [88] Giles J M, Black A E, Bischoff J E. Anomalous rate dependence of the preconditioned response of soft tissue during load controlled deformation. *Journal of Biomechanics*, 2007, 40(4): 777–785.
- [89] Vogel H G, Hilgner W. Influence of age and of desmotropic drugs on the step phenomenon observed in rat skin. *Archives of Dermatological Research*, 1979, 264(2): 225–241.
- [90] Arumugam V, Naresh M D, Sanjeevi R. Effect of strain rate on the fracture behaviour of skin. *Journal of Biosciences*, 1994, 19(3): 307–313.
- [91] Jamison C E, Marangoni R D, Glaser A A. Viscoelastic properties of soft tissue by discrete model characterization. *Journal of Biomechanics*, 1968, 1(1): 33–36.
- [92] Vogel H G, Hilgner W. The “step phenomenon” as observed in animal skin. *Journal of Biomechanics*, 1979, 12(1): 75–81.

- [93] Cohen R E, Hooley C J, McCrum N G. Viscoelastic creep of collagenous tissue. *Journal of Biomechanics*, 1976, 9(4): 175–184.
- [94] Haut R C. The sensitivity of skin to strain rate of loading. 7th Annual Meeting of the American Society of Biomechanics. Rochester, 1983.
- [95] Daly C H. Biomechanical properties of dermis. *Journal of Investigative Dermatology*, 1982, 79(Suppl. 1): 17s–20s.
- [96] Li J T, Armstrong C G, Mow V C. The effect of strain rate on mechanical properties of articular cartilage in tension. *ASME Biomechanics Symposium*, 1983: 117–120.
- [97] Lakes R S, *Viscoelastic Solids*. Boca Raton: CRC Press, 1998.
- [98] Fung Y C. Stress-strain history relations of soft tissues in simple elongation//Fung Y C, Perrone N, Anliker M. *Biomechanics: Its Foundations and Objectives*. Englewood Cliffs: Prentice-Hall, 1971: 181–208.
- [99] Ledoux W R, Blevins J J. The compressive material properties of the plantar soft tissue. *Journal of Biomechanics*, 2007, 40(13): 2975–2981.
- [100] Decraemer W F, Maes M A, Vanhuyse V J, et al. A non-linear viscoelastic constitutive equation for soft biological tissues based upon a structural model. *Journal of Biomechanics*, 1980, 13(7): 559–564.
- [101] Moon D K, Woo S L, Takakura Y, et al. The effects of refreezing on the viscoelastic and tensile properties of ligaments. *Journal of Biomechanics*, 2006, 39(6): 1153–1157.
- [102] Defrate L E, Li G. The prediction of stress-relaxation of ligaments and tendons using the quasi-linear viscoelastic model. *Biomechanics and Modeling in Mechanobiology*, 2007, 6(4): 245–251.
- [103] Funk J R, Hall G W, Crandall J R, et al. Linear and quasi-linear viscoelastic characterization of ankle ligaments. *Journal of Biomechanical Engineering*, 2000, 122(1): 15–22.
- [104] Woo S L Y, Simon B R, Kuei S C, et al. Quasi-linear viscoelastic properties of normal articular cartilage. *Journal of Biomechanical Engineering*, 1980, 102(2): 85–90.
- [105] Simon B R, Coats R S, Woo S L Y. Relaxation and creep quasilinear viscoelastic models for normal articular cartilage. *Journal of Biomechanical Engineering*, 1984, 106(2): 159–164.
- [106] Sarver J J, Robinson P S, Elliott D M. Methods for quasi-linear viscoelastic modeling of soft tissue: Application to incremental stress-relaxation experiments. *Journal of Biomechanical Engineering*, 2003, 125(5): 754–758.
- [107] Johnson G A, Tramaglino D M, Levine R E, et al. Tensile and viscoelastic properties of human patellar tendon. *Journal of Orthopaedic Research*, 1994, 12(6): 796–803.
- [108] Carew E O, Talman E A, Boughner D R, et al. Quasi-linear viscoelastic theory applied to internal shearing of porcine aortic valve leaflets. *Journal of Biomechanical Engineering*, 1999, 121(4): 386–392.
- [109] Lin H C, Kwan M K, Woo S L Y. On the stress relaxation properties of anterior cruciate ligament (ACL). *Advances in Bioengineering*, 1987: 5–6.

- [110] Kwan M K, Lin T H, Woo S L. On the viscoelastic properties of the antero-medial bundle of the anterior cruciate ligament. *Journal of Biomechanics*, 1993, 26(4-5): 447–452.
- [111] Myers B, McElhaney J, Nightingale R, et al. Experimental limitations of quasi-linear theory, and a method for reducing these effects. *Advances in Bioengineering*, 1991, BED-20: 139–142.
- [112] Dortmans L J, Sauren A A, Rousseau E P. Parameter estimation using the quasi-linear viscoelastic model proposed by Fung. *Journal of Biomechanical Engineering*, 1984, 106(3): 198–203.
- [113] Nigul I, Nigul U. On algorithms of evaluation of Fung's relaxation function parameters. *Journal of Biomechanics*, 1987, 20(4): 343–352.
- [114] Gimbel J A, Sarver J J, Soslowsky L J. The effect of overshooting the target strain on estimating viscoelastic properties from stress relaxation experiments. *Journal of Biomechanical Engineering*, 2004, 126(6): 844–848.
- [115] Abramowitch S D, Woo S L. An improved method to analyze the stress relaxation of ligaments following a finite ramp time based on the quasi-linear viscoelastic theory. *Journal of Biomechanical Engineering*, 2004, 126(1): 92–97.
- [116] Puso M A, Weiss J A. Finite Element implementation of anisotropic quasi-linear viscoelasticity using a discrete spectrum approximation. *Journal of Biomechanical Engineering*, 1998, 120(1): 62–70.
- [117] Kenedi R M, Gibson T, Evans J H, et al. *Tissue mechanics*. *Physical Medical Biology*, 1975, 20(3): 699–717.
- [118] Barbenel J C, Evans J H. The time-dependent mechanical properties of skin. *Journal of Investigative Dermatology*, 1977, 69(3): 318–320.
- [119] Purslow P P, Wess T J, Hukins D W L. Collagen orientation and molecular spacing during creep and stress-relaxation in soft connective tissues. *Journal of Experimental Biology*, 1998, 201(1): 135–142.
- [120] Haut R C, Little R W. A constitutive equation for collagen fibers. *Journal of Biomechanics*, 1972, 5(5): 423–430.
- [121] Lanir Y. A microstructure model for the rheology of mammalian tendon. *Journal of Biomechanical Engineering*, 1980, 102(4): 332–339.
- [122] Pioletti D P, Rakotomanana L R. On the independence of time and strain effects in the stress relaxation of ligaments and tendons. *Journal of Biomechanics*, 2000, 33(12): 1729–1732.
- [123] Yang W, Fung T C, Chian K S, et al. Viscoelasticity of esophageal tissue and application of a QLV model. *Journal of Biomechanical Engineering*, 2006, 128(6): 909–916.
- [124] Oyen M L, Cook R F, Stylianopoulos T, et al. Uniaxial and biaxial mechanical behavior of human amnion. *Journal of Materials Research*, 2005, 20(11): 2902–2909.
- [125] Dunn M G, Silver F H. Viscoelastic behavior of human connective tissues: Relative contribution of viscous and elastic components. *Connective Tissue Research*, 1983, 12(1): 59–70.

- [126] Woo S L Y, Lee T Q, Gomez M A, et al. Temperature dependent behaviour of the canine medial collateral ligament. *Journal of Biomechanical Engineering*, 1987, 109(1): 68–71.
- [127] Rigby R B, Hirai R, Spikes J D, et al. The mechanical properties of rat tail tendon. *The Journal of General Physiology*, 1959, 43: 265–283.
- [128] Sobol E, Sviridov A, Omel’chenko A, et al. Laser reshaping of cartilage. *Biotechnology and Genetic Engineering Reviews*, 2000, 17: 553–578.
- [129] Gaon M D, Wong B J F. Measurement of the elastic modulus of porcine septal cartilage specimens following Nd:YAG laser treatment. *Lasers in Medical Science*, 2003, 18(3): 370–379.
- [130] Wong B J F, Milner T E, Anvari B, et al. Measurement of radiometric surface temperature and integrated backscattered light intensity during feedback controlled laserassisted cartilage reshaping. *Lasers in Surgery and Medicine*, 1998, 13(1): 66–72.
- [131] Wong B J F, Milner T E, Kim H K, et al. Characterization of temperature dependent biophysical properties during laser mediated cartilage reshaping. *IEEE Journal of Selected Topics in Quantum Electronics*, 1999, 5(4): 1095–1102.
- [132] Karamzadeh A M, Wong B J F, Milner T E, et al. Temperature distributions in Nd:YAG (=1.32 mm) laser-irradiated cartilage grafts accompanied by cryogen spray cooling. *Society of Photo-Optical Instrumentation Engineers*, 1999, 3601: 422–433.
- [133] Chao K K, Ho K H, Wong B J. Measurement of the elastic modulus of rabbit nasal septal cartilage during Nd:YAG laser irradiation. *Lasers in Surgery and Medicine*, 2003, 32(5): 377–383.
- [134] Brinkmann R, Radt B, Flamm C, et al. Influence of temperature and time on thermally induced forces in corneal collagen and the effect on laser thermokeratoplasty. *Journal of Cataract and Refractive Surgery*, 2000, 26(5): 744–754.
- [135] Silver F H, Freeman J W, DeVore D. Viscoelastic properties of human skin and processed dermis. *Skin Research and Technology*, 2001, 7(1): 18–23.
- [136] Silver F H, Christiansen D L, Snowhill P B, et al. Role of storage on changes in the mechanical properties of tendon and self-assembled collagen fibers. *Connective Tissue Research*, 2000, 41(2): 155–164.
- [137] Silver F H, Horvath I, Foran D J. Viscoelasticity of the vessel wall: The role of collagen and elastic fibers. *Critical Reviews in Biomedical Engineering*, 2001, 29(3): 279–301.
- [138] Huang D, Chang T R, Aggarwal A, et al. Mechanisms and dynamics of mechanical strengthening in ligament-equivalent fibroblast-populated collagen matrices. *Annals of Biomedical Engineering*, 1993, 21(3): 289.
- [139] Fung Y C. *Biomechanics: Mechanical Properties of Living Tissue*. New York: Springer-Verlag, 1981.
- [140] Potts R O, Breuer M M. The low strain viscoelastic properties of skin. 3rd International Symposium on Bioengineering of the Skin. Philadelphia, 1981.
- [141] Sanjeevi R, Somanathan N, Ramaswamy D. A viscoelastic model for collagen fibres. *Journal of Biomechanics*, 1982, 15(3): 181–183.

- [142] Vogel H G. Age dependent mechanical and biochemical changes in the skin. *Bioeng Skin*, 1988, 4: 75–81.
- [143] Mansour J M, Davis B R, Srouf M, et al. Effects of ribose on the tensile behavior of skin: Application to a theory of aging. *Proceedings of ASME Biomechanics Symposium*, 1991: 299–302.
- [144] Wainwright S A, Biggs W D, Curry J D, et al. *Mechanical Designs in Organisms*. London: Edward Arnold, 1976.
- [145] Wilkes G L, Brown I A, Wildnauer R H. The biomechanical properties of skin. *CRC Critical Reviews in Bioengineering*, 1973, 1(4): 453–495.
- [146] Minns R J, Soden P D, Jackson D S. The role of the fibrous components and the ground substance in the mechanical properties of biological tissues: A preliminary investigation. *Journal of Biomechanics*, 1973, 6(2): 153–165.
- [147] Wells S M, Langille B L, Lee J M, et al. Determinants of mechanical properties in the developing ovine thoracic aorta. *American Journal of Physiology*, 1999, 277(4): H1385–H1391.
- [148] Nishimura M, Yan W, Mukudai Y, et al. Role of chondroitin sulfate-hyaluronan interactions in the viscoelastic properties of extracellular matrices and fluids. *Biochimica et Biophysica Acta*, 1998, 1380(1): 1–9.
- [149] Rochdi A, Foucat L, Renou J P. Effect of thermal denaturation on water-collagen interactions: NMR relaxation and differential scanning calorimetry analysis. *Biopolymers*, 1999, 50(7): 690–696.
- [150] Klavuhn K G. Epidermal protection: A comparative analysis of sapphire contact and cryogen spray cooling. *Laser Hair Removal Technical Note No. 1*, 2001.
- [151] Basinger B, Aguilar G, Nelson J S. Effect of skin indentation on heat transfer during cryogen spray cooling. *Lasers in Surgery and Medicine*, 2004, 34(2): 155–163.

PART IV SKIN THERMAL PAIN

Chapter 11

Skin Thermal Pain Mechanism

11.1 Introduction

Skin plays a variety of important roles including sensory, thermoregulatory and host defense, etc, which are essential in protecting the inside human body. However, in extreme environment, uncomfortable feeling or pain sensation is evocated due to extreme hot or cold. Obviously, skin fails in protecting the human body when the temperature is out of normal physiological range. Furthermore, in medicine, with advances in electromagnetic technologies such as laser and microwave, various thermal therapeutic methods have been widely used to cure disease/injury involving skin tissue. The associated problem of pain relief has nonetheless limited the further application and development of these thermal treatments.

As one of the most important sensations, pain sensation has been studied extensively for a long time over a range of scales, from molecular level (such as ion channel) to the entire human neural system level. Thermal stimulation, as one of the three main stimulations for pain (thermal, mechanical and chemical), has been widely used in the pain study^[1], such as the examination of tissue injury and sensitization mechanisms, and the quantification of therapeutic effects of pharmacological, physical, and psychological interventions^[2,3]. However, the understanding of the underlying mechanisms of thermal pain is still far from clear, the main reason being that pain is influenced by many factors, including both physiological factors such as stimulus intensity^[4,5] and duration^[6~8], and psychological factors such as attention^[9~11] and empathy^[12].

This chapter aims to provide a comprehensive description of the skin thermal mechanism, and is organised as follows. First, definition of pain and its classification, and pain pathways is introduced in Section 11.2. Since the pain sensation involved in this book is mainly nociceptive pain, the physiology and transduction function of nociceptors is described in detail in the Section 11.3. Afterwards, available theories are presented, including gate control

theory (GCT) and neuromatrix theory.

11.2 Definition of Pain and Pain Pathways

11.2.1 What is pain?

The International Association for the Study of Pain defines pain as: “an unpleasant sensory and emotional experience associated with actual or potential tissue damage, or described in terms of such damage”. Generally, pain can be classified as ① nociceptive pain: activation or sensitization of peripheral nociceptors; ② inflammatory pain: damaged tissue, inflammatory and tumor cells release chemical mediators which activate or modify the stimulus response properties of nociceptor afferents; ③ neuropathic pain: result of injury or acquired abnormalities of peripheral or central neural structures. In this book, we mainly focus on the nociceptive pain.

11.2.2 Pain pathways

The physiology of nociceptive pain has been studied extensively^[13~17]. The pain pathway is schematically shown in Figure 11.1 and can be simply described as ① transduction: when a stimulus is applied to the skin, the nociceptors located there trigger action potentials by converting the physical energy from a noxious thermal, mechanical, or chemical stimulus into

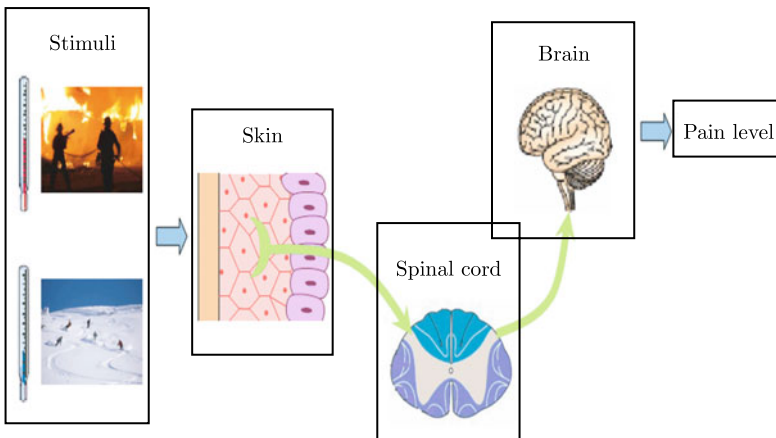


Figure 11.1 Skin thermal pain pathway: stimulus (hot/cold) → skin (the energy of thermal stimulus is converted into electrical energy via nerve impulses) → spinal cord & brain (the signals are transmitted to the dorsal horn of the spinal cord and brain, where they are modulated and perceived as pain sensation)(by permission of Elsevier)

electrochemical energy; ② transmission: the signals are subsequently transmitted in the form of chains of action potentials (similar to pulse trains) via nerve fibers from the site of transduction (periphery) to the dorsal horn of the spinal cord, which then activates the associated transmission neuron; ③ perception: the appreciation of signals arriving in higher structures as pain; ④ modulation: descending inhibitory and facilitatory input from the brain that influences (modulates) nociceptive transmission at the level of the spinal cord.

11.3 Anatomy and Physiology of Nociceptors

As the starting part of pain sensation pathway, the transduction function of nociceptors is described in detail in this section. Nociceptors, the special receptor for pain sensation, are the first cells in the series of neurons leading to the sensation of nociceptive pain^[18]. Nociceptors transduce mechanical, chemical and/or thermal energy to ionic current (noxious stimuli into depolarizations that generate action potentials), conduct the action potentials from the peripheral sensory site to the synapse in the central nervous system, and convert the action potentials into neurotransmitter release at the presynaptic terminal (frequency modulation)^[19].

11.3.1 Nociceptors for pain

Peripheral nerves include myelinated afferent $A\delta$ fibers and $A\alpha$ & $A\beta$ fibers, as well as unmyelinated C afferent fibers, as schematically shown in Figure 11.2. However, $A\beta$ fibers only respond to non-noxious, low density mechanical stimuli. Most nociceptors are either $A\delta$, or C fibers, while thermal pain sensations are mediated by both thin myelinated $A\delta$ and unmyelinated C fibers^[20].

$A\delta$ fiber nociceptors have medium-diameter (2~6 μm), lightly myelinated peripheral axons with intermediate conduction velocities (12~30 m/s). In comparison, C fibers have conduction velocities in the range 0.5~2 m/s whilst the rapidly conducting, large-diameter $A\beta$ fibers have conduction velocities ranging from 30 to 100 m/s^[15,21]. The conduction velocity is directly related to fiber diameter^[14], with the conduction velocities of $A\delta$ and C fibers accounting for the first (fast) and second (slow) pain responses, respectively^[14], as schematically show in Figure 11.3. C fiber nociceptors have small-diameter (0.4~1.2 μm), unmyelinated, slowly conducting axons and small (< 30 μm)-diameter cell bodies. Anatomically, most C fibers fall into one of two categories^[22]: one contains pro-inflammatory peptides and

is regulated by nerve growth factor; the other is nonpeptidergic and can be identified histologically. For example, for the 225 mechanosensitive afferent fibers identified in mouse glabrous skin, 106 were classed as $A\beta$ fibers, 51 as $A\delta$ fibers, and 68 as C fibers, with mean velocity of 22.2m/s, 7.1m/s and 0.7 m/s, respectively^[23]. For comparison, the conduction velocities of $A\beta$, $A\delta$ and C fibers of a peripheral nerve of the upper limb in normal human subjects were 69.1m/s, 10.6m/s and 1.2 m/s, respectively^[24].

Primary afferent axons




	$A\alpha$ and $A\beta$ fibres	Thermal threshold
	Myelinated Large diameter Proprioception light touch	None
<hr/>		
	$A\delta$ fibre	
	Lightly myelinated Medium diameter Nociception (mechanical, thermal, chemical)	$\approx 53^\circ\text{C}$ Type I $\approx 43^\circ\text{C}$ Type II
<hr/>		
	C fibre	
	Unmyelinated Small diameter Innocuous temperature, itch Nociception (mechanical, thermal, chemical)	$\approx 43^\circ\text{C}$

Figure 11.2 Different peripheral nociceptors and their features, including $A\alpha$, $A\beta$, $A\delta$ and C^[14] (by permission of Nature Publishing Group)

Furthermore, the so-called “silent” nociceptors have also been found, which in general cannot be activated^[25~42]. For example, in the survey of cutaneous C fibers, Bessou & Perl^[25] found that only 10% of the skin sample was inexcitable while Lynn & Carpenter^[26] and Pini & Baranowski^[27] found up to 28% of the nerve units in rat skin were inexcitable. Under conditions of inflammation or tissue injury, however, these silent nociceptors are sensitized and activated by a variety of chemical mediators^[30,31,37,43~46]. This recruitment of previously silent nociceptors under pathological states may contribute to temporal and spatial summation and considerably enhances the C fiber afferent barrage to the dorsal horn. It may also contribute both to primary hyperalgesia due to heat and pressure after chemical irritation, and secondary hyperalgesia as a consequence of central sensitization^[15,30,41,42].

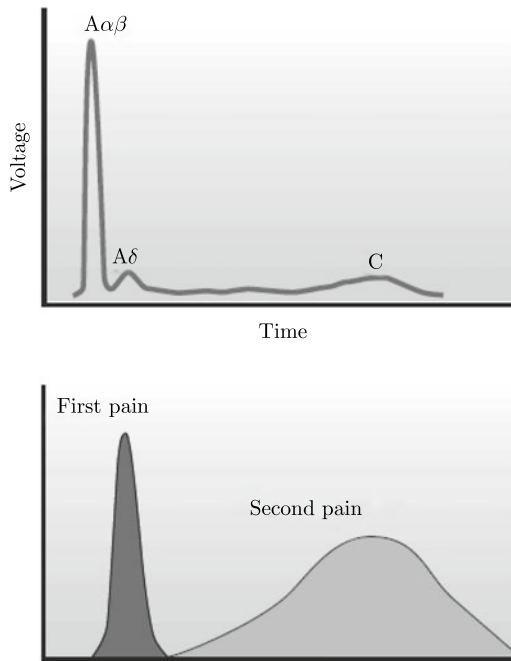


Figure 11.3 First and second pain response^[14](by permission of Nature Publishing Group)

11.3.2 Modalities of stimulation to nociceptors

According to the response to different stimulations, nociceptors can be further classified as: C and $A\delta$ mechanoheat nociceptors (CMH, AMH); C and $A\delta$ high threshold mechanoreceptors (CM, AM); C and $A\delta$ chemoreceptors; C and $A\delta$ polymodal nociceptors; C and $A\delta$ cold nociceptors; C and $A\delta$ mechanoinsensitive (silent) nociceptors. Besides, C fibers respond only to heating (CH) has also been found^[30]. For example, in the study of cutaneous sensory receptors in the skin of rat hindpaw, Leem et al.^[47] classed about 70% of $A\delta$ nociceptors as mechanical nociceptors, 20% as mechanoheat nociceptors, and 10% as mechanocoldnociceptors. In the thirty-two identified single C fibers, eleven had polymodal receptors, eight were only sensitive to mechanical stimuli, two were only sensitive to heat stimuli, and 11 were insensitive to both^[34].

The cutaneous nociceptors responding to thermal stimulations are largely polymodal, as they can be activated by thermal, mechanical, and/or chemical stimuli, and belong to six classes of distinctive afferents^[48,49]: ① C cold nociceptors ($< 10\text{ }^{\circ}\text{C}$); ② A cold and possible C cold afferents ($> 20\text{ }^{\circ}\text{C}$);

- ③ type I AMH ($> 53^{\circ}\text{C}$); ④ type II AMH ($> 46^{\circ}\text{C}$, mediator of first pain);
 ⑤ C warm afferent ($> 40^{\circ}\text{C}$); ⑥ CMH ($> 45^{\circ}\text{C}$, mediator of second pain).

11.3.3 Distribution of nociceptors in skin tissue

The skin is a large sense organ of the external environment. Numerous encapsulated and free sensory nerve endings within the skin respond to stimuli for temperature, pressure, touch, and pain. These perceptions are a consequence of variable combinations of three types of sensory receptor: mechanoreceptors for touch, vibration, pressure; thermal receptors for temperature; and nociceptors for pain.

Nociceptors with sensory terminals in skin have been widely studied since Burgess & Perl^[50] and Bessou & Perl^[25]. As for nociceptors in skin, C, $A\delta$ and $A\beta$ fibers are typically present in proportions about 70%, 10% and 20%, respectively, though these ratios may vary^[15]. Each of these fibers is attached to a receptor in the skin which may be a Meissner's corpuscle, a Pacinian corpuscle, a Ruffini or Krause end-organ or, for the great majority (60%~70%), a free nerve ending. Many unmyelinated C fibers can be traced far into the epidermal layer. Vertical sections reveal that free nerve endings emerge from superficial dermal nerve plexuses running beneath the epidermis into epidermis^[51], as shown by points in Figure 11.4 (a). The study of myelinated mechanical nociceptor endings in cat hairy skin showed that the free nerve endings for pain receptors exist around a depth of $50\ \mu\text{m}$ ^[52], while the receptors effective in mediating the pain sensation are calculated to be at a depth of approximately $200\ \mu\text{m}$ ^[53]. In comparison, the receptor depth in the hairskin of monkey estimated from responses to ramped stimuli ranged from 20 to $570\ \mu\text{m}$, with a mean of $201\ \mu\text{m}$ ^[54,55].

It has been found that C fibers have a higher density of distribution than $A\delta$ fibers^[56,57]. Depending on the species and the methods for quantification, the density distribution of C terminals is approximately $2\sim 8/\text{mm}^2$ while that of $A\delta$ fibers is less than $1/\text{mm}^2$ ^[58].

11.3.4 Ion channels of nociceptors

All the essential functions of nociceptors depend on ion channels^[13,19], which are integral membrane proteins found in all cells that mediate the selective passage of specific ions or molecules across a cell membrane^[59]. The ion channels that have been found in nociceptors include: heat activated channels^[60~63]; capsaicin receptor^[64,65], ATP-gated channels^[66~69]; Proton-gated channels or acid-sensing channels^[70~72]; nociceptor-specific voltage-

gated Na^+ channels^[73], mechanosensitive channels, amongst others. In spite of these different channels, they are generally converted from closed to open states or “gated” by mainly three types of stimulus, namely, thermal (hot or cold), mechanical, and chemical stimuli, with thresholds of 43°C and about 0.2MPa for the first two. Although not directly gated by stimuli, channels that are gated by changes in transmembrane voltage form a very important class of channels. These voltage-gated channels that respond to membrane depolarization or hyperpolarization are central to the generation and transmission of electrical signals along nerve axons^[74].

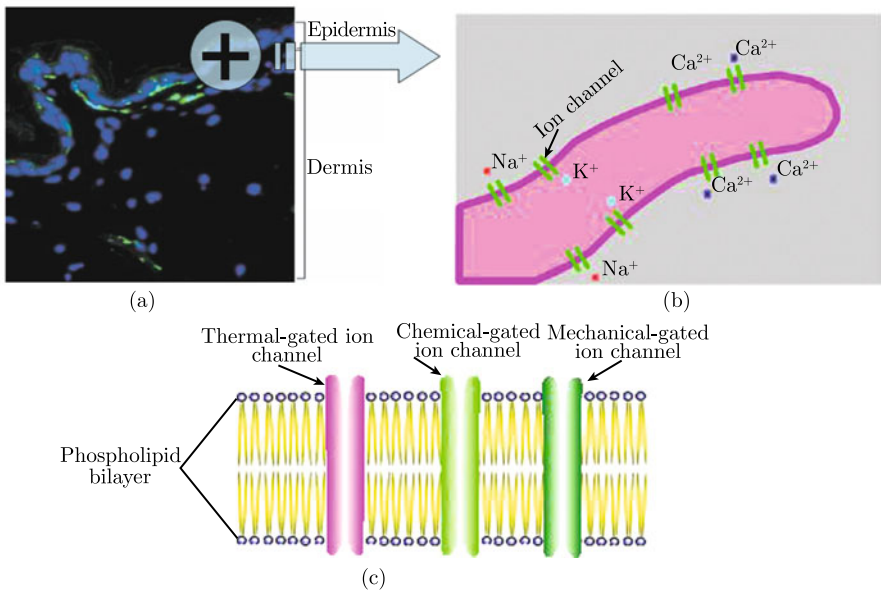
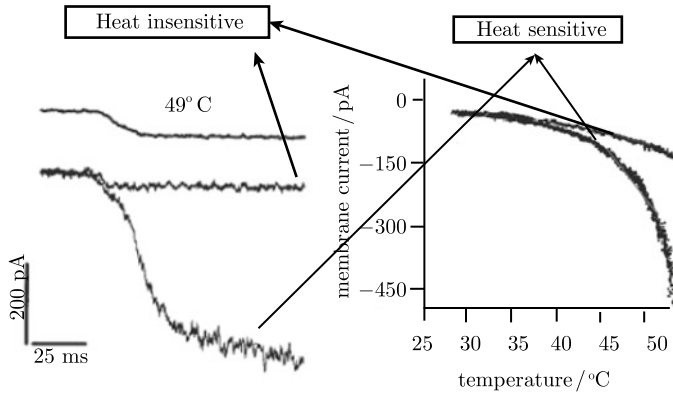


Figure 11.4 Schematic of nociceptor transduction: if the thermal stimulus surpasses the thermal threshold of nociceptors [points in (a)^[51]], the heat current will be induced due to the opening of the corresponding ion channels in (b), and the action potential is triggered; the thermal stress and thermal-damage-induced release of some chemical mediators may also open corresponding mechanically- and chemically-gated channels in (c) if it is larger than the mechanical threshold (by permission of Nature Publishing Group)

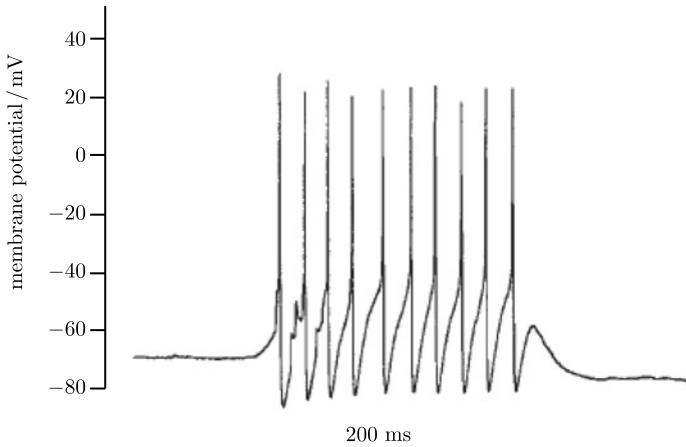
When a noxious stimulus is applied to a nociceptor (larger than the threshold), the corresponding ion channels will be opened, as shown in Figure 11.5, which will induce a heat current through the nociceptor membrane and increase the membrane voltage. When the membrane voltage increases more than the threshold, the current will then open more channels in a positive feedback mode that results in the depolarization of the membrane, generat-

ing eventually the action potential. For example, when a thermal loading is applied to a nociceptor, the heat activated channels will be opened. The corresponding heat current and action potential are shown in Figure 11.5(a) and (b), respectively.



(a)

49°C



(b)

Figure 11.5 Action potential triggered by a thermal stimulus^[75]: (a) application of a rapid step change in temperature elicits an inward current in both heat-sensitive and heat-insensitive nociceptive neurons, but it is much smaller for heat-insensitive neurons; (b) a train of action potentials initiated in a nociceptive neuron in culture by application of a brief heat stimulus (by permission of National Academy of Sciences, U.S.A.)

Although a tremendous amount of work has been done on the histomorphology and electrophysiology of skin thermal pain nerve circuits, the exact coupling between neural and thermomechanical participations is yet precisely known.

11.4 Theories of Thermal Pain

11.4.1 Gate control theory

Early pain theories did not taken the brain into account, e.g. the so-called pain-pleasure theory proposed by René Descartes¹⁾ in seventieth century, where pain is thought to be simply a direct response to a stimulus. However, this theory failed to explain many pain phenomena. A number of other theories have been also proposed to explain the neural mechanisms associated with pain^[76], among which the gate control theory, proposed by Melzack & Wall in 1965^[77], was more successful than many others in explaining the important features of pain process. It was the turning point in pain research and the basis for many of the subsequent advances in the understanding of pain. Figure 11.6 (a) shows a schematic of the original version of the theory. In general, it is the small (C, A δ) fibers that carry information about noxious stimuli whilst the role of the large (A β) fibers is to carry information about less intense mechanical stimuli. As the signal from the (C, A δ) fibers is routed through substantia gelatinosa (SG) to central transmission (T) cells and onwards, the double inhibition (indicated by the minus signs) strengthens the signal. The signal from the A β fibers, however, is diminished in strength when routed through SG. The gate control system is therefore described as follows:

(1) When there is no stimulus, the small activity of the small fibers tends to keep the gate somewhat open and the very small activity of the large fibers is not enough to close it;

(2) When a small stimulus is applied to the skin, the activity of the large fibers becomes relatively more intense although both types of fiber become more active, which tends to close the gate and results in passing through of a smaller proportion of the barrage;

(3) When the stimulus is strengthened, the activity of both small and large fibers gets increase equally, which does not change the gate;

(4) When the stimulus is maintained for a period of time, the natural adaptation of the L cells makes both fibers less active, which causes the gate

1) René Descartes was a highly influential French philosopher, mathematician, scientist, and writer.

to open further;

(5) When the stimulus is still maintained but the L cells are kept active through (vibration), the gate tends to close.

The theory was later modified by Melzack & Wall^[78], as shown in Figure 11.6(b). The new model included excitatory (white circle) and inhibitory (black circle) links from SG to T-cells as well as descending inhibitory control from some brainstem structures. The round knob at the end of the inhibitory link implies that its actions may be presynaptic, postsynaptic, or both. All connections are excitatory, except the inhibitory link from SG to T-cells.

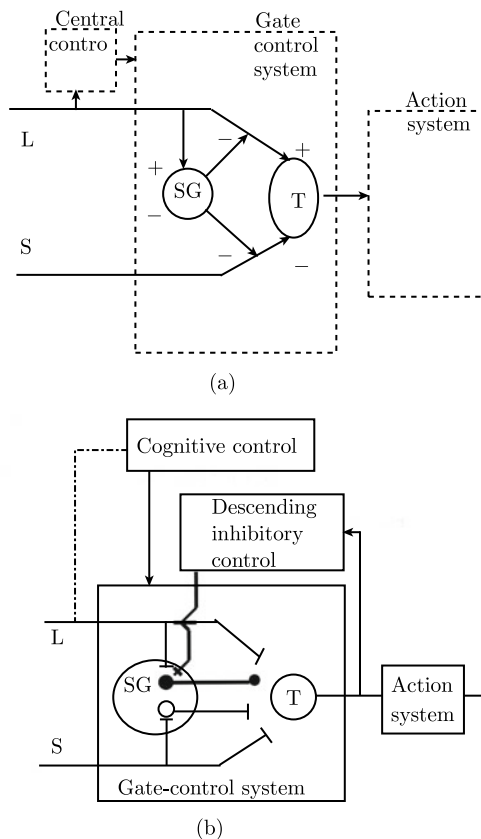


Figure 11.6 Schematic of the (a) Gate-control theory and (b) its modified version

11.4.2 Neuromatrix theory

The neuromatrix theory was proposed by Melzack in 1999^[79], which integrates multiple inputs to produce the output pattern that evokes pain. The

body-self neuromatrix comprises a widely distributed neural network that includes somatosensory, limbic, and thalamocortical components, as shown in Figure 11.7. In the figure, it is schematically depicted as a circle containing smaller parallel networks that contribute to the sensory discriminative (S), affective-motivational (A), and evaluative-cognitive (E) dimensions of pain experience. The synaptic architecture of the neuromatrix is determined by genetic and sensory influences, and the “neurosignature” output of the neuromatrix (patterns of nerve impulses of varying temporal and spatial dimensions) is produced by neural programs, which is genetically built into the neuromatrix to determine the particular qualities and other properties of the pain experience and behaviour.

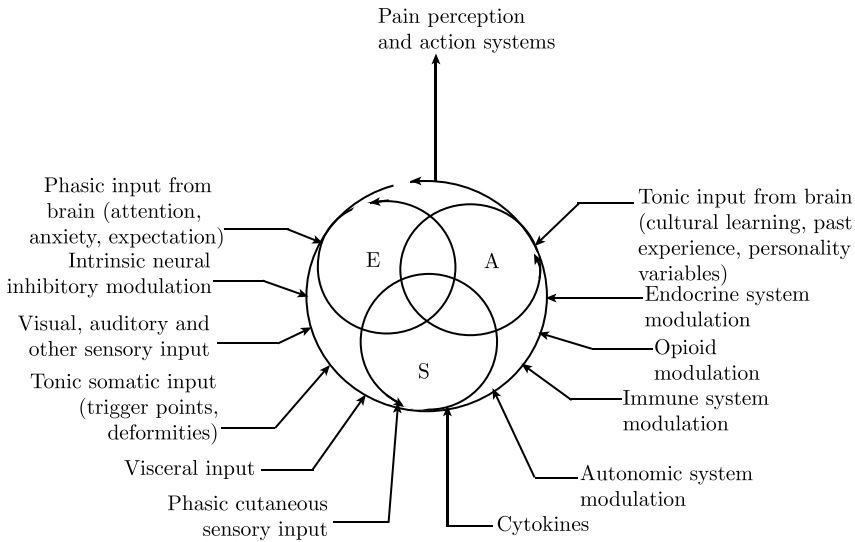


Figure 11.7 The body-self neuromatrix^[79](by permission of Elsevier)

There are several inputs that act on the neuromatrix programs and contribute to the output neurosignature, given as: ① sensory inputs from somatic receptors (phasic cutaneous, visceral and tonic somatic inputs); ② visual and other sensory inputs that influence the cognitive interpretation of the situation; ③ phasic and tonic cognitive and emotional inputs from other areas of the brain; ④ intrinsic neural inhibitory modulation inherent in all brain function; ⑤ the activity of the body’s stress-regulation systems.

References

- [1] Towell A D, Purves A M, Boyd S G. CO₂ laser activation of nociceptive and

- non-nociceptive thermal afferents from hairy and glabrous skin. *Pain*, 66(1): 79–86.
- [2] Borckardt J J, Anderson B, Andrew Kozel F, et al. Acute and long-term VNS effects on pain perception in a case of treatment-resistant depression. *Neurocase*, 2006, 12(4): 216–220.
 - [3] Mao-Ying Q L, Cui K M, Liu Q, et al. Stage-dependent analgesia of electroacupuncture in a mouse model of cutaneous cancer pain. *European Journal of Pain*, 2006,10(8): 689–694.
 - [4] LaMotte R H, Campbell J N. Comparison of responses of warm and nociceptive C-fiber afferents in monkey with human judgments of thermal pain. *Journal of Neurophysiology*, 1978,41(2): 509–528.
 - [5] Torebjork H E, LaMotte R H, Robinson C J. Peripheral neural correlates of magnitude of cutaneous pain and hyperalgesia: Simultaneous recordings in humans of sensory judgments of pain and evoked responses in nociceptors with C-fibers. *Journal of Neurophysiology*, 1984,51(2): 325–339.
 - [6] Pertovaara A, Kaupila T, Hmlinen M. Influence of skin temperature on heat pain threshold in humans. *Experimental Brain Research*, 1996,107(3): 497–503.
 - [7] Nielsen J, Arendt-Nielsen L. The importance of stimulus configuration for temporal summation of first and second pain to repeated heat stimuli. *European Journal of Pain*, 1998,2(4): 329–341.
 - [8] Pertovaara A. The influence of stimulus temperature rise rate, adapting temperature, and stimulus duration on suprathreshold responses evoked by noxious heat in the glabrous skin of the limb comparison of neuronal discharge in the rat spinal dorsal horn with human sensations. *Experimental Brain Research*, 1999,126(4): 482–494.
 - [9] Miron D, Duncan G H, Bushnell M C. Effects of attention on the intensity and unpleasantness of thermal pain. *Pain*, 1989,39(3): 345–352.
 - [10] Jones A K, Derbyshire S W. Reduced cortical responses to noxious heat in patients with rheumatoid arthritis. *Annals of the Rheumatic Diseases*, 1997,56(10): 601–607.
 - [11] Brooks J C, Nurmikko T J, Bimson W E, et al. MRI of thermal pain: Effects of stimulus laterality and attention. *NeuroImage*, 2002,15(2): 293–301.
 - [12] Kakigi R, Inui K, Tran D T, et al. Human brain processing and central mechanisms of pain as observed by electro- and magneto-encephalography. *Journal of Chinese Medical Association*, 2004,67(8): 377–386.
 - [13] Caterina M J, Julius D. Sense and specificity: A molecular identity for nociceptors. *Current Opinion in Neurobiology*, 1999,9(5): 525–530.
 - [14] Julius D, Basbaum A I. Molecular mechanisms of nociception. *Nature*, 2001, 413 (6852): 203–210.
 - [15] Millan M J. The induction of pain: An integrative review. *Progress in Neurobiology*, 1999,57(1): 1–164.
 - [16] Brooks J, Tracey I. From nociception to pain perception: Imaging the spinal and supraspinal pathways. *Journal of Anatomy*, 2005,207(1): 19–33.

- [17] Cesare P, McNaughton P A. Peripheral pain mechanisms. *Current Opinion in Neurobiology*, 1997,7: 493–499.
- [18] Sherrington C S. *The Integrative Action of the Nervous System*. New York: Scribner, 1906.
- [19] McCleskey E W, Gold M S. Ion channels of nociception. *Annual Review of Physiology*, 1999,61: 835–856.
- [20] Meyer R A, Campbell J N, Raja S N. Peripheral neural mechanisms of nociception//Wall P D, Melzack R. *Textbook of Pain*. London: Churchill, 1994: 13–44.
- [21] Harper A A, Lawson S N. Conduction velocity is related to morphological cell type in rat dorsal root ganglion neurons. *The Journal of Physiology (London)*, 1985,359: 31–46.
- [22] Snider W D, McMahon S B. Tackling pain at the source: New ideas about nociceptors. *Neuron*, 1998,20(4): 629–632.
- [23] Cain D M, Khasabov S G, Simone D A. Response properties of mechanoreceptors and nociceptors in mouse glabrous skin: An in vivo study. *Journal of Neurophysiology*, 2001,85(4): 1561–1574.
- [24] Tran T D, Lam K, Hoshiyama M, et al. A new method for measuring the conduction velocities of Aβ-, Aδ- and C-fibers following electric and CO₂ laser stimulation in humans. *Neuroscience Letters*, 2001,301(3): 187–190.
- [25] Bessou P, Perl E R. Response of cutaneous sensory units with unmyelinated fibers to noxious stimuli. *Journal of Neurophysiology*, 1969,32: 1025–1043.
- [26] Lynn B, Carpenter S E. Primary afferent units from the hairy skin of the rat hind limb. *Brain Research*, 1982,238(1): 29–43.
- [27] Pini A, Baranowski R, Lynn B. Longterm reduction in the number of C-fibre nociceptors following capsaicin treatment of a cutaneous nerve in adult rats. *European Journal of Neuroscience*, 1990,2(1): 89–97.
- [28] Schaible H G, Grubb B D. Afferent and spinal mechanisms of joint pain. *Pain*, 1993,55(1): 5–54.
- [29] Cervero F, Meyer R A, Campbell J N. A psychophysical study of secondary hyperalgesia: Evidence for increased pain to input from nociceptors. *Pain*, 1994,58(1): 21–28.
- [30] Schmidt R, Schmelz M, Forster C, et al. Novel classes of responsive and unresponsive C nociceptors in human skin. *Journal of Neuroscience*, 1995,15(1): 333–341.
- [31] Siddall P J, Cousins M J. Spinal pain mechanisms. *The Spine Journal*, 1997,22(1): 98–104.
- [32] Treede R D, Meyer R A, Campbell J N. Myelinated mechanically insensitive afferents from monkey hairy skin: Heat-response properties. *Journal of Neurophysiology*, 1998,80(3): 1082–1093.
- [33] Torebjork E. Subpopulations of human C-nociceptors and their sensory correlates. 9th World Congress on Pain. Seattle: IASP Press, 2000: 199–206.
- [34] Watanabe M, Toma S, Murakami M, et al. Assessment of mechanical and

- thermal thresholds of human C nociceptors during increases in skin sympathetic nerve activity. *Clinical Neurophysiology*, 2002,113(9): 1485–1490.
- [35] McMahon S, Koltzenburg M. The changing role of primary afferent neurones in pain. *Pain*, 1990,43(3): 269–272.
- [36] McMahon S B, Koltzenburg M. Novel classes of nociceptors: Beyond Sherrington. *Trends in Neurosciences*, 1990,13(6): 199–201.
- [37] Koltzenburg M, Torebjork H E. Pain and hyperalgesia in acute inflammatory and chronic neuropathic conditions. *Lancet*, 1995,345(8957): 1111.
- [38] Treede R D, Meyer R A, Raja S N, et al. Peripheral and central mechanisms of cutaneous hyperalgesia. *Progress in Neurobiology*, 1992,38(4): 397–421.
- [39] Messlinger K. What is a nociceptor? *Anaesthetist*, 1997,46(2): 142–153.
- [40] Gee M D, Lynn B, Cotsell B. Activity-dependent slowing of conduction velocity provides a method for identifying different functional classes of C-fibre in the rat saphenous nerve. *Neuroscience*, 1996,73(3): 667–675.
- [41] Kress M, Rodl J, Reeh P W. Stable analogues of cyclic AMP but not cyclic GMP sensitize unmyelinated primary afferents in rat skin to heat stimulation but not to inflammatory mediators, in vitro. *Neuroscience*, 1996,74(2): 609–617.
- [42] Schmidt R, Schmelz M, Torebjork H E, et al. Mechano-insensitive nociceptors encode pain evoked by tonic pressure to human skin. *Neuroscience*, 2000,98(4): 793–800.
- [43] Reeh P W, Bayer J, Kocher L, et al. Sensitization of nociceptive cutaneous nerve fibers from the rat's tail by noxious mechanical stimulation. *Experimental Brain Research*, 1987,65(3): 505–512.
- [44] Sengupta J N, Gebhart G F. Mechanosensitive properties of pelvic nerve afferent fibers innervating the urinary bladder of the rat. *Journal of Neurophysiology*, 1994,72(5): 2420–2430.
- [45] Sengupta J N, Gebhart G F. Characterization of mechanosensitive pelvic nerve afferent fibers innervating the colon of the rat. *Journal of Neurophysiology*, 1994,71(6): 2046–2060.
- [46] Dmitrieva N, McMahon S B. Sensitisation of visceral afferents by nerve growth factor in the adult rat. *Pain*, 1996,66(1): 87–97.
- [47] Leem J W, Willis W D, Chung J M. Cutaneous sensory receptors in the rat foot. *Journal of Neurophysiology*, 1993,69(5): 1684–1699.
- [48] Simone D A, Kajander K C. Responses of cutaneous A-fiber nociceptors to noxious cold. *Journal of Neurophysiology*, 1997,77(4): 2049–2060.
- [49] Arendt-Nielsen L, Chen A C N. Lasers and other thermal stimulators for activation of skin nociceptors in humans. *Clinical Neurophysiology*, 2003,33(6): 259–268.
- [50] Burgess P R, Perl E R. Myelinated afferent fibres responding specifically to noxious stimulation of the skin. *The Journal of Physiology (London)*, 1967,90(3): 541–562.
- [51] Patapoutian A, Peier A M, Story G M, et al. Thermo TRP channels and beyond: Mechanisms of temperature sensation. *Nature Reviews Neuroscience*, 2003,4(8): 529–539.

- [52] Kruger L, Perl E R, Sedivec M J. Fine structure of myelinated mechanical nociceptor endings in cat hairy skin. *The Journal of Comparative Neurology*, 1981,198(1): 137–154.
- [53] Stoll A M, Greene L C. Relationship between pain and tissue damage due to thermal radiation. *Journal of Applied Physiology*, 1959,14(3): 373–382.
- [54] Tillman D B, Treede R D, Meyer R A, et al. Response of C fibre nociceptors in the anaesthetized monkey to heat stimuli: Correlation with pain threshold in humans. *The Journal of Physiology*, 1995,485 (3): 767–774.
- [55] Tillman D B, Treede R D, Meyer R A, et al. Response of C fibre nociceptors in the anaesthetized monkey to heat stimuli: Estimates of receptor depth and threshold. *The Journal of Physiology*, 1995,485 (3): 753–765.
- [56] Ochoa J, Mair W G. The normal sural nerve in man. I. Ultrastructure and numbers of fibres and cells. *Acta Neuropathol (Berlin)*, 1969,13(3): 197–216.
- [57] Tran T D, Inui K, Hoshiyama M, et al. Conduction velocity of the spinothalamic tract following CO₂ laser stimulation of C-fibers in humans. *Pain*, 2002,95(1-2): 125–131.
- [58] Lynn B, Baranowski R A. Relative numbers and properties of cutaneous nociceptors in different species//Schmidt R F, Schaible H G, Vahle-Hinz C. *Fine Afferent Nerve Fibers and Pain*. Weinheim: VCH, 1987: 86–94.
- [59] Alberts B, Bray D, Lewis J, et al. *Molecular Biology of the Cell*. New York: Garland, 1994.
- [60] Cesare P, McNaughton P A. A novel heat-activated current in nociceptive neurons and its sensitization by bradykinin. *Proceedings of the National Academy of Sciences. USA*, 1996, 93(26): 15435–15439.
- [61] Dittert I, Vlachova V, Knotkova H, et al. A technique for fast application of heated solutions of different composition to cultured neurones. *Journal of Neuroscience Methods*, 1998,82(2): 195–201.
- [62] Kirschstein T. Coexpression of heat-evoked and capsaicin-evoked inward currents in acutely dissociated rat dorsal root ganglion neurons. *Neuroscience Letters*, 1997,231(1): 33–36.
- [63] Nagy I, Rang H. Noxious heat activates all capsaicin-sensitive and also a sub-population of capsaicin-insensitive dorsal root ganglion neurons. *Neuroscience*, 1999,88(4): 995–997.
- [64] Nagy I, Rang H P. Similarities and differences between the responses of rat sensory neurons to noxious heat and capsaicin. *The Journal of Neuroscience*, 1999, 19(24): 10647–10655.
- [65] Caterina M J, Rosen T A, Tominaga M, et al. Capsaicin-receptor homologue with a high threshold for noxious heat. *Nature*, 1999,398(6726): 436–441.
- [66] Burnstock G. A unifying purinergic hypothesis for the initiation of pain. *The Lancet Neurology*, 1996,347(9015): 1604–1605.
- [67] Burnstock G, Wood J N. Purinergic receptors: Their role in nociception and primary afferent neurotransmission. *Current Opinion in Neurobiology*, 1996,6(4): 526–532.
- [68] Hamilton S G. ATP and pain. *Pain Practice*, 2002,2(4): 289–294.

- [69] Hilliges M, Weidner C, Schmelz M, et al. ATP responses in human C nociceptors. *Pain*, 2002,98(1-2): 59–68.
- [70] Krishtal O A, Pidoplichko V I. A receptor for protons in the nerve cell membrane. *Neuroscience*, 1980,5(12): 2325–2327.
- [71] Krishtal O A, Pidoplichko V I. A receptor for protons in the membrane of sensory neurons may participate in nociception. *Neuroscience*, 1981,6(12): 2599–2601.
- [72] Waldmann R. Proton-gated cation channels: Neuronal acid sensors in the central and peripheral nervous system. *Advances in Experimental Medicine and Biology*, 2001,502: 293–304.
- [73] Waxman S G, Dib-Hajj S, Cummins T R, et al. Sodium channels and pain. *Proceedings of the National Academy of Sciences. USA*, 1999,96: 7635–7639.
- [74] Elmore D E. Investigations of Ion Channel Structure-Function Relationships Using Molecular Modeling and Experimental Biochemistry [Ph. D. Thesis]. California: California Institute of Technology, 2004.
- [75] Cesare P, Moriondo A, Vellani V, et al. Ion channels gated by heat. *Proceedings of the National Academy of Sciences. USA*, 1999,96(14): 7658–7663.
- [76] Guyton A C, Hall J E. *Textbook of Medical Physiology*. 10th Edition. Philadelphia: WB Saunders, 2000.
- [77] Melzack R, Wall P D. Pain mechanisms: A new theory. *Science*, 1965,150(699): 971–979.
- [78] Melzack R, Wall P D. *The Challenge of Pain*. New York: Basic Book, 1983.
- [79] Melzack R. From the gate to the neuromatrix. *Pain*, 1999,Suppl. 6: S121–S126.

Chapter 12

Physiological Features of Pain Sensation

12.1 Introduction

It is well known that pain sensation exhibits physiological and psychological features and is influenced by many factors such as the strength of the noxious stimulus, state of the organism, and environmental variables. As engineers, we want to know the different features of skin thermal pain and how they are induced. This will be helpful for engineers to apply engineering methods to solve biological and neural problems. In this chapter we mainly discuss the physiological features of pain sensation, and psychological features are not included in this chapter.

12.2 Role of C and A δ Nociceptors

Information about noxious events in the periphery is signaled to the spinal cord in unmyelinated (C fiber) and myelinated A α / β and A δ fiber (A fiber) nociceptors. Differences in the physiology of myelinated and unmyelinated nociceptors^[1] suggest that they play different roles in the pain experience.

In order to understand the different roles of A and C fibers in pain sensation, a multitude of techniques have been developed. There are generally four different selective activations of nociceptors based on their different characteristics^[2]: ① difference in resistance to ischemic compression block; ② difference in threshold; ③ difference in distribution density; ④ selective pathology of A δ fibers. For example, selective block of A or C fiber conduction can be accomplished with local anesthetics or pressure/ischemia^[3]. Low and high noxious skin heating rates preferentially activate C or A nociceptors, respectively^[4]. Yarnitsky & Ochoa^[5] found that for low rates of temperature rise ($< 2.0^\circ\text{C/s}$), pain threshold is signaled by C fiber activity. There appears to be a clear difference in the response thresholds between A δ and C nociceptors in monkeys^[6]: the response thresholds for most A δ

nociceptors were less than 0°C , whereas those of most C nociceptors were more than 0°C ^[7]. This supports the notion that C nociceptors contribute to the sensation of dull pain produced by cold stimuli ($\geq 0^{\circ}\text{C}$) and that A δ nociceptors contribute to pricking pain evoked by cold stimuli ($< 0^{\circ}\text{C}$) and by skin freezing. The threshold, magnitude and reaction time of heat pain best correlate with the activity of C nociceptors recorded in monkeys and in humans^[8], and are not altered significantly by the conduction block of A δ fibers^[9]. It has also been found that the C fibers responsive to intense and painful, cold stimuli are located along vein walls, whereas the thermosensory A δ fibers responsive to cooling are localized cutaneously^[10].

With various techniques, the different roles in the pain experience have been studied. Generally speaking, upon exposure of the skin to a noxious stimulus, myelinated A δ fibers elicit a rapid, first phase of pain, which is “sharp” in nature, whereas unmyelinated C fibers evoke a second wave of “dull” pain^[11]. However, the micro-stimulation of C polymodal fibers also produced dull pain^[12] depending on the skin areas they innervate. Besides, psychophysical studies of first and second pain produced by heat have shown that first pain is quickly suppressed with repeated heating^[13]. Furthermore, the myelinated and unmyelinated nociceptive primary afferents play different roles in the establishment and maintenance of secondary hyperalgesia^[14], suggesting that they have different functions in chronic pain states. With regard to the affective component of the pain experience, recent reports that A and C fiber inputs activate distinct brainstem circuits suggest that the precise pattern of autonomic responses evoked by noxious stimulation depends upon the relative contributions of A and C nociceptor-evoked activity^[15]. McMullan & Lumb^[16] found that descending control has differential effects on the central processing of A versus C nociceptive input.

However, considerable controversy also exists concerning the true selectivity of this technique^[17]. For example, LaMotte & Thalhammer^[18] found no differences in the responses of A δ and C polymodal nociceptors to noxious cold reaching 2°C . Harrison & Davis^[19] found the absolute thresholds at different cooling rates become more similar with the C fiber estimate than with the A δ fiber estimate but still vary with cooling rate. In normal individuals, a cold stimulus delivered during experimental A fiber block feels hot and burning, suggesting a complex interaction between A and C fiber primary afferents^[20]. In studies of a small sample of C and A δ nociceptors in rat, Simone & Kajander^[21] found that the response thresholds for cold stimuli and the responses evoked by suprathreshold stimuli did not differ from each other.

As for cold pain, it is likely that pricking pain produced by cold stimuli is mediated, at least in part, by excitation of $A\delta$ nociceptors. C fiber nociceptors may also contribute to the sensation of cold pain, because a portion of C nociceptors in animals^[22] and humans^[23] was excited by noxious cold.

12.3 Influence of Stimulus Temperature on Pain

It is well known that the magnitude of temperature has a great effect on pain. For example, LaMotte & Campbell^[24] found that heat pain increases monotonically with stimulus intensities between 40 °C and 50 °C, whilst Torebjork et al.^[8] observed a linear relationship between the mean responses of CMHs (C fiber mechano-heat nociceptors) recorded in awake humans and median ratings of pain over the temperature range of 39~51°C. It was also shown that the intensity of cold pain is linearly correlated with that of a cold stimulus^[25]. For example, Georgopoulos^[26] found that the stimulus-response functions were approximately linear, with mean slopes of power functions of 1.15 while Simone & Kajander^[6] obtained a slope of 1.07.

12.4 Influence of Nociceptors Depth

Haimi-Cohen et al.^[27] found that the receptor threshold temperature was 45 °C when the receptor layer was set between the epidermis and the dermis; however, Tillmann et al.^[28] found the value of 40.4 °C at a depth of 200 μm for a heat stimulus having the same magnitude. Tillman et al.^[29] also found that the heat threshold for C fiber mechano-heat nociceptors was determined by receptor depth.

12.5 Influence of Temperature Change Rate on Pain

It has been shown that higher firing frequencies are evoked by higher rates of temperature change in warm and cold-specific afferents^[30]. However, studies on the effect of stimulus ramp rate on suprathreshold pain sensation have given conflicting results.

It has been found that the threshold increases with faster rates of change in skin temperature^[31]. For example, Lynn^[32] found lower thresholds for rates of 0.2 than for 2.0 °C/s in rabbits. The surface temperature thresholds were found to be 41.9 °C for stimulus ramp rate of 5.8 °C/s, 40.1 °C for rate of 0.85 °C/s, and 39.6 °C for rate of 0.095 °C/s^[28]. Treede et al.^[33] found that the threshold for detecting an action potential in the C fiber of the monkey increased with ramp rate in the range of 0.1°C/s, 1.0°C/s and

10.0 °C/s. Defrin et al.^[4] found that the pain threshold difference was as large as 4 °C measured in the range of 0.5~40 °C/s, and a much steeper stimulus-response function for pain sensation was observed for stimuli with a faster rise rate, while the slopes for the slow rate resemble those of the power functions for C fibers discharge evoked by noxious heat in rats.

Bessou & Perl^[34] found higher discharge rates in cat polymodal nociceptors for faster heating rates. In humans, faster heating rates to suprathreshold temperatures evoke higher C fiber activity and higher peak magnitude estimates of pain^[35]. Tillman et al.^[29] found that the peak discharge frequency of CMHs during the heat ramp increased with stimulus ramp rate.

Harrison & Davis^[19] found that faster rates (0.5°C/s, 1°C/s or 2 °C /s) of cooling increased the thresholds and decreased the supra-threshold indices of pain. The same results have been reported previously by Croze & Duclaux^[36].

However, others found no influence of the temperature change rate^[37]. For example, Corze et al.^[38] observed no change in nociceptor threshold between rates of 0.2°C/s and 1.5 °C/s in monkey; Nielsen & Arendt-Nielsen^[39] did not find any change in human C nociceptor firing threshold between the three rates of temperature rise used (0.3°C/s, 2.0°C/s and 6.0 °C/s); and Pertovaara^[37] found that the magnitudes of sensory and spinal neuronal response were independent of the stimulus ramp rate (2.5°C/s, 5.0°C/s, and 10.0 °C/s).

Conflicting results have also been reported. For example, with increasing rate of rising temperature stimuli, Yarnitsky et al.^[35] found the magnitude estimates of pain increased, while Nielsen & Arendt-Nielsen^[40] observed a decrease in the magnitude estimate.

Possible explanations

(1) At low rise rates of the stimulus temperature, the threshold responses may be based on the activation of unmyelinated C fibers^[41], whereas, at high rise rates, they may be based on the activation of thin myelinated A δ fibers^[42]. For example, the pressure block of A δ fibers caused a dramatic elevation of pain threshold for fast rise stimuli while had no influence on the threshold for slow rise stimulation^[4]. However, there are results in humans^[35] and in monkeys^[29] showing that increased response rates can also be recorded from C fibers when the rate of rise of noxious thermal stimulation is increased.

(2) Reaction time factors were proposed as a possible explanation^[43]. Since there is a delayed diffusion of heat energy into nociceptor endings, a higher stimulus temperature is needed to produce C fiber activation and pain sensation with an increase in stimulus ramp rate^[29]. Consequently, heat

pain threshold determined using this reaction time-based method is markedly elevated^[5].

(3) The influence of stimulus ramp rate on heat pain threshold can be explained by an artifact caused by the long delay in the arrival of a peripheral afferent volley at the brain^[5].

(4) Different methods used: the increase of pain threshold with increasing stimulus ramp rate was found only with subject-controlled ascending stimuli (method of limits) but not with experimenter-controlled, predetermined stimulus ramps (method of levels)^[44].

(5) The discrepancies in results for the effect of ramp rate on heat-evoked responses may be caused by the different experimental parameters used^[37]. An increase in pain magnitude estimates and in peak discharge frequency of primary afferent nociceptors were observed when slower ramp rates were used, while the mechanisms causing an increase in neuronal discharge frequency may have been saturated when higher rates were used. A possible explanation relates to the size of the area stimulated since different sizes have been used^[39]. It is suspected that heating larger surfaces might induce greater skin warming, through higher energy input and lesser heat dissipation.

(6) At the higher ramp rate, a faster transducing or conducting population of primary afferent fibers was recruited^[41] and a faster rate produced a higher maximum discharge and a more synchronized volley in primary afferents^[37].

(7) The different response obtained with slow and fast rise stimuli may be a result of the temporal parameters of the presented stimuli^[4].

12.6 Temporal Summation

12.6.1 Wind up

Wind up review^[45]:

The temporal summation of repetitive noxious stimuli, or wind up, refers to the enhancement of perceived pain intensity when noxious stimuli are delivered repetitively above a critical rate^[46]. When peripheral afferent C fibers are activated repetitively at frequencies greater than about 0.3 Hz, wide dynamic range (WDR) neurons show progressively increasing responses to unchanging or diminishing afferent inputs^[47].

Not only are the phenomena of wind up and temporal summation of pain intensity regarded as dependent on activation of C afferents^[46], but also it has seemed likely that stimulation of nociceptors is required^[48]. However, the temporal summation of thermal sensation to very strong levels of pain

could be produced by the repetition of a stimulus that produced only sensations of warmth when presented at frequencies of being equal and less than 0.14 Hz^[48]. This finding opens the possibility that the temporal summation to painful levels does not depend on the activation of nociceptors. Alternatively, some nociceptors may be activated by temperatures that elicit only sensations of warmth, or nociceptor activity may be recruited especially by brief contacts of the preheated thermode at frequencies more than 0.14 Hz. Convincing evidence has been provided by a demonstration that peripheral nociceptor discharge is suppressed progressively by repetitive stimulation that produces wind up of central cells^[47]. Using ramped thermal stimulation^[49] or brief contacts by a preheated thermode^[48], an NMDA receptor antagonist^[50], clearly attenuated temporal summation.

However, central neurons with receptive fields common to the two sites of alternating stimulation receive input at 0.33 Hz, which does produce summation for stimulation of a single site. The amount of summation from alternation should be less than that obtained from stimulation of a single site at 0.33 Hz, unless the peripheral receptive fields overlap extensively. Also, the central summation could be enhanced by an NMDA-receptor-sensitive expansion of the central receptive fields^[51]. Peripheral sensitization of each site could be enhanced by mutual influences on the sites from a lateral spread of inflammation^[52], but secondary hyperalgesia adjacent to a cutaneous injury is not revealed by thermal stimulation^[53]. In the experiment of Vierck et al.^[48], evidence in favor of central summation was obtained by the finding that alternating stimulation of adjacent sites on the thenar eminence at 0.33 Hz produced temporal summation that was intermediate in rate, and had an amount between those obtained with stimulation of either site alone at ISIs of 3 s or 6 s. This finding is suggestive of central radiation but contrasts with another study using alternating ramped stimulation of adjacent sites on hairy skin that produced temporal summation in excess of that observed with stimulation at a single site^[47]. Thus for the paradigm involving extended series of stimuli to one site and then another, repetitive excitation of a subset of SI cortical neurons that are maximally excited at the first site would suppress the activity of neurons with partially overlapping receptive fields that are less effectively excited at the first site than at the second site. In contrast, for alternating stimulation of the same sites, the two subsets of neurons with partially overlapping receptive fields would be activated to some extent at a rate of 0.33 Hz, which could produce some temporal summation.

Possible explanations

- (1) The sensitization is presumed to be attributable to central mechanisms,

because the effect requires input from C nociceptors that reveal a declining response amplitude with stimulus repetition^[47], and because the increased response magnitudes for central neurons or exaggerated behaviours in animal models of nociceptive sensitivity can be attenuated by NMDA receptor antagonists^[54].

(2) The temporal summation has been shown to be centrally mediated^[48].

(3) The temporal summation of heat pain was strongly influenced by the ISIs and cannot be explained by small increases in skin temperature between taps or by heat storage throughout a stimulus series^[55].

(4) The temporal summation for psychophysical and neural responses to heat is dependent on activation of C nociceptors and is dependent in part on activation of NMDA receptors^[56].

(5) In the dorsal horn of the spinal cord, wherein the primary processing of nociceptive information occurs, NMDA receptors are activated by glutamate released from nocisponsive afferent fibers. Their activation plays a key role in the induction of neuronal sensitization, a process underlying prolonged painful states^[57].

(6) Repetitive firing in axons can lead to their subexcitability and reduced conduction velocity, due to prolonged hyperpolarization^[58].

12.6.2 Fatigue

Although much attention has been directed at nociceptor sensitization, relatively little attention has been devoted to the reciprocal property, i.e., fatigue.

The mean response of C fiber nociceptors to 3 s heat stimuli applied to the hand with an interstimulus interval of 25 s declines by 60% from the first to the second stimulus^[24]. When a similar stimulus paradigm is applied to human subjects, a similar decline in the magnitude of pain^[24] and nociceptor response^[8] is observed.

Primary nociceptive afferents exhibit pronounced adaptation for physical as well as chemical stimuli^[59]. Peripheral adaptation of nociceptive nerve endings is compensated by central summation (i.e., wind up)^[47]. Since wind up is specific for wide dynamic range (WDR) neurones, heat responses of nociceptive-specific neurones showed adaptation whereas WDR neurones in the spinal cord did not^[60]. Compensation of peripheral adaptation to yield a constant pain sensation may be the major function of wind up.

Nociceptive primary afferents act as proportional and differential sensors, exhibiting pronounced albeit slow adaptation ($\tau \approx 2.5$ s) when stimulated

with mechanical or heat stimuli^[61]. Recovery from this adapted state takes 10 min or longer^[62] and affects the dynamic response more than the static response^[33]. This long-lasting reduction of nociceptor discharge is called “suppression”.

The adaptation and suppression of nociceptive afferent action potential discharges may occur at two stages of the neural encoding process: ① transduction of physical stimuli into generator potentials and ② transformation of generator potentials into trains of action potentials. Whereas adaptation in the transformation process is supported by decreased conduction velocity^[58] and reduced kinetics of sensory neuron-specific sodium channels^[63], there is no evidence for adaptation in the transduction process so far. The transduction process for noxious heat stimuli has been studied using dissociated neurons from dorsal root ganglia (DRG) as models of their own terminals^[64~67]. Brief heat stimuli (< 1 s) were found to elicit inward currents (I_{heat}) in DRG neurons which did not adapt^[68], and were reproducible with stimulus repetition at short intervals^[69]. Heat stimuli with slowly increasing temperatures revealed a threshold temperature of about 43 °C to evoke I_{heat} in DRG neurons^[64]. The correlate of adaptation in the transduction process would be the inactivation of I_{heat} upon constant stimulation; suppression would be visible as tachyphylaxis upon repeated stimulation.

Slugg et al.^[70] found that the C fibers demonstrated a significant fatigue in response to mechanical stimuli when the interstimulus interval between the paired stimuli was less than or equal to 150s, whereas the A fibers did not demonstrate a significant fatigue until the interstimulus interval was less than or equal to 30 s. This fatigue could result from changes in stimulus transmission, stimulus transduction, spike initiation, and spike propagation^[70]. It should be noticed that, however, Garell et al.^[71], in their study of feline nociceptors, did not observe a similar adapting response.

12.7 Influence of Stimulus Duration

With an increase in the duration of the noxious heat stimulus, the heat pain threshold is decreased^[37], activation of CMHs decreased^[28] and the sensory magnitude estimate of suprathreshold heat pain and the spinal neural responses were considerably increased^[37].

However, in these studies, the stimulus-duration changes always entailed an associated change in the delivered energy^[72]. By using lasers with the same energy but different duration applied to skin, it was found that shorter stimulus durations yielded steeper slopes in the skin temperature profiles and

higher pain ratings^[72].

Coghill et al.^[60] reported that pain did not decrease substantially during the course of prolonged, repetitive nociceptive stimulation, the responses of NS neurons declined significantly, whereas both WDR neurons alone were sufficient to evoke both sensory intensity and affective responses to prolonged pain.

Pertovaara^[37] found that the onset latencies of pain reactions and spinal neuronal responses were independent of the peak stimulus duration, whereas the latency of the maximum discharge in spinal neurons increased with prolongation of the peak stimulus. Moreover, the peak frequency of spinal neuronal response increased significantly with prolongation of the heat stimuli after spinalization, but not in animals with an intact spinal cord. Iannetti et al.^[72] found shorter stimulus durations shortened the latency.

Possible explanations

The contribution of biophysical mechanisms at the tissue level, transduction characteristics of nociceptive endings, and central synaptic summation mechanisms as underlying causes for this phenomenon are still under debate^[29].

There are several alternative explanations for the increased cumulative impulse count and a consequent higher pain magnitude estimate with longer stimuli^[37].

(1) With prolonged stimuli and a prolonged diffusion of heat, the temperature at the level of subepidermally located nociceptors should be gradually increased, leading to higher activation of nociceptors^[73] and higher effective temperature at the location of the receptor terminals, because as the stimulus duration increases, the skin surface temperature needed to achieve a given temperature at the depth of the receptor decreases^[74]. However, recent results indicate that the cumulative storage of heat in subepidermal tissue with repetitive heat stimulation does not play a significant role in the development of enhanced pain sensation^[48].

(2) The prolonged stimuli may activate a different population of nociceptors (type I AMHs) than brief stimuli^[37]. Electrophysiological studies demonstrate that, nociceptive C fibers and type II AMHs have a peak discharge near the stimulus onset during prolonged suprathreshold stimuli, whereas type I AMHs have a slowly increasing discharge frequency during prolonged stimuli^[33].

(3) The gradual diffusion of heat to wider subepidermal areas during prolonged stimulation might produce a gradual increase in the size of nociceptor

population recruited (spatial summation effect)^[37].

(4) The well-known “wind up” phenomenon in central neurons. The increases in sensory magnitude estimates and in total impulse count of WDR neurons with prolonged stimuli were, however, less than expected than if there had been a linear relationship between the sensory or neuronal response and the duration of the stimulus.

(5) With repetitive heat stimuli, a suppression of primary afferent nociceptor discharge and a concomitant heat pain sensation has been demonstrated in human subjects^[75], which may explain the smaller increase in heat-evoked responses than expected on the basis of a linear model^[37].

(6) Repetitive stimuli with high frequencies can induce the release of chemical substances that may account for many phenomena such as adaptation and sensitization^[76].

(7) Sensitization of high threshold mechanoreceptors with myelinated axons by repeated heating^[77].

12.8 Spatial Summation

Spacial summation (SS) refers to an increase in pain perception when larger areas of stimulation are used^[78]. A positive SS effect for non-painful thermal stimuli has been observed^[79]. For example, it has been found that the spatial characteristics of thermal sensation maintained that warm sensation is subject to considerable spatial summation^[80].

However, existing results regarding the existence of spatial summation for pain perception are contradictory. Early studies reported little or no spatial summation for painful cold and heat stimuli^[81], while the important role of spatial summation for pain coding has been demonstrated both in psychophysical^[82] and clinical studies^[83].

Studies show that increasing the area of noxious stimulation results in a decrease in pain threshold^[84] or an increase in perceived pain intensity^[82]. Spatial summation in these studies was examined by applying either a single stimulus with an increasing area^[84], or an increasing number of stimuli (1~3) of a fixed size^[85].

A single discharge of an individual nocisponsive fiber is not perceived as noxious and many nocisponsive units need to be recruited over a period of time for “pain” to be experienced, and actual pain thresholds are higher in man than the thresholds for activation of individual nociceptors^[57].

Dipping the entire hand in 18 °C water during one minute induced a transient faint pain whilst decreasing cutaneous temperature at a rate of 1.3 °C/s

with a 6.5 cm² area provokes a pricking pain only at about 10°C^[36]. Gronroos et al.^[86] found that the minimal energy per surface area needed to produce a pain sensation was lower with a larger stimulus surface. Nielsen & Arendt-Nielsen^[85] found that the mean heat pain threshold decreased significantly from 45.6 to 43.5 °C as the stimulus dermatome area was increased from minimum (3.14 cm²) to maximum (15.70 cm²). Staud et al.^[87] examined the characteristics of SS by progressive immersion of the fingers, hand, and forearm in a heated water bath, similar to previous SSP studies^[82], taking into account the contribution of pain inhibitory mechanisms like DNIC^[88]. There is a significant increase in pain ratings when the stimulus areas are increased from 0.21 to 2.10 cm² or from 1 to 3 cm²^[89].

Experiments using multiple stimuli report that SS exists both within and between dermatomes, although the largest separation distance between stimuli tested was 10 cm^[90]. Defrin et al.^[4] demonstrated that when stimulus separation exceeds a given distance (10 cm) SS is no longer evident even if the stimuli are applied within the same dermatome. To complicate the matter further, Lautenbacher et al.^[91] found no significant effect of area for the ratings of the supra-threshold stimuli.

Possible explanations

(1) A minimal quantity of warm receptors has to be activated for nociception. Green & Cruz^[92] reported that in normal skin areas devoid of warm sensation, noxious thermal stimulation produces only a pricking sensation. Furthermore, the spatial summation of pain threshold is not observed when nonnoxious thermal sensations are impaired^[93].

(2) The neurophysiological mechanisms of SSP are complex, which include pain coding of central nociceptive neurons that are dependent both on impulse frequency and the number of central neurons recruited^[94].

(3) The spatial summation of perceived heat pain intensity may be attributed to the reduced heat pain threshold^[91].

(4) SS and SD of pain are mutually exclusive phenomena and that C and A δ nociceptors are probably similarly involved in both processes^[4]. However, Gronroos et al.^[86] found that following the impairment of function in nociceptive C fibers, the spatial summation of argon laser-induced pain was enhanced.

(5) The possible recruitment of inhibitory mechanisms by nociceptive stimuli such as diffuse noxious inhibitory controls (DNIC): the more intense the conditioning nociceptive stimuli are, the more active the inhibitory response becomes^[95]. DNIC rely on intense or painful conditioning stimulation

of one part of the body to inhibit pain in another part^[96]. For example, in humans, DNIC were shown to reduce heat pain stimuli to the face, when the volunteers also immersed their hand in cold water (5 °C)^[97], and the progressive immersion of the hand and arm in hot water causes the nociceptive input from the hand to inhibit the effects of nociceptive input from the arm^[82].

(6) Microneurographic data indicate that only the summated activation of C nociceptors causes a conscious perception of pain in humans^[98].

12.9 Hyperalgesia and Tissue Damage

Damage to tissue causes cells to break down and release a number of tissue byproducts and mediators that activate nociceptor free nerve endings. Some of these substances activate nociceptors but most sensitize nociceptors (hyperalgesia). Peripheral sensitization amplifies signal transmission and thereby contributes to central sensitization and clinical pain states.

Hyperalgesia to cold as well as to heat and mechanical stimuli occurs following a mild freeze injury to the skin^[99]. Generally, it is believed that secondary hyperalgesia in man is restricted to mechanical stimuli^[100].

Some studies found no change in heat pain threshold in the zone of secondary hyperalgesia^[101], while other studies demonstrated lowered heat pain thresholds in the normal skin adjacent to burn and freeze injuries^[102], and in skin adjacent to capsaicin injections^[103].

However, unchanged pain thresholds do not imply unchanged suprathreshold pain responses^[104]. Hardy et al.^[105] demonstrated that heat pain was more than doubled in the zone with secondary hyperalgesia compared with normal skin on the control arm. Increased pain ratings to contact heat stimuli were reported by Thalhammer & LaMotte^[106] in skin adjacent to burn injuries (56°C, 7 s) delivered to the volar forearm. Secondary hyperalgesia to heat has been demonstrated in animal studies^[107]. Pedersen & Kehlet^[108] found significant hyperalgesia to heat within the zone of secondary hyperalgesia to punctate mechanical stimuli after a burn injury in hairy skin.

Thermal injury influenced the heat pain sensation^[52]. Heat injury produced an immediate fall in heat pain threshold^[108] and increase in pain sensitivity^[109].

Bleehen & Keele^[110] proposed that ATP released from damaged cells contributes to pain caused by tissue damage. It has been found that ATP applied to blisters causes pain^[110], and fractions of cell cytosol causing pain when applied to blisters are mostly composed of ATP^[111]. There have also been reports demonstrating ATP-evoked pain in whole animals^[112].

In skin, the mechanical threshold of all unmyelinated nociceptors diminishes when pH drops, whereas low-threshold mechanosensors are unaffected by pH^[113]. A subset (38%) of CMH nociceptors actively fire action potentials in response to decreasing pH, exhibiting a clear dose-response relation between firing frequency and pH^[113]. Bevan & Yeats^[114] showed that a transient proton-activated current activated in sensory neurons below pH 7 was followed by a sustained current seen only when pH dropped further, to pH 6 and below. Pain due to inflammation, infection, or ischemia is not transient, and may be due to the large, persisting current that is evoked when extracellular pH drops below 6 has been proposed to underlie the pain of these conditions, but this presumes that such low pH is reached^[115].

Possible explanations

(1) The primary hyperalgesia which ensues upon tissue injury can be accounted for by changes in the transduction sensitivity, responsiveness and activity of peripheral nociceptors and by the recruitment of “silent” nociceptors^[57]. For example, Thalhammer & LaMotte^[106] found the existence of outlying terminal endings that are normally unresponsive to non-injurious mechanical or heat stimuli but become responsive to these stimuli following injury.

(2) The secondary hyperalgesia to heat found by Hardy et al.^[105] was suggested by Ali et al.^[100] to be caused by the increased skin temperatures in the area of flare, as higher skin temperatures would be reached with a certain amount of energy when the starting point is warmer.

(3) Upon peripheral nerve injury, a reduction of inhibitory interneurone tone in the dorsal horn exacerbates sensitized states and further enhances nociception^[57].

(4) Although hyperalgesia is mediated in part by sensitization of nociceptors at the site of injury, sensitization of spinal dorsal horn neurons also contributes to hyperalgesia^[116]. For example, enhanced responses of spinal dorsal horn neurons to heat and cold stimuli following mild freeze injury to the skin was observed^[117].

(5) Junger et al.^[118] showed that full-thickness burns cause extensive tissue damage and edema, and can sensitize nearby unburned skin. Full-thickness burns activate and/or sensitize C nociceptors, thus probably leading to pain.

(6) It is likely that primary hyperalgesia results from a combination of peripheral and central sensitization^[119]. However, thus far it has only been possible to demonstrate sensitization of nociceptors to heat^[8], and not me-

chanical stimuli, in the zone of primary hyperalgesia after skin injuries^[106].

(7) An additional mechanism, which may contribute to primary hyperalgesia without lowering the nociceptor thresholds, is the recruitment of silent nociceptors and previously insensitive nociceptor branches leading to the expansion of receptive fields^[120~122].

(8) Secondary hyperalgesia most likely reflects enhanced responsiveness of CNS neurons to nociceptor input^[123], whereas touch-evoked pain or mechanical allodynia in normal tissue surrounding an injury most likely reflects sensitization of CNS neurons to low threshold mechanoreceptor input^[124].

(9) Xu et al.^[125] found that a novel, NMDA-mediated activation of on-cells is required for secondary thermal hyperalgesia in acute inflammation.

(10) Meyer & Campbell^[126] found that burn damage resulted in the increased sensitivity of the A fibers, decreased sensitivity of the C fibers, and increased pain sensibility (hyperalgesia) in the human. This shows that it is the A fiber, not C fiber, which mediates the hyperalgesia. On the other hand, it was found that C fiber codes for the intensity of thermal pain near pain threshold (43~48 °C) on the glabrous skin of uninjured hand. Above 48 °C, myelinated nociceptors also contribute to pain sensation.

12.10 Influence of Origin of Skin(Different Part in Body)

Unlike thermal and mechanical thresholds, Hardy et al.^[73] found relatively little difference in the pain sensitivity of different test areas, except for the thick glabrous skin of the finger pads and the heel, and the upper leg to be slightly more sensitive than the abdomen. Lynn & Perl^[127] found that the heat pain threshold in the leg is 0.3~1.0 °C higher than that in neck and abdomen. Experiments have also been carried out to determine heat pain threshold in four skin regions (cheek, glabrous skin of hand, hairy forearm, leg) of eight healthy human subjects^[128]. No significant difference in heat pain sensitivity was found between comparable sites on the upper versus lower extremities, or between left and right sides^[129]. There was great variation of pain sensitivity of different body parts in all volunteers, irrespective of age and sex, while body length did not influence thermal and pain perception thresholds^[130].

Harrison & Davis^[19] found: ① cold thresholds were lower (i.e., occurred at higher absolute temperatures) for the hairy skin of the dorso-lateral hand in comparison with the glabrous skin of the thenar eminence; ② exponents for supra-threshold ratings fit to power functions were larger for the glabrous skin site than the hairy skin site, regardless of cooling rate or dimension

of pain measured. Hagander et al.^[131] found that the thenar eminence is less sensitive to cold pain but otherwise the hand and the foot are equally sensitive to thermal pain. In the method of limits, cold pain showed lower thresholds in the foot than hand^[132], and cold thresholds were significantly higher in the thenar eminence compared to the forearm^[133].

12.11 Influence of Skin Type

Experimental findings in a variety of species have revealed differences in the innervation of glabrous and hairy skin by noxious thermal stimulus^[129]. For example, it has been found that hairy but not glabrous CMH nociceptors readily sensitize following a burn injury^[134], and the heat pain threshold for hairy skin in human is lower than those for glabrous skin^[133]. However, in both human hairy and glabrous skin, C fiber stimulation predominantly elicited sensations of dull pain and burning pain^[12];

Harrison & Davis^[19] found pain ratings for stimulation of glabrous skin began later than that for hairy skin, then increased at a faster rate to reach equal and often higher maximum pain ratings during maintained noxious cold stimulation. Pain ratings for the two sites were mostly equal initially during rewarming, but glabrous skin pain ratings decreased at a faster rate once the thermode had returned to baseline. Most subjects perceived more prickle at their hairy test site than their glabrous test site, especially during the rewarming phase.

Conversely, other studies found no differences between skin types in the heat response^[135]. Davis^[20] found relatively similar pain intensity profiles in the intact hairy and glabrous skin for cold pain. Stevens & Chou^[135] also found no differences in cold threshold.

Possible explanations

(1) Anatomical differences may provide an explanation for the differences found in the sensitivity of hairy and glabrous skin^[19]. It has long been known that hairy and glabrous skin differ in composition, sympathetic innervation and, possibly, the location and density of receptors mediating noxious cold sensation^[136]. In general, glabrous skin is five-fold thicker and has more epidermal layers compared to hairy skin^[137], which may affect the rate of heat transfer to the nociceptors. In support of this hypothesis, no difference was found between skin types for peak pain ratings^[19]. However, if skin thickness was the sole factor involved, ratings should have increased at similar rates once the threshold had been exceeded. In fact, power function analysis revealed that glabrous skin ratings rose significantly faster above the

threshold^[19].

(2) The difference may be due to the differences in the peripheral innervation densities of the nerves subserving the two skin types^[18]. For example, Hensel^[138] reported a higher density of cold spots on the dorsolateral hand compared to the thenar eminence in humans. Fleischer et al.^[139] also observed that cold-sensitive C fibers were significantly more common in glabrous skin compared to hairy skin in rat. Treede et al.^[33] found 46 AMHs and 21 CMH in hairy skin and only 59 AMHs and 10 CMHs in glabrous skin.

(3) Sympathetic activity may be a possible reason for the different psychophysical affects in different skin types. Artificially induced sweating has been shown to reduce human cold thresholds for the thenar eminence but not hairy skin^[141]. This sweating may result from secretion of the sympathetically innervated eccrine sweat glands, which are more abundant in glabrous skin sites^[141]. Thus increased sweating in glabrous skin may affect the heat transfer rate through the skin, thereby increasing the threshold measurements^[19].

(4) Primary afferent nociceptor conduction velocities subserving glabrous skin sites have been reported to be faster than those subserving hairy skin sites for both AMH nociceptors^[33] and monkey cold-sensitive afferents^[142]. However, it should be noticed that other studies found no differences between skin types in the conduction velocities of CMH nociceptors^[33].

(5) Another important factor is the proximity of cold stimulus at the two test sites to superficial veins, which are innervated by cold-sensitive nociceptors^[143]. These polymodal venous receptors are thought to contribute to the pain but not the thermal sensations evoked by cooling the skin. However, the greater responses at the hairy sites during the rewarming phase suggest that central mechanisms may also be a factor. Furthermore, during the A fiber block most subjects experienced substantially greater cold-evoked pain whereas the effect of the block at the hairy sites was variable. These results further illustrate that the differences between sensation elicited from stimulation at glabrous and hairy skin is a result of a complex interaction of peripheral and central factors^[22].

(6) Primary afferent recordings in monkey indicate that different nociceptors innervate hairy and glabrous skin^[33]. AMH nociceptors that are presumed to play a role in heat pain perception are found in hairy but not glabrous skin, which is consistent with the absence of first pain to heat in glabrous skin.

12.12 Gender Difference

Sex differences have been reported for many pain-related responses. For

instance, women are at greater risk for pain disorders such as fibromyalgia^[144]. Women also report more widespread pain, more pain-related affective symptoms^[145], and more frequent daily pain^[146].

Sex differences have also been investigated in laboratory settings. No statistically significant differences in pain perception thresholds were demonstrated between the genders^[147].

However, other studies have shown differences in pain perception or tolerance^[148]: there is generally higher pain threshold among males while women generally showed greater sensitivity for thermal pain. For example, Lautenbacher & Rollman^[149] found that there were no sex differences in heat pain thresholds but significant sex differences in electrical pain. Many of these researchers noted that a confounding problem may be that women are more likely to report pain than men^[150], which may also be true across different cultural norms^[151].

Sex differences in facial responses to pain have hardly been investigated, and only in very few studies on facial expression of pain was “sex” included in analyses. Whereas no significant sex differences in facial expression of pain were found in two different studies^[152], Guinsburg et al.^[153] reported increased facial pain responses in female neonates. However, systematic investigations of sex differences in facial expression of pain in adult subjects have been lacking so far.

Lang et al.^[154] reported that facial expression of emotions corresponded much better to self-report in women than in men. Kunz et al.^[155] found that men and women differed neither in self-report ratings nor in facial responses during tonic heat stimulation. However, sex had a considerable impact on the relationship between these variables. Whereas no significant correlations at all were found for men, several significant correlations were observed in woman. For that reason, Kunz et al.^[155] argued that future studies investigating the relationship between self-report and nonverbal pain behaviours should consider sex as an important modulating factor.

Possible explanations

While some researchers emphasize socialization^[156] or emotional responsiveness^[157] as potential mechanisms for the sex difference, others have highlighted biological factors^[158] or pain-coping^[159].

(1) Females had significantly greater activation of the contralateral prefrontal cortex when compared to the males, and volume of interest comparison also suggested greater activation of the contralateral insula and thalamus in the females^[160].

(2) Females evinced lower thresholds than males for the method of levels assessments with both slow and fast rates of rise, while no sex differences emerged for the threshold assessed via the method of limits^[161].

(3) Finer sensory-discriminative capacity may explain the greater perceptual responses of females to painful stimuli^[162].

(4) Catastrophizing may be a possible reason for sex differences^[163]. During a cold pressor task, females reported more pain and displayed more pain behaviour than males, effects which became non-significant when catastrophizing was controlled^[164].

(5) One plausible explanation for these incongruous results is the preponderance of unidimensional pain measures used in previous studies, which address only the magnitude of pain^[162]. If females and males differ more along one of the dimensions, then assessment procedures which do not directly assess the different dimensions of pain would be expected to yield inconsistent findings.

(6) Resting blood pressure may contribute to the gender difference in pain sensitivity^[165]. Male exhibited higher resting blood pressure than females, and the resting blood pressure was found to be inversely associated with pain sensitivity^[166].

12.13 Influence of Age

Somatosensory thresholds clearly increase in the elderly, and there is a decreased somatosensitivity in the elderly^[167].

Although age-associated declines in other sensory modalities are well documented^[135], such as pressure^[168], cold^[169], and ischemia^[170], and the effects of aging on the experience of clinical pain seem relatively clear, the effects of aging on pain perception remain unclear and existing results of laboratory studies of pain are conflicting^[167].

Some researchers reported no age-associated differences in heat pain thresholds^[171] and no age-related changes in regard to spatial summation of heat pain^[167], while others reported increased thermal pain thresholds (decreased sensitivity) in the elderly^[172], stronger temporal summation to heat pain in elder subjects than younger ones^[171] and higher ratings of the intensity and unpleasantness of thermal pain^[171].

Possible explanations

It seems that the effects of age on pain responses may vary as a function of the stimulus^[171].

(1) Aging may differentially affect the various types of afferent fiber that

convey information concerning pain^[172]. Senescent demyelination may produce decrements in myelinated fiber conduction velocity^[173]. Greater reductions in the density of myelinated relative to unmyelinated fibers appear with advancing age^[174]. Elderly adults rely predominantly on C fiber input whereas younger adults utilize additional input from A δ fibers^[172].

(2) The length of the afferent pathways seems to influence the degree of age-related changes in heat pain perception, resulting in a distal-proximal pattern of age-dependent decline^[175]. However, altered receptor properties were suggested to explain the age-related decline^[176].

(3) The age effect on pain may be accounted for by decrements in endogenous pain inhibitory systems or reduced CNS plasticity on the part of the older adults^[177]. Since temporal summation is modulated by endogenous pain inhibitory systems^[178], the finding, that endogenous pain inhibition (i.e. DNIC) appeared to be reduced in the elderly^[179], is noteworthy.

(4) These contradicting results may be explained by methodological differences between studies, like age distribution, size and sex ratios of samples, clinical conditions included and the use of different methods of experimental pain assessment^[167].

12.14 Summary

Van Hees & Gybels^[180] found that a mechanical stimulus that evokes the same level of activity in C fiber nociceptors as a heat stimulus causes less pain than the heat stimulus. They explained this discrepancy as possible due to spatial summation. Since tissue deformation due to heating or cooling is used by some researchers to explain pain^[181]. It has also been shown that the thermal stress due to skin surface heating maybe surpasses the threshold value of mechanical pain^[182].

Besides, it has been found that mechanoreceptors can be evoked by extremely cold stimulus temperatures and this response has been argued not be specific to absolute temperature, but may be due to small mechanical changes in the skin that may occur as a consequence of vasoconstriction^[6].

References

- [1] Lawson S N. Phenotype and function of somatic primary afferent nociceptive neurones with C-, Adelta- or Alpha/beta-fibres. *Experimental Physiology*, 2002, 87(2): 239-244.
- [2] Plaghki L, Mouraux A. How do we selectively activate skin nociceptors with a high power infrared laser? *Physiology and biophysics of laser stimulation*.

- Neurophysiologie Clinique, 2003,33(6): 269–277.
- [3] Nahra H, Plaghki L. The effects of A-fiber pressure block on perception and neurophysiological correlates of brief non-painful and painful CO₂ laser stimuli in humans. *European Journal of Pain*, 2003, 7(2): 189–199.
 - [4] Defrin R, Givon R, Raz N, et al. Spatial summation and spatial discrimination of pain sensation. *Pain*, 2006, 126(1): 123–131.
 - [5] Yarnitsky D, Ochoa J L. Studies of heat pain sensation in man: Perception thresholds, rate of stimulus rise and reaction time. *Pain*, 1990,40(1): 85–91.
 - [6] Simone D A, Kajander K C. Responses of cutaneous A-fiber nociceptors to noxious cold. *Journal of Neurophysiology*, 1997,77(4): 2049–2060.
 - [7] Simone D A, Marchettini P, Caputi G, et al. Identification of muscle afferents subserving sensation of deep pain in humans. *Journal of Neurophysiology*, 1994, 72(2): 883–889.
 - [8] Torebjork H E, LaMotte R H, Robinson C J. Peripheral neural correlates of magnitude of cutaneous pain and hyperalgesia: Simultaneous recordings in humans of sensory judgments of pain and evoked responses in nociceptors with C-fibers. *Journal of Neurophysiology*, 1984, 51(2): 325–339.
 - [9] Yarnitsky D, Ochoa J L. Differential effect of compression-ischæmia block on warm sensation and heat-induced pain. *Brain*, 1991, 114(Pt 2): 907–913.
 - [10] Chen C C, Rainville P, Bushnell M C. Noxious and innocuous cold discrimination in humans: Evidence for separate afferent channels. *Pain*, 1996, 68(1): 33–43.
 - [11] Belemonte C, Cervero F. *Neurobiology of Nociceptors*. Oxford: Oxford University Press, 1996.
 - [12] Ochoa J, Torebjork E. Sensations evoked by intraneural microstimulation of C nociceptor fibres in human skin nerves. *The Journal of Physiology*, 1989, 415: 583–599.
 - [13] Price D D, Dubner R. Mechanisms of first and second pain in the peripheral and central nervous systems. *Journal of Investigative Dermatology*, 1977, 69(1): 167–171.
 - [14] Magerl W, Fuchs P N, Meyer R A, et al. Roles of capsaicin-insensitive nociceptors in cutaneous pain and secondary hyperalgesia. *Brain*, 2001, 124(9): 1754–1764.
 - [15] Lumb B M, Parry D M, Semenenko F M, et al. C-nociceptor activation of hypothalamic neurones and the columnar organisation of their projections to the periaqueductal grey in the rat. *Experimental Physiology*, 2002, 87(2): 123–128.
 - [16] McMullan S, Lumb B M. Midbrain control of spinal nociception discriminates between responses evoked by myelinated and unmyelinated heat nociceptors in the rat. *Pain*, 2006,124(1-2): 59–68.
 - [17] Wall P D, McMahon S B. Microneuronography and its relation to perceived sensation. A critical review. *Pain*, 1985, 21(3): 209–229.
 - [18] LaMotte R H, Thalhammer J G, Robinson C J. Peripheral neural correlates of magnitude of cutaneous pain and hyperalgesia: A comparison of neural

- events in monkey with sensory judgments in human. *Journal of Neurophysiology*, 1983, 50(1): 1–26.
- [19] Harrison J L K, Davis K D. Cold-evoked pain varies with skin type and cooling rate a psychophysical study in humans. *Pain*, 1999, 83: 123–135.
- [20] Davis K D. Cold-induced pain and prickle in the glabrous and hairy skin. *Pain*, 1998, 75(1): 47–57.
- [21] Simone D A, Kajander K C. Excitation of rat cutaneous nociceptors by noxious cold. *Neuroscience Letters*, 1996, 213(1): 53–56.
- [22] LaMotte R H, Thalhammer J G, Torebjork H E, et al. Peripheral neural mechanisms of cutaneous hyperalgesia following mild injury by heat. *Journal of Neuroscience*, 1982, 2(6): 765–781.
- [23] Campero M, Serra J, Ochoa J L. C-polymodal nociceptors activated by noxious low temperature in human skin. *Journal of Physiology*, 1996, 497(2): 565–572.
- [24] LaMotte R H, Campbell J N. Comparison of responses of warm and nociceptive C-fiber afferents in monkey with human judgments of thermal pain. *Journal of Neurophysiology*, 1978, 41(2): 509–528.
- [25] Chery-Croze S. Relationship between noxious cold stimuli and the magnitude of pain sensation in man. *Pain*, 1983, 15(3): 265–269.
- [26] Georgopoulos A P. Stimulus-response relations in high-threshold mechanothermal fibers innervating primate glabrous skin. *Brain Research*, 1977, 128(3): 547–552.
- [27] Haimi-Cohen R, Cohen A, Carmon A. A model for the temperature distribution in skin noxiously stimulated by a brief pulse of CO₂ laser radiation. *Journal of Neuroscience Methods*, 1983, 8(2): 127–137.
- [28] Tillman D B, Treede R D, Meyer R A, et al. Response of C fibre nociceptors in the anaesthetized monkey to heat stimuli: Estimates of receptor depth and threshold. *The Journal of Physiology*, 1995, 485(3): 753–765.
- [29] Tillman D B, Treede R D, Meyer R A, et al. Response of C fibre nociceptors in the anaesthetized monkey to heat stimuli: Correlation with pain threshold in humans. *Journal of Physiology*, 1995, 485(3): 767–774.
- [30] Duclaux R, Kenshalo D R. Response characteristics of cutaneous warm receptors in the monkey. *Journal of Neuroendocrinology*, 1980, 43(1): 1–15.
- [31] Palmer S T, Martin D J, Steedman W M, et al. C- and Adelta-fibre mediated thermal perception: Response to rate of temperature change using method of limits. *Somatosensory and Motor Research*, 2000, 17(4): 325–333.
- [32] Lynn B. The heat sensitization of polymodal nociceptors in the rabbit and its independence of the local blood flow. *The Journal of Physiology*, 1979, 287: 493–507.
- [33] Treede R D, Meyer R A, Raja S N, et al. Evidence for two different heat transduction mechanisms in nociceptive primary afferents innervating monkey skin. *The Journal of Physiology*, 1995, 483(3): 747–758.
- [34] Bessou P, Perl E R. Response of cutaneous sensory units with unmyelinated fibers to noxious stimuli. *Journal of Neuroendocrinology*, 1969, 32: 1025–1043.

- [35] Yarnitsky D, Simone D A, Dotson R M, et al. Single C nociceptor responses and psychophysical parameters of evoked pain: Effect of rate of rise of heat stimuli in humans. *Journal of Physiology*, 1992, 450: 581–592.
- [36] Croze S, Duclaux R. Thermal pain in humans: Influence of the rate of stimulation. *Brain Research*, 1978, 157(2): 418–421.
- [37] Pertovaara A. The influence of stimulus temperature rise rate, adapting temperature, and stimulus duration on suprathreshold responses evoked by noxious heat in the glabrous skin of the limb: Comparison of neuronal discharge in the rat spinal dorsal horn with human sensations. *Experimental Brain Research*, 1999, 126(4): 482–494.
- [38] Croze S, Duclaux R, Kenshalo D R. The thermal sensitivity of the polymodal nociceptors in the monkey. *The Journal of Physiology*, 1976, 263(3): 539–562.
- [39] Nielsen J, Arendt-Nielsen L. The influence of rate of temperature change and peak stimulus duration on pain intensity and quality. *Somatosensory and Motor Research*, 1998, 15(3): 220–229.
- [40] Nielsen J, Arendt-Nielsen L. The importance of stimulus configuration for temporal summation of first and second pain to repeated heat stimuli. *European Journal of Pain*, 1998, 2(4): 329–341.
- [41] Yeomans D C, Proudfit H K. Nociceptive responses to high and low rates of noxious cutaneous heating are mediated by different nociceptors in the rat: Electrophysiological evidence. *Pain*, 1996, 68(1): 141–150.
- [42] Pertovaara A, Morrow T J, Casey K L. Cutaneous pain and detection thresholds to short CO₂ laser pulses in humans: Evidence on afferent mechanisms and the influence of varying stimulus conditions. *Pain*, 1988, 34(3): 261–269.
- [43] Severin F, Lehmann W P, Strian F. Subjective sensitization to tonic heat as an indicator of thermal pain. *Pain*, 1985, 21(4): 369–378.
- [44] Pertovaara A, Kauppila T, Hamalainen M M. Influence of skin temperature on heat pain threshold in humans. *Experimental Brain Research*, 1996, 107(3): 497–503.
- [45] Herrero J F, Laird J M A, Lopez-Garcia J A. Wind-up of spinal cord neurones and pain sensation: Much ado about something. *Progress in Neurobiology*, 2000, 61(2): 169–203.
- [46] Li Z, Morris K F, Baekey D M, et al. Responses of simultaneously recorded respiratory-related medullary neurons to stimulation of multiple sensory modalities. *Journal of Neurophysiology*, 1999, 82(1): 176–187.
- [47] Price D D, Hu J W, Dubner R, et al. Peripheral suppression of first pain and central summation of second pain evoked by noxious heat pulses. *Pain*, 1977, 3(1): 57–68.
- [48] Vierck C J, Cannon R L, Fry G, et al. Characteristics of temporal summation of second pain sensations elicited by brief contact of glabrous skin by a preheated thermode. *Journal of Neurophysiology*, 1997, 78(2): 992–1002.
- [49] Price D D, Bush F M, Long S, et al. A comparison of pain measurement characteristics of mechanical visual analogue and simple numerical rating scales. *Pain*, 1994, 56(2): 217–226.

- [50] Church J, Lodge D, Berry S C. Differential effects of dextrorphan and levorphanol on the excitation of rat spinal neurons by amino acids. *European Journal of Pharmacology*, 1985, 111(2): 185–190.
- [51] Ren K. Wind-up and the NMDA receptor: From animal studies to humans. *Pain*, 1994, 59(2): 157–158.
- [52] LaMotte R H, Lundberg L E, Torebjork H E. Pain, hyperalgesia and activity in nociceptive C units in humans after intradermal injection of capsaicin. *The Journal of Physiology*, 1992, 448: 749–764.
- [53] Simone D A, Baumann T K, LaMotte R H. Dose-dependent pain and mechanical hyperalgesia in humans after intradermal injection of capsaicin. *Pain*, 1989,38(1): 99–107.
- [54] Meller S T, Dykstra C, Pechman P S, et al. Ethanol dose-dependently attenuates NMDA-mediated thermal hyperalgesia in the rat. *Neuroscience Letters*, 1993,154(1-2): 137–140.
- [55] Mauderli A P, Vierck C J, Cannon R L, et al. Relationships between skin temperature and temporal summation of heat and cold pain. *Journal of Neurophysiology*, 2003,90(1): 100–109.
- [56] Graven-Nielsen T, Aspegren K S, Henriksson K G, et al. Ketamine reduces muscle pain, temporal summation, and referred pain in fibromyalgia patients. *Pain*, 2000,85(3): 483–491.
- [57] Millan M J. The induction of pain: An integrative review. *Progress in Neurobiology*, 1999,57(1): 1–164.
- [58] Serra J, Campero M, Ochoa J, et al. Activity-dependent slowing of conduction differentiates functional subtypes of C fibres innervating human skin. *The Journal of Physiology*, 1999,515(3): 799–811.
- [59] Meyer R A, Campbell J N, Raja S N. Peripheral neural mechanisms of nociception// Wall P D, Melzack R. *Textbook of Pain*. London: Churchill, 1994: 13–44.
- [60] Coghill R C, Mayer D J, Price D D. Wide dynamic range but not nociceptive-specific neurons encode multidimensional features of prolonged repetitive heat pain. *Journal of Neurophysiology*, 1993,69(3): 703–716.
- [61] Schneider W, Slugg R M, Turnquist B P, et al. An electromechanical stimulator system for neurophysiological and psychophysical studies of pain. *Journal of Neuroscience Methods*, 1995,60(1-2): 61–68.
- [62] Treede R D, Meyer R A, Campbell J N. Myelinated mechanically insensitive afferents from monkey hairy skin: Heat-response properties. *Journal of Neurophysiology*, 1998,80(3): 1082–1093.
- [63] Waxman S G, Dib-Hajj S, Cummins T R, et al. Sodium channels and pain. *Proceedings of the National Academy of Sciences. USA*, 1999,96: 7635–7639.
- [64] Vyklicky L, Vlachová V, Vitásková Z, et al. Temperature coefficient of membrane currents induced by noxious heat in sensory neurones in the rat. *Journal of Physiology*, 1999,517(1): 181–192.
- [65] Kirschstein T, et al. Coexpression of heat-evoked and capsaicin-evoked inward currents in acutely dissociated rat dorsal root ganglion neurons. *Neuroscience Letters*, 1997,231(1): 33–36.

- [66] Kirschstein T, Greffrath W, Büsselberg D, et al. Inhibition of rapid heat responses in nociceptive primary sensory neurones of the rat by vanilloid receptor antagonists. *Journal of Neurophysiology*, 1999,82(6): 2853–2860.
- [67] Nagy I, Rang H. Noxious heat activates all capsaicin-sensitive and also a sub-population of capsaicin-insensitive dorsal root ganglion neurons. *Neuroscience*, 1999,88(4): 995–997.
- [68] Cesare P, McNaughton P A. A novel heat-activated current in nociceptive neurons and its sensitization by bradykinin. *Proceedings of the National Academy of Sciences. USA*, 1996, 93(26): 15435–15439.
- [69] Guenther S, Reeh P W, Kress M. Rises in $[Ca^{2+}]_i$ mediate capsaicin- and proton-induced heat sensitization of rat primary nociceptive neurons. *European Journal of Neurophysiology*, 1999,11(9): 3143–3150.
- [70] Slugg R M, Meyer R A, Campbell J N. Response of cutaneous A- and C-fiber nociceptors in the monkey to controlled-force stimuli. *Journal of Neurophysiology*, 2000,83(4): 2179–2191.
- [71] Garell P C, McGillis S L, Greenspan J D. Mechanical response properties of nociceptors innervating feline hairy skin. *Journal of Neurophysiology*, 1996,75(3): 1177–1189.
- [72] Iannetti G D, Leandri M, Truini A, et al. Delta nociceptor response to laser stimuli: Selective effect of stimulus duration on skin temperature, brain potentials and pain perception. *Journal of Clinical Neurophysiology*, 2004,115(11): 2629–2637.
- [73] Hardy J D, Wolff H G, Goodell H. Pricking pain threshold in different body areas. *Proceedings of the Society for Experimental Biology and Medicine*, 1952: 425–427.
- [74] Wu G, Campbell J N, Meyer R A. Effects of baseline skin temperature on pain ratings to suprathreshold temperature-controlled stimuli. *Pain*, 2001,90(1-2): 151–156.
- [75] Adriaensen H, Gybels J, Handwerker H O, et al. Suppression of C-fibre discharges upon repeated heat stimulation may explain characteristics of concomitant pain sensations. *Brain Research*, 1984,302(2): 203–211.
- [76] Brown A C. Sensory processes: Thermal sensation//Patton H D, Fuchs A F, Hille B, et al. *Textbook of Physiology*. Philadelphia: WB Saunders, 1989: 305–308.
- [77] Fitzgerald M, Lynn B. The sensitization of high threshold mechanoreceptors with myelinated axons by repeated heating. *Journal of Neurophysiology*, 1977,265(2): 549–563.
- [78] Raja S N, Meyer R A, Ringkamp M, et al. Peripheral neural mechanisms of nociception// Wall P D, Melzack R. *Textbook of Pain*. 4th Edition. London: Churchill, 1999: 11–57.
- [79] Kandel E R, Schwartz J H, Jessel T M. *Principles of Neural Science*. 4th Edition. New York: McGraw-Hill, 2000.
- [80] Dyck P J, Zimmerman I, Gillen D A, et al. Cool, warm, and heat-pain detection thresholds: Testing methods and inferences about anatomic distribution of receptors. *Neurology*, 1993,43(8): 1500–1508.

- [81] Murgatroyd D. Spatial Summation of Pain for Large Body Areas. Defence Atomic Support Agency Report, 1964: 1568
- [82] Marchand S, Arsenault P. Spatial summation for pain perception: Interaction of inhibitory and excitatory mechanisms. *Pain*, 2002,95(3): 201–206.
- [83] Stohler C S, Kowalski C J. Spatial and temporal summation of sensory and affective dimensions of deep somatic pain. *Pain*, 1999,79(2-3): 165–173.
- [84] Defrin R, Ronat A, Ravid A, et al. Spatial summation of pressure pain: Effect of body region. *Pain*, 2003,106(3): 471–480.
- [85] Nielsen J, Arendt-Nielsen L. Spatial summation of heat induced pain within and between dermatomes. *Somatosensory and Motor Research*, 1997,14(2): 119–125.
- [86] Gronroos M, Reunala T, Pertovaara A. Influence of selective nerve fiber blocks on argon laser-induced thermal pain in the human skin. *Neuroscience Letters*, 1996,211(2): 143–145.
- [87] Staud R. Predictors of clinical pain intensity in patients with fibromyalgia syndrome. *Current Rheumatology Reports*, 2004,6(4): 281–286.
- [88] Price D D. Characteristics of second pain and flexion reflexes indicative of prolonged central summation. *Experimental Neurology*, 1972,37(2): 371–387.
- [89] Douglass D K, Carstens E, Watkins L R. Spatial summation in human thermal pain perception: Comparison within and between dermatomes. *Pain*, 1992,50(2): 197–202.
- [90] Price D D, McHaffie J G, Larson M A. Spatial summation of heat-induced pain: Influence of stimulus area and spatial separation of stimuli on perceived pain sensation intensity and unpleasantness. *Journal of Neurophysiology*, 1989,62(6): 1270–1279.
- [91] Lautenbacher S, Nielsen J, Andersen T, et al. Spatial summation of heat pain in males and females. *Somatosensory and Motor Research*, 2001,18(2): 101–105.
- [92] Green B G, Cruz A. “Warmth-insensitive fields”: Evidence of sparse and irregular innervation of human skin by the warmth sense. *Somatosensory and Motor Research*, 1998,15(4): 269–275.
- [93] Defrin R, Ohry A, Blumen N, et al. Sensory determinants of thermal pain. *Brain*, 2002,125(3): 501–510.
- [94] Price D D. Psychological mechanisms of pain and analgesia: Progress in pain research and management. Seattle: IASP Press, 1999: 1–248.
- [95] Watanabe S, Kakigi R, Hoshiyama M, et al. Effects of noxious cooling of the skin on pain perception in man. *Journal of the Neurological Sciences*, 1996,135(1): 68–73.
- [96] Bouhassira D, Gall O, Chitour D, et al. Dorsal horn convergent neurones: Negative feedback triggered by spatial summation of nociceptive afferents. *Pain*, 1995,62(2): 195–200.
- [97] Talbot J D, Duncan G H, Bushnell M C. Effects of diffuse noxious inhibitory controls (DNICs) on the sensory-discriminative dimension of pain perception. *Pain*, 1989,36(2): 231–238.

- [98] Gybels J, Handwerker H O, Van Hees J. A comparison between the discharges of human nociceptive nerve fibres and the subject's ratings of his sensations. *The Journal of Physiology*, 1979,292: 193–206.
- [99] Paulson P E, Minoshima S, Morrow T J, et al. Gender differences in pain perception and patterns of cerebral activation during noxious heat stimulation in humans. *Pain*, 1998,76(1-2): 223–229.
- [100] Ali Z, Meyer R A, Campbell J N. Secondary hyperalgesia to mechanical but not heat stimuli following a capsaicin injection in hairy skin. *Pain*, 1996,68(2-3): 401–411.
- [101] Warncke T, Stubhaug A, Jorum E. Ketamine, an NMDA receptor antagonist, suppresses spatial and temporal properties of burn-induced secondary hyperalgesia in man: A double-blind, cross-over comparison with morphine and placebo. *Pain*, 1997,72(1-2): 99–106.
- [102] Kilo S, Schmeltz M, Koltzenburg M, et al. Different patterns of hyperalgesia induced by experimental inflammation in human skin. *Brain*, 1994,117 (2): 385–396.
- [103] Wallace M S, Laitin S, Licht D, et al. Concentration-effect relations for intravenous lidocaine infusions in human volunteers: Effects on acute sensory thresholds and capsaicin-evoked hyperpathia. *Anesthesiology*, 1997,86(6): 1262–1272.
- [104] Arendt-Nielsen L, Nielsen J, Petersen-Felix S, et al. Effect of racemic mixture and the (S)-isomer of ketamine on temporal and spatial summation of pain. *British Journal of Anaesthesia*, 1996,77(5): 625–631.
- [105] Hardy J D, Wolff H G, Goodell H. Experimental evidence on the nature of cutaneous hyperalgesia. *The Journal of Clinical Investigation*, 1950,29(1): 115–140.
- [106] Thalhammer J G, LaMotte R H. Spatial properties of nociceptor sensitization following heat injury of the skin. *Brain Research*, 1982,231(2): 257–265.
- [107] Lawand N B, Willis W D, Westlund K N. Excitatory amino acid receptor involvement in peripheral nociceptive transmission in rats. *European Journal of Pharmacology*, 1997,324(2-3): 169–177.
- [108] Pedersen J L, Kehlet H. Secondary hyperalgesia to heat stimuli after burn injury in man. *Pain*, 1998,76(3): 377–384.
- [109] Andrew D, Greenspan J D. Mechanical and heat sensitization of cutaneous nociceptors after peripheral inflammation in the rat. *Journal of Neurophysiology*, 1999,82(5): 2649–2656.
- [110] Bleehen T, Keele C A. Observations on the algogenic actions of adenosine compounds on the human blister base preparation. *Pain*, 1977,3(4): 367–377.
- [111] Bleehen T, Hobbiger F, Keele C A. Identification of algogenic substances in human erythrocytes. *The Journal of Physiology*, 1976,262(1): 131–149.
- [112] Sawynok J, Reid A. Peripheral adenosine 50-triphosphate enhances nociception in the formalin test via activation of a purinergic p2X receptor. *European Journal of Pharmacology*, 1997,330(2-3): 115–121.
- [113] Steen K H, Reeh P W, Anton F, et al. Protons selectively induce lasting

- excitation and sensitization to mechanical stimulation of nociceptors in rat skin, *in vitro*. *Journal of Neurophysiology*, 1992,12(1): 86–95.
- [114] Bevan S, Yeats J. Protons activate a cation conductance in a subpopulation of rat dorsal root ganglion neurones. *Journal of Physiology*, 1991,433: 145–161.
- [115] McCleskey E W, Gold M S. Ion channels of nociception. *Annual Review of Physiology*, 1999,61: 835–856.
- [116] Baranauskas G, Nistri A. Sensitization of pain pathways in the spinal cord: Cellular mechanisms. *Progress in Neurobiology*, 1998,54(3): 349–365.
- [117] Khasabov S G. Enhanced responses of spinal dorsal horn neurons to heat and cold stimuli following mild freeze injury to the skin. *Journal of Neurophysiology*, 2001,86(2): 986–996.
- [118] Junger H, Moore A C, Sorkin L S. Effects of full-thickness burns on nociceptor sensitization in anesthetized rats. *Burns*, 2002,28(8): 772–777.
- [119] Sang C N, Gracely R H, Max M B, et al. Capsaicin-evoked mechanical allodynia and hyperalgesia cross nerve territories. Evidence for a central mechanism. *Anesthesiology*, 1996,85(3): 491–496.
- [120] Schmidt R, Schmelz M, Forster C, et al. Novel classes of responsive and unresponsive C nociceptors in human skin. *Journal of Neurophysiology*, 1995,15(1): 333–341.
- [121] Schmelz M, Schmidt R, Ringkamp M, et al. Limitation of sensitization to injured parts of receptive fields in human skin C-nociceptors. *Experimental Brain Research*, 1996,109(1): 141–147.
- [122] Schmelz M, Schmidt R, Ringkamp M, et al. Sensitization of insensitive branches of C nociceptors in human skin. *The Journal of Physiology*, 1994, 480(2): 389–394.
- [123] Cervero F, Meyer R A, Campbell J N. A psychophysical study of secondary hyperalgesia: Evidence for increased pain to input from nociceptors. *Pain*, 1994,58(1): 21–28.
- [124] Koltzenburg M, Handwerker H O, Torebjork H E. The ability of humans to localise noxious stimuli. *Neuroscience Letters*, 1993,150(2): 219–222.
- [125] Xu M, Kim C J, Neubert M J, et al. NMDA receptor-mediated activation of medullary pro-nociceptive neurons is required for secondary thermal hyperalgesia. *Pain*, 2007,127(3): 253–262.
- [126] Meyer R A, Campbell J N. Myelinated nociceptive afferents account for the hyperalgesia that follows a burn to the hand. *Science*, 1981,213(4515): 1527–1529.
- [127] Lynn B, Perl E R. A comparison of four tests for assessing the pain sensitivity of different subjects and test areas. *Pain*, 1977,3(4): 353–365.
- [128] Pertovaara A, Kojo I. Influence of the rate of temperature change on thermal thresholds in man. *Experimental Neurology*, 1985,87(3): 439–445.
- [129] Taylor D J, McGillis S L, Greenspan J D. Body site variation of heat pain sensitivity. *Somatosensory and Motor Research*, 1993,10(4): 455–465.
- [130] Meh D, Denislic M. Quantitative assessment of thermal and pain sensitivity. *Journal of the Neurological Sciences*, 1994,127(2): 164–169.

- [131] Hagander L G, Midani H A, Kuskowski M A, et al. Quantitative sensory testing: Effect of site and skin temperature on thermal thresholds. *Journal of Clinical Neurophysiology*, 2000,111(1): 17–22.
- [132] Meier P M, Berde C B, DiCanzio J, et al. Quantitative assessment of cutaneous thermal and vibration sensation and thermal pain detection thresholds in healthy children and adolescents. *Muscle Nerve*, 2001,24(10): 1339–1345.
- [133] Greenspan J D, Taylor D J, McGillis S L. Body site variation of cool perception thresholds, with observations on paradoxical heat. *Somatosensory and Motor Research*, 1993,10(4): 467–474.
- [134] Campbell J N, Meyer R A. Sensitization of unmyelinated nociceptive afferents in monkey varies with skin type. *Journal of Neurophysiology*, 1983,49(1): 98–110.
- [135] Stevens J C, Choo K K. Temperature sensitivity of the body surface over the life span. *Somatosensory and Motor Research*, 1998,15(1): 13–28.
- [136] Okamoto T, Iwase S, Sugeno Y, et al. Different thermal dependency of cutaneous sympathetic outflow to glabrous and hairy skin in humans. *European Journal of Applied Physiology*, 1994,68(6): 460–464.
- [137] Cormack D H. The integumentary system//Lippincott J B. *Ham's Histology*. Philadelphia: WB Saunders, 1987: 450–474.
- [138] Hensel H. *Thermal Sensation and Thermoreceptors in Man*. Illinois: Springfield, 1982.
- [139] Fleischer E, Handwerker H O, Joukhadar S. Unmyelinated nociceptive units in two skin areas of the rat. *Brain Research*, 1983,267(1): 81–92.
- [140] Hilz M J, Claus D, Balk M, et al. Influence of caffeine, sweating and local hyperemiasis on “Marstock” thermotesting. *Acta Neurologica Scandinavica*, 1992,86(1): 19–23.
- [141] Lever W F, Schaumburg-Lever G. *Histology of the skin*//Lippincott J B. *Histopathology of the Skin*. Philadelphia: WB Saunders, 1990.
- [142] Iggo A. Cutaneous thermoreceptors in primates and sub-primates. *Journal of Physiology (London)*, 1969,200: 403–430.
- [143] Klement W, Arndt J O. Pain but no temperature sensations are evoked by thermal stimulation of cutaneous veins in man. *Neuroscience Letters*, 1991,123(1): 119–122.
- [144] Unruh A M. Gender variations in clinical pain experience. *Pain*, 1996, 65(2-3): 123–167.
- [145] Keefe F J, Lefebvre J C, Egert J R, et al. The relationship of gender to pain, pain behavior, and disability in osteoarthritis patients: The role of catastrophizing. *Pain*, 2000,87(3): 325–334.
- [146] Bassols A, Bosch F, Banos J E. How does the general population treat their pain? A survey in Catalonia, Spain. *Journal of Pain and Symptom Management*, 2002,23(4): 318–328.
- [147] Yosipovitch G, Meredith G, Chan Y H, et al. Do ethnicity and gender have an impact on pain thresholds in minor dermatologic procedures? A study on thermal pain perception thresholds in Asian ethnic groups. *Skin Research and Technology*, 2004,10(1): 38–42.

- [148] Fillingim R B, Edwards R R, Powell T. Sex-dependent effects of reported familial pain history on recent pain complaints and experimental pain responses. *Pain*, 2000,86(1-2): 87–94.
- [149] Lautenbacher S, Rollman G B. Sex differences in responsiveness to painful and non-painful stimuli are dependent upon the stimulation method. *Pain*, 1993,53(3): 255–264.
- [150] Keogh E, Hatton K, Ellery D. Avoidance versus focused attention and the perception of pain: Differential effects for men and women. *Pain*, 2000,85(1-2): 225–230.
- [151] Lawlis G F, Achterberg J, Kenner L, et al. Ethnic and sex differences in response to clinical and induced pain in chronic spinal pain patients. *Spine*, 1984,9(7): 751–754.
- [152] Prkachin K M. The consistency of facial expressions of pain: A comparison across modalities. *Pain*, 1992,51(3): 297–306.
- [153] Guinsburg R, de Araujo Peres C, Branco de Almeida M F, et al. Differences in pain expression between male and female newborn infants. *Pain*, 2000,85(1-2): 127–133.
- [154] Lang P J, Greenwald M K, Bradley M M, et al. Looking at pictures: Affective, facial, visceral, and behavioral reactions. *Psychophysiology*, 1993,30(3): 261–273.
- [155] Kunz M, Gruber A, Lautenbacher S. Sex differences in facial encoding of pain. *Journal of Pain*, 2006,7(12): 915–928.
- [156] Riley J L, Gilbert G H. Orofacial pain symptoms: An interaction between age and sex. *Pain*, 2001,90(3): 245–256.
- [157] Berkley K J. Sex differences in pain. *Behavioral and Brain Sciences*, 1997,20: 371–380.
- [158] Fillingim R B. Sex, gender and pain: Women and men really are different. *Curr Rev Pain*, 2000,4(1): 24–30.
- [159] Myers C D, Riley III J L, Robinson M E. Psychosocial contributions to sex-correlated differences in pain. *Clinical Journal of Pain*, 2003,19(4): 225–232.
- [160] Paulson P E, Minoshima S, Morrow T J, et al. Gender differences in pain perception and patterns of cerebral activation during noxious heat stimulation in humans. *Pain*, 1998,76(1-2): 223–229.
- [161] Fillingim R B, Maddux V, Shackelford J A. Sex differences in heat pain thresholds as a function of assessment method and rate of rise. *Somatosensory and Motor Research*, 1999,16(1): 57–62.
- [162] Fillingim R B, Maixner W, Kincaid S, et al. Sex differences in temporal summation but not sensory-discriminative processing of thermal pain. *Pain*, 1998,75(1): 121–127.
- [163] Edwards R R, Haythornthwaite J A, Sullivan M J, et al. Catastrophizing as a mediator of sex differences in pain: Differential effects for daily pain versus laboratory-induced pain. *Pain*, 2004,111(3): 335–341.
- [164] Sullivan M J L, Tripp D A, Santor D. Gender differences in pain and pain behavior: The role of catastrophizing. *Cognitive Therapy and Research*, 2000,24(1): 121–134.

- [165] Fillingim R B, Maixner W. The influence of resting blood pressure and gender on pain responses. *Psychosomatic Medicine*, 1996,58(4): 326–332.
- [166] Fillingim R B, Maixner W, Bunting S, et al. Resting blood pressure and thermal pain responses among females: Effects on pain unpleasantness but not pain intensity. *International Journal of Psychophysiology*, 1998,30(3): 313–318.
- [167] Lautenbacher S, Kunz M, Strate P, et al. Age effects on pain thresholds, temporal summation and spatial summation of heat and pressure pain. *Pain*, 2005,115(3): 410–418.
- [168] Woodrow K M, Friedman G D, Siegelau A B, et al. Pain tolerance: Differences according to age, sex and race. *Psychosomatic Medicine*, 1972,34(6): 548–556.
- [169] Walsh N E, Schoenfeld L, Ramamurthy S, et al. Normative model for cold pressor test. *American Journal of Physical Medicine and Rehabilitation*, 1989,68(1): 6–11.
- [170] Edwards R R, Fillingim R B. Age-associated differences in responses to noxious stimuli. *Journals of Gerontology Series A: Biological Sciences and Medical Sciences*, 2001,56(3): M180–M185.
- [171] Edwards R R, Fillingim R B. Effects of age on temporal summation and habituation of thermal pain: Clinical relevance in healthy older and younger adults. *Journal of Pain*, 2001,2(6): 307–317.
- [172] Chakour M C, Gibson S J, Bradbeer M, et al. The effect of age on A delta- and C-fibre thermal pain perception. *Pain*, 1996,64(1): 143–152.
- [173] Sato T, Oda H. Progress in pain therapy: Acupuncture (including acupuncture anesthesia and percutaneous electrotherapy). *Kango Gijutsu*, 1985,31(5): 579–585.
- [174] Gibson S J, Farrell M. A review of age differences in the neurophysiology of nociception and the perceptual experience of pain. *The Clinical Journal of Pain*, 2004,20(4): 227–239.
- [175] Lautenbacher S, Strian F. Sex differences in pain and thermal sensitivity: The role of body size. *Percept Psychophys*, 1991,50(2): 179–183.
- [176] Meliala A, Gibson S J, Helme R D. The effect of stimulation site on detection and pain thresholds in young and older adults//IXth World Congress on Pain. Seattle: IASP Press, 1999: 559.
- [177] Zheng Z, Gibson S J, Khalil Z, et al. Age-related differences in the time course of capsaicin-induced hyperalgesia. *Pain*, 2000,85(1-2): 51–58.
- [178] Price D D, Staud R, Robinson M E, et al. Enhanced temporal summation of second pain and its central modulation in fibromyalgia patients. *Pain*, 2002,99(1-2): 49–59.
- [179] Edwards R R, Fillingim R B, Ness T J. Age-related differences in endogenous pain modulation: A comparison of diffuse noxious inhibitory controls in healthy older and younger adults. *Pain*, 2003,101(1-2): 155–165.
- [180] Van Hees J, Gybels J. C nociceptor activity in human nerve during painful and non painful skin stimulation. *Journal of Neurology, Neurosurgery and*

- Psychiatry, 1981,44(7): 600–607.
- [181] Reuck A V S, Knight J. Touch, Heat and Pain. London: Churchill, 1966.
- [182] Xu F, Wen T, Seffen K A, et al. Biothermomechanics of skin tissue. *Journal of the Mechanics and Physics of Solids*, 2008, 56(5): 1852–1884.

Chapter 13

Skin Thermal Pain Modeling

13.1 Introduction

As one of the most important sensations, pain sensation has been studied extensively for a long time over a range of scales, from molecular level to the entire human neural system level. Thermal stimulation, as one of the three main stimulations for pain (thermal, mechanical and chemical stimuli), has been widely used in the pain study^[1], such as the examination of tissue injury and sensitisation mechanisms, and the quantification of therapeutic effects of pharmacological, physical, and psychological interventions^[2,3]. However, the understanding of the underlying mechanisms of thermal pain is still far from clear, the main reason being that pain is influenced by many factors, including both physiological factors and psychological factors.

Although the utilization of computational models in the field of pain has been very limited and attempts at modeling pain have generally focused on acute pain, there are strong arguments for mathematical modeling of pain^[4,5]: ① it can handle extremely complex theories; ② the model can be used to predict behaviours which had perhaps previously gone unnoticed; ③ the method is non-invasive. So far several mathematical models have been developed at different levels: at the molecular level and cellular level^[4,6~12]; and at the level of network of neurons^[13,14]. However, none of these models have considered morphological plausibility and the biothermomechanical response of skin tissue, or correlated the external stimulus parameters directly with the pain sensation level, and no transmission process has been considered. All these issues will be addressed in this chapter.

For simplicity, this study only attempts to model superficial nociceptive acute pain (i.e., neuropathic pain and chronic pain are not considered). Additionally, psychological factors that may influence pain are not modeled.

In this chapter, a holistic mathematical model for quantifying skin thermal pain was developed, by using biothermomechanical models of skin tissue developed in previous chapters and considering the current biophysical and

neurological mechanisms of pain sensation. From the review in Chapter 11, we know that classic descriptions of pain typically include four processes, namely, transduction, transmission, perception and modulation. The holistic model is thus composed of three sub models: model of transduction, model of transmission, and model of perception and modulation, as schematically shown in Figure 13.1.

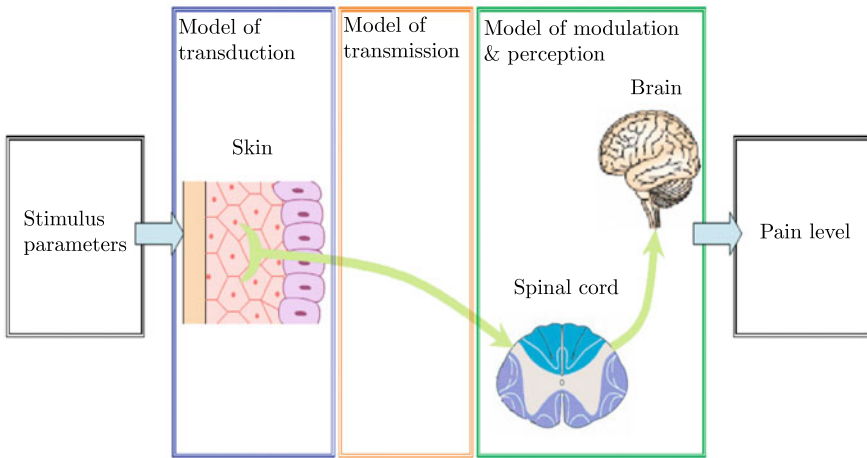


Figure 13.1 Schematic of the holistic skin thermal pain model
(by permission of Elsevier)

The model development was first presented in detail. Then the model was used to explain some physiological features of skin thermal pain. A short summary was given in the last part.

13.2 Model of Transduction

In this section, with emphasis placed on the transduction function of nociceptors, the development of nociceptor transduction model is presented.

13.2.1 Model development

Although a tremendous amount of work has been done on the histomorphology and electrophysiology of nerve circuits of skin thermal pain, the exact coupling between neural and thermomechanical participations is yet precisely known. According to the mechanism of nociceptor transduction, as described in Chapter 11, the proposed model is composed of three sub-models: biothermomechanical model of skin tissue, model of current generation, and model of frequency modulation. Each of these models is presented in detail below.

1) Biothermomechanical model of skin tissue

It is now widely accepted that thermal pain is decided by temperature at the location of nociceptor, not that at the skin surface^[15,16]. Besides, thermal damage causes the cells to break down and to release a number of tissue byproducts and mediators, which will activate and sensitize nociceptors^[17]. Further, thermally induced stresses due to non-uniform temperature distributions may also lead to the sensation of thermal pain, in addition to the pain generated by heating alone. Our numerical results in Chapter 6 also showed that the stress induced by heating may exceed the mechanical threshold of nociceptors.

The thermomechanical model of skin tissue developed in Chapter 4 and Chapter 9 was used here. It should be noted here that the skin is assumed to be a thermo-elastic material although viscoelasticity has been shown to play an important role in the mechanical behaviour of skin^[18~21] and touch sensation^[22~25]. Since the thermal induced strain level will be very small, the assumption of thermo-elasticity is reasonable.

2) Model of current generation

As described above, pain signal starts from the current induced by the opening of ion channels in nociceptors. Since ion channels are generally gated by three different stimuli (thermal, mechanical and chemical stimuli), there are correspondingly three different currents. The total current may be calculated as

$$I_{st} = I_{heat} + I_{chem} + I_{mech} \quad (13.1)$$

where I_{heat} , I_{chem} and I_{mech} are the currents due to the opening of thermally-, chemically-, and mechanically-gated ion channels, respectively.

Thermally-gated channels

The heat current (I_{heat}) is assumed to be a function of nociceptor temperature (T_n) and thermal pain threshold (T_t), given as

$$I_{heat} = f_h(T_n, T_t) \quad (13.2)$$

Here, T_t is assumed to be 43°C ^[26,27].

Chemically-gated channels

The chemical current (I_{chem}) is assumed to depend on the thermal damage degree of skin tissue (Deg)

$$I_{chem} = f_c(Deg) \quad (13.3)$$

Mechanically-gated channels

The mechanical current (I_{mech}) is assumed to be a function of the stress at the location of nociceptor (σ_n) and mechanical pain threshold (σ_t)

$$I_{\text{mech}} = f_m(\sigma_n, \sigma_t) \quad (13.4)$$

where σ_t is assumed to be 0.2MPa^[28].

3) Model of frequency modulation

When the evoked current overpasses the threshold, action potential is generated. It is now accepted that the intensity of external stimulation is carried through the frequency of these impulses (f_s), not the exact magnitude or shape of the signal, which can be calculated as

$$f_s = f_{\text{fm}}(I_{\text{st}}) \quad (13.5)$$

Unfortunately, there exists no study to quantify the current-frequency relation. We need, therefore, to choose a model for the generation of action potential. Although there has been no analysis of the nociceptor kinetics, all neurons have been found to behave qualitatively similar to that described by the Hodgkin-Huxley (H-H) model^[29]. This model was established by Hodgkin and Huxley in 1952 and has been shown to provide an excellent phenomenological description of nerve excitation. Their work on the squid giant axon was awarded a Nobel price in physiology and medicine (together with Eccles in 1963) and is until today one of the key achievements in cellular biophysics. Various H-H-form models have also been developed for modeling human sensations such as mechanical^[30~34] and thermal sensations^[35,36]. Although the H-H model is original for unmyelinated nerve fiber (axon), it is used here for skin nociceptors which are found both unmyelinated (C fiber) and myelinated (A fiber). This is reasonable since the H-H model has been extended, with relatively minor modifications, to myelinated axons^[37] and muscle fibers^[38,39].

The electrical behaviour of membrane in the basic H-H model can be represented by the network shown in Figure 13.2(a). The through membrane electrical current is induced by either charging the membrane capacity or transport of ions through the resistances in parallel with capacity. The ionic current is composed of three components, namely, current carried by sodium, current carried by potassium ions, and a small “leakage current” carried by chloride and other ions. Mathematically, the model can be described as

$$C_m \frac{dV_m}{dt} = I_{\text{st}} + I_{\text{Na}} + I_{\text{K}} + I_{\text{L}} \quad (13.6)$$

where V_m is membrane potential (depolarization positive) (mV); t is time (ms); C_m is membrane capacity per unit area ($\mu\text{F}/\text{cm}^2$); I_{st} is stimuli induced current density, positive outward ($\mu\text{A}/\text{cm}^2$); I_{Na} , I_{K} and I_{L} are sodium,

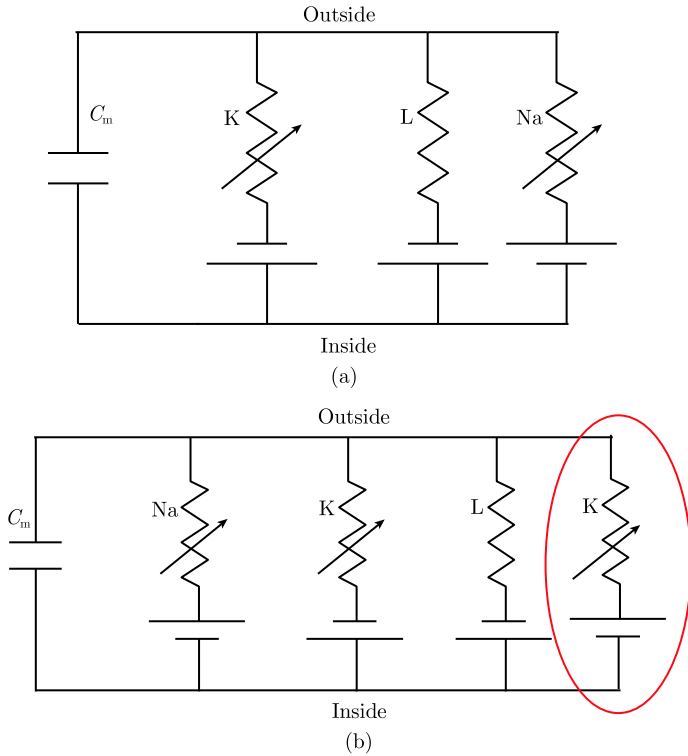


Figure 13.2 (a) Original Hodgkin and Huxley model and (b) revised H-H model (by permission of ASME)

potassium and leakage current components ($\mu\text{A}/\text{cm}^2$), respectively. Each of the above three ionic currents is driven by a force, which may conveniently be measured as an electrical potential difference and a permeability coefficient (conductance)^[29]. The conductances of ionic currents are regulated by voltage dependent activation and inactivation variables (gating variables), which are given as

$$\frac{dx}{dt} = \frac{x_\infty(V_m) - x}{\tau_x(V_m)} \text{ or } \frac{dx}{dt} = \alpha_x(1 - x) - \beta_x x \quad (13.7)$$

here x is gating variable; $\tau_x = x_{\text{fac}} [1/(\alpha_x + \beta_x)]$, $x_\infty = \alpha_x/(\alpha_x + \beta_x)$ where α_x and β_x are called rate constants (s^{-1}); $x_\infty(V_m)$ is steady-state voltage dependent activation function of x , and $\tau_x(V_m)$ is voltage-dependent time constant. Furthermore, $x_\infty(V_m)$ and $\tau_x(V_m)$ can be calculated as^[40]

$$x_\infty(V_m) = 1/\{1 + \exp[(V_m - \vartheta_x)/\sigma_x]\} \quad (13.8)$$

$$\tau_x(V_m) = x_{\text{fac}} \{ \tau_x / \cosh [(V_m - \vartheta_x) / (2\sigma_x)] \} \quad (13.9)$$

where $x_\infty(V_m)$ is steady-state value and is a sigmoidal function with half activation (or inactivation) at $V_m = \vartheta_x$ and a slope that is proportional to $1/\sigma_x$; $\tau_x(V_m)$ is time constant and has a bell-shaped curve with maximum at $V_m = \vartheta_x$ and a half-width determined by σ_x ; and x_{fac} is scaling factor. Thus, each gating variable is described by only three parameters, which, in principle, can be measured experimentally.

13.2.2 Preliminary results and model revision

At current understanding, it is not sure of the highly nonlinear neural impulse initiation component in the response characteristics of nociceptors. We will first apply a simple model to quantify the neural impulse initiation. The input is thermal stimulus at the location of nociceptors, and the output is time history of nerve impulse initiated, from which the frequency can be derived.

1) Preliminary results

For preliminary study, the standard H-H model is used for the modeling, which incorporates three kinds of channels, as shown in Figure 13.2(a). The voltage-gated sodium channels mediate the rapid increase in Na^+ conductance during the initial phase of action potentials, while the voltage-gated noninactivating potassium channels (delayed rectifiers) are responsible for the shape of action potentials, as the outward current through these channels repolarizes the membrane potential. The leak channels contribute to the resting membrane potential. The model is given as^[29]

$$C_m \frac{dV_m}{dt} = I_{\text{st}} + \bar{g}_{\text{Na}} m^3 h (E_{\text{Na}} - V_m) + \bar{g}_{\text{K}} n^4 (E_{\text{K}} - V_m) + g_{\text{L}} (E_{\text{L}} - V_m) \quad (13.10)$$

where E_{Na} , E_{K} and E_{L} are the corresponding reversal potentials for sodium, potassium and leakage current components given by the Nernst equation (mV), respectively; \bar{g}_{Na} , \bar{g}_{K} and g_{L} are the maximal ionic conductance through sodium, potassium and leakage current components (ms/cm^2), respectively. The various voltage- and time-dependent parameters (m, n, h) are defined as shown in Equations (13.11) and (13.12), where α_x and β_x can be calculated as^[29]

$$\begin{aligned} \alpha_n &= -0.01 (V_m + 50) / \{ \exp [- (V_m + 50) / 10] - 1 \}, \\ \beta_n &= 0.125 \exp [- (V_m + 60) / 80] \end{aligned} \quad (13.11)$$

$$\begin{aligned} \alpha_m &= -0.1 (V_m + 35) / \{ \exp [- (V_m + 35) / 10] - 1 \}, \\ \beta_m &= 4 \exp [- (V_m + 60) / 18] \end{aligned} \quad (13.12)$$

$$\alpha_h = 0.07 \exp[-(V_m + 60)/20], \quad \beta_h = 1/\{\exp[-(V_m + 30)/10] + 1\} \quad (13.13)$$

At the preliminary stage, only heat-gated ion channels are considered for the generation of stimulation current I_{st} . Unfortunately, there is yet no experimentally obtained quantitative relationship between stimuli and current available in the literature, and there is no consensus of any standard model for this. However, it has been shown that the current is exponentially proportional to the stimulus^[41], as shown in Figure 2.9(a), so that the following relation may be assumed:

$$I_{st} = I_{heat} = \left[C_{h1} \exp \frac{(T_n - T_t)/T_t}{C_{h2}} + C_{h3} \right] \times H(T_n - T_t) \quad (13.14)$$

where C_{h1} , C_{h2} and C_{h3} are constants, and $H(x)$ is the Heaviside function. With the current input range in mind, the constants are chosen as $C_{h1} = 0.382 \mu\text{A}/\text{cm}^2$, $C_{h2} = 0.064 \mu\text{A}/\text{cm}^2$, $C_{h3} = -0.355 \mu\text{A}/\text{cm}^2$. The current-temperature relation predicted from Equation (13.14) is plotted in Figure 13.3.

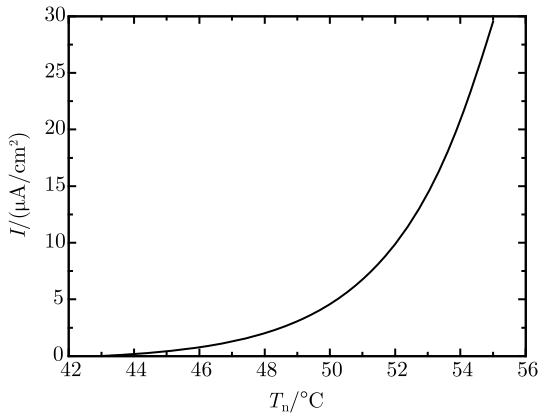


Figure 13.3 Current-temperature relationship

As for the original H-H model itself, there exists a threshold current for action potential generation, which varies with the choice of the different parameters in the model. In order to account for this, a shift current (I_{shift}) is added to Equation (13.14) to ensure that action potential is generated when $T_n \geq T_t$ while none is generated if $T_n < T_t$

$$I_{st} = I_{heat} = \left[C_{h1} \exp \frac{(T_n - T_t)/T_t}{C_{h2}} + C_{h3} + I_{shift} \right] \times H(T_n - T_t) \quad (13.15)$$

The whole group of governing equations are solved using an explicit Runge-Kutta formula and the Dormand-Prince pair^[42] under MATLAB;

the parameters given by Hodgkin and Huxley for squid axon^[43] are selected: $C_m = 1.0\mu\text{F}/\text{cm}^2$, $E_{\text{Na}} = 55\text{mV}$, $E_{\text{K}} = -72\text{mV}$, $\bar{g}_{\text{Na}} = 120\text{ms}/\text{cm}^2$, $\bar{g}_{\text{K}} = 36\text{ms}/\text{cm}^2$, $G_{\text{L}} = 0.3\text{ms}/\text{cm}^2$, $x_{\text{fac}} = 1$.

The membrane potential and frequency responses under stimuli of different nociceptor temperatures (T_n) and of duration of 0.4 seconds are presented in Figure 13.4(a) and (b). From the figure, it can be seen that the persistent stimulus results in an ongoing firing of action potentials, where both the frequency and amplitude of generated action potential are governed by the stimulus' strength.

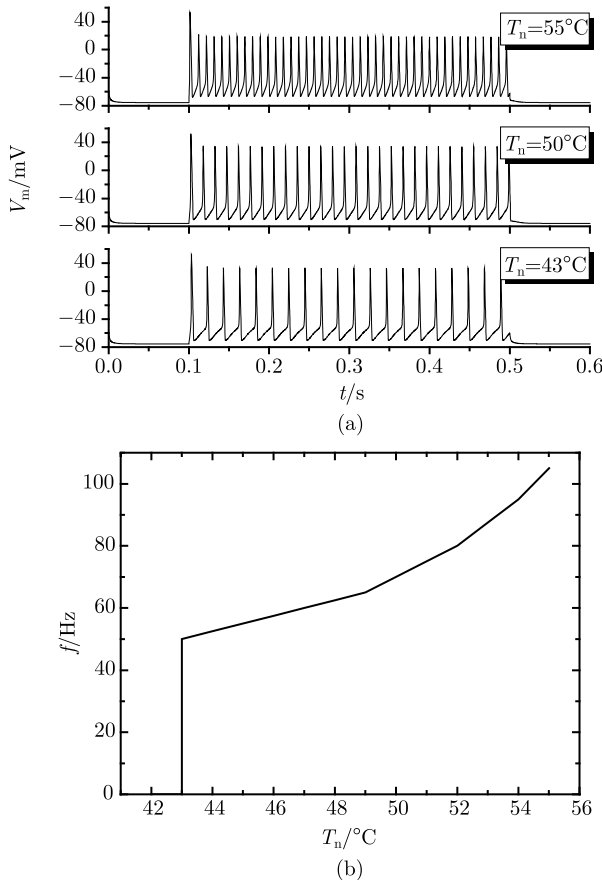


Figure 13.4 Influence of nociceptor temperature on (a) membrane potential and (b) frequency responses in H-H model (by permission of ASME)

The mechanism of action potential generation in the H-H model can be explained as^[29]: ① application of a noxious stimulus induced a stimulation current (positive), which causes depolarization of the membrane;

② with the rise in membrane potential, the activation of the sodium conductance increases, which results in the rapid entry of positive ions into the cell; ③ during the upwards wing in membrane potential the sodium conductance become inactivate while the potassium conductance becomes activated, which slows the inward flow of sodium ions and increases the outward flow of potassium ions; ④ an action potential peak is achieved when these two current are equal, after which the membrane potential rapidly returns toward the resting level and beyond due to the overpass of the sodium current by the potassium current; ⑤ finally the membrane potential recovers back to the resting potential due to the long time constant of the potassium conductance in this voltage region.

The frequency increases nonlinearly with increasing stimulation intensity [see Figure 13.4(b)]: from 50Hz at $T_n = 43^\circ\text{C}$ to 105Hz at $T_n = 55^\circ\text{C}$. However, when compared with experimental observations of nociceptors in mouse glabrous skin, as shown in Figure 13.5(a) and (b), this variation of frequency with stimulus intensity predicted by the preliminary model differs in two major respects. The first one is that the minimum nerve impulse frequency predicted by the model is much larger than the afferent units as observed in experiments^[44~47]. For example, Figure 13.5(b) gives a frequency range of 0~8Hz when the heat stimulus is in the range of 35~51°C, which is much smaller than the model prediction in Figure 13.4. Meyer &

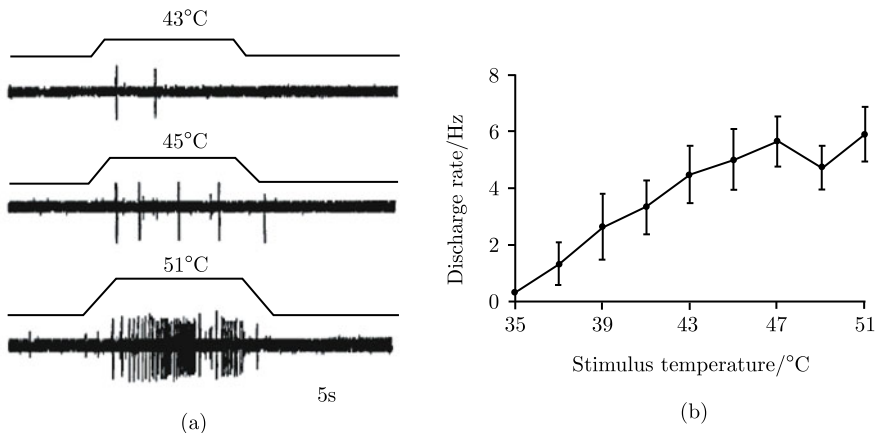


Figure 13.5 Experimental observations of the responses of *C* nociceptors in mouse glabrous skin to heat stimuli^[27] (a): responses of a single *C* nociceptor evoked by heat stimuli of 43°C, 45°C, and 51°C (response threshold to heat was 43°C) (b) the relationship between the mean discharge rate and the same stimulus temperatures (by permission of the American Physiological Society)

Campbell^[45] also found that under a skin surface stimulus of 53°C, the maximum discharging frequency of CMH nociceptors is about 10Hz while AMH has a max value of 20Hz. Similar results have also been obtained elsewhere for other sensory terminals, which are found to fire at a rate much slower than the Hodgkin-Huxley equations, even down to 1Hz or 2Hz^[43,48,49]. It is therefore necessary to decrease the rate of the channel kinetics. The second major discrepancy is that the firing frequency jumps discontinuously to a nonzero value rather than rising continuously at the threshold temperature, as can be seen from Figure 13.4(b): when $T_n < T_{th}$, there is no repetitive response, while at higher intensities, the nociceptor suddenly begins firing a train of impulses at a relatively high rate (50Hz). However, this phenomenon has not been observed in nociceptors, as shown in Figure 13.5(b).

2) Model revision

Several methods can be adopted to solve the problems associated with the preliminary model. The first one is to change the rates of existing channels in the H-H equations themselves. When the rate of channel kinetics is decreased by decreasing the rates, a very high membrane resistance in the threshold range is produced and thus a lower firing frequency can be achieved^[25,50,51]. However, modifying the rates alone does not change the fundamental nature of channel kinetics. The qualitative form of simulated frequency responses with different rates are very similar to that with the original equations^[25], while frequency in the lower range becomes extremely sensitive to stimulus intensity^[50]. There are several other potential ways for solving the problems with the original H-H model and we adopt the following two in this study.

(1) Consideration of temperature influence

Temperature is one of the most important factors which regulate neuronal activities^[52,53]. Several membrane properties have been found to be temperature dependent^[54,55], such as generation threshold^[56~59], resting membrane potential, membrane resistance (input impedance)^[60,61], gating kinetics of ion channels^[29,62,63], and hence the generation^[64,65] and the shape and amplitude^[66,67] of action potentials. For example, as the temperature is increased, it was found that the duration of action potential is reduced and its amplitude decreased^[67]. However, the original H-H model was developed as approximations of experimental results measured at temperature of 6.3°C. In order to consider the temperature effect, the following revisions are adopted.

Temperature corrections of rate constants

In order to consider temperature effect on the gating factor of activation speed of ionic channel, Equation (13.7) in the H-H model can be adjusted by

adding a temperature coefficient C_{Tx} , given as

$$\frac{dx}{dt} = C_{Tx} \frac{x_{\infty}(V_m) - x}{\tau_x(V_m)} \quad (13.16)$$

The temperature coefficient C_{Tx} depends on the difference of actual temperature T and laboratory temperature T_0 , defined as

$$C_{Tx} = (Q_x)^{(T-T_0)/10} \quad (13.17)$$

where Q_x is a special constant that gives the acceleration in membrane behaviour when the temperature is increased by 10°C . Hodgkin & Huxley found $Q_{10} = 3$ to be an adequate coefficient for squid membranes with $T_0 = 6.3^\circ\text{C}$ ^[29]. In this study, $T_0 = 32^\circ\text{C}$ is chosen as the reference temperature, since it coincides with the lower temperature limits in most neurophysiological experiments^[40] and lies within the reasonable physiological range of human body.

Temperature corrections of maximum conductances

The maximum conductances should also be considered as temperature dependent, especially in the simulation of processes near the threshold region of stimulation^[59,60,67,68]. Different formats of correcting factor have been suggested^[60,68]. Hodgkin et al.^[68] suggested a correction factor of $Q_x^{(T-6.3)/10}$, where Q_x was found to be in the range of $1 \sim 1.5$ for giant axon^[68]. According to Moore's experiments^[60], Fitzhugh^[59] suggested another factor, $C_1 [1 + C_2 (T - 6.3)]$, for temperature induced changes in ionic conductances, where $C_1 = 4$ is the ratio between the ionic conductances of axon at 6.3°C and the values used by Hodgkin and Huxley, while $C_2 = 0.061$ is the changing rate of conductance with temperature.

In this study, with reference temperature of 32°C , the format suggested by Hodgkin et al^[68] is adopted

$$C_{Tx2} = Q_x^{(T-32)/10} \quad (13.18)$$

Temperature corrections of reversal membrane potential

The reversal membrane potentials of ion channels are determined with the Nernst equation, which is temperature dependent. The temperature-dependent reversal membrane potential V_{Na} and V_K can be calculated as^[35]

$$V_{Na} = 10^3 \times \frac{R(T + 273.15)}{F} \ln([Na]_e / [Na]_i) \quad (13.19)$$

$$V_K = 10^3 \times \frac{R(T + 273.15)}{F} \ln([K]_e / [K]_i) \quad (13.20)$$

where $[K]_e$ and $[K]_i$ are external and internal concentration of potassium ions; $[Na]_e$ and $[Na]_i$ are external and internal concentration of sodium ions, and they are given as $[K]_e = 20\text{mM}^1$, $[K]_i = 400\text{mM}$, $[Na]_e = 440\text{mM}$ and $[K]_i = 50\text{mM}$ respectively^[69]; $F = 9.6485 \times 10^4\text{C/mol}$ is the Faraday constant; $R = 8.314\text{J}/(\text{mol}\cdot\text{K})$ is the universal gas constant. The normal condition is set as $T = 32^\circ\text{C}$, $V_{Na} = 57.19\text{mV}$ and $V_K = -78.78\text{mV}$. The reversal potential of $E_L = -63.79\text{mV}$ is obtained by adjusting E_L so that the -60mV equilibrium membrane potential is achieved.

For a preliminary modeling, Equations (13.17)~(13.20) are adopted with $Q_x = 3$ for Equation (13.17) and $Q_x = 1.5$ for Equation (13.18). However, in the stimulus range $T_n = 43 \sim 55^\circ\text{C}$, no action potential generation can be achieved. This phenomenon is known as “heat block” or “temperature block”, as observed in experiments^[66,70~72]. It is mainly due to the comparatively large values of Q_x in Equations (13.17) and (13.18), which are derived from experimental data of squid axon. For mammalian nerves, it has been found that Q_x is comparatively smaller, for example $Q_{10} = 1.3$ was assumed for the maximum conductances of thermal receptor^[36]. In view of these, $Q_x = 1.2$ is chosen for both Equations (13.17) and (13.18). The results are presented in Figure 13.6(a) and (b). The rise of temperature causes a fastened time course and lower amplitudes of generated action potentials. However, compared with Figure 13.5, a firing frequency jump to a nonzero value still exists. This can be solved by the addition of new ion channels, as illustrated below.

(2) Addition of transient K^+ channels

It has been known that neurons in higher organisms have different electrophysiological properties much more than the squid axon studied by Hodgkin & Huxley, which has been shown to be mainly due to the large variety of different ion channels^[43,73,74]. The presence of transient K^+ channels have been shown to regulate the discharge patterns of neurons^[43,75~81]. Transient K^+ channels are then added to our model, as schematically shown in Figure 13.2(b). The system can be described mathematically as

$$C_m \frac{dV_m}{dt} = I_{st} + \bar{g}_{Na} m^3 h (E_{Na} - V_m) + \bar{g}_K n^4 (E_K - V_m) + g_L (E_L - V_m) + I_{K2} \quad (13.21)$$

which with an additional current I_{K2} for the second potassium channel is different from Equation (13.10). There are different forms of K^+ conductance. One of the most used was the fast transient K^+ current (also called A-current I_A), which has been experimentally observed early in crab^[77] and

1) $1\text{mM} = 0.001\text{mol/L}$.

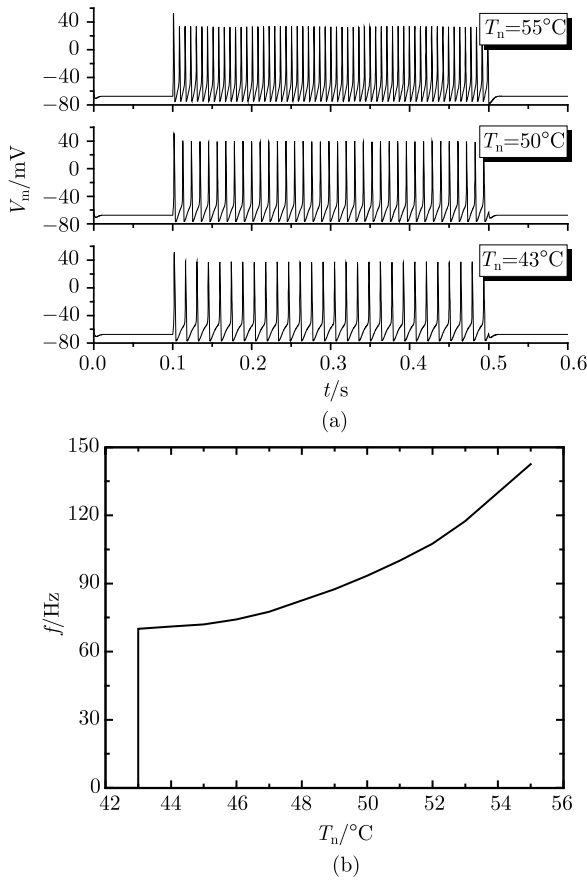


Figure 13.6 Response of (a) membrane potential and (b) frequency response in H-H model under different stimulus intensities (by permission of ASME)

molluscan neurons^[82], and later in a variety of neurons that display repetitive firing^[40,83,84]. Connor & Stevens^[85] suggested that the potassium A -current can be expressed by

$$I_{K2} = I_A = \bar{g}_A A^3 B (V_A - V_m) \tag{13.22}$$

where $\bar{g}_A = 47.7\text{ms/cm}^2$, A and B are factors having the same functional significance as factors m and h of the sodium conductance system, given as^[75]

$$\tau_A \frac{dA}{dt} + A = A_\infty, \quad A_\infty = \left\{ 0.0761 \frac{\exp [(V_m + 94.22)/31.84]}{1 + \exp [(V_m + 1.17)/28.93]} \right\}^{1/3}$$

$$\tau_A = A_{\text{fac}} \left\{ 0.3632 + \frac{1.158}{1 + \exp [(V_m + 55.96)/20.12]} \right\} \tag{13.23}$$

$$\tau_B \frac{dB}{dt} + B = B_\infty, \quad B_\infty = \left\{ \frac{1}{1 + \exp [(V_m + 53.3)/14.54]} \right\}^4$$

$$\tau_B = B_{\text{fac}} \left\{ 1.24 + \frac{2.678}{1 + \exp [(V_m + 50)/16.027]} \right\} \quad (13.24)$$

Due to the additional channel, the -60 mV equilibrium membrane potential has been achieved by readjusting the reversal potential of leak current E_L . The parameters used for the revised model are: $C_m = 2.8\mu\text{F}/\text{cm}^2$, $\bar{g}_{\text{Na}} = 120\text{ms}/\text{cm}^2$, $\bar{g}_K = 36\text{ms}/\text{cm}^2$, $G_L = 0.3\text{ms}/\text{cm}^2$, $A_{\text{fac}} = B_{\text{fac}} = 7.0$, $m_{\text{fac}} = h_{\text{fac}} = 0.263$ and $n_{\text{fac}} = 2.63$.

The membrane potential and frequency responses under stimulus of different nociceptor temperatures (T_n) are given in Figure 13.7(a) and (b). Compared with experimental observations of nociceptors, as shown in Figure 13.5,

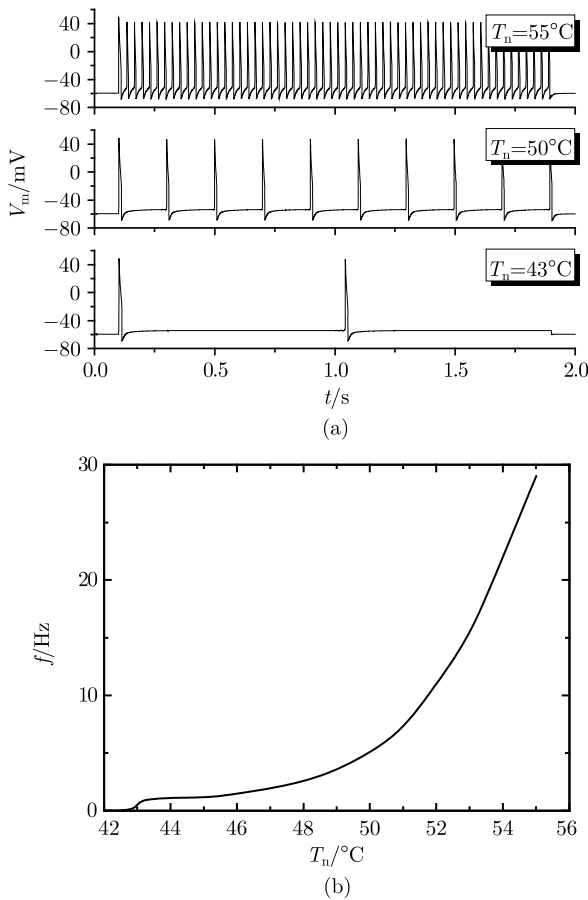


Figure 13.7 Response of (a) membrane potential and (b) frequency response in revised H-H model under different stimulus intensities (by permission of ASME)

it can be seen from Figure 13.7 that a good agreement has been achieved for both response shape and intensity-response relationship. In particular, with the revised model, the predicted neural impulse rate is comparable to that of the actual nociceptors. Exponential growth of response frequency with increasing stimulus intensity has also been observed in *C* nociceptors in monkey skin^[46].

The large decrease in response frequency can be explained as the modified sequence of events (described in H-H model) due to the addition of transient potassium conductance^[40,79]. Immediately following the action potential and after hyperpolarizing potential, as the membrane starts to depolarize, A -currents (I_A) is activated and an outward potassium current flows in a direction opposite the applied current, which slows the rate of depolarization on the first spike and prolongs the membrane hyperpolarization. This leads to increased inter-spike intervals and, therefore, serves as a damper on the generation of action potentials. Shortly afterward, however, the inactivation of I_A begins, which allows the membrane to slowly depolarize. For stronger input pulses, the rise in I_A is increasingly by-passed as the membrane potential moves more rapidly through its voltage range of activation.

In summary, by considering the temperature effect and adding transient K^+ channels to the original H-H model, frequency response behaving in a manner consistent with experimental observation has been achieved. The application of the revised model is given in the next section through case study.

It should be noted here that in developing our model, given the limited knowledge about noxious stimuli-sensitive ion channels and our desire for simplicity, a simple approximation between the noxious stimuli applied to the nociceptors and the generator current has been assumed, although it would be desirable to incorporate the actual noxious stimuli-sensitive ion channels into the model for compatibility with other models of excitable membranes. However, the addition of actual ion channels can not be achieved until more is known about these channels. The H-H model adopted in our model is original for unmyelinated nerve fiber (axon), while nociceptors are found both unmyelinated (*C* fiber) and myelinated (*A* fiber).

13.3 Model of Transmission

The model of transmission is to simulate the transmission of noxious stimulus triggered neural signals from the skin along the respective fibers to the spinal cord and brain. Since the intensity of the stimulation is carried through

firing rate (frequency) of these impulses, the actual shape, amplitude and duration of the single spike are not taken into account. The time for this transmission (t_t) will be obtained according to the conduction velocity and corresponding nerve length.

The model of transmission is to simulate the transmission of noxious stimulus triggered neural signals from the skin along the respective fibers to the spinal cord and brain. Since the intensity of the stimulation is carried through firing rate of these impulses, the actual shape, amplitude and duration of the single spike are not taken into account. The time for this transmission (t_t) will be obtained according to the conduction velocity and corresponding nerve length.

13.3.1 Nerve length (L_n)

Since at present study, skin is considered under only very small size thermal loading, or only localized stimuli, all fibers connected with the skin nociceptors can be postulated to have the same length. Here a length of 1 m was chosen, which is about the distance between a finger and the spinal cord^[86].

$$L_n = 1\text{m} \quad (13.25)$$

13.3.2 Conduction velocity (v_c)

The conduction velocity (v_c) is found to be directly related to fiber diameter (D)^[87]. Here a linear relationship is assumed between v_c and D , given as

$$v_c = v_{cN} = c_d D \quad (13.26)$$

where v_{cN} is the conduction velocity under normal condition; D is the diameter of the nerve fibre; c_d is the coefficient between diameter and velocity.

In addition to fiber diameter, temperature has also found to influence the nerve conduction velocity. For example, cold has been found to reduce the conduction velocity and the rate of reduction of conduction velocity is identical for slow and fast fibers^[88,89].

$$v_c = v_{cT} = c_T v_{cN} \quad (13.27)$$

where v_{cT} is the velocity when the fibre is in a environment of temperature T ; c_T is the influence factor of temperature on conduction velocity. c_T is given by Paintal^[88,89], which was obtained from data in the cat. Here it is assumed that the resulting rules were also applicable to human peripheral nerves.

13.3.3 Transmission time (t_t)

When the nerve length and conduction velocity are known, the time latency can then be calculated with the following equations:

$$t_t = L_n/v_c \quad (13.28)$$

In cold environment

$$t_t = \frac{L_{co}}{v_c (1 - x_{co}/100)} + \frac{L_f - L_{co}}{v_c} \quad (13.29)$$

13.4 Model of Modulation and Perception

When the signal is transmitted to the dorsal horn of the spinal cord and brain, where the signal is modulated and perceived as pain sensation. Gate control theory (GCT)^[90] is used here to describe the modulation and perception process of skin thermal pain.

13.4.1 GCT

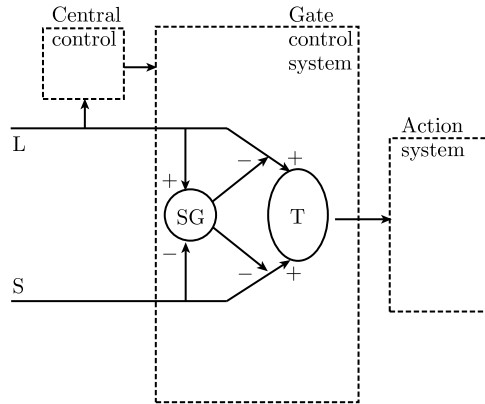
A number of theories have been proposed to explain the neural mechanisms associated with pain^[91], among which the gate control theory, proposed by Melzack & Wall in 1965^[90], was more successful than previous ones in explaining some features of pain process. It was the turning point in pain research and the basis for many of the advances in the understanding of pain. Figure 13.8(a) shows the schematics of the original version of the theory. In general, it is the small (C, A δ) fibers that carry information about noxious stimuli and the role of the large (A β) fibers is to carry information about less intense mechanical stimuli. As the signal from the C, A δ fibers is routed through substantia gelatinosa (SG) to central transmission (T) cells and onwards, the double inhibition (indicated by the minus signs) actually strengthens the signal. The signal from the A β fibers, however, is diminished in strength when routed through SG.

The gate control system is described as follows:

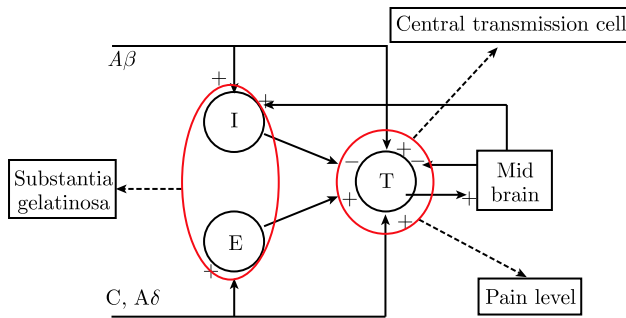
(1) When there is no stimulus, the small activity of the small fibers tends to keep the gate somewhat open and the very small activity of the large fibers is not enough to close it.

(2) When a small stimulus is applied to the skin, the activity of the large fibers gets relatively more increase although both types of fibers get more active, which tends to close the gate and results in passing through of a smaller proportion of the barrage.

(3) When the stimulus is strengthened, the activity of the small and the large fibers gets equal increase, which doesn't change the gate.



(a)



(b)

Figure 13.8 The schematic of the gate control theory: (a) basic schematic of the gate-control theory (b) that used in the mathematical model of pain (by permission of Elsevier)

(4) When the stimulus is maintained for a period of time, the natural adaptation of the L cells makes them less active, which causes the gate to open further.

(5) When the stimulus is still maintained but the L cells are kept active through (vibration), the gate tends to close.

13.4.2 Mathematical model

The GCT, as shown in Figure 13.8(b), has been used to extrapolate the relevant features and translated into a mathematical model by Britton & Skevington^[4,10~12]. It was then subjected to four simulations for verification: ① simulation consisting of constant small fibre input with variable large fibre input, which was to ascertain the inhibitory effect of the large fibre input, as evidence for this had been anecdotal due to the difficulty in

obtaining experimentally independent stimulation of large and small fibres; ② simulation involving small fibre input only, which was to establish that as the small fibre input is increased the T_{cell} output also increases at a rate “slightly greater than linear”; ③ simulation involving the phenomenon of wind-up^[92], which occurs following repeated stimulation of C fibres resulting in a progressive increase in the T-cell response; ④ simulation of ramp-off, which occurs when the peripheral stimulus is removed causing a pulse of pain^[93].

The mathematical description of GCT is given as

$$\tau_i \dot{V}_i = -(V_i - V_{i0}) + g_{li}(x_1) + g_{mi}(x_m) \quad (13.30)$$

$$\tau_e \dot{V}_e = -(V_e - V_{e0}) + g_{se}(x_s, V_e) \quad (13.31)$$

$$\tau_t \dot{V}_t = -(V_t - V_{t0}) + g_{st}(x_s) + g_{lt}(x_1) + g_{et}(x_e) - g_{it}(x_i) - g_{mt}(x_m) \quad (13.32)$$

$$\tau_m \dot{V}_m = -(V_m - V_{m0}) + g_{tm}(x_t) \quad (13.33)$$

where subscripts i, e, t and m stand for inhibitory SG cell, excitory SG cell, T-cell and midbrain, respectively; τ_t is the time constant, V_t is membrane potential; V_{t0} is initial membrane potential; x_t is the firing frequency; x_1 and x_s are signals (frequency) from large and small fibres, respectively; the functions g_{tm} represent the effects of the inputs (t) to a cell (m) on its steady state slow potential.

The firing frequency x_t at which the cell fires is a function of its slow potential, so that $x_t = f(V_t)$, given as

$$f(V_m) = [K(V_m - V_{\text{thr}})/(-V_{m0})] H(V_m - V_{\text{thr}}) \quad (13.34)$$

where H is the usual Heaviside function; K is a constant; V_{thr} is the firing threshold potential (taken as -55 mV). The output from the T-cell is taken to be in direct relation to the pain experience, such that if the T-cell exceeds its firing threshold ($V_t \geq -55$ mV) then the noxious signal is transmitted to the next relay point. If the noxious signals reach the cortex then they are perceived as pain.

With the parameters given by Britton & Skevington^[4,10~12], Equations (13.30)~(13.33) can be rewritten as:

$$0.7\dot{V}_i = -(V_i + 70) + 60 \tanh(\theta_{li}x_1) + 40 \tanh[f_m(V_m)] \quad (13.35)$$

$$0.7\dot{V}_e = -(V_e + 70) + 40 \tanh(\theta_{se}x_s) \{1 + 3 \tanh[4f_e(V_e)]\} \quad (13.36)$$

$$0.7\dot{V}_t = -(V_t + 70) + 40 \tanh [(1 - \theta_{se}) x_s] + 40 \tanh [(1 - \theta_{ii}) x_1] \\ + 40 \tanh [f_e (V_e)] - 40 \tanh [f_i (V_i)] - 40 \tanh [f_m (V_m)] \quad (13.37)$$

$$0.7\dot{V}_m = -(V_m + 70) + 40 \tanh [f_t (V_t)] \quad (13.38)$$

where $\tanh [4f_e (V_e)]$ is the Nmethyl-D-aspartate (NMDA) component of the equation. The NMDA receptor has been argued to be responsible for phenomena in pain sensation such as wind-up, where the response of a neuron increases progressively as the neuron is repeatedly stimulated. θ_{ii} and θ_{se} are the proportions of the inputs that pass through interneurons in the SG and correspondingly $(1 - \theta_{ii})$ and $(1 - \theta_{se})$ are the proportions passing through to the T-cell.

Whilst the model produced expected results in line with the literature, certain assumptions were made in order to simplify the model. The assumptions used are^[4,10~12]: ① the cell potentials in the model are the slow potentials, or moving time-averages of membrane potentials at the soma, and the firing frequency of a particular cell is assumed to be a function of its slow potential; ② any long term effects such as plasticity are neglected; ③ each T-cell is simulated by one C or A δ and one A β nerve fibre from the skin (with frequencies x_s and x_1 respectively) and one inhibitory and one excitatory SG cell; ④ the potentials V_k depend on the frequencies of impulses arriving at their dendrites from various sources, and on the dendrites and synaptic junctions themselves, whose properties we shall assume to be constant over the time scales; ⑤ the system is linear; ⑥ the cells don't fire until their potential reaches some threshold, and that above this threshold the firing frequency is an increasing function of slow potential; ⑦ the function must also saturate.

13.5 Results and Discussion

13.5.1 Description of problem

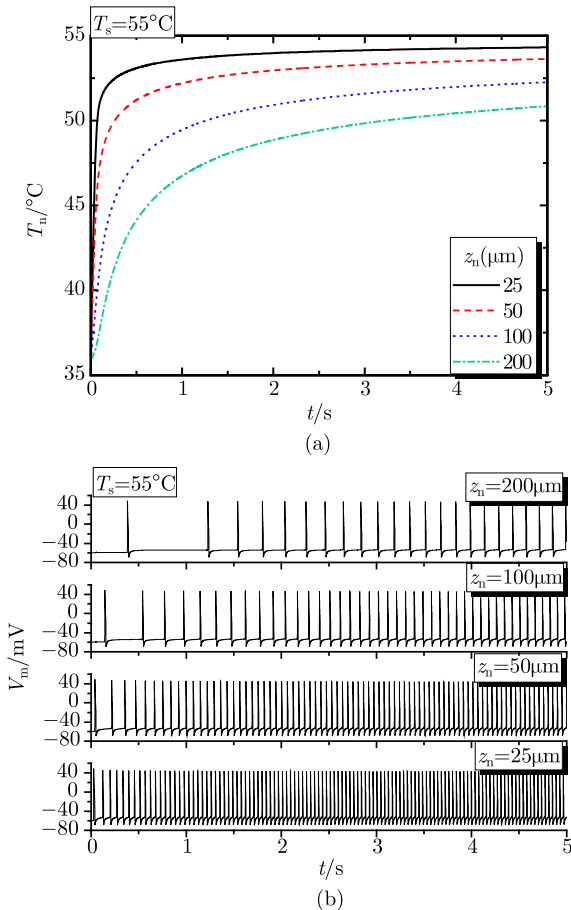
In this section, a case study of skin heating with constant surface temperature is carried out to illustrate the applicability of the developed holistic thermal pain model. The skin is initially kept at constant temperature. At $t = 0$, its surface initially at normal temperature is suddenly taken into contact with a hot source of constant temperature T_s for 5 s (i.e., the surface temperature is instantaneously raised to T_s). The depth of nociceptor is assumed to vary in the range of $25\mu\text{m} \leq z_n \leq 200\mu\text{m}$. With the skin thermo-mechanical model introduced earlier, the temperature history of nociceptor is obtained first, which is then used as the input for the neural model. The

nociceptors are assumed to be C fibres with conduction velocity of 1m/s.

The skin is divided into four layers with different properties: stratum corneum, epidermis, dermis and subcutaneous fat. Blood perfusion is only considered in the dermis layer while metabolic heat generation is considered in all four layers. The relevant parameters used for both heat transfer and thermal stress analyses are summarized in Table 6.1 and Table 6.4.

13.5.2 Influence of nociceptor depth

Nociceptors located at four different depths ($z_n = 25\mu\text{m}, 50\mu\text{m}, 100\mu\text{m}, 200\mu\text{m}$) are considered with stimulus $T_s = 55^\circ\text{C}$. With the skin thermo-mechanical model, the temperature history of nociceptor is first obtained, as given in Figure 13.9(a), which is then used as the input of the pain model. The corresponding neural responses and pain level are shown in



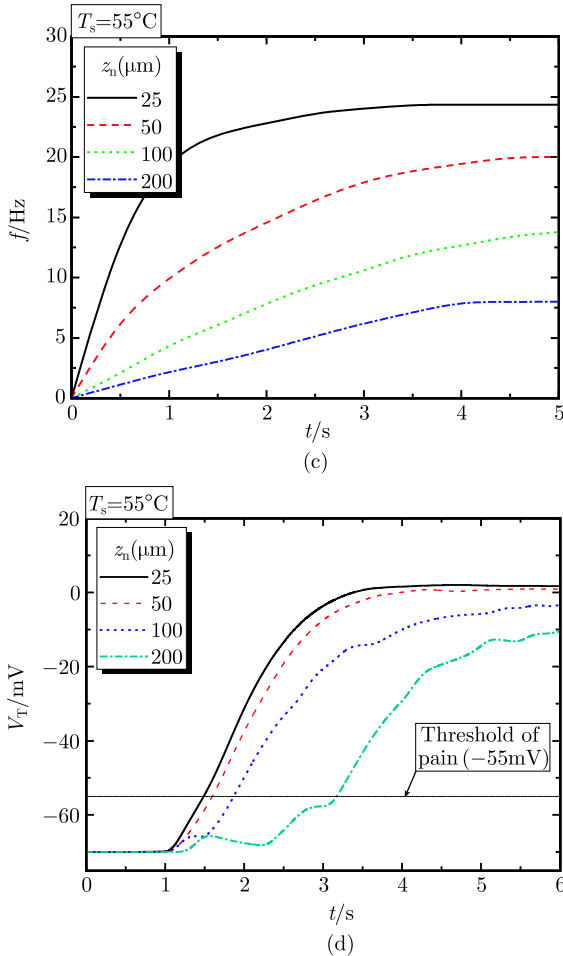


Figure 13.9 Influence of nociceptor location on transduction: (a) temperature (b) membrane voltage variation (c) frequency response (d) pain level (by permission of Elsevier)

Figure 13.9(b)~(d). From Figure 13.9(a), it can be seen that temperature at the location of nociceptor increases nearly exponentially with heating, tending eventually to a constant value with time. The temperature at nociceptor located closer to skin surface is much larger, e.g. at $t = 5s$ the temperature at $z_n = 25\mu m$ is almost $5^\circ C$ higher at $z_n = 200\mu m$. The variation of membrane voltage with time is plotted in Figure 13.9(b). The generation frequency of action potential spikes increases with time and, similar to that of temperature, it tends to a constant value. At the same time the frequency increases as the nociceptor depth is reduced, which can be better seen from frequency

history shown in Figure 13.9(c). It has been shown that the pain level is decided by signal frequency: Torebjork et al.^[94] observed a linear relationship between the mean responses of CMHs recorded in awake humans and the median ratings of pain. Therefore, it can be seen from our results that the pain level, as shown in Figure 13.9(d), is higher if the nociceptor is located closer to the surface of skin under the same stimulus intensity. This may be used to explain why different pain thresholds were obtained by different studies for the same stimulus^[15,16].

It should be noted here that there is a clear latency about 1 s as shown in Figure 13.9(d) due to the transmission. Similar results have also been experimentally observed. For example, Campbell & LaMotte^[95] found that, the median time to detection of temperature stimuli ranging from 39 to 51°C was in the range of 0.7~1.1s for the finger tip and 0.4~1.1s for the arm.

13.5.3 Influence of stimulus intensity

Naturally, it is expected that the magnitude of skin surface temperature has a great effect on pain. Figure 13.10(a)~(c) plot the temperature, membrane voltage variation, frequency responses and as functions of time for selected values of skin surface temperature, with the nociceptor fixed at $z_n = 50\mu\text{m}$. The nociceptor temperature increases much quicker under higher surface heating temperature, with the temperature difference between T_n almost equal to that of T_s for $t > 1\text{s}$ [see Figure 13.10(a)]. This temperature difference is better shown in plots of spikes densities, as can be seen from Figure 13.10(b) and (c).

The stimulus intensity–pain level relation is shown in Figure 13.11 in near threshold range. It can be found that there is a nearly linear relation in the temperature range studied. Similar results have been observed in literature. For example, LaMotte & Campbell^[46] found that heat pain increases monotonically with stimulus intensities between 40°C and 50°C and Torebjork et al.^[94] observed a linear relationship between mean responses of CMHs recorded in awake humans and median ratings of pain over the temperature range of 39~51°C. It was also shown that the intensity of cold pain is linearly correlated with that of a cold stimulus^[96~100]. For example, Georgopoulos^[97,98] found that the stimulus-response functions were approximately linear, with mean slopes of power functions of 1.15 while Simone & Kajander^[101] obtained a slope of 1.07.

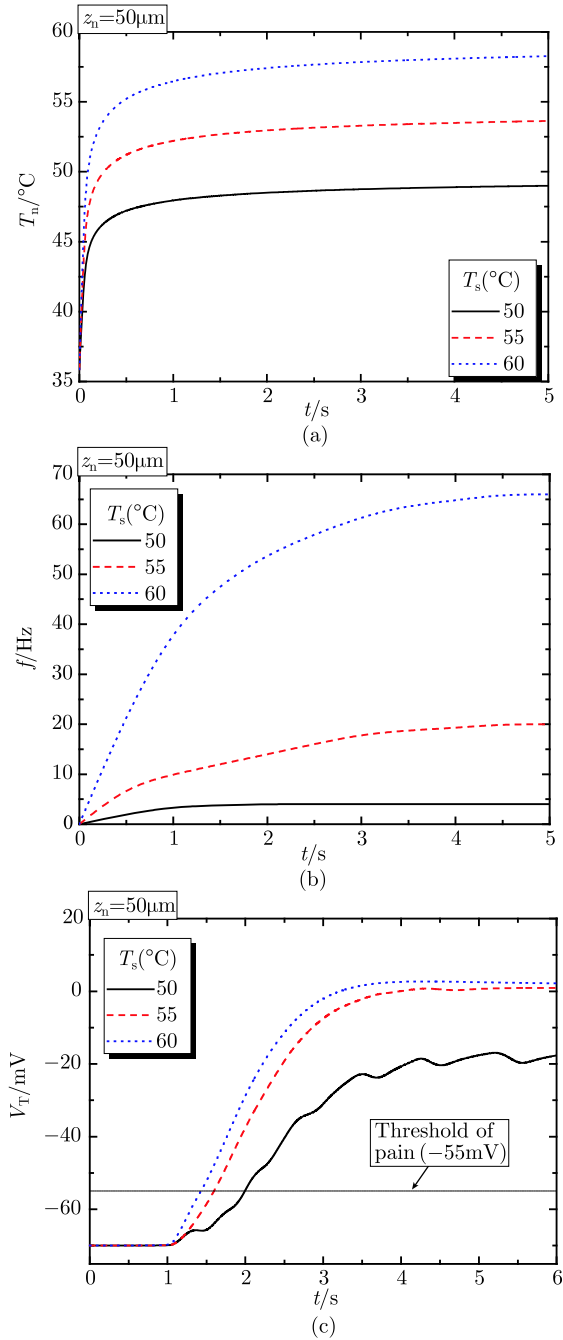


Figure 13.10 Influence of stimulus intensity on nociceptor transduction: (a) temperature (b) membrane voltage variation (c) frequency response (by permission of Elsevier)

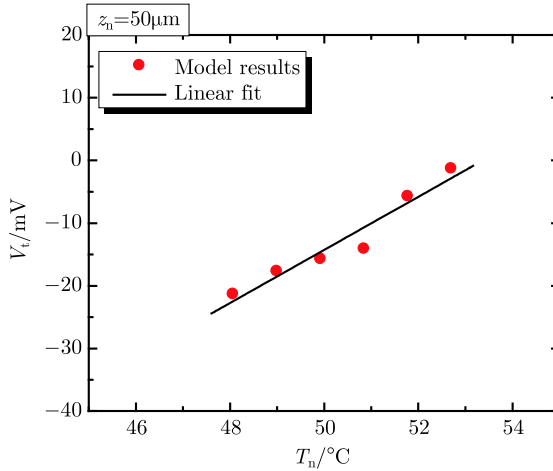


Figure 13.11 Stimulus intensity-pain level relation (by permission of Elsevier)

13.5.4 Role of thermal stress and thermal damage

To examine the rule of thermal stress and thermal damage, currents due to the opening of chemical-gated (I_{chem}) and mechanical-gated (I_{mech}) ion channels are added to the stimulation current (I_{st}). The result obtained with this current ($I_{\text{st}} = I_{\text{heat}} + I_{\text{chem}} + I_{\text{mech}}$) are then compared with that considering only I_{heat} . Since no experimental data are available, a simple linear relationship between generated currents and stimuli has been assumed for both I_{chem} and I_{mech} , given as

$$I_{\text{chem}} = C_c (Deg) \quad (13.39)$$

$$I_{\text{mech}} = C_m (\sigma_n - \sigma_t) / \sigma_t \quad (13.40)$$

where $C_c = C_m = 20 \mu\text{A}/\text{cm}^2$ is assumed.

The skin is initially kept at constant temperature. At $t = 0$, the skin surface initially at normal temperature is suddenly taken into contact with a hot source of constant temperature $T_s = 55^\circ\text{C}$ (i.e., the surface temperature is instantaneously raised to 55°C); after contacting for 5s, the hot source is removed and the skin is cooled by natural convection of environmental air [$T_e = 25^\circ\text{C}$, $h = 7\text{W}/(\text{m}^2 \cdot \text{K})$] for 5s. The nociceptors are assumed to be located at a depth of $50 \mu\text{m}$.

The thermomechanical responses of skin tissue are plotted as functions of time in Figure 13.12(a)~(c), while the comparison between neural responses of the nociceptor and pain level with and without considering I_{chem} and I_{mech} are given in Figure 13.13(a)~(c). It can be seen from these results that, during heating the pain level (frequency) increases continually,

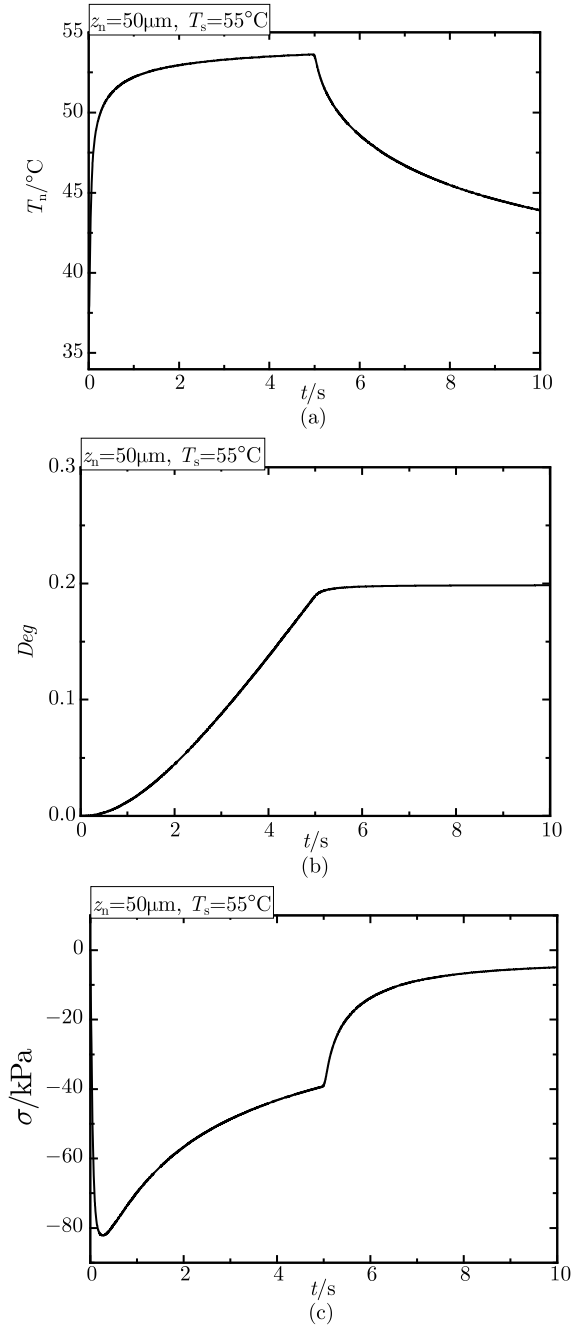


Figure 13.12 Thermo-mechanical responses at location of nociceptor:

(a) temperature (b) thermal damage degree (c) thermal stress

(by permission of Elsevier)

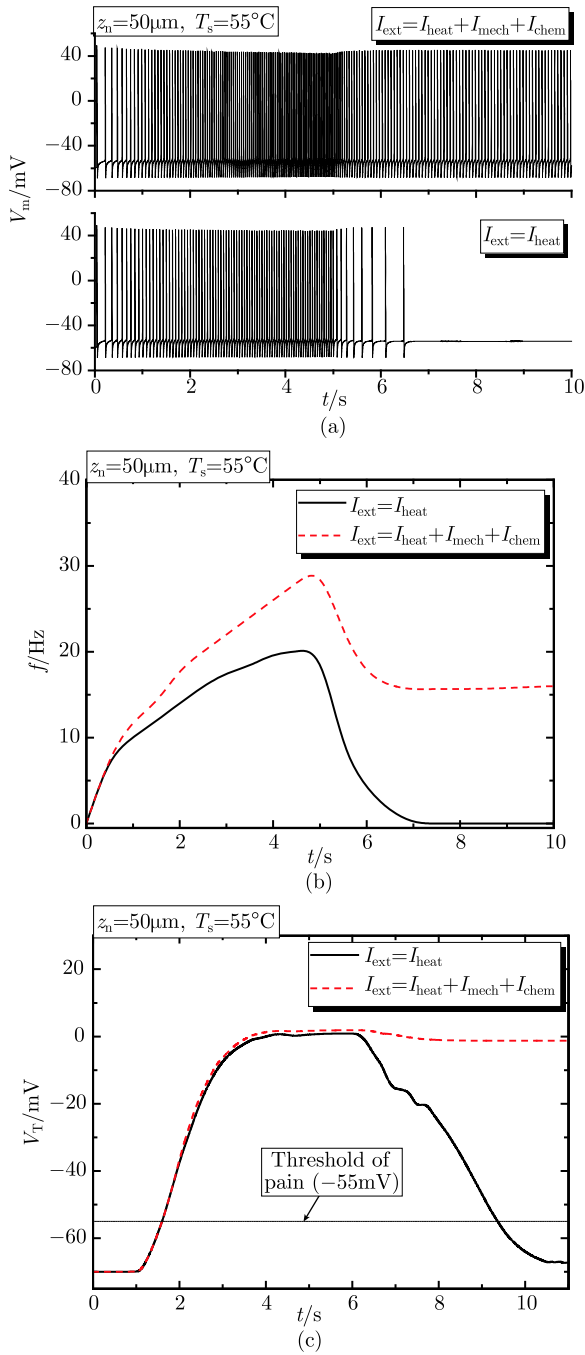


Figure 13.13 Role of thermal stress and thermal damage: (a) membrane voltage variation (b) frequency response (c) pain level (by permission of Elsevier)

peaking at about $t = 5\text{s}$. Although heating is stopped at $t = 5\text{s}$, there is still generation of action potential for both cases since temperature at the nociceptor location is still higher than the threshold [see Figure 13.12(a)]. For the model without considering I_{chem} and I_{mech} , after the peak, the pain level decreases quickly due to the decrease of temperature and, at about $t = 7\text{s}$, the generation of action potential stops due to the decrease of T_n below the threshold. In comparison, the pain level obtained from the model with I_{chem} and I_{mech} included is still high despite of the ending of heating; even during the heating process, the model predicts a higher frequency than that predicted from the model considering I_{heat} alone. This is mainly attributed to the thermal damage (I_{chem}), since the thermal stress is smaller than the mechanical threshold of nociceptor [see Figure 13.12(c)] so that $I_{\text{mech}} = 0$. Thermal damage has been accumulated in skin tissue during heating, which is an irreversible process. Thus the thermal damage will cause the cells to break down and release a number of tissue byproducts and mediators that keep the chemically-gated ion channels fully opened. This explains why people still feel pain even when a noxious heat source has been removed from our skin, a common phenomenon called hyperpathia.

13.5.5 Role of non-Fourier thermal behaviour

1) Description of the problem

The skin is initially kept at constant temperature. At $t = 0$, its surface initially at normal temperature is suddenly taken into contact with a hot source of constant temperature $T_s = 60^\circ\text{C}$ (i.e., the surface temperature is instantaneously raised to T_s); after contacting for 5s, the hot source is removed and the skin is cooled by cold water ($T_s = 15^\circ\text{C}$) for 10s. The depth of nociceptor is assumed to be $z_{\text{noc}} = 50\mu\text{m}$, which is in the reasonable range of experimental measurement^[15,16]. Using the skin bioheat transfer model, the temperature history of the nociceptor is obtained first, which is then used as input for the neural model.

2) Thermal behaviour

The temperature distributions at the end of heating ($t = 5\text{s}$) and cooling ($t = 15\text{s}$) along skin depth, as predicted by using different bioheat transfer models, are shown in Figure 13.14. As a whole, the temperature decreases along skin depth during heating and increases during cooling, except for that of thermal wave model at $t = 15\text{s}$. As shown in Figure 13.14, the thermal relaxation time τ_q tends to induce an abrupt step in the temperature (i.e., a wave-front is introduced), which separates the heated surface area from

the unheated inner area. It is noticed that a sudden temperature drop for heating or a step for cooling at the skin surface occurs with the DPL model.

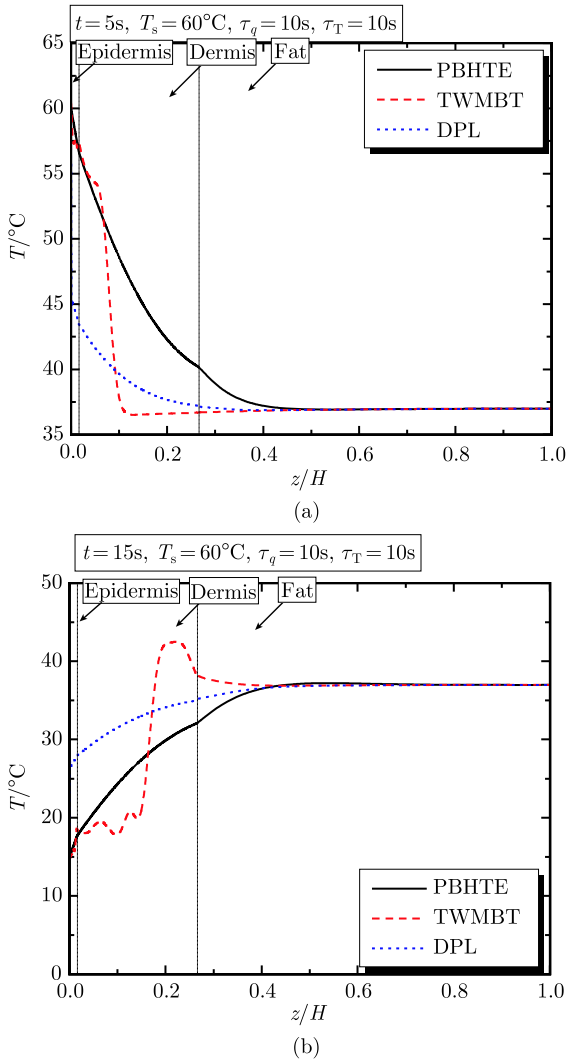
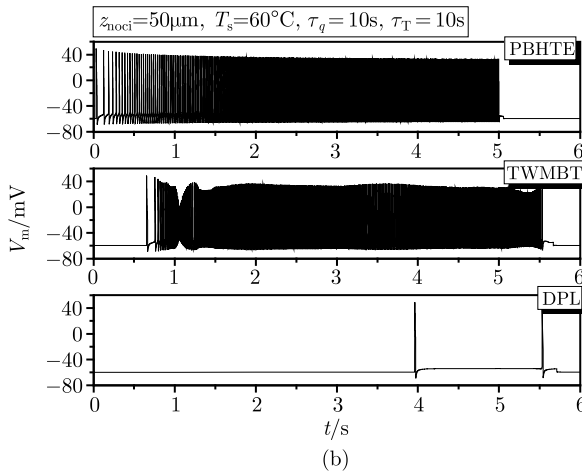
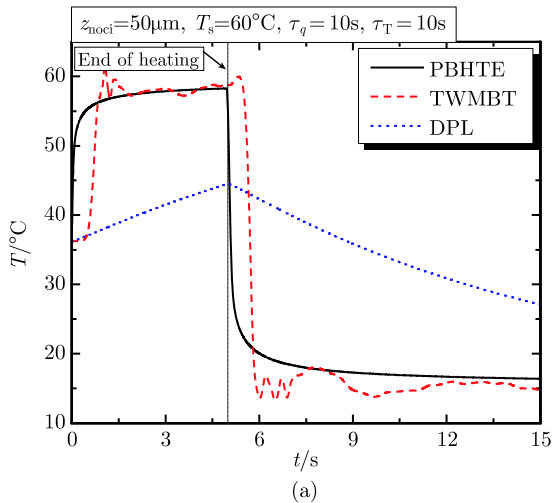


Figure 13.14 Comparison of predictions of temperature distribution along skin depth from different models: (a) at $t = 5\text{s}$ (b) at $t = 15\text{s}$ (by permission of Elsevier) (PBHTE: Pennes model; TWMBT: thermal wave model; DPL: dual-phase lag model)

3) Comparison of the thermal-neural responses

Comparison between the thermal-neural responses of nociceptors predicted with different models is presented in Figure 13.15(a) for temperature, in Figure 13.15(b) for membrane voltage variation, and in Figure 13.15(c)

for frequency response. From Figure 13.15(a), it can be seen that the nociceptor temperature increases nearly exponentially during heating, tending eventually to a constant value with time. With the thermal wave model, the tissue temperature inside the body is undisturbed during the initial stage of heating before jumping instantaneously, which may be viewed as the wave front emerging from the finite propagation of thermal wave or the existence of relaxation time τ_q . The unchanged tissue temperature during the initial stage may be attributed to the non-thermally consumption related biological activities^[102]. The predictions from the DPL model differ from those of both Pennes model and thermal wave model. Unlike the thermal wave model, no wave behaviour is observed in the DPL models as expected, but a non-Fourier



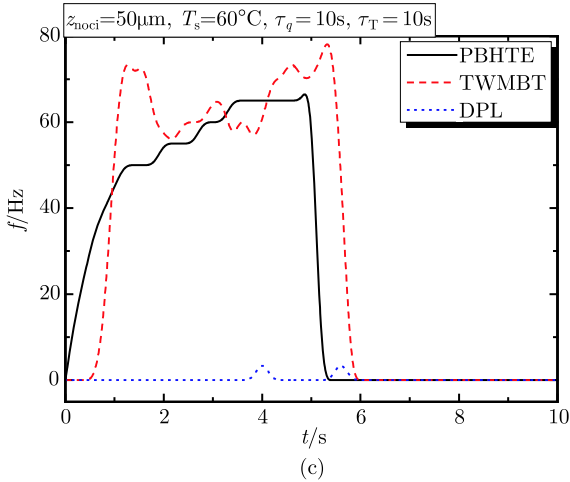


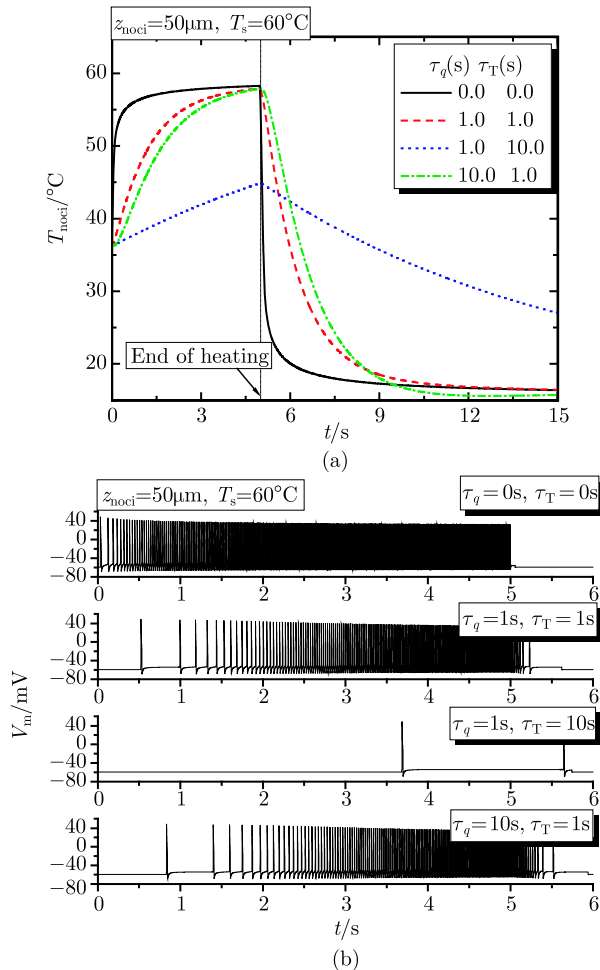
Figure 13.15 Comparison of predictions of the thermal-neural response of nociceptors from different models: (a) temperature, (b) membrane voltage variation, and (c) frequency response (by permission of Elsevier)

diffusion-like behaviour exists due to the second thermal relaxation time τ_T whose effect is to weaken the thermal wave, thereby destroying the sharp wave front.

The large differences amongst the predicted temperatures from different models can cause significant deviations in membrane voltage variation and frequency response of nociceptors, as can be seen from Figure 13.15(b) and (c). For the results predicted from both the Pennes model and the thermal wave model, the generation frequency of action potential spikes increases with time and, similar to temperature, it tends to a constant value. Note that there is a clear latency (about 0.6 s) for neural response predicted by the thermal wave model, as shown in Figure 13.15(b) and (c). Similar results have also been experimentally observed^[95]. This means that non-Fourier thermal behaviour may play a role in the latency phenomenon, which has previously been attributed to signal transmission along nerve fibers^[103]. However, with the DPL model, only two action potentials can be observed. This can be explained by the corresponding temperature as shown in Figure 13.15(a), where the nociceptor temperature is less than the threshold (43°C) during most of the heating period. It has been established that pain level is decided by signal frequency^[94]. Therefore, it can be seen from our results that, for the same heating condition, both the Pennes model and the thermal wave model predict relatively high levels of pain (frequency), and there is little pain predicted from the DPL model.

4) Effect of thermal relaxation time

To investigate the effect of τ_q and τ_T on the thermal-neural response of nociceptors, calculations with different values of thermal relaxation time have been performed with the DPL model. The results are presented in Figure 13.16(a) for temperature, in Figure 13.16(b) for membrane voltage variation, and in Figure 13.16(c) for frequency response. As can be seen from Figure 13.16(a), no obvious wave-fronts are found in all the cases studied: the sharp wave-fronts due to τ_q are smoothed by the promoting conduction of τ_T , and the effect is more noticeable with increasing values of τ_T . This is attributable to the stronger dissipation from the mixed derivative term ($\tau_T k \nabla^2 \partial T / \partial t$) due to the existence of τ_T , as shown in Equation (13.9), which leads to the non-Fourier diffusion-like conduction.



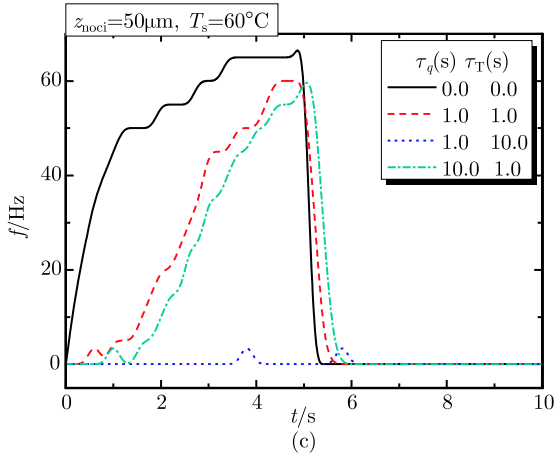


Figure 13.16 Effect of τ_T and τ_q on the predictions of thermal-neural response of nociceptors from DPL model: (a) temperature, (b) membrane voltage variation, and (c) frequency response (by permission of Elsevier)

From the membrane voltage variation and frequency response shown in Figure 13.16(b) and (c), it can be seen that, with τ_T fixed at 1s, the latency of neural response increases with increasing τ_q : when $\tau_q = 1$ s, the time for the generation of the first action potential is $t \approx 0.5$ s, which delays to $t \approx 0.8$ s when $\tau_q = 10$ s. This suggests that it is τ_q , rather than τ_T , that dominates the wave-like behaviour of the thermal-neural response of nociceptors in skin tissue.

13.6 Summary

In summary, this chapter presented the result of skin thermal pain modeling. A holistic mathematical model for quantifying skin thermal pain has been developed, by using the thermomechanical models developed in Chapter 6 and considering the current biophysical and neurological mechanisms of pain sensation, where the concepts of bioengineering are coupled with established methods in neuroscience, and the biological behaviour of skin is re-casted in engineering systems parlance. The model development has been made consistent with the known morphology and physiology of skin tissue. The model is composed of three interconnected parts: peripheral modulation of noxious stimuli, which converts the energy from a noxious thermal stimulus into electrical energy via nerve impulses; transmission, which transports these neural signals from the site of transduction in the skin to the spinal cord and brain; and modulation and perception in the spinal cord and brain.

It has been demonstrated that the model is capable of capturing the essential properties of experimentally measured frequency responses. With this model, the intensity of thermal pain can be predicted directly in terms of the character of the noxious stimuli: as a corollary, for a given thermal treatment profile, a given medical procedure can be determined how painful (or not) it becomes. The mechanism of skin thermal pain can be better understood and some features of pain sensation can be explained, such as hyperpathia.

References

- [1] Arendt-Nielsen L, Chen A. Lasers and other thermal stimulators for activation of skin nociceptors in humans. *Clinical Neurophysiology*, 2003, 33(6): 259–268.
- [2] Borckardt J J, Anderson B, Andrew Kozel F, et al. Acute and long-term VNS effects on pain perception in a case of treatment-resistant depression. *Neurocase*, 2006, 12(4): 216–220.
- [3] Mao-Ying Q L, Cui K M, Liu Q, et al. Stage-dependent analgesia of electroacupuncture in a mouse model of cutaneous cancer pain. *European Journal of Pain*, 2006, 10(8): 689–694.
- [4] Britton N F, Skevington S M. On the mathematical modeling of pain. *Neurochemical Research*, 1996, 21(9): 1133–1140.
- [5] Picton P D, Campbell J A, Turner S J. Modelling chronic pain: An initial survey. 8th International Conference on Neural Information Processing. Shanghai, 2001: 1267–1270.
- [6] Fors U, Ahlquist M L, Skagerwall R, et al. Relation between intradental nerve activity and estimated pain in man: A mathematical model. *Pain*, 1984, 18(4): 397–408.
- [7] Fors U G, Ahlquist M L, Edwall L G, et al. Evaluation of a mathematical model analysing the relation between intradental nerve impulse activity and perceived pain in man. *International Journal of Biomedical Computing*, 1986, 19(3–4): 261–277.
- [8] Fors U G, Edwall L G, Haegerstam G A. The ability of a mathematical model to evaluate the effects of two pain modulating procedures on pulpal pain in man. *Pain*, 1988, 33(2): 253–264.
- [9] Fors U G, Sandberg H H, Edwall L G, et al. A comparison between different models of the relation between recorded intradental nerve impulse activity and reported pain in man. *International Journal of Biomedical Computing*, 1989, 24(1): 17–28.
- [10] Britton N F, Chaplain M A, Skevington S M. The role of N-methyl-D-aspartate (NMDA) receptors in wind-up: A mathematical model. *IMA Journal of Mathematics Applied in Medicine and Biology*, 1996, 13(3): 193–205.
- [11] Britton N F, Skevington S M. A mathematical model of the gate control theory of pain. *Journal of Theoretical Biology*, 1989, 137(1): 91–105.

- [12] Britton N F, Skevington S M, Chaplain M A J. Mathematical modeling of acute pain. *Journal of Theoretical Biology*, 1995, 3(4): 1119–1124.
- [13] Minamitani H, Hagita N. A neural network model of pain mechanisms computer simulation of the central neural activities essential for the pain and touch sensations. *IEEE Transactions on Systems Man and Cybernetics*, 1981, 11: 481–493.
- [14] Haeri M, Asemani D, Gharibzadeh S. Modeling of pain using artificial neural networks. *Journal of Theoretical Biology*, 2003, 220(3): 277–284.
- [15] Tillman D B, Treede R D, Meyer R A, et al. Response of C fibre nociceptors in the anaesthetized monkey to heat stimuli: Correlation with pain threshold in humans. *The Journal of Physiology*, 1995, 485(3): 767–774.
- [16] Tillman D B, Treede R D, Meyer R A, et al. Response of C fibre nociceptors in the anaesthetized monkey to heat stimuli: Estimates of receptor depth and threshold. *The Journal of Physiology*, 1995, 485(3): 753–765.
- [17] Junger H, Moore A C, Sorkin L S. Effects of full-thickness burns on nociceptor sensitization in anesthetized rats. *Burns*, 2002, 28(8): 772–777.
- [18] Kirkpatrick S J, Chang I, Duncan D D. Viscoelastic anisotropy in porcine skin: Acousto-optical and mechanical measurements. *International Society for Optical Engineering*, 2005, 34: 174–183.
- [19] Khatyr F, Imberdis C, Vescovo P, et al. Model of the viscoelastic behaviour of skin in vivo and study of anisotropy. *Skin Research and Technology*, 2004, 10(2): 96–103.
- [20] Wu J Z, Dong R G, Smutz W P, et al. Non-linear and viscoelastic characteristics of skin under compression: Experiment and analysis. *Biomedical Material Engineering*, 2003, 13(4): 373–385.
- [21] Silver F H, Freeman J W, DeVore D. Viscoelastic properties of human skin and processed dermis. *Skin Research and Technology*, 2001, 7(1): 18–23.
- [22] Moy G, Singh U, Tan E, et al. Human psychophysics for teletactation system design. *The Electronic Journal of Haptics Research*, 2000, 1(3): 1–20.
- [23] Wu J Z, Krajnak K, Welcome D E, et al. Analysis of the dynamic strains in a fingertip exposed to vibrations: Correlation to the mechanical stimuli on mechanoreceptors. *Journal of Biomechanics*, 2006, 39(13): 2445–2456.
- [24] Gulati R J, Srinivasan M A. Human fingerpad under indentation I: Static and dynamic force response. *ASME New York*, 1995: 261–262.
- [25] Pawluk D T V. A Viscoelastic Model of the Human Fingerpad and a Holistic Model of Human Touch [Ph. D. Thesis]. Cambridge: Harvard University, 1997.
- [26] Patapoutian A, Peier A M, Story G M, et al. Thermo TRP channels and beyond: Mechanisms of temperature sensation. *Nature Reviews Neuroscience*, 2003, 4(8): 529–539.
- [27] Cain D M, Khasabov S G, Simone D A. Response properties of mechanoreceptors and Nociceptors in mouse glabrous skin: An in vivo study. *Journal of Neurophysiology*, 2001, 85(4): 1561–1574.
- [28] James N C, Richard A M. *Neurobiology of Nociceptors*. Oxford: Oxford University Press, 1996.

- [29] Hodgkin A L, Huxley A F. A quantitative description of membrane current and its application to conduction and excitation in nerve. *The Journal of Physiology*, 1952, 117(4): 500–544.
- [30] Pawluk D, Howe R. A holistic model of human touch. 5th Annual CNS Meeting. Saskatoon, 1996.
- [31] Nemoto I, Miyazaki S, Saito M, et al. Behavior of solutions of the hodgkin-huxley equations and its relation to properties of mechanoreceptors. *Biophysical Journal*, 1975, 15(5): 469–479.
- [32] Miftakhov R N, Wingate D L. Electrical activity of the sensory afferent pathway in the enteric nervous system. *Biological Cybernetics*, 1996, 75(6): 471–483.
- [33] Takeuchi E, Yamanobe T, Pakdaman K, et al. Analysis of models for crustacean stretch receptors. *Biological Cybernetics*, 2001, 84(5): 349–363.
- [34] Torkkeli P H, French A S. Simulation of different firing patterns in paired spider mechanoreceptor neurons: The role of Na(+) channel inactivation. *Journal of Neurophysiology*, 2002, 87(3): 1363–1368.
- [35] Lv Y G, Liu J. Interpretation on thermal comfort mechanisms of human bodies by combining Hodgkin-Huxley neuron model and Pennes bioheat equation. *Forschung im Ingenieurwesen*, 2005, 69(2): 101–114.
- [36] Braun H A, Huber M T, Anthes N, et al. Noise-induced impulse pattern modifications at different dynamical period-one situations in a computer model of temperature encoding. *Biosystems*, 2001, 62(1-3): 99–112.
- [37] Frankenhaeuser B, Huxley A F. The action potential in the myelinated nerve fiber of *xenopus laevis* as computed on the basis of voltage clamp data. *The Journal of Physiology*, 1964, 171(2): 302–315.
- [38] Noble D. Applications of Hodgkin-Huxley equations to excitable tissues. *Physiological Reviews*, 1966, 46(1): 1–50.
- [39] Adrian R H, Chandler W K, Hodgkin A L. Voltage clamp experiments in striated muscle fibres. *The Journal of Physiology*, 1970, 208(3): 607–644.
- [40] Wechselberger M, Wright C L, Bishop G A, et al. Ionic channels and conductance-based models for hypothalamic neuronal thermosensitivity. *American Journal of Physiology: Regulatory, Integrative and Comparative Physiology*, 2006, 291(3): R518–R529.
- [41] Cesare P, Moriondo A, Vellani V, et al. Ion channels gated by heat. *Proceedings of the National Academy of Sciences*, 1999, 96(14): 7658–7663.
- [42] Dormand J R, Prince P J. A family of embedded Runge-Kutta formulae. *Journal of Computational and Applied Mathematics*, 1980, 6: 19–26.
- [43] Hille B. *Ionic Channels of Excitable Membranes*. Sunderland: Sinauer Associates, 1992.
- [44] Adriaensen H, Gybels J, Handwerker H O, et al. Suppression of C-fibre discharges upon repeated heat stimulation may explain characteristics of concomitant pain sensations. *Brain Research*, 1984, 302(2): 203–211.
- [45] Meyer R A, Campbell J N. Myelinated nociceptive afferents account for the hyperalgesia that follows a burn to the hand. *Science*, 1981, 213(4515): 1527–1529.

- [46] LaMotte R H, Campbell J N. Comparison of responses of warm and nociceptive C-fiber afferents in monkey with human judgments of thermal pain. *Journal of Neurophysiology*, 1978, 41(2): 509–528.
- [47] Treede R D, Meyer R A, Campbell J N. Myelinated mechanically insensitive afferents from monkey hairy skin: Heat-response properties. *Journal of Neurophysiology*, 1998, 80(3): 1082–1093.
- [48] Fuortes M G, Mantegazzini F. Interpretation of the repetitive firing of nerve cells. *The Journal of General Physiology*, 1962, 45(6): 1163–1179.
- [49] Jack J J B, Noble D, Tsien R W. *Electric Current Flow in Excitable Cells*. London: Oxford University Press, 1975: 305–378.
- [50] Dodge F A. On the transduction of visual, mechanical, and chemical stimuli. *International Journal of Neuroscience*, 1972, 3(1): 5–14.
- [51] Shapiro B I, Lenherr F K. Hodgkin-Huxley axon. Increased modulation and linearity of response to constant current stimulus. *Biophysical Journal*, 1972, 12(9): 1145–1158.
- [52] Radmilovich M, Fernández A, Trujillo-Cenóz O. Environment temperature affects cell proliferation in the spinal cord and brain of juvenile turtles. *The Journal of Experimental Biology*, 2003, 206(17): 3085–3093.
- [53] Xu H, Robertson R M. Effects of temperature on properties of flight neurons in the locust. *Journal of Comparative and Physiological Psychology*, 1994, 175: 193–202.
- [54] Chandler W K, Meves H. Rate constants associated with changes in sodium conductance in axons perfused with sodium fluoride. *Journal of Physiology*, 1970, 211(3): 679–705.
- [55] Joyner R W. Temperature effects on neuronal elements. *Fed Proc*, 1981, 40(14): 2814–2818.
- [56] Sjodin R A, Mullins L J. Oscillatory behavior of the squid axon membrane potential. *The Journal of General Physiology*, 1958, 42(1): 39–47.
- [57] Guttman R. Effect of temperature on the potential and current thresholds of axon membrane. *The Journal of General Physiology*, 1962, 46(2): 257–266.
- [58] Guttman R. Temperature characteristics of excitation in space-clamped squid axons. *The Journal of General Physiology*, 1966, 49(5): 1007–1018.
- [59] Fitzhugh R. Theoretical effect of temperature on threshold in the Hodgkin-Huxley nerve model. *The Journal of General Physiology*, 1966, 49(5): 989–1005.
- [60] Moore J W. Temperature and drug effects on squid axon membrane ion conductances. *Fed Proc*, 1958, 17: 113.
- [61] Cao X J, Oertel D. Temperature affects voltage-sensitive conductances differentially in octopus cells of the mammalian cochlear nucleus. *Journal of Neurophysiology*, 2005, 94(1): 821–832.
- [62] Bezanilla F, Taylor R E. Temperature effects on gating currents in the squid giant axon. *Biophysical Journal*, 1978, 23(3): 479–484.
- [63] Zhao Y, Boulant J A. Temperature effects on neuronal membrane potentials and inward currents in rat hypothalamic tissue slices. *The Journal of Physiology*, 2005, 564(7): 245–257.

- [64] Rosenthal J J, Bezanilla F. A comparison of propagated action potentials from tropical and temperate squid axons: Different durations and conduction velocities correlate with ionic conductance levels. *The Journal of Experimental Biology*, 2002, 205(12): 1819–1830.
- [65] Volgushev M, Vidyasagar T R, Chistiakova M, et al. Membrane properties and spike generation in rat visual cortical cells during reversible cooling. *The Journal of Physiology (London)*, 2000, 522(1): 59–76.
- [66] Hodgkin A L, Katz B. The effect of temperature on the electrical activity of the giant axon of the squid. *The Journal of Physiology*, 1949, 109: 240–249.
- [67] Cocherová E. The Temperature Relationship in the Modified Hodgkin-Huxley Model of the Nerve Fibre. 12th International Scientific Conference Radioelektronika. Bratislava, 2002: 132–135.
- [68] Hodgkin A L, Huxley A F, Katz B. Measurement of current-voltage relations in the membrane of the giant axon of Loligo. *The Journal of Physiology*, 1952, 116(4): 424–448.
- [69] Hodgkin A L. *The Conduction of the Nervous Impulses*. Liverpool: Liverpool University Press, 1964.
- [70] Rattay F. *Electrical Nerve Stimulation*. Wien: Springer-Verlag, 1990.
- [71] Bremer F, Titeca J. Etude Oscillographique De La Paralyse Thermique Du Nerf. *Archives Internationales De Physiologie Et De Biochimie*, 1946, 54(3): 237–272.
- [72] Huxley A F. Ion movements during nerve activity. *The New York Academy of Sciences*, 1959, 81: 221–246.
- [73] Llinás R, Mühlethaler M. Electrophysiology of guinea-pig cerebellar nuclear cells in the in vitro brain stem-cerebellar preparation. *The Journal of Physiology*, 1988, 404: 241–258.
- [74] Koch C. *Biophysics of Computation*. New York: Oxford University Press, 1999.
- [75] Connor J A, Walkter D, McKown R. Neural repetitive firing modifications of the hodgkin-huxley axon suggested by experimental results from crustacean axons. *Biophysical Journal*, 1977, 18(1): 81–102.
- [76] Rush M E, Rinzel J. The potassium a-current, low firing rates and rebound excitation in hodgkin-huxley models. *Bulletin of Mathematical Biology*, 1995, 57(6): 899–929.
- [77] Connor J A, Stevens C F. Voltage clamp studies of a transient outward membrane current in gastropod neural somata. *The Journal of Physiology (London)*, 1971, 213(1): 21–30.
- [78] Kanold P O, Manis P B. A physiologically based model of discharge pattern regulation by transient K^+ currents in cochlear nucleus pyramidal cells. *Journal of Neurophysiology*, 2001, 85(2): 523–538.
- [79] Hewitt M J, Meddis R. A computer model of dorsal cochlear nucleus pyramidal cells: Intrinsic membrane properties. *Journal of the Acoustical Society of America*, 1995, 97(4): 2405–2413.
- [80] Kernell D, Sjöholm H. Repetitive impulse firing: Comparisons between neurone models based on “voltage clamp equations” and spinal motoneurons.

- Acta Physiol Scand, 1973, 87(1): 40–56.
- [81] Rothman J S, Manis P B. The roles potassium currents play in regulating the electrical activity of ventral cochlear nucleus neurons. *Journal of Neurophysiology*, 2003, 89(6): 3097–3113.
- [82] Hagiwara S, Kusano K, Saito N. Membrane changes in Onchidium nerve cell in potassium rich media. *The Journal of Physiology (London)*, 1961, 155(3): 470–489.
- [83] Rudy B. Diversity and ubiquity of K channels. *Neuroscience*, 1988, 25(3): 729–749.
- [84] Sheng M, Liao Y J, Jan Y N, et al. Presynaptic A-current based on heteromultimeric K⁺ channels detected in vivo. *Nature*, 1993, 365(6441): 72–75.
- [85] Connor J A, Stevens C F. Prediction of repetitive firing behaviour from voltage clamp data on an isolated neurone soma. *The Journal of Physiology*, 1971, 213(1): 31–53.
- [86] De Medinaceli L, Hurpeau J, Merle M, et al. Cold and post-traumatic pain: Modeling of the peripheral nerve message. *Biosystems*, 1997, 43(3): 145–167.
- [87] Julius D, Basbaum A I. Molecular mechanisms of nociception. *Nature*, 2001, 413(6852): 203–210.
- [88] Paintal A S. Effects of temperature on conduction in single vagal and saphenous myelinated nerve fibres of the cat. *The Journal of Physiology (London)*, 1965, 180(1): 20–49.
- [89] Paintal A S. The influence of diameter of medullated fibres of cats on the rising and falling phases of the spike and its recovery. *The Journal of Physiology (London)*, 1966, 184(4): 791–811.
- [90] Melzack R, Wall P D. Pain mechanisms: A new theory. *Science*, 1965, 150(699): 971–979.
- [91] Guyton A C, Hall J E. *Textbook of Medical Physiology*. 10th Edition. Philadelphia: WB Saunders, 2000.
- [92] Mendell L M. Physiological properties of unmyelinated fiber projection to the spinal cord. *Experimental Neurology*, 1966, 16(3): 316–332.
- [93] Humphries S A, Johnson M H, Long N R. An investigation of the gate control theory of pain using the experimental pain stimulus of potassium iontophoresis. *Percept Psychophys*, 1996, 58(5): 693–703.
- [94] Torebjork H E, LaMotte R H, Robinson C J. Peripheral neural correlates of magnitude of cutaneous pain and hyperalgesia: Simultaneous recordings in humans of sensory judgments of pain and evoked responses in nociceptors with C-fibers. *Journal of Neurophysiology*, 1984, 51(2): 325–339.
- [95] Campbell J N, LaMotte R H. Latency to detection of first pain. *Brain Research*, 1983, 266(2): 203–208.
- [96] Iggo A. Cutaneous heat and cold receptors with slowly conducting (C) afferent fibres. *Quarterly Journal of Experimental Physiology*, 1959, 44(4): 362–370.
- [97] Georgopoulos A P. Functional properties of primary afferent units probably

- related to pain mechanisms in primate glabrous skin. *Journal of Neurophysiology*, 1976, 39(1): 71–83.
- [98] Georgopoulos A P. Stimulus-response relations in high-threshold mechanothermal fibers innervating primate glabrous skin. *Brain Research*, 1977, 128(3): 547–552.
 - [99] Chery-Croze S. Painful sensation induced by a thermal cutaneous stimulus. *Pain*, 1983, 17(2): 109–137.
 - [100] Chery-Croze S. Relationship between noxious cold stimuli and the magnitude of pain sensation in man. *Pain*, 1983, 15(3): 265–269.
 - [101] Simone D A, Kajander K C. Responses of cutaneous A-fiber nociceptors to noxious cold. *Journal of Neurophysiology*, 1997, 77(4): 2049–2060.
 - [102] Liu J, Chen X, Xu L X. New thermal wave aspects on burn evaluation of skin subjected to instantaneous heating. *IEEE Transactions on Biomedical Engineering*, 1999, 46(4): 420–428.
 - [103] Plaghki L, Mouraux A. How do we selectively activate skin nociceptors with a high power infrared laser? *Physiology and biophysics of laser stimulation. Clinical Neurophysiology*, 2003, 33(6): 269–277.

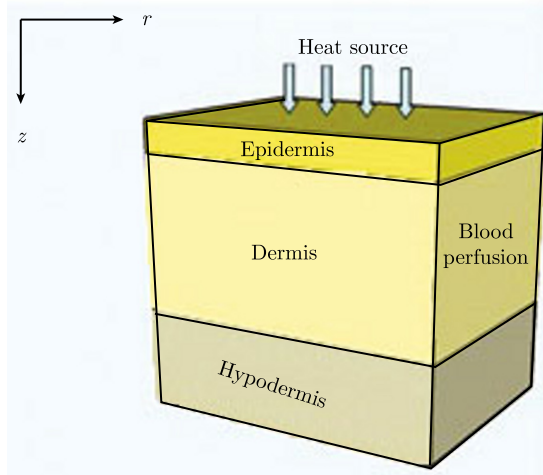


Figure 2.1 Structure of human skin

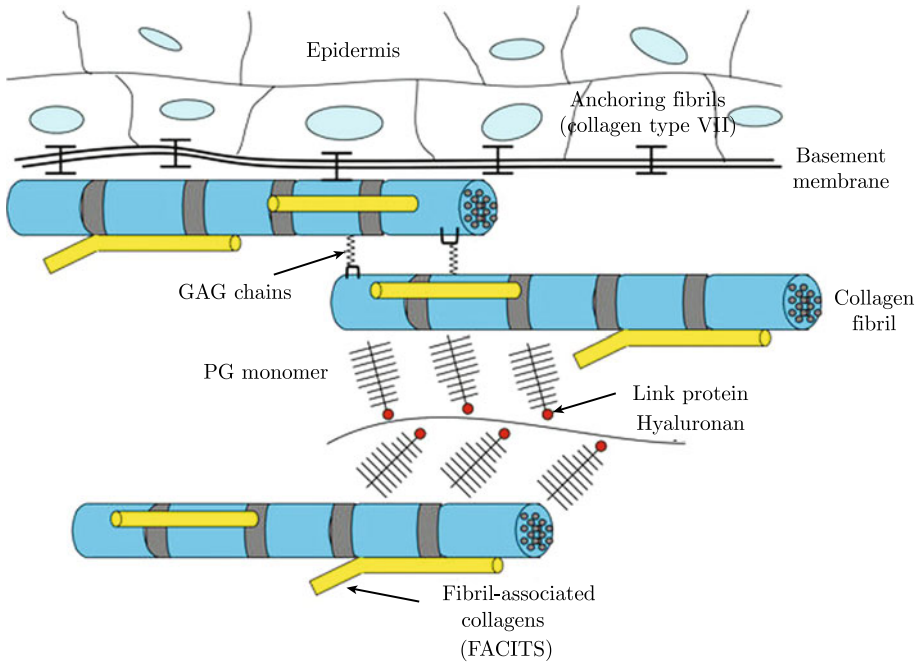


Figure 2.2 Macromolecular components of skin

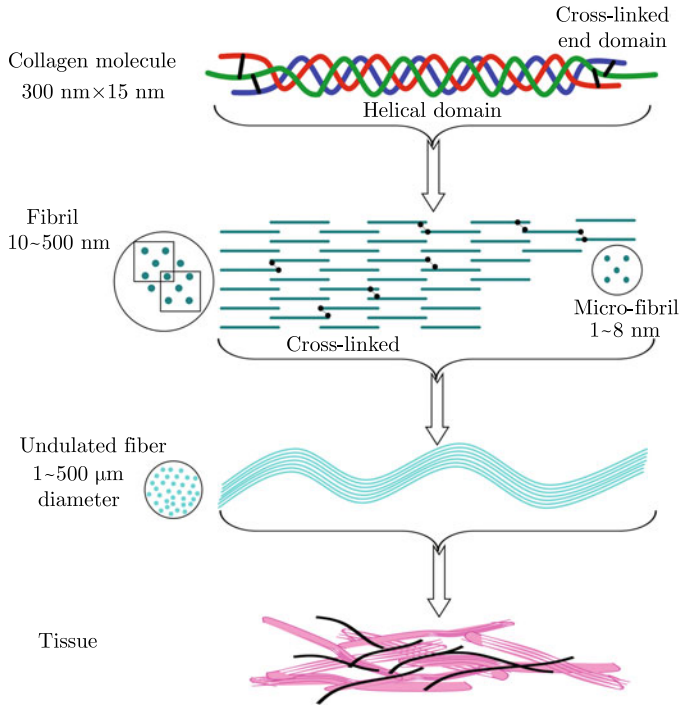


Figure 2.3 Molecular/fibrillar configuration of Type I collagen

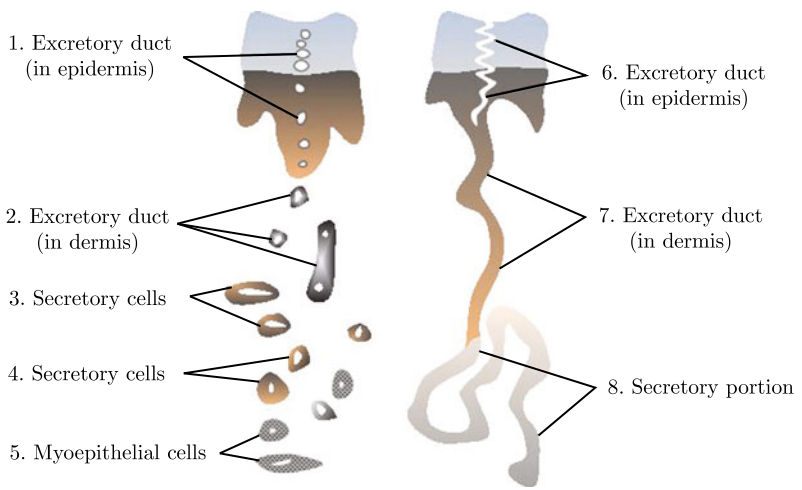


Figure 2.8 Sweat gland in skin

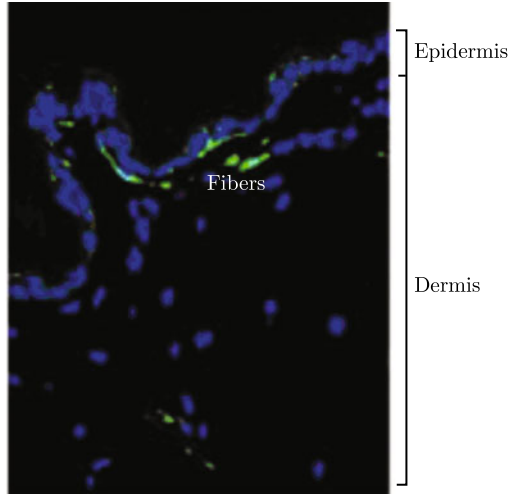


Figure 2.9 Histological section of free nerve endings in skin^[28]
 (by permission of Nature Publishing Group)

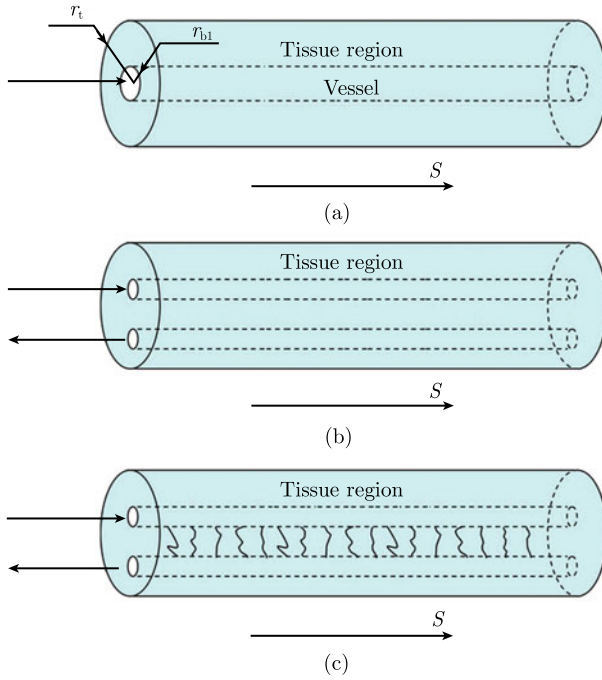


Figure 3.1 Vessel configurations of vascular models: (a) unidirectional vessel configuration; (b) countercurrent vessel configuration; (c) large/small/large vessel configuration

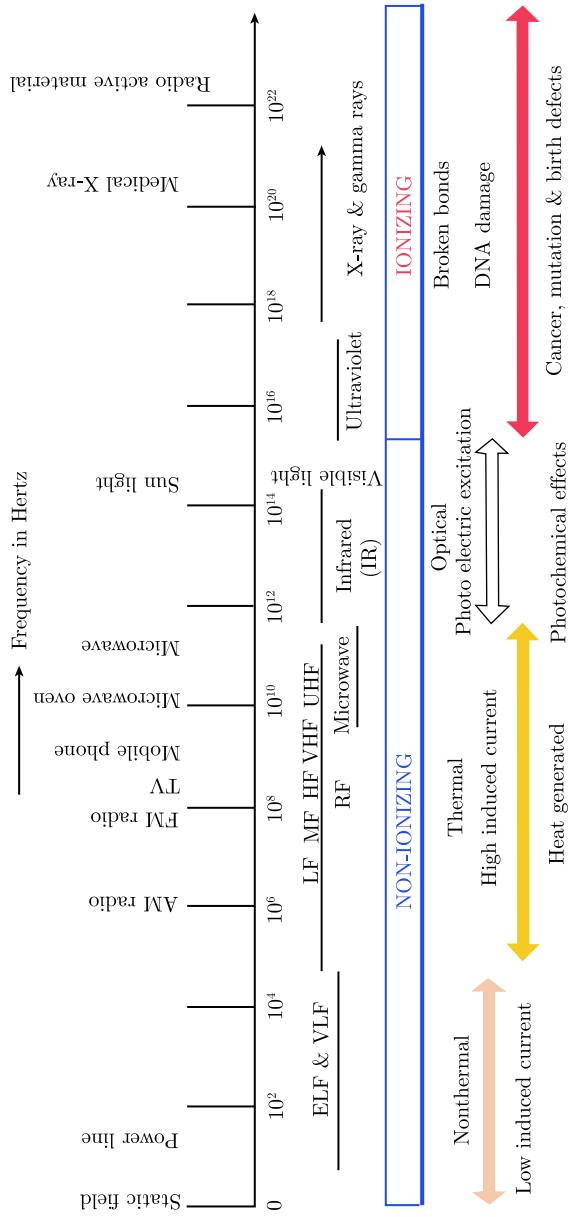


Figure 3.3 Electromagnetic spectrum^[59] (by permission of the author)

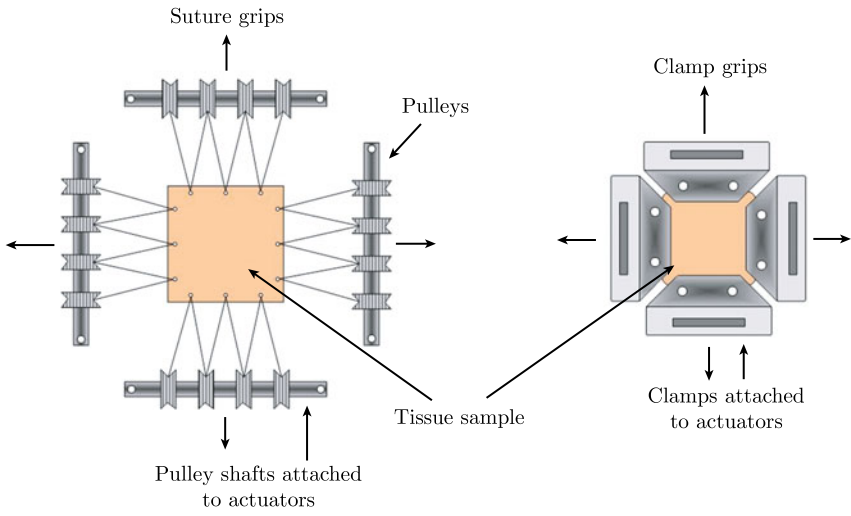


Figure 6.3 Different holding methods

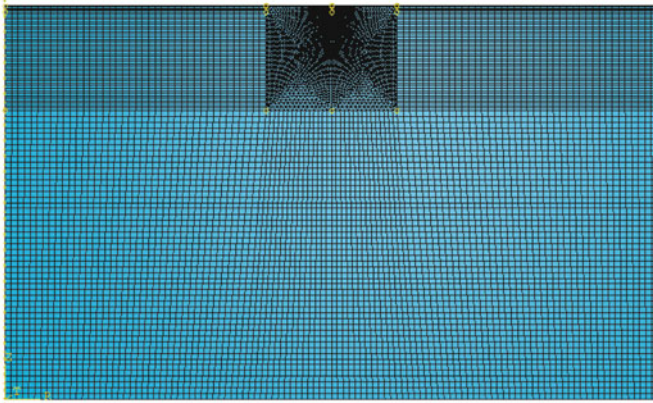


Figure 9.4 Mesh of the skin model in Figure 9.3 (by permission of Elsevier)

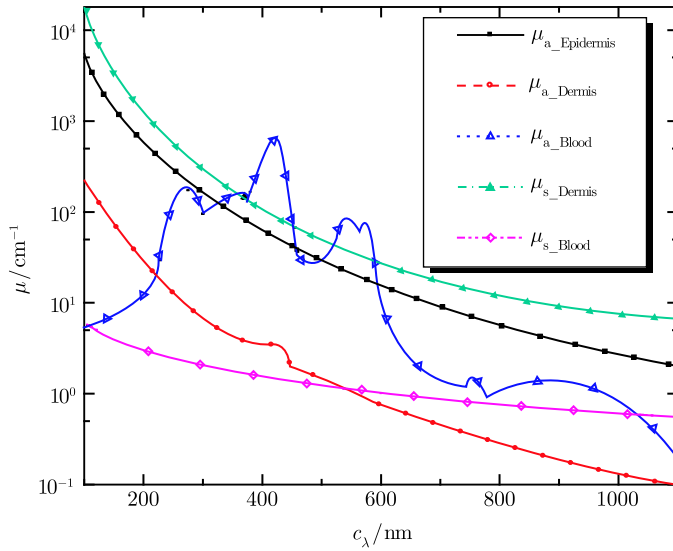


Figure 9.19 Optical properties of different skin layers (by permission of Elsevier)

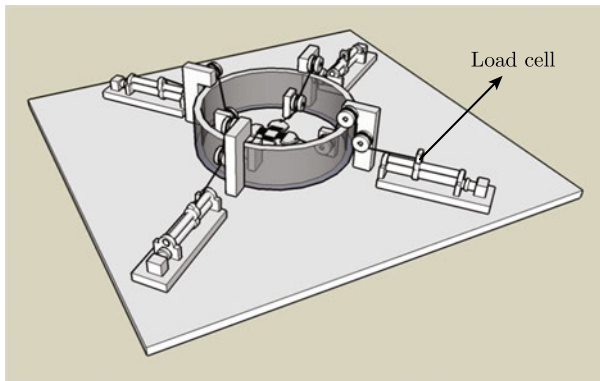


Figure 10.2 Loading subsystem of the hydrothermal tensile testing system: user-defined loading, such as isometric tension tests and isotonic tension tests, can be achieved through the pulley system



Figure 10.3 Practical implementation of Figure 10.1

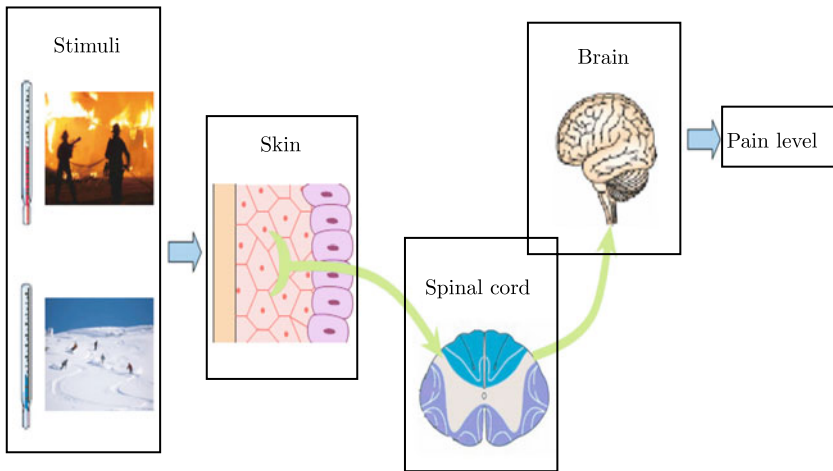


Figure 11.1 Skin thermal pain pathway: stimulus (hot/cold) → skin (the energy of thermal stimulus is converted into electrical energy via nerve impulses) → spinal cord & brain (the signals are transmitted to the dorsal horn of the spinal cord and brain, where they are modulated and perceived as pain sensation)
(by permission of Elsevier)

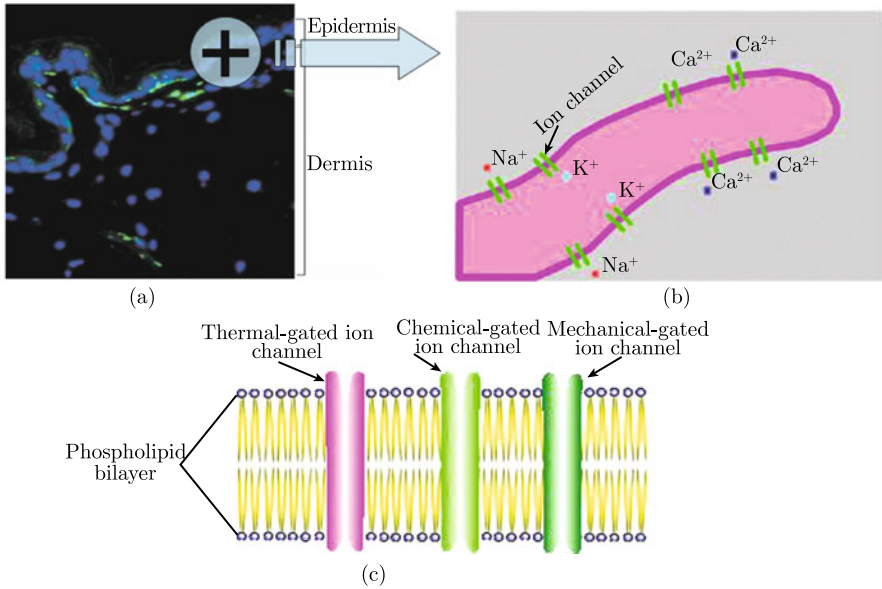


Figure 11.4 Schematic of nociceptor transduction: if the thermal stimulus surpasses the thermal threshold of nociceptors [points in (a)^[51]], the heat current will be induced due to the opening of the corresponding ion channels in (b), and the action potential is triggered; the thermal stress and thermal-damage-induced release of some chemical mediators may also open corresponding mechanically- and chemically-gated channels in (c) if it is larger than the mechanical threshold (by permission of Nature Publishing Group)

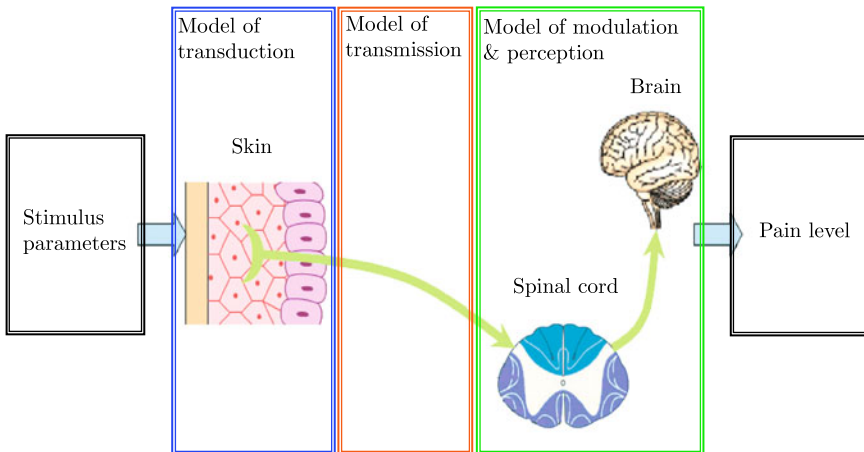


Figure 13.1 Schematic of the holistic skin thermal pain model (by permission of Elsevier)